PIONEER OUTER PLANETS ORBITER

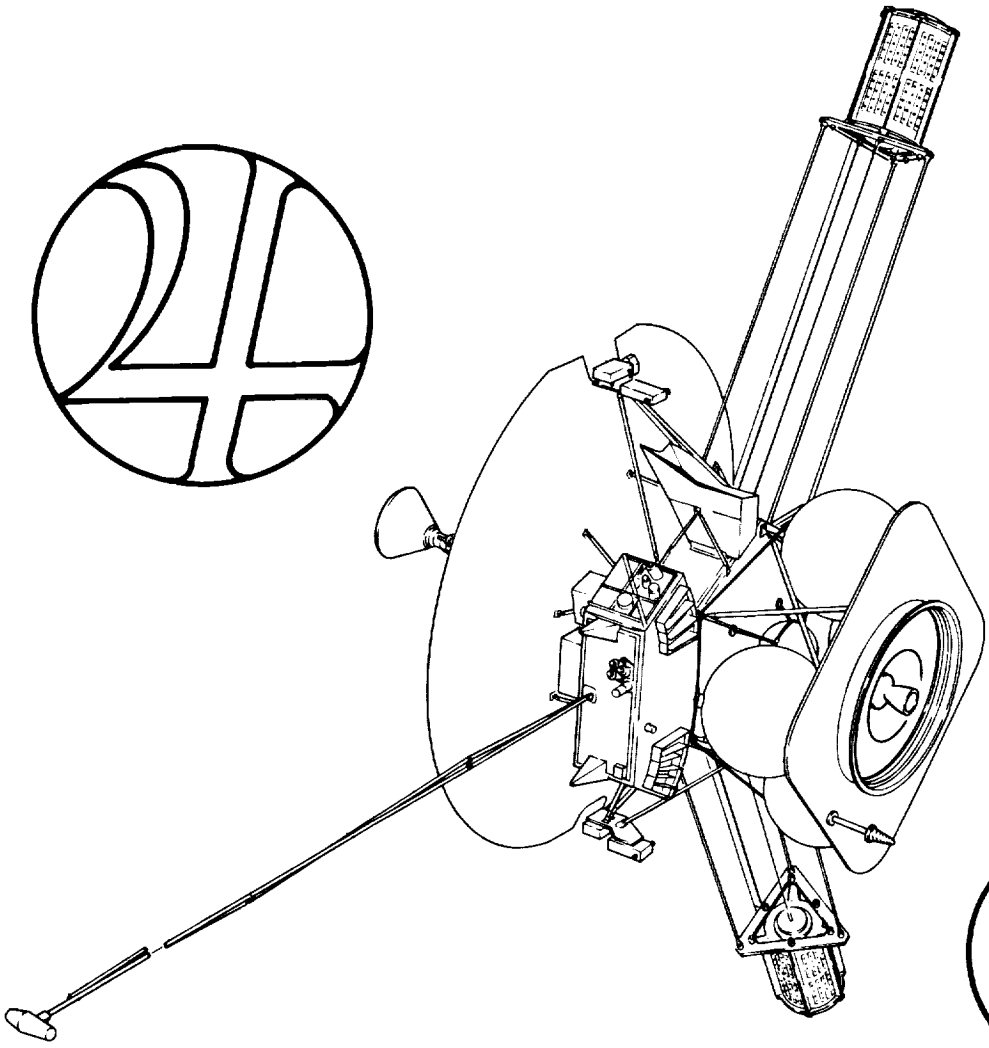

NATIONAL AERONAUTICS AND SPACE ADMINISTRATION
AMES RESEARCH CENTER
MOFFETT FIELD, CALIFORNIA

10 December 1974

THIS REPORT CONSISTS OF A MAIN VOLUME

AND A SEPARATE VOLUME OF APPENDICES

CONTENTS

		Page
NOTATION		xvii
1.	INTRODUCTION	1-1
1.1	Mission Description	1-2
1.1.1	Mission Objectives	1-2
1.1.2	Launch	1-2
1.1.3	Post Launch	1-3
1.1.4	Interplanetary	1-3
1.1.5	Planetary Approach and Orbit Injection	1-4
1.1.6	Planetary Orbit Phase	1-4
1.2	Pioneer 10 and 11 Description	1-5
1.2.1	System-Level Description	1-5
1.2.2	Propulsion and Attitude Control	1-7
1.2.3	Electric Power	1-7
1.2.4	Thermal Control	1-7
1.2.5	Communications	1-9
1.2.6	Data Handling	1-11
1.3	Related Documents	1-11
1.4	Organization of the Report	1-12
2.	SUMMARY OF DESIGN REQUIREMENTS	2-1
2.1	Mission Requirements	2-1
2.1.1	Environmental Factors	2-1
2.1.2	Mission Categories	2-7
2.2	Spacecraft Design	2-10
2.2.1	Mechanical Requirements	2-10
2.2.2	Electrical Requirements	2-13
2.2.3	Thermal Requirements	2-14
2.2.4	Data and Communication Requirements	2-14
2.2.5	Propulsion Requirements	2-15

CONTENTS (CONTINUED)

		Page
2.3	Interfaces	2-17
2.3.1	Launch Vehicle	2-17
2.3.2	Deep Space Network	2-18
2.3.3	RTG Power Sources	2-19
3.	SPACECRAFT SYSTEM DESIGN	3-1
3.1	Configuration	3-1
3.1.1	Design Approach	3-1
3.1.2	Jupiter Orbiter Configuration	3-7
3.1.3	Saturn Orbiter Configuration	3-20
3.1.4	Alternate Orbiter Configurations	3-20
3.2	Mass Properties	3-24
3.2.1	Spacecraft Weight Summary	3-24
3.2.2	Mass Properties Requirements	3-24
3.2.3	Mass Properties Summary	3-24
3.2.4	Subsystem Weight Estimates	3-24
3.3	Electrical Block Diagram	3-32
3.4	Electrical Power Budget	3-34
3.5	Dynamic Characteristics	3-37
3.5.1	Attitude Stability	3-37
3.5.2	Nutation Effects due to Injection and Spacecraft Separation	3-40
3.5.3	Appendage Deployment Dynamics	3-41
3.5.4	Nutation Effects due to ΔV and Precession Maneuvers	3-45
3.6	Variation of Spin Rate	3-49
3.6.1	Proposed Spin Rate Profile	3-49
3.6.2	Effects of Spin Rate Reduction	3-51
3.6.3	Effects of Spin Rate Increase	3-54
3.6.4	Redundant Spin/Despin Thruster Pair	3-55

CONTENTS (CONTINUED)

		Page
3.7	Orbit Insertion Thrust Level	3-55
3.8	Telemetry Allocations	3-58
3.9	Command Assignments	3-63
4.	SUBSYSTEM DESIGN	4-1
4.1	Structure	4-1
4.1.1	Equipment Compartment	4-2
4.1.2	Propulsion Bay and Interstage Structure	4-2
4.1.3	High-Gain Antenna Support	4-5
4.1.4	RTG Support Assembly	4-5
4.1.5	Magnetometer Boom Assembly	4-5
4.2	Thermal Control	4-9
4.2.1	Thermal Control Design Approach	4-9
4.2.2	Thermal Control Heaters	4-17
4.2.3	Spacecraft-RTG Thermal Interface	4-18
4.3	Propulsion	4-19
4.3.1	Requirements	4-19
4.3.2	Candidate Configurations	4-21
4.3.3	Preferred Subsystem Description	4-27
4.4	Attitude Control	4-30
4.4.1	Requirements	4-30
4.4.2	Functional Description	4-31
4.4.3	Orbiter Mission Considerations	4-34
4.4.4	Roll Attitude Signal Generation	4-35
4.4.5	Operation at Extended Solar Ranges	4-42
4.4.6	Spin Rate Variations	4-42
4.4.7	Experiment Drive Assembly	4-46
4.4.8	Restrictions in Performing Maneuvers	4-48
4.4.9	Subsystem Modification Summary	4-49

CONTENTS (CONTINUED)

		Page
4.5	Electrical Power	4-50
4.5.1	Subsystem Description	4-50
4.5.2	RTG's	4-52
4.5.3	Power Control Unit	4-52
4.5.4	Shunt Regulator/Radiator	4-53
4.5.5	Inverter Assembly	4-54
4.5.6	CTRF	4-55
4.6	Command Distribution	4-56
4.6.1	Summary Description	4-56
4.6.2	Digital Decoder Unit	4-58
4.6.3	Command Distribution Unit	4-58
4.7	Data Handling	4-63
4.7.1	Summary Description	4-63
4.7.2	Digital Telemetry Unit (DTU)	4-67
4.7.3	Data Storage Unit	4-72
4.8	Communications	4-75
4.8.1	Functional Requirements	4-75
4.8.2	Summary Description	4-76
4.8.3	Telemetry Link Performance Trades	4-79
4.8.4	Dual Frequency Transmission	4-80
4.8.5	Telemetry System Optimization	4-81
4.8.6	Ranging	4-82
4.8.7	Hardware Implementation	4-84
5.	SPACECRAFT PERFORMANCE	5-1
5.1	Accommodation of Scientific Instruments	5-1
5.1.1	Mechanical	5-1
5.1.2	Thermal	5-2
5.1.3	Electrical	5-2
5.1.4	Signals to the Instruments	5-3
5.1.5	Data from the Instruments	5-3
5.1.6	Pointing and Scanning Capabilities	5-11

CONTENTS (CONTINUED)

		Page
5.2	Attitude Control Performance	5-12
5.2.1	Operational Modes	5-12
5.2.2	Stored Program	5-13
5.2.3	Thruster Selection	5-14
5.2.4	Control Effectivity	5-15
5.2.5	Spin Rate	5-15
5.2.6	Stellar Reference	5-16
5.3	Propulsion Performance	5-16
5.3.1	Functions of Primary and Auxiliary Propulsion Subsystems	5-16
5.3.2	Bipropellant System Performance	5-17
5.3.3	Monopropellant System Performance	5-17
5.4	Power Subsystem	5-19
5.5	Communications Capability	5-20
5.5.1	Uplink	5-20
5.5.2	Downlink	5-22
5.6	Reliability and Extended Life Capability	5-27
5.6.1	Fail-Safe Design Policy	5-27
5.6.2	Single-Point Failures	5-28
5.6.3	Wear-Out Life	5-29
5.6.4	Radiation and Micrometeoroid Environment	5-30
5.6.5	Reliability Analysis	5-31
5.6.6	Reliability Improvements	5-42
6.	MISSION PERFORMANCE OF THE JUPITER ORBITER	6-1
6.1	Launch Opportunities	6-1
6.2	Selection Criteria for Earth-Jupiter Trajectories	6-3
6.3	Departure Energy and Arrival Velocity for the 1981, 1983 and 1985 Launch Opportunities	6-5
6.4	Retro-Propulsion Performance Characteristics and Tradeoffs	6-7
6.5	Launch Vehicle Performance	6-9

CONTENTS (CONTINUED)

		Page
6.6	Launch Phase	6-10
	6.6.1 Launch Constraints	6-10
	6.6.2 Declination of Departure Asymptote	6-11
	6.6.3 Launch Azimuth and Parking Orbit Caost Time	6-12
6.7	Selected Nominal Earth-Jupiter Transfer Trajectories	6-14
	6.7.1 Trajectory Characteristics	6-14
	6.7.2 Trajectory Time History, Pointing Angles and Communication Distances	6-14
6.8	Jupiter Orbit Insertion	6-17
	6.8.1 Orbit Insertion Retro Velocity Requirements	6-17
	6.8.2 Effects of Finite Thrust Acceleration and Constant Thrust Direction	6-17
	6.8.3 ΔV Penalty for Finite Thrust Orbit Insertion at Jupiter	6-20
6.9	Jupiter Orbit Characteristics	6-22
	6.9.1 Orbit Size	6-22
	6.9.2 Eccentricity	6-22
	6.9.3 Orbit Periods	6-22
	6.9.4 Inclination	6-23
	6.9.5 Orbit Perturbations	6-23
	6.9.6 Satellite Encounter Orbits	6-24
6.10	Orbit Corrections	6-28
6.11	Navigation	6-32
	6.11.1 Navigational Requirements	6-33
	6.11.2 Pioneer 10 and 11 Orbit Determination Accuracy	6-34
	6.11.3 Accuracy of Saturn Approach Navigation	6-36
	6.11.4 Effect of Encounter Accuracy on Capture Orbit Characteristics	6-37
	6.11.5 In-Orbit Navigation	6-40
	6.11.6 Approach Guidance Maneuver	6-40
6.12	Operational Sequences and Time Lines	6-41
	6.12.1 Summary of Operational Sequence for a Typical Mission	6-41

CONTENTS (CONTINUED)

		Page
6.12.2	Post-Launch Operations	6-41
6.12.3	Spacecraft Maneuver Operations	6-41
6.12.4	Typical Operations in Jupiter Orbit	6-45
6.13	Performance Summary	6-48
6.13.1	Orbit Performance Chart	6-48
6.13.2	Spacecraft Performance Summary in 1982 and 1985 Sample Missions	6-50
7.	MISSION PERFORMANCE OF THE SATURN ORBITER	7-1
7.1	Launch Opportunities, Launch Phase Characteristics, Departure and Arrival Velocity	7-1
7.2	Selected Nominal Earth-Saturn Transfer Trajectories	7-5
7.3	Saturn Orbit Insertion	7-8
7.3.1	Orbit Insertion Retro Velocity Requirements	7-8
7.3.2	Influence of Ring Particle Impact Hazard on Orbit Selection	7-10
7.3.3	Effect of Finite Thrust Acceleration and Constant Thrust Direction	7-12
7.3.4	Orbit Insertion in the Earth-Pointing Mode	7-14
7.4	Saturn Orbit Characteristics	7-15
7.5	Navigation	7-16
7.6	Operational Sequence	7-17
7.7	Performance Summary	7-17
8.	CONCLUSIONS	8-1
	REFERENCES	R-1
	APPENDIX A - SCIENTIFIC INSTRUMENTS	A-1
	APPENDIX B - MISSION ANALYSIS	B-1
	APPENDIX C - ELECTRONIC PIECE PARTS FAILURE RATES	C-1
	APPENDIX D - STRUCTURAL LOADS ON APPENDAGES DUE TO COMBINED SPIN AND THRUST EFFECTS	D-1
	APPENDIX E - CANDIDATE RTG POWER SOURCES	E-1

ILLUSTRATIONS

		Page
1-1	Pioneer F/G Spacecraft	1-6
1-2	General Arrangement of the Pioneer F/G Equipment Compartment	1-8
1-3	Pioneer F/G Spacecraft Functional Block Diagram	1-10
2-1	Estimated Impacts Sustained During Saturn Ring Crossing	2-3
2-2	Model and Actual Proton Fluences in Jovian Radiation Environment	2-6
2-3	Mission Categories	2-11
3-1	Principal Axis Control Approach of Pioneer Spacecraft with Asymmetrical RTG Deployment	3-3
3-2	Jupiter Orbiter Configuration	3-8
3-3	Jupiter Orbiter Propulsion Bay	3-10
3-4	Propulsion Structural and Tank Support Configuration	3-12
3-5	Jupiter Orbiter Equipment Bay Layout	3-14
3-6	Rotational Mounting of Optical Sensors	3-17
3-7	Saturn Orbiter Propulsion Bay Configuration	3-21
3-8	Alternate Spacecraft and Propellant Tank Support Configurations	3-22
3-9	Functional Block Diagram	3-33
3-10	Updated Orbiter Stability Performance	3-39
3-11	Wobble Damper Performance	3-39
3-12	Deployment Simulation Model	3-43
3-13	Time History of (a) Wobble Angle, (b) Body Rates and (c) Boom Moments During Simultaneous Deployment of Appendages	3-46
3-14	Pointing Errors Caused by Main Thrust Maneuver	3-47
3-15	Representative Spin Rate Profile	3-50
3-16	Spacecraft Precession from Magnetic and Gravity Gradient Disturbances at Low Spin Rates	3-53

ILLUSTRATIONS (CONTINUED)

		Page
3-17	Wobble Damper Time Constant Variation with Spin Rate	3-54
3-18	Thrust Level Considerations (Jupiter Orbiter)	3-57
4-1	RTG Deployment and Support Structure of Pioneer F, G	4-6
4-2	Scissors Type Magnetometer Boom	4-8
4-3	Typical Louver Performance Plot	4-10
4-4	Thermal Control by Louvered Platform with Open Propulsion Bay	4-11
4-5	Thermal Control by Use of Side-Viewing Second Surface Mirrors	4-12
4-6	Thermal Control by Louvered Platform and Open Truss	4-13
4-7	Thermal Control by Side Louvers	4-14
4-8	Thermal Control by Means of Heat Pipe	4-14
4-9	Relative Performance of Candidate Propulsion Systems	4-21
4-10	Acceleration Forces Acting on Deboost Propellant During Thrust	4-24
4-11	Alternate Pressurization Systems	4-25
4-12	Propulsion System Schematic	4-27
4-13	Propulsion Subsystem ΔV Performance Capability	4-29
4-14	Attitude Control Subsystem Functional Block Diagram	4-32
4-15	Attitude Control Subsystem Component Placement	4-33
4-16	Roll Angle Error Vs. Sun Look Angle	4-36
4-17	Spin Rate Change Due to Jovian Magnetic Field	4-38
4-18	Auxiliary Roll Reference Signal Generation	4-40
4-19	Magnetometer Phase Angle Delay Circuitry Block Diagram	4-41
4-20	Maximum Normalized Wobble Amplitude Vs. Inertia Ratio	4-44
4-21	Automatic Spin Up/Down Logic	4-45

ILLUSTRATIONS (CONTINUED)

		Page
4-22	Harmonic Drive Configuration	4-47
4-23	Functional Diagram of Experiment Drive Assembly	4-48
4-24	Power Subsystem Block Diagram	4-50
4-25	PCU Simplified Block Diagram	4-53
4-26	Simplified Shunt Schematic	4-53
4-27	Shunt Dissipation Characteristics	4-54
4-28	Inverter Assembly Schematic	4-55
4-29	TRF-Regulator Block Diagram	4-56
4-30	Command Subsystem Functional Block Diagram	4-57
4-31	Command Distribution Unit Functional Block Diagram	4-59
4-32	Command Memory Processor Block Diagram	4-62
4-33	Clock Detector Block Diagram	4-64
4-34	Data Handling Subsystem Block Diagram	4-65
4-35	Mainframe Organization	4-66
4-36	DTU Functional Block Diagram (Pioneer 10/11 Configuration)	4-69
4-37	Data Storage Unit Functional Diagram and Interfaces	4-74
4-38	Memory Module Block Diagram	4-75
4-39	Communication Subsystem Functional Block Diagram	4-77
4-40	Telemetry Link Performance with Modulation Index and Transmitter Power as Parameters	4-83
4-41	Antenna Feed Configurations	4-84
4-42	S-Band Transmitter Driver Block Diagram	4-86
4-43	Motorola X-Band Transmitter (MMM-73) Modified for Pioneer Outer Planets Orbiter Application	4-88
4-44	TRW S-Band Transmitter Modified for Pioneer Outer Planets Orbiter X-Band Driver Application	4-90

ILLUSTRATIONS (CONTINUED)

		Page
5-1	Mainframe Organization	5-5
5-2	Science Subcommutator Organization	5-7
5-3	Line-Scan Imaging Capabilities and Data Rate Requirements	5-9
5-4	RTG Performance Predictions	5-20
5-5	Uplink Communications Performance	5-21
5-6	Downlink Communications Performance	5-22
5-7	Telemetry Bit Rate Vs. Range Profile (Jupiter Orbiter)	5-25
5-8	Reliability Vs. Time Histories of the Pioneer F/G, Jupiter, and Saturn Orbiter Missions	5-33
5-9	Structure Subsystem Reliability Block Diagram	5-36
5-10	Hydrazine Propulsion Reliability Block Diagram	5-37
5-11	Bipropellant System Reliability Block Diagram	5-38
5-12	Thermal Subsystem Reliability Block Diagram	5-39
5-13	Attitude Control Subsystem Reliability Block Diagram	5-40
5-14	Data Handling Subsystem Reliability Block Diagram	5-40
5-15	Communications Subsystem Reliability Block Diagram	5-41
5-16	Electrical Power Subsystem Reliability Block Diagram	5-41
5-17	Command Subsystem Reliability Block Diagram	5-42
6-1	Launch Opportunities for Jupiter and Saturn Orbiter Missions in the 1970's and 1980's	6-1
6-2	Variation of Injection Energy Requirements with Launch Year for 400-, 500-, and 600-Day Earth-Jupiter Transfers	6-2
6-3	Variation of Jupiter Approach Velocity V_∞ with Launch Year for the 400-, 500-, and 600-Day Earth-Jupiter Transfers	6-4
6-4	Launch Energy and Arrival Velocity Characteristics for 1981 through 1983 Earth-Jupiter Trajectories	6-6
6-5	Launch Energy and Jupiter Approach Velocity Characteristics for Various Trip Times; 1981 Launch Opportunity	6-6

ILLUSTRATIONS (CONTINUED)

		Page
6-6	ΔV Capability Vs. Injected Weight	6-7
6-7	ΔV Performance Limits	6-8
6-8	Titan IIIE/Centaur D-1T/TE 364-4 Injection Performance	6-9
6-9	Declination of Departure Asymptote Vs. Trip Time for Earth-Jupiter Trajectories	6-11
6-10	Minimum Southerly Azimuth Angles at ETR Vs. Departure Inclination δ	6-12
6-11	Weight Penalty Due to Off-East Launch for Two Values of Injection Energy	6-13
6-12	Orbital Coast Time Requirements	6-13
6-13	Sample Earth-Jupiter Trajectories	6-15
6-14	Communication Distance and Earth-Spacecraft-Sun Angle Vs. Time Druing Cruise for Sample Earth Jupiter Trajectory (Launch: 1 January 1982)	6-16
6-15	Relative Sun, Earth, and Jupiter Positions During Orbital Phase of Sample Missions 1 and 2	6-16
6-16	Characteristics of Orbits about Jupiter	6-18
6-17	Effective ΔV Change with Change in V_∞ for Jupiter Orbits	6-19
6-18	ΔV Penalty for Finite Thrust Orbit Insertion at Jupiter	6-20
6-19	Jupiter Orbit Insertion in Earth Pointing Mode: Deviation Angle (Δ) and Cosine Loses (ΔV_L) Vs. Trip Time	6-21
6-20	Options of Orbit Inclination Attainable at Orbit Insertion	6-24
6-21	Satellite Alignments	6-25
6-22	Three-Satellite Encounter	6-26
6-23	Plane Change Maneuver Parameters Vs. Targeting Angle	6-29
6-24	Geometry of Orbit Plane Inclination	6-30
6-25	1σ Dispersion Ellipses at Jupiter Vs. Days before Encounter for (a) Pioneer 10, (b) Pioneer	6-35
6-26	Semi-Major Axis of Dispersion Ellipse in $\overline{B}$-Plane for Saturn Approach; Earth-Based Radio Navigation Only	6-37

ILLUSTRATIONS (CONTINUED)

		Page
6-27	Orbit Adjustment	6-46
6-28	Updating of Earth-Pointing During Orbital Phase	6-47
6-29	Jupiter Orbit Insertion Performance Chart	6-49
7-1	Variation of Injection Energy Requirements with Launch Year for 500- to 1625-Day Earth-Saturn Trajectories	7-2
7-2	Variation of Saturn Approach Velocity V_∞ with Launch Year for 500- to 1625-Day Earth-Saturn Transfers	7-3
7-3	Launch Energy and Arrival Velocity Characteristics for 1982, 1984, and 1986 Earth-Saturn Trajectories	7-4
7-4	Declination of Departure Asymptote Vs. Trip Times for Earth-Saturn Trajectories	7-4
7-5	Sample Earth-Saturn Trajectories (Projected into Ecliptic)	7-6
7-6	Communication Distance and Earth-Spacecraft-Sun Angle Vs. Time During Cruise for Sample Earth-Saturn Trajectory (Launch: 5 January 1983)	7-7
7-7	Relative Sun, Earth, and Saturn Positions During Orbital Phase of Sample Missions 1 and 2	7-8
7-8	Characteristics of Orbits about Saturn	7-9
7-9	Effective ΔV Change in V_∞ for Saturn Orbits	7-9
7-10	Geometry of Saturn Orbit with Periapsis Located Symmetrically Between Nodes	7-11
7-11	Boundary of Permissible Aim Angles and Orbit Inclinations	7-13
7-12	ΔV Reduction Through Lowering of Periapsis Distance	7-13
7-13	Saturn Orbit Insertion in Earth-Pointing Mode: Deviation Angle (Δ) and Cosine Losses (ΔV_L) Vs. Trip Time.	7-14
7-14	Saturn Orbit Insertion Performance Chart	7-18

TABLES

		Page
1-1	Pioneer F/G Spacecraft Subsystem Parameter Summary	1-9
2-1	Suggested Payload Complements for Mission Classes	2-12
2-2	Tracking and Data Acquisition Stations of the DSIF	2-18
2-3	DSS Primary Telecommunication Parameters (Nominal)	2-20
2-4	Scientific Payload Complement	2-22
3-1	List and Location of Payload Instruments for Jupiter Orbiter (Preliminary Selection)	3-15
3-2	Weight Summary	3-25
3-3	Mass Properties Requirements Versus Capabilities	3-26
3-4	Mass Property Summary	3-26
3-5	Electrical Power Requirements	3-35
3-6	Pulse Loads	3-37
3-7	Balanced Boom System Deployment Schemes	3-42
3-8	Deployment Simulation Results	3-44
3-9	Nutation Build-Up Due to Precession Maneuver	3-49
3-10	Telemetry Allocations	3-59
3-11	Command List	3-64
4-1	Summary of Minimum Margins of Safety	4-3
4-2	Candidate Structural Materials and Significant Material Properties	4-4
4-3	Thermal Control Heaters	4-18
4-4	Candidate Long Burn Time Thrusters	4-23
4-5	Accuracy of a Magnetometer Roll Reference	4-40
4-6	Attitude Control Subsystem Modification Summary	4-49
4-7	Electric Power Subsystem Functional Characteristics	4-51
4-8	Electric Power Subsystem Physical Characteristics	4-51

TABLES (CONTINUED)

		Page
4-9	Command Distribution Unit - Function Summary	4-60
4-10	CDU Configuration Summary	4-64
4-11	DTU Characteristics	4-68
4-12	DSU Characteristics	4-68
4-13	Data Handling Subsystem Bit Rates	4-71
4-14	Candidate Data Storage Units	4-73
4-15	Communication Subsystem Modification	4-78
4-16	Summary Characteristics of Candidate X-Band Transmitter Driver	4-89
4-17	X-Band TWT Development Status	4-92
5-1	Signals Available to Scientific Instruments	5-4
5-2	Data from the Scientific Instruments	5-4
5-3	Scientific Instrument Data Handling Capability	5-5
5-4	Program Storage Parameters	5-14
5-5	Nominal Maneuver Rates	5-15
5-6	Summary of Bipropellant System Performance	5-17
5-7	Summary of Monopropellant System Performance	5-18
5-8	Telemetry Link Design Control Summary	5-23
5-9	S-Band and X-Band Pointing Errors	5-26
5-10	Life-Limited or Time-Variable Components	5-30
5-11	Summary of Equipment Changes to Pioneer F/G for the Jupiter and Saturn Orbiter Missions	5-32
5-12	System Reliability Summary	5-33
5-13	Hydrazine Thruster Failure Rates	5-34
5-14	Bipropellant System Failure Rates	5-35
5-15	Propulsion Activity and Duty Cycling	5-36

TABLES (CONTINUED)

		Page
5-16	Selected Reliability Improvements for Individual Spacecraft Units	5-42
6-1	Selected Earth-Jupiter Sample Trajectories	6-14
6-2	Representative Satellite Tour Encounter Histories	6-27
6-3	ΔV-Budget for Representative Jupiter Orbit Missions	6-31
6-4	Pioneer 10 and 11 Encounter Accuracy Projections	6-35
6-5	Effect of Periapsis Dispersions on Capture Orbit Characteristics	6-39
6-6	Capture Orbit Characteristics of the Mariner Mars (1971) Mission	6-39
6-7	Flight Operations Summary. Three-Satellite Encounter Mission	6-42
6-8	Performance Summary of Jupiter Orbiter	6-51
7-1	Selected Earth-Saturn Sample Trajectories	7-5
7-2	Upper Bound of Number of Hits Sustained by Propulsion Stage During Saturn Ring Plane Crossing	7-10
7-3	Performance Summary of Saturn Orbiter	7-19

NOTATION

ACS	Attitude Control Subsystem
AGC	Automatic Gain Control
ARC	Ames Research Center
AU	Astronomical Unit (150×10^6 kilometers)
BOL	Beginning of Life
CDU	Command Distribution Unit
CEA	Control Electronics Assembly
c.g.	Center-of-Gravity
c.m.	Center-of-Mass
CSP	Conscan Signal Processor
CTRF	Central Transformer-Rectifier-Filter Unit
DDU	Digital Decoder Unit
DSA	Despin Sensor Assembly
DSIF	Deep Space Instrumentation Facility
DSL	Duration and Steering Logic
DSN	Deep Space Network
DSS	Deep Space Station
DSU	Data Storage Unit
DTU	Digital Telemetry Unit
EDA	Experiment Drive Assembly
EM	Electromagnetic
EOL	End of Life
ETR	Eastern Test Range
HPG	High Power Generator
I	Moment of Inertia

I_{sp}	Specific Impulse
JPL	Jet Propulsion Laboratory
K	Inertia Ratii
	$\left[\frac{I_z - I_x}{I_y} \cdot \frac{I_z - I_y}{I_x}\right]^{1/2}$
keV	Thousand Electron Volts
M	Body-Fixed Precessing Moment
MeV	Million Electron Volts
MHW	Multi-Hundred Watt RTG's
n	Number of Spin Revolutions Between Precession Pulses
NRZ-L	Nonreturn to Zero (level)
PCU	Power Control Unit
RHU	Radioisotope Heater Unit
RPM	Revolutions per Minute
RTG	Radioisotope Thermoelectric Generator
SCT	Spin Control Thruster
SPC	Sensor and Power Control
SPSG	Spin Period Section Generator
SRA	Stellar Reference Assembly
SSA	Sun Sensor Assembly
TCA	Thruster Cluster Assembly
TWTA	Travelling Wave Tube Amplifier
VPT	Velocity/Precession Thruster
α	Normalized Apoapsis Radius (r_a/r_o)
β	Normalized Periapsis Radius (r_p/r_o)

NOTATION (CONTINUED)

η	Inertia Ratio (I_y/I_z)
ξ	Inertia Ratio (I_x/I_z)
ω_s	Spin Rate

1. INTRODUCTION

This document describes a spacecraft based on Pioneer 10/11 technology, which can perform orbiter missions of the outer planets (Jupiter and beyond). Use of the spacecraft at Uranus or beyond would take a trip time of at least seven years from earth and a launch vehicle more powerful than the Titan/Centaur. Therefore in this document the Pioneer Outer Planets Orbiter is considered only for missions to Jupiter and Saturn.

The major spacecraft modifications from the Pioneer 10/11 design are the following:

- Addition of a MMH/N_2O_4 propulsion system for the orbit insertion maneuver, and for later orbit adjustments. Up to 2.3 km/s velocity increment is available at Jupiter, 1.4 km/s at Saturn. Four propellant tanks are mounted below the present equipment compartment, and a 90-lbf thruster is employed.

- Addition of X-band downlink transmission to the existing S-band two-way communications. 23-watt transmitted power will provide expected downlink data rates of 32,768 bits per second from Jupiter, and 8192 from Saturn.

- Replacement of the four Pioneer 10/11 SNAP-19 radioisotope thermoelectric generators (RTG's) by two multi-hundred watt (MHW) units. This change provides increased initial power (300 watts compared with 160) and enough power at mission end (265 watts at Jupiter, 242 watts at Saturn) for the increased communications and payload requirements.

The nominal mission durations are as follows:

Target Planet	Jupiter	Saturn
Transit time from earth	2.5 years	5.0 years
Time in orbit	1.0 years	1.0 years
Total mission time	3.5 years	6.0 years

The spacecraft as described may be launched by the Titan 3E/Centaur D-1T/TE-364-4 launch vehicle at annual opportunities in the 1980's. The retro-propulsion system permits entry into useful orbits at both planets, with periapsis at three or more planetary radii from the planet centers — adequate to avoid Jupiter's most intense radiation and Saturn's rings. The provisions for instrument weight and power and the data transmission capability will support a comprehensive scientific payload, including remote sensing instruments as well as particles and fields detectors. In particular, medium to high resolution images in visible and near infrared light can be obtained by a line scan camera employing a linear array of solid-state photodetectors which scans the scene as a consequence of the spacecraft's spinning motion.

1.1 MISSION DESCRIPTION

This section presents a brief synopsis of a typical Pioneer Orbiter mission to the planet Jupiter. A launch in the December 1981 opportunity is assumed.

1.1.1 Mission Objectives

The objectives of Jupiter orbiter missions can vary significantly. However the prominent elements of scientific interest at this time are the following:

- Investigation of the magnetosphere. This includes magnetic field measurements, plasma and electric field experiments to define bow shock and magnetopause regions, and particle detectors to refine the characterization of outer magnetospheric populations as well as the higher intensity inner trapped radiation belts.

- Remote sensing of Jupiter. Detectors in infrared, visible, and ultraviolet wavelengths can obtain a great variety of information about the characteristics of the atmosphere of the planet. Perhaps the most valuable information is in the form of images, with varying combinations of spatial, spectral, and temporal resolution.

- Similar remote sensing of Jovian satellites. Here it is a solid surface that we expect to see rather than an atmosphere.

- Other atmospheric measurements — by observing the sun at the onset of solar eclipse, and by RF occultation techniques.

To accommodate these objectives a 3 x 80 R_J orbit of intermediate inclination (40 degrees) is adopted for this typical mission. This combination of periapsis radius and inclination will keep the exposure to radiation below levels destructive to the spacecraft equipment, will permit orbital entry in an earth-line mode of thrusting without a large penalty in propulsive efficiency, and will permit significant exploration north and south of the geographic and magnetic equatorial planes. The 33-day period of the orbit is short enough to allow repeated passages through the inner magnetosphere and numerous favorable imaging opportunities.

1.1.2 Launch

The 1981 launch to Jupiter has a departure asymptote from the earth of zero to slightly negative declination, calling for coast times in parking orbit of about 16 to 26 minutes, if launched from CKAFS in Florida within a typical launch azimuth range of 90 to 114 degrees. Thus liftoff would be in early afternoon, local time. After Titan burn and staging and Centaur first burn, the flight vehicle would coast the required time, entering the earth's shadow in the process. The second Centaur burn, followed by Centaur staging and third stage firing places the orbiter spacecraft on a trajectory for Jupiter.

1.1.3 Post Launch

Following separation from the spent TE-364-4 stage, the spacecraft performs the following events, either by ground command or by automatic initiation by the on-board sequencer:

- Reduction of spin rate from ~60 rpm (used for third stage firing) to ~16 rpm
- Ordnance firing to release appendages (two RTG's and the magnetometer boom) followed by deployment of these appendages (spin rate decreases to ~5 rpm)
- Precession of the spacecraft from the injection attitude to an interim attitude more closely sun pointing, producing a more benign thermal environment and satisfactory short range communications.

Scientific instruments to be used in the interplanetary phase can be turned on, calibrated, and checked out as desired.

1.1.4 Interplanetary

The interplanetary phase of the mission is occupied by spacecraft operations and experiment operations. The spacecraft operations are primarily concerned with trajectory control and attitude control.

Trajectory control is effected by propulsive ΔV maneuvers, first to correct for the injection error resulting from launch vehicle operation, and subsequently to correct for maneuver errors, tracking errors, and minor perturbations to the trajectory. Attitude control provides proper orientation for the trajectory correction maneuvers when they are performed, and to contribute to optimum thermal conditions and communications performance during the long intervening cruise portions of the mission. Earth-pointing gives the highest spacecraft antenna gain for communications, and is the preferred orientation for most of the cruise phase, subject to reasonable intervals (~one week) between attitude updating maneuvers. However for a month or two after launch, the communication range is short enough that a low-gain antenna provides satisfactory communications. Therefore, an interim attitude is selected during this period which is closer to sun pointing. This shades side- and aft-viewing portions of the spacecraft from direct sunlight, thereby avoiding a more extreme thermal environment. After two months the sun and earth are within 26 degrees (as seen from the spacecraft), and earth-pointing is satisfactory for both purposes.

The experiment operations during the interplanetary portion of the mission depend on the applicability of the payload of the Jupiter orbiter to investigations in this region. Certainly studies of the solar wind and of solar and galactic energetic particles are germane during this phase, as well as further studies of small particle populations and asteroids.

1.1.5 Planetary Approach and Orbit Injection

As the spacecraft approaches the target planet a terminal trajectory correction may have to be performed to attain the desired encounter conditions for orbit insertion. Remaining trajectory errors relative to the planet can be determined with sufficient accuracy from earth-based radio navigation aided by the focusing effect of the strong planetary gravity field of Jupiter (or Saturn). The highest navigational accuracy is achieved if tracking and orbit determination is continued until just a few days before the encounter. Small terminal guidance maneuvers can be accomplished without a change from the nominal earth pointing spacecraft spin axis orientation by using axial ΔV thrusters or the circumferential spin/despin thrusters (the latter in a pulsed thrusting mode).

Orbit injection at the time of closest approach (periapsis) to the target planet will also be performed in the earth pointing mode for greater operational simplicity, and to avoid loss of high-gain communications coverage during this critical mission event. Mission analysis shows that by imposing appropriate constraints on the time of arrival, on the orbital parameters to be achieved and on the retro-thrust duration (i.e., the total impulse and the retro-propulsion thrust level) the injection maneuver can be performed at fixed earth-pointing attitude with a high propulsive efficiency.

The choice of orbit dimensions and inclination is constrained by the scientific objectives of the mission, by the available ΔV capability (i.e., small periapsis radius and large eccentricity reduce the ΔV magnitude) and by the environment existing at close vicinity of the planet. Periapsis distances of 3 planet radii are a likely choice to avoid excessive radiation dosages at Jupiter and hazards due to ring-particle impact at Saturn.

1.1.6 Planetary Orbit Phase

An extended planetary orbit phase is desirable for maximum scientific data yield. Nominally, orbital phases of one-year duration are assumed for the Jupiter and Saturn orbit missions. The highly eccentric orbits typically achievable with the available ΔV capability may have orbital periods in excess of 60 days (in the case of the Saturn mission) thus permitting only six orbital passes (or fewer) in the course of one year. The large apoapsis distances inherent in this mission profile have the advantage of permitting repeated excursions to the outer regions of the magnetosphere, the magnetopause and the bow shock where temporal and spatial changes of interactions with the interplanetary medium and the solar wind can best be observed.

Changes of orbital characteristics may be desired for increasing the scientific yield of the mission, including the achievement of close encounters with some of the planetary satellites. Adjustments of the orbit period can be performed by subsequent trim maneuvers near periapsis, variation of the periapsis by maneuvers near the apoapsis (both consistent with maintaining an earth-fixed spacecraft orientation). Plane change maneuvers can be performed most effectively near apoapsis, but require a reorientation of the spin axis. The preferred thrust orientation would be perpendicular to the orbit plane. Orbital characteristics can also be changed

deliberately through gravity perturbations at close encounters with planetary satellites. In any event, the orbit changes will be limited by the propulsive capability of the spacecraft remaining after orbit insertion and by the constraints of environmental hazards to be anticipated in close vicinity of the planet.

1.2 PIONEER 10 AND 11 DESCRIPTION

The Pioneer Outer Planets Orbiter configuration is derived from the Pioneer F/G spacecraft. Pioneer F, now designated Pioneer 10, was launched in March 1972 for the first flyby of Jupiter. Pioneer G, now designated Pioneer 11, was launched in April 1973. The Pioneer F/G spacecraft design is described in this section.

1.2.1 System-Level Description

Figure 1-1 shows the prominent physical features of the Pioneer F/G spacecraft. It is a highly reliable spacecraft of simple, straightforward design with many of its components and subsystems already having demonstrated successful performance on earlier missions. It has a thermally-controlled equipment compartment with two sections, one hexagonally shaped, and containing electronic units and the propellant tank, and the other a bay containing most of the scientific sensors and their associated electronics. Several sensors, including the magnetometer and two meteoroid detectors are externally mounted.

Forward of the equipment compartment is a 9-foot diameter parabolic reflector for the high-gain antenna. Mounted on a tripod structure forward of the reflector are the medium-gain antenna and the feed for the high-gain antenna.

Three appendages are stowed within a 9-foot cylindrical envelope at launch; they are shown in their deployed positions attained within an hour after launch. Two pairs of RTG's are extended approximately 6 feet at 120 degrees spacing. The magnetometer sensor is located on the end of a long folding boom which, in the deployed condition, extends 17 feet radially from the instrument side of the equipment compartment. The RTG's are retained in a stowed position for launch next to the equipment compartment and under the antenna reflector.

Six 1-pound hydrazine thrusters are located in three clusters near the perimeter of the 9-foot reflector. Four thrusters are aligned parallel to the spin axis for precession and velocity correction maneuvers; two thrust tangentially for spin control. Other external features include a mast-mounted omnidirectional antenna directed aft, and a sun sensor mounted near one of the thruster assemblies which determines the spacecraft's position in the spin cycle. Two large light shields are associated with the stellar reference assembly and with an optical asteroid/meteoroid detector.

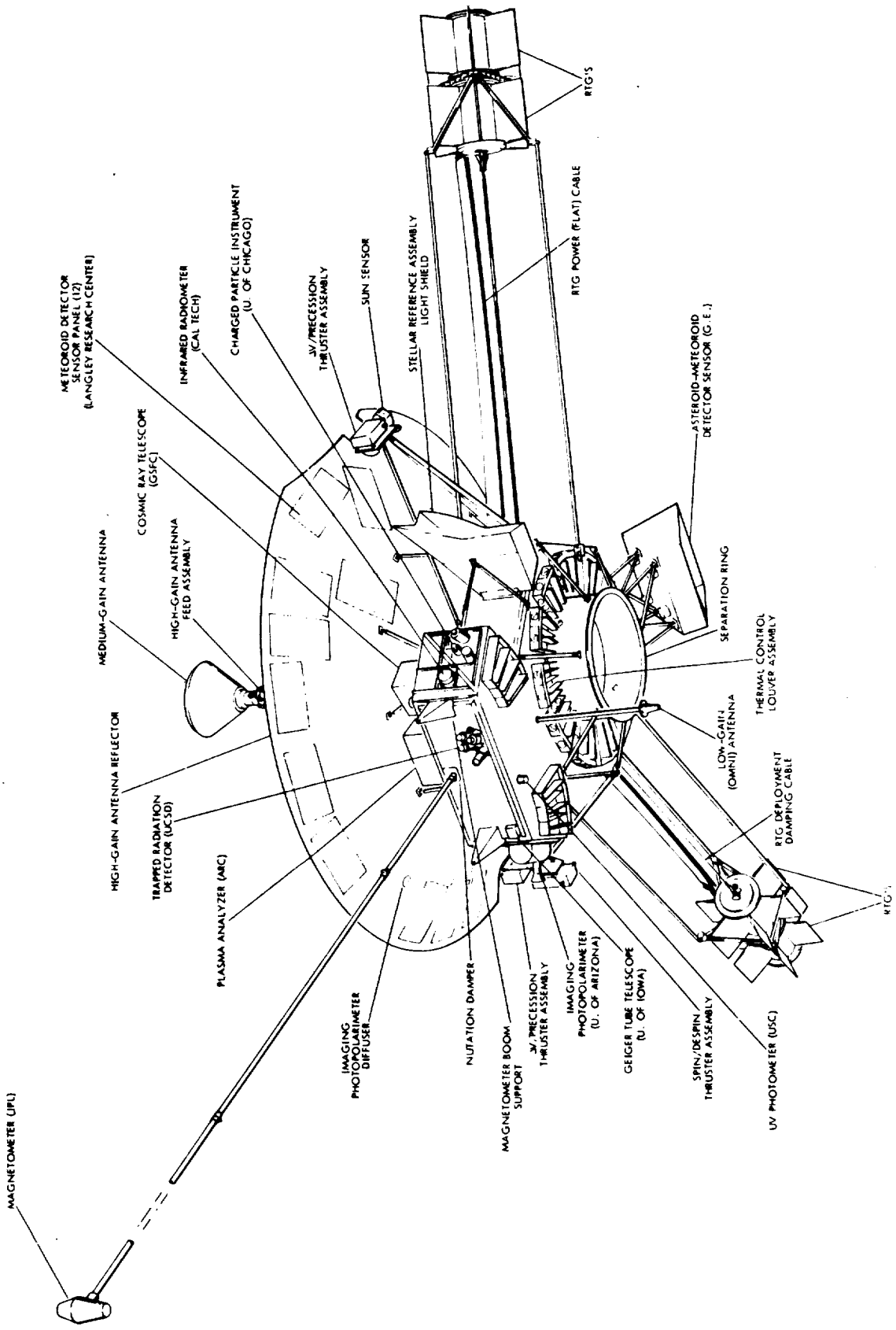

Figure 1-1. Pioneer F/G Spacecraft

Figure 1-2 shows the arrangement within the spacecraft equipment compartment. Most of the spacecraft electronic assemblies are located in the central hexagonal portion of the compartment, surrounding a 16.5-inch diameter hydrazine tank. Most of the scientific instruments' electronic units and internally-mounted sensors are in an instrument bay mounted on a structure of aluminum honeycomb which provides support and meteoroid protection and is covered with insulation which, together with louvers under the mounting platform, provides thermal control.

Table 1-1 summarizes the major parameters characterizing this spacecraft. A functional block diagram is shown in Figure 1-3.

1.2.2 Propulsion and Attitude Control

The spacecraft is attitude stabilized by spinning about an axis which is parallel to the axis of the 9-foot reflector; the nominal cruise spin rate is 4.8 rpm. During the major portion of the mission the spacecraft is maintained in an earth pointing attitude for proper aiming of the narrow beam high-gain antenna. Periodic attitude adjustments are required throughout the mission to compensate for the variation in the heliocentric longitude of the earth-spacecraft line. In addition, correction of launch vehicle injection errors to provide the desired Jupiter encounter trajectory may be required. These velocity vector adjustments will necessitate reorienting the spacecraft to direct the thrust in the desired direction. The orientation of the spin axis is altered in precession steps achieved by pulsed firing of two thrusters forming a couple. The precession maneuvers can be open-loop, for orientations toward or away from earth pointing, or closed-loop for homing on the uplink RF transmission from the earth.

1.2.3 Electric Power

A unique characteristic of this spacecraft is the use of RTG's as the primary source of electric power, making it a sun-independent vehicle. Each of the four space-proven SNAP-19 RTG's converts five to six percent of the heat released from plutonium dioxide fuel to electric power. RTG power is greatest at 4.2 volts; an inverter boosts this to 28 volts for distribution. RTG life is degraded at low currents; therefore, voltage is regulated by shunt dissipation of excess power.

1.2.4 Thermal Control

The equipment compartment is insulated from extreme heat influx with aluminized mylar and Kapton blankets. Adequate warmth is provided by dissipation of 70 to 120 watts of electric power by electronic units within the compartment. Louvers located below the mounting platform regulate the release of this heat and thus maintain temperatures in the vicinity of the spacecraft equipment and scientific instruments within operating limits. External component temperatures are controlled, where necessary, by appropriate coating and, in some cases, by radioisotope or electrical heaters.

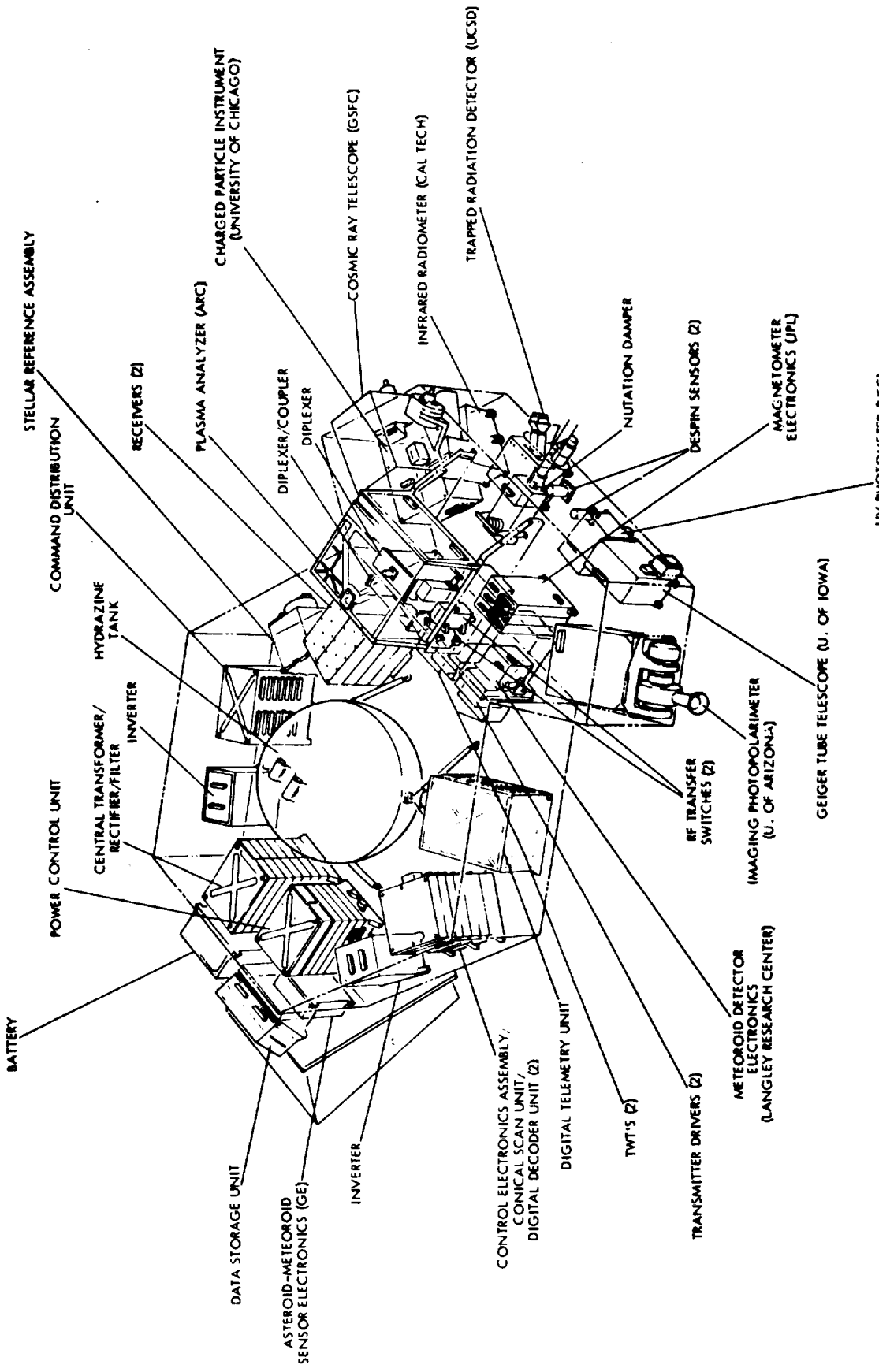

Figure 1-2. General Arrangement of the Pioneer F/G Equipment Compartment

Table 1-1. Pioneer F/G Spacecraft Subsystem Parameter Summary

Power

- Four radioisotope thermoelectric generators — 4.2 volts
  - Pioneer 10 (at launch) — 166 watts
  - Minimum (after 2.5 years) — 120 watts
- Internal distribution — 28 Vac, 28 Vdc

Stabilization, Propulsion

- Spin-stabilized - 4.8 rpm
- Spin axis directed at earth (cruise)
- References
  - Sun and star (optical)
  - Earth (rf)
- Precession
  - Open-loop to and from earth pointing
  - Closed-loop (conscan) earth tracking (uplink RF)
- Six hydrazine thrusters (1 pound)
  - Pulsed - precession, spin control
  - Continuous - ΔV for trajectory correction
  - 200 m/sec ΔV capability

Communications

- Antennas (uplink and downlink)
  - 9-ft parabolic reflector (33 dBi)
  - 16-in. horn (13 dBi)
  - Log conical spiral (aft hemisphere)
- S-band frequencies
- 8-watt TWT amplifiers
- 1024 bps telemetry capability at Jupiter

Data

- Bit rates, 16 to 2048 bps (integral powers of two)
- Data formats (192 bits/frame)
  - Two science main frames
  - One science subcommutated
  - Four engineering main frames (or subcommutated)
  - 16 special (combined) science main frames
- Data storage - 49,152 bits

Commands

- 255 discrete commands available
  - Up to 5 stored
- One bps command rate
- 22-bit command message
- Hamming (15, 11) coded

Weight Summary

RTG power sources	120 pounds
Scientific instruments	66
Propellant	61
Other spacecraft	317
Total	564

1.2.5 Communications

The communications subsystem provides for: 1) uplink and downlink communications; 2) doppler coherence of the downlink carrier signal with the uplink carrier signal; and 3) generation of the conical scan signal for closed-loop precession of the spacecraft spin axis towards earth. S-band carrier frequencies, compatible with the Deep Space Network (DSN) are used in conjunction with a PCM/FSK/PM modulation format of the uplink carrier and PCM/PSK/PM modulation of the downlink using a single subcarrier. The high-gain antenna is used to achieve a high telemetry data rate as the communication distance increases. The coupled medium-gain/omnidirectional antennas with fore and aft elements respectively, provide broad angle communications at intermediate and short ranges.

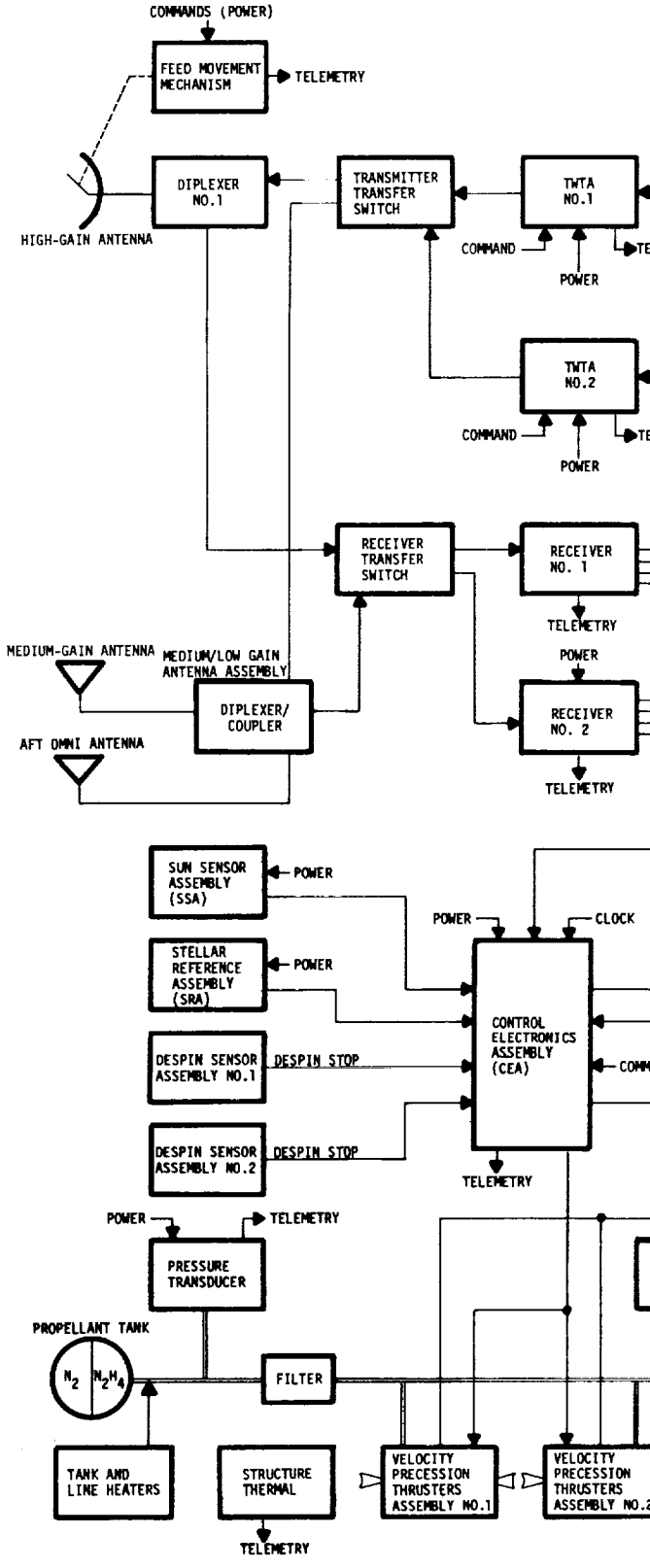
COMMANDS (POWER)
FEED MOVEMENT MECHANISM
TELEMETRY
DIPLEXER NO.1
TRANSMITTER TRANSFER SWITCH
TWTA NO.1
HIGH-GAIN ANTENNA
COMMAND
POWER
TWTA NO.2
COMMAND
POWER
RECEIVER TRANSFER SWITCH
RECEIVER NO. 1
TELEMETRY
POWER
MEDIUM-GAIN ANTENNA
MEDIUM/LOW GAIN ANTENNA ASSEMBLY
DIPLEXER/ COUPLER
RECEIVER NO. 2
AFT OMNI ANTENNA
TELEMETRY
SUN SENSOR ASSEMBLY (SSA)
POWER
POWER
CLOCK
STELLAR REFERENCE ASSEMBLY (SRA)
POWER
CONTROL ELECTRONICS ASSEMBLY (CEA)
DESPIN SENSOR ASSEMBLY NO.1
DESPIN STOP
DESPIN SENSOR ASSEMBLY NO.2
DESPIN STOP
TELEMETRY
POWER
TELEMETRY
PRESSURE TRANSDUCER
PROPELLANT TANK
N_2
N_2H_4
FILTER
TANK AND LINE HEATERS
STRUCTURE THERMAL
TELEMETRY
VELOCITY PRECESSION THRUSTERS ASSEMBLY NO.1
VELOCITY PRECESSION THRUSTERS ASSEMBLY NO.2

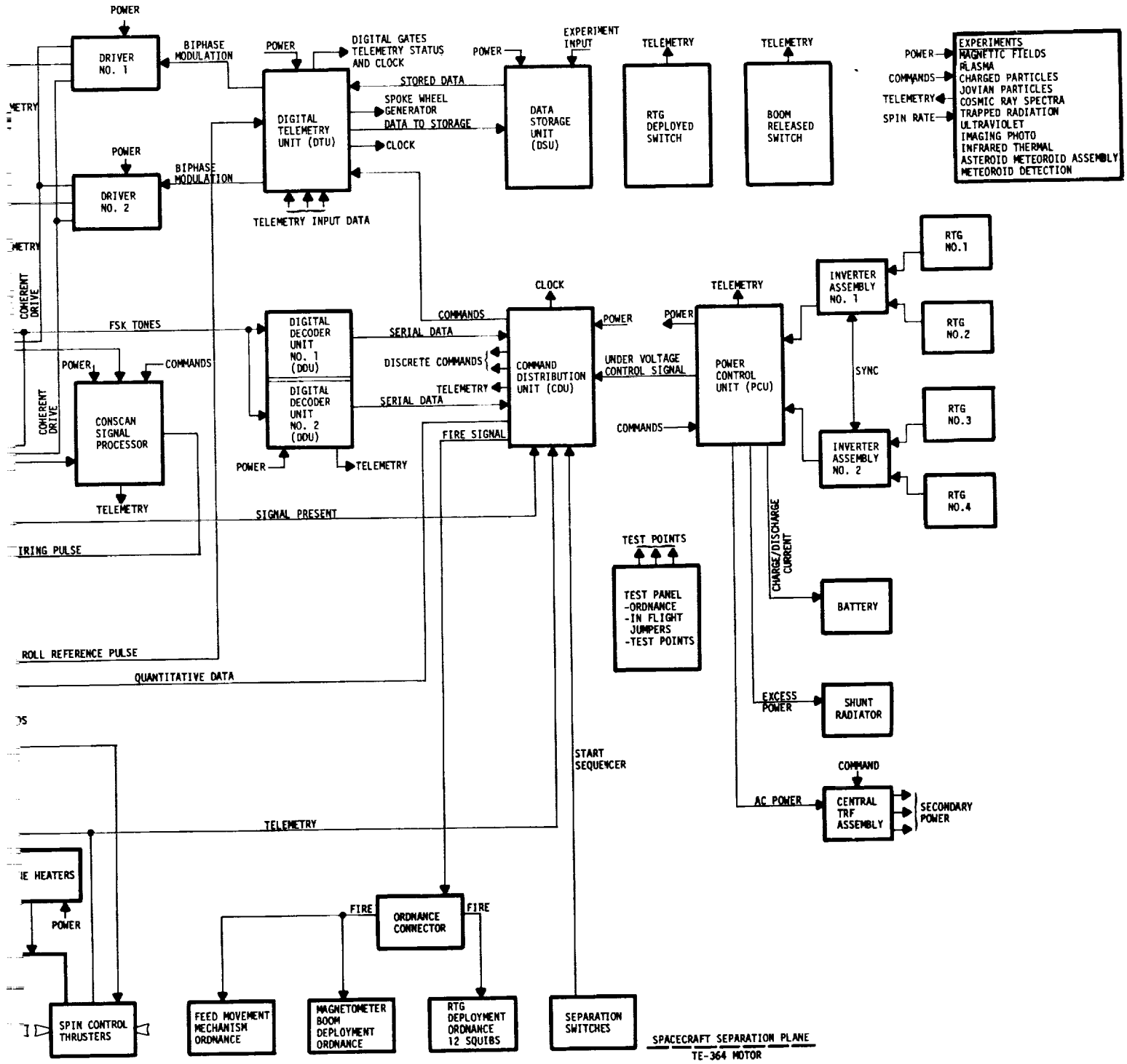

Figure 1-3. Pioneer F/G Spacecraft Functional Block Diagram

Two frequency-addressable phase-lock receivers are connected to the two antenna systems through a ground commanded transfer switch and two diplexers, providing access to the spacecraft via either signal path. The receivers and antennas are interchangeable through a transfer switch either by ground command or automatically after a preselected fixed period of inactivity.

Except when inhibited by command, the receiver which is locked to an uplink signal provides a phase coherent drive signal to either of the two redundant transmitter drivers which are connected to redundant 8-watt traveling wave tube amplifiers (TWTA's). In the absence of an uplink signal, the activated driver automatically switches to a self-contained auxiliary oscillator. The TWTA's are coupled to both antenna systems via a transfer switch and the two diplexers.

A closed-loop RF angle tracking, or conscan system is used to acquire and maintain the earth pointing attitude. The spinning spacecraft automatically provides the signal for closed-loop precession by tilting the receiving antenna beam with respect to the spin axis. This antenna gain variation amplitude-modulates the received uplink carrier, producing an error signal which indicates both the amplitude and direction of the pointing error. The high-gain antenna feed can be offset by ground command to provide the tilt; the medium-gain antenna is permanently tilted.

The amplitude-modulated RF signal is coherently detected by the receiver automatic gain control (AGC). The conscan signal processor (CSP) conditions the resultant conscan signal and generates a thruster firing pulse which precesses the spacecraft in a direction to reduce the pointing error.

1.2.6 Data Handling

Scientific and engineering telemetry data are time-multiplexed and formatted into a binary bit stream in the DTU. The unit converts analog inputs into 6-bit digital words, convolutional codes formatted data and generated an NRZ-L biphase modulated 32-kHz square wave. The DTU operates at eight bit rates (16 to 2048 bps in binary increments), three modes, and 23 format combinations to process 290 data inputs.

Convolutional coding is introduced into the telemetry link to permit more information to be transmitted at a given power and within a prescribed error rate criterion. The coding, or noncoding of the telemetry data, is controllable by ground command. A sequential decoding process, performed at the ground station reconstructs error-free data for telemetry link conditions well beyond acceptable limits without coding.

1.3 RELATED DOCUMENTS

The design of the Pioneer Outer Planets Orbiter evolved from that of Pioneer F/G as a baseline with a number of modifications already contemplated for the Outer Planets Pioneer spacecraft. The following documents describe those configurations and may serve as additional references:

1. "Pioneer F/G Spacecraft Operational Characteristics Study" Final Report. TRW Systems Report 71-7531.9-14, 23 April 1971 (Reference 1). A comprehensive document on design features and operational characteristics of Pioneer F/G.

2. "The Pioneer Mission to Jupiter NASA Report SP-268, Washington, 1971 (Reference 2). A brief description of the Pioneer F/G missions, the scientific objectives, payload instruments, the spacecraft and its support system.

3. "Outer Planets Pioneer Spacecraft" NASA/Ames Research Center Report, dated 23 March 1973, and Revision 1, dated 15 April 1974 (Reference 3). A document describing the design of advanced Pioneer spacecraft for outer planet flyby, orbiter and probe missions. This document (Revision 1) also contains updated characteristics of Pioneer 10/11.

4. "Extended Life Outer Planets Pioneer Spacecraft" NASA/Ames Research Center Report, dated 5 March 1974 (Reference 4). A comprehensive review document of recommended approaches to extend mission life of Pioneer F/G type spacecraft as required for outer planet missions exceeding the basic 2.5-year mission life requirement of the baseline spacecraft.

5. "Study of Follow-On Pioneer Missions to Jupiter" TRW Systems Report 20406-6006-RO-00 dated 13 August 1971 (Reference 5). A preliminary study similar in scope to the present report (but excluding Saturn orbiter missions). The report explores alternate design approaches, one of which being similar to the configuration described in the present document.

1.4 ORGANIZATION OF THE REPORT

Section 2 presents a summary of mission requirements, spacecraft design requirements and interface constraints. The discussion of mission requirements includes environmental characteristics and constraints to be met by the spacecraft design as well as scientific objectives and mission categories. The spacecraft design objectives covered in this section include mechanical and electrical requirements, in general, and specific requirements of thermal control, data handling and communications subsystems and the added deboost propulsion subsystem.

Section 3 describes the Pioneer Outer Planets Orbiter spacecraft from the system design standpoint. It covers the configurations of the Jupiter and Saturn orbiters, mass properties, dynamic characteristics and overall electrical design. The electrical power budget, telemetry allocations and command assignments are also covered in this section. The section also includes a listing of principal mission event sequences.

Section 4 presents a detailed description of the Pioneer Outer Planets Orbiter subsystems and considers design options not included in the selected baseline system design approach.

Section 5 discusses spacecraft performance in terms of accommodation of scientific instruments and capabilities of attitude control, electrical power, data handling and storage, and communications. It also includes a detailed discussion of projected reliability characteristics, taking into account the extended mission life of the Pioneer orbiter spacecraft compared to the Pioneer F/G design which is based on a nominal mission duration of only 2.5 years.

Sections 6 and 7 present mission performance characteristics of the spacecraft in the Jupiter and Saturn orbiter missions, respectively, considering launch opportunities in the early and middle 1980's. These sections also discuss performance constraints and tradeoffs between alternate mission modes and indicate the rationale for selection of a set of nominal mission profiles. The section draws on mission analysis data available from other documents, and on more detailed mission characteristics presented in Appendix B.

Section 8 presents concluding remarks regarding the overall capabilities of Pioneer as a baseline configuration for future outer planet orbiter missions in the framework of planetary exploration objectives of the 1970's and 1980's.

Several appendixes are included to provide support material on scientific instruments, mission analysis, reliability and structural load characteristics for several of the foregoing sections.

2. SUMMARY OF DESIGN REQUIREMENTS

2.1 MISSION REQUIREMENTS

2.1.1 Environmental Factors

Some design features and operational modes of the Pioneer orbiter spacecraft, different from those of Pioneer F/G, are dictated by the changed environment in which this spacecraft must operate. These environmental conditions are discussed below with emphasis on major differences from the Jupiter flyby mission environment.

2.1.1.1 Launch Environment

The Titan III E/Centaur/TE-364-4 acoustic and vibration environment is included in the specification PC 210.03 to which Pioneer F/G was developed and qualified. Thus, no requalification of the spacecraft for the new launch vehicle is necessary. However, the increased mass moments of the longer and much heavier orbiter spacecraft introduce greater structural/dynamic loads on the launch vehicle and third stage adapter. The McDonnell Douglas DSV-3-17A spin table which is used to spin up the TE 364-4 solid motor and payload before separation from the burned-out Centaur stage, and the standard 37- by 31-inch attach fitting on top of the TE 364-4 stage require structural strengthening to support the heavy Pioneer orbiter spacecraft. Additional structural analysis of these interfaces is required as part of the future design studies of the Pioneer orbiter and its launch vehicle.

The vehicle follows a launch and injection sequence different from Pioneer 10 and 11 since up to 30 minutes of coasting in parking orbit is required prior to the interplanetary injection burn. This is followed by a possible delay of appendage deployment to permit verification and control of deployment events from the ground. Prolonged (up to 80 minutes) thermal radiation of the stowed RTG units on adjacent portions of the flight vehicle can be of some concern, but adverse effects are avoided by selecting an appropriate RTG deployment and venting sequence.

2.1.1.2 Thermal Environment

The only concern with an adverse initial thermal environment different from that for Pioneer 10/11 in this mission arises from a possible prolonged exposure of the propulsion bay to a side-sun condition during the first 50 days after launch, if the flight spacecraft is maintained in an earth-pointing mode for medium- and high-gain communication coverage. However, to minimize thermal load problems during this mission phase, a compromise with communication requirements can be made by orienting the spacecraft away from earth and closer to the sun and relying on omni-antenna coverage for downlink communications. This mode provides adequate bit rates during the first 50 to 60 days of the mission.

2.1.1.3 Micrometeoroid Environment

The Pioneer orbiter spacecraft will be exposed to a varied micrometeoroid environment in interplanetary space, including cometary and asteroidal particles which present a potential hazard because of the possibility of penetration of mission-critical components. Exposure to micrometeoroid flux will be a matter of concern both during the interplanetary cruise and during the extended orbital phase.

Prior to the asteroid belt crossing by Pioneer 10 and 11 it was generally assumed that the particle flux in this region was many times denser than at earth's distance from the sun. Consequently, these spacecraft were designed to withstand the estimated relatively high flux at the densest part of the asteroid belt, 2.5 AU (10^{-13} particles per cubic meter of mass greater than 10^{-3} grams) in accordance with NASA's micrometeoroid spatial density model defined in SP-8069 (Reference 6).

Precautions taken in the Pioneer 10/11 spacecraft design to preclude a catastrophic collision include the following:

a) Double-walled (honeycomb core) aluminum panels for the equipment platform and side panels offer weight-effective barriers to meteoroid masses of concern.

b) Component baseplates add to the protection provided by the platform

c) Exterior propellant lines are routed along the side of the strut opposite from the probable direction of impingement. Armalon fabric provides protection in exposed areas.

Actually, the meteoroid impact measurements obtained by Pioneer 10 and 11 indicate that the penetration flux was smaller by a factor of 3 in the asteroid belt than it was near 1 AU while the NASA model suggested that it would be greater by a factor of 5. Secondly, the penetration flux measured by Pioneer 10 was nearly two orders of magnitude greater near Jupiter than predicted in the NASA model.

These results are of great importance to the design of the outer planets orbiter spacecraft, particularly since they represent actual penetration measurements on exposed sheet metal samples of two thicknesses, rather than visual observation of particles encountered.

In the outer planet orbiter the protection of the propellant and pressurant tanks against catastrophic meteoroid impacts is a requirement that can be met by providing an aluminum honeycomb sandwich panel and Armalon protective blankets to cover the exposed tankage areas. The earth-pointing orientation of the spacecraft during the interplanetary cruise as well as during the orbital phase has the effect of exposing primarily the aft-facing spacecraft exterior to the predominant micrometeoroid flux owing to the relative geometry of spacecraft and particle motion. Hence the addition of the meteoroid penetration shield on that side is effective during both mission phases.

The mission profile is designed to avoid prolonged spacecraft exposure to the particle flux in the immediate vicinity of the respective target planet. In the case of the Saturn mission the orbital characteristics will be chosen so as to avoid crossing, or moving in the equatorial plane (the plane of Saturn's rings) at distances closer than about 3 planet radii. If impact measurements are performed during the orbital phase it will be possible to modify the mission profile to avoid repeated passages at low periapsis distances if an excessive particle flux density should be found.

Based on the current NASA model of particle flux density in Saturn's rings (NASA SP-8091, Reference 7) an estimated upper bound was calculated for the number of impacts sustained during Saturn's ring plane crossing, at a distance of 2.3 planet radii and under representative encounter conditions. The result is shown as a solid line in Figure 2-1. The graph also presents a much less conservative estimate of the number of impacts sustained, using a 90th percentile particle flux estimate (dashed line). The upper bound of the number of particles of 0.01 gram or larger striking the protective shield would be about three per ring crossing. The 90th percentile flux estimate projects only 0.3 particle impacts. Note that the assumed ring crossing distance of 2.3 Saturn radii is also on the conservative side since this would be at the perimeter of the visible outer ring (A). It appears therefore that even with highly conservative assumptions as to the meteoroid flux encountered at Saturn the impact hazard can be met without excessive shielding requirements. It should also be noted that just inside the perimeter of ring A or R = 2.29 R_S, i.e., 600 km closer to the planet, the estimated particle number density in NASA's model is six times greater than at 2.30 R_S.

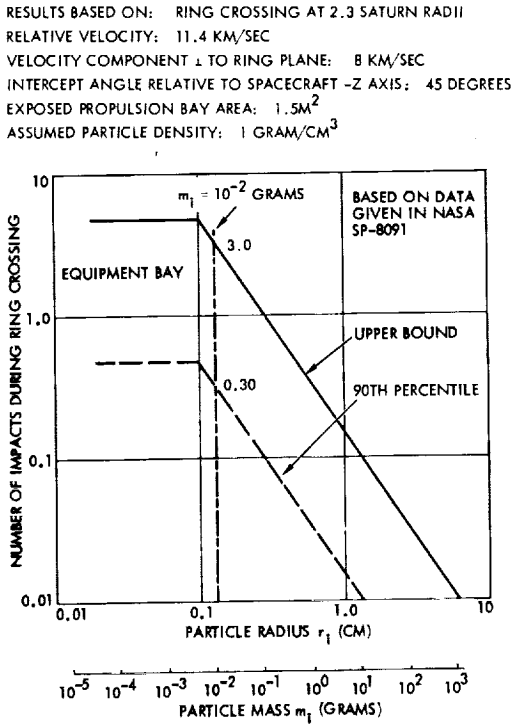

Figure 2-1. Estimated Impacts Sustained During Saturn Ring Crossing

Actually, the results obtained indicate that unless a more severe particle environment in the outer ring area is established by the current series of DSIF radar observations of Saturn, the probability of damage during ring plane crossing can be made reasonably small.

2.1.1.4 Radiation Environment

Radiation Environment Near Jupiter

The trapped radiation belts of Jupiter constitute a potential major hazard for close-in flyby, orbiter and entry probe missions. Since in the projected orbiter missions the orbital eccentricity is generally high ($e > 0.8$), due to propellant limitations, the governing parameters are periapsis radius and the number of orbital revolutions. Orbital inclination and location of the nodal line also have a significant influence.

Considerations regarding the radiation hazard and possible protection of the spacecraft against radiation damage may be summarized as follows:

- Radiation damage to transistors from the proton component of the Jovian radiation belt will curtail the life for low periapsis orbits (periapsis $<2\ R_J$). The "nominal" and "maximum" radiation environment referred to in the following paragraphs represent recent estimates of the most likely Jovian environment and the maximum possible radiation intensity, respectively.

- The uncertainty in the radiation flux about Jupiter, translates to an uncertainty in the calculated lifetime in orbit. Estimated lifetimes in orbit range from less than 0.1 to more than 10 revolutions for a "radiation hardened" system depending on orbital parameters.

- Radiation hardening of a system entails a) component selection, b) circuit design to withstand a higher flux before circuit failure, and c) selective shielding of the more susceptible components.

- With minor modifications it will be possible to harden the Pioneer spacecraft design to survive more than four low periapsis orbits ($R_J < 1.2$) in the Jovian "nominal" radiation environment.

- To increase lifetime in orbit to more than one revolution (based on the "maximum" environment) in the low periapsis orbits, an intensive radiation hardening program is required. The program would entail partial redesign of circuits to make use of less radiation susceptible components, and the addition of shields around selected assemblies.

The presence and intensity of trapped-radiation belts surrounding Jupiter are inferred from observations of radio noise in the decimeter range of wavelengths emanating from Jupiter. However, various characterizations of the radiation belt model differ widely in intensity, energy, and spatial distribution, and even in whether electrons or protons are the dominant species.

In the most recent models, high-energy protons are most critical in terms of potential damage to spacecraft components, as their energy range and intensity have been increased greatly over earlier estimates, and their spatial range extended. Figure 2-2 shows proton fluence (integrated exposure in a single orbital passage) for several models as a function of the radius of closest approach.

Flux models proposed by Neil Divine of the Jet Propulsion Laboratory in early 1971 were based on earth observations of HF and UHF radio emissions generated near Jupiter. Fluences of 20 MeV equivalent protons due to "nominal" and "maximum" models are shown in Figure 2-2. They differ by two orders of magnitude for low periapsis orbits, and by three or more orders at higher periapsis radii.

The Jupiter Radiation Workshop (July 1971) postulated an even more intense proton environment. This is due primarily to the observation that the Jovian ionosphere is likely to extend to higher radial distances (40 to 80 R_J) because of the low molecular weight of the Jovian atmosphere and the high rate of planetary rotation. The resulting flux models (known as the BKTC models) differ by 2.5 orders of magnitude, depending on the fraction of solar wind particles being trapped. These models also are spatially the most extensive. Flux levels drop off as $r^{-3.2}$, leading to fluences dropping off as $\beta^{-1.7}$, where β is the periapsis radius expressed in Jovian radii, as shown in Figure 2-2.

Pioneer 10 Encounter Results

The Divine model was the best estimate of Jupiter's radiation environment at the time of initiation of the Pioneer F/G program, October 1969. Proton fluxes were not identified for energies above 4 MeV. Because protons do not penetrate at 4 MeV and below, electrons were more critical than protons in influencing the spacecraft design. Actually, the Pioneer 10 and 11 spacecraft are estimated to be capable of exposure to 20 MeV equivalent proton fluences of 10^{11} particles/cm^2 before major component damage would occur.

Results from Pioneer 10's encounter with Jupiter's radiation fields shown in Figure 2-2 indicate that for its approach geometry and periapsis (2.84 Jupiter radii) the radiation levels were below the damage threshold of the active devices with the possible exception of a decrease in the sensitivity of the stellar reference assembly.

While results of Pioneer 10's encounter with Jupiter's radiation fields tend to indicate a lower susceptibility to damage than expected, many other factors should be examined. Recent analysis of data obtained from Pioneer 10 show a high concentration of energetic protons in a disk perpendicular to

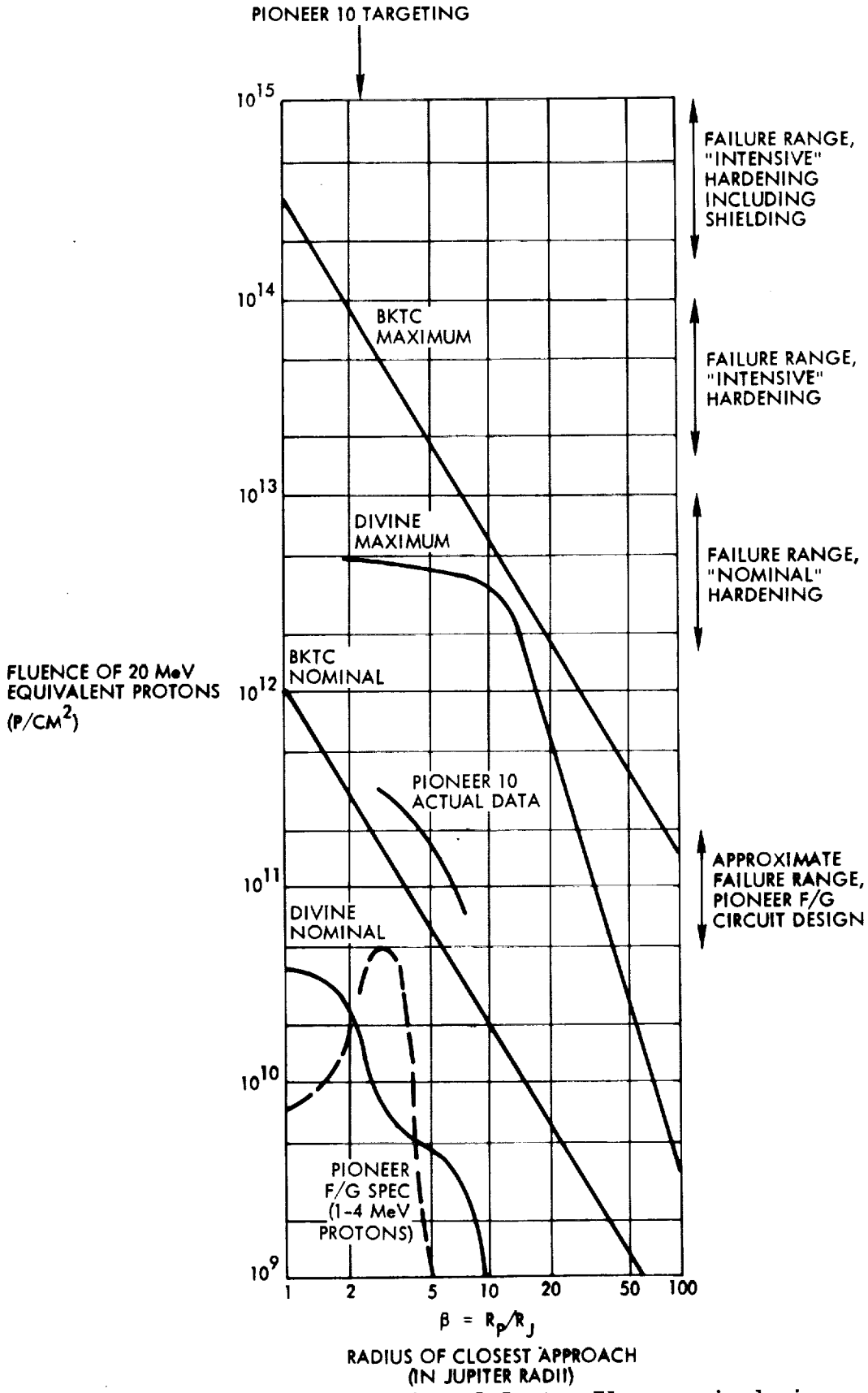

Figure 2-2. Model and Actual Proton Fluences in Jovian Radiation Environment

the planet's axis of rotation. In addition, there is evidence that both temporal and spatial variations exist in the magnetodisk. These findings postulate a host of encounter conditions worse than those observed. In light of these findings, the selection of the approch trajectory and periapsis for a Jupiter orbiter becomes increasingly important from a reliability standpoint. This is especially true for an orbiter for which the dwell time within the radiation fields is significant.

Radiation Environment Near Saturn

The existence of radiation belts at Saturn has been postulated based on the observation of UHF radio emission from this planet and on the assumption that the mechanism of producing radiation belts in the presence of strong magnetic fields is similar to that at Jupiter. However, as discussed in the Design Criteria Documents NASA SP-8091 and SP-8103 it is plausible that the number density, flux and energy of radiation belt particles are much weaker than at Jupiter. With large spacecraft flyby distances of at least 3 Saturn radii, it is unlikely that radiation belt exposure should present a significant hazard to the spacecraft. However, from a scientific standpoint observation of charged particle flux and energy during closest approach is definitely an important objective.

It is of interest to note that existing models of Saturn's radiation belt predict that the presence of ring particles tends to depopulate the radiation belt at distances below 2.3 R_S. At the nominal periapsis distance of 3 R_S and during approach to and departure from periapsis the spacecraft traverses regions where trapped particle characteristics should be measurable.

2.1.2 Mission Categories

Jupiter and Saturn orbiter missions will make major contributions to a number of diverse areas of scientific interest in the target planets, their environment and satellites. The ultimate scientific payloads for these missions will properly represent several of these interests. Ideally, the spacecraft design is capable of accepting any payload; but in practice, the spacecraft design, selection of orbit, and payload complement may all be chosen to emphasize some areas of interest at the expense of others.

This section summarizes the classes of scientific interest and objectives which may be addressed by the orbiter missions, and identifies mission categories which, by virtue of their orbital characteristics, cater to some objectives more than to others.

2.1.2.1 Study of the Planets Jupiter and Saturn

The objective is to conduct exploratory investigations of the appearance, size, mass, magnetic properties, and dynamics of the planets Jupiter and Saturn.

This is best accomplished in the case of the Jupiter mission from a spacecraft in an elliptic orbit with a periapsis of 1 to 4 R_J and apoapsis of 10 to 100 R_J. Periapsis >4 R_J may be desirable in order to avoid the threat of the Jovian radiation belt. Because orbital constraints are minimum for the satisfaction of this objective, it will generally be possible to combine a study of the planet with one or more of the other objectives discussed below.

The spacecraft would carry instruments to observe, both visually and in the infrared, motions in the atmosphere of Jupiter and measure the particles, fields and radio emissions in the near Jupiter environment. The experiments that emphasize planetary science include high-resolution video, IR spectrometers and radiometers, and UV spectrometers and photometers. The visual imaging experiments should receive high priority for this mission.

The study of cloud motions which in turn will lead to critical information regarding the dynamics of the atmospheres of the major planets requires visual imaging over a broad range of horizontal scales. The visual imaging, therefore, can begin at a distance of 20 planetary radii or more, and continue until the spacecraft approaches periapsis.

Displacements of planetary-scale features in the equatorial zone relative to nonequatorial regions will be of interest. In addition, the imaging system should be adjustable to provide high resolution on selected features. Resolution of as little as a few kilometers at closest approach is desirable for observations of the limb. This will provide information on aerosol distribution and cloud stratification. The images should be acquired in stereo pairs in order to determine the relative heights and motions of clouds.

Thermal imaging should form an integral part of the Jovian imaging experiment. In nonhomogeneous, convective atmospheres, upward mass motions transport heat from hotter to cooler regions. At a sufficiently high level, this heat is radiated to the outside, and it can be measured remotely by an infrared sensor. The temperature field can then be correlated with the visual field to provide further information regarding motions within the atmosphere. Thus, an infrared imaging experiment system should be included with the visual experiment.

Similar considerations apply to the observational objectives in a Saturn orbiter mission, except the observation of the rings, their structure, density and photometric characteristics adds new geometrical constraints on orbit selection.

2.1.2.2 Study of Planetary Satellites

The objective of this mission is to supplement the study of the planet Jupiter with a study of the appearance, size, mass, and dynamics of the satellites of Jupiter. The most sophisticated approach — but certainly not the only approach — is to use an orbit which encounters several satellites in successive orbits. This generally requires plane change maneuvers. Similar considerations apply at Saturn.

The most important measurements on the satellites are deduced from imaging. The objectives of the imaging experiment should be to measure the diameter, and therefore the mean densities of the satellites, to resolve basic geologic structures such as impact craters, volcanic structures, mountain chains, etc., if possible, and resolve the question of the possession of the atmospheres by the larger satellites. This may require radio occultation measurements combined with polarimetry, in addition to imagery.

2.1.2.3 Atmospheric Studies; Jupiter Skimmer Package

A possible, though difficult to achieve mission objective is to probe the atmosphere of Jupiter at an altitude of less than 1000 km. The initial periapsis would be lowered from 1.1 R_J to as low a value as possible (<1.01 R_J). The orbit can be at any inclination. This orbit requires a minimum of propellant for injection. An entry probe would be used, carrying a mass spectrometer to sample the composition of the atmosphere as well as instruments to determine temperature, density, pressure, and physical and chemical properties of the clouds. Additional instrumentation on the orbiting spacecraft would be designed to measure fields and particles over a wide energy range and to detect decametric radio emissions.

A prime objective for the low periapsis mission is the determination of the relative abundance and isotopic ratios of hydrogen, helium, carbon and heavy elements up to mass 40. An atmospheric skimmer experiment complement should consist of a mass spectrometer, a retarding potential analyzer and a photoelectron detector to directly study the upper Jovian atmosphere.

The principal problem of mission feasibility is survival of the orbiter in the severe radiation environment known to exist at the very low altitudes being considered. One possibility is to place the perihelion location at a point where the particle flux density can be assumed to be reduced as a result of the sweeping effect of the upper atmosphere and the symmetrical reflection of trapped particles traveling along the planet's magnetic field lines. Repeated short exposures of the orbiter to greater particle flux densities on crossing the radiation belts at higher altitudes while approaching or receding from periapsis cannot be avoided, but could be tolerated if critical components are designed with adequate radiation hardening.

2.1.2.4 Magnetospheric Studies: Magnetic Fields and the Radiation Belts

Elliptical orbits about Jupiter or Saturn will be suitable for a mapping and study of the magnetosphere. A high apogee orbit would permit studies of the magnetospheric boundary, while high inclination orbits would yield the greatest amount of coverage of the planets' magnetic fields and radiation belts.

Jupiter is the only planet, other than the earth, known to have belts of electrically charged particles temporarily trapped by the external magnetic field of the planet. Because of this, a prime objective of the

exploration of Jupiter should be a detailed study of the external magnetic field and charged-particle populations in the vicinity of the planet. This information will be most valuable if concomitant observations of the nonthermal radio emissions originating through correlated phenomena are made in situ. These observations include:

- Interaction of the solar wind and natural satellites with the planetary magnetosphere and trapped radiation phenomena
- The nature of the solar wind and magnetic fields at great distances from the planet
- Galactic and solar cosmic rays.

Of particular interest are orbit modifications, achievable by gravitational perturbations due to close satellite encounters, which change the orientation of the line of apsides relative to the sun line such that different regions of the bow shock and the magnetotail can be explored during the same mission. These mission options which require sophisticated satellite approach navigation capabilities and repeated orbital correction maneuvers are under active study by NASA/Ames Research Center and JPL (Reference 8).

2.1.2.5 Summary of Mission Types (for Jupiter Orbiter)

Orbits that would satisfy all scientific objectives of Jupiter orbiter missions have been categorized into four orbit types. Figure 2-3 outlines the characteristics of each orbit and the dominant scientific objectives to be satisfied by each orbit type. For example, a mission aimed specifically at studying the satellites would not be suitable for an atmospheric skimmer mission. Such a mission would also not be ideal for studies of the magnetospheric boundary of Jupiter. Suggested payload complements and weight estimates for the four mission categories are listed in Table 2-1.

2.2 SPACECRAFT DESIGN

The spacecraft design must meet the requirements of the Jupiter and Saturn orbiter missions, emphasizing commonality of design features for the two missions, and relying as much as possible on the existing Pioneer F/G configuration. Design modifications imposed by these missions include primarily the added orbit insertion and adjustment maneuver capability, increased electrical power and communication performance, accommodation of added experiments, and extended mission life.

2.2.1 Mechanical Requirements

- Provision for attaching to and interfacing with an externally mounted propulsion stage. Several design concepts are investigated in Section 3.1.

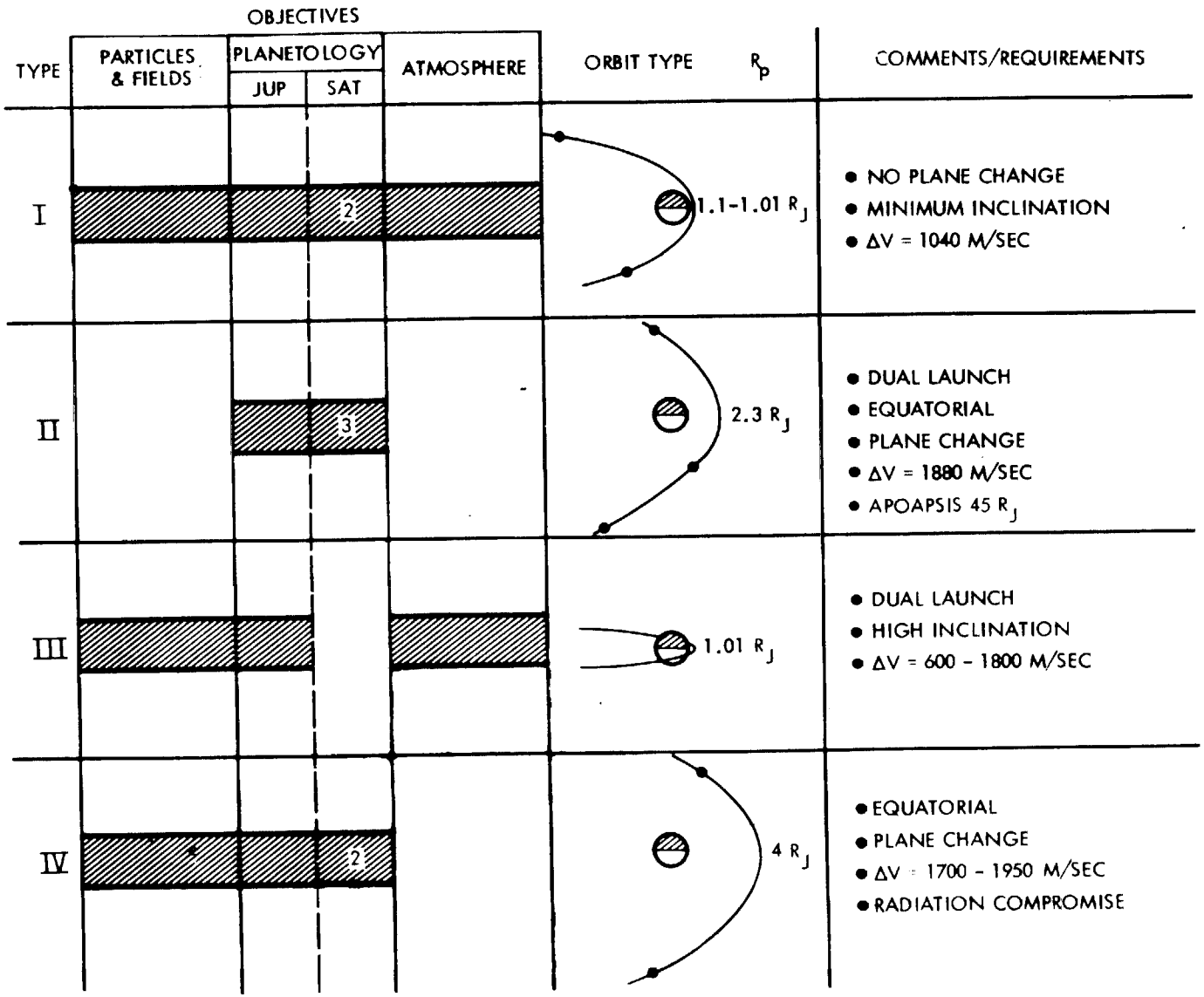

Figure 2-3. Mission Categories

Table 2-1. Suggested Payload Complements for Mission Classes

Mission	I				II				III				IV			
Objectives																
Jupiter	x				x				x				x			
Satellites (maximum number)	x (2)				x (3)								x (2)			
Atmosphere	x								x							
Magnetosphere	x								x				x			
Periapsis (R_J)	1.01				2.3				1.01				≥4			
Orbit inclination	Minimum				Zero				High				Zero			
Instruments (weights in pounds)																
1. Jupiter and Satellites																
Visible imager	15	15	25	45	35	35	45	45			15	25	20	25	35	45
Infrared instrument	8.5	8.5	16.5	16.5	16.5	20	28	36	6	8.5	16.5	16.5	8.5	16.5	28	36
Ultraviolet instrument	6	6	6	14.5	15	15	15	20	2.5	6	15	15	6	7	15	20
Absolute photometer					3.5	3.5	3.5	3.5		3.5				3.5	3.5	3.5
2. Atmosphere																
Skimmer*	24	24	27	30					24	30	30	30				
3. Magnetosphere																
Magnetometer	6	6	6	6		6	6	6	6	6	6	6	6	6	6	6
Charged particle detector	6.5	10	10	10		6.5	6.5	6.5	8.5	10	10	10	6.5	6.5	6.5	8.5
RF receiver	4	4	6.5	6.5		4	6.5	6.5	4	6.5	6.5	25	4	6.5	6.5	6.5
Plasma analyzer		12	12	12				12	12	12	12	12	12	12	12	12
Plasma wave detector		3.5	3.5	3.5			3.5	3.5	3.5	3.5	3.5	3.5	3.5	3.5	3.5	3.5
Suprathermal detector				3.5					3.5	3.5	3.5	3.5	3.5	3.5	3.5	3.5
Total weight (pounds)	70	89	112.5	147.5	70	90	114	139	70	89.5	118	146.5	70	90	119.5	144.5

*Includes: mass spectrometer, retarded potential analyzer and photoelectron detector.

- A rotationally mounted (articulated) sensor package is required to accommodate selected instruments with limited field-of-view capability. This feature will be used to best advantage during the orbital phase to permit a wide range of viewing angles of the planet and its satellites.

- In contrast to Pioneer F/G, the orbiter spacecraft center-of-mass does not lie in the plane of the deployable appendages. Therefore the mass unbalance created by asymmetrical deployment of the RTG's must be compensated by addition of a deployment counterweight to prevent a tilt of the principal axis of inertia and maintain continuous earth pointing.

- Meteoroid protection for the added propulsion tanks is required to minimize the possibility of impacts which may cause mission-catastrophic penetrations.

- The potentially larger nutation angles that can develop during the despin and deployment phases and the increased end masses supported by the deployment arms in the case of the orbiter spacecraft combine to impose substantially larger structural loads on these arms, under worst case conditions, than for Pioneer F/G. Previous analysis has shown that the concept of simultaneous release of the three deployment arms leads to acceptable control of deployment-induced wobble and boom root bending moments.

- Consideration must be given to reinforcement of the several appendages to withstand the orbit insertion deceleration. Whereas Pioneer F/G has been designed for 0.04 g, the orbiter will experience 0.1 g (assuming a 100-lbf thruster).

- To prevent excessive nutation angle buildup following separation from the launch vehicle but prior to appendage deployment, a sufficiently large ($\geq$1.1) spin moment of inertia/transverse moment of inertia ratio must be maintained. The inclusion of the external propulsion stage is a destabilizing factor in meeting this criterion.

2.2.2 Electrical Requirements

- Additional payload power requirements derived from the increased number and type of instruments.

- Significantly increased data rate transmission capability to satisfy imaging objectives is dependent upon substantial increases in primary power allocation for the transmitter.

- Provide sufficient primary power to supply the electrical heaters required to control the operating temperature of the propulsion stage.

- The power source should be sized to permit deletion of the battery which would degrade spacecraft system reliability for these long duration missions.

2.2.3 Thermal Requirements

- Provide heat rejection capability to accommodate the increased science payload and transmitter heat dissipation requirements with reduced radiating area. (The external propulsion stage effectively blocks the platform area formerly occupied by louvers on Pioneer F/G.)

- A hybrid combination of radioisotope heater units (RHU's) and thermostatically controlled electric heaters is required to heat the propulsion stage.

2.2.4 Data and Communication Requirements

A preliminary review of the command, telemetry, and data storage requirements was made to determine the extent of modifications required to meet the orbiter mission objectives.

2.2.4.1 Command

Changes in the command subsystem derive from:

- Enhanced communications performance, i.e., the addition of X-band transmission equipment

- Additional data handling and storage requirements

- Accommodation of the revised science payload complement

- Accommodation of the external propulsion stage requirements.

2.2.4.2 Command Storage

The command memory feature of Pioneer F/G provides the capability of storing a maximum of five command messages and their associated time delays for later sequential execution. Enlargement of command memory capacity may be essential for execution of certain time-dependent functions such as orbit insertion and other maneuvers, and controlling scientific experiments when the spacecraft is occulted by the planet. Other operational procedures such as instrument calibration and mode selection may be greatly simplified with the aid of the command memory. An improved unit, providing increased capacity, redundancy, and time resolution is contemplated for the orbiter application.

2.2.4.3 Communications

To achieve high data rate capability at extended interplanetary communication ranges is a requirement that has been addressed in the Outer

Planets Pioneer spacecraft design study. The same approach can be taken in the Jupiter and Saturn orbiter spacecraft to obtain the highest possible bit rate (approximately 33 kbit/s) consistent with retaining as much of the simplicity, reliability, and technology of Pioneer F/G as possible, constrained by the available electrical power. The inclusion of an X-band transmission capability to provide the prime telemetry support is the most straightforward solution within the constraints cited to provide the desired improvement in link gain.

Retention of an S-band downlink capability is imperative, however, because it:

- Supports tracking and telemetry operations during launch, ascent, and initial Deep Space Station acquisition phases of the mission.
- Provides continuous communications during off earth-pointing maneuvers (at limited ranges).
- Permits routine data acquistion from the DSN 26-meter diameter antenna network.
- Serves as a backup data link (at reduced bit rate) for the X-band system.
- Provides increased assurance of continuous telemetry coverage in the event that the spacecraft attitude "drifts" beyond the X-band beamwidth.

2.2.4.4 Data Storage

Data storage capacity significantly greater than the 50-kilobit core memory of Pioneer F/G is dictated primarily by the requirements of:

- Serving as a buffer for image system data until they can be transmitted to earth at the prevailing data rate
- Recording data during earth occultation.

The memory capacity must be designed to accommodate a multiple line scan imaging experiment wherein the data is stored until they can be transmitted to the ground. A representative 150,000-element picture with 10 bits/pixel encoding is assumed, thus requiring approximately 1.5 megabits of storage. It is further assumed that only one picture will be stored at a time.

2.2.5 Propulsion Requirements

The propulsion subsystem is required to provide impulse for attitude control and midcourse maneuvers, similar to the Pioneer F/G subsystem. For the contemplated orbiter missions, however, a much greater total

impulse capacity must be provided for orbit insertion and adjustment. This added requirement dictates a large increase in the propellant load, relative to Pioneer F/G and has a major impact on the propulsion subsystem design. The relative magnitude of the velocity increments required for the principal maneuvers is shown below:

	Jupiter (1982)	Saturn (1986)
Orbit insertion	1.8 km/s	1.35 km/s
Orbit plane change	300 m/s	200 m/s
Midcourse corrections	40 to 50 m/s	40 to 50 m/s

Previous studies have shown that a minimum ΔV capability of 800 m/s can be implemented by straightforward modifications to the basic Pioneer F/G hydrazine subsystem. This capability is much lower than the above stated ΔV requirements. Consequently, it will be necessary to implement an externally mounted deboost system with higher performance than is obtainable from monopropellant hydrazine. Moreover, the system must be capable of repeated operations, as dictated by the maneuvers shown above. Tradeoffs leading to a selection of the preferred system will be discussed in subsequent sections.

The choice of deboost thrust level must take into account orbit insertion maneuver efficiency on one hand, and structural loads on the deployed appendages on the other. Although low thrust is desirable to minimize redesign of the appendages and their support structure (Pioneer F/G appendages were designed to withstand axial acceleration of 0.04 g) the acceleration should be sufficiently large to avoid significant performance losses during the orbit insertion maneuver.

In the interest of maintaining an uninterrupted command and telemetry capability at large earth-spacecraft distances, the spacecraft must normally remain earth-oriented at all times. Off-earth pointing will be permitted for initial midcourse maneuvers and for certain in-orbit maneuvers essential to accomplishing mission objectives, such as orbital plane changes and orbit modifications and corrections related to planetary encounters (see Section 6.11).

New spin rate maneuvers are planned for the orbiter missions which were not necessary for Pioneer F/G. They are:

- Spinup from the nominal 4.8 rpm to 15 rpm prior to high-thrust ΔV maneuvers
- Despin from 15 rpm to 4.8 rpm
- Despin from 4.8 rpm to 2 rpm to increase image resolution
- Spinup from 2 rpm to 4.8 rpm.

2.3 INTERFACES

2.3.1 Launch Vehicle

The launch vehicle for the Outer Planets Pioneer Orbiter missions is the Titan 3E/Centaur D-1T/TE-364-4. The launch vehicle for the Pioneer 10 and 11 spacecraft was the Atlas SLV-3C/Centaur D-14/TE-M-364-4. Thus the launch vehicle has a new first stage, a modified second stage, and the same third stage, as the previous Pioneers for Jupiter.

2.3.1.1 Nose Fairing and Envelope

The Viking nose fairing is to be used with the launch vehicle for these missions. While the 10-foot diameter fairing for Pioneers 10 and 11 (based on the OAO fairing) attaches to the forward end of the Centaur, the 14-foot diameter Viking fairing encloses the Centaur and attaches to the forward end of the Titan.

The dynamic envelope available for the spacecraft is increased from 109 to 150 inches in diameter. However, because the spacecraft design is not changed from the Pioneer F/G design except where necessary, the orbiter spacecraft does not occupy any space outside the 109-inch limit.

2.3.1.2 Payload Capability

The weight which can be sent to either Jupiter or Saturn by the launch vehicle for the orbiter mission is discussed in Section 6.5.

2.3.1.3 Coast Capability

For the typical Jupiter and Saturn mission opportunities considered, launches occur between December and May. With the launch site at ETR, and with launch azimuths restricted to the usual range of about 90 to 114 degrees, these departures can be reached by the direct ascent mode or by an orbital ascent mode with a short coast time. The coast periods generally do not exceed 25 minutes. The Centaur stage will have this capability.

2.3.1.4 Mechanical Environment

The acoustic and vibration environment of the launch vehicle, while greater in some frequency bands than the Atlas, falls within the envelope specified for the qualification and acceptance testing of the Pioneer F and G spacecraft in Specification PC210.03, Pioneer F and G Spacecraft Specification.

2.3.1.5 Launch Vehicle Adapter

The adapter connecting the flight spacecraft to the TE-364-4 stage is the standard 37-inch diameter by 31-inch adapter.

2.3.1.6 Umbilical

Because of the use of RTG's as the spacecraft electrical power source, and because RF communications with the spacecraft are used for inserting commands and monitoring results, no umbilical cable is necessary for spacecraft operations from RTG installation – normally about 30 hours before the launch window of the first launch day – until separation from the launch vehicle. However, ground power (at 28 VDC) is required to support all spacecraft test operations on the launch vehicle prior to RTG installation.

2.3.2 Deep Space Network

The Deep Space Network (DSN), established by the NASA Office of Tracking and Data Acquisition under the system management and technical direction of the Jet Propulsion Laboratory (JPL), provides two-way communications with the spacecraft. The Deep Space Stations (DSS's) and the telecommunications interface through the RF link with the spacecraft, providing tracking, telemetry, and command support, is known as the Deep Space Instrumentation Facility (DSIF).

2.3.2.1 DSIF

The DSIF consists of a world-wide network of Deep Space Stations equipped with 26-meter diameter antennas and a network of 64-meter diameter antenna stations equipped with phase-lock receiving systems and high-power transmitters to provide radio communications with the spacecraft. The stations are located approximately 120 degrees apart in longitude, assuring that a spacecraft in or near the ecliptic will always be in the field-of-view of at least one station and for several hours each day may be seen by two stations. Stations comprising the DSIF are identified in Table 2-2.

Table 2-2. Tracking and Data Acquisition Stations of the DSIF

Location	DSS	DSS Serial Designation	Antenna	
			Diameter m (ft)	Type of Mounting
California	Pioneer	11	26 (85)	Polar
	Echo	12	26 (85)	Polar
	Mars	14	64 (210)	Az-El
Australia	Weemala (formerly Tidbinbilla)	42	26 (85)	Polar
	Ballima (formerly Booroomba)	43	64 (210)	Az-El
Australia	Honeysuckle Creek	44	26 (85)	X-Y
South Africa	Hartebeesthoek	51	26 (85)	Polar
Spain	Robledo	61	26 (85)	Polar
	Cebreros	62	26 85)	Polar
	Robledo	63	64 (210)	Az-El

The Pioneer Outer Planets Orbiter mission requires the periodic support of both networks to accomplish the various phases: the 26-meter network establishes the initial two-way acquisition, conducts routine cruise-phase TT&C operations, and provides a backup capability for the 64-meter stations; adequate telemetry bit rates from the vicinity of Jupiter and Saturn require the X-band capability available only at the 64-meter stations.

All DSS's operate at S-band frequencies: 2110-2120 MHz for earth-to-spacecraft transmission and 2290-2300 MHz for spacecraft-to-earth transmission. In addition, the 64-meter network is capable of receiving spacecraft signals in the X-band (8402-8441 MHz). DSS performance parameters which are critical to achieving compatibility with the spacecraft communications subsystem are given in Table 2-3.

2.3.3 RTG Power Sources

The radioisotope thermoelectric generator (RTG) identified for the Pioneer Outer Planets Orbiter missions is the multi-hundred watt (MHW) RTG which is currently under development for the LES 8 and 9 spacecraft to be launched in 1974 and is designated for use on the Mariner-Jupiter-Saturn spacecraft to be launched in 1977.

The RTG unit to be employed weighs 85 pounds and has a diameter of 15.7 inches and a length of 23 inches. It contains $Pu^{238}O_2$ as the heat source, producing 2400 watts of thermal power. A shell containing a matrix of silicon-germanium thermocouples converts 150 watts (soon after launch) into electric power which is delivered at 28 volts. A more detailed description of the RTG characteristics is given in Appendix E.

2.3.3.1 Physical Arrangement

Two units are to be carried on each flight spacecraft, one on each side. The RTG units are in a stowed position, just outboard of the equipment compartment side panel, during launch. Soon after the spacecraft is separated from the launch vehicle, the RTG's are released to deploy some seven feet radially to their location for the remainder of the mission.

This remote location (a) minimizes accumulated interaction between the radioisotope and the components and instruments aboard the spacecraft, (b) establishes a favorable moment of inertia ratio for the spacecraft, and (c) virtually eliminates a thermal interaction between the RTG's and the other elements of the spacecraft.

2.3.3.2 Mechanical Interface

Each RTG unit is attached to a mounting plate by three bolts. The mounting plate is attached to the equipment compartment by bolts, when stowed; at deployment these bolts are severed by bolt cutters. The mounting plate is connected to the equipment compartment by guide rods.

Table 2-3. DSS Primary Telecommunication Parameters (Nominal)

Parameter		Station Configuration			
	S-Band Uplink	S-Band Downlink	S-Band Uplink	S-Band Downlink	X-Band Downlink
Frequency range (MHz)	2110-2120	2290-2300	2110-2120	2290-2300	8402-8441
Antenna gain (dBi)[1]	51.8	53.3	60.4	61.3	71.5
Antenna beamwidth (deg)	0.36	0.33	0.15	0.14	0.038
Polarization	RCP	RCP	RCP	RCP	RCP
RF power output, maximum (kw)	20	N/A	400	N/A	N/A
System noise temperature (^{o}K)	N/A	54	N/A	36	47
Coherent downlink frequency	N/A	240/221 x uplink	N/A	240/221 x uplink	880/221 x uplink
Receiver noise bandwidth, minimum (Hz)	N/A	10.8	N/A	10.8	1
Uncoded data rate, maximum (bps)	10	2500[2]	10	33,000[3]	33,000[3]
Convolutional coded data rate, maximum (bit/s)	N/A	2048	N/A	2048[4]	2048[4]

[1]Antenna elevation angle, 10 degrees

[2]Upper limit constrained by 4800 bps high speed data line

[3]Upper limit constrained by 50 kbps data lines

[4]Upper limit constrained by sequential decoding capability

2.3.3.3 Thermal Interface

The thermal interface of the RTG's with the spacecraft is significant only until deployment. Before launch, cooled air appropriately directed within the shroud keeps the RTG's below vacuum-operating temperatures, and keeps adjacent spacecraft temperatures low.

From liftoff to deployment (about 1.5 hours) temperatures of the RTG's and spacecraft will rise. Internal RTG temperatures are kept low by delaying the venting of the inert fill gas until after deployment. Adjacent spacecraft surfaces may have to withstand temperatures approaching 450°F. Appropriate coatings and Kapton insulation will be applied as necessary.

2.3.3.4 Electrical Interface

Power is transferred from the RTG's at 28 VDC via a cable which is drawn from a slack box as the RTG is deployed. The spacecraft maintains the bus voltage at this value by dissipating excess power in a shunt circuit.

2.3.3.5 Nuclear Radiation

The nuclear radiation of the RTG's is composed primarily of gamma-ray photons in the energy range, 10 to 1000 keV and neutrons in the energy range, 1.5 to 5 MeV.

The only significant impact of the gamma rays is the potential interference with scientific instruments sensitive to radiation at this energy. This type of interference, affecting instruments measuring intermediate-energy nuclear particle fluxes at low intensities, has been resolved on Pioneer F/G; the interfering flux levels are increased less than 50 percent on the Pioneer Outer Planets Orbiter spacecraft.

Neutron radiation should be examined for potential damage to components and materials. On the orbiter missions the longer duration and greater isotope weight will raise total neutron fluences at typical equipment compartment locations from 1.7×10^{10} to 7×10^{10} n/cm^2. However, for components utilized, 10^{12} or 10^{13} n/cm^2 would be the threshold of concern, so no impact is foreseen.

2.3.4 Scientific Instruments

2.3.4.1 Payload Complement Selection

A variety of scientific experiments may be accommodated by the orbiter spacecraft configurations defined in Section 3.1. Payload complements with weights ranging from 70 to 120 pounds were considered, compatible with the weight and power constraints of the Jupiter and Saturn orbiters (see also Appendix A).

Table 2-4 lists representative payload complements for the two missions. This selection is only tentative and requires further study as plans for the outer planet orbiter missions develop. However, as sample payload complements they can be used to identify relevant payload interface requirements.

Table 2-4. Scientific Payload Complements

Instrument	Pioneer 10/11		Jupiter Orbiter		Saturn Orbiter		Data Rate (bits/s)
	Weight (lb)	Power (W)	Weight (lb)	Power (W)	Weight (lb)	Power (W)	
Magnetospheric Particles and Fields							
Magnetometer	5.9	3.1	6.0	4.0	5.2	4.0	25
Plasma analyzer	12.0	4.5	12.0	5.0	11.5	5.0	50
Charged particle	7.2	2.4	10.0	4.0			
Geiger tube telescope	3.6	0.8	—	—	12.6	6.0	
Cosmic ray telescope	7.1	2.8	—	—			
Suprathermal particle detector	—	—	3.5	2.0	—	—	10
RF sweep receiver	—	—	6.5	3.0	—	—	250
Plasma wave detector	—	—	3.5	2.0	—	—	10
Trapped radiation detector	3.9	2.1	—	—	—	—	
Subtotal	39.7	15.7	41.5	20.0	29.3	15.0	
Planetology							
Infrared	4.4	1.2	12.0	4.0	6.0	4.0	1,000
Ultraviolet	1.5	1.0	10.0	3.0	6.0	3.0	200
Photopolarimeter	9.5	3.5	—	—	—	—	
Imaging							
Line-scan imaging system			25.0	16.0	25.0	16.0	10^6
Subtotal	15.4	5.7	47.0	23.0	37.0	23.0	
Meteoroid Detectors	11.0	2.5	—	—	3.7	1.0	
Unspecified	—	—	31.5	14.0	—	—	<12,000
Total	66.1	23.9	120.0	57.0	70.0	39.0	

2.3.4.2 Payload Interface Requirements

The Jupiter Orbiter payload weight, power, and telemetry requirements represent significant increases from the Pioneer 10 payload, which is also shown in Table 2-4 for comparison. Three of the instruments — the magnetometer, plasma analyzer, and charged particle instrument — are identical to, or only slightly modified from, the corresponding instruments carried by Pioneers 10 and 11. Their interface requirements remain essentially unchanged. The remaining six identified instruments are new.

Of these, only the line-scan imaging system imposes interface requirements that have an appreciable impact on the spacecraft system design. These special requirements include:

a) High data transfer rates, typically 1.3 megabits/s if the frame size is 3.35 x 3.35 degrees and the spacecraft rotation rate is 5 rpm (assuming 10-bit parallel transfer to buffer storage).

b) High data buffer storage capacity – approximately 1.5 megabits per frame with linear encoding (10 bits/pixel).

c) Rotational mount to vary the cone angle, as required for planet and satellite viewing (also required for the infrared spectrometer and the ultraviolet photometer)

d) Careful selection of mounting area on spacecraft to avoid stray light effects and to provide a wide pointing field of view

e) Mode switching for multispectral options

f) Special provisions to shield sensor elements from inadvertent exposure to the sun and to protect the objective lens against extended exposure to potential micrometeoroid damage.

Some of the line-scan imaging system requirements, including mode switching, line-of-sight rotation, and clear field-of-view, are similar to those imposed by the imaging photopolarimeter of Pioneers 10 and 11 which is not included in the orbiter payload. Other interface aspects of the line-scan imaging system are less demanding. It does not require the frequent cone angle changes of the photopolarimeter, and ground data processing is less complex to reconstruct image frames.

Most of the instruments can be accommodated in either of two dedicated payload compartments or by the same external mounting provisions (e.g., magnetometer, meteoroid sensors, and plasma analyzer).

The interface requirements for the Saturn orbiter payload are similar to those described above for the Jupiter orbiter configuration, although fewer instruments can be accommodated because of the smaller weight capability.

3. SPACECRAFT SYSTEM DESIGN

3.1 CONFIGURATION

Selection of the Pioneer Outer Planets Orbiter configuration is governed by the following design considerations and criteria:

- Retention of the Pioneer F/G configuration or its derivative, the Outer Planets Pioneer spacecraft, as building block, modified as required for the orbiter missions
- Provision of adequate propulsive maneuver capability for planetary orbit insertion and orbit changes
- Effective accommodation of science payload in terms of weight, space and power capacity, sensor articulation, data handling, storage and telemetry capability
- System reliability commensurate with extension of mission life to 3.5 years for the Jupiter orbiter, 6 years for the Saturn orbiter
- Simplicity and cost economy in system design, implementation and operation.

The evolution of the Pioneer orbiter from the baseline Pioneer F/G via the Outer Planets Pioneer spacecraft (Reference 3) has been previously outlined in Section 1.3. In the selected orbiter design concept to be described in this section many design features of Pioneer F/G are retained intact or with modifications that have already been identified in the design of the Outer Planets Pioneer. The only major departures from the existing designs are those related to the accommodation of the new propulsion system and the scientific payload instruments.

3.1.1 Design Approach

In the earlier study of Pioneer Jupiter orbit missions performed by TRW Systems (Reference 5) several design alternatives of adding the required large propulsion capability to the baseline Pioneer F/G spacecraft were investigated. The design concept designated as Configuration 2 in that study is applicable in a modified version to the requirements of the outer planets orbiter spacecraft. Principal features of this configuration, consisting of a modified Pioneer F/G spacecraft with an added propulsion stage, are reflected in the orbiter design concept to be described below.

Questions of principal interest in this design approach involve

- Feasibility of using the basic Pioneer F/G configuration with only small modifications
- Accommodation of the large externally stored propellant mass

- Control of mass properties which are significantly altered from those of Pioneer F/G by the addition of the propulsion stage.

These questions are addressed in the following paragraphs.

Retention of the Basic Pioneer F/G Configuration

A principal design objective is to retain the basic structural configuration of Pioneer F/G embodied by the hexagonal equipment bay and the attached payload bay, the high-gain antenna dish, antenna feed and support structure and the deployment provisions of the RTG support booms and magnetometer boom.

In contrast to the layout of the previously defined Configuration 2 where the RTG booms are deployed in diametrally opposite directions, the preferred configuration retains the asymmetrical deployment concept of Pioneer F/G where RTG booms are located 120 degrees apart, partly balanced by the deployed magnetometer boom which extends in a direction 120 degrees from the RTG's. This permits retention of the RTG guide rod location, attach fittings and stowage provisions, but imposes constraints on the control of mass properties dissimilar from those of Pioneer F/G, to prevent tilting of the principal axis relative to the spacecraft centerline.

In the case of Pioneer F/G the asymmetrical deployment of the RTG booms introduces a lateral shift in the spacecraft center-of-mass, but this does not cause a tilt of the principal axis, because the center of mass is tightly controlled to remain within the deployment plane of the RTG's and the magnetometer boom. With the principal axis offset but remaining parallel to the spacecraft centerline at all times, continuous earth pointing of the high-gain antenna can be assured (see Figure 3-1a).

In the case of the Pioneer orbiter configuration the asymmetrical RTG deployment must be fully compensated by a deployment counterweight added to the tip of the magnetometer boom, such that the mass center of the spacecraft proper always remains on the spacecraft centerline, lined up with the mass center of the attached stage, to avoid a principal axis tilt (see Figure 3-1b). The alignment remains unaffected by propellant depletion since this only has the effect of shifting the total center of mass along the Z axis, closer to the mass center of the spacecraft proper.

Propulsion System Accommodation

To provide a 2000 m/s ΔV capability to a spacecraft with 800 pounds of inert weight requires 800 to 1000 pounds of propellant depending on the specific impulse characterizing the propulsion system.

The objective of retaining the baseline Pioneer F/G configuration rules out internal storage of this amount of propellant because of the limited space available in the existing equipment compartment. The

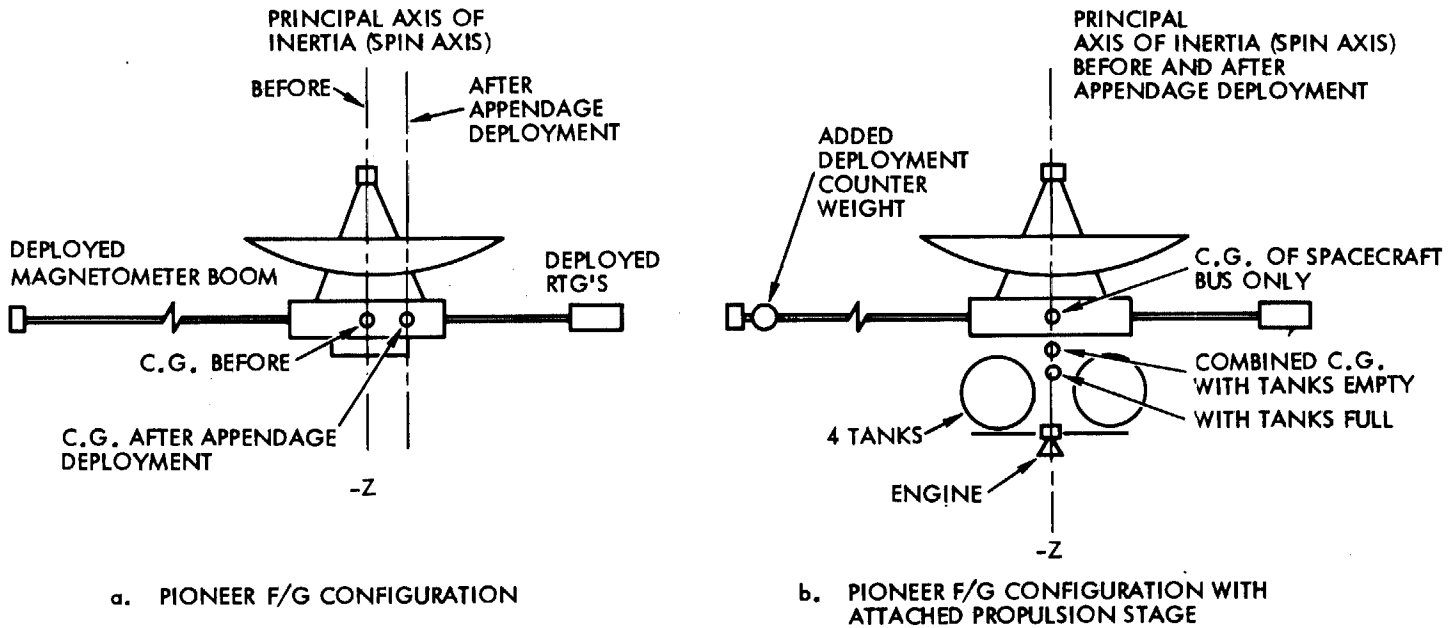

Figure 3-1. Principal Axis Control Approach of Pioneer Spacecraft with Asymmetrical RTG Deployment (120-degree Separation Angle)

maximum size to which the present 16.5-inch hydrazine tank of Pioneer F/G could be enlarged is 25 to 28 inches providing a maximum prepellant capacity of 300 pounds. Assuming monopropellant hydrazine with I_{sp} = 225 seconds this would provide a maneuver capacity of only 800 to 850 m/s which is marginal, at best, for a Jupiter orbit mission and inadequate for a Saturn orbiter. This minimum capability Pioneer orbiter defined in TRW's previous study and designated as Configuration 1 thus does not meet the specified mission requirements.

The externally attached propulsion stage used in the selected orbiter configuration has two distinct advantages. It provides ample propellant storage capacity limited only by injected weight performance of the launch vehicle. It also provides the option (not offered by a simple internally mounted propellant tank) of using a bipropellant system with higher I_{sp} performance than monopropellant hydrazine. The specific impulse of MMH/N_2O_4, the bipropellants used by the Mariner 9 Mars Orbiter, is 290 seconds. This reduces the propellant weight required for a specified maneuver capability by nearly 30 percent, compared with monopropellant hydrazine.

A prerequisite for storing the unequal amounts of oxidizer and fuel mass symmetrically with respect to the spin axis and achieving a favorable moment of inertia ratio for the spin-stabilized vehicle is to use at least four spherical tanks for mass balance. Only if toroidal propellant tanks were to be used could the desired mass distribution be attained with two tanks in tandem arrangement. This option was not selected because it would require additional development in tankage and expulsion system technology (see below).

Four spherical tanks arranged symmetrically at the corners of a rectangle, square or rhomboid can be used to achieve the desired mass distribution characteristics with the fuel and the oxidizer tanks located at alternate corners.

The preferred configuration uses a rhomboid arrangement, with the larger dimension aligned with the spacecraft Y axis. This yields favorable moment-of-inertia ratios during the predeployment phase, while minimizing field of view obstruction of articulated science sensors. This configuration also reduces blockage of thermal radiation from louvered areas at the bottom surface of the two payload compartments.

Control of Mass Properties

The following design criteria apply to the control of mass properties of the spacecraft/stage combination:

- Mass balance of the stored propellant such that the stage center of mass is maintained on the spacecraft centerline during all mission phases, with fully loaded, partially depleted and empty propellant tanks.

- Mass balance of the deployed appendages such that the center of mass of the spacecraft proper is maintained on the spacecraft centerline before, during and after deployment.

- Mass balance of the rotationally mounted sensor package to prevent products of inertia being generated by sensor orientation changes.

- Sufficiently large spin moment of inertia (I_z) compared to transverse moments of inertia (I_x, I_y) during the critical predeployment phase to avoid dynamic instability and hence the accrual of excessive nutation angles during this phase and the initial part of the deployment phase.

The first two criteria have been previously mentioned and can be met by attention to balanced appendage deployment and proper placement of the propellant storage tanks.

A deployment counterweight of approximately 25 pounds placed at the tip of the magnetometer boom prevents displacement of the center of mass of the spacecraft proper along the -X axis due to the asymmetrical RTG boom deployment.

Regarding propellant mass balance, the large difference of fuel and oxidizer mass of the MMH/N_2O_4 bipropellant system (i.e., approximately 60 percent N_2O_4 versus 40 percent MMH) requires a configuration of at least four tanks, with the fuel tanks and oxidizer tanks placed in opposite locations, respectively.

The concept of using only two spherical tanks either side-by-side as in the 3-axis stabilized Mariner 9 orbiter or in tandem was found to be impractical from a mass distribution standpoint (see References 9 and 10).

An alternate concept of using two toroidal tanks in tandem arrangement (see References 9 and 11) proves to be feasible but requires advances in propulsion system technology not necessary when using conventional spherical propellant tanks.

The selected 4-tank bipropellant propulsion stage configuration closely resembles a configuration developed and qualified for an earth satellite program and constitutes a minimum risk approach.

Custom Stage Design for the Saturn Orbiter

Because of the higher launch energy required for Saturn missions the maximum injected gross spacecraft weight is 800 to 900 pounds less than that of Jupiter missions for the launch years and flight times being contemplated, as determined by the Titan IIIE/Centaur launch vehicle capability. This limits the maximum propellant capacity of the Saturn orbiter to about half of the capacity of the Jupiter orbiter (see Sections 6 and 7).

This limitation in propellant capacity is the more severe because orbit injection at Saturn will occur at a relatively greater distance from the planet than in the Jupiter orbit mission, probably at least 3 planet radii, so as to reduce the hazard of ring particle impact. Increasing the distance of the orbit injection point reduces the effectiveness of the maneuver, causing the capture orbit to be more eccentric.

In view of these factors it is critically important in the Saturn orbiter mission to use the available propellant in a manner which yields the highest possible ΔV capability.

The design approach adopted for the Saturn orbiter is to minimize the spacecraft inert weight by reducing the size and weight of the propulsion system, thereby maximizing the achievable ΔV capability, rather than using the same configuration as for the Jupiter orbiter with offloaded tanks.

The increase in ΔV capability due to reduction of dry weight (with the gross spacecraft weight held constant) is given by

$$\frac{\partial \Delta V}{\partial W_e} = - \frac{I_{sp}\, g}{W_e} = -3.4 \frac{m/s}{lb}$$

where

W_e = 850 pounds = estimated dry weight

I_{sp} = 292 seconds = specific impulse of MMH/N_2O_4 propulsion system.

The relative ΔV increase is given by

$$\frac{\partial\, \Delta V/\Delta V_{ref}}{\partial\, W_e/W_{e_{ref}}} = - \frac{1}{\ell n\, (W_o/W_{e_{ref}})} = -2.0$$

The subscript ref designates reference values of ΔV and W_e, and the nominal gross weight W_o is assumed to be 1400 pounds. Under the assumed conditions a 5 percent reduction in dry weight yields an increase of 10 percent in ΔV capability.

These results reflect two factors: (1) the available propellant mass increases by the amount saved in dry weight and (2) the maneuver effectiveness increases inversely with dry weight reduction. Thus an estimated 30-pound reduction in stage dry weight (tankage, pressurant and structural weight) increases the ΔV capacity by 100 m/s, providing an appreciable performance improvement of the Saturn orbiter.

A further advantage associated with using smaller propellant tanks in the Saturn orbiter configuration, rather than off-loading propellant, is the avoidance of propellant sloshing during the launch phase. This reduces dynamic loads on the expulsion bladders, tank and support structure and thus simplifies system development and test requirements.

3.1.2 Jupiter Orbiter Configuration

The selected design concept of the Pioneer Jupiter orbiter is shown in Figure 3-2. The side view (bottom drawing) shows the spacecraft with its externally attached propulsion bay in the stowed configuration mounted on top of the launch vehicle's third stage, the TE 364-4 solid motor. The interstage is a standard 37-inch diameter cylindrical adapter to which the spacecraft is fastened by a Marman clamp.

Spacecraft loads are transferred through an open trusswork support structure and adapter ring to the interstage mounting flange. In addition, the adapter ring directly supports the four spherical propellant tanks and four struts that hold the 93-pound main retro-engine.

The spacecraft is housed within the 14-foot diameter Viking shroud, the standard nose fairing for Titan III E/Centaur class boosters. Actually, with the maximum lateral dimensions, determined by the 9-foot diameter high-gain antenna dish as in Pioneer F/G, the vehicle would fit into the Centaur/Pioneer F/G shroud. Thus, the Viking shroud provides more than ample space, both longitudinally and laterally. A potential weight advantage, estimated as about 100 pounds, would accrue from the use of the smaller Centaur/Pioneer shroud, if this shroud were to be adapted to the Titan IIIE/Centaur class boosters. However, no such plans are currently under consideration.

The plan view, at the top of Figure 3-2, shows the spacecraft in stowed and deployed configuration. The deployment principle illustrated in this view is essentially the same as in Pioneer F/G. The RTG booms and the magnetometer boom are extended by centrifugal action under the control of restraint cables, attached to viscous deployment dampers.

Each RTG boom consists of three guide rods which slide in guide fittings mounted to the top and bottom of the equipment bay. The four SNAP-19 radioisotope generator units of Pioneer F/G have been replaced by the new higher performance multi-hundred watt (MHW) RTG units, one on each RTG boom.

The magnetometer boom, deployed along the +X axis opposite the RTG booms, is reinforced against bending in the X-Y plane by the addition of a scissors-type linkage. This reinforcement is required because

1) Higher bending loads are acting on the structure as the boom is deployed simultaneously with the RTG booms, starting at a spin rate of 15 rpm

FOLDOUT FRAME

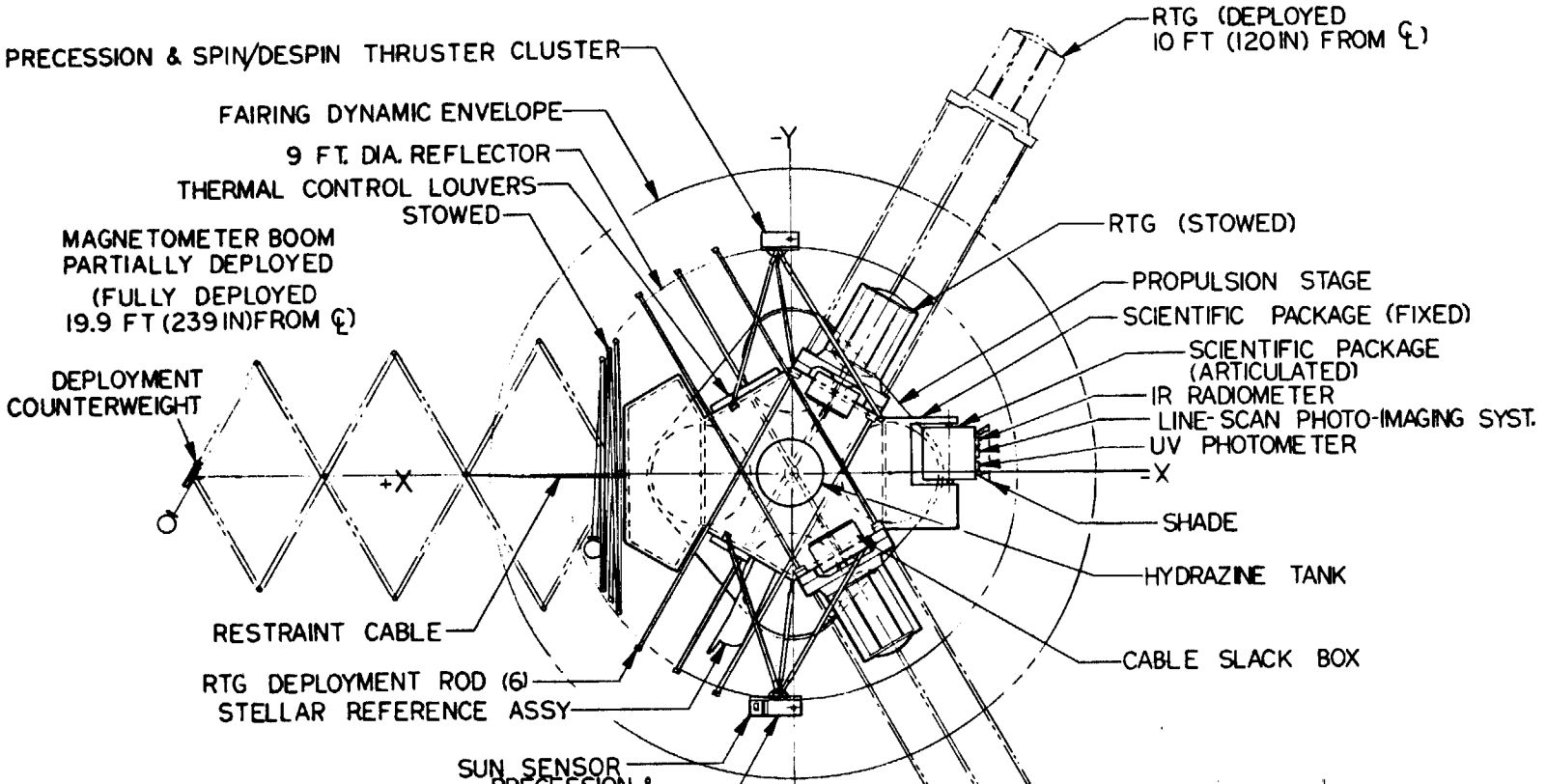

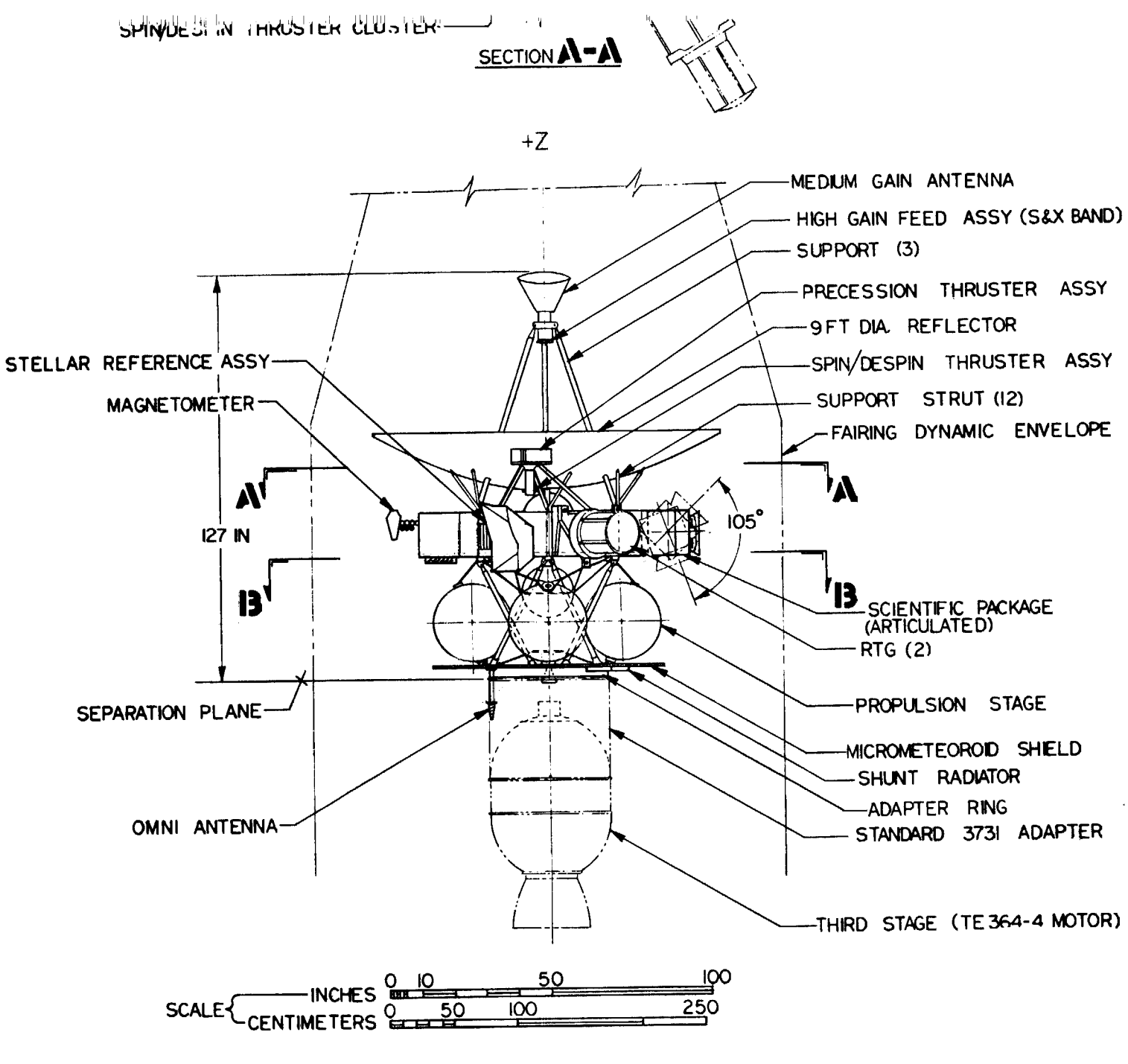

Figure 3-2. Jupiter Orbiter Configuration

2) Addition of a 25-pound deployment counterweight near the tip of the magnetometer boom, required to maintain the center of mass of the spacecraft proper on the Z axis (see Section 3.1.1), also increases the structural load acting on the boom during deployment.

The drawings in Figure 3-3 show details of the support truss, the tank mounting provisions and the attach fittings by which the concentrated tankage and truss loads are transferred to the adapter ring. The adapter ring is designed to spread these loads more uniformly over the interstage mounting flange.

It is evident from the design drawings that the orbiter configuration retains many design features of the baseline Pioneer F/G spacecraft. These are:

- The hexagonal central equipment bay and +X axis extension used to house payload instruments
- The RTG and magnetometer booms and their stowage and deployment provisions (with modifications as discussed above)
- The 9-foot parabolic high-gain antenna dish, support truss and antenna feed structure
- The medium- and low-gain antennas
- The fore-aft pointing ΔV precession thrusters and the tangential spin/despin thrusters mounted near the rim of the high-gain antenna dish, as well as their support struts. A pair of spin/despin thrusters has been added as discussed below. A small lateral shift of the thruster assemblies was necessary to align the ΔV/precession thrusters with the center-of-mass location on the spacecraft Z axis and thus to avoid precession torques around the Y axis in the new configuration.
- The 16.5-inch hydrazine tank inside the central equipment bay. The tank mounting structure has been modified slightly to conform with the support structure of the added nitrogen pressurant tank located below the equipment platform.
- The star reference assembly and sun sensor assembly at locations essentially unchanged from Pioneer F/G.

Configuration features (other than the propulsion stage and support structure) that are new or have been adapted from the Outer Planets Pioneer spacecraft are summarized as follows:

- Addition of a second extension bay on the -X side of the hexagonal central equipment compartment. This extension bay

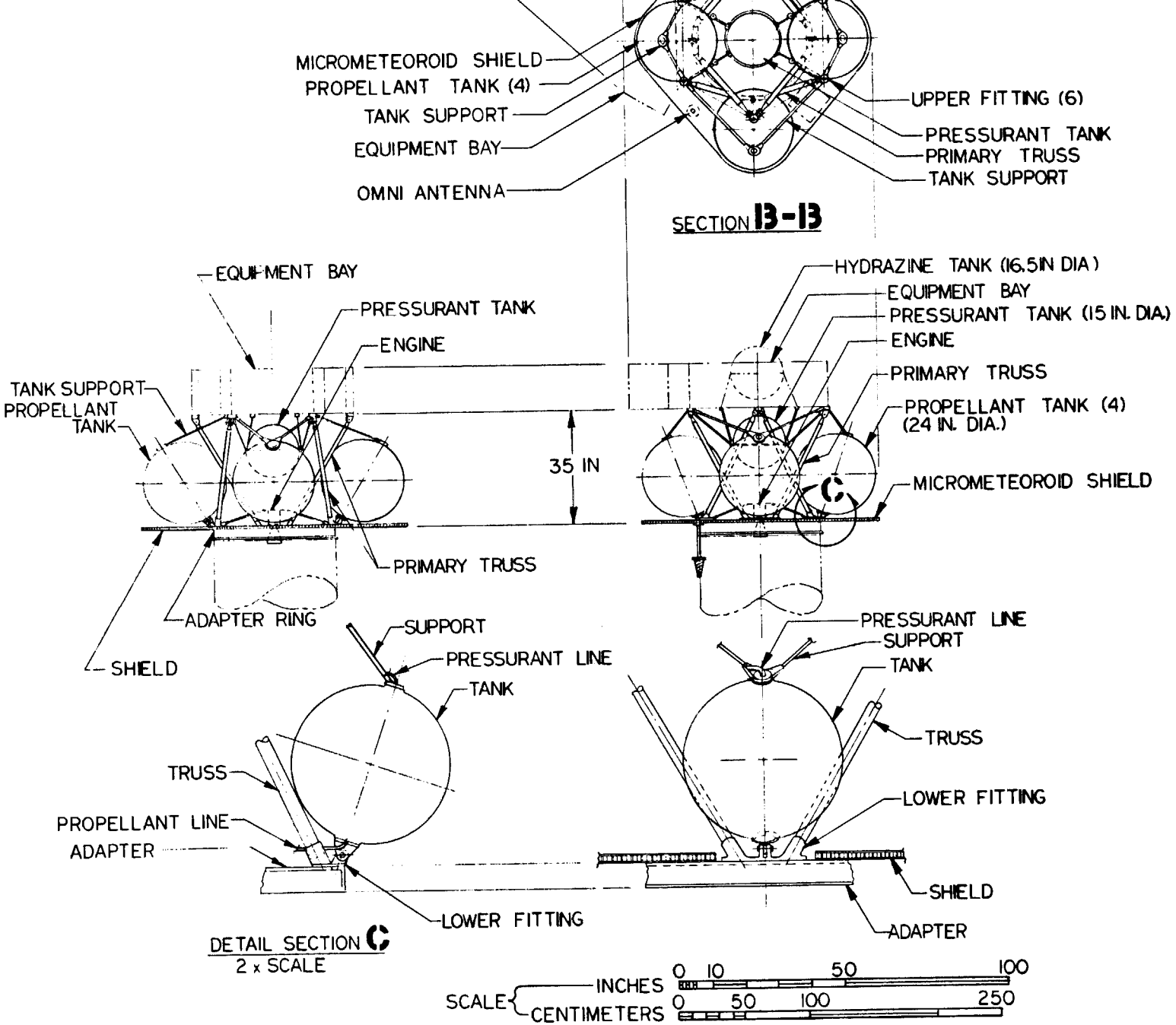

Figure 3-3. Jupiter Orbiter Propulsion Bay (Detail)

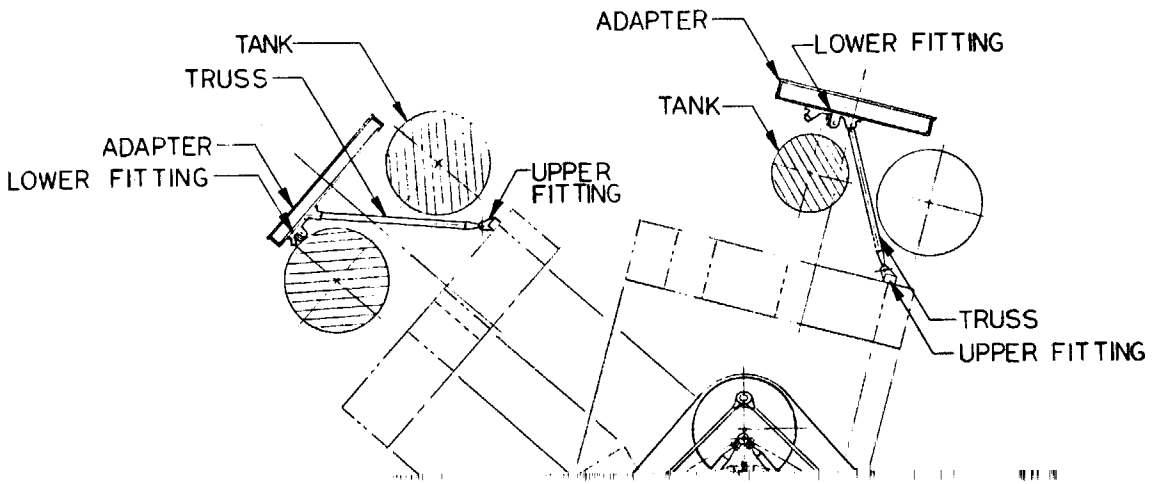
TANK
TRUSS
ADAPTER
LOWER FITTING
UPPER FITTING
ADAPTER
LOWER FITTING
TANK
TRUSS
UPPER FITTING

houses payload equipment and subsystem components and supports a 1-axis rotatable sensor package.

- Modification of the equipment platform support structure. The 25-inch spacecraft adapter ring of the original Pioneer F/G configuration has been eliminated. An eight-member truss has been attached below the central equipment bay to support the ring-mounted new GN_2 pressurant tank and the equipment platform in lieu of the 25-inch adapter ring.

- Change in location of the thermal control louvers: because of thermal radiation blockage by the attached propulsion stage most aft-facing thermal control louvers of Pioneer F/G have been eliminated and louvers added to several side walls of the equipment compartment and extension bays.

- Change of the antenna feed structure to accommodate the new dual S-band/X-band communication system, adapted from the Outer Planets Pioneer design.

- Replacement of four SNAP-19 RTG's by two MHW units, as previously discussed.

- Modification and reinforcement of the magnetometer boom structure and addition of deployment counterweight, as previously discussed.

- Addition of a micrometeoroid shield of 1-inch thick aluminum honeycomb at the bottom of the new propulsion bay. This shield protects the propellant tanks against particles approaching from the aft hemisphere, the principal approach direction of asteroidal micrometeoroids during the outbound passage. Protection against particles approaching from all other directions is provided by the spacecraft proper (front hemisphere) and by Armalon blankets wrapped around the sides of the propulsion stage (not shown in design drawing).

Other design features of the Jupiter orbiter not listed above are briefly described in the following paragraphs.

Structure

The structural support concept is illustrated in Figure 3-4 by a simplified perspective sketch. The eight-member support truss provides a direct load path from the six hard-points at the corners of the equipment compartment to the interstage adapter ring.

Axial loads of the four polar-mounted propellant tanks are also transferred directly to the adapter ring. Lateral loads are transferred via transverse trusses to the top of the central support structure.

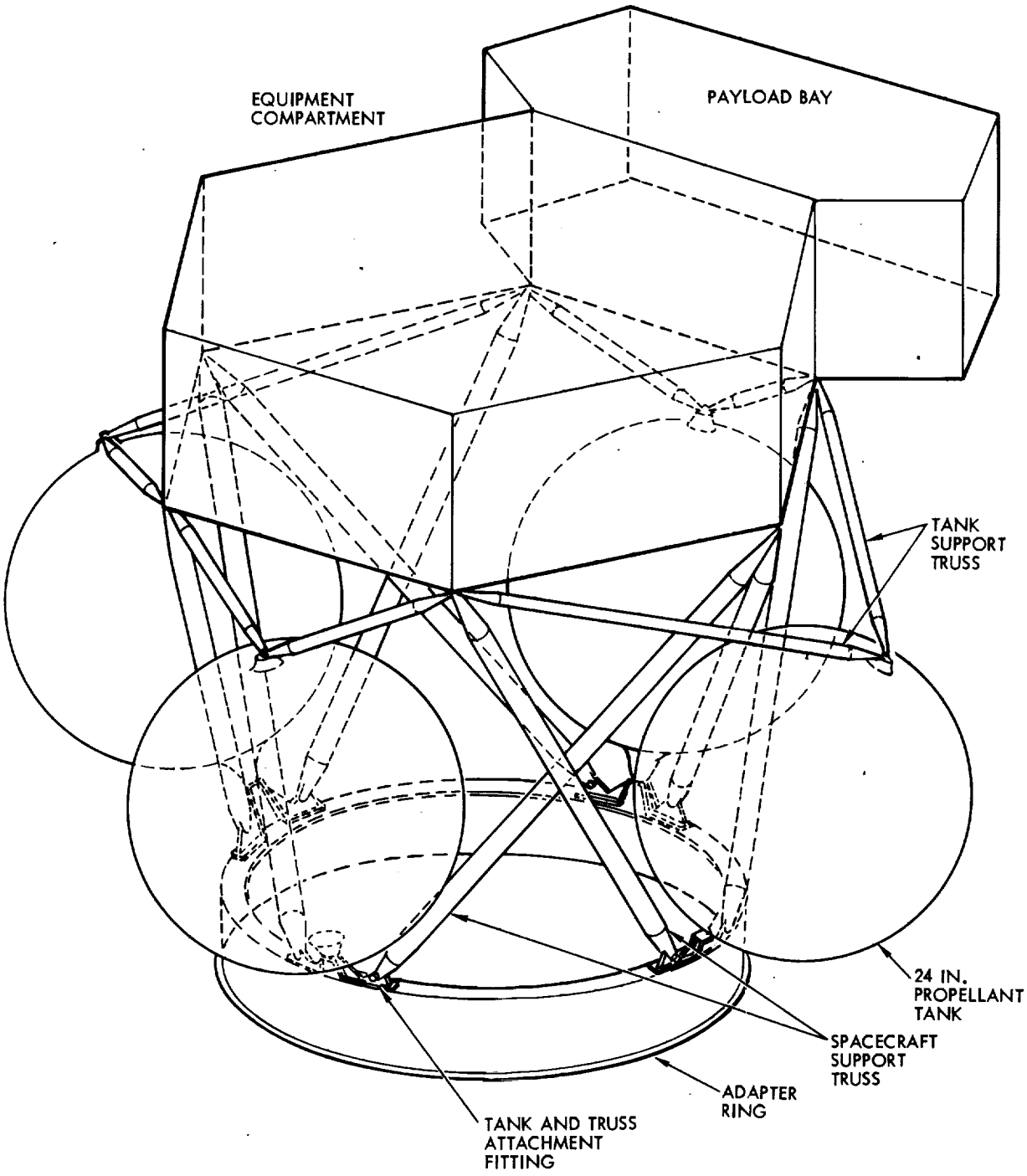

Figure 3-4. Propulsion Structural and Tank Support Configuration

This structural design approach was adopted to separate the load paths of the propulsion stage almost completely from those of the spacecraft proper and thus to avoid placing stresses due to spacecraft loads on the propellant tanks.

The structure is configured to facilitate assembly, handling and testing of the propulsion stage as a separate module and to simplify its integration with the spacecraft proper by minimizing the number of mechanical interface joints.

The relatively large propellant tank separation achieved by outward tilt of the tank support axes is required to increase the Z axis moment of inertia in the stowed configuration so as to improve the spin stability margin during the predeployment and initial deployment phases, as previously discussed. This choice of tank locations also facilitates placement of the eight main spacecraft support struts within the constraints given by the dimensions of the adapter ring and the hexagonal array of attach points at the equipment compartment.

Equipment and Science Compartments

Figure 3-5 shows the internal layout of the central equipment compartment and the extension bays used for scientific payload equipment.

A change of the equipment compartment layout from that used in Pioneer F/G by rearrangement of electronic components was necessitated by:

- Modified mass balance requirements due to change in the mass of deployable items (heavier RTG's, added magnetometer structure and tip mass) and the addition of the -X axis extension bay
- Changes and relocation of several payload elements
- Changes in several subsystem components
- Elimination of the storage battery used in Pioneer F/G
- Relocation of thermal control louvers from the bottom of the equipment compartment to the side walls (because of thermal radiation blockage in aft direction by the added propulsion stage).

Louvered side wall space is limited because two outer walls of the equipment compartment are blocked by RTG's (when stowed), a third one is partly blocked by the stellar reference assembly and light shade. However, since only components with high power rating such as the S-band and X-band transmitters require direct access to a louvered mounting plate the available louvered area is sufficient. As shown in the drawing, most of the other units can be mounted either on interior surfaces, i.e., the partitions separating the equipment compartment from the extension bays, or on the

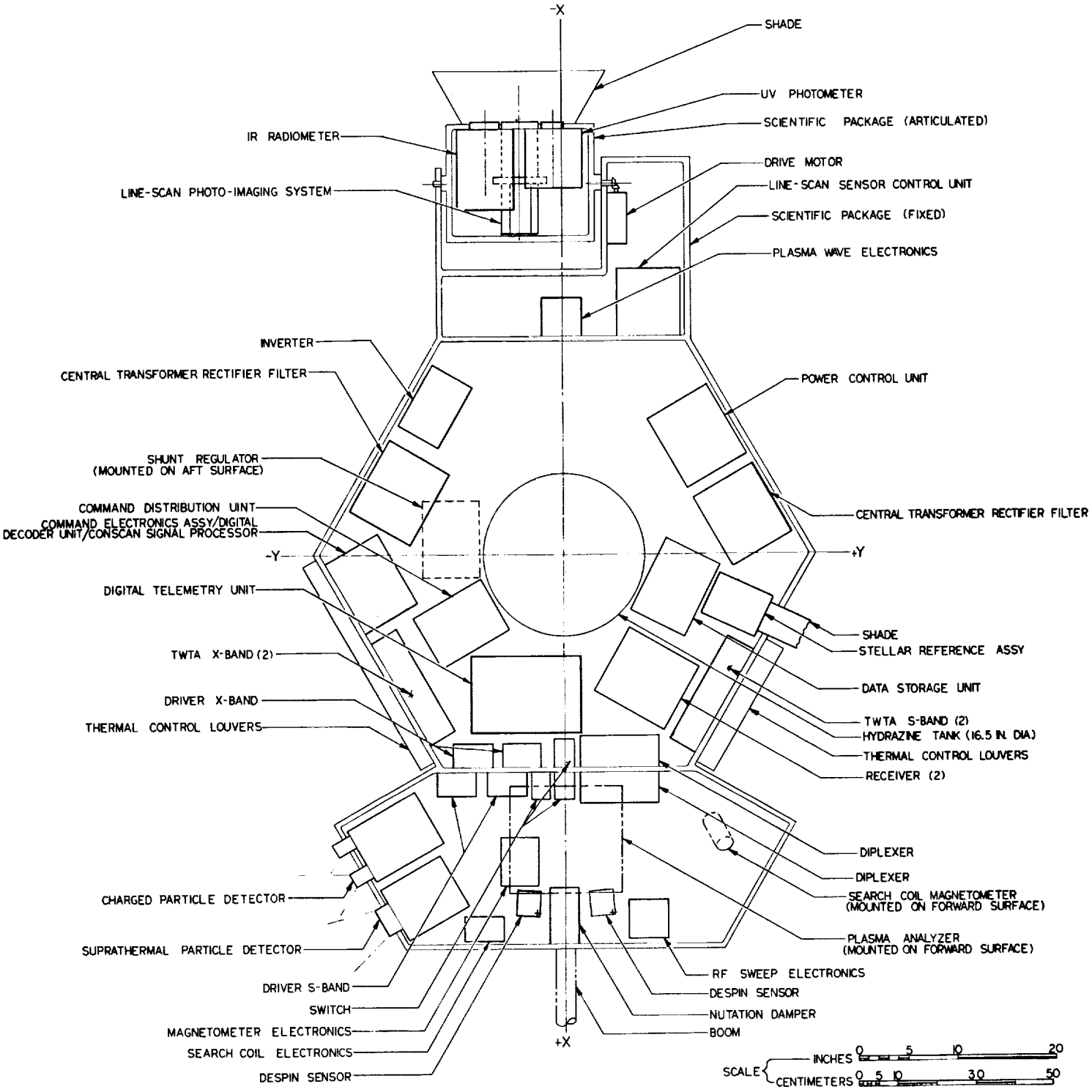

Figure 3-5. Jupiter Orbiter Equipment Bay Layout

equipment platform, where heat dissipation is provided by conductive and/or radiative coupling. Additional space for thermal louvers is available at the bottom and sides of the two extension bays to serve electronic units associated with payload instruments.

The change from aft-mounted to side-mounted louvers imposes an operational constraint, limiting the exposure of the spacecraft to side-sun illumination at the beginning of the mission. This constraint can be met effectively by allowing the spacecraft to point off earth during the first 50 days of the mission, using the medium/low-gain antenna for uplink and downlink communications, to avoid prolonged side-sun illumination. This operation mode also required in the Saturn Uranus entry probe mission was analyzed and is described in Reference 12).

Science payload instruments are located in the extension bays on both sides of the central equipment compartment. Several sensors are located externally on deployable appendages and three electro-optical instruments are housed in the rotational sensor package extending from the add-on payload bay on the -X side.

Table 3-1 lists the payload instruments tentatively selected for the Jupiter orbiter and their respective location on the spacecraft. These instruments account for about 75 percent of the total allocated payload weight capacity. The two payload bays provide additional mounting space and access to unobstructed viewing ports for use by other still unspecified payload instruments.

Table 3-1. List and Location of Payload Instruments for Jupiter Orbiter (Preliminary Selection)

Experiment	Estimated Weight (lb)	Location of Sensor	Location of Electronics
Magnetometer	6.0	Magnetometer boom	Bay 1
Plasma analyzer	12.0	Forward of bay 1	At sensor location
Charged particle instrument	10.0	Bay 1	At sensor location
Suprathermal particle detector	3.5	Bay 1	At sensor location
RF emission detector (including RF sweep receiver)	10.5	Tip of RTG boom	Bay 1
Plasma wave detector	3.5	Magnetometer boom	Bay 1
IR radiometer	12.0	Articulated package (bay 2)	At sensor location
UV photometer	10.0		At sensor location
Line scan imaging system	25.0		Bay 2
Subtotal	92.5		
Unassigned capacity	27.5		
Total	120.0		

Note: Bay 1 located on +X side; bay 2 located on -X side.

Two externally-mounted sensors listed in Table 3-1 but not shown in the design drawings Figures 3-2 and 3-5 are the plasma wave detector and the RF emission detector. Both are lightweight deployable antennas. The plasma wave detector similar to the antenna flown on Explorer would be mounted most likely on one of the hinges of the magnetometer boom, deployed by spring action in the direction perpendicular to the boom and parallel to the Y axis. The RF emission detector consists of two whip antennas extending from the ends of the RTG arms. After spring-actuated deployment their tip-to-tip distance will be 40 feet.

The externally-mounted plasma analyzer is the same instrument being carried by Pioneers 10 and 11. It is located above the equipment platform with its aperture facing in the direction of the sun through a viewing port in the high-gain antenna dish as in Pioneers 10 and 11.

The articulated sensor package rotatable around an axis parallel to the spacecraft Y axis is provided to permit effective observation of the planet and its satellites from a wide range of orbital positions. The instruments included in the package are the line-scan imaging system, the infrared radiometer and the ultraviolet photometer.

In the configuration shown in Figure 3-5 the three instruments are boresighted to share the same cone angle of observation. Other arrangements are conceivable which would allow the sensors to view in different directions. The axis of rotation selected here permits viewing over a cone angle range of 135 degrees, limited in forward direction by the high-gain antenna dish (40-degree cone angle) and in aft direction by the propulsion bay enclosure (175-degree cone angle) as shown in Figure 3-2. Viewing at cone angles closer to the +Z axis than 40 degrees would generally not be useful because of solar stray light interference, except during sun occultation periods. Viewing at angles closer than 5 degrees from the -Z axis does not produce useful images by spin-scanning instruments.

Figure 3-6 shows sketches of various sensor articulation options, one of which (option 1) is comparable to the arrangement of the imaging photopolarimeter in Pioneer F/G. Rotation around the spacecraft X axis (option 5) which was proposed in the previous Pioneer Jupiter orbiter study (Reference 5) would be unfavorable in the selected configuration because of partial field of view obstruction and stray light effects produced by the RTG booms. The rotational sensor package configuration shown in Figures 3-2 and 3-5 partly integrated with the extension bay has the advantage of compact, lightweight design permitting reasonably simple implementation of thermal control and environmental protection. During launch and propulsion phases when exhaust products must be kept from impinging on the optical surfaces the package is reoriented such that the sensor apertures are covered by a stationary protective lid. This protection can also be used during the cruise phase when the instruments are inactive.

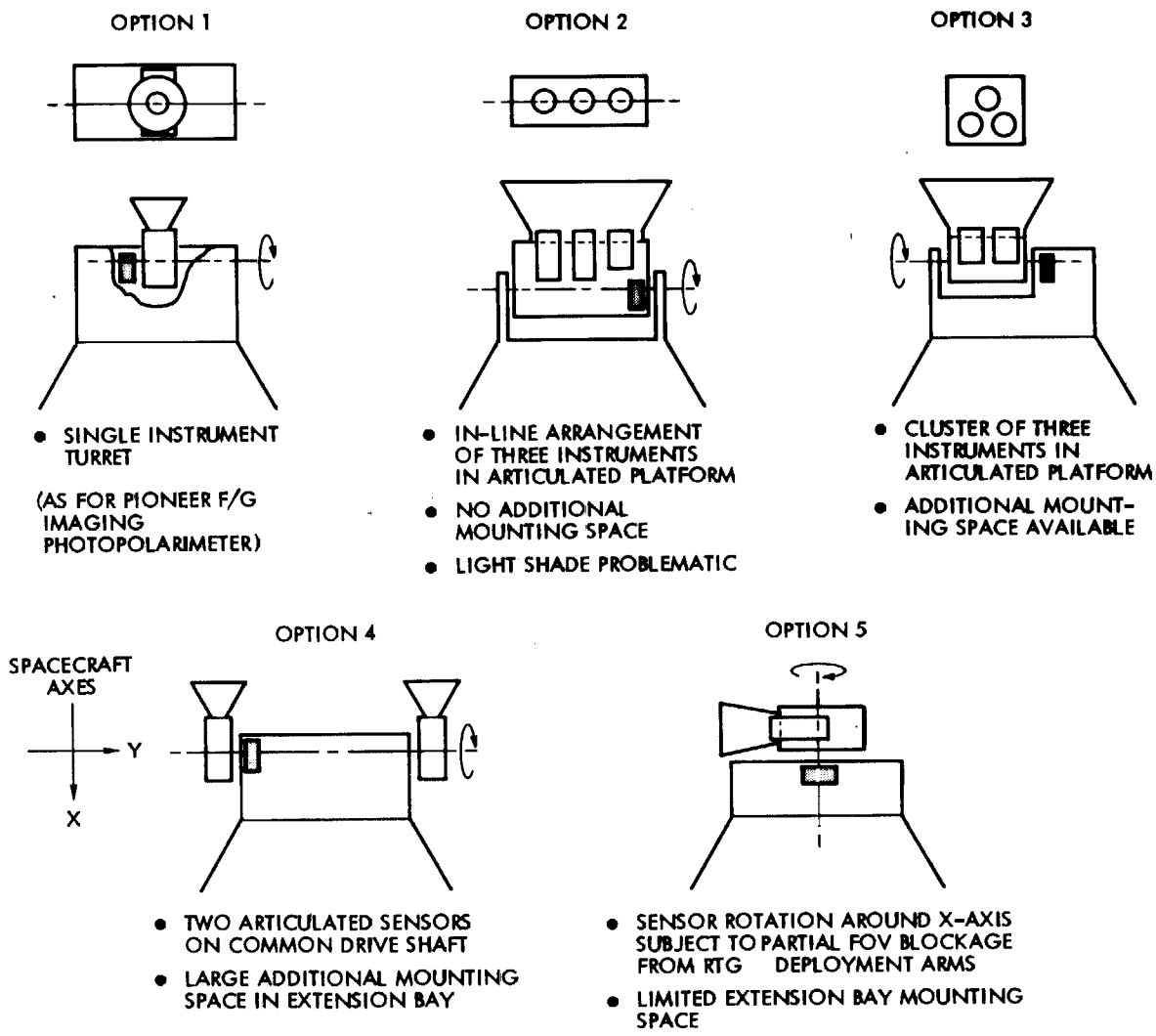

Figure 3-6. Rotational Mounting of Optical Sensors

Propulsion

The configuration of the externally mounted main propulsion system has been discussed before. It comprises four 24-inch diameter propellant tanks, one 15-inch high pressure nitrogen pressurant tank, propellant and pressurant feed lines and valve assemblies, and a 94-lb_f main axial thruster. In order to reduce attitude perturbations due to thrust axis misalignment it is necessary to increase the spin rate from the nominal value of 4.8 rpm to 15 rpm whenever the main engine is used.

The Pioneer F/G monopropellant hydrazine system to be used for attitude control and orbit correction maneuvers is left essentially unchanged. The 16.5-inch diameter tank located at the center of the equipment compartment is retained although a propellant load of 50 pounds (20 percent below full capacity) is the maximum amount required in either the Jupiter or Saturn mission. As in Pioneer F/G the system operates in a simple blowdown mode.

The arrangement of the axial ΔV and precession thrusters and the circumferential spin/despin thrusters is the same as in Pioneer F/G except for the addition of a second pair of spin/despin thrusters on the opposite side of the antenna dish. Since the spacecraft center of mass is located up to 20 inches lower than the circumferential thrusters, a spin-up or despin maneuver executed by using only a single thruster would have an appreciable unwanted nutation effect. By using two thrusters on opposite sides of the antenna dish this effect can be avoided.

The second pair of spin/despin thrusters also provides a backup capability for critically important repeated spin-up and despin maneuvers during the orbital phase. These maneuvers are required to increase the spin rate at times of main thrust operation, to decrease the spin rate at times of planetary imaging operations and to return the spacecraft to the nominal spin rate at the end of each departure from the nominal mode.

Thermal Control

As on Pioneer F and G, the spacecraft is wrapped in thermal blankets and the equipment compartment is thermally isolated from all external appendages by supporting them with nonmetallic materials of low-thermal conductance, to minimize uncontrolled heat loss.

Independent thermal control is applied to the spacecraft proper and the external propulsion system and thermal coupling is held to a minimum. The propulsion system is maintained at a lower temperature than the equipment compartment, with electric and isotope heater units added to each propellant tank.

The use of side-mounted rather than aft-facing thermal louvers in the equipment compartment and the constraint against prolonged side-sun exposure has been previously discussed in this section. To further reduce thermal load variations in the equipment compartment, the heat-dissipating portion of the shunt regulator circuits is placed outside the compartment (see Figure 3-5). The shunt radiator is removed from the side-mounted

location used in Pioneer F/G and placed at the bottom of the propulsion stage meteoroid shield.

Attitude Control

The stellar reference and sun sensor assemblies are used in the same manner as in Pioneer F/G to generate roll reference pulses and the location of these sensors is left unchanged. A search coil magnetometer is added as an auxiliary roll reference sensor to substitute for the stellar reference assembly in close vicinity of Jupiter when radiation effects are expected to interfere with normal operation of the SRA. This magnetometer located outside the equipment compartment senses the planet's strong magnetic field and generates roll reference pulses to a distance of 10 planet radii under most of the orbital positions and relative orientations of the spacecraft anticipated in the mission. The location of this sensor outside the equipment compartment is illustrated in Figure 3-5.

The spin/despin and the ΔV/precession thruster clusters are mounted in a similar manner as on Pioneer F/G at the spacecraft Y axis. A nutation damper, actuated by the magnetometer boom's motion in the X-Z plane, is used as on Pioneer F and G, with a modification for operation at lower spin rates, as will be discussed in Section 3.6.

Communications

The location and installation of the high-gain and medium-gain antenna systems are like those of Pioneer F and G. The conical log spiral low-gain antenna is mounted to a mast, located aft of the propulsion stage and separation plane with its tip extending 24 inches beyond the adapter ring.

As in Pioneer F/G, the high-gain antenna reflector is mounted to the hexagonal equipment compartment by 12 fiberglass struts. The medium-gain antenna and high-gain antenna feed assembly are supported by three fiberglass struts mounted to alternate corners of the hexagonal compartment. It is expected that the inclusion of X-band capability to the high-gain antenna feed will have no effect on the basic support structure.

As can be seen in Figure 3-5, the arrangement and locations of the S-band TWTA, diplexer, diplexer/coupler, RF transfer switches, and transmitter drivers, are similar to those of the Pioneer F/G spacecraft, minimizing physical changes and line losses in the communications and antenna systems.

Electric Power

The Pioneer F/G basic RTG support structure is retained in the new configuration except for small modifications required to accommodate the two MHW radioisotope generators which replace the four SNAP-19 units and to reinforce the support arm guide fittings. The RTG mounting provisions are changed to fit the MHW units.

The externally mounted battery of Pioneer F and G has been eliminated since all peak loads can be readily accommodated by the increased power capacity of the new RTG's. The other components of the electric power subsystem — inverter assemblies, power control unit, CTRF, and external shunt — are shown in Figure 3-5 in locations appropriate to the equipment layout of the new configuration.

3.1.3 Saturn Orbiter Configuration

As previously discussed, the Saturn orbiter configuration differs from that of the Jupiter orbiter only by the smaller size of the added bipropellant stage. With a tank size of 19 inches a maximum usable propellant load of 560 pounds can be accommodated compared to 1150 pounds for the 24-inch tanks used in the Jupiter orbiter.

Figure 3-7 shows the modified propulsion stage configuration for the Saturn orbiter. The length of the stage plus support structure has been reduced by 4 inches to 36 inches, and the maximum lateral dimension in Y direction by 10 inches, to 70 inches. The shorter length permits a reduction of the support strut cross-section and other weight saving measures. The principal weight reduction accrues from the smaller tankage and N_2 pressurant mass.

The layout of the equipment and payload compartments remains unchanged from the configuration used in the Jupiter orbiter except for the omission of several payload instruments. The allocated payload weight capacity has been reduced by 50 pounds from that of the Jupiter orbiter, allowing a total payload capacity of 70 pounds for the Saturn orbiter. Instruments to be omitted are probably some of the particle and fields sensors included in the payload complement tentatively selected for the Jupiter orbiter. It is also anticipated that a reduction of the estimated line-scan camera weight will be possible to reduce the total payload weight to the allocated capacity of 70 pounds. However, the articulated sensor package used in the Jupiter orbiter should be retained if at all possible.

3.1.4 Alternate Orbiter Configurations

Several alternate configurations of the propulsion stage and spacecraft support structure were considered before adopting the design concept described above.

Omitting from this discussion any configurations with obvious mass distribution problems (such as two-sphere configurations) and those with unconventional tank shapes (such as toroids) referred to in Section 3.1.1 there remain several viable candidate design concepts with different tank placement, different tank mounting provisions and different support truss arrangements. Figure 3-8 shows several such design options that were investigated in some detail, all of which utilize four spherical propellant tanks arranged in a square configuration.

In Configuration A the propellant tanks are located on bisectors between the spacecraft X and Y axes. The tanks are supported by polar mounts as in the selected configuration described previously. This layout

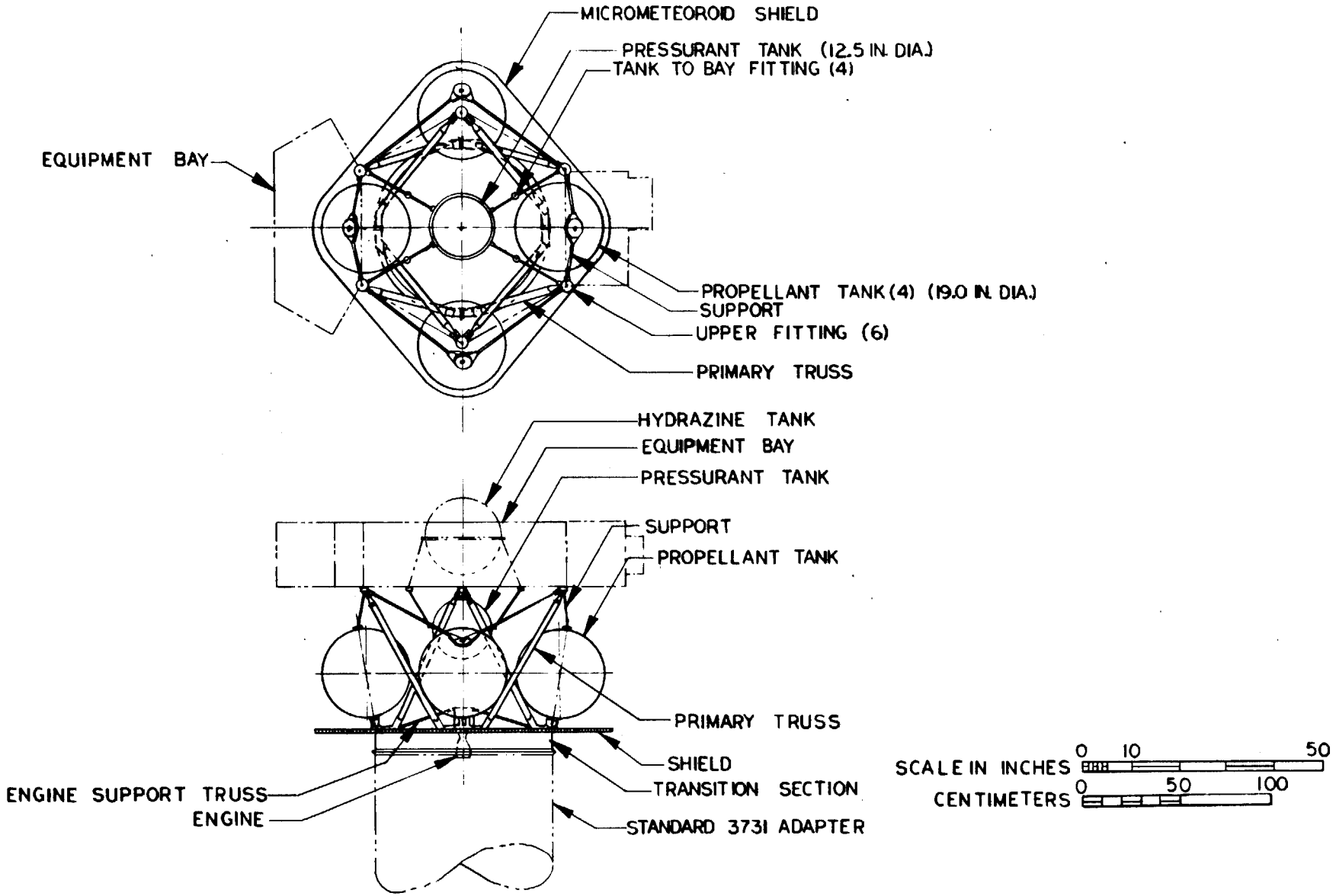

Figure 3-7. Saturn Orbiter Propulsion Bay Configuration

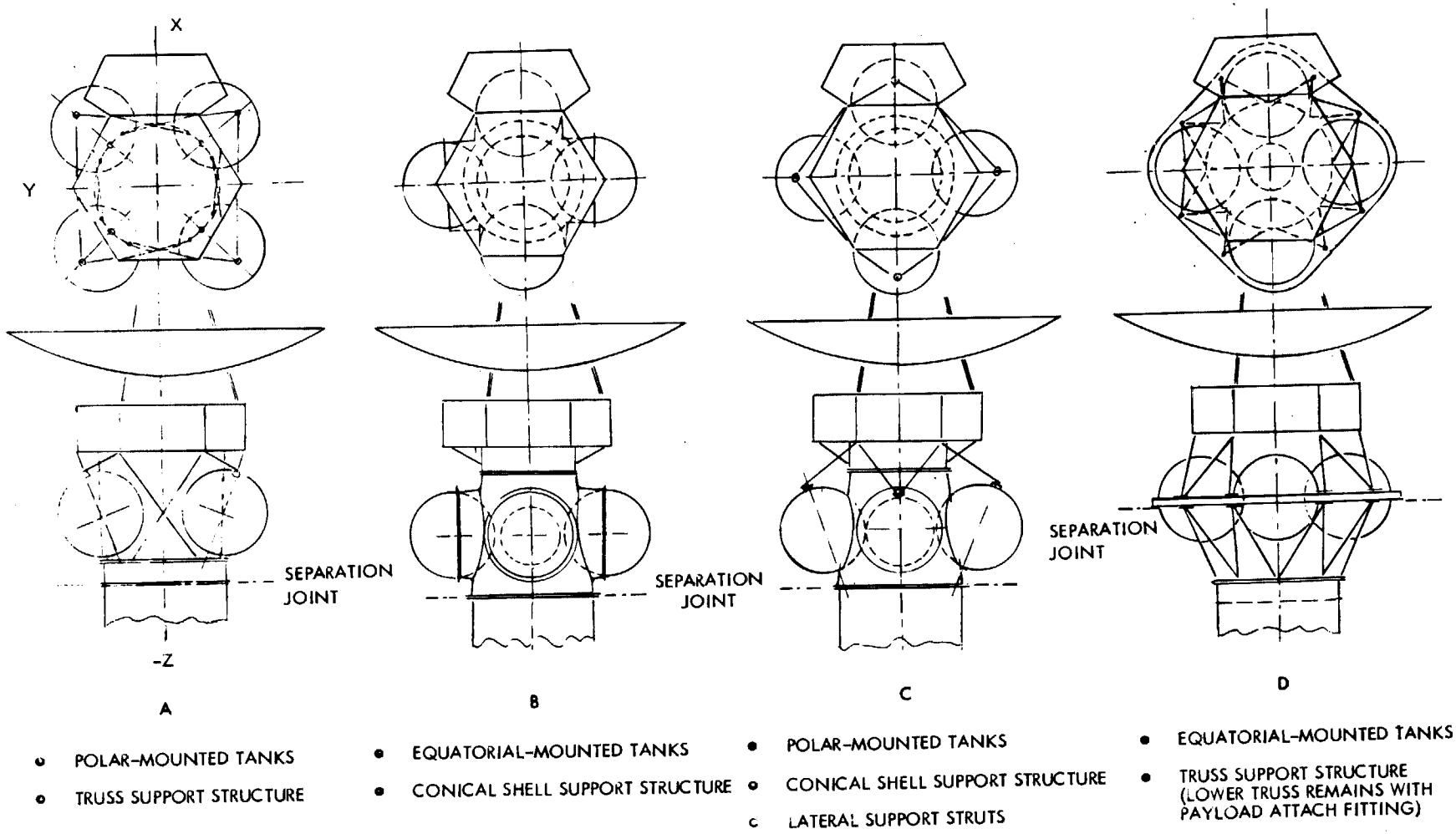

Figure 3-8. Alternate Spacecraft and Propellant Tank Support Configurations

has the disadvantage that the unequal masses of fuel and oxidizer introduce an appreciable rotation of the two principal axes of inertia from the desired alignment with the X and Y axes of the spacecraft. As a consequence the tanks must be separated by a greater distance from each other than in the selected rhomboid arrangement in order to obtain comparable moment of inertia ratios (and hence, spin stability margin) prior to appendage deployment. The lateral dimensions of the stage structure would thus become somewhat larger than with the preferred rhomboid arrangement.

Configuration B uses a conical shell as central support structure. This cone is attached to the cylindrical adapter ring that supports the equipment platform as in the original Pioneer F/G design. The four propellant tanks are attached to this center cone by individual equatorial mounts, with each tank tied securely to its mount by meridional straps. This configuration has a simple structural interface with the Pioneer spacecraft centerbody, requiring almost no modification of the original configuration. However the load distribution in the conical support structure, the tank mounting rings and the spherical tanks, themselves, is difficult to analyze, and an extensive development and test program may be required for this design to assure structural integrity.

Configuration C uses a central support cone similar to Configuration B but provides polar mounts for the propellant tanks similar to the selected configuration and Configuration A. The upper tank mounts are supported from four corners of the hexagonal centerbody by four pairs of lateral support struts. The lower tank mounts rest on pedestals which distribute the concentrated load over the mounting flange of the center cone comparable to the tank load distribution technique used in the selected configuration (and Configuration A). The design is attractive because it achieves a favorable load path separation and retains the Pioneer F/G support structure with almost no modification. However its structural interface with the centerbody is not as simple as in Configuration B. The structural weights of Configurations A, B and C are comparable.

In the last configuration illustrated in Figure 3-8 (Configuration D) the propellant tanks are supported by equatorial mounting rings rather than by polar mounts. This design uses a clover-leaf shaped tank support platform from which trusses extend to the spacecraft, above, and to the launch vehicle cylindrical adapter, below. The separation joint is located at the tank support platform. This design resembles the Mariner 9 stage support structure except for accommodating four rather than two propellant tanks. The weight of structural elements that remain attached to the flight spacecraft after separation is slightly reduced in this configuration. However, the structural concept and the design of the separation joint involve greater complexity than the selected truss structure.

3.2 MASS PROPERTIES

3.2.1 Spacecraft Weight Summary

A summary weight statement for the Pioneer Jupiter and Saturn orbiter configurations is presented in Table 3-2. The corresponding data for the Pioneer F/G system and the baseline Outer Planets Pioneer configuration are included in this table for comparison.

3.2.2 Mass Properties Requirements

Limits have been established for spacecraft mass properties in order to satisfy the launch vehicle accuracy, attitude control, and antenna pointing requirements consistent with a sequence of events representative of a flyby or multiple planet mission. These mass properties limits are presented in Table 3-3.

3.2.3 Mass Properties Summary

Mass properties of the two orbiter configurations are summarized in Table 3-4. Pioneer F/G parameter values are given for comparison. The configurations satisfy the criteria established in Table 3- .

3.2.4 Subsystem Weight Estimates

Estimated weight breakdowns for each subsystem of the Pioneer Outer Planets Orbiter are presented below compared with the corresponding weights of Pioneer F/G and the Outer Planets Pioneer. Separate weights are stated for the Jupiter and Saturn orbiters where appropriate.*

Weights given for Pioneer F/G are based on actual measurements of Pioneer 10 subsystems. Weight estimates derived from these data for the advanced Pioneer configurations can therefore be regarded as realistic values with good confidence.

Structure

	Pioneer F/G	Outer Planets Pioneer	Jupiter (Saturn) Orbiter
Primary Structure			
Platform assembly	18.5	20.4	20.4
Frame assembly	8.6	10.6	10.6
Separation assembly and tank support	13.9	17.0	10.0
Propulsion bay and adapter ring	---	---	45.0 (40.0)

*All weights will be given in pounds.

Table 3-2. Weight Summary

Subsystem	Pioneer F/G Weight (lb)	Outer Planets Pioneer		Jupiter Orbiter		Saturn Orbiter		Remarks[2]
		Δ Weight (lb)	Weight (lb)	Δ Weight[1] (lb)	Weight (lb)	Δ Weight[1] (lb)	Weight (lb)	
Structure								
• Primary	41	+7	48	+45	86	+40	81	Added propulsion stage and equipment compartment; meteoroid protection
• Secondary and meteoroid protection	41	+4	45	+32	73	+32	73	
• RTG support	22	+3	25	+2	24	+2	24	
Electrical power	39	-14	25	-15	24	-15	24	No battery; reduced PCU and inverters
RTG's	120	+50	170	+50	170	+50	170	New RTG system (two MHW's)
Command	38	+2	40	+11	49	+11	49	Increased cabling and stored commands
Data handling	10	+6	16	+9	19	+9	19	Increased DSU capacity
Communications	68	+24	92	+25	93	+25	93	Added X-band transmission
Attitude control	13	+1	14	+6	19	+6	19	
Propulsion (dry)	23	+7	30	+108	131	+79	102	Added propulsion stage
Thermal control	16	+3	19	+17	33	+17	33	Added insulation and louvers
Balance weight provisions	6	+3	9	+8	14	+6	12	Heavier spacecraft
Deployment counterweight	-	+25	25	+25	25	+25	25	Maintain c.g. on longitudinal axis
Spacecraft Weight (Dry)[3]	437	+126	563	+327	764	+286	723	
Pressurant and unusable propellant	2	+1	3	+38	40	+18	20	Added propulsion stage
Usable propellant	59	+32	91	+1143	1202	+491	550	Added propulsion stage
Scientific experiments	66	+24	90	+54	120	+4	70	
Spacecraft Weight (Wet)	564	+182	747	+1562	2126	+799	1363	
Adapter	30	+5	35	+35	65	+20	50	
Spacecraft System (Total)	594	+188	782	+1597	2191	+819	1413	

(1) Δ weight data are increments above corresponding values of Pioneer F/G.

(2) Remarks apply to Jupiter and Saturn orbiters. However, some of the weight increments are in common with Outer Planets Pioneer spacecraft.

(3) Excludes scientific experiments.

Table 3-3. Mass Properties Requirements Versus Capabilities

Requirement	Capability
1. Spacecraft plus third stage	
• Limit third stage injection errors	
Spacecraft c.g. offset ≤ 0.050 inch	0.015 inch
Spacecraft spin principal axis parallel to Z axis within 0.003 radian	0.002 radian
Spacecraft plus third stage I_z/I_x and $I_z/I_y \leq 0.90$	0.71
2. Stowed spacecraft	
• Attitude stability:	
$I_z/I_x \geq 1.1$	1.6
$I_z/I_y \geq 1.1$	1.5
3. Deployed spacecraft	
• Attitude stability:	
$I_z/I_x \geq 1.1$	2.1
$I_z/I_y \geq 1.1$	1.6
• Limit cruise mode pointing error	
Spin principal axis parallel to Z axis within 0.15 degree	0.06 degree
• Limit pointing error during ΔV:	
c.g. X-Y location known to ≤ 1.6 inch	0.25 inch
• Limit nutation during precession	
$K = K_o \pm 0.05$	< 0.01
$K = \left[(I_z - I_x)(I_z - I_y)/I_x I_y\right]^{1/2}$	0.91

Table 3-4. Mass Property Summary

Spacecraft Configuration	Weight (lb)	Center of Gravity[1] (in.)			Moments of Inertia (slug-ft²)			MOI RATIOS			K[2]
		$\bar{X}$	$\bar{Y}$	$\bar{Z}$	I_x	I_y	I_z	$\frac{I_z}{I_x}$	$\frac{I_z}{I_y}$	$\frac{2I_z}{I_x+I_z}$	
Pioneer 10[3]											
Stowed	564	0	0	19.2	71	63	101	1.4	1.6	1.5	0.49
Deployed (B.O.L.)	564	-6.3	0	19.2	287	188	443	1.5	2.3	1.9	0.86
Deployed (E.O.L.)[4]	504	-7.1	0	19.4	287	187	442	1.5	2.3	1.9	0.86
Jupiter Orbiter											
Stowed	2151	0	0	28.1	314	269	345	1.1	1.3	1.2	0.17
Deployed (B.O.L.)	2151	0	0	28.1	622	735	1119	1.8	1.5	1.7	0.65
Deployed (E.O.L.)	949	0	0	39.8	455	626	963	2.1	1.5	1.8	0.78
Saturn Orbiter[5]											
Stowed	1368	0	0	30.0	191	197	245	1.3	1.2	1.3	0.26
Deployed (B.O.L.)	1368	0	0	30.0	500	633	1019	2.0	1.6	1.8	0.78
Deployed (E.O.L.)	818	0	0	40.4	435	615	930	2.1	1.5	1.8	0.76

[1] C.G. position $\bar{Z}$ is referenced to spacecraft separation plane
$\bar{X}$ and $\bar{Y}$ are measured from geometric centerline

[2] $K = \left[(I_z - I_x/I_y)(I_z - I_y/I_x)\right]^{1/2}$

[3] Pioneer 10 data from actual measurements or calculations, provided for comparison

[4] B.O.L., E.O.L. = Beginning or End of Life, respectively

[5] Mass properties of Saturn orbiter configuration are preliminary estimates, i.e., less well defined than those of Jupiter orbiter

Secondary Structure				
Side panels and interior bulkhead	12.1	13.4	13.4	
Cover panels	7.1	8.3	8.3	
Thruster support assemblies	5.8	5.8	5.8	
Magnetometer support assembly	7.6	8.6	13.6	
Miscellaneous and attach hardware	7.2	7.2	7.2	
Wobble damper	1.2	1.2	1.2	
Micrometeoroid protection	---	---	15.0	
Articulated sensor platform	---	---	8.0	
RTG Support Assemblies	22.4	24.4	24.4	
Total	104.4	117.9	182.9	(177.9)

The largest contribution to the weight growth in the structure subsystem is due to the added propulsion bay and adapter ring. In the Jupiter orbiter this increment is five pounds greater than in the Saturn orbiter.

Other structural weight contributions are due to the following items: a honeycomb sandwich panel required to provide micrometeoroid protection for the added propulsion stage; increased support for the heavier RTG's; and reinforcement of the magnetometer boom structure. Elimination of the adapter ring of the original Pioneer F/G reflects in a small negative weight increment (3.9 pounds) in the orbiter configurations.

Electrical Power

	Pioneer F/G		Outer Planets Pioneer		Jupiter (Saturn) Orbiter	
RTG's	(4)	120.0	(2)	170.0	(2)	170.0
Power control unit		10.9		6.0		6.0
Battery		5.3		---		---
Inverters	(2)	10.2	(1)	5.0	(1)	5.0
Central transformer-rectifier-filter		11.8		11.8		11.8
Strip heater (shunt radiator)		0.8		0.8		0.8
Total		159.0		193.6		193.6

The electrical power subsystem weight shows a net increase of 34.6 pounds both in the Outer Planets Pioneer and Outer Planets orbiter

configurations. This is attributed primarily to the heavier RTG's which account for 50 pounds. This is partially offset by elimination of the battery, an inverter, and simplification of the PCU.

Command Subsystem

	Pioneer F/G	Outer Planets Pioneer	Jupiter (Saturn) Orbiter
Digital decoder unit	1.7	1.7	1.7
Command distribution unit	8.8	9.0	11.0
Cabling and connectors	27.0	29.5	36.0
Total	37.5	40.2	48.7

The increased number of connectors and length of cable runs account for most of the 11.2-pound increase in command subsystem weight of the Outer Planets Orbiter spacecraft. No changes are planned for the DDU; minor changes to the CDU to implement additional commands will be accomplished with the presently available but unused circuitry.

Data Handling

	Pioneer F/G	Outer Planets Pioneer	Jupiter (Saturn) Orbiter
Digital telemetry unit	6.8	6.8	6.8
Data storage unit	3.3	12.0	12.0
Total	10.1	18.8	18.8

The significantly increased DSU capacity reflects in an approximately 9-pound increase in data handling subsystem weight.

Communications

	Pioneer F/G		Outer Planets Pioneer		Jupiter (Saturn) Orbiter	
Receiver	(2)	10.2	(2)	10.2	(2)	10.2
Transmitter driver	(2)	2.8	(4)	5.6	(4)	5.6
TWTA (S-band)	(2)	8.0	(2)	8.0	(2)	8.0
TWTA (X-band)		---	(2)	18.0	(2)	18.0
Conical scan processor		1.0		1.0		1.0
High-gain antenna		33.4		33.4		33.4
Medium-gain antenna		3.7		3.7		3.7
Low-gain antenna		0.7		0.7		1.2
Diplexers and coupler		4.3		4.3		4.3

Switches	(2)	1.3	(3)	1.9	(3)	1.9
Waveguide		---		2.0		2.0
RF cabling		3.0		3.5		3.5
Total		68.4		92.3		92.8

The increase in communication subsystem weight both in Outer Planets Pioneer and Outer Planets Orbiter is the result of adding redundant X-band transmitters (TWTA's and drivers) and the associated waveguide and switch to interconnect with the high-gain antenna.

Deletion of the feed movement mechanism presently configured on Pioneer F/G is offset by a heavier dual X- and S-band feed.

Attitude Control

		Pioneer F/G	Outer Planets Pioneer	Jupiter (Saturn) Orbiter
Control electronics assembly		5.1	6.0	6.0
Stellar reference assembly		2.6	2.6	2.6
Stellar reference assembly light shade		3.4	3.4	3.4
Sun sensor assembly		1.1	1.1	1.1
Despin sensor assembly	(2)	0.4	0.4	0.4
Search coil magnetometer		---	---	1.5
Experiment drive assembly for articulated sensor		---	---	4.0
Total		12.6	13.5	19.0

Attitude control subsystem weight in increased by 6.4 pounds in the Outer Planets Orbiter. This includes the weight of the articulated platform drive motor and electronics, as well as the search coil magnetometer which has been added as auxiliary roll attitude sensor.

Thermal Control

	Pioneer F/G	Outer Planets Pioneer	Jupiter (Saturn) Orbiter
Insulation	11.1	12.5	24.1
Thermal louvers	4.3	5.8	6.3
RHU and support (sun sensor)	0.6	0.6	0.6

Heaters, propellant tank(s)	0.3	0.3	1.5
Heater, articulated sensor package	---	---	0.3
Total	16.3	19.2	32.8

The thermal control subsystem weight is increased by 13.0 pounds to provide insulation for the propulsion stage and the added equipment compartment including the articulated sensor package. The addition of louvers on the added equipment compartment and the externally mounted shunt regulator circuits is partly offset by the elimination of aft-facing louver assemblies used in Pioneer F/G. The net louver weight increase is estimated as 2.0 pounds.

Propulsion

	Pioneer F/G		Outer Planets Pioneer		Jupiter (Saturn) Orbiter		
Hydrazine System (Midcourse Trim and ACS)							
Propellant tank	(1)	10.7	(1)	15.6		10.7	
Fill/drain valves		0.4		0.4		0.4	
Filters		0.5		0.5		0.5	
Pressure transducer		0.4		0.4		0.4	
Temperature transducer		0.1		0.1		0.1	
Thruster assemblies	(3)	9.0	(3+)*	10.5	(4)	12.0	
Lines/fittings		0.6		0.7		0.7	
Line heater assembly		1.4		1.4		1.4	
Subtotal (dry)		23.1		29.6		26.2	
Propellant, usable		59.2		91.0		50.0	
Propellant, residual		0.8		1.0		0.7	
Pressurant		1.0		1.5		1.0	
Subtotal (wet)		84.1		123.1		77.9	
Bipropellant System							
Pressurant tank						30.0	(15.0)
Propellant tanks						54.0	(40.0)
Fill/drain valves						0.7	(0.7)
Pressure transducers						1.0	(1.0)

Filters				1.7	(1.7)
Pressure regulator				2.6	(2.6)
Check valves				0.6	(0.6)
Burst disks				0.5	(0.5)
Isolation valves				1.4	(1.4)
Deboost thruster assembly				8.3	(8.3)
Lines and fittings				4.0	(4.0)
Subtotal (dry)				104.8	(75.8)
Propellant (MMH), usable			435.0		(190.0)
Propellant (MMH), residual			7.0		(3.0)
Propellant (N_2O_4), usable			717.0		(310.0)
Propellant (N_2O_4) residual			11.0		(5.0)
Pressurant (GN_2)			20.0		(10.0)
Subtotal (wet)			1294.8		(593.8)
Total propulsion system (dry)	23.1	29.6	131.0		(102.0)
Total propulsion system (wet)	84.1	123.1	1372.7		(671.7)

The hydrazine propulsion system weight of both the Jupiter and Saturn orbiters is estimated to be 6.2 pounds less than in Pioneer F/G reflecting a 9.3-pound decrease in propellant partly offset by the addition of a second pair of spin/despin thrusters.

Balance Weight

A balance weight allowance of 14.0 pounds is estimated to be adequate in the orbiter configurations to control the radial center of gravity and the products of inertia. This is an 8-pound increase over that actually required by Pioneer F.

In addition, a deployment counterweight not required in Pioneer F/G is used in the Outer Planets Pioneer and Outer Planets Orbiter magnetometer booms. This counterweight is estimated to be 25 pounds.

3.3 ELECTRICAL BLOCK DIAGRAM

The system design, reflected in the block diagram of Figure 3-9, retains the same basic electrical design concepts and techniques proven on the Pioneer F/G spacecraft. However the orbiter mission requirements exceed the Jupiter flyby mission in two major areas:

- The requirement for increased propulsive capability to enter into and adjust the orbit about Jupiter or Saturn
- Increased support for the complement of scientific instruments, including increased weight and power, greater data storage and transmission capability, spin rate versatility, and variable cone angle control for the pointing of remote sensors. This added requirement applies only to the extent that the payload is augmented beyond the particles and fields type of instruments.

Requirements involving additions to, or modifications of, the baseline Pioneer F/G block diagram are discussed in detail in Section 4.

Those subsystem elements which are impacted by the new requirements are cross-hatched in the block diagram. The principal design modifications are summarized below.

An external propulsion stage, capable of velocity increments in the range of 2000 meters per second, has been attached to the aft end of the main equipment compartment with a stabilized truss network. Four propellant tanks, a pressurant tank, and a 100-lbf thrust retro-engine comprise the major items of the bipropellant system (monomethyl-hydrazine and nitrogen-tetroxide) utilizing existing technology.

The existing S-band telemetry transmission capability is augmented by a standby-redundant X-band system to achieve the appreciably higher data rates required to support the imaging instrument at the extreme communication ranges occurring during orbital operations. This implementation has already been adopted for the baseline Outer Planets Pioneer spacecraft.

The major change to the data handling subsystem is the replacement of the limited capacity (50 kilobits) Pioneer F/G core memory with a modular solid-state unit configured to store 1.5 megabits. The significantly expanded data storage is essential to buffer photo-imaging system data acquired at a rate of 1.3 megabit per second during an exposure of several tenths of a second for delayed retrieval at the prevailing telemetry link transmission rate. The digital telemetry unit is modified to accommodate the higher bit rates (to 33 kilobits per second).

Increased operational complexity associated with substantial round-trip light-time delay (3.5 hours at Saturn), orbit insertion and adjustment, and instrument programming led to selection of an improved command memory (integral with the command distribution unit). The new command

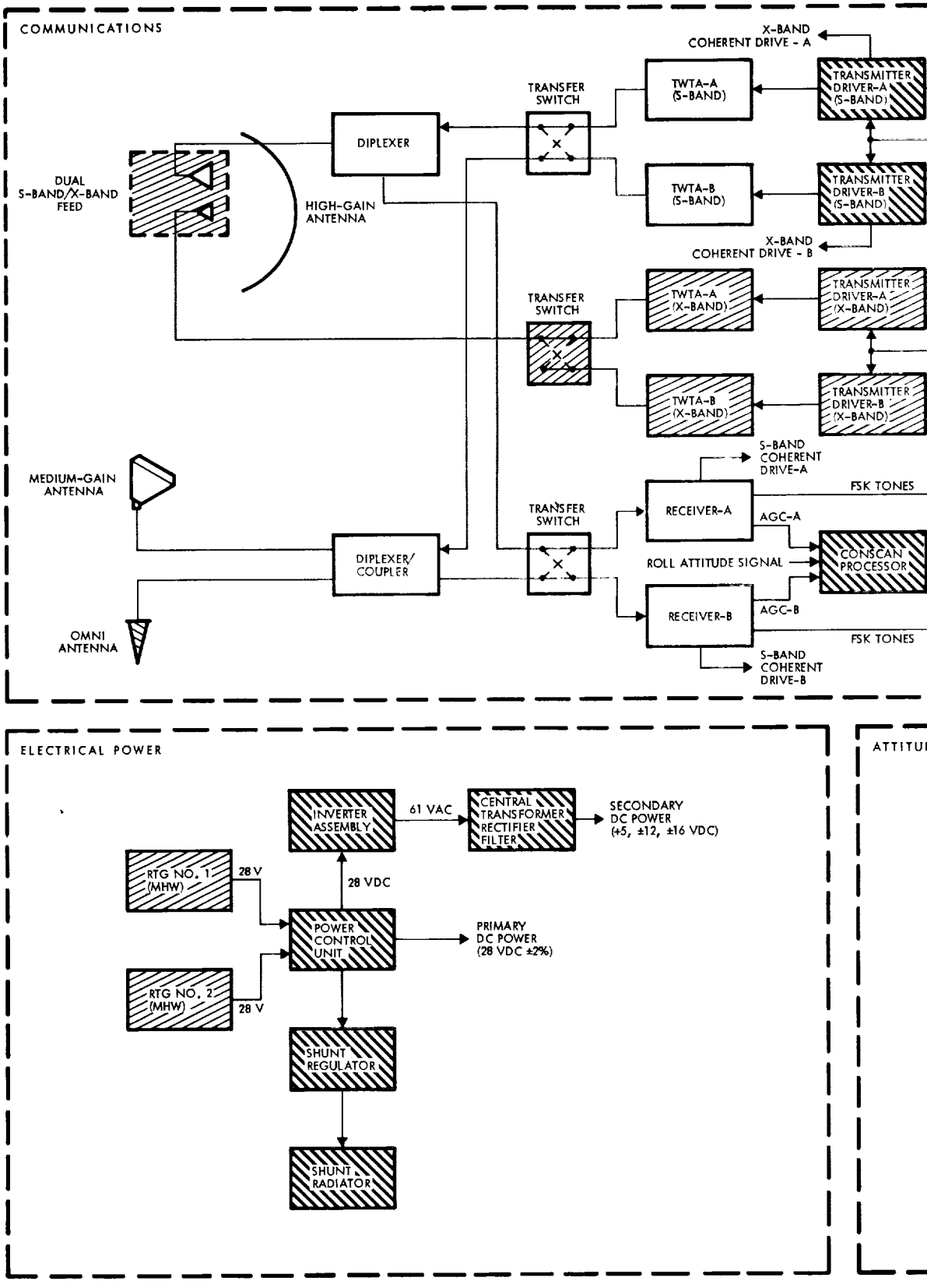

FOLDOUT FRAME

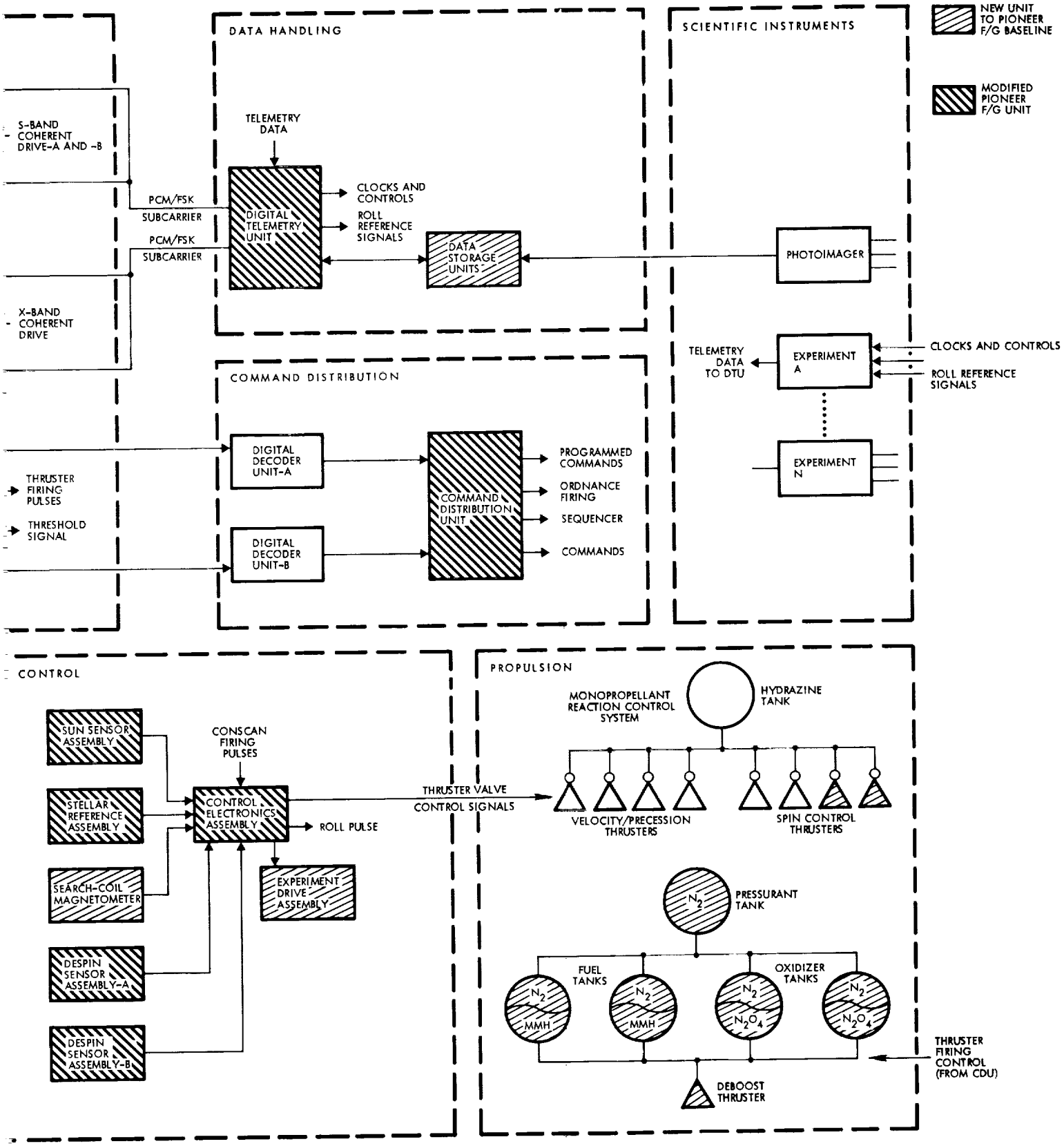

Figure 3-9. Functional Block Diagram

FOLDOUT FRAME 2

memory is capable of storing 32 discrete commands (16 each in redundant programmers) and associated time tags, providing a maximum delay period of 36 hours with a resolution of 2 seconds.

Significantly increased electrical power requirements arising from the X-band transmitter and the contemplated science payload dictate replacing the four SNAP-19 RTG's (160 watts) with two multi-hundred-watt (MHW) units providing approximately 300 watts at launch. The increased RTG supply voltage (from 4.2 to 28 VDC) simplifies power processing with a concomitant reduction in weight, power, and cost. Moreover, ample power margin is available to permit deletion of the battery.

The attitude control subsystem generally uses the same control modes and control sequence logic as the baseline Pioneer F/G configuration. However, the sun and star sensors have been augmented with a search-coil magnetometer to generate roll pulses when the spacecraft is in close proximity to the planet and the primary references are inoperative. In addition, an experiment drive assembly has been added to provide cone angle control for planetology instruments requiring variable viewing capability.

Modifications of subsystem interfaces occur in several areas of the system as a result of changes described above. The modifications involve primarily the flow of command signals and telemetry input data. The changes also affect power distribution and control.

3.4 ELECTRICAL POWER BUDGET

The electrical power requirements of the Pioneer Outer Planets Orbiter spacecraft are listed in Table 3-5 for end-of-mission conditions. Power requirements for Pioneer F/G and the Outer Planets Pioneer baseline configuration are also tabulated for convenient reference. Power requirements that can be met with only one of the two RTG's functioning during the orbital phase are also listed (columns 3 and 5) indicating the minimum system capability under partial power failure.

Principal items of increased power requirement in the orbiter spacecraft include:

- Addition of dual-mode X-band transmitter
- Heater power for the propulsion stage
- Increased experiment power
- Increased data storage capacity.

Inverter losses are lower than in the case of Pioneer F/G since the 28 VDC power bus, operating directly from the MHW RTG's provides primary power to subsystems and science instruments without conversion penalties, as discussed in Section 4.5.

Table 3-5. Electrical Power Requirements

Load \ Power (watts)	Pioneer F/G	Outer Planets Pioneer	Jupiter Orbiter (End of Mission)		Saturn Orbiter (End of Mission	
		2 RTG's	1 RTG (MHW)	2 RTG's	1 RTG (MHW)	2 RTG's
Secondary DC Power						
Communications						
Receivers (2)	3.4	3.4	3.4	3.4	3.4	3.4
Driver, S-band	1.3	1.3	1.3	1.3	1.3	1.3
Driver, X-band	N/A	0.5	0.0	2.5	0.0	2.5
Conscan processor	1.2	1.2	1.2	1.2	1.2	1.2
Attitude Control						
Control electronics assembly	2.7	3.2	3.5	3.5	3.5	3.5
Sun sensor assembly	0.2	0.2	0.2	0.2	0.2	0.2
Stellar reference assembly	0.3	0.3	0.3	0.3	0.3	0.3
Magnetometer reference	N/A	N/A	0.5	0.5	0.5	0.5
Command						
Command distribution unit	3.1	3.6	3.6	3.6	3.6	3.6
Digital decoder unit	1.3	1.3	1.3	1.3	1.3	1.3
Data Handling						
Digital telemetry unit	3.7	4.2	4.2	4.2	4.2	4.2
Data storage unit	0.6	4.0	4.0	4.0	4.0	4.0
Subtotal (CTRF output)	17.8	23.2	23.5	26.0	23.5	26.0
Secondary AC Power						
CTRF losses[1]	10.4	13.6	15.3	15.3	15.3	15.3
Subtotal (inverter output)	28.2	36.8	37.3	41.3	37.3	41.3
Primary DC Power						
Communications						
TWTA, S-band (8 watts)	27.8	27.8	27.8	27.8[3]	27.8	27.8[3]
TWTA, X-band	N/A	43.0[2]	0.0	60.2	0.0	60.2
Attitude Control						
Control electronics assembly	0.4	0.4	0.4	0.4	0.4	0.4
Electrical Power						
Inverter loss (30 VDC)[4]	N/A	4.0	4.5	5.0	4.5	5.0
Battery electronics	0.1	N/A	N/A	N/A	N/A	N/A
Shunt regulator heater[5]	N/A	N/A	4.0	4.0	4.0	4.0
Propulsion						
Transducers	0.2	0.4	1.5	1.5	1.5	1.5
Propulsion heaters	4.0	4.0	24.0	24.0	24.0	24.0
Command						
Command distribution unit	0.2	0.2	0.2	0.2	0.2	0.2
Experiments						
Experiments	24.0	45.0	21.9	60.0	9.9	35.0
Science package heater	N/A	N/A	7.0	7.0	7.0	7.0
Subtotal (28 VDC loads)	56.7	124.8	91.3	190.1	79.3	165.1
Cable losses (spacecraft)	0.6	0.6	1.0	1.0	1.0	1.0
RTG Power						
RTG cable losses[6]	4.2	1.0	0.4	1.1	0.4	0.9
PCU plus minimum shunt losses	7.7	3.0	3.0	3.0	3.0	3.0
Inverter loss (4.2 VDC)[7]	13.3	N/A	N/A	N/A	N/A	N/A
Spacecraft System Total	110.7	166.2	133.0	236.5	121.0	211.3
Total RTG Output[8]	124.0	250.0	133.0	265.0	121.0	242.0
Power Margin	13.3	83.8	0.0	28.5	0.0	30.7

Notes:

(1) CTRF efficiency - 63 percent

(2) X-band TWTA low power mode - 12 watts RF output (min.)

(3) X-band TWTA high power mode - 22 watts RF output (min.)

(4) Inverter efficiency - 88 percent

(5) Heater power for external regulator

(6) RTG cable resistance - 0.016 ohms/cable

(7) 4.2 VDC inverter efficiency - 86 percent

(8) End-of-mission lifetimes assumed: Pioneer F/G - L + 2.5 years, Outer Planets Pioneer - L + 5 years; Jupiter Orbiter - L + 3.5 years; Saturn Orbiter - L + 6 years.

During the lifetime of the contemplated orbiter missions the MHW generator system provides a power margin sufficient to handle all anticipated steady and pulse loads without a battery. Even greater margin is achieved if S- and X-band transmitters are not operated simultaneously. Conversely, in the event that one of the two MHW RTG's fails, alternative operational modes, involving duty cycling of transmitters or experiments, are available to ensure operational flexibility in continuing to meet mission objectives.

With nominal operating conditions (column 4), the Jupiter orbiter spacecraft can support 60 watts of science instruments and the high power mode X-band transmitter (22 watts RF output), leaving an adequate margin of 28.5 watts for pulse loads. If one RTG should fail, approximately 22 watts can be allocated to scientific instruments but operation is constrained to S-band transmission with an attendant reduction in data rate, as tabulated in column 3.

The power margins at Saturn are somewhat less due to the increased RTG degradation associated with the longer mission lifetime. Consequently the science payload is reduced to approximately 10 watts with S-band transmission, assuming one RTG has failed.

The power budget given in Table 3-5 is actually quite conservative since not all of the loads representing the most critical phase of the mission from the power requirements point of view, need to operate simultaneously. Items in this category include S-band or X-band drivers and TWTA's, propulsion heaters, some of the experiments, the data storage unit, and the conscan processor. These may be duty-cycled or turned off temporarily to reduce the total load, as required.

Table 3-6 lists the pulse loads occurring during the mission, based on Pioneer F/G characteristics. With the exception of the battery heater and feed movement mechanism, which are deleted, these loads are representative of the orbiter mission requirements. Actually, none of the pulse loads need to overlap since they are all ground commanded and may be sequenced accordingly. The transfer switches, used to interconnect transmitters and receivers with the antennas would, in general, only be actuated in case of a transmitter or receiver failure. Initiation of this action can be commanded with experiments turned off, if necessary.

Table 3-6. Pulse Loads

Function	Pulse Load (watts)	
	Pioneer F/G	Pioneer Outer Planets Orbiter
Experiments (command initiated)	3-4	3-4
Transfer switch (command initiated)	14 (50 ms)	14 (50 ms)
Thruster pair (every firing)	11.2	11.2
Spacecraft battery heater (command initiated)	1.2	N/A
Feed movement mechanism (command initiated)	4.3	N/A
Experiment ordnance (one time only)	6	6
CDU ordnance	0.5	0.5
Experiment Drive Assembly	N/A	6.5

3.5 DYNAMIC CHARACTERISTICS

Spacecraft dynamic characteristics which have a significant effect on system performance are examined in this section. These include:

- Attitude stability and pointing accuracy of the deployed spacecraft
- Deployment dynamics
- Nutation damping
- Wobble due to thrust misalignment.

Because of the large change in mass distribution from the original Pioneer F/G design, including some mass increase of the deployed appendages, a new analysis of dynamic characteristics was performed in which the influence of the appendages' structural flexibility had to be taken into account to obtain realistic spin stability criteria.

3.5.1 Attitude Stability

Spin stabilization is used to maintain the inertial orientation of the spacecraft's Z axis as in Pioneer F and G. The initial spin motion is provided by a Centaur-mounted spin table which spins up the spacecraft and third stage to approximately 60 rpm. During the first three minutes after Centaur separation, including 45 seconds of TE-364-4 thrusting and a two-minute and 15-second wait period for residual thrusting to decay, the spacecraft is spinning about an axis of minimum moment of inertia. In this

configuration, energy dissipation due to propellant sloshing causes nutation to increase. Starting with a nutation angle of 2.5 degrees induced by third stage thrusting this will increase the angle by less than 0.5 degree.

During the interval between third stage separation and appendage deployment (23 minutes in the case of Pioneer 11) the spacecraft possesses only a small margin of stability since the moment of inertia (I_z) around the Z axis is not much greater than the transverse moments I_x and I_y (see Table 3-4). With completion of the RTG and magnetometer boom deployment the spacecraft attains a more stable configuration, and the nutation angle, having increased by several degrees during the interim, begins to decay. The damping time constant is of the order of 10 minutes.

The large increase of the center-body moments of inertia and the increase of the tip masses supported by the deployment booms can produce large boom deflections that tend to reduce the spacecraft stability margin compared to that of a rigid spacecraft with otherwise the same mass distribution. Thus, stability criteria of a rigid body which require that the spin moment of inertia be larger than the two transverse moments of inertia are no longer sufficient to assure stability in the case of a spacecraft with flexible appendages. Deviations from the dynamic stability of a rigid spacecraft are still greater if, in the limit, the appendages are considered as articulated (hinged) rather than flexible booms.

Results of a simplified (linearized) stability analysis of a spinning spacecraft with added deboost stage and flexible appendages based on the mass properties of the modified Pioneer spacecraft and representative spring and damping characteristics of its flexible magnetometer and RTG booms are shown in Figures 3-10 and 3-11.

Figure 3-10 shows stability boundaries of the spacecraft with flexible (solid curve) and rigid appendages (dashed curve) in a graph of propulsion stage weight versus center-of-mass location relative to the spacecraft's appendage deployment plane. The range of operating conditions of the Jupiter and Saturn orbiters from beginning to end of life are also indicated in the graph showing the respective stability margins (expressed in terms of the distance to the boundary location). It is apparent from the results that an increase in retro-stage mass for a given center-of-mass location tends to reduce the stability margin since the transverse moments of inertia, I_x and I_y, are being increased relative to the spin moment-of-inertia, I_z, such that the moment-of-inertia ratios approach unity, i.e., the critical value in the case of the rigid body system.

Actually, the nominal design range indicated in the diagram is stable for rigid as well as flexible appendages, but the stability margin decreases as much as 30 percent (10 inches) for the case of flexible appendages. This comparison illustrates the importance of using the flexible-body rather than the rigid-body dynamics model for the stability analysis of this spacecraft design.

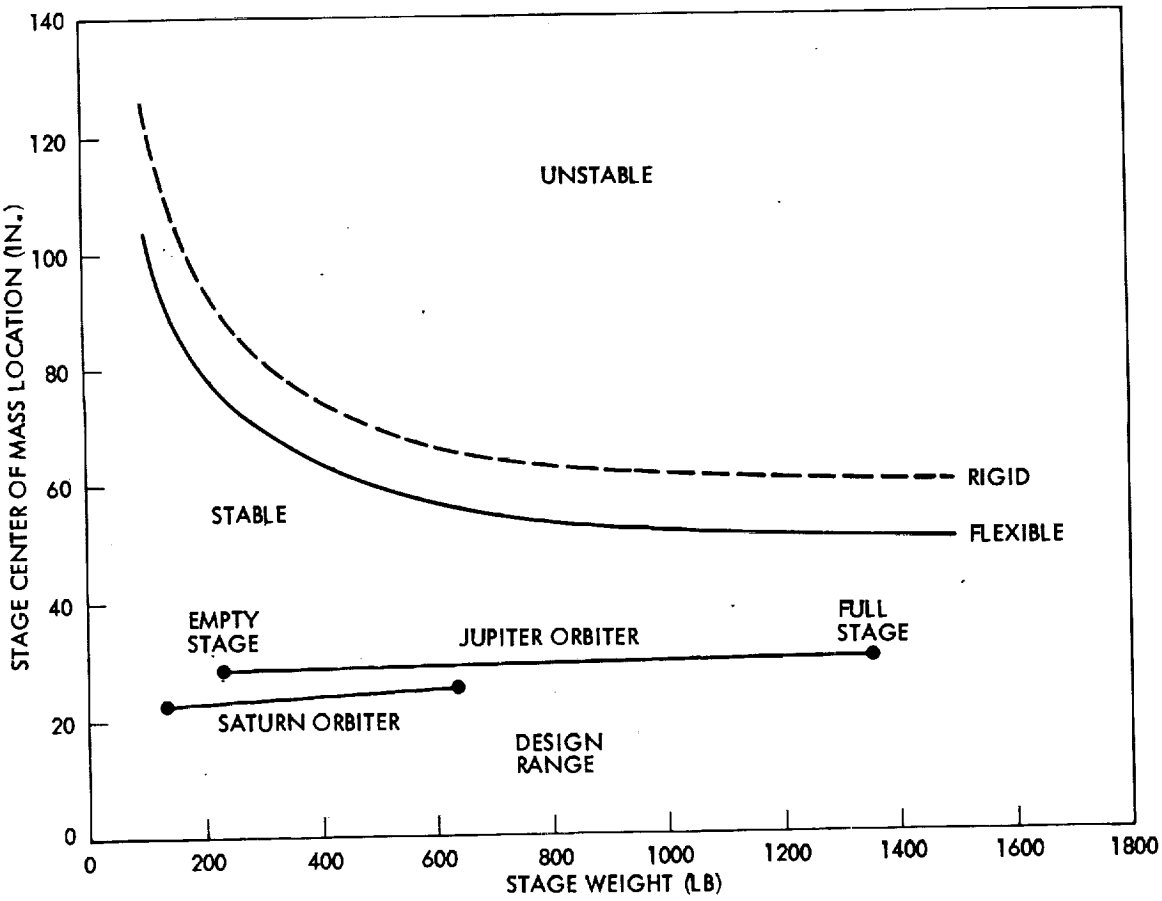

Figure 3-10. Updated Orbiter Stability Performance

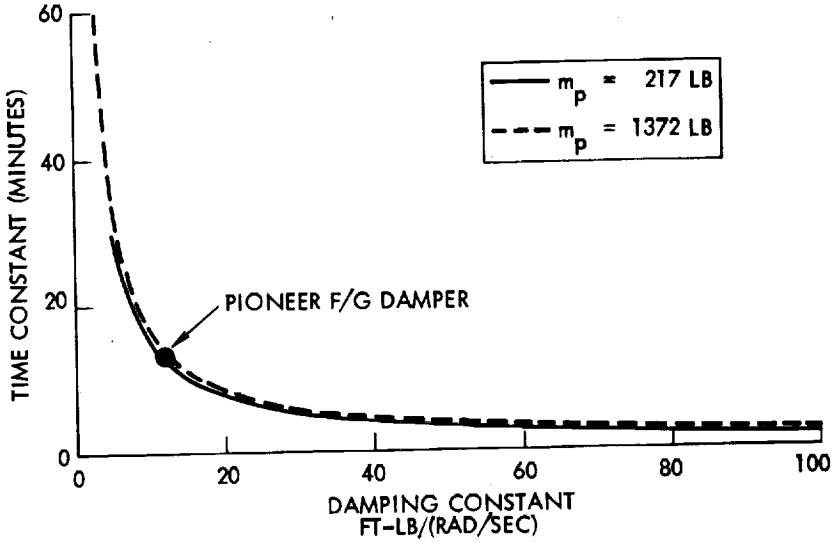

Figure 3-11. Wobble Damper Performance

Figure 3-11 shows the nutation damping time constant as function of the damping constant of the magnetometer boom wobble damper constant for the case of the Jupiter orbiter. It is seen that the present damper of Pioneer F/G will provide a 13-minute damping time constant and that smaller values can be obtained simply by increasing the damper constant. Differences between the results of rigid-body and flexible-body analysis are practically negligible.

Other results obtained from the analysis of a spacecraft with flexible appendages can be qualitatively summarized as follows:

- The increased tip masses of the RTG and magnetometer booms tend to increase the stability margin compared to a system with the original tip masses used in Pioneer F/G.
- Flexural stiffness variation of the RTG booms has a strong effect on stability in the range of low stiffness coefficients less than half the nominal Pioneer F/G values. At larger values the system's stability is comparable to that of a rigid body.
- Flexural stiffness of the magnetometer boom has much less influence on the stability margin. In effect the boom acts as if articulated.
- An increase in wobble damper constant has no effect on the stability margin but reduces wobble decay time.

3.5.2 Nutation Effects due to Injection and Spacecraft Separation

Accuracy of third stage injection is dependent upon mass properties of the combined third stage/spacecraft vehicle, thrust vector misalignment with respect to the vehicle's center of mass and spin rate. For the purpose of this analysis it is assumed that the initial spin rate is the same as in Pioneer F/G (60 rpm) and that the mass properties of the combined third stage/spacecraft configuration are consistent with spin stability during injection, as in Pioneer F/G.

Computer simulations of injection, in which it is conservatively assumed that a constant, body-fixed, transverse torque of 14,900 pounds x 0.10 inch = 1,490 inch-pounds acts throughout the entire third stage thrusting duration, indicate that the induced errors will not exceed the following values:

- Angular dispersion of velocity vector = 0.48 degree
- Reduction in magnitude of velocity vector = negligible
- Nutation angle (from thrust misalignment only) = 2.5 degrees.

Correction of the velocity vector misalignment is readily achieved during the first midcourse maneuver.

Following separation of the spacecraft from the third stage, the resultant nutation angle is:

$$\nu = \nu_0 \frac{I_{t2}\, I_{s1}}{I_{t1}\, I_{s2}}$$

where I_{s1} and I_{t1} are the spin and transverse moments of inertia of the combined third stage/spacecraft vehicle and I_{s2} and I_{t2} are the spin and transverse moments of inertia of the separated spacecraft. ν_0 and ν are the nutation angles prior to and following separation, respectively. For the Pioneer orbiter configuration, the estimated 3.0-degree wobble angle prior to separation would decrease to 1.8 degrees according to the above equation. Due to tipoff error the angle will actually be somewhat larger.

The despin maneuver that must precede appendage deployment to avoid unduly large dynamic loads on appendage structures increases the wobble angle remaining after spacecraft separation in the ratio of initial to interim spin rates, ω_1/ω_2. The value of the interim spin rate ω_2 to be achieved by the despin maneuver is governed by the requirement that the subsequent appendage deployment result in a final spin rate ω_3, nominally 4.8 rpm as in Pioneer F/G. Conservation of angular momentum during the deployment maneuver thus establishes the interim spin rate ω_2 as 15.7 rpm. Consequently the increase in nutation angle during the despin maneuver is in the ratio

$$\frac{\omega_1}{\omega_2} = \frac{60}{15.7} = 3.8$$

The resulting nutation angle is $\nu_2 = 3.8\ \nu_1 = 6.9$ degrees. Appendage deployment can be accomplished with this nutation angle as initial condition. (Actually, the Pioneer F/G design can accommodate appendage deployment with initial nutation angles of 10 to 15 degrees.)

3.5.3 Appendage Deployment Dynamics

The mass distribution of the bus/debooster combination implies less favorable spin stability characteristics compared to the baseline Pioneer F/G in the initial stowed configuration and during deployment, before the magnetometer boom becomes effective as a nutation damper. The potentially larger nutation angles that can develop during the deployment phase and the increased tip masses supported by the deployment arms in the case of the Pioneer orbiter spacecraft combine to impose substantially larger structural loads on these arms under worst case conditions than in the case of Pioneer F/G.

Balanced deployment of the three appendages is necessary to maintain the spacecraft center of mass on the geometrical centerline during the entire deployment process, thereby avoiding a significant tilt of the principal axis of inertia and the buildup of large nutation angles.

A preliminary analysis was conducted a) to assess requirements for structural reinforcement of the deployment booms and b) to define alternatives to the sequential deployment technique of Pioneer F and G (where the RTG booms were deployed before the magnetometer boom) to reduce the dynamic loads.

The four deployment concepts analyzed in this study are compared in Table 3-7. The first is the concept used on Pioneer F and G. It is the simplest, but also the least satisfactory, under the dynamic characteristics of the Pioneer orbiter spacecraft configuration.

Table 3-7. Balanced Boom System Deployment Schemes

Model	Mode of Operation	Advantages/Disadvantages
1. Sequential	Present Pioneer F/G scheme. RTG's first, then magnetometer boom	Least complex, permits considerable principal axis shift and wobble buildup
2. Simultaneous	All booms released simultaneously	Reduced wobble buildup but more complex implementation
3. "Tuned" simultaneous	All booms released simultaneously; lock-up achieved at same time	Requires matched dampers
4. Synchronous	Deployment controlled to maintain principal axis parallel to Z axis continuously	Best control of wobble, but most complex in implementation

The fourth concept which may require feedback or other complex techniques of implementation, such as operation from a common deployment damper mechanism, obviously would be most effective in eliminating lateral excursions of the center of mass during deployment, and thus would minimize wobble buildup.

The second and third concepts actually involve open-loop control, based on the assumption that simultaneous release of all deployment arms leads to nearly simultaneous deployment. Model 3 ("tuned" simultaneous deployment) is an idealized system calling for damper matching with a precision which cannot actually be realized in practice. It was included among the four analytical models studied to indicate the best performance of Model 2.

Figure 3-12 shows a schematic of the dynamic model used to simulate deployment dynamics. Basically, the model consists of four bodies. The central body (Body 1) represents the bus plus the deboost stage. Body 2 represents the magnetometer boom assembly, Body 3 represents the -Y axis RTG boom assembly and Body 4 represents the +Y axis RTG boom assembly. Body 1 is allowed a full 6 degrees of freedom while Bodies 2, 3, and 4 are assumed to be point masses capable of radial translation on rigid, massless bars oriented along their respective boom axes. The translational rates of Bodies 2, 3 and 4 are controlled passively by means of

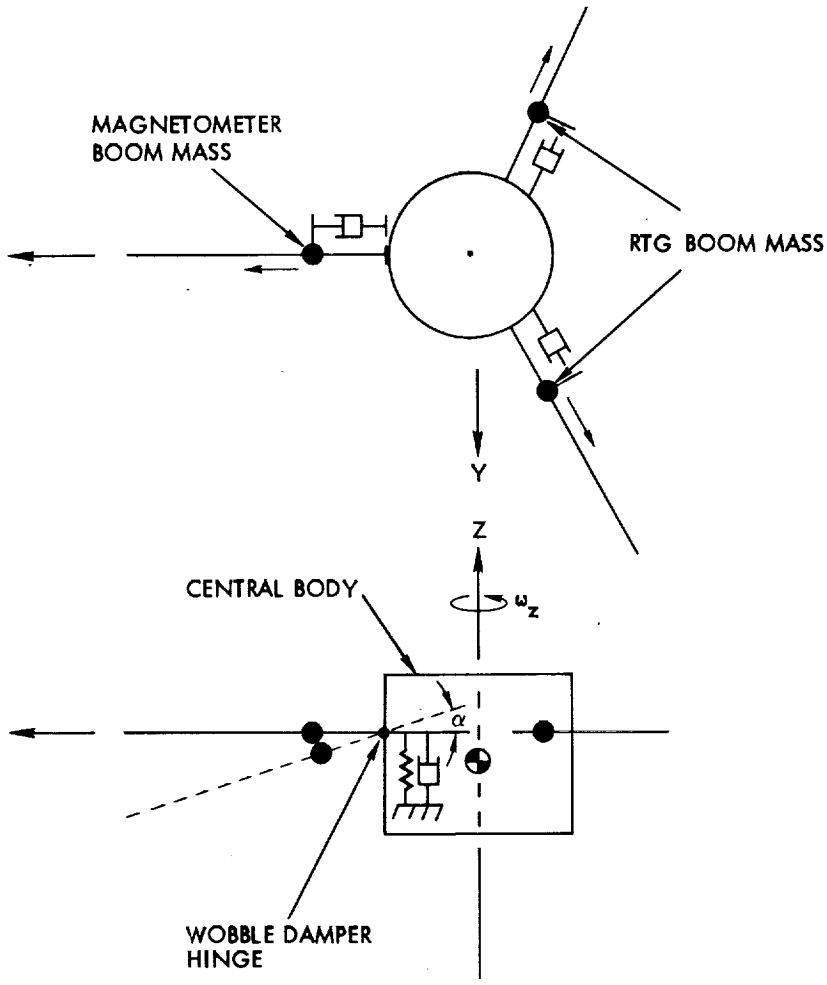

Figure 3-12. Deployment Simulation Model

linear, velocity proportional deployment dampers. In addition to its translational motion, the magnetometer boom system (Body 2) is allowed a rotational degree of freedom at its wobble damper hinge in order to simulate the transient effects of the damper and the shock loads induced when the magnetometer boom impacts the damper stops at $\pm$3 degrees.

Nominal initial conditions for the deployment process include a spin rate (ω_z) of 15.7 rpm (1.644 rad/sec), and an initial wobble angle of 9 degrees; the 9-degree wobble angle implies initial transverse rates of $\omega_x = \pm 0.32$ rad/sec or $\omega_y = \pm 0.27$ rad/sec.

Results of this preliminary analysis are briefly summarized here. Simultaneous deployment was found to lead to acceptable control of deployment-induced wobble and bending moments at the root of the deployment booms.

Even with highly conservative assumptions on magnitude of initial wobble angles and angular rates the simultaneous deployment concept holds

excursion amplitudes to less than 25 degrees. "Tuned" simultaneous deployment does not appear to be much superior to the simpler "untuned" case, even under the assumption that RTG deployment is completed twice as fast as the magnetometer boom deployment.

Table 3-8 presents the results of several deployment simulations performed with various termination conditions. Specifically, termination occurred when any one of the appendages reached its fully deployed length: "simultaneous" indicates that all three appendages latch at approximately the same time; "magnetometer boom out 1/2 length" indicates that the magnetometer boom is deployed approximately 1/2 when the RTG/s latch; "magnetometer boom stowed" indicates that the magnetometer boom is not released and only the RTG's are allowed to deploy (i.e., the present Pioneer F/G scheme). "RTG boom out 1/2 length" indicates that the RTG's are deployed approximately 1/2 when the magnetometer boom latches.

Table 3-8. Deployment Simulation Results

Case No.	Termination Conditions	Initial Rates (rad/sec)		Wobble Damper	Maximum Boom Moments (in. lb)		Maximum Wobble (deg)
		$\omega_x(0)$	$\omega_y(0)$		Magnetometer	RTG	
1	Simultaneous	0	0	Caged	48	40	0.95
2	Simultaneous	0.32	0	Caged	102	133	13
3	Magnetometer boom out 1/2 length	0.32	0	Caged	55	124	12
4	Magnetometer boom stowed (sequential deployment)	0.32	0	-	-	220	20.7
5	Magnetometer boom out 1/2 length	0.32	0	Active	90	124	12
6	Magnetometer boom out 1/2 length	0	0.27	Active	69	112	10.6
7	RTG boom out 1/2 length	0.32	0	Active	202	146	20.4
8	Simultaneous	0.32	0	Active	175	130	12.5

*Caged wobble damper: magnetometer boom assumed as cantilevered
Active wobble damper: magnetometer boom hinged with limit stops at ±3 degrees

The "maximum boom moments" indicated in Table 3-8 are the maximum instantaneous RSS values of the "despin moment" (root boom moment about an axis parallel to the spin axis) and the "wobble moment" (root boom moment about an axis perpendicular to both the spin axis and the boom axis). It should be noted that these root moments are conservative as they do not reflect the flexibility of the booms.

From Table 3-8, it is apparent that conditions where magnetometer deployment leads RTG deployment should be avoided. In addition, it is noted that load conditions are reduced if the RTG's deploy faster than the magnetometer instead of simultaneously as might be expected. However, sequential deployment (Case 4) with the magnetometer boom stowed until

completion of RTG deployment leads to the highest RTG boom moments and wobble angles and must be avoided. This case would also involve unacceptable initial conditions for the subsequent magnetometer boom deployment phase.

Figure 3-13a, b, c shows representative time histories of wobble angles, angular rates and RSS root moments of the three appendages obtained under deployment conditions of Case 3 (see Table 3-8).

A comparison of the maximum dynamic magnetometer boom and RTG boom bending moments obtained by this analysis with steady state bending moments due to axial thrust acceleration during retro-engine firing is of interest to assess their relative magnitude from a structural load standpoint. Worst case bending moments introduced by 100 lbf of axial thrust acting on the spacecraft with nearly empty propellant tanks are of the order of 300 in.-lb for the magnetometer boom, and 700 in.-lb for the RTG booms, i.e., they are 3 to 6 times greater than the dynamic loads occurring in the preferred simultaneous deployment mode, as indicated in Table 3- . Thus, booms and attachment fittings of Pioneer F/G design which must be reinforced structurally to withstand the maximum thrust acceleration loads should be more than adequate to withstand the dynamic loads occurring in the deployment phase. (See Section 3.7, 4.1 and Appendix D for additional discussion of load characteristics and structural design.)

3.5.4 Nutation Effects due to ΔV and Precession Maneuvers

Midcourse corrections, deboost and orbit change maneuvers introduce a buildup of precession and nutation angles due to body-fixed torques resulting from thrust vector-to-c.g. misalignment. Nutation angles also build up as an unavoidable side effect of precession maneuvers. After completion of these maneuvers the nutation angles will decay gradually through wobble damper action.

ΔV Maneuvers

An upper bound on the pointing error occurring during ΔV maneuvers by the retro-engine is given by

$$\alpha \leq 57.3 \frac{2T}{(I_z - I_x)\, S^2}$$

where

α is the pointing error (degree)

T is the thrust vector misalignment torque (ft-lb)

I_z, I_x are spacecraft moments of inertia (slug-ft^2)

S is the spin rate (rad/sec)

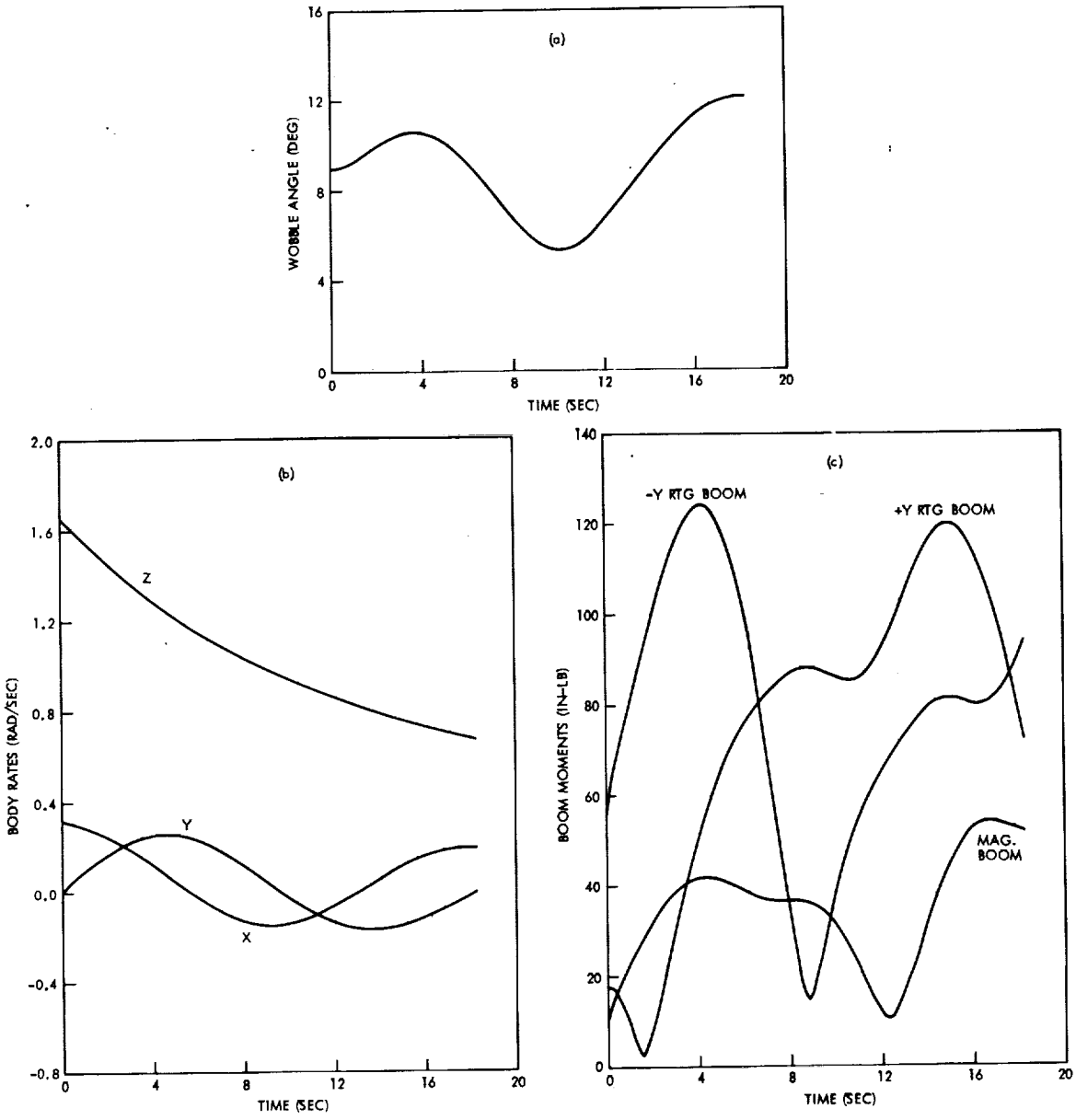

Figure 3-13. Time History of (a) Wobble Angle, (b) Body Rates and (c) Boom Moments During Simultaneous Deployment of Appendages (see Table 3-8, Case 3)

The total thrust vector misalignment torque T is estimated as follows:

$$T = (\text{thrust}) \times \left\{(\text{c.g. location tolerance})^2 + \left[(\text{thrust vector angular misalignment}) \times (\text{thruster-to-c.g. Z-axis displacement})\right]^2\right\}^{1/2}$$

$$= 100 \text{ pound } \left[0.10 \text{ in.}^2 + (0.004 \text{ rad} \times 39 \text{ in.})^2\right]^{1/2}$$

$$= 18.9 \text{ in.-lb}$$

The worst-case misalignment torque assumed here occurs when the propellant tanks are nearly empty such that the thruster-to-c.g. Z-axis displacement is at a maximum. The moment-of-inertia difference $(I_z - I_x)$ varies between 497 and 509 slug-ft^2 from the beginning to the end of the mission (see Table 3-4). With the above data the maximum value of the pointing error α is found to vary with spin rate as shown in Figure 3-14 by a solid line. Data in this graph apply to the Jupiter as well as the Saturn orbiter configuration.

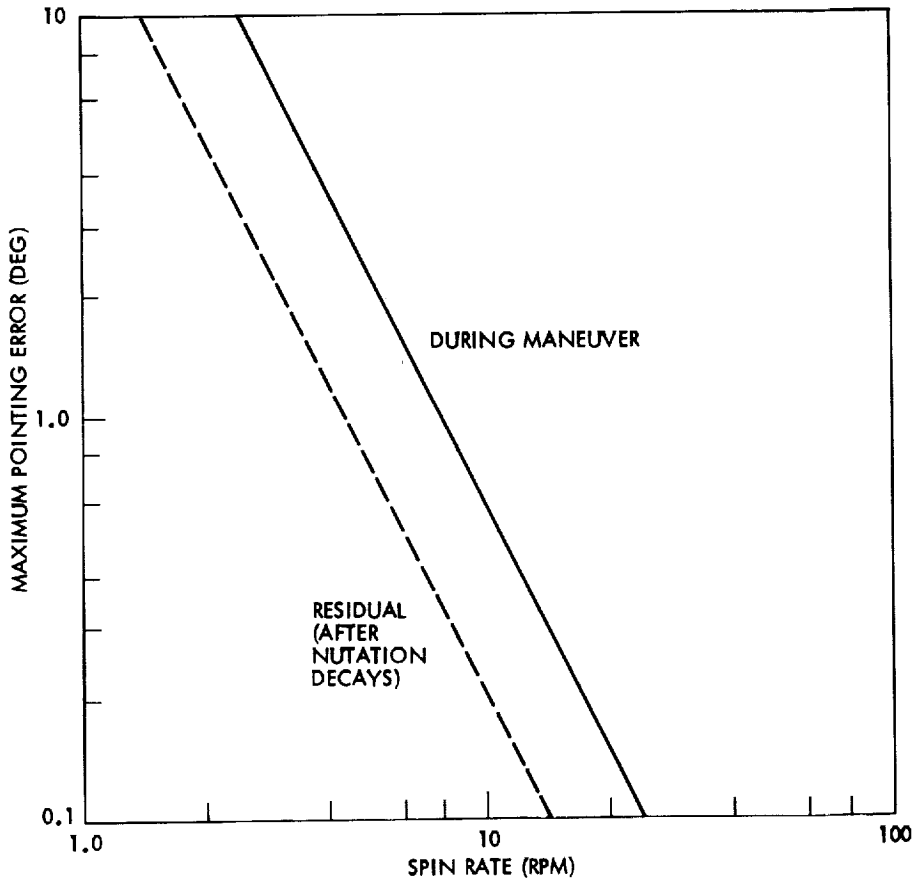

Figure 3-14. Pointing Errors Caused by Main Thrust Maneuvers

After thrust termination, the wobble portion of α will decay exponentially with a time constant of about 10 minutes, leaving a residual pointing error β, which is bounded by the expression

$$\beta \leq 57.3 \frac{2T}{I_z S^2}$$

This error varies with spin rate as shown by the dotted line in Figure 3- . The value of I_z used here is 963.2 slug-ft^2 (see Table 3-4).

These pointing errors will be reduced by spinning up the spacecraft from the nominal spin rate of 4.8 rpm prior to main thruster firing. As discussed in Sections 3.6 and 3.7, the selected spin rate is 15 rpm. At this spin rate the resulting pointing error upper bounds are

$$\alpha = 2.61 \text{ degrees}$$

$$\beta = 0.911 \text{ degree}$$

Spin rate variations due to worst-case axial thrust misalignment can be as large as ± 2 rpm during a large ΔV maneuver with a duration of 25 to 30 minutes. This effect is comparatively small for the selected maneuver-phase spin rate of 15 rpm. However, if a spin rate of only 10 rpm were selected, a 2 rpm deviation could be significant in causing a large (56 percent) increase in maximum pointing errors.

Precession Maneuvers

The moment-of-inertia ratios of the spacecraft in the deployed state (as per Table 3-4) are:

$$\xi = \frac{I_x}{I_z} = \begin{matrix} 0.556 \\ 0.472 \end{matrix} \qquad \eta = \frac{I_y}{I_z} = \begin{matrix} 0.654 \\ 0.649 \end{matrix} \qquad \begin{matrix} \text{(for full tanks)} \\ \text{(for empty tanks)} \end{matrix}$$

These ratios affect the nutation buildup during pulsed precession maneuvers in a manner which may differ slightly from Pioneer F/G behavior.

The nutation frequency (in body coordinates) is K times the spin rate, where K is given by

$$K = \left[\frac{I_z - I_y}{I_x} \cdot \frac{I_z - I_x}{I_y}\right]^{1/2} = \left[\frac{1-\eta}{\xi} \cdot \frac{1-\xi}{\eta}\right]^{1/2} = \begin{matrix} 0.650 \text{ (full tanks)} \\ 0.778 \text{ (empty tanks)} \end{matrix}$$

This compares with K = 0.86 for Pioneer F/G. The decrease reflects primarily the addition of the propulsion stage to the basic Pioneer spacecraft configuration.

In pulsed precession maneuvers, nutation can build up to a factor of $|\csc(nK\pi)|$ times the precession step size, where n is the number of spin revolutions between precession pulses. For programmed open-loop precession maneuvers, a pulse is fired every revolution, so with n = 1 the factor is decreased from 2.5 to 1.1 and 1.56 for full and empty tanks, respectively, compared to Pioneer F/G when K is reduced from 0.86 to 0.65 and 0.78. The precession step size itself is reduced to a factor of 0.40 to 0.46 times its value in Pioneer F/G, because the same thrusters are used but the spin moment of inertia has been increased. Thus the maximum nutation amplitude during such a maneuver generally decreases.

In Table 3-9 the precession and nutation characteristics of the Pioneer Jupiter orbiter are compared with those of Pioneer 10 and the Outer Planets Pioneer spacecraft design. These characteristics and their relation to attitude control system operation will be further discussed in Section 4.4.

Table 3-9. Nutation Build-Up Due to Precession Maneuver

	Pioneer 10	Outer Planets Pioneer	Pioneer Jupiter Orbiter	
			Start of Mission	End of Mission
Coefficient K	0.86	0.91	0.65	0.78
Precession step size (0.125-sec pulses)				
Full tank	0.31°	0.17°	0.12°	0.14°
Empty tank	0.12°	0.06°	0.05°	0.06°
Nutation build-up factor	2.5	3.6	1.1	1.56
Maximum nutation				
Full tank	0.78°	0.61°	0.13°	0.22°
Empty tank	0.30°	0.22°	0.06°	0.09°

3.6 VARIATION OF SPIN RATE

3.6.1 Proposed Spin Rate Profile

The spacecraft spin rate will be varied repeatedly during the mission as needed to meet pointing and experiment scan rate requirements. A proposed profile of spin rates versus time is illustrated in Figure 3-15, and requirements which dictate the choice of spin rates are indicated in the graph. After the initial despin maneuver and appendage deployment which reduces the spin rate to the nominal value of 4.8 rpm, the spacecraft maintains this rate during the cruise to the target planet, except during

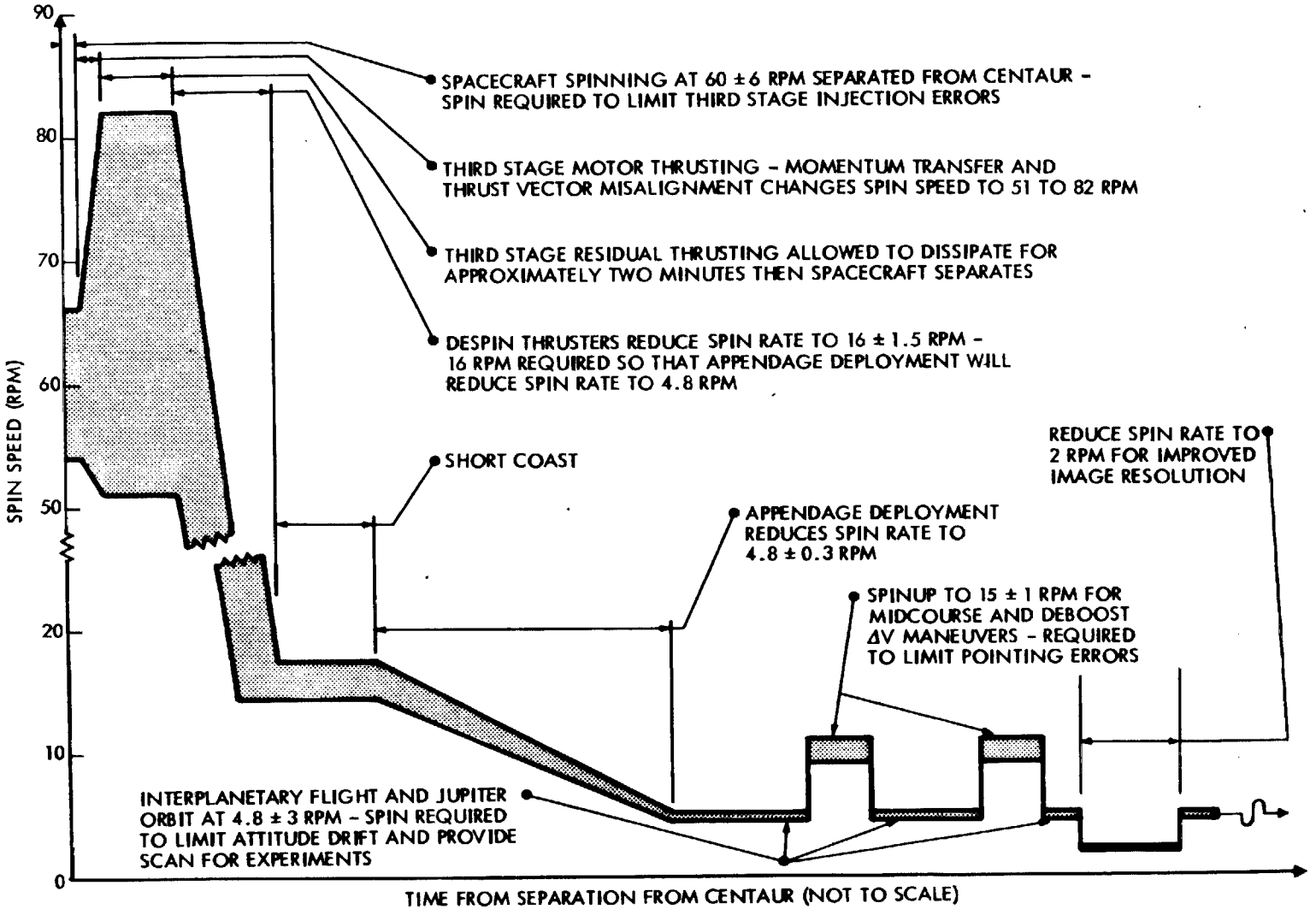

Figure 3-15. Representative Spin Rate Profile

high thrust midcourse maneuvers when a higher spin rate is desired (15 rpm in this example) to assure accurate thrust vector pointing. A high spin rate is also used during planetary orbit insertion, subsequent orbit trims and plane change maneuvers. During the orbital phase the spin rate may be periodically reduced for improved TV camera image resolution whenever the spacecraft is in a favorable viewing position close to the planet. After each periapsis passage the spacecraft resumes the normal operating mode at a spin rate of 4.8 rpm. With highly eccentric orbits typical for the mission, and with orbit periods that may exceed 30 days, the spacecraft will actually spend almost all of the orbital phase in the normal mode.

It should be noted that the high-resolution solid-state array line scan camera contemplated for the Pioneer orbiter spacecraft has sufficient sensitivity to operate at the nominal spin rate at Jupiter, but would require a reduced spin rate of about 2 rpm for operating most effectively at Saturn.

Spacecraft design considerations and operating characteristics involved in changing the spin rate upward or downward as indicated in Figure 3-15 will be discussed in the following sections.

3.6.2 Effects of Spin Rate Reduction

Reduction of the spin rate from the nominal value of 4.8 rpm has two major effects upon the attitude control subsystem. First, the reduction decreases the angular momentum so that external disturbance torques acting normal to the spin axis have a greater effect in precessing the spin axis. Second, the Pioneer F/G attitude control subsystem was designed to operate only within a limited range of spin rates other than nominal. Operation at spin rates outside this range requires modification to some attitude control units and subassemblies (see Section 4.4).

Disturbance Torque Effects

Predominant sources of attitude disturbance in a planetary orbit are gravity gradient and magnetic torques. The greatest effect occurs near periapsis.

The gravity gradient torques about the spacecraft's X, Y and Z body axes are given by

$$T_{ggx} = \frac{3\mu_J}{R^3} (I_z - I_y)\, r_{by}\, r_{bz}$$

$$T_{ggy} = \frac{3\mu_J}{R^3} (I_x - I_z)\, r_{bz}\, r_{bx}$$

$$T_{ggz} = \frac{3\mu_J}{R^3} (I_y - I_x)\, r_{bx}\, r_{by}$$

where

μ_J = gravitational constant of the planet

R = distance from planet's center to the spacecraft center of mass

I_x, I_y, I_z = principal moments of inertia of the spacecraft

r_{bx}, r_{by}, r_{bz} = direction cosines of the radius vector $\overline{R}$ (in spacecraft coordinates)

Notice that these torques vary as the inverse cube of the radial distance from the planet center and depend upon the differences in moments of inertia. The angle between the spin axis and the radial vector varies periodically with each orbital pass. Also, spin about the Z axis causes periodic changes in the projection of the radial direction on the body axes.

A magnetic torque is caused by interaction of the planet's and the spacecraft's magnetic fields. This torque is given by

$$\overline{T}_m = \overline{M} \times \overline{B}$$

where

$\overline{M}$ = spacecraft magnetic dipole moment

$\overline{B}$ = planet's magnetic field vector

The strength of the field varies inversely as the cube of the radial distance between the spacecraft and the planet's center.

The combined effect of these two disturbances was evaluated for the case of a Jupiter orbiter assuming moments of inertia and magnetic properties of Pioneer F/G. As a worst case example a skimmer orbit was selected. A magnetic field strength of 10 gauss at Jupiter's surface was assumed. Maximum precession angles accumulating per orbital pass due to each perturbing effect were combined in an RSS-sense with an initial pointing uncertainty of 0.2 degree (conscan dead zone). The resulting change in pointing angle is shown in Figure 3-16. As seen in the graph, the precession buildup is small in the range of the higher spin speeds, e.g., >3 rpm, but becomes more pronounced as speed is decreased. At 1 rpm spin rate the pointing error accruing per orbital period is 0.6 degree. Permissible error limits for S- and X-band operation are indicated in the graph. The precession exceeds the error limit for X-band below approximately 1.25 rpm. These estimates can be regarded as quite conservative since actually the average magnetic field strength at Jupiter's surface is only about 4 gauss (based on Pioneer 10 encounter data), and the Pioneer orbiter's susceptibility to precessing perturbation torques is less than Pioneer F/G's with the spin moment of inertia being more than twice as large.

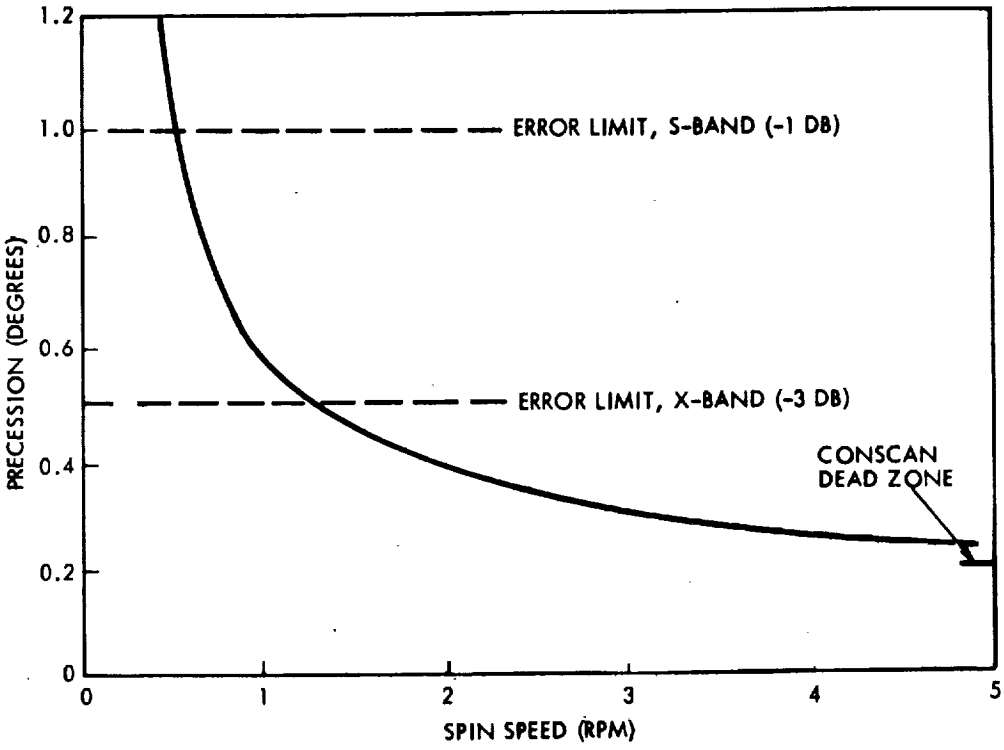

Figure 3-16. Spacecraft Precession from Magnetic and Gravity Gradient Disturbances at Low Spin Rates

Nutation Damping

Another impact of operation at low spin rate involves the performance of the nutation (wobble) damper. The Pioneer F/G design provides a time constant of 10 minutes or less at 4.8 rpm. The time constant would rise to 100 minutes at 2 rpm. This is illustrated in Figure 3-17. A second curve in this diagram shows the increased effectiveness of the wobble damper due to addition of a large tip mass (deployment counterweight) on the magnetometer boom. The time constant of this configuration is approximately 14 minutes at 2 rpm.

Should it become necessary to reduce the time constant under these conditions, there exist several alternatives for modification of the existing damper so as to tune its response characteristics for more effective performance at low spin rates.

Effect on Attitude Control Subsystem Operation

The attitude control subsystem designed to operate near the nominal spin rate at 4.8 rpm cannot accommodate the low spin rates considered here without requiring some modifications. These modifications involving primarily the control electronics assembly, the conscan signal processor,

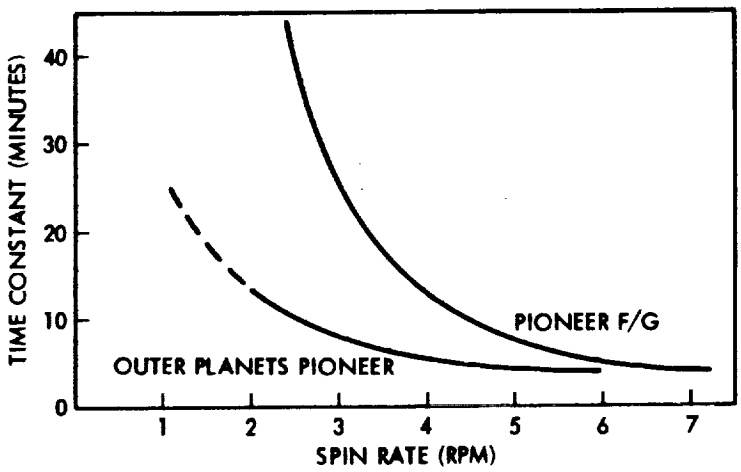

Figure 3-17. Wobble Damper Time Constant Variation with Spin Rate

as well as the roll attitude timer and spin period sector generator in the digital telemetry unit will be discussed in Section 4.4.

3.6.3 Effects of Spin Rate Increase

Operation at increased spin rate has the primary objective of reducing the pointing error due to thrust vector misalignment during high-thrust maneuver phases. This was previously discussed in Section 3.5 (see Figure 3-14).

As a beneficial side effect, a stiffening of the large flexible appendages against deflection due to thrust loads occurs because of increased centrifugal action at the higher spin rates (see Reference 13). Typically, the deflection of the 15-ft magnetometer boom due to a 0.1 g axial acceleration is reduced by about 50 percent at the spin rate of 10 rpm. This in turn reduces asymmetrical mass distribution due to boom deflection and, hence, tilting of the principal axis of inertia with respect to spacecraft body axes. Preliminary analysis indicates that the worst case tilt angle occurring for a 100 lbf thrust force and empty propellant tanks is about 0.5 degree at 10 rpm, but only 0.25 degree at 15 rpm spin rate. Effects of increased spin rate on structural loads and deformations due to axial thrust will be discussed in greater detail in Appendix D.

The recommended spin rate at which the spacecraft should operate during high-thrust maneuver phases is 15 rpm (rather than 10 rpm as proposed in the previous Jupiter orbiter study, Reference 5). This selection is based on the greater pointing accuracy and greater stiffening obtainable at the higher spin rate and the fact that unwanted spin rate variations due to thrust vector misalignment (2 rpm in the worst case as discussed in Section 3.5) have a less significant effect in this case. 15 rpm is the upper limit of the range of off-nominal spin rates that can

be accommodated by the baseline Pioneer F/G without attitude control system modifications. All attitude control related subsystems also can function nominally within this range of spin rates. Register and counter lengths require no modifications, although quantization errors will increase assuming that the counter drive pulse rates are maintained at their original values.

The conical scan signal processing accuracy is spin rate dependent. The number of signal averaging cycles is based upon the inertia properties of the configuration and signal-to-noise considerations. The latter requires reassessment at the higher spin rate, since less time is spent averaging out noise, and some degradation in signal-to-noise ratio can be expected. Actually, the use of conscan in closed-loop precession maneuvers, which is used rarely even under nominal operating conditions, can be avoided entirely during high spin rate operation because of the short time intervals involved.

3.6.4 Redundant Spin/Despin Thruster Pair

Because of the frequent spin-up and despin operations required in the orbiter missions (e.g., at least six spin-up/despin cycles for high thrust maneuvers and a similar number of cycles for repeated low spin rate operations during the orbit phase), it is essential that a redundant pair of spin/despin thrusters be added to the orbiter configuration to increase the mission success probability.

Actually, these thrusters are only partially redundant, since longitudinal c.g. shifts due to propellant depletion would cause an undesirably large amount of precession coupling unless the spin or despin thrusters are used in pairs. However, in the event of failure of one of the added thrusters it is still possible, albeit at the price of greater operational complexity and propellant expenditure, to compensate the coupling effect by appropriate use of precession thrusters.

3.7 ORBIT INSERTION THRUST LEVEL

The selection of the thrust level for the high-thrust engine is based on conflicting considerations. In favor of a high thrust level are:

a) Greater efficiency in orbit insertion maneuvers or major orbit change maneuvers at periapsis as the maneuver approaches the idealized "impulsive transfer"

b) Reduction in maneuver duration and engine burn time

In favor of a low thrust level are

c) Less wobble buildup due to unavoidable thrust-line/center-of-mass offsets

d) Lower structural loads on deployed structures

e) Lighter propulsion components and lower electric power requirement for valve operation, heaters, etc.

Considerations a), c), and d) are the most important ones. However, the wobble buildup at high thrust levels can be countered by increasing the spin rate during high-thrust maneuvers (see Section 3.6.3), so that consideration c) is not governing.

The tradeoff between a) the ΔV penalty due to finite thrust level ("gravity loss") and d) structural penalty to accommodate high accelerations is illustrated in Figure 3-18 for the case of the Jupiter orbiter. The center of the figure shows acceleration levels sustained during firing of a high-thrust engine of 50, 100 and 200 lbf thrust level. The lower acceleration limit occurs when the tanks are full, the upper limit when they are empty. The top of the figure shows the ΔV penalty for an orbit entry maneuver of given magnitude at a 2 R_J periapsis for V_∞ = 6 km/sec. (For details refer to Section 6.8.2.) At the bottom are seen accelerations that would be acceptable for the existing Pioneer F/G deployed structures, or if straightforward reinforcement is applied. A 100 lbf thrust level will incur ΔV penalties of probably no more than 30 to 40 meters/sec with orbit entry maneuvers up to 2000 m/sec, while structural penalties are modest.

Orbit insertion penalties for the Saturn orbiter are considerably smaller (about 10 m/sec) as discussed in Section 7.3.4.

The structural limits indicated at the bottom of Figure 3-18 should only be considered as qualitative. Actually, the concern with potentially large bending moments acting on flexible appendages due to large thrust accelerations and heavy tip masses is mitigated to some extent by the stiffening effect due to centrifugal action at increased spin rates as discussed in the preceding section (see also Section 4.1 and Appendix D). This factor contributed to the selection of 15 rpm as the recommended spin rate during high-thrust maneuvers.

These considerations show that the choice of an existing engine with 90 to 100 lbf thrust level as retro-engine for the Pioneer orbiter (see Section 4.3) is consistent with the preferred operating range identified in Figure 3-18.

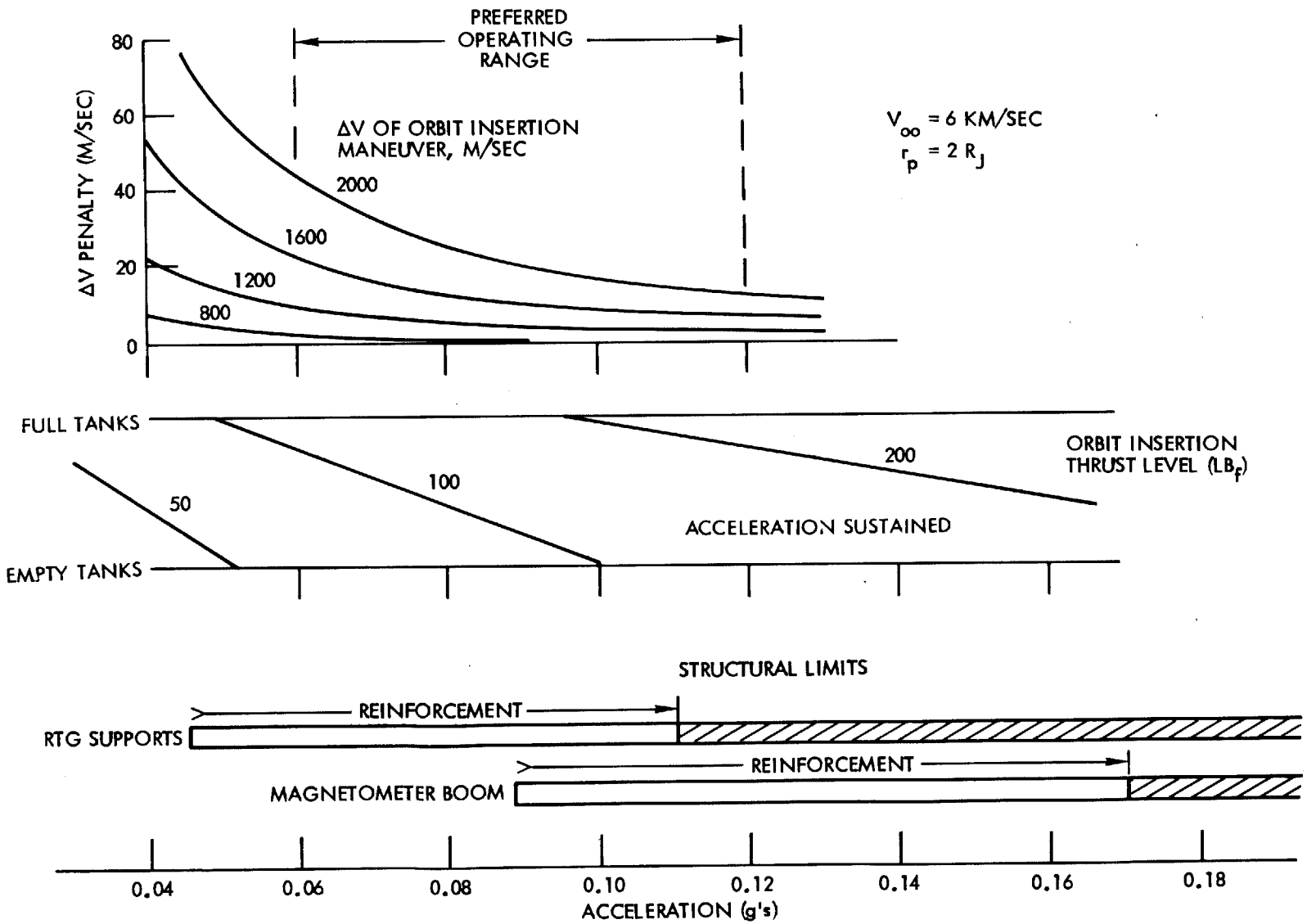

Figure 3-18. Thrust Level Considerations (Jupiter Orbiter)

3.8 TELEMETRY ALLOCATIONS

Table 3-10 identifies the list of telemetry measurements required to monitor and control the spacecraft performance. The majority of measurement sources are identical to Pioneer F/G and are retained intact. These have been augmented with telemetry allocations for new functions peculiar to the orbiter mission, e.g., the X-band transmitters and the bipropellant stage.

The telemetry measurements are identifed as bilevel, analog, or digital signals. Bilevel measurements provide indications of operational status of spacecraft subsystems and scientific instruments such as switching and position functions. Analog signals include voltage, temperature, and current measurements. Digital measurements provide quantitative information from the measurement sources.

Table 3-10. Telemetry Allocations

Telemetry Measurement Source	Number Required	Bilevel	Digital	Analog
COMMAND DISTRIBUTION				
Decoder A addressed	1	X		
Decoder A addressed	1	X		
Command memory enable/disable status	1	X		
Command memory 1 contents - command 8 bits	1		X	
Command memory 2 contents - command 8 bits	1		X	
Command memory 1 contents - time 8 bits	1		X	
Command memory 2 contents - time 8 bits	1		X	
Command memory 1 contents - time 8 bits	1		X	
Command memory 2 contents - time 8 bits	1		X	
Command memory 1 contents - routing 3 bits	1		X	
Command memory 2 contents - routing 3 bits	1		X	
Command execute flip-flop status	1	X		
Spacecraft separation status	1	X		
Ordnance safe/arm relay status (prime)	1	X		
Ordnance safe/arm relay status (redundant)	1	X		
Capacitor bank charge status	1	X		
OIM ordnance safe/arm motor status	4	X		
Overload protection status	1	X		
CDU +5 V bus select status	1	X		
Magnetometer boom release status	1	X		
Magnetometer boom extend/retract status	1	X		
RTG-1 deploy status	1	X		
RTG-2 deploy status	1	X		
Ordnance safe/arm	1	X		
Ordnance safe/arm	1	X		
Ordnance safe/arm	1	X		
Ordnance safe/arm	1	X		
Sequencer status	1	X		
Sequencer power status	1	X		
Undervoltage override	1	X		
Command processor memory status	1	X		
ELECTRICAL POWER				
Shunt bus current	1			X
Bus current	1			X
Bus voltage	1			X
Bus voltage (exp scale)	1			X
CTRF A/inverter B transfer on/off	1	X		
CTRF B/inverter A transfer on/off	1	X		
TRF +5 VDC output CDU bus A	1			X
TRF +5 VDC output CDU bus B	1			X
RTG-1 current	1			X
RTG-2 current	1			X
RTG-1 voltage	1			X
RTG-2 voltage	1			X
DATA HANDLING				
MU 1 on/off status	1	X		
MU 2 on/off status	1	X		
MU 3 on/off status	1	X		
MU 4 on/off status	1	X		
MU 5 on/off status	1	X		
DTU redundancy A/B status	1	X		
Data coding mode (convolutional encoder on/off)	1	X		
Mode I.D.	3		X	
Bit rate I.D.	3		X	
Format I.D.	5		X	
Extended frame counter I.D. words	1		X	
SPSG mode select (ACS, average, nonaverage)	2	X		
Roll pulse/roll-index pulse PH error word	1		X	
Spin period measurement words	3		X	
A/D calibration voltage, low	1			X
A/D calibration voltage, medium	1			X
A/D calibration voltage, high	1			X
Roll attitude timer words	2		X	
SPSG roll reference (0 deg/180 deg)	1	X		
DSU configuration select status word	1		X	

Table 3-10. Telemetry Allocations (Continued)

Telemetry Measurement Source	Number Required	Bilevel	Digital	Analog
COMMUNICATIONS				
Receiver A AGC conscan	1			X
Receiver B AGC conscan	1			X
Receiver reverse enable status	1	X		
Receiver A signal presence status	1	X		
Receiver B signal presence status	1	X		
Receiver A OSC status	1	X		
Receiver B OSC status	1	X		
Receiver A loop stress	1			X
Receiver B loop stress	1			X
Receiver A VCO temperature	1			X
Receiver B VCO temperature	1			X
Receiver A signal strength	1			X
Receiver B signal strength	1			X
Receiver A AGC	1			X
Receiver B AGC	1			X
Driver A temperature (S-band)	1			X
Driver B temperature (S-band)	1			X
Transmitter A on/off status (S-band)	1	X		
Transmitter B on/off status (S-band)	1	X		
Conscan A sin θ	2		X	
Conscan A cosine θ	.2		X	
Conscan threshold mode status	1		X	
Conscan thruster phase output status	1		X	
Conscan signal threshold	1	X		
Conscan on/off status	1	X		
Conscan to DSL	1	X		
Converter temperature, S-band TWTA-A	1			X
Converter temperature, S-band TWTA-B	1			X
Converter temperature, X-band TWTA-A	1			X
Converter temperature, X-band TWTA-B	1			X
Cathode current, S-band TWTA-A	1			X
Cathode current, S-band TWTA-B	1			X
Cathode current, X-band TWTA-A	1			X
Cathode current, X-band TWTA-B	1			X
Helix current, S-band TWTA-A	1			X
Helix current, S-band TWTA-B	1			X
Helix current, X-band TWTA-A	1			X
Helix current, X-band TWTA-B	1			X
Power output monitor, S-band TWTA-A	1			X
Power output monitor, S-band TWTA-B	1			X
Power output monitor, X-band TWTA-A	1			X
Power output monitor, X-band TWTA-B	1			X
TWTA-1 temperature (S-band)	1			X
TWTA-2 temperature (S-band)	1			X
TWTA-1 temperature (X-band)	1			X
TWTA-2 temperature (X-band)	1			X
Driver A temperature (X-band)	1			X
Driver B temperature (X-band)	1			X
Transmitter A on/off status (X-band)	1	X		
Transmitter B on/off status (X-band)	1	X		
Receiver switch position	1	X		
Transmitter switch position (S-band)	1	X		
Transmitter switch position (X-band)	1	X		
THERMAL				
RTG-1 fin root temperature	1			X
RTG-2 fin root temperature	1			X
RTG-1 hot junction temperature	1			X
RTG-2 hot junction temperature	1			X
Temperature hexagonal platform -X axis	1			X
Temperature hexagonal platform -X, +Y	1			X
Temperature hexagonal platform +X, -Y	1			X
Temperature hexagonal platform +X axis	1			X
Temperature experiment platform +X axis	1			X
Temperature experiment platform +X, -Y	1			X
Temperature experiment platform -X axis	1			X
Temperature experiment platform -X, +Y	1			X
Shunt regulator compartment temperature	1			X

Table 3-10. Telemetry Allocations (Continued)

Telemetry Measurement Source	Number Required	Bilevel	Digital	Analog
ATTITUDE CONTROL				
ACS sequence status (note 1)	1		X	
Clock select (note 2)	1		X	
Roll pulse present status	1		X	
Sun sensor temperature	1			X
CEA power status (note 3)	1		X	
Reference select (note 4)	1		X	
ACS registers inhibit status	1		X	
Precession register 1 status (arm/disarm)	1		X	
Delta V register status (arm/disarm)	1		X	
Precession register 2 status (arm/disarm)	1		X	
Precession pair select (axial)	1	X		
Pulse length select (note 5)	1		X	
Delta V pair select	2		X	
Spin control direction status	2	X		
SCT delta V mode status	2	X		
Number 1 precession magnitude	2		X	
Number 1 precession magnitude redundant	2		X	
Number 1 precession angle	2		X	
Delta V magnitude	2		X	
Delta magnitude redundant	2		X	
Delay register	1		X	
Number 2 precession magnitude	2		X	
Number 2 precession magnitude redundant	1		X	
Number 2 precession angle	2		X	
Delta V/SCT pair select	1		X	
SRA temperature	1			X
Star delay	2		X	
Star count	1		X	
Experiment drive assembly position counter	3		X	
Experiment drive assembly - SW 1 position	1	X		
Experiment drive assembly - SW 2 position	1	X		
Experiment drive assembly - SW 3 position	1	X		
Auxiliary roll reference SW position	4	X		
PROPULSION				
Monopropellant System				
VPT firing status	4	X		
SCT firing status	4	X		
SCT thruster pulse count	4		X	
VPT thruster pulse count	4		X	
Propellant supply pressure	1			X
Thruster temperatures	9			X
Nitrogen tank temperature	1			X
Propellant supply temperature	1			X
Spin control thruster 1 pulse count	1		X	
Spin control thruster 2 pulse count	1		X	
Spin control thruster 3 pulse count	1		X	
Spin control thruster 4 pulse count	1		X	
PSA line temperature, +Y	1			X
PSA line temperature, -Y	1			X
Bipropellant System				
Isolation valve position indication	2	X		
Propellant supply pressure	1			X
Oxidizer tank pressure	1			X
Fuel tank pressure	1			X
Oxidizer tank temperature	2			X
Fuel tank temperature	2			X
Pressurant tank temperature	1			X
Thruster temperature	1			X
Fuel valve position	2	X		
Oxidizer valve position	2	X		
Thruster motor valve position	1	X		
Thruster firing status	1	X		

Table 3-10. Telemetry Allocations (Continued)

Telemetry Measurement Source	Number Required	Bilevel	Digital	Analog
SCIENCE				
Summary Preliminary Allocations				
Experiments	30	X		
Experiments	22			X
Experiments	8		X	
Instrument Allocations				
Spin scan imager				
Power on/off status	1	X		
Housekeeping	TBD	X		
Housekeeping	TBD			X
Charged particle instrument				
Power on/off status	1	X		
Housekeeping	TBD	X		
Housekeeping	TBD			X
Data word line	1		X	
Suprathermal particle detector				
Power on/off status	1	X		
Housekeeping	TBD	X		
Housekeeping	TBD			X
Data word line	1		X	
RF sweep receiver				
Power on/off status	1	X		
Housekeeping	TBD	X		
Housekeeping	TBD			X
Data word line	1		X	
UV spectrometer				
Power on/off status	1	X		
Housekeeping	TBD	X		
Housekeeping	TBD			X
Data word line	1		X	
Magnetometer				
Power on/off status	1	X		
Data word line	1		X	
Plasma analyzer				
Power on/off status	1	X		
Housekeeping	TBD	X		
Housekeeping	TBD			X
Data word line	1		X	
IR radiometer				
Power on/off status	1	X		
Housekeeping	TBD	X		
Housekeeping	TBD			X
Data word	1		X	
Plasma wave detector				
Power on/off status	1	X		
Housekeeping	TBD	X		
Housekeeping	TBD			X
Data word line	1		X	

NOTES TO TABLE

1. ACS Sequence Status

000	Reset
100	Delay number 1
010	Precession number 1
110	Delay number 2
001	Delta velocity
101	Delay number 3
011	Precession number 2
111	Not used

2. Clock Select

11	Normal reset (A&B)
01	Clock A (A only)
10	Clock B (B only)
00	Reset reverse (B&A)

3. CEA Power Status

000	Mode A - standby (no power on)
100	Mode C - partial 1 (DSLA power on, DSLB and PSE power off)
010	Mode D - partial 2 (DSLB power on, DSLA and PSE power off)
110	Not used
001	Mode B - storage (PSE power on, DSLA and DSLB power off)
101	Mode E - total 1 (PSE and DSLA power on, DSLB power off)
011	Mode F - total 2 (PSE and DSLB power on, DSLA power off)
111	Not used

4. Reference Select Status

00	Error
01	Magnetometer
10	Sun B
11	Sun A

5. Pulse Length

000	Not used
001	0.03125 sec
010	Not used
011	0.125 sec
100	2.0 sec
101	Not used
110	1.0 sec
111	0.5 sec

3.9 COMMAND ASSIGNMENTS

The command list, organized by spacecraft subsystem is shown in Table 3-11. Command assignments are identical to Pioneer F/G wherever practical. However, the unique requirements required to support the orbiter missions have been included.

Commands are categorized as serial, pulse, or state. Serial commands are routed to the DTU, CEA, command memory processor, and the DSU according to the following routing address code.

Routing Address Code	Destination
000	Not used
001	CDU real-time commands
010	CDU command memory data
011	DSU command data
100	DTU command data
101	ACS command data
110	Experiment drive assembly
111	Not used

The DTU and DSU serial commands are decoded internally. A breakdown of these commands is shown in the command list; to distinguish them from discrete commands they are identified as digital commands. Pulse commands initiate modes, operations, fire ordnance, etc. State commands are typically used to control power to various units, such as the scientific instruments and to enable/disable various spacecraft functions.

Table 3-11. Command List

Command Title	Number Required	Pulse	Serial	State	Digital
COMMAND DISTRIBUTION					
Memory address counter reset	1	X			
Memory time counter reset	1	X			
Execute stored sequence	1	X			
Stop stored sequence	1	X			
Memory time register update	1		X		
Memory address pre-set	1		X		
Spacecraft ordnance safe	1	X			
Spacecraft ordnance arm	1	X			
Safe OIM ordnance	1			X	
Arm OIM ordnance	2			X	
Fire OIM ordnance	2	X			
Overload protection on	1	X			
Overload protection off	1	X			
Memory - command processor 1 select	1	X			
Memory - command processor 2 select	1	X			
CDU select 5 VDC bus A	1	X			
CDU select 5 VDC bus B	1	X			
Release magnetometer boom - ordnance	1	X			
All experiments off	1	X			
Start sequencer	1	X			
Sequencer inhibit	1	X			
Sequencer enable	1	X			
RTG/magnetometer deployment	1	X			
RTG/magnetometer deployment (redundant)	1	X			
-Y line heater off	1			X	
-Y line heater on	1			X	
+Y line heater off	1			X	
+Y line heater on	1			X	
Receiver signal present override	1	X			
Receiver signal present reset	1	X			
ELECTRICAL POWER					
CTRF A/inverter B transfer off/on	2	X			
CTRF B/inverter A transfer off/on	2	X			
RTG relay reset	1	X			
Inverter-A relay	2	X			
Inverter-B relay	2	X			
DATA HANDLING					
MU 1 on/off	2				X
MU 2 on/off	2				X
MU 3 on/off	2				X
MU 4 on/off	2				X
MU 5 on/off	2				X
Real time mode	1				X
Telemetry store mode	1				X
Memory readout mode	1				X
Select and enable MU No. 1	1				X
Select and enable MU No. 2	1				X
Select and enable MU No. 3	1				X
Select and enable MU No. 4	1				X
Select and enable MU No. 5	1				X
Select DSU store DTU data only	1				X
DTU redundancy A	1	X			
DTU redundancy B	1	X			
Coded data mode	1				X
Uncoded data mode	1				X
Bit rate - 32 bits/s	1				X
Bit rate - 64 bits/s	1				X
Bit rate - 256 bits/s	1				X
Bit rate - 1024 bits/s	1				X
Bit rate - 4096 bits/s	1				X
Bit rate - 8192 bits/s	1				X
Bit rate - 16,384 bits/s	1				X
Bit rate - 32,768 bits/s	1				X

Table 3-11. Command List (Continued)

Command Title	Number Required	Pulse	Serial	State	Digital
DATA HANDLING (CONTINUED)					
Format A	1				X
Format B	1				X
Format C	1				X
Format C - 1	1				X
Format C - 2	1				X
Format C - 3	1				X
Format C - 4	1				X
Format A/D - 1	1				X
Format A/D - 2	1				X
Format A/D - 3	1				X
Format A/D - 4	1				X
Format B/D - 1	1				X
Format B/D - 2	1				X
Format B/D - 3	1				X
Format B/D - 4	1				X
Roll reference 0 deg	1				X
Roll reference 180 deg	1				X
Spin averaging mode	1				X
Non-averaging mode	1				X
ACS mode SPSG	1				X
Memory halt mode	1				X
Memory continue mode	1				X
COMMUNICATIONS					
Receiver reverse inhibit	1	X			
Receiver reverse enable	1	X			
Receiver A coherent mode on	1			X	
Receiver A coherent mode off	1			X	
Receiver B coherent mode on	1			X	
Receiver B coherent mode off	1			X	
Transmitter A on (S-band)	1	X			
Transmitter A off (S-band)	1	X			
Transmitter B on (S-band)	1	X			
Transmitter B off (S-band)	1	X			
Conscan to DSL enable	1	X			
Conscan to DSL inhibit	1	X			
Conscan on	1	X			
Conscan off	1	X			
Conscan 0 deg output	1	X			
Conscan 180 deg output	1	X			
Conscan threshold high	1	X			
Conscan threshold low	1	X			
TWTA-A (S-band) to high-gain antenna	1	X			
TWTA-A (S-band) to medium-gain antenna	1	X			
Receiver A to high-gain antenna	1	X			
Receiver A to medium-gain antenna	1	X			
TWTA-A (X-band) to antenna	1	X			
TWTA-B (X-band) to antenna	1	X			
Transmitter-A on (X-band)	1	X			
Transmitter-A off (X-band)	1	X			
Transmitter-B on (X-band)	1	X			
Transmitter-B off (X-band)	1	X			
ATTITUDE CONTROL					
Sequence execute	1	X			
Sequence inhibit	1	X			
Sequence override	1	X			
Sequence reset	1	X			
Sequence step	1	X			
Duration/steer logic A select (DSL A on, B off)	1	X			
Duration/steer logic B select (DSL B on, A off)	1	X			

Table 3-11. Command List (Continued)

Command Title	Number Required	Pulse	Serial	State	Digital
ATTITUDE CONTROL (CONTINUED)					
PSE on, DSL off (standby power on)	1	X			
Program storage and execute off	1	X			
Arm register 1 (No. 1 precession magnitude/angle)	1	X			
Arm register 2 (Delta V/delay)	1	X			
Arm register 3 (No. 2 precession magnitude/angle)	1	X			
Pulse length 1	1	X			
Pulse length 2	1	X			
Pulse length 3	1	X			
Pulse length 4	1	X			
Pulse length 5	1	X			
Delta V pair 1 select (axial)	1	X			
Delta V pair 2 select (axial)	1	X			
Delta V pair 3 select (transverse)	1	X			
Delta V pair 4 select (transverse)	1	X			
Spin direction up (transverse)	1	X			
Spin direction down (transverse)	1	X			
Precession pair 1 select	1	X			
Precession pair 2 select	1	X			
Precession pulse, 0 deg (axial)	1	X			
Precession pulse, 90 deg (axial)	1	X			
Precession pulse, 180 deg (axial)	1	X			
Precession pulse, 270 deg (axial)	1	X			
Real-time spin pulse	1	X			
Real-time precession pulse (axial)	1	X			
Real-time spin/Delta V pulse (transverse)	1	X			
Real-time axial Delta V pulse	1	X			
SCT/Delta V mode select	1	X			
Clock reset	1	X			
Sensor select sun A	1	X			
Sensor select sun B	1	X			
Time frequency select A	1	X			
Time frequency select B	1	X			
Despin start	1	X			
Sensor select star	1	X			
Sensor select magnetometer	1	X			
Sensor select clock	1	X			
Automatic star mode	1	X			
Star gate enable	1	X			
Star gate disable	1	X			
Star delay up - least significant	1	X			
Star delay up - most significant	1	X			
Star delay down - least significant	1	X			
Star delay down - most significant	1	X			
Star time gate enable	1	X			
Star time gate decrement	1	X			
Star time gate increment	1	X			
Experiment drive assembly - set No. of steps, n	1				
Experiment drive assembly - set No. of steps/pulse	1				
Experiment drive assembly - set rate m	1				
Experiment drive assembly - SW 1 open	1	X			
Experiment drive assembly - SW 1 close	1	X			
Experiment drive assembly - SW 2 open	1	X			
Experiment drive assembly - SW 2 close	1	X			
Experiment drive assembly - SW 3 open	1	X			
Experiment drive assembly - SW 3 close	1	X			

Table 3-11. Command List (Continued)

Command Title	Number Required	Pulse	Serial	State	Digital
PROPULSION					
Isolation valve open	1	X			
Isolation valve close	1	X			
Isolation valve (redundant) open	1	X			
Isolation valve (redundant) close	1	X			
Multicycle fuel valve open	1	X			
Multicycle fuel valve close	1	X			
Multicycle fuel valve (redundant) open	1	X			
Multicycle fuel valve (redundant) close	1	X			
Multicycle oxidizer valve open	1	X			
Multicycle oxidizer valve close	1	X			
Multicycle oxidizer valve (redundant) open	1	X			
Multicycle oxidizer valve (redundant) close	1	X			
Thrust motor valve open	1	X			
Thrust motor valve close	1	X			
Bipropellant tank heaters	4			X	
Bipropellant thruster heater	1			X	
Science					
Summary Preliminary Allocations					
Total commands (pulse)		X			
Total commands for orbiter experiments (state)				X	
Proposed Allocations					
Spin scan imager	2			X	
Power on/off	2			X	
Discrete commands	TBD	X			
Charged particle instrument					
Power on/off	2			X	
Discrete commands	TBD	X			
Suprathermal particle detector					
Power on/off	2			X	
Discrete commands	TBD	X			
RF sweep receiver					
Power on/off	2			X	
Discrete commands	TBD	X			
UV spectrometer					
Power on/off	2			X	
Discrete commands	TBD	X			
Magnetometer					
Power on/off	2			X	
Discrete commands	TBD	X			
Plasma analyzer					
Power on/off	2			X	
Discrete commands	TBD	X			
IR radiometer					
Power on/off	2			X	
Discrete commands	TBD	X			
Plasma wave detector					
Power on/off	2			X	
Discrete commands	TBD	X			

4. SUBSYSTEM DESIGN

4.1 Structure

The structure subsystem carries primary flight loads, provides the physical interface to the launch vehicle, and includes secondary mounting provisions for all spacecraft assemblies. A major new addition to the Pioneer F/G original spacecraft structure is the support truss which accommodates the bipropellant retro-propulsion subsystem. The structure includes provisions for meteoroid and thermal protection of critical components. It incorporates access provisions to facilitate integration, assembly, and maintenance. The structure subsystem also includes all deployment mechanisms as well as any required balance weights. The structure must survive the powered-flight environment and other environments that currently apply to the Pioneer F/G spacecraft (see NASA/ARC Specification PC-210.02 for further definition of design environments). It must also sustain the thrust acceleration loads acting on the deployed appendages during major maneuver phases.

The structure subsystem of the selected Pioneer orbiter configuration described in Section 3.1 (see Figures 3-2 and 3-3) consists of the modified Pioneer F/G spacecraft structure and the added support structure for the spacecraft and the new retro-propulsion subsystem. The support structure also referred to as propulsion bay includes an interstage adapter ring which is attached to the 37 x 31 inch launch vehicle upper stage adapter. The cylindrical 25 x 13 inch adapter ring used in the Pioneer F/G configuration is eliminated.

Principal modifications to the Pioneer F/G spacecraft structure are summarized as follows:

- An added rectangular compartment on the -X axis accommodates the increased science payload, including the articulated optical sensor package
- The internal equipment is rearranged for appropriate mass balance and to accommodate new instruments
- Louvered equipment compartment side panels are used for equipment mounting to permit unobstructed thermal radiation, since radiation in aft direction is partially blocked by the added propulsion stage.
- The 25-inch diameter fiberglass interstage, separation ring flange and boron filament-epoxy platform support struts are eliminated. A structural truss is added to support the platform, the hydrazine propellant tank and the new GN_2 pressurant tank
- The two larger multi-hundred watt RTG units which replace the four Pioneer F and G RTG units are supported by structurally strengthened deployment arms

- The magnetometer boom and damper are modified to provide sufficient strength for deboost loads and higher deployment taking into account the added tip mass loads

- An aluminum honeycomb sandwich panel closeout is added at the 37-inch diameter separation ring flange to provide micrometeoroid protection at the aft end of the propulsion stage.

4.1.1 Equipment Compartment

The equipment compartment previously illustrated in Figure 3-5 consists of three sections

- The hexagonal center section

- The hexagonal experiment bay (on the +X axis)

- An added rectangular extension bay (on the -X axis) which also supports an articulated optical sensor package.

The first two sections are essentially of the same construction as in Pioneer F/G. The add-on bay is of similar construction. The primary structural elements consist of aluminum honeycomb material for the floor and side panels, tied together with an external box structure employing angle sections and fittings. Since some of the side walls in the modified configuration are used as equipment mounting panels the honeycomb sandwich face sheets are increased in thickness from 0.010 to 0.016 inch, and the core thickness is increased from 0.50 to 0.75 inch.

The equipment layout (see Figure 3-5) is arranged to take into consideration such factors as static and dynamic balance, moment-of-inertia ratios, thermal control requirements, sensor fields of view, ease of assembly and minimum cable length. Changes in the distribution of components in the equipment compartment from the Pioneer F/G layout are dictated in part by functional modifications of the system for the orbiter mission, viz., the addition of the retro-propulsion bay, the new RTG units, the addition of an X-band communication capability and the change of scientific payload equipment. However, even with these modifications the arrangement of subsystems and experiments, and the support of external structure and appendages, including their deployment provisions, remain quite similar to the corresponding features of Pioneer F/G.

4.1.2 Propulsion Bay and Interstage Structure

The truss structure which houses the propulsion bay and supports the spacecraft on top of the launch vehicle is shown in the design drawings, Figures 3-2 and 3-3. A perspective view is shown in Figure 3-4. The lower end of this structure mates with the standard 37 x 31 inch launch vehicle third stage attach fitting. The upper end is attached to the structure of the spacecraft centerbody at the corners of the main hexagonal equipment compartment.

The 37-inch diameter interstage adapter ring distributes the concentrated loads of the four propellant tanks and eight support struts nearly uniformly for transfer to the mounting flange of the launch vehicle attach fitting. Load distribution is aided by four mounting fixtures which spread the tank and truss loads laterally over the upper adapter ring flange (see Figure 3-4) and the 6-inch cylindrical height of the ring structure.*

Load paths across the propulsion bay and support structure are separated into principal spacecraft loads, transferred through the trusswork to the adapter ring, and principal propellant tank loads, carried directly by this ring. The upper mounting bosses of the four propellant tanks are canted outward to give the desired lateral mass distribution of the propulsion bay. They are held by four pairs of connecting struts which transfer lateral (secondary) tank loads to the equipment compartment support points and from here into the main support truss. This design precludes a load transfer of the main spacecraft structure into the propellant tanks.

The support structure is designed to accommodate maximum longitudinal loads of +9.3 and -3.5 g and lateral loads of $\pm$3.9 g. Dimensions and margins of safety of the structural elements and their critical failure modes are listed in Table 4.1. The estimated structural weight is 33.2 pounds assuming aluminum construction.

Table 4-1. Summary of Minimum Margins of Safety

Structural Element	Critical Failure Mode	Margin of Safety
Primary struts (2-in. dia. x 0.040-in. wall)	Compression yield	0.60
Tank support struts (1-in. dia x 0.040-in. wall)	Compression yield	0.24
Lower ring (2-1/2 x 2-1/2 angle with lip)	Flange crippling	0.18
Cross beam (I section)	Flange crippling	0.34

Thermal isolation requirements may favor a change to titanium or fiberglass struts and tank support fittings in order to reduce thermal conductivity of the structure. Use of fiberglass, having a lower stiffness to sensity ratio (E/ρ) compared to aluminum, introduces a structural weight penalty in exchange for obtaining the desired thermal isolation characteristics. Table 4-2 summarizes the thermal conductivity and stiffness to

*The design drawings, Figures 3-2 and 3-3, show an earlier version with only 4-inch cylindrical height.

Table 4-2. Candidate Structural Materials and Significant Material Properties

	K (BTU ft/hr-ft^2 ^{o}F)	E (10^6 PSI)	ρ (lb/in.^{3})	E/ρ (10^6 in.)
Aluminum	96	10.7	0.1	107
Stainless Steel	3.5	16.0	0.16	100
Stainless steel	10	26	0.286	91
Fiberglass	0.09	3	0.061	50
Graphite/Epoxy	38/9	12.3	0.067	205
Boron/Epoxy	1	35	0.075	467

K = thermal conductivity
E = elastic modulus
ρ = density

density ratio (E/ρ) for several representative structural materials. Next to fiberglass, boron/epoxy composite material exhibits lower conductivity than the others but a significantly higher E/ρ ratio. A structural weight penalty of up to 10 percent may accrue depending on the degree of thermal isolation to be attained.

The propulsion bay and interstage structure is designed as a self-contained module to facilitate separate handling and testing prior to integration with the remainder of the spacecraft. A removable upper frame is substituted to provide rigidity to the trusswork during these operations.

In addition to supporting the spacecraft proper and the propellant tanks the structure also provides support for the 100-pound main engine mounted at the bottom of the propulsion bay and the 15-inch GN_2 pressurant tank at the top. The truss holding the pressurant tank also provides support to the center of the equipment bay platform, substituting for the cylindrical 25-inch adapter ring originally provided in the Pioneer F/G structural design.

At the bottom of the propulsion bay the structure is closed out with a 1-inch thick aluminum honeycomb sandwich panel which provides micrometeoroid protection and reinforces the interstage adapter ring. This panel also provides mounting space for the omni-directional antenna boom relocated from its original location at the aft equipment platform, and the shunt radiator panel (see Figure 3-2).

4.1.3 High-Gain Antenna Support

The 9-foot diameter reflector, high-gain antenna feed assembly, and medium-gain S-band antenna are all supported via struts mounted directly to the hexagonal section of the equipment compartment. The strut arrangement is identical to the Pioneer F/G.

One potential modification is the addition of attach fittings on one of the feed support struts for the new X-band waveguide between the TWTA and the feed. Modifications to the feed assembly itself are described in Section 4.8.

4.1.4 RTG Support Assembly

The RTG selected for the Jupiter and Saturn orbiter missions necessitates some change in the RTG deployment hardware even though the deployment concept remains unchanged. The MHW units are 50 pounds heavier than the four SNAP-19 RTG's of the Pioneer F/G spacecraft. The increased weight, the fact that there are two units rather than four, and the changed mounting geometry require modifications of the RTG support structure. Figure 4-1 shows the Pioneer F/G support structure and deployment mechanism. The orbiter configuration replaces the bipod truss and the triangular fitting by a mounting plate.

The main thrust maneuvers at acceleration levels as large as 0.12 g acting on the deployed RTG's impose greatly increased bending loads on the RTG deployment arms, particularly with end masses that are 42 percent heavier than in Pioneer F/G. The tradeoff between performance requirements, favoring a large thrust force, and structural stiffening requirements for the deployed appendages was discussed in Section 3.7. Preliminary analysis of bending and buckling loads in the deployment arm guide rods (see Appendix D) indicates that doubling of the tube wall thickness from 0.03 inch (used in the Pioneer F/G guide rods) to 0.06 inch will be adequate with the higher centrifugal load in the deployment arms due to increased spin rate (15 rpm) during thrust phases. This guide rod reinforcement increases the total weight by about three pounds. The deployment guides and retention fittings on the equipment compartment also require strengthening to accommodate the larger structural loads on the RTG booms.

4.1.5 Magnetometer Boom Assembly

In Section 3.1 various solutions for control of the spacecraft principal axes of inertia were discussed. The selected approach involved the addition of a 25-pound counterweight to the magnetometer boom.

A preliminary structural investigation of the present Pioneer F/G magnetometer boom was conducted to determine whether the boom would tolerate the added counterweight under the more demanding deployment loads and large axial thrust accelerations. The results of the investigation indicated that although the present design concept may be feasible, the added boom structural weight necessary to withstand the higher loads makes the present design insufficient.

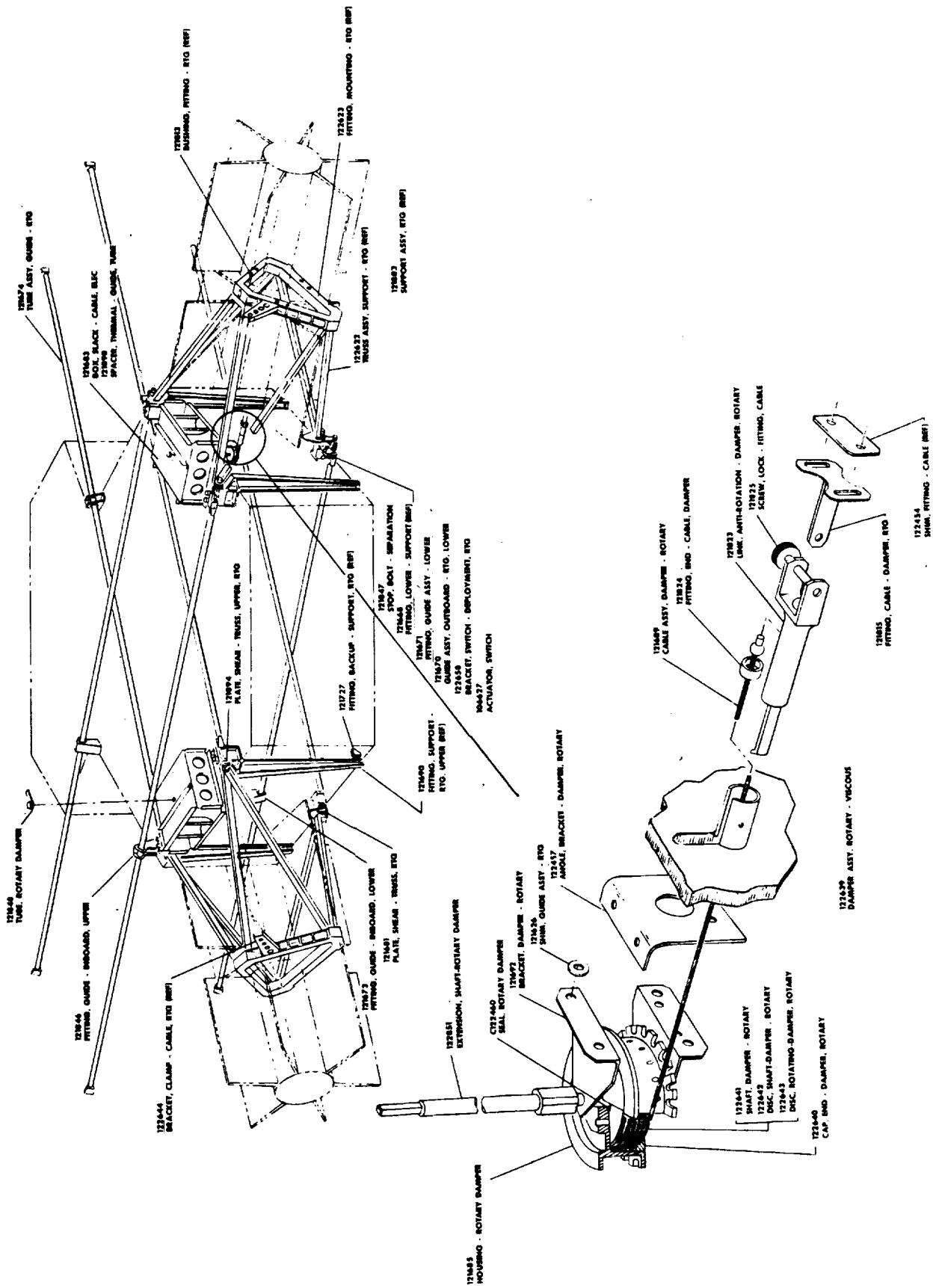

Figure 4-1. RTG Deployment and Support Structure of Pioneer F, G

Investigation of the effect on the magnetometer boom design of the addition of the counterweight, the initiation of deployment at a higher spacecraft spin rate, and the bending loads due to large thrust acceleration shows that the following items have to be considered:

- Higher launch loads (vibration, quasi-static acceleration)
  - support structure
  - boom structure
- Higher deployment loads
  - deployment damper
  - boom structure
  - release loads
  - centrifugal forces
  - Coriolis forces
  - latch loads
- Higher loads in deployed configuration
  - axial thrust acceleration up to 0.12 g
  - boom as cantilever beam
  - wobble damper and pivot mechanism.

In Pioneer F/G the primary portions of the magnetometer boom are designed for loads experienced at the initiation of deployment. Loaded portions of the boom at the stowed boom support points are designed by launch vibration loads.

Structural loads generated during boom deployment are from three effects:

1) The energy release due to the preload in the tie-down mechanism

2) The centrifugal force on the boom, magnetometer and counterweight

3) Lateral forces due to Coriolis acceleration.

To accommodate the increased deployment and thrust loads a redesign of the boom structure and support provisions is required. To retain as much of the present design concept as possible the following steps were considered:

1) Release the boom in two stages, i.e., release the preload in the center tie prior to release of the boom from the spacecraft to reduce the initiation-of-deployment loads

2) Replace the present deployment damper with one that would tie to the outer boom segment, which incorporates the counterweight. This would tend to unload the boom constraint cables, and thus unload the boom structure.

3) Reduce the rate of deployment by increasing the deployment damper's viscous damping constant, in order to reduce Coriolis accelerations.

An alternative magnetometer boom design would be to incorporate a scissors type deployment mechanism as shown in Figure 4-2. The scissors concept allows a controlled symmetrical deployment while considerably reducing the loads in the boom tube segments. The fully deployed boom will have the same structural and mechanical characteristics as the present design concept.

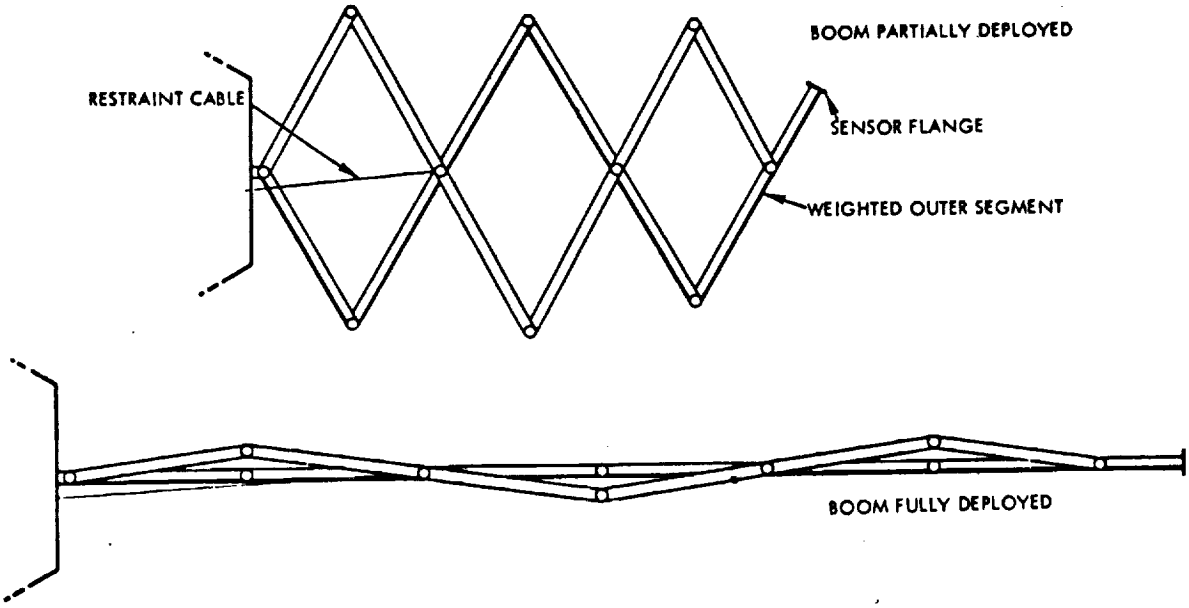

Figure 4-2. Scissors Type Magnetometer Boom

Although the scissors mechanism provides structural stiffening against deployment loads acting in the X, Y plane it does not provide reinforcement against thrust acceleration loads acting in the -Z direction, since only the primary boom will have locked joints when fully deployed. However, increasing the spin rate to 15 rpm during thrust phases in effect provides boom stiffening through centrifugal action, with the resultant force at the tip mass inclined only 4 to 5 degrees against the X, Y plane.

Actually the hinged magnetometer boom can be deflected without bending to an excursion of ± 3 degrees from the X axis, reaching a limit stop on the wobble damper assembly at this point. This means that the bending deflection of the boom is only as large as to permit the boom tip to align itself with the resultant force vector, requiring a differential angle of only 1 to 2 degrees, at the time of worst-case axial acceleration loads, when the propellant tanks are nearly empty.

An analysis of boom deflection characteristics under the influence of increased spin rate is given in Appendix D. It can be shown that a spin rate of at least 15 rpm is required to reduce the tilt of the principal axis of inertia due to differential tip mass deflections of the

magnetometer boom and RTG booms to angles of less than 0.25 degree, desirable for maintenance of accurate thrust vector pointing and for accurate antenna beam pointing at earth during the propulsion phase.

An alternative approach of retracting the magnetometer boom during the thrust phase is impractical because of the required mass balance against the deployed RTG booms. Retraction of all three booms is unattractive because it would require a more complicated design of the deployment mechanisms, exposing the system to the possibility of serious new failure modes.

4.2 THERMAL CONTROL

The thermal control subsystem provides the necessary thermal environment for the spacecraft components and scientific instruments throughout the mission including earth shadowing during launch, interplanetary flight, and solar eclipse during orbital operations. For the anticipated environment, temperatures in the vicinity of the internally located scientific instruments will be maintained between 0 and 90°F.

4.2.1 Thermal Control Design Approach

The thermal control concept is predicated on conservation of internal heat generated by the electronic components through the use of high performance insulation and accommodation of the variation in solar intensity and direction by means of temperature-sensitive louvers. Additional factors influencing the thermal survival of the spacecraft include variations in RTG output power and material and surface properties. During the prelaunch operations there is a substantial variation in the thermal control mechanism since conduction and convection replace radiative transfer as the predominant processes for thermal control. To accommodate these variations, the spacecraft utilizes a combination of passive elements (coatings, insulation), semiactive elements (louvers) and active elements (heaters). The final choice of the various elements involves full-scale model testing, computer modeling, and full-scale qualification testing of flight quality hardware.

Important features of the thermal control subsystem of the Pioneer Outer Planets Orbiter include:

- The equipment and propulsion sections are thoroughly insulated to make them as independent of the sun as possible.
- Active control for the equipment and experiment bays by the use of bimetal-actuated louvers over second surface mirrored radiating areas mounted to the side walls. A somewhat larger total louver area is required because of solar absorptance when the sun sees the side of the spacecraft near the beginning of the mission.
- Twenty-four layer insulation blankets are provided for the propulsion compartment. The compartment is thermally isolated from the other sections.

- A hybrid combination of RHU's and thermostatically controlled electric heaters is used to heat the propulsion section. Preliminary sizing of this combination requires 22 watts of RHU heat and 12 watts of thermostatically controlled electric heat in combination with an 8-watt thermostatically controlled electric heater and 8 watts of RHU power on the bipropellant valve.

- The thermostatically controlled electric heater power requirement for the equipment section consists of 3.4 watts for the lines, 1 watt for the propellant tank and 7 watts for the articulated science package.

The Pioneer F/G louver system consists of 30 individually actuated blades or vanes, 24 of which are positioned radially around the interstage adapter and 6 of which are mounted on the aft side of the experiment platform. Each trapezoidal blade is supported on the larger end by a bimetallic spring/actuator housing assembly and on the smaller end by a lexan bearing assembly which, for the two-bladed assemblies, is contained in the interstage ring. Each blade is constructed from 0.156-inch aluminum honeycomb core with 2-mil aluminum face sheets. The overall blade thickness is approximately 0.160 inch. Functionally, the louver system acts to control the heat rejection of the radiating platform by varying the angular position of a set of highly reflective blades or shutters. A bimetallic spring, radiatively coupled to the platform, provides the motive force for altering the angle of each blade. In a closed condition the heat rejection of the platform is minimized by virtue of the "blockage" of the blades while open louvers provide the platform with a nearly unobstructed view of space. A typical louver angle-spring temperature plot is shown in Figure 4-3.

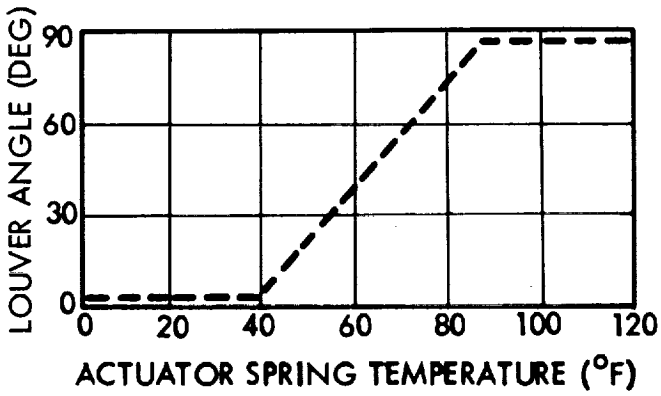

Figure 4-3. Typical Louver Performance Plot

4.2.1.1 Candidate Configurations

In the orbiter configuration the addition of the propulsion bay has the effect of partially blocking thermal radiation from the bottom side of the equipment bay. Various design approaches, shown schematically in

Figures 4-4 through 4-8, were considered to achieve satisfactory thermal control of the equipment compartment. These approaches are described below.

Louvered Platform/Open Propulsion Section (Figure 4-4). This concept relies on a cold propulsion section to remove equipment heat by radiation from the platform. This requires a maximum average propellant section temperature of about 28°F during hot case conditions. For cold case conditions, the equipment platform louvers would be closed.

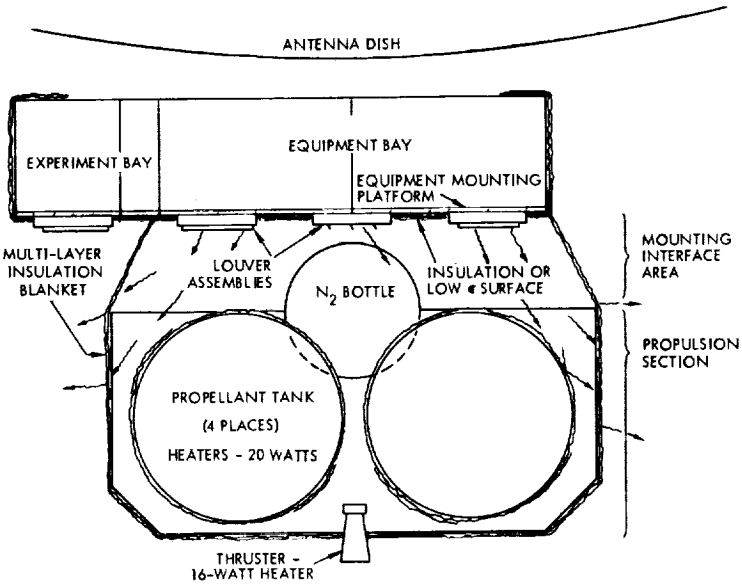

Figure 4-4. Thermal Control by Louvered Platform with Open Propulsion Bay

Advantages	Disadvantages
• Retains current Pioneer approach with aft louvers	• Requires greatly increased louver area
• No limitations on propellant section mounting interface	• Requires high tank heater power
	• Depends on predictable and consistent insulation heat loss

Second Surface Mirror (Figure 4-5). Heat is transferred by radiation from the equipment platform to the rear of the circumferential second surface mirror panels. Since this surface has a low absorptivity/emissivity (α/ϵ) ratio, the effect of solar variations is minimized. A 50-watt platform heater is required to adjust for changing equipment power dissipation. The propulsion section is isolated and insulated. Tanks are insulated and heated by controlled heaters.

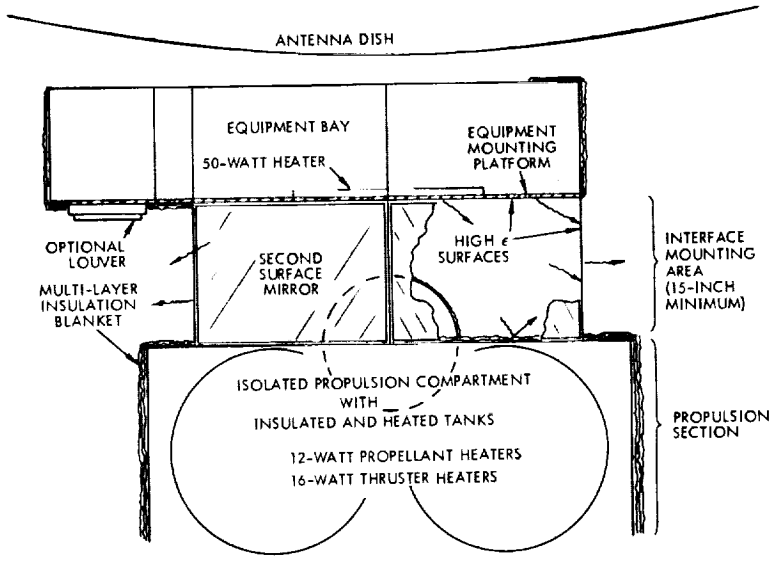

Figure 4-5. Thermal Control by Use of Side-Viewing Second Surface Mirrors

Advantages	Disadvantages
• Simplicity	• Requires substantial heater power late in RTG life
• No weight penalty	• Requires an 18-inch deep propellant section interface area
• Minimum tank heat	

Louvered Platform/Open Truss (Figure 4-6). Insulation on the upper surface of the propellant section is shadowed during the forward-sun condition maintained for most of the mission. Since the aft surfaces have an unobstructed view to space, the open truss acts as an effective re-radiation heat sink for the platform. Changes in platform heat load are handled by the aft-facing louvers. Reflected insolation into the louvers is unacceptable, however, so a side-sun attitude must be avoided. Two solutions to the complex reflection/re-radiation situation in the intersection area were analyzed:

a) High emissivity re-radiation surfaces — most platform heat is absorbed by the outer insulation blanket and re-radiated to space either directly or by reflection from the low antenna dish

and

b) Low emissivity re-radiation surfaces — the platform heat follows the same path, but most is reflected by the surfaces to space.

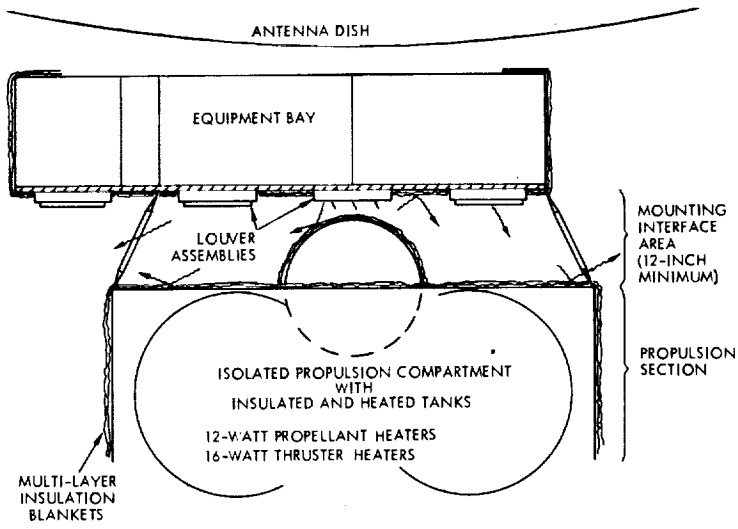

Figure 4-6. Thermal Control by Louvered Platform and Open Truss

Case a) is the most effective. Again, the propulsion section is isolated and insulated. The tanks are heated.

Advantages	Disadvantages
• Retains current Pioneer approach with aft louvers	• Restricts attitude during mission
• Minimum heater power	• Requires a 12-inch deep propellant section interface area

Side Louvers (Figure 4-7). The equipment compartment side walls are used as the heat sink with this approach, providing an unblocked radiative path to space. On the other hand, as they are exposed to solar radiation during the side-sun conditions, a somewhat greater louver area may be necessary and special care must be taken to ensure that a satisfactory α/ϵ ratio can be obtained. The aft surface of the experiment bays are not appreciably blocked by the propulsion section and may retain louver assemblies. The propulsion section is isolated and insulated.

Advantages	Disadvantages
• Minimum heater power	• Requires remounting of heat producing components on the side walls
• No limitations on propellant section mounting interface	• May require increased louver area

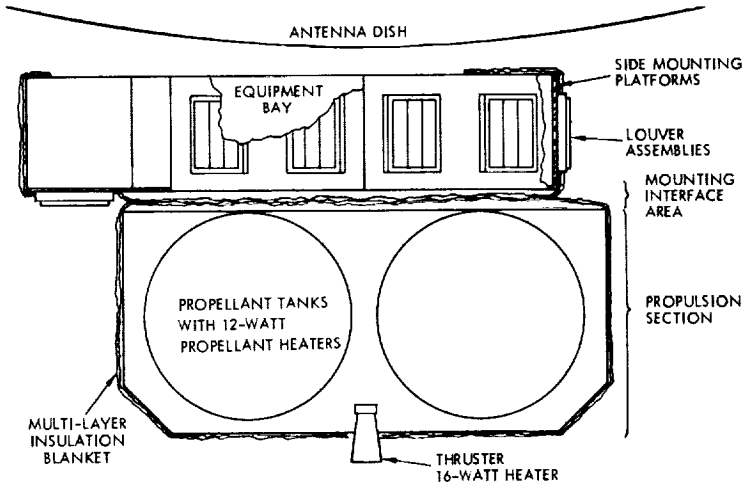

Figure 4-7. Thermal Control by Side Louvers

Heat Pipes (Figure 4-8). This concept is based on transferring heat from the equipment platform to the aft end of the spacecraft with axially-oriented heat pipes. Radial heat pipes could be used to collect the heat from the platform and distribute it over the aft radiator. It is possible to use louvers over the radiator, but a better approach would be to use a controllable heat pipe. Complexity is not increased and greatly improved effectiveness would be obtained. Heat pipes are currently considered a state-of-the-art development. However, this approach may be considered as a practical alternative for missions in the 1980's.

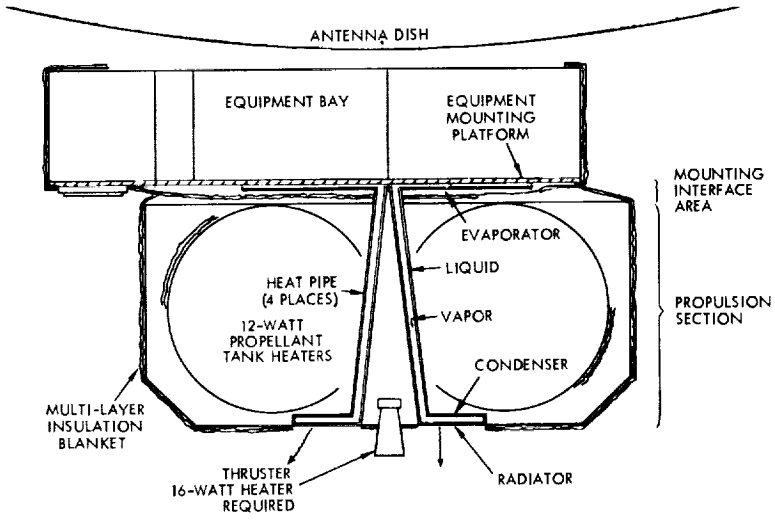

Figure 4-8. Thermal Control by Means of Heat Pipe

Advantages	Disadvantages
• Minimum heater power	• Development effort required
• Simplicity	• Possible weight penalty
• No limitations on propellant section mounting interface	
• Retains aft radiator concept	

Recommended Approach. The side louver approach has been selected for the orbiter because it not only satisfies thermal requirements but also because it ensures the best structural configuration and also one that meets the required dynamic balance conditions.

4.2.1.2 Shunt Regulator Relocation

In order to minimize the temperature problems associated with larger RTG power variations during the orbiter mission, the spacecraft equipment compartment thermal control system incorporates the maximum possible BOL-to-EOL RTG power change control capability. This maximum control capability is achieved by minimizing the change in internal equipment compartment heat dissipation over the mission lifetime. Locating the shunt regulators external to the equipment compartment eliminates a 58-watt heat dissipation change from BOL to EOL conditions. The equipment compartment internal electronic heat dissipation remains essentially constant from BOL to EOL (six years) even though the RTG power output varies from 300 to 242 watts when both RTG's are operative.

The loss of one RTG can be tolerated on the orbiter vehicle even though the RTG and equipment compartment EOL internal electronic heat dissipation decreases by 50 percent. This decrease in RTG power output can only be tolerated if the shunt regulators are located external to the equipment compartment. The equipment compartment internal electronic heat dissipation would decrease 60 percent from BOL (two RTG's) to EOL (one RTG) if the shunt regulators were located inside the PCU as was done on Pioneer F/G.

Locating the shunt regulators external to the equipment compartment does require a 4-watt thermal control heater for these units. The added thermal control heater maintains the shunt regulators above the -70°F minimum temperature limit at EOL when the normal unit heat dissipation approaches zero. Bimetal-actuated louvers are mounted to the shunt regulator radiator plate to minimize EOL required thermal control heater power. The shunt regulators are mounted to a radiating plate mounted to the aft surface of the hexagonal experiment bay. The radiating plate is conductively and radiatively decoupled from the platform with fiberglass insolators and multilayer insulation, respectively. The shunt regulator radiator plate aft surface is painted white and has a louver assembly

attached to it facing aft to control the heat loss to space. The 4-watt thermostatically controlled heater distributes the heat across the radiator plate (turn-on -60°F, turn-off -50°F).

4.2.1.3 1.0 AU Side-Sun Power Decrease

The Pioneer F/G equipment compartment internal electronic heat dissipation is maintained at maximum levels during 1.0 AU side-sun environmental conditions at BOL to obtain maximum science and engineering data. During 1.0 AU side-sun conditions the equipment compartment absorbs approximately 38 watts of additional solar heat compared to 1.0 AU front-sun conditions. The equipment compartment louvers are sized to handle this additional side-sun heat influx. When front-sun conditions are achieved, the equipment compartment net heat input decreases 38 watts (19 percent of 1.0 AU side-sun total) and temperatures decrease approximately 24°F.

In order to maximize the orbiter spacecraft capability to handle RTG BOL to EOL power output changes, it is recommended that the equipment compartment thermal control system should be designed (louver area sizing) to satisfy 1.0 AU front-sun power conditions. If the equipment compartment internal electronic heat dissipation can be reduced during 1.0 AU side-sun conditions to offset the increased absorbed solar heat, the net heat input can be reduced to below the design point 1.0 AU front-sun full power conditions. This approach will eliminate the approximate 38-watt reduction in internal heat input associated with sun angle changes from BOL to EOL. An interim quasi sun-pointing attitude during the first two months following launch, discussed in Section 1.1.4, will meet the requirements. Alternative techniques are described below.

Turning off the X-band transmitter during 1.0 AU side-sun conditions (first 50 days of mission) will more than offset the 38-watt increase in absorbed solar heat input compared to 1.0 AU front-sun conditions. The S-band transmitter should be able to handle all engineering and science data requirements during this time period. If additional electronic heat dissipation reductions were required to hold 1.0 AU side-sun temperature below 1.0 AU front-sun maximum design limit values, some experiments could be turned off, further reducing internal equipment compartment heat dissipation (planetary instruments would not normally be powered at this time).

The powered-down 1.0 AU side-sun approach is not applicable to the Pioneer F/G design because the shunt regulators are located internal to the equipment compartment. If the transmitter or experiments are turned off under 1.0 AU side-sun conditions, the major portion of the excess power will be dissipated in the shunt regulators in the power control unit (PCU). The net heat dissipation in the equipment compartment will not be decreased appreciably; only the distribution will change, concentrating the heat in the PCU.

4.2.2 Thermal Control Heaters

4.2.2.1 Monopropellant System

In order to handle RTG output power variations, the propellant tank and line heaters employed on Pioneer F/G should be retained intact on the orbiter configuration. Redundant resistance wire heaters (1.0 watt) on the tank and each of two internal propellant lines (0.5 watt) prevent freezing of the hydrazine. The heaters are controlled by series-redundant thermostats. Each of the internal line circuits also include a 0.2 watt spot heater near the wall.

Each of two line heater assemblies which are routed external to the equipment compartment consists of a 1-watt primary heater circuit and a redundant secondary circuit, similar to those used on the tank. They are designed to maintain the temperature above $45^{o}F$.

Three radioisotope heater units (RHU's) provide thermal energy (1 watt per unit) to prevent freezing of the hydrazine in each of the four thruster cluster assemblies during non-operating periods.

4.2.2.2 Bipropellant System

The basic approach to thermal control of the bipropellant system is utilization of both electrical and isotope heaters. The RHU's provide a major portion of the thermal input with the electrical heaters used to accommodate worst-case conditions.

Preliminary sizing of this hybrid combination requires 22 watts of RHU heat and 12 watts of thermostatically controlled electric heat for the propellant and oxidizer tanks. An additional 8 watts of RHU power and 8 watts of electrical heater power are recommended for the 100-pound thruster engine.

4.2.2.3 Summary Heater Requirements

Table 4-3 summarizes the thermal control heater requirements for the orbiter mission; the Pioneer F/G heater complement is given to illustrate similarities as well as deviations from the flight-proven configuration.

It should be emphasized that the allocation between electrical heaters and RHU's given here is a compromise. An all-electric thermostatically controlled system gives the optimum thermal solution; the hybrid RHU approach is the lowest cost approach, but it creates thermal and local particle radiation problems.

Table 4-3. Thermal Control Heaters

Power (watts) / Requirement	Pioneer F and G		Pioneer Outer Planets Orbiter	
	Electric*	RHU	Electric*	RHU
Propulsion Heaters				
Monopropellant system				
External lines	2		2	
Internal lines	1.4		1.4	
Tank	1		1	
One-pound thrusters		9		12
Bipropellant system				
Tanks	-	-	12	22
100-pound thruster	-	-	8	8
Other Heaters				
Battery**	1.6	-	-	-
Sun sensor assembly	-	2	-	2
Shunt regulator	-	-	4	-
Magnetometer	-	1	-	1
External science package	-	-	7	-
Total	6	12	35.4	45

*Thermostatically controlled electric heaters.

**May be commanded on before battery use.

4.2.3 Spacecraft-RTG Thermal Interface

The thermal interfaces requiring special attention are:

- Blockage of the RTG heat rejection system by the spacecraft and its components
- Heating of the spacecraft and its components during on-stand and during launch
- High temperatures during launch and prior to deployment.

The interference by the spacecraft in the space environment can be minimized by deploying the RTG's away from the spacecraft. However, during on-stand conditions when the RTG's are in the stowed position there may be critical areas requiring special insulation. On Pioneer F and G it was determined that heating effects in the stowed position and during launch were more critical on the high-gain antenna and side panels of the spacecraft. The side panel insulation was modified and thermal insulators were incorporated in the RTG support structure to reduce the heat leakage into the spacecraft compartment. The back side of the antenna is polished aluminum to reduce localized heating effects. In addition, air conditioning ducts to direct air flow were used on-stand to carry away the heat generated by the RTG's. The air conditioning minimized local heat effects on the spacecraft and prevented RTG over-temperature during the launch phase between liftoff and RTG deployment.

The extent to which internal heat generation is a problem is determined primarily by the RTG fuel loading and the heat rejection temperatures. Each MHW generates 2400 watts of heat of which approximately 150 watts is converted into electrical energy. This is a considerable increase over the Pioneer F/G SNAP-19 unit which develops 650 thermal watts. Outer case temperature for the MHW is estimated to be 590^{o}F in vacuum as compared to 329^{o}F for the SNAP-19 generator. Based on natural convection heat transfer coefficients the MHW case temperature in air is reduced to 536^{o}F. The temperature can be further reduced by using directed air flow or gaseous nitrogen in the launch vehicle fairing. The air conditioning load for the orbiter configuration will nevertheless be considerably higher than that provided for Pioneer F/G.

Temperature predictions derived from the above RTG conditions indicate that the insulation directly opposite the end of the RTG may reach 455^{o}F. This estimate is considered conservative since the steady-state value may not be reached prior to RTG deployment; moreover the temperature of the end of the RTG is probably less than the assumed value for the outer case. However, the 3-mil Kapton insulation installed in this critical area is able to withstand 500^{o}F and no problem is anticipated.

Insulation adjacent to the RTG side reaches only 315^{o}F with direct solar impingement. Kapton face sheets are also recommended here although the thermal problem is not as severe.

4.3 PROPULSION

4.3.1 Requirements

The primary modification of the Pioneer F/G design for use in an outer planet orbiter is the addition of sufficient propulsion capability for orbit insertion and other maneuvers. To account for midcourse corrections, orbit insertion, and possible orbit change maneuvers, a range of 0.7 to 2.3 km/s velocity change capability is appropriate for the Pioneer Jupiter orbiter spacecraft. A total ΔV range of 1.1 to 1.7 km/s is appropriate for the Saturn orbiter.

Two approaches to meeting these ΔV requirements have been considered (see also Section 3.1). The first approach uses an enlarged internally mounted propellant tank. The monopropellant hydrazine capacity of Pioneer F/G can be expanded to achieve as much as 0.8 km/s capability. This would require the tank diameter to be enlarged to 25 inches, the maximum that can be accommodated without extensive structural changes. Separate ullage tanks for the pressurant would be used to maximize volumetric efficiency. A higher thrust engine must be added for efficient orbit insertion. While it minimizes the modifications to the Pioneer F/G configuration, this approach can only accommodate some of the contemplated Jupiter orbiter missions — those in which periapsis is low and apoapsis is high — but none of the Saturn orbiter missions.

In the second design approach the required propulsion capability is provided by an externally mounted propulsion stage large enough to accommodate the more ambitious Jupiter orbiter missions as well as the Saturn missions. This second approach also permits the use of the more efficient bipropellant propulsion technology. Physically the stage is attached to the aft end of the spacecraft and consists of the bipropellant tanks, deboost engine, structural support, thermal control insulation and heaters. The monopropellant hydrazine system with its complement of 1-lbf thrusters is retained in the spacecraft center section and is used for spin control and precession functions, as well as for small ΔV maneuvers.

The Jupiter and Saturn orbiter configurations differ mainly in their stage propellant capacity. The Jupiter orbiter requires 800 to 1040 pounds of propellant while 400 to 650 pounds is adequate for Saturn requirements. One approach is to provide for 1040 pounds capacity and off-load, as required, for the Saturn orbiter mission. However, the tighter weight constraints of this mission would be met more advantageously by a smaller size propulsion stage without excess capacity.

The propulsion subsystem requirements for the Jupiter and Saturn orbiter missions are summarized as follows:

- Precession and spin control maneuvers are to be performed by the monopropellant system
- Large ΔV maneuvers are to be performed by the bipropellant system
- Small ΔV maneuvers are to be executed by the monopropellant system. To eliminate reorientation requirement for midcourse and orbit change maneuvers of arbitrary ΔV-vector direction axial and spin/despin thrusters will be used in combination.

The ΔV requirements derive from launch vehicle injection errors, uncertainties in the knowledge of the planet's ephemeris, orbit injection errors, and orbit change requirements. Spin control and precession requirements are estimated based on operational experience from Pioneers 10 and 11.

The tradeoff considerations leading to the preferred configuration for the deboost stage are discussed in the following sections.

4.3.2 Candidate Configurations

4.3.2.1 Propellant Systems

Four candidate propellant systems were evaluated:

- Solid rockets
- Monopropellant hydrazine
- Space-storable cryogenic bipropellant
- Earth-storable bipropellant.

The relative performance of these systems is shown in Figure 4-9.

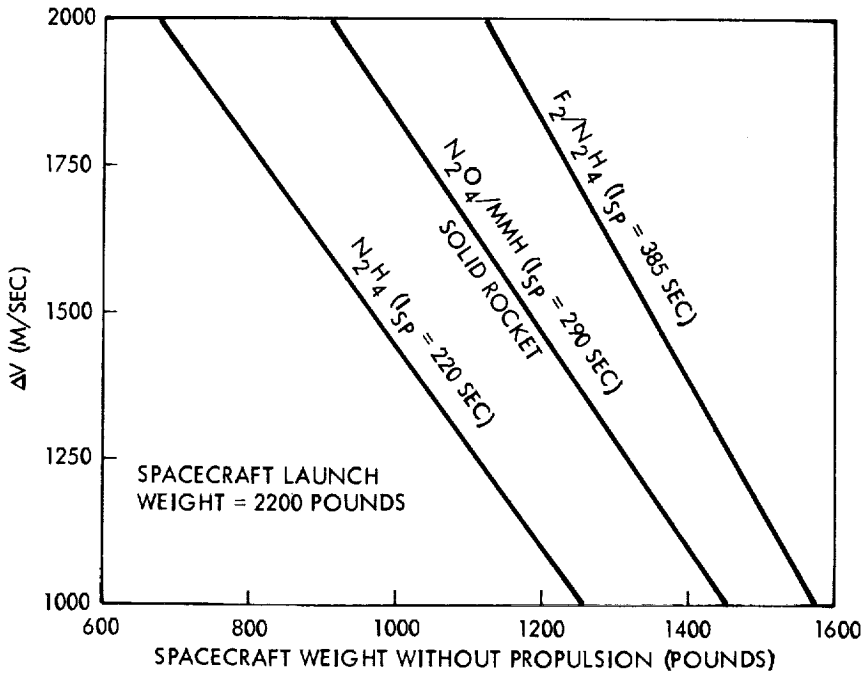

Figure 4-9. Relative Performance of Candidate Propulsion Systems

Solid propellant rocket motors offer high storage density which is desirable for volume-limited spacecraft. However, they have several disadvantages for the orbiter spacecraft. Major structural and thermal control design modifications to the spacecraft would be necessary. Several solid motors would be required to permit repeated firings. The units would have to be fired in pairs to avoid thrust vector offset. Thrust levels would have to be restricted to the 50-100 lbf range to limit structural loads on appendages. The long burn times necessary to achieve the required large total impulse at the desired low thrust level exceed

the capability of available solid rockets and would necessitate a new nozzle/throat development program. Solid motor reliability under prolonged space exposure is questionable and has not previously been required or demonstrated. From a programmatic standpoint, therefore, a solid rocket motor is a relatively expensive approach for this application.

A monopropellant hydrazine system would only be marginal on account of its low specific impulse (I_{sp} = 225 sec) although it would permit propellant commonality for use in the main retropropulsion engine and in the auxiliary thrusters.

Space storable bipropellant systems using liquid fluorine as oxidizer and hydrazine as fuel offer the potential of greatly increased specific impulse (I_{sp} = 360 to 385 sec) but would involve the greater complexity of handling and storing the oxidizer as a cryogenic liquid in a nonvented tank at storage temperatures of 110°K. Such systems have been under preliminary development by JPL (Reference 14) and elsewhere. Major additional development would be required to achieve flight-ready status for this new technology. Since the high performance of space storable bipropellants is not essential to the Pioneer Outer Planet Orbiter missions their use is not recommended for this application.

Earth storable bipropellant systems have been proven on both NASA and military spacecraft and can be implemented with off-the-shelf hardware and existing technology. System development from initial design to delivered flight hardware can be accomplished within 15-20 months. Moreover the achievable performance is adequate for the orbiter missions. Therefore the monomethyl-hydrazine/nitrogen tetroxide (MMH/NTO) bipropellant deboost system is recommended for the Pioneer Outer Planets Orbiter spacecraft.

It would be desirable to use pure hydrazine as the fuel to achieve commonality of propellant usage for the monopropellant and bipropellant systems. However, the fuel in the proposed system (MMH), although using a hydrazine base, contains significant amounts of hydrocarbons which would degrade the catalyst in catalytic thrusters.

Development of a bipropellant deboost thruster utilizing only hydrazine as the fuel is feasible. Several successful demonstration units have been tested by JPL. However, thruster development would increase program costs far beyond the costs saved by deleting the existing monopropellant system hydrazine tankage. Therefore development of a bipropellant system with hydrazine as the fuel is not recommended.

4.3.2.2 Deboost Thruster

Several candidate thrusters for the bipropellant system (see Table 4-4) with thrust levels from 25 to 300 lbf were considered. However, the range of tolerable acceleration levels during deboost is constrained at the high end by appendage structural limitation and at the

Table 4-4. Candidate Long Burn Time Thrusters

Source	Thrust Level (lb)	Program Background
Marquardt	25	--
TRW	90	USAF
Bell Aerosystems	100	USAF
Marquardt	100	NASA/Apollo
Rocketdyne	300	NASA/Mariner Mars '71

low end by thrust inefficiency. The 25-lbf units imposing thrust accelerations of 0.01 to 0.03 g would result in excessive ΔV loss due to extended firing time. The 300-lbf units would induce accelerations of 0.15 to 0.3 g, i.e., values beyond the capability of the RTG and magnetometer support structure without extensive design changes. Units operating in the 90-100 lbf thrust range are characterized by nominal ΔV losses in the range of only 25 m/s and acceptable accelerations of 0.05 to 0.1 g.

The 90-lbf TRW thruster with a specific impulse of 292 seconds is flight-qualified for the required propellant loads and burn times. The unit is radiation-cooled to accommodate the long burn durations (3200 to 4400 seconds) required for a 1100- to 1500-pound propellant load. The Marquardt R4D thruster (100 lbf) is also a suitable candidate for this application.

4.3.2.3 Tankage

Tankage considerations for the stage include:

- Number of tanks
- Tank shape
- Tank material

A bipropellant system requires at least two propellant tanks. However, as discussed in Section 3.1, the unequal masses of oxidizer and propellant being stored necessitate the use of pairs of oxidizer and propellant tanks in a symmetrical quadrilateral arrangement to achieve dynamic balance of the spinning spacecraft regardless of the state of propellant depletion.

The four 24-inch propellant tanks for the Jupiter orbiter configuration accommodate up to 1170 pounds of MMH/NTO at an oxidizer-to-fuel mixture ratio of 1.65 (728 pounds NTO, 442 pounds MMH). This mixture permits

the use of oxidizer and fuel tanks of equal volumes and a nearly optimal thruster I_{sp} of 292 seconds. Therefore, only one tank size needs to be procured for each orbiter which affords a program cost advantage.

Spherical tanks were selected over oblong tanks because of more favorable mounting height and suitability to yield the desired mass distribution by appropriate tank-to-tank separation, as discussed in Section 3.1. Although no spherical tanks of the required 24- and 19-inch size are currently available off-the-shelf, new procurement of these spherical tank sizes presents no problems.

Heat-treated 6Al-4V titanium offers the lowest tankage weight and is free of magnetic property problems. Stainless steel tanks are less expensive to fabricate but have two potential disadvantages: greater weight and unfavorable magnetic properties.

4.3.2.4 Expulsion Device

Several approaches as to the choice of propellant acquisition method were explored. The principal alternatives are passive versus active expulsion devices such as bladders. The 4.8-rpm spacecraft spin rate is sufficient to orient the propellants over the outlet port in the absence of a bladder and maintain a positive propellant pressurant interface. Figure 4-10 presents the radial and axial accelerations acting on the propellant during deboost thrusting, and the propellant surface angle

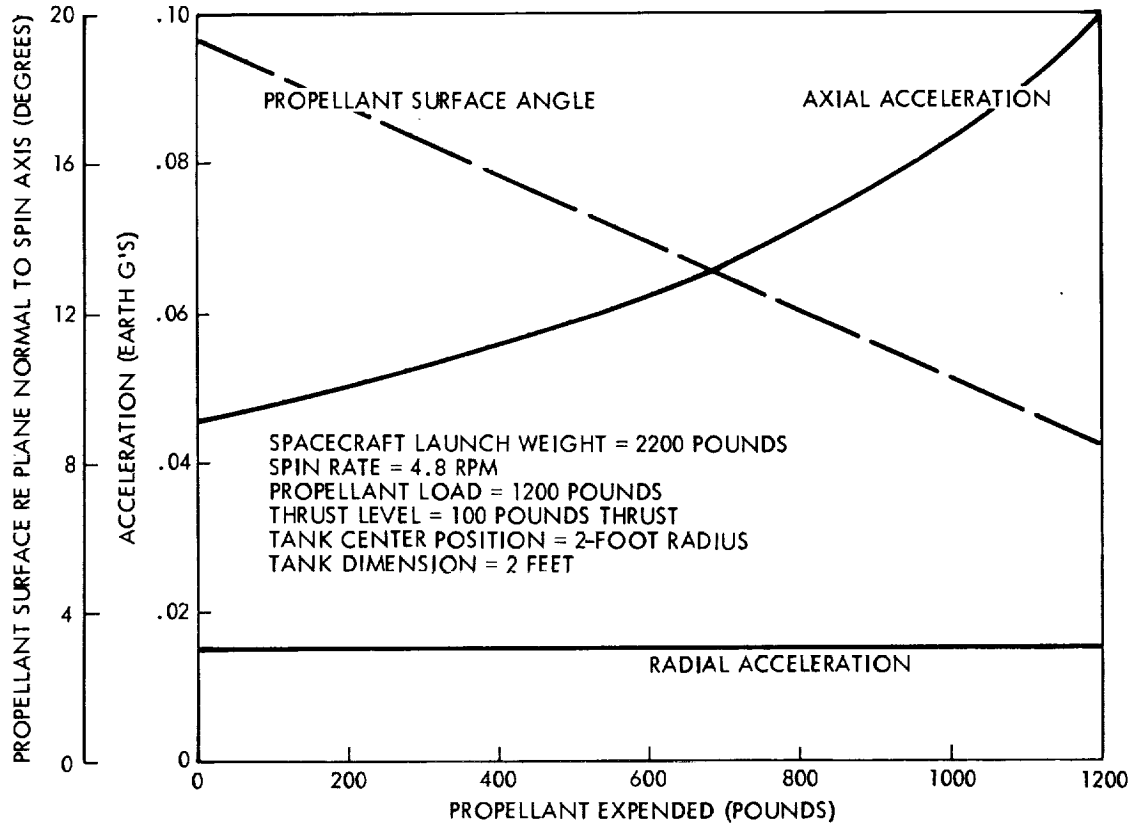

Figure 4-10. Acceleration Forces Acting on Deboost Propellant During Thrust

relative to a plane normal to the spin axis. Although a conospheroid ("teardrop") tank could be used without an expulsion device it is difficult to support structurally and, more importantly, it exhibits higher energy dissipation due to propellant slosh. This energy dissipation is undesirable during third stage burn when the combined transverse/longitudinal (I_x/I_z) moment-of-inertia ratio is less than 1. Therefore, the conospheroid is not recommended.

Passive expulsion by surface tension devices and/or appropriate location of single or multiple outlets is a promising reliable and lightweight design approach. However, it requires additional development and test. As a more conservative approach, a Teflon bladder is recommended to provide propellant orientation in the spherical tanks. Teflon is compatible with both the fuel and oxidizer, thus allowing a single tank procurement and interchangeability.

4.3.2.5 Regulated Pressurization System

Pressure regulation is typically required for bipropellant systems. A common pressurization system (both fuel and oxidizer pressurized from the same source) is recommended for the fuel and oxidizer tanks (Figure 4-11). This approach has been used on a bipropellant system for a flight-qualified earth-orbital spacecraft program. It is more cost and weight effective than the independent pressurization scheme as it minimizes the number of tanks, valves, regulators, etc.

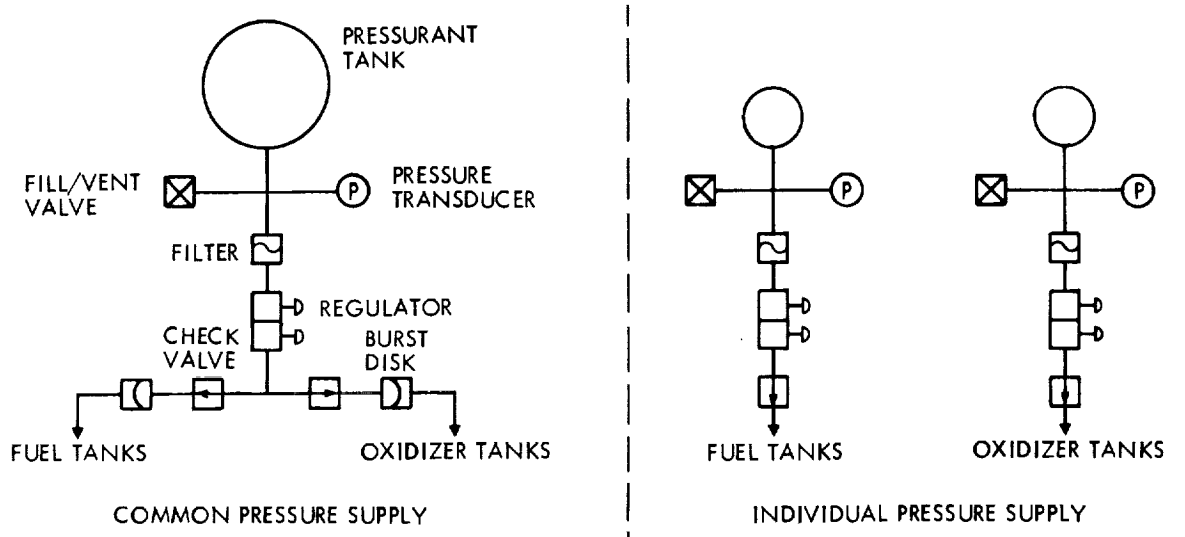

Figure 4-11. Alternate Pressurization Systems

Teflon bladders are somewhat permeable to both the fuel and the oxidizer. Therefore, with a common pressurant system it is necessary to prevent mixing of the hypergolic fuel and oxidizer in the pressurant plumbing. The recommended approach involves the use of burst disks to

positively isolate the fuel and oxidizer in the launch phase of the mission when the propellant tanks are full and the vibration environment is most severe. The burst disks are ruptured upon the first use of the deboost system. Isolation during the remainder of the mission is provided by check valves.

Isolation of the high-pressure supply from the low-pressure propellant tanks is required due to the long mission duration and the relatively poor sealing characteristics of pressure regulators. Two isolation approaches were considered: squibs and multicycle valves. The selection narrowed to the multicycle valves (either latching type or solenoid) which offer the maximum mission flexibility (essentially unlimited activations) and least weight and cost. The weight and cost of the required squibs would be incompatible with the number of anticipated restarts.

Either nitrogen or helium is satisfactory for use as pressurant gas. Approximately 20 pounds of nitrogen would be required, compared to only 3 pounds of helium. The weight savings with helium is appreciable, if the science can tolerate possible minute quantities of helium in the atmosphere surrounding the spacecraft due to leakage. In view of this uncertainty nitrogen is recommended at this time.

4.3.2.6 Hydrazine System Pressurization

The Pioneer F and G hydrazine subsystem utilizes blowdown pressurization. Use of the regulated pressure from the bipropellant system to pressurize the monopropellant system is an alternate approach. This has the potential advantage of improving the impulse predictability (constant tank pressure) of attitude control/midcourse trim maneuvers.

The attendant disadvantages are small increases in subsystem weight (approximately 3 pounds) and cost (15 to 20 thousand dollars per subsystem) due to the addition of parallel redundant tank isolation valves and associated command circuitry. Reliability may be adversely affected by the added items. The isolation valves are required to preclude regulator leakage failure from overpressurizing and possibly bursting the hydrazine tank. The isolation valves may be commanded open prior to each hydrazine thruster firing, or the hydrazine tank can be equipped with a pressure switch to activate the isolation valves open/closed at preset pressure levels.

Both the current blowdown technique and the pressure-regulated approach offer essentially the same ΔV capability. The average tank pressure with blowdown pressurization is approximately 225 psia, which coincides with the regulator pressure setting. Therefore, neither pressurization technique offers an appreciable performance advantage.

Based on the above considerations, the Pioneer F/G blowdown pressurization technique is retained for the orbiter configuration.

4.3.3 Preferred Subsystem Description

The bipropellant deboost propulsion system schematic is presented in Figure 4-12. A single 1900-cubic inch tank fabricated from 6Al-4V heat-treated titanium is used to store the high-pressure nitrogen gas. Series-redundant pressure regulators provide a constant operating pressure to the oxidizer and fuel tanks which must deliver constant propellant flow rates (mixture ratios) to achieve the rated thruster performance. The recommended regulators were developed for the Apollo program and have been used on earth-orbiting spacecraft.

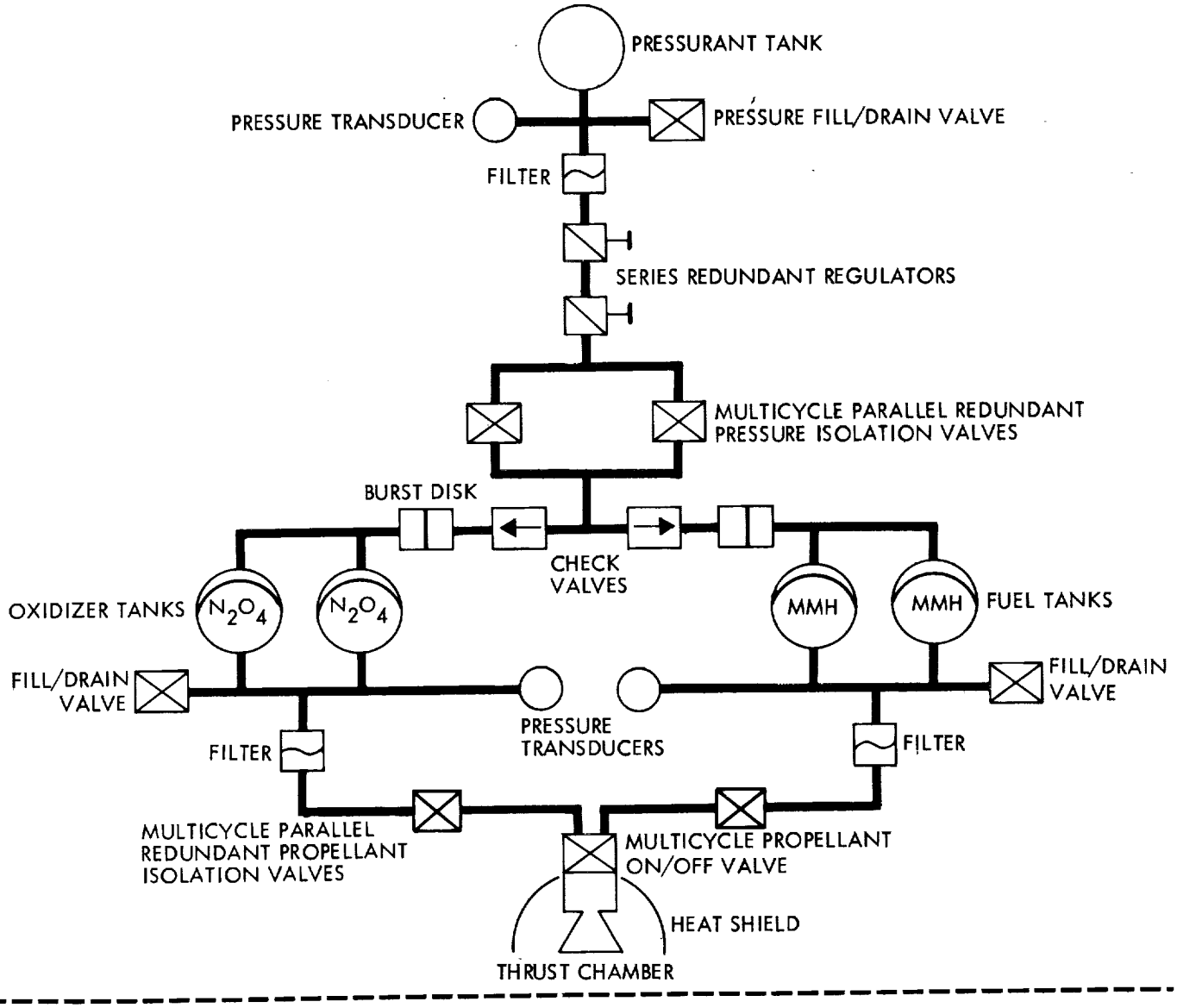

Figure 4-12. Propulsion System Schematic

Two parallel-redundant multicycle valves (latching type) isolate the high/low pressure systems. The regulators are not designed for the low leakage sealing that is required during periods of deboost system inactivity, i.e., during cruise and orbital operations. Excessive leakage into the low-pressure system prior to an appreciable propellant expenditure would result in propellant tank overpressurization and possibly tank rupture. The isolation valves are commanded open prior to deboost thrusting and closed following the maneuver. These valves also feature position (open/closed) telemetry indicators.

It is essential to prevent the hypergolic fuel and oxidizer from mixing in the common pressurant supply plumbing. Burst disks (100 psid rupture) provide this isolation during the early phase of the mission when the propellant tanks are fully loaded and propellant slosh is the most severe (booster firing and staging). The burst disks will rupture upon the first actuation of the deboost system (opening of the isolation valves). Check valves effect propellant isolation during the remainder of the mission. The check valves allow gas flow from the high- to low-pressure systems, and prevent reverse flow. The burst disks and check valves are available from an earth-orbiting spacecraft program.

Four tanks are used to store propellant: two for fuel and two for oxidizer. Each tank utilizes a Teflon bladder for positive expulsion. The Teflon bladders are designed to accommodate launches with off-loaded propellants. Each pair of tanks is plumbed with two Pioneer F and G fill-drain valves and a modified pressure transducer. Two valves facilitate tank drainage: one valve is used to supply a low-pressure gas above the liquid inside the bladder; the other is used for propellant outflow. The pressure transducer is a modified version of the Pioneer F and G unit and is used to monitor propellant supply pressures.

The outlets of common propellant tanks are manifolded and routed to a wire-mesh type propellant filter. Both the fuel and oxidizer tanks will be isolated from the deboost thruster by parallel redundant multicycle valves. These latching-type valves are actuated by ground command prior to each maneuver.

The deboost thruster assembly recommended is a 90-lbf unit developed by TRW with a minimum specific impulse of 292 seconds. The assembly consists of a torque motor actuated valve and a radiation shield. The thruster is radiation cooled and has been qualified for propellant loads and burn times in excess of the Jupiter and Saturn orbiter requirements.

Section 3.2.4 presents the propulsion subsystem weight breakdown for the Jupiter and Saturn orbiter missions.

Thermal control for the bipropellant system is discussed in detail in Section 4.2. The basic approach is a hybrid combination of electrical and isotope heaters. The isotope heaters provide a major percentage of the thermal input; the electrical heaters accommodate worst case conditions and provide a conservative design margin for analytical uncertainties.

The power requirements for the subsystem, exclusive of heaters, are summarized below:

Item	Required Power (W)
Pressure transducers	1.5
Monopropellant hydrazine thruster valve (pair)	11.2
Pressure isolation valves	0*
Deboost thruster valve	15.0

*Momentary power required for each actuation, approximately 60 watts for 50 msec.

4.3.3.1 Subsystem Performance

Figure 4-13 shows performance capabilities of the bipropellant and monopropellant subsystems for the Jupiter and Saturn orbiters. Monopropellant performance is presented in terms of ΔV capability under conditions where the bipropellant tanks are full and empty. However, only 50 percent or less of the available hydrazine propellant mass can be used for ΔV maneuvers, the rest is allocated to attitude control functions, as will be discussed in Section 5.3.

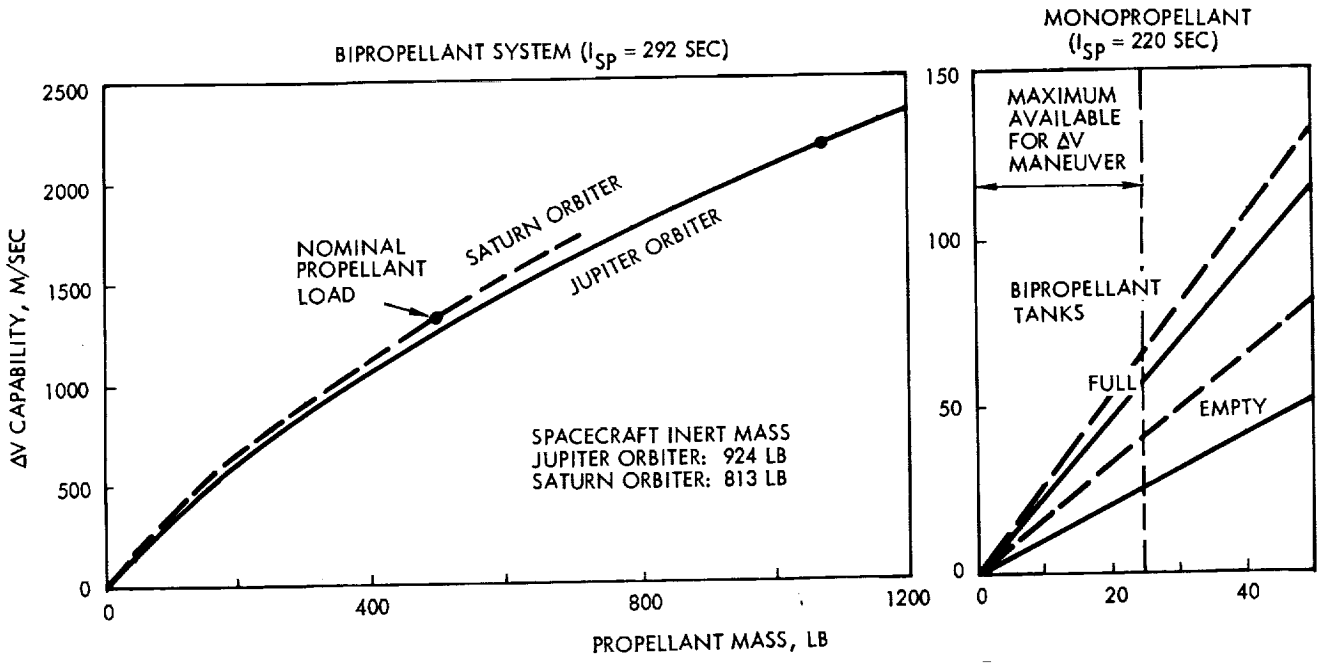

Figure 4-13. Propulsion Subsystem ΔV Performance Capability

4.4 ATTITUDE CONTROL

4.4.1 Requirements

Various orientations of the spacecraft are required to accomplish the mission. During the major portion of the flight an earth-pointing attitude is necessary for the narrow beam of the high-gain antenna to illuminate earth and maintain optimum communications. Since the geocentric celestial longitude of the spacecraft varies continuously throughout the mission, it is necessary to make attitude adjustments to compensate for this variation. In addition, some adjustment of the velocity vector may be required during the interplanetary flight to provide the desired planetary trajectory and orbital characteristics. These velocity vector adjustments require thrust in a particular direction, and, with thrusters in a fixed relationship to the spacecraft, reorientations of the spacecraft may be necessary to achieve maximum propulsive efficiency.

Changes in the spin rate are also required. The spin rate after injection by the launch vehicle will be approximately 60 rpm and must be reduced to about 16 rpm before deployment of the appendages. Subsequent deployment of the RTG's and magnetometer boom further reduces the spin rate to a nominal 4.8 rpm. Attitude and velocity changes may also produce small changes in spin rate which will need correction to maintain the spin rate within required limits. Additionally, propulsive operations with the bipropellant system require spin-up to 15 rpm to reduce pointing errors whereas a reduced spin rate (2 rpm) caters to the requirements of sensitivity-limited instruments.

Attitude, velocity, trim, and spin rate changes during the mission are accomplished in conjunction with monopropellant hydrazine thrusters, part of the propulsion subsystem. Two clusters of thrusters positioned on opposite sides of the spacecraft near the edge of the high-gain antenna reflector are employed for attitude changes and velocity corrections parallel to the spin axis. Each cluster contains a forward-facing nozzle and a rearward-facing nozzle. Spin rate changes and velocity corrections normal to the spin axis are accomplished by two additional thruster clusters with tangentially aligned nozzles. The redundant spin/despin thruster (SCT) set provides the following features:

- Eliminates the body-fixed torque arising from firing one SCT
- Adds redundancy for the multiple spin control requirements
- Adds redundancy for lateral ΔV maneuvers
- Avoids transient spin rate changes by firing ΔV pulses simultaneously.

The timing of the thrust pulses for precession of the spin axis in a desired direction is obtained by reference to signals provided by sun or star sensors. Attitude changes can be accomplished open-loop by ground command or closed-loop by homing of the spacecraft on the uplink RF signal

received from earth. The duration of thrust for velocity and spin rate changes is established by ground calculations and transmitted to the spacecraft and stored for execution on command. This storage information can be combined to perform a precession-velocity change-precession sequence with suitable time intervals in the sequence and to provide a completely automated velocity vector adjustment with return to a selected spacecraft orientation.

The closed-loop precession (conscan) maneuver may be used periodically for accurate realignment of the spin axis toward earth. The medium-gain and high-gain antennas will be used, respectively, for coarse and fine homing on the uplink communication signal. For the conscan maneuver, the axis of the medium-gain antenna and the feed of the high-gain antenna are permanently offset from the spin axis and provide an amplitude-modulated signal when the spin axis is not aligned with the earth. This signal is processed and times the firing of the thrusters to cause the desired precession to orient the spin axis toward earth.

4.4.2 Functional Description

A functional block diagram of the subsystem is given in Figure 4-14. The location of the major components of the attitude control system (ACS) on the spacecraft is shown in Figure 4-15. Although part of the propulsion subsystem, the thrusters are integral with the ACS and are also shown. A functional description of the principal ACS components is summarized below.

4.4.2.1 Control Electronics Assembly (CEA)

The CEA is the central processor for the ACS and contains four subassemblies. The sensor and power control (SPC) subassembly processes the magnetometer, stellar, and sun reference signals, provides logic for selecting the desired sensor and controls the experiment drive assembly. It switches power to the remaining two subassemblies of the CEA. The SPC also provides timing control and clock references to the CEA.

A program storage and execution (PSE) subassembly stores and executes (upon command) open-loop precession and velocity programs. Provision is made to automatically precess the spacecraft to its original attitude following a velocity increment required by a midcourse maneuver.

Two duration and steering logic (DSL) subassemblies provide redundant thruster valve driving capability. When appropriately commanded, each DSL meters out the proper pulse length and steers the pulse(s) to the selected valve drivers for executing any of the required maneuvers.

4.4.2.2 Sun Sensor Assembly (SSA)

The SSA provides sun pulses to establish a reference plane for open-loop precession. It also serves as a roll reference for indexing the experiments.

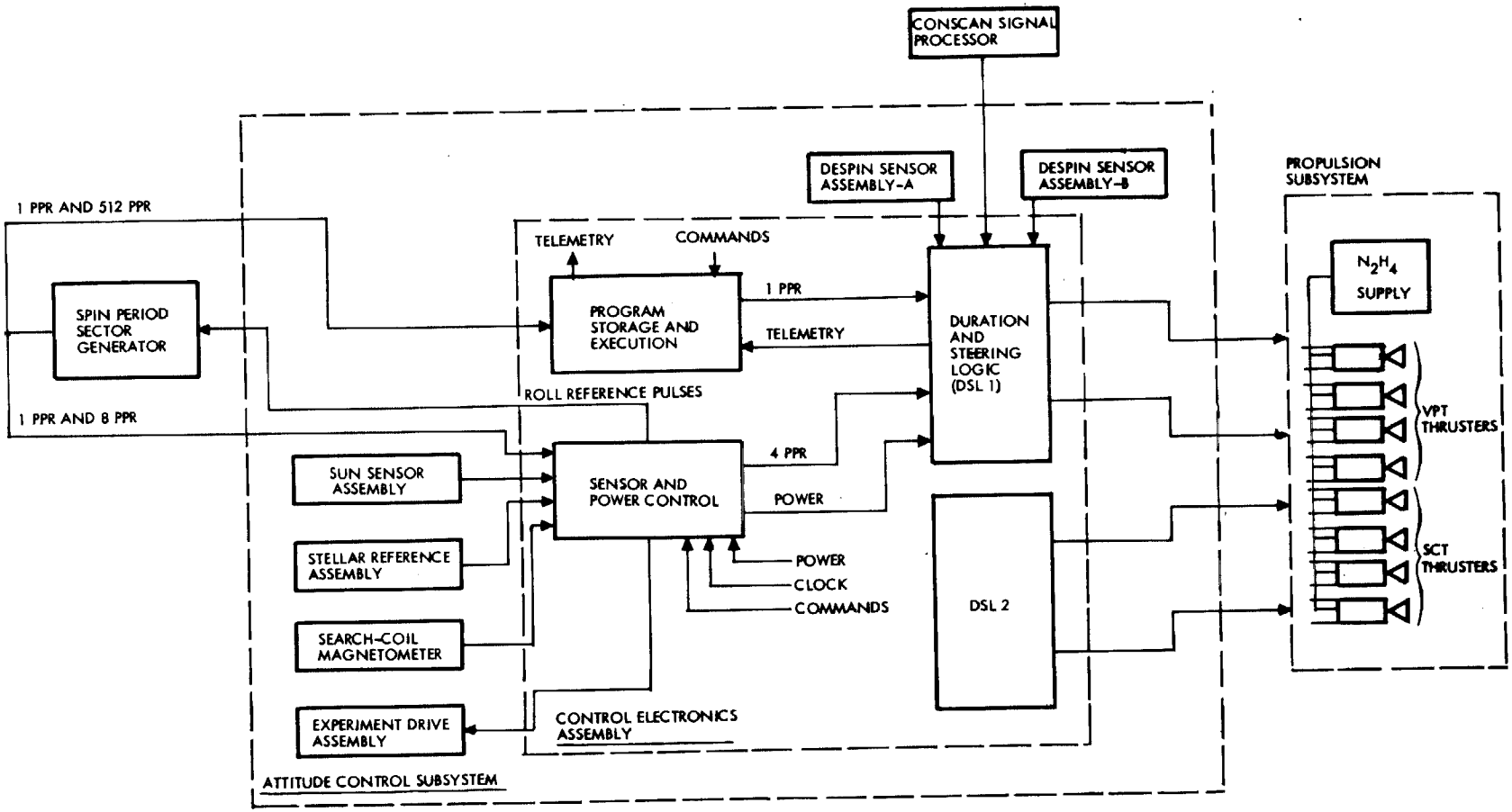

Figure 4-14. Attitude Control Subsystem Functional Block Diagram

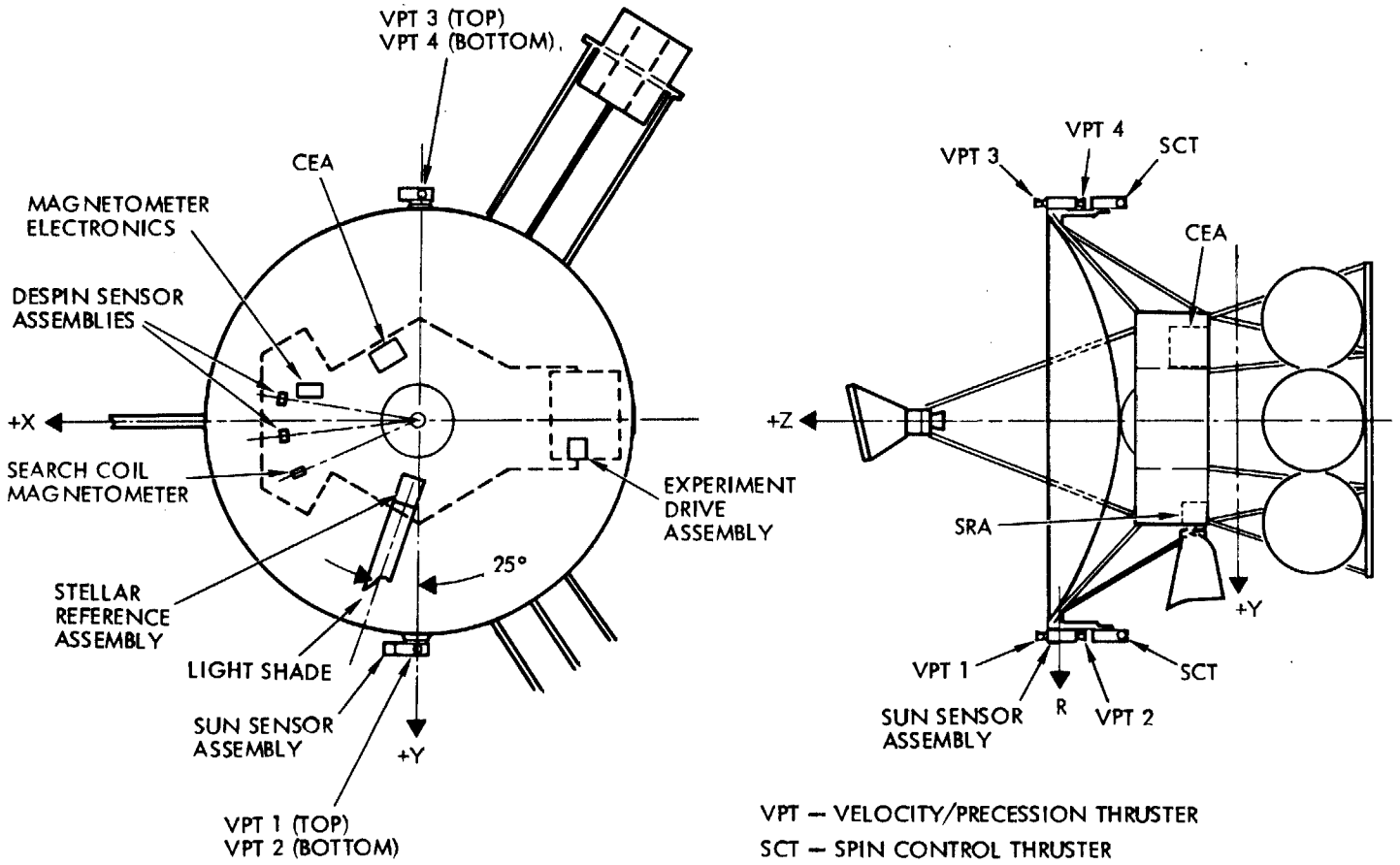

Figure 4-15. Attitude Control Subsystem Component Placement

The SSA is mounted at the edge of the high-gain antenna reflector, parallel to the Y axis. The sun sensor detects the sun as it passes through the Z-Y plane and issues a pulse. The SSA consists of three channels with overlapping fields of view covering sun look angles from 1 to 170 degrees relative to the positive spin axis.

4.4.2.3 Stellar Reference Assembly (SRA)

The SRA is a nonredundant unit mounted within the spacecraft compartment (except for its stray light shade). The primary star selected for reference purposes is Canopus, but other sources such as planets, asteroids, and the sun may be detected. A single pulse is issued when a source enters the field of view. The light shade prevents sunlight reflected from the spacecraft structure, appendages, or the planet from affecting the star detection.

4.4.2.4 Magnetometer Roll Reference Sensor

A search-coil magnetometer serves as an auxiliary sensor to complement the SSA and SRA in providing roll reference information in the vicinity of Jupiter or Saturn.

4.4.2.5 Despin Sensor Assembly (DSA)

Redundant DSA's, mounted within the equipment compartment, provide a signal to terminate despin when the spin speed drops below a rate compatible with safe deployment of the RTG's and the magnetometer boom. The DSA senses centrifugal acceleration and provides a bilevel (switch) output.

4.4.3 Orbiter Mission Considerations

The ACS configuration is derived directly from the flight-proven Pioneer F/G design. However, the orbiter missions impose additional requirements which necessitate modification of some of the units and the incorporation of two additional assemblies. These mission-peculiar requirements include:

1) Provision for roll reference indexing in proximity to Jupiter and Saturn

2) Compatibility with solar ranges between 1 and 10 AU

3) Operation at spin rates over a range from 2 to 15 rpm

4) Incorporation of drive mechanism and control electronics for articulated instrument package

5) Restrictions in performing maneuvers

4.4.4 Roll Attitude Signal Generation

The angular orientation of the spacecraft with respect to the ecliptic plane is required for many functions. As on Pioneers F and G, the roll reference pulse signal is utilized to index attitude control related maneuvers to an inertially fixed direction and to provide a means of indexing scientific experiment data. An accurate reference is required throughout the mission, from time of injection into the transfer orbit to the multiple orbit revolutions about Jupiter or Saturn.

A roll reference is required for the following functions:

- Conscan signal processing
- Open-loop attitude precession maneuvers
- Determination of spin speed
- Indexing scientific experiments in conjunction with the spin period sector generator (SPSG).

Pioneer F and G utilizes a sun sensor assembly and a stellar reference assembly to provide such reference. The sun sensor provides sun pulses to establish a reference plane for open-loop precession maneuvers but can serve as a redundant roll sensor for indexing scientific experiments. The star sensor, on the other hand, provides the primary roll reference for indexing experiments and can be used as a closed-loop precession reference or as an open-loop precession reference for small maneuvers.

The Pioneer F and G sun sensor assembly, which is mounted at the edge of the high-gain antenna, is comprised of three channels with an overall field of view from 1 degree of the +Z axis to 10 degrees of the -Z axis parallel to the spacecraft YZ plane. As the sun is detected passing through the YZ plane a pulse is issued. This sensor is designed to operate over a wide spin speed range (2 to 85 rpm) and by thresholding the processed detector output, can discriminate against the albedo of both earth and Jupiter or Saturn, and thus provide a reliable roll reference with a minimum of logic.

The referencing error of this sensor is heavily dependent upon the sun look angle: the angle subtended by the +Z spacecraft axis and the spacecraft-sun line. Figure 4-16 presents the nominal Pioneer F and G SSA accuracy (bias and jitter) as a function of this angle. At small look angles, e.g., several degrees, the expected roll angle error bias and jitter can easily exceed 1 degree. Moreover, as the sun look angle is further decreased, the sensitivity grows, resulting in substantial inaccuracy of the roll angle reference. Additionally, this sensor becomes unusable when the planet occults the sun, a regular occurrence in orbits of small to medium inclination. Therefore, this sensor may not have utility when close to the planet.

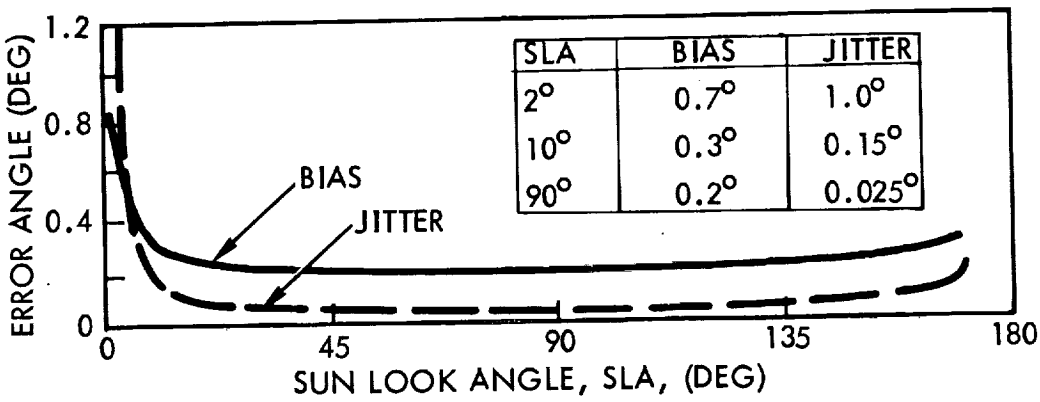

Figure 4-16. Roll Angle Error Vs. Sun Look Angle

The stellar reference assembly is mounted with a field of view +19 degrees from the perpendicular to the spacecraft spin axis and 0.5 degree wide. A single pulse is issued when a source enters this field of view. The primary star is Canopus with logic (recovery network) for discrimination against very bright objects, viz, the planet limb, sun, and planetary satellites. Special star gate logic within the CEA eliminates interference from stars of brightness comparable to Canopus after Canopus has been acquired.

This sensor provides an accurate roll reference, having a bias error (RSS) of approximately 0.16 degree with jitter less than 0.6 degree. It is susceptible (as are most other optical sensors) to radiation belt interference near Jupiter. (Also, it is unlikely that a light shade design will be found which keeps albedo from interfering with the SRA's ability to keep locked on Canopus at all points of a low periapsis orbit.) In spite of the star gating logic within the CEA, the recovery network in the SRA electronics and Canopus pulse replacement logic and automatic sensor switching logic of Pioneer F and G, there is a high probability that this sensor will be inoperative during the deep penetration of the radiation belts, particularly in Jovian orbits. Thus, the need for an auxiliary means of generating a roll reference is established.

4.4.4.1 Auxiliary Roll Reference Approaches

Free-Running Clock. In this approach, the existing Pioneer F and G crystal controlled clock would be used in conjunction with the SPSG. Under the assumption that the spacecraft spin rate is constant, the spin period will remain unchanged. By accurately measuring the spin period, and initializing the clock start by a star or sun pulse, an accurate extrapolation of the roll reference could be achieved.

$$\Delta\phi = \dot{\phi}_M t_c - \dot{\phi} t + \epsilon_o$$

where

$\dot{\phi}_M$ = measured spin rate

$\dot{\phi}$ = actual spin rate

t_c = "clock time"

t = actual time

ϵ_0 = initialization error.

Making a first order approximation, the roll reference error is simply

$$\Delta\phi = \Delta\dot{\phi}\, t + \dot{\phi}\, \Delta t + \epsilon_0$$

where

$$\Delta\dot{\phi} = \dot{\phi}_M - \dot{\phi} \text{ and } \Delta t = t_c - t$$

The Pioneer F and G clock accuracy is approximately 1.5 parts/10^5 (≈two seconds/day). The roll rate determination accuracy is determined by quantization within the spin period sector generator. In the spin averaging mode, the averaging is performed over 64 revolutions, with a clock rate of 8192 pps. Thus, at the nominal spin rate of 4.8 rpm, the quantization step will lead to a spin rate error of one part in 6.5×10^6, which corresponds to a roll reference drift of 0.38 degree/day.

An auxiliary reference will be required only near Jupiter or Saturn, within 5 planetary radii, for example. For the range of proposed orbits, this reference would be used no more than approximately 12 hours each orbit. The expected roll reference accuracy is 20 degrees at the nominal spin rate, and approximately 8 degrees at the reduced spin rate (2 rpm). Note that the inaccuracy is dependent almost entirely upon the clock inaccuracy; initialization errors and quantization of the roll rate are negligible contributors.

The spin rate, however, cannot be expected to remain at its initial value. Eddy currents induced within the spacecraft by the planetary magnetic field will tend to reduce the spin rate. The retardation depends upon the design of the spacecraft, the magnetic field strength encountered at the planet, and the orbit (primarily the periapsis radius). Figure 4-17 shows the spin rate retardation, on a per orbit basis, as a function of magnetic field strength at the surface of Jupiter and the normalized radius at periapsis (R_p/R_J). It assumes spacecraft eddy-current properties based on Pioneer F and G.

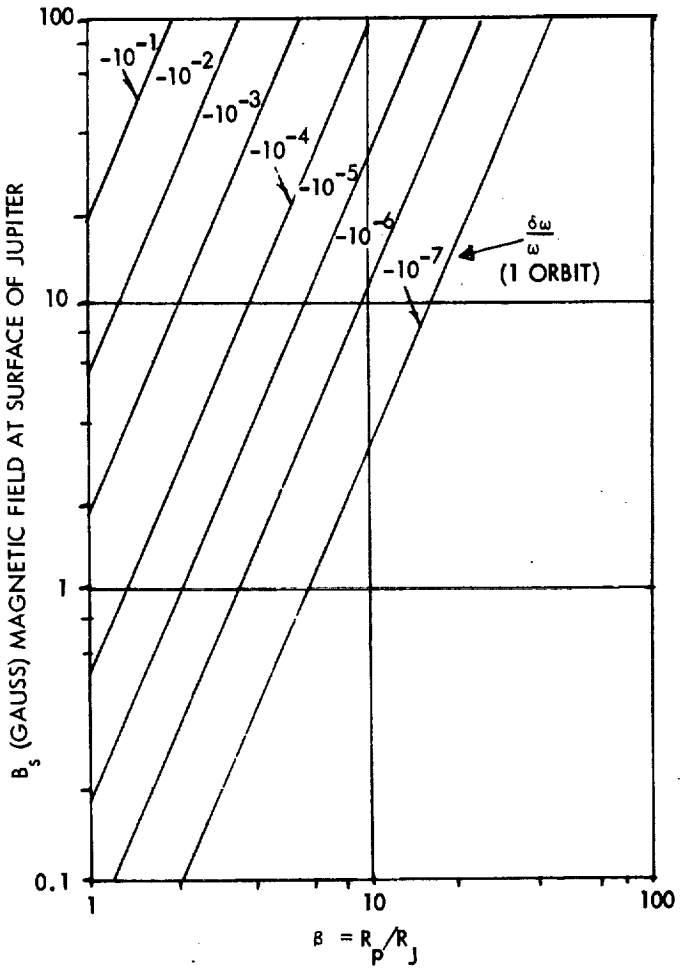

Figure 4-17. Spin Rate Change Due to Jovian Magnetic Field

For B_S = 4 gauss (extrapolation of Pioneer 10 measurement) and a skimmer orbit, in one orbit the spin speed will reduce by approximately 0.3 percent. At larger values of periapsis distance, the spin rate is reduced to a lesser extent, for example, for β = 3 the spin rate reduction is only approximately 0.003 percent/orbit.

The error in roll reference as a function of orbital position (or time) depends upon the orbit parameters and is somewhat tedious to evaluate. However, to demonstrate the effect of the spin rate change, consider a segment of a Jovian orbit, commencing from periapsis. From a symmetry argument, the cumulative spin speed change at periapsis (assuming initialization of the clock at $R \geq 5\ R_J$) will be about one-half the total spin speed change/orbit. Thus, from periapsis, the roll reference will undergo a rotation equal to the spin speed error multiplied by the elapsed time. For β = 3 and an initial spin rate of 4.8 rpm, this rotation is approximately 3 degrees/hour for short time intervals near periapsis.

Magnetometer Roll Reference Sensor. A search coil magnetometer, a simple device unaffected by radiation, can be utilized to provide a roll reference on the spinning spacecraft.

Characteristics of a typical device suitable for this application include:

Weight	1.5 pounds
Power	0.5 watt
Size	
Electronics	2 x 4 x 5 inches
Coil	1 inch diameter x 4 inches length
Sensitivity	0.01 gauss at ≥ 2 rpm

The coil is mounted so that its plane is parallel to the spin axis. With rotation of the spacecraft (and coil), an alternating signal is generated in the coil, of amplitude proportional to the magnetic field component normal to the spin axis. The zero crossings of the signal index two points in each spin rotation related to the local magnetic field. direction.

The accuracy of this method should be independent of distance from Jupiter (provided the field strength exceeds the threshold of the device) but will be influenced by the shape of the magnetic field and the orientation of the spacecraft orbit. A nonorthoganality of the magnetic flux lines at their intersection with the orbit plane must be assumed. Thus, as the spacecraft travels around the planet the angle between the detected zero corssings and the desired roll reference pulses will change as a function of time. This can be precalculated and commanded into the system as a programmed correction.

The expected accuracy of the magnetometer sensor for various Jovian orbits is shown in Table 4-5. For equatorial and high inclination orbits the field component normal to the spin axis should dominate. If the spin axis and flux lines are parallel (a possibility during portions of intermediate inclination orbits) no change in the field can be detected and hence the sensor cannot provide a continuous reference. The expected accuracy is based upon a consideration of the factors described above, with an improvement of in excess of 50 percent after the magnetic field has been mapped over several orbits. Since little is known about the magnetic field of Saturn (or even whether there is one of sufficient intensity), this approach may not work there.

The minor disadvantages of the magnetometer can be circumvented by combining it with the free-running clock approach. Instead of operating the magnetometer as an absolute indicator of roll orientation, its output can be utilized to periodically update the spin rate used to drive (open-loop) the spin period sector generator. The updating can be performed as often as deemed necessary and would adjust the spin rate measurement near periapsis where the majority of any spin retardation will occur.

Table 4-5. Accuracy of a Magnetometer Roll Reference

Orbit	Planetary Magnetic Field Characteristics			
	Component ⊥ Spin Axis	Direction Throughout Orbit	Expected Accuracy (deg)	
			First Orbit	Later**
Equatorial	Dominates	Constant (North)	10	4
Intermediate inclination	May vanish*	Varies	10-20	4-10
High inclination	Dominates	Varies	15	6

*At particular points, in orbit of particular inclination

**After mapping the Jovian field

4.4.4.2 Roll Reference Implementation

Figure 4-18 shows how the auxiliary roll reference technique discussed above can be implemented with minimum impact to the Pioneer F/G configuration. The modifications consist of expanding the roll pulse inputs to the SPSG (part of the data handling subsystem) to accept 1) magnetometer zero-crossing pulses and 2) "clock" pulses. Two registers, a comparator, a counter, and several switches are also added.

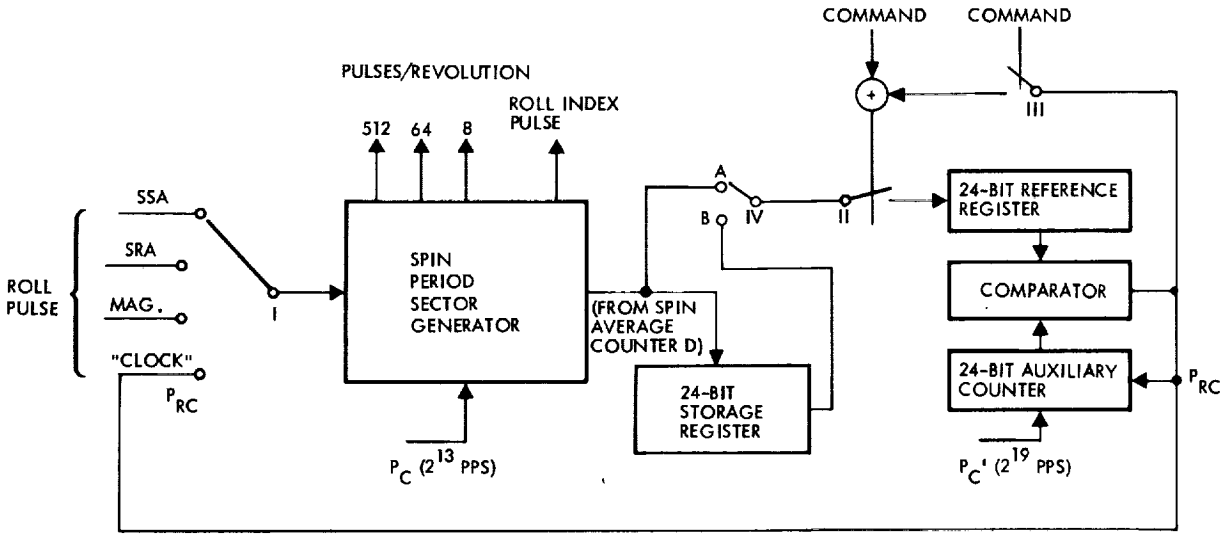

Figure 4-18. Auxiliary Roll Reference Signal Generation

During periods when the spacecraft-planet distance exceeds, for example, 5 planetary radii, the SPSG is operated identically to Pioneer F and G with the SSA or SRA providing the roll pulses. For lesser distances the SPSG is put in the spin averaging mode. Sixty-four spin revolutions later, the average spin period is transferred from the SPSG 24-bit spin average counter D into the auxiliary 24-bit reference register (switch position II closed). Subsequently, switch I is switched to the "clock" position and switch II is then opened. (Over the next spin revolution, the outputs of the SPSG are, of course, determined by the previous history.) The auxiliary 24-bit counter (driven by the clock rate of 2^{19} pps) is compared with the auxiliary register and at equality, a "clock" reference pulse P_{RC} is issued to simulate the roll reference to the SPSG and reset the 24-bit counter to zero. This comparison is continued as long as required using the contents of the 24-bit register as the spin period base.

The circuitry required to provide the angular delay in the sensed magnetic field zero crossings so that they coincide with the desired reference pulse orientation is shown in Figure 4-19. For sizing purposes, it has been assumed that the desired resolution of this delay angle is 0.7 degree (or 1/512 of a revolution, so that the 512 ppr can be used). The desired angle delay can be preset into a 9-bit register. The "field" pulses can then be delayed as follows: each field pulse causes the register contents to transfer into a 9-bit counter which counts at 512 ppr. The expiration of the count causes the delayed field pulse to be generated.

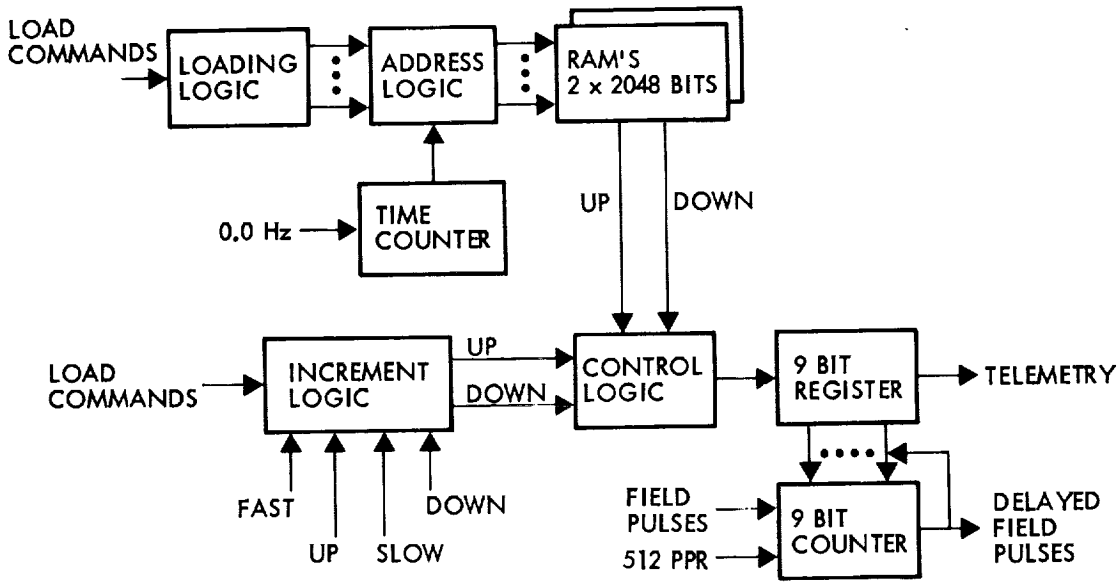

Figure 4-19. Magnetometer Phase Angle Delay Circuitry Block Diagram

The register can be preset by commands. Since the angle must vary as a function of time, this is not sufficient and an angle/time program must also be stored. The angle variation maximum is assumed as 360 degrees/day. If the maximum rate of change of angle is four times the average daily rate of change of angle, then this rate is 1 degree/minute. If the angular increments are 0.7 degree, then the time increments can be 0.7 minute. Since 0.7 minute is 1/2048 of one day, then 2^{11} time increments must be stored.

At each time increment, either the register must be 1) incremented up one pulse (0.7 degree), 2) decremented down one pulse, or 3) not changed. This information can be coded as 2 bits. The stored program is therefore 2048 x 2 bits in size. This can be contained in two 2048-bit random access memory (RAM) chips. These chips are addressed by readout by a time counter operating at 0.024 Hz (0.7 minute period). The RAM's are loaded by ground commands.

An updating of the roll period measurement to compensate for potential spin rate retardation due to eddy currents can be accomplished using the magnetometer as a source of roll pulses. The magnetometer input in Figure 4-18 is selected and switch IV is commanded to position B. Switches II and III are open. The SPSG is commanded to the spin-averaging mode. After 64 revolutions, the contents of spin average counter D are transferred to the 24-bit storage register. Then switch I is moved to the "clock" position and switch III is closed. Note that since switch II is still open, the 24-bit reference register contains its original input. At the next equality of the reference register and the 24-bit counter, the pulse P_{RC} (in addition to referencing the SPSG and resetting the 24-bit counter) will close switch II and transfer the contents of the storage register to the reference register. Switch III is then opened. The period of spin rotation is updated without an instantaneous shift in the pulse timing.

4.4.5 Operation at Extended Solar Ranges

The Pioneer F/G SSA is designed to operate over solar distances from 0.9 to 6.0 AU, which is compatible with the requirements of the Jupiter orbiter mission. This device is applicable to the Saturn mission as well, with modifications to the associated electronics to accommodate the 70 percent reduction in solar radiation power density experienced at 10 AU. The required changes consist of adjusting the threshold level and the detector loading (which determines the magnitude of the output as a function of the input). This is consistent with the operational constraint to maintain an earth-pointing attitude at extended ranges for uninterrupted downlink communications.

4.4.6 Spin Rate Variations

During the contemplated orbiter missions, the spacecraft spin rate will be varied, as needed, to meet pointing and experiment scan rate requirements. Section 3.6 discusses the mission requirements which lead to the increased range of spin rates and the impact on the spacecraft design.

The Pioneer F/G ACS was designed to operate within a range about the nominal spin rate: 4.8 rpm ± 10 percent. Departures from this operating range will necessitate modifications to the ACS and other subsystems, with the number of required changes increasing as the spin speed operating range is broadened.

4.4.6.1 Spin Rate Decrease

A minimum spin rate of 2 rpm has been selected for the orbiter, based upon the rationale in Section 3.6, as a satisfactory compromise between improved imaging resolution and the pointing error buildup induced by magnetic and gravity gradient disturbances. Without momentum augmentation, 1.5 rpm would be approximately the minimum tolerable spin rate without exceeding pointing requirements imposed by the narrow beam X-band communication antenna. Therefore, only the CEA and the conscan processor require modification.

Control Electronics Assembly. The Pioneer F/G star time gate circuit includes a 6-bit time gate register and a 6-bit ripple counter. Used in conjunction with the 4-Hz drive pulse rate, the maximum time gate is 16 seconds which corresponds to a spin rate of 3.75 rpm. To accommodate a spin rate reduction to 2 rpm, both the time gate register and ripple counter require a 1-bit length increase to 7 bits. The transfer gates (between the time gate register and ripple counter) must be increased accordingly.

The star-delay logic of Pioneer F/G contains a 12-bit delay register and 12-bit ripple counter. The ripple counter (which contains the complement of the delay register) is clocked at 256 Hz, providing a maximum delay of 16 seconds corresponding to a spin rate of 3.75 rpm. Operation at 2 rpm requires an increase in the length of the ripple counter and the delay register to 13 bits with a corresponding change in the number of transfer gates.

Conscan Signal Processor. The changes to this unit (which is part of the communications subsystem but treated here for completeness) involve increases in register and accumulator lengths to prevent overflow at the lower spin speed. The following circuits require length increases of 1 bit to operate at a spin rate of 2 rpm:

- A cos θ accumulator
- A sin θ accumulator
- Amplitude estimator
- Division logic
- Amplitude comparator.

The orbiter configuration has inertia properties substantially different from those of Pioneer F and G. The conscan signal processor estimates the magnitude and phase of the earth-pointing angle error by digital integration and processing over n - 1 spin revolutions and, if

the error exceeds the selected deadzone, emits an appropriately timed firing pulse during the next spin revolution. The number of revolutions, n, between successive thruster firings is chosen to limit the wobble amplitude, i.e., the wobble induced by one firing will tend to be cancelled, not reinforced, by the next firing.

The normalized expression for peak wobble amplitude is

$$\frac{P_{max}}{\text{Precession step size}} = \frac{1}{|\sin Kn|}$$

where

$$K = \sqrt{K_x K_y} = \sqrt{\frac{(I_z - I_y)}{I_x} \cdot \frac{(I_z - I_x)}{I_y}}$$

Figure 4-20 shows this normalized ratio for two values of n over the expected range of K values. It is evident that no single value for n is adequate. The n value used by the conscan signal processor must be command-selectable between 3 and 4. The digital integration will then be performed over two spin revolutions with a firing (if necessary) during the third or fourth spin revolution. The initial value of n will be 4, with a switch to n = 3 when the tanks are about half full.

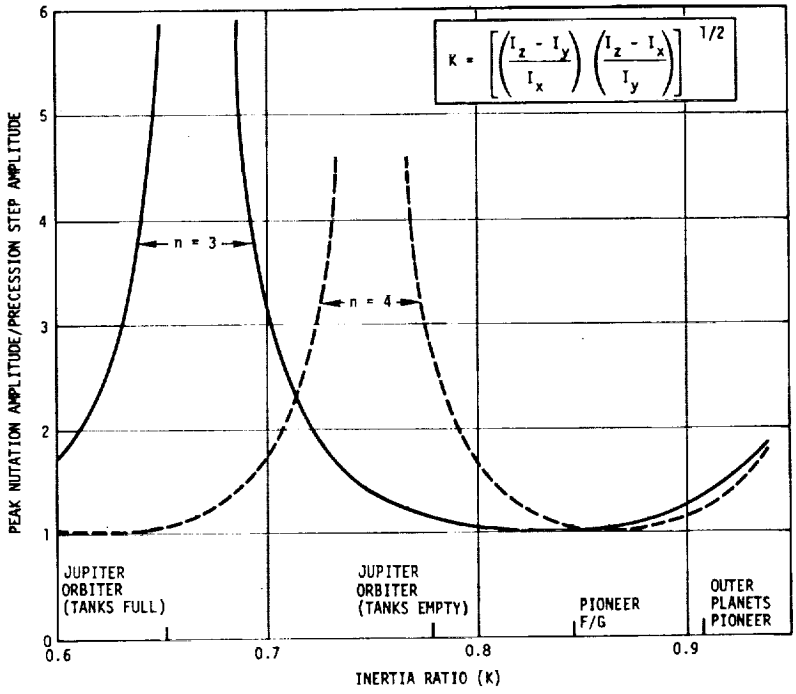

Figure 4-20. Maximum Normalized Wobble Amplitude Vs. Inertia Ratio

Paired Despin Thrusters. The spin control clusters lie substantially forward of the plane of the center of gravity. During firing of a single spin thruster, a sizeable precession torque would be generated, in addition to the spinup (or despin) torque which is commanded. This body-fixed disturbance torque would induce undesirable wobble. To eliminate this condition, the thrusters are operated in pairs to produce a couple. This is accomplished with a minor modification to the DSL select logic to accommodate the two additional valve drivers.

4.4.6.2 Spin Rate Increase

An increase in the spin rate to 15 rpm is desirable for all velocity change maneuvers involving the 90 lb_f axial engine. The higher spin rate should be limited to this occurrence so that precession does not need to be done at the higher speed (which requires more propellant) and so that modifications do not need to be made in other equipment (such as the stellar reference assembly, the conscan signal processor, and the spin period sector generator).

The spin speed increase to 15 rpm and reduction back to 4.8 rpm must be automatic just before and after the ΔV firing and must occur just after the initial programmed precession and just before the return precession. This function can be most easily made automatic, not by timed firings of spin/despin thrusters but by onboard measurement of the spin period.

In the circuit shown in Figure 4-21, the timing between sun pulses defines the actual period. Fixed one-shots define the 4.8 rpm (12.5 sec) and 15 rpm (4 sec) periods. Spin-up occurs while the actual period is >4 seconds and despin occurs while the actual period is >12.5 seconds. Termination is thus automatic.

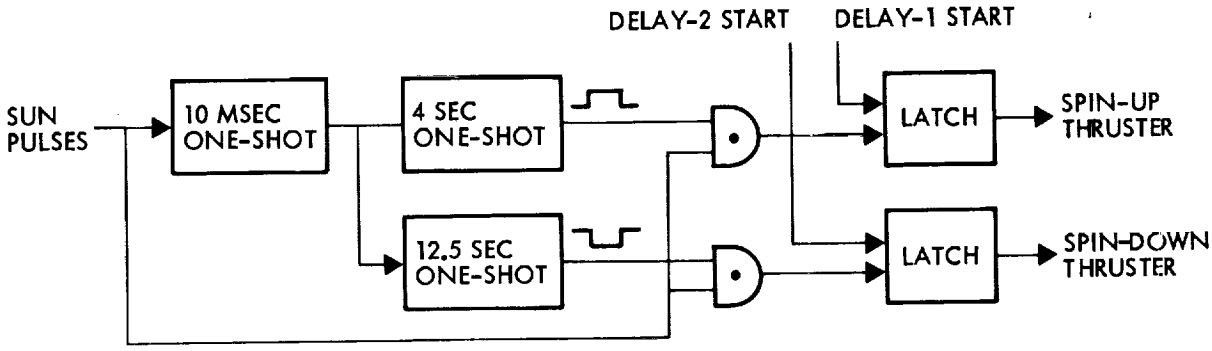

Figure 4-21. Automatic Spin Up/Down Logic

The determination of the start of spin-up or despin can be obtained from the start of the second delay (spin-up) and the start of the third delay (despin) in the program registers of the PSE. These delay times must be set long enough to accommodate the spin speed change (a few minutes) plus the damping of resulting wobble.

4.4.7 Experiment Drive Assembly

The experiment drive assembly (EDA) provides single-axis gimballing capability to the articulated external science package located at the -X axis. The deployed package is rotated through a 180-degree range about an axis parallel to the Y axis allowing any cone angle from 0 to 180 degrees.

The selected drive unit contains a stepper motor with integrally attached gearhead, a harmonic drive, and support bearings. A 90-degree/step permanent magnet stepper motor is used as the prime mover. This motor step angle is reduced by 6000 to obtain an output stepping resolution of 0.015 degree. The reduction is achieved with a gearhead of approximately 50:1 ratio integral to the motor and a harmonic drive of 121:1 ratio.

The motor has a cylindrical permanent magnet rotor, magnetized across the diameter. The permanent magnet rotor poles align with the electromagnetic field of the stator when a winding is excited. The stator field is rotated by sequential excitation of the stator coils. With each reorientation of the stator field, the rotor realigns with this field in a stepping motion. Reversing the sequence in coil excitation reverses the direction of the rotor rotation. Energized holding torque of large value is provided by steady-state energization of a winding. When de-energized, the permanent magnet rotor poles will remain aligned with the salient poles of the stator to provide a residual magnetic detent.

The output motion of the gearhead is reduced further by another stage of gear reduction. The harmonic drive was selected to obtain high reduction ratio and high torque capacity in a small package and to obtain low backlash. The harmonic drive, depicted in Figure 4-22 consists of three elements: the circular spline, the flexspline, and the wave generator. The circular spline is a rigid internal toothed ring. This meshes with the flexspline, a thin flexible ring of slightly smaller diameter with external teeth. The wave generator consists of a ball bearing with thin races which have been deflected into an elliptical shape by the elliptical hub on which the bearing is mounted. When the hub and inner race are rotated, the shape of the outer ring rotates at the same speed. In the basic harmonic drive configuration as a speed reducer, the wave generator is the input element. As the wave generator rotates, it imparts the ellipse-like shape to the non-rigid flexspline. The shape of the flexspline, but not the flexspline itself, rotates at the input speed of the wave generator. This action forces the flexspline teeth into engagement with the circular spline teeth. Since the flexspline has two teeth less than the circular spline, a relative motion results between the two members as the wave generator advances the position of teeth engagements. The circular spline is held stationary to the case and the flexspline becomes the output member.

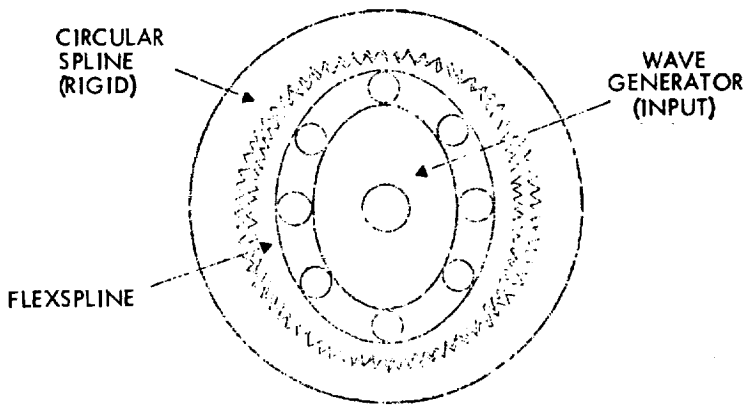

Figure 4-22. Harmonic Drive Configuration

The physical characteristics of the experiment drive are summarized below.

	Experiment Drive Assembly	Drive Electronics
Weight, pounds	4	0.1
Power, watts	6.2 energized, 0 unenergized	0.25
Size, inches	4.25 diameter by 4.25 length	3 x 3 (1 board)

A functional diagram of the drive logic appears in Figure 4-23. The drive can be slewed through a given angle at a specific pulse rate or can be reindexed a multiple of the stepping size every spacecraft rotation. To command the drive to move the package through an angle n (0.015) degrees with a step every 2/m seconds, the parameter n is loaded into the 14-bit step counter A and m is loaded into the step rate register logic D. (This logic, not shown in detail, divides down the input clock rate, 16 pps, and issues output pulses every 16/8m seconds). Switch positions 1 and 2 are normally closed. The pulses from the step rate logic are inputs to the stepper motor drive electronics and the step counter. Each pulse energizes the stepper motor, causing a science package rotation of 0.015 degrees and reducing the step count by one. When the contents of the step counter reaches zero, the step rate logic inhibits the pulse train and the stepper drive remains at the previously commanded position. The accumulated position counter (16 bits) stores the position of the drive. This is telemetered for indexing experiment data.

The drive is reindexed every spacecraft revolution using the filtered roll pulse from the spin period sector generator (SPSG) to trigger the step rate logic. The roll pulse is delayed via the present delay logic B (so that reorientation will occur while the science package is pointed away from the object to be scanned). The total number of steps per spacecraft revolution is preset into the step/roll pulse logic C. The output

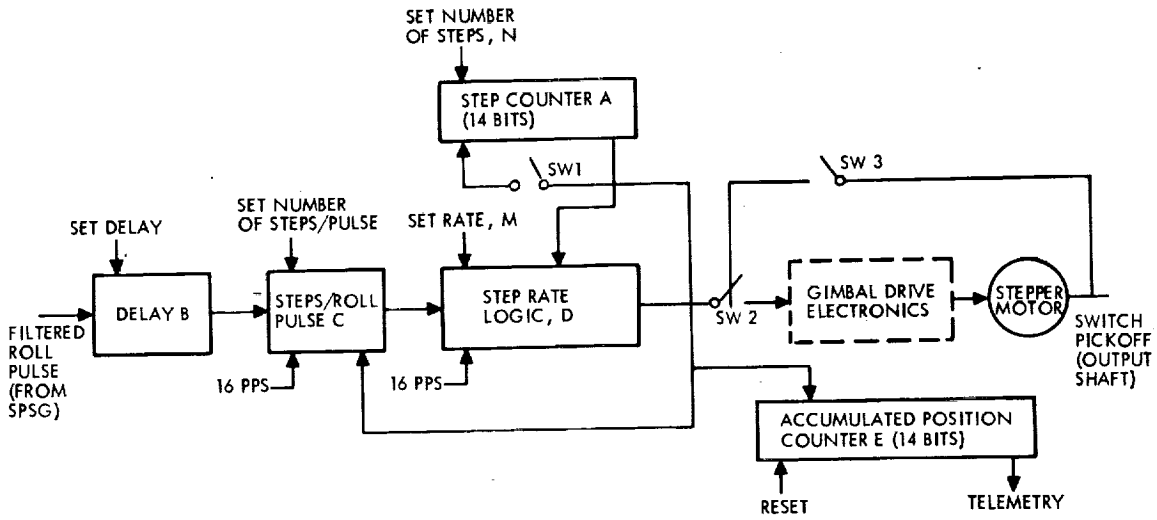

Figure 4-23. Functional Diagram of Experiment Drive Assembly

pulses from the step rate register logic D are fed back to C. In operation, the delay roll pulse initializes the step/roll pulse logic C at the preset value which, in turn, enables the step rate register logic D. The gimbal drive is commanded at the given step rate with each step also counting down the preset value in C. When the count in C reaches zero the step rate logic is inhibited. The process continues with each roll pulse from the SPSG.

This implementation does not require a resolver for position control or indexing. In the unlikely event of loss of reference, the drive can be commanded open-loop toward the central orientation (null) by opening switch 2. A single switch type pickoff indicates when the null is reached, and with switch 3 closed, will interrupt additional drive pulses from the drive electronics. (A telemetered discrete signals the completed re-indexing at null.) The accumulated position counter can then be reset to correspond to the null.

4.4.8 Restrictions in Performing Maneuvers

There are some restrictions in the performance of maneuvers for the midcourse corrections, orbital injection and orbital adjustments that need to be considered. Some of these maneuvers may involve the use of the 90 lb_f axial engine and in this case require the reorientation of the spacecraft for proper thrust orientation.

Reorientations imply the loss of communications and therefore all of these maneuvers must be done under stored program control. The stored program will involve a delay, a precession, a spin-up, a delay, the velocity correction, a despin, a delay, and a return precession.

Reorientations also imply that the phase reference during the maneuver cannot be the stellar reference assembly or the magnetometer, since both would require a changing delay angle as a function of orientation. The free-running clock cannot be used since the spin speed change resulting from any thruster firing (misalignments) is too great.

This leaves only the sun sensor as a possible phase reference. Maneuvers can therefore only be performed in sunlight. Two mission phases are thereby excluded. One is planetary eclipse of the sun. The second is when the sun-spacecraft-earth angle becomes too small (<1 degree) for the sun sensor to produce accurate pulses. These periods of earth-sun conjunction occur approximately each 200 days for a duration of approximately 10 days (near Jupiter) to approximately 20 days near Saturn. Precession into the rearward (10-degree half-angle) conical blind spot of the sun sensor must also be avoided.

During the conjunction periods the free-running clock can provide the phase reference for science as long as no thruster firings are permitted.

4.4.9 Subsystem Modification Summary

Table 4-6 summarizes the design changes to the Pioneer F/G attitude control subsystem required for the orbiter mission.

Table 4-6. Attitude Control Subsystem Modification Summary

Unit	Modification
Control Electronics Assembly	
• Sensor and power control	Add signal processing circuitry for search-coil magnetometer, and angle delay circuits
	Add experiment drive assembly elements
• Duration and steering logic	Add two valve drivers for redundant SCT assembly
	Modify valve select logic to drive SCT with programmed ΔV signals
	Add automatic spin up/down logic
Despin Sensor Assembly (2)	Select operating point at 0.25 g to terminate despin at 15.7 rpm
Sun Sensor Assembly	Adjust threshold and sensor loading for operation at 10 AU (Saturn mission only)
Experiment Drive Assembly	New item - single axis gimbal for articulated science package
Search-Coil Magnetometer	New item - auxiliary roll reference

4.5 ELECTRICAL POWER

4.5.1 Subsystem Description

The electrical power subsystem processes power received from the RTG's and supplies it to other spacecraft equipment and to the scientific instruments. The orbiter configuration, shown in Figure 4-24, consists of two multi-hundred-watt (MHW) RTG's, a power control unit (PCU), an inverter assembly, a central-transformer-rectifier-filter (CTRF) unit, and an externally mounted shunt regulator and shunt radiator. The PCU, in conjunction with the shunt regulator, regulates the primary DC bus to 28 volts ±2 percent, provided the available RTG power exceeds load demand. The PCU also provides cross-strapping of the RTG's, fault isolation for the RTG's and loads, and power system diagnostic telemetry. The CTRF, in conjunction with the inverter assembly, provides conditioned secondary power to the spacecraft loads. All experiment loads are supplied from the regulated 28-volt primary bus. Table 4-7 summarizes the functions of these components and identifies the required modifications to the existing Pioneer F/G design. A comparison of the physical characteristics of these components with those of Pioneer F/G is given in Table 4-8.

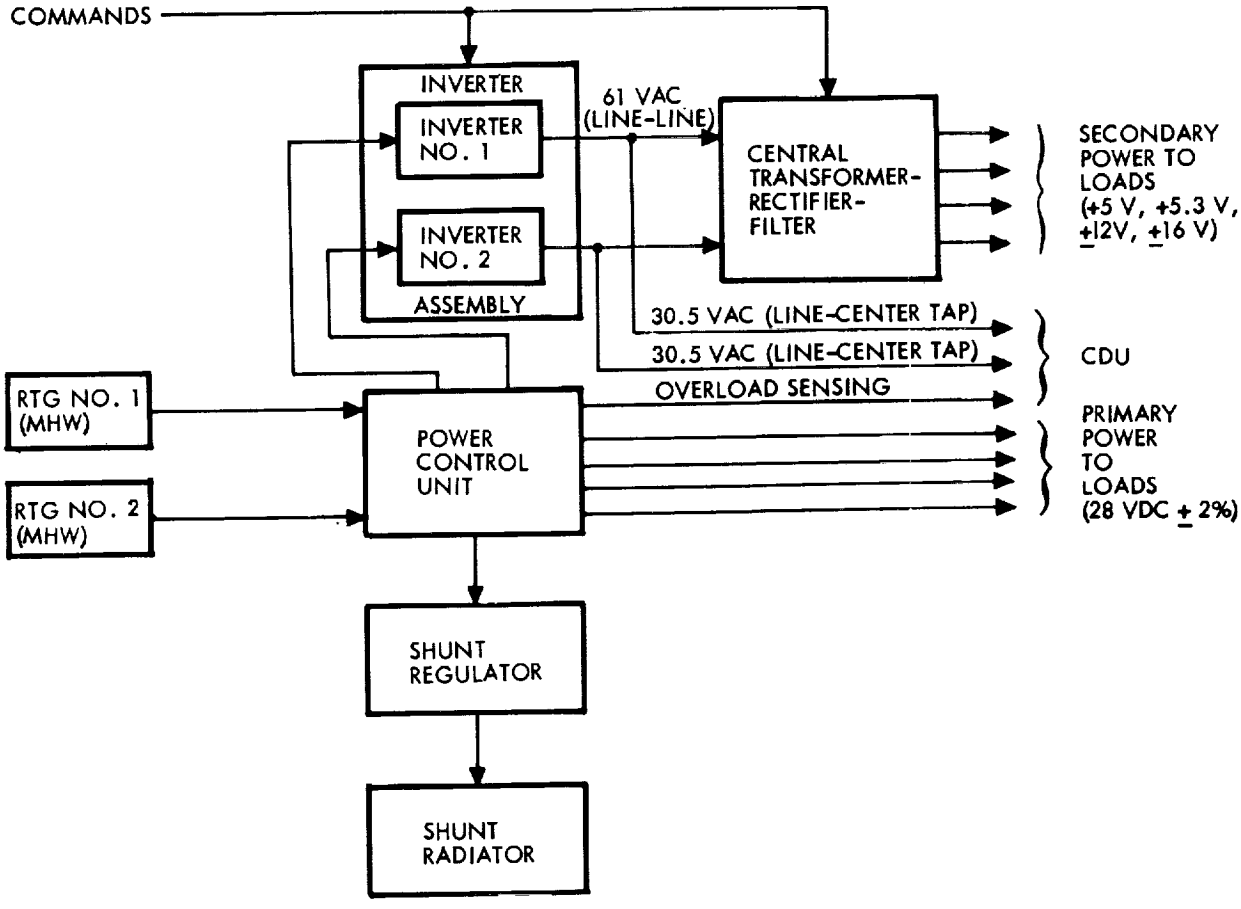

Figure 4-24. Power Subsystem Block Diagram

Table 4-7. Electric Power Subsystem Functional Characteristics

Component	Function	Modification to Pioneer F/G Design
RTG	Power source	Replace four 40-watt, 4.2-volt SNAP-19 units with two 150-watt, 28-volt MHW units
Power Control Unit	Cross-strap RTG units Provide RTG fault isolation Distribute primary DC power to loads Provide power circuit protection Regulate DC bus to 28 VDC ±2% Control dissipation of excess RTG power Provide overload sensing Condition power subsystem diagnostic telemetry	Remove battery charger, battery discharge regulator Remove shunt regulator Modify control logic, DC bus filter, telemetry conditioning Add RTG fault control logic, RTG cross-strapping, load distribution circuits
Shunt Regulator	In conjunction with shunt radiator, dissipate excess RTG power	Increase capability to dissipate 75 watts Repackage for mounting external to equipment compartment
Shunt Radiator	In conjunction with shunt regulator, dissipate excess RTG power	Increase dissipation capability to 250 watts
Inverter Assembly	Invert 28 VDC to 61 VAC, 2.5 kHz for input to CTRF Supply AC to CDU for ordnance capacitance charging Provide inverter fault isolation	Modify transformer and power stages to accept 28 VDC instead of 4.2 VDC Delete RTG telemetry circuits Reconfigure reverse current relays to provide AC bus switching for CTRF input Add redundant oscillator
CTRF	Provide conditioned and regulated DC power at several voltages to spacecraft loads Provide current limiting at each output	Increase number of data storage unit TRF slices Increase capacity of attitude control TRF's Add X-band transmitter driver TRF's Assemble existing, modified and new TRF's to form two separate TRF units

Table 4-8. Electric Power Subsystem Physical Characteristics

Component	Pioneer F/G				Orbiter Spacecraft			
	No. of Units	Size (in.) Length x Width x Height	Weight (lb) Each	Weight (lb) System	No. of Units	Size (in.) Length x Width x Height	Weight (lb) Each	Weight (lb) System
RTG	4	15.7 dia x 11.1	30.1	120.4	2	15.7 dia x 23.0	85.0	170.0
Power Control Unit	1	6.0 x 8.0 x 9.3	10.9	10.9	1	6.0 x 8.0 x 5.8	7.3	7.3
Inverter Assembly	2	4.5 x 6.0 x 7.0	5.1	10.2	1	4.5 x 6.0 x 7.0	5.1	5.1
Shunt Regulator	N/A	Part of PCU	N/A	N/A	1	6.0 x 8.0 x 1.6	2.2	2.2
Shunt Radiator	1	12.5 x 15.0 x 1.9	0.8	0.8	1	243 square in.	1.0	1.0
Central TRF Unit A	1	6.0 x 8.0 x 11.3	11.8	11.8	1	6.0 x 8.0 x 6.8	7.2	7.2
Central TRF Unit B		Not applicable			1	6.0 x 8.0 x 6.8	7.2	7.2
Battery	1	10.6 x 8.2 x 2.7	5.2	5.2		Not applicable		
Spacecraft Total				159.3				200.0

The Pioneer orbiter electrical power requirements to be met by the power subsystem design were previously discussed in Section 3.4 (see Table 3-5).

4.5.2 RTG's

A description of the various candidate RTG systems considered for the Pioneer outer planets orbiter is given in Appendix E.

The selected RTG for the orbiter mission is the MHW providing an estimated beginning-of-life power output of 150 watts at 28 VDC. Two of these units will be required to support the maximum steady-state Jupiter-orbiter load of 237 watts plus 14 watts for the maximum pulsed load (see Section 3.4). The characteristics of the MHW unit and an alternative candidate, the SNAP-19 HPG, are given in Appendix E. The two RTG's are expected to provide a total power of 160 watts during ground operations, 300 watts at beginning of life in vacuum, and decreasing to 265 watts after 3.5 years of operation.

4.5.3 Power Control Unit

The PCU provides central power conditioning, regulation, and distribution for the subsystem, as shown in Figure 4-25. Specifically, it performs the following functions:

- Combines the two RTG inputs to form a DC bus. This bus distributes power to the TWTA's, pulse loads, scientific instruments and heaters
- Controls shunt dissipation to regulate the DC bus to 28 VDC $\pm$2 percent
- Provides fault isolation for the RTG's
- Provides bus overload sensing
- Conditions subsystem diagnostic telemetry
- Provides fused branch circuits for scientific instruments.

Bus regulation is accomplished by a closed-loop regulation technique which uses majority-voting voltage-error amplifiers where the output current is linearly varied in response to the bus voltage error signal. If the RTG power capability exceeds the load demand, the bus voltage will rise above the deadband and the shunt will be enabled. The shunt regulator limits the bus voltage by dissipating a portion of the excess power in the power transistor stages and the remainder in a resistive shunt radiator (parallel redundant resistors).

Shunt regulation is compatible with RTG operating requirements necessitating operation near the maximum power point to minimize excessive internal temperatures which would accelerate performance degradation.

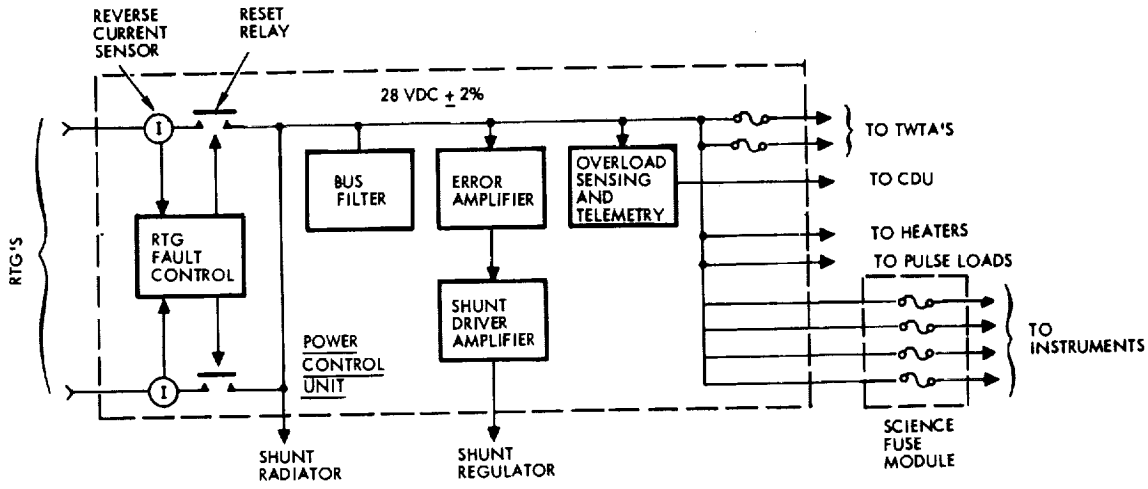

Figure 4-25. PCU Simplified Block Diagram

This method also minimizes shunt losses under mission conditions where the available RTG output equals the load requirements. Thereafter, as further RTG degradation occurs, load power can be maintained equal to or less than the source capability by ground command.

4.5.4 Shunt Regulator/Radiator

The Pioneer 10/11 shunt regulator slice consists of six power transistors, arranged in a 2 x 3 series-parallel array to preclude catastrophic single part failures, as shown in the simplified schematic, Figure 4-26.

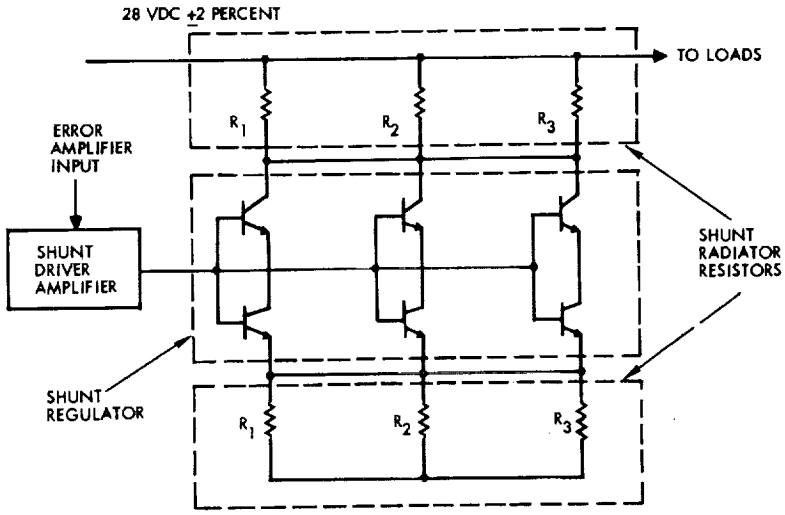

Figure 4-26. Simplified Shunt Schematic

The shunt current requirements for the orbiter mission are appreciably higher than for Pioneer F/G: approximately 10 amperes for an undervoltage condition which disconnects all loads not essential to spacecraft survival, and assuming maximum RTG power (300 watts) is available.

Each series string of transistors is capable of handling 2.25 amperes of shunt current. The Pioneer F/G design, therefore, is limited to 4.5 amperes with one string failed. Consequently, the orbiter shunt regulator must be modified to provide supplemental shunt transistor strings to increase the power dissipation capability. This may be accomplished by the addition of transistors to the existing shunt slice or, alternatively, mounted in individual housings to facilitate their placement.

Electrically, the approaches are identical. Since the shunt regulator is removed from the PCU for mounting external to the equipment compartment and will require repackaging, the most straightforward solution is incorporation of the additional power transistors in the new shunt regulator.

The apportionment of power dissipation between the shunt regulator and shunt radiator as a function of shunt current is shown in Figure 4-27.

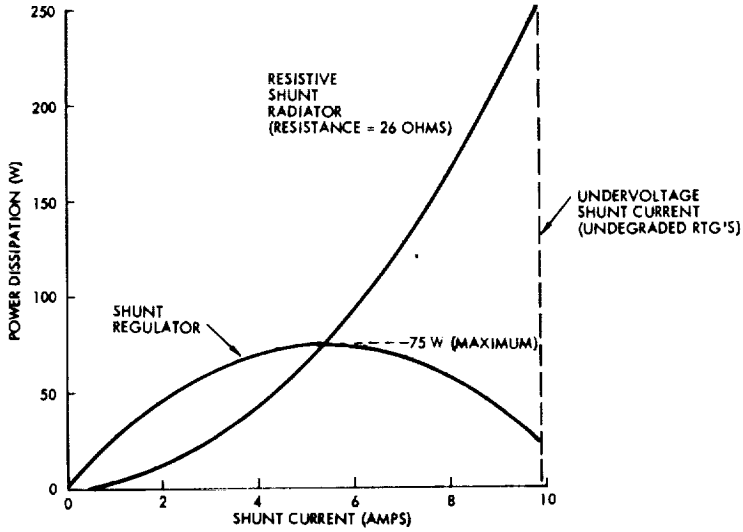

Figure 4-27. Shunt Dissipation Characteristics

In the absence of an RTG failure and with the predicted degradation rates, the power subsystem will operate in the shunting mode for the entire orbiter mission. Excess RTG power capability is readily determined from the shunt current telemetry sensor.

4.5.5 Inverter Assembly

Dual inverters housed in the inverter assembly operate in parallel from the 28 VDC bus, as shown in the schematic on Figure 4-28. Fuses at each inverter input protect against faults within the inverter assembly.

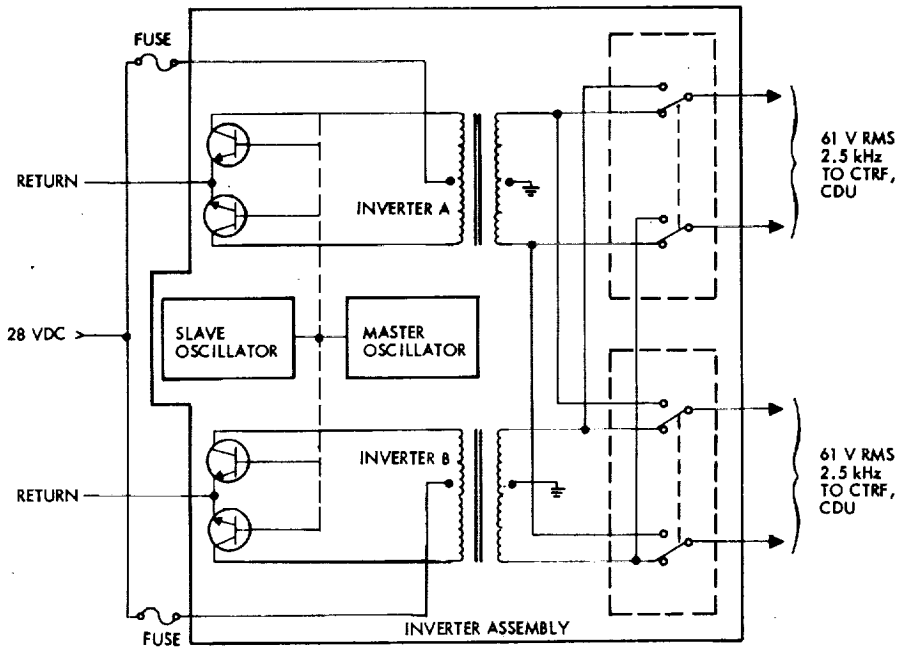

Figure 4-28. Inverter Assembly Schematic

Redundant oscillators synchronize the inverter switching. Normally the inverters are driven by the master oscillator. Switchover to the slave oscillator is automatic should the other fail.

The cross-strapping relays at the inverter output allow switching of the redundant CTRF slices to the alternate inverter should one inverter fail. Moreover, either inverter can drive the entire CTRF, if required.

The inverter assembly is a modified Pioneer F/G design. The majority of design changes are necessitated by the requirement to operate from the 28-volt bus instead of from the 4.2-volt RTG output. The deletion of the RTG telemetry circuits permits the addition of the redundant oscillator.

4.5.6 CTRF

The CTRF is comprised of individual transformer-isolated power supplies for each subsystem which convert the 61-volt rms AC bus to DC voltages tailored to the user requirements. Each power supply is packaged in a separate but identical housing (slice) which facilitates their addition and removal to readily adapt to mission requirements. A block diagram of a typical TRF-regulator slice is illustrated in Figure 4-29.

Each voltage output (with the exception of two outputs to non-redundant subsystem units) has a separate TRF-regulator. Automatic or command switching between redundant TRF-regulators is provided, as required.

Two types of regulators are used. Series-dissipative regulators are used for all voltages where the current requirements are less than

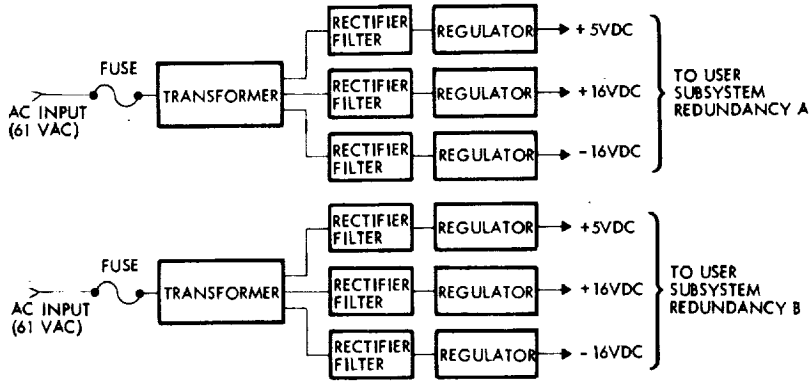

Figure 4-29. TRF-Regulator Block Diagram (Typical)

100 mA. A switching regulator is used for the +5-volt outputs where the current requirements exceed 100 mA. This approach limits power dissipation and increases the efficiency.

The CTRF provides two types of fault isolation. In the event of a secondary fault the user output is current limited to prevent an excessive power demand from propagating back to the inverter and the main bus. In addition, the input to each slice is fused to clear CTRF shorts from the AC bus.

The majority of Pioneer F/G CTRF slices are directly adaptable to the orbiter configuration. However, modifications to the ACS and DSU slices are required and the X-band transmitter drivers will require an additional slice.

4.6 COMMAND DISTRIBUTION

The command subsystem provides the capability of controlling the operating modes of the spacecraft equipment and scientific instruments from information received in RF transmission to the spacecraft and from signals generated on-board at discrete events. The command subsystem consists of redundant command decoders (DDU) and a command distribution unit (CDU). A functional block diagram of the subsystem is shown in Figure 4-30. The configuration is identical to that employed on Pioneer F/G, with relatively minor modifications to the CDU to accommodate additional requirements peculiar to the outer planets orbiter mission.

4.6.1 Summary Description

Commands are transmitted to the spacecraft with a PCM/FSK/PM modulation of the uplink S-band carrier signal at a rate of 1 bit/s. Twenty-two bits are transmitted from the ground for a single command message. Two bits are used for selecting the decoder, three bits are used for command routing, and eight bits for command information. The remainder are used for processing and verification of the command. The activated spacecraft receiver demodulates the carrier and provides the frequency shift key (FSK)

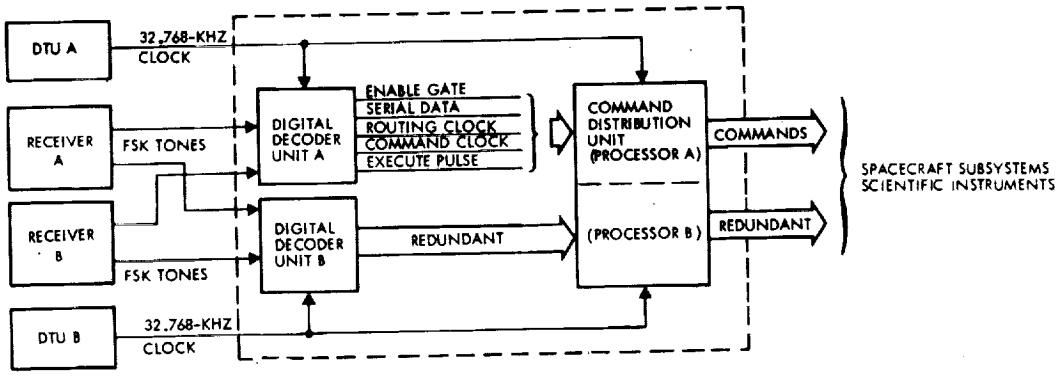

Figure 4-30. Command Subsystem Functional Block Diagram

tones to the command decoders. The addressed decoder converts the FSK tones to digital data and performs a verification operation with the command message to reduce the probability of executing wrong commands. The decoder forwards the routing address, command message and, if the command is properly verified, an execute pulse to the command distribution unit. If the command is not properly verified by the decoder the execute pulse is inhibited and the CDU does not act on the command message.

The CDU processes and distributes all commands to the spacecraft equipment and scientific instruments. Two basic types of output are provided by the command distribution unit. One type is a serial data output to a specified user. The routing portion of the command message identifies the user and the 8 bits of command information provide the serial data. The other output is a signal applied to any one of 255 discrete lines for initiating specific functions. The routing portion of the message signifies this discrete type of output and the 8 bits of command information identify the particular one of the possible 255 discrete commands. The CDU also has the capability of being programmed by the routing and command messages to store up to 32 discrete commands and their associated time tags for later execution with up to 36 hours delay. This feature permits the commands to be sent and verified by telemetry before execution and will be particularly useful at extended ranges when the communication time is appreciable. In addition, the command distribution unit will provide a sequence of commands that will be activated at preset intervals by a sequencer which will be initiated automatically by separation of the spacecraft from the launch vehicle.

In the event of an overload condition on the primary electrical bus, the CDU will sequentially disconnect power to the various subsystems which are not essential to spacecraft survival. Restoration of these loads is by ground command.

The CDU also provides for the automatic switching of the two antenna system inputs to the redundant receivers if a preset interval elapses without ground station contact. If either receiver is activated before the time delay period, the circuit is reset.

The command subsystem provides parallel on-line redundancy. Receivers (part of the communications subsystem), digital decoder units, and the command distribution unit (internally redundant) are always powered. No single-failure will prevent the receipt and execution of commands.

4.6.2 Digital Decoder Unit

The Pioneer F/G DDU and command message format are directly applicable to the orbiter spacecraft configuration without modification. The DDU interfaces with the receivers and with the CDU are compatible and flight-proven.

4.6.3 Command Distribution Unit

The CDU is a centralized unit that performs command processing and supplementary functions for the entire spacecraft. Figure 4-31 shows a functional block diagram of the CDU. Table 4-9 summarizes the functions performed by the CDU. The following sections describe the changes to the Pioneer F/G design required for the orbiter spacecraft.

4.6.3.1 Thruster Counters

The thruster counter provides an indication of the number of firings executed by the velocity/precession thrusters (VPT) and the spin control thrusters (SCT). The Pioneer F/G VPT counters are capable of counting a maximum of 64 firings before recycling; the SCT counters recycle after two firings. In addition to firing count, the counter circuitry provides real-time telemetry indication of when the thrusters are firing.

During an orbiter mission, spacecraft spin rate will be varied several times, as needed, to meet pointing and experiment scan rate requirements. Moreover, the spin control thrusters may be used in a pulse mode to effect spacecraft velocity corrections (ΔV) normal to the spin axis while keeping an earth-pointing attitude. Consequently, the orbiter spacecraft is equipped with a redundant pair of SCT's to enhance the reliability of these operations. Two additional counters are provided to indicate the status and number of firings.

When the SCT's are used to support a ΔV maneuver, pulses are issued each spacecraft revolution for a preselected time interval. It is desirable, therefore, to expand the maximum count capability of each of the four SCT's from 2 to 64. The required signal processing circuitry is identical to that used for the four VPT's. Word allocations in the telemetry format must also be increased.

4.6.3.2 Command Memory Processor

The stored command feature is particularly convenient for orbiter missions — greatly simplifying ground operational procedures and increasing flexibility for activating various configuration and mode changes when the spacecraft is occulted by the planets. The Pioneer F/G command memory

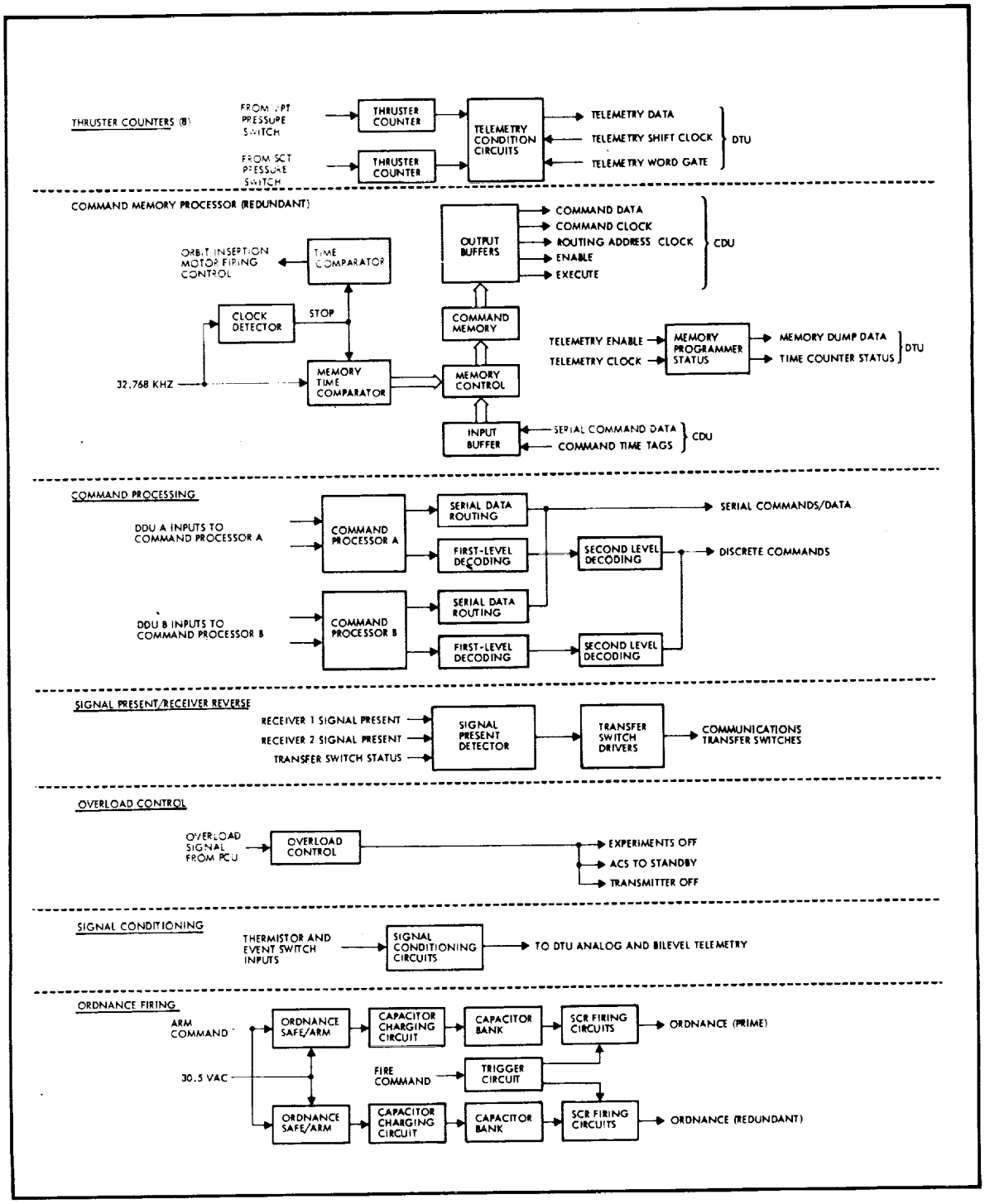

Figure 4-31. Command Distribution Unit Functional Block Diagram

Table 4-9. Command Distribution Unit - Function Summary

Function	Initiation	Operating Time	Description	Characteristics
Thruster Firing Control	Thruster pressure switch closure	During thruster firing periods	Detect and store thruster firing counts	Count up to 64 firings of each thruster: 4 velocity/precession thrusters, 4 spin control thrusters
Command Memory	Ground command - "Execute stored sequence"	Dependent upon time tags stored in time registers	Store 32 commands that can be initiated following stored time delays	Storage: 16 commands with redundancy, 32 commands total Time resolution: ±2 seconds Maximum time delay: 36 hours
Command Processing	Upon receipt of command signal from DDU via command link	22 seconds, maximum 20 seconds, minimum per command	Accept, process, and distribute real-time commands	255 discrete commands Up to 7 serial commands Command word: 8 bits Redundant processors
Signal Present Control	Absence of receiver signal indicating loss of lock	After elapse of 36.4 hours	Signal present control for automatic switching of receivers/antennas	16 pps clock from DTU "Signal present" resets countdown Enable/inhibit by ground command
Overload Control	Signal from 28 VDC bus sensor in PCU	300 ms, maximum	Overload control to turn off nonessential power	Sequenced events: Experiments off - 60 ms delay ACS standby - 180 ms delay Experiments off - 300 ms delay Control off (reset - 420 ms delay)
Signal Conditioning	Continuous monitoring	Continuous	Signal conditioning of switch positions and thermistors for telemetry	Passive resistor components for switch positions Resistor linearization for thermistors Conditioned output: 0 to 3 VDC
Ordnance Firing	Ground commands	During armed period and firing time	Control ordnance safe, arm and firing functions	Capacitor discharge method, redundant capacitor banks Recharge time: 3 minutes

consists of five command messages and their associated time delays for later sequential execution. The relatively limited capacity of the existing design, coupled with timing resolution of only 128 seconds and lack of redundancy, led to selection of a new design to meet the more complex operational requirements of outer planet orbital missions.

The preferred command memory processor, shown in Figure 4-32, is capable of storing 32 discrete commands (16 each in redundant programmers) and associated time tags, providing a maximum delay of 36 hours with a resolution of two seconds. This design permits the memory "stack" to be executed in an order different from that in which the commands were stored. Further, the stored commands are not destroyed following execution, thereby simplifying repetitive operational sequences and minimizing the need for periodic mandatory real-time commands.

The 32-command capacity was selected to optimize the use of standard 256-bit C-MOS chips (identical to the device recommended for the data storage unit) and offers substantial reserve for potential increase in requirements. Active redundancy precludes late execution (or failure to execute) due to single-point failures, affording fail-safe operation for critical events such as orbit insertion motor firing. The redesigned command memory processor is repackaged in the existing CDU slice.

Command memory operation is divided into three phases: programmer data load, memory verify, and command processing. Data loading consists of inserting data into the C-MOS memory. The memory itself is subdivided into two sectors — one for time codes and one for commands. Each can be controlled individually. Sixteen bits of time data are loaded 1 bit at a time into random-access memory (RAM) No. 1 successive addresses; 8 bits of command data into RAM-2.

Memory verify is a complete readout or retrieval of the memory contents through telemetry for bit-by-bit comparison on the ground. The readout begins at address 0 and progresses sequentially through the 256 address locations.

After data load and verify, command processing is initiated upon receipt of an execute command. The stored time for each command is compared every two seconds with the 16-bit time counter for equality. When equality is detected, the command data in the command register is serially transferred at a rate of 64 bits/s to the CDU processor for further processing and execution. An execute pulse, delayed by 50 milliseconds, is routed to the processor for execution of the stored command. Command processing requires that the two address counters operate together with the bit/word counter providing control information for the memory. This complete time comparison is conducted in about 8 msec and permits loading of stored commands in a random fashion. The time counter can be preset by ground command in addition to reset to zero, or the counter can be reset by one of the stored commands. This enhances program flexibility.

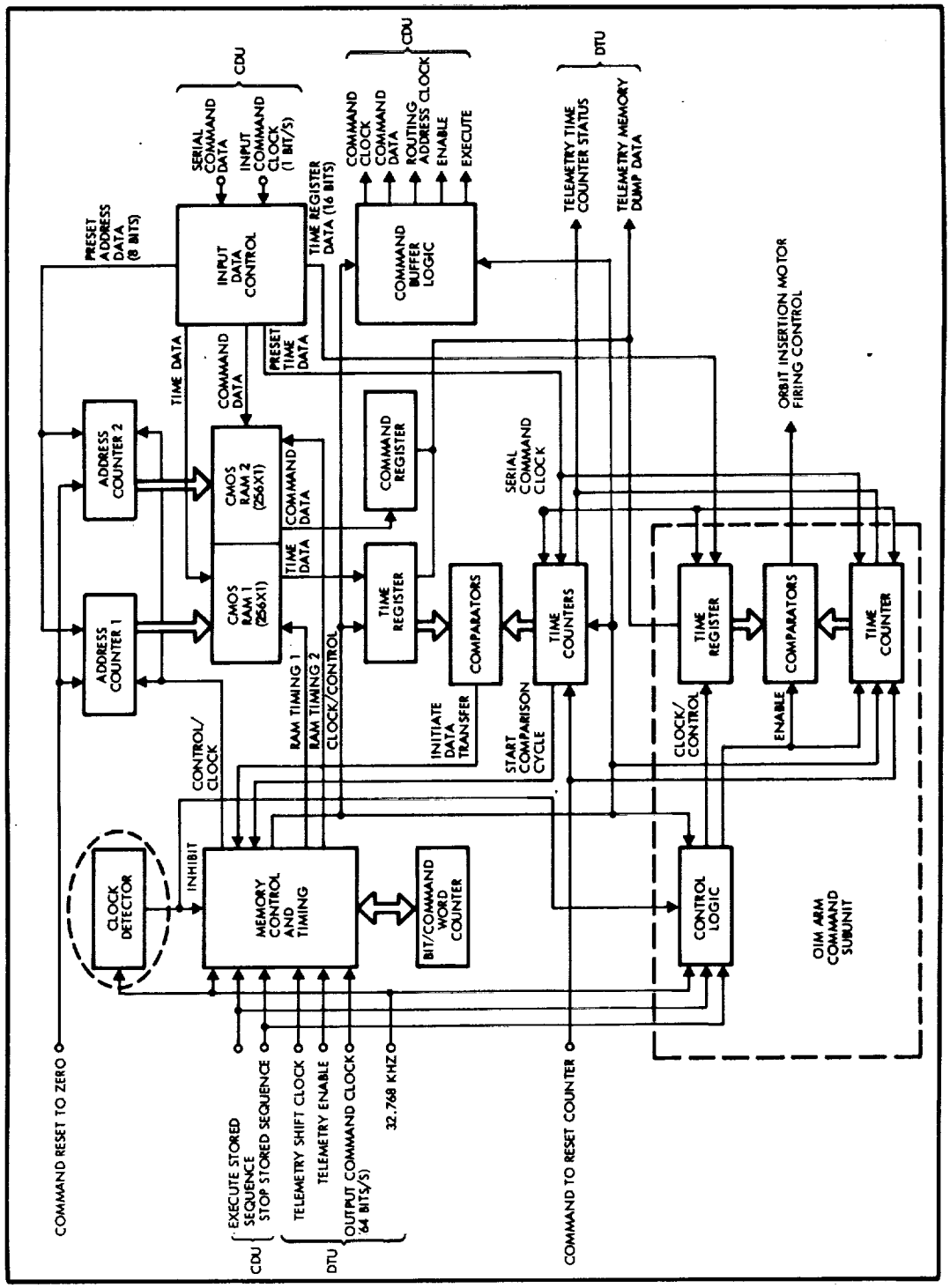

Figure 4-32. Command Memory Processor Block Diagram (Typical of Two Redundant Boards)

Fail-safe stored command operation is essential for reliable activation of the bipropellant propulsion stage. This is achieved by using a clock detector (depicted in Figure 4-33) which will inhibit the command memory processor if the 32-kHz clock source shifts frequency due to a failure in the countdown chain. The detector integrates the 32-kHz signal and converts it to a DC level proportional to frequency which is compared to a preset value. Clock frequency increase greater than 20 percent triggers the inhibit signal. Thus, premature firing due to fast clocks is avoided. All other single-point failures are precluded by using a separately generated arm command. This arm command is isolated from the other 16 commands. Note that there are two arm commands (primary and backup) and two fire commands (primary and backup) configured so that no single-point failure can cause an early, late, or no-fire condition.

4.6.3.3 Command Processing

The CDU is capable of processing 255 discrete commands whereas less than 190 commands have been implemented for Pioneer F/G. Thirty-four of the unused discretes are available without modification to accommodate increased orbiter spacecraft requirements; the remainder can be made available by the addition of integrated circuits on existing circuit boards.

4.6.3.4 Signal Present Control

Signal-present detection circuitry is provided to automatically switch antenna inputs to the redundant receiver, after a preset interval, to preclude a lock-out condition if a receiver fails and the spacecraft attitude is not favorable for reception of uplink commands with the antenna connected to the operative receiver. A limitation of the Pioneer F/G CDU design resulted in either a 36-hour or 72-hour period, depending on the previous position of the receiver transfer switch. Inclusion of a simple logic function to monitor the transfer switch position will ensure that the preset delay remains invariant, regardless of the initial position of the switch.

4.6.3.5 CDU Configuration Summary

Implementation of the previously described modifications to the Pioneer F/G CDU necessitates change to five of the eight slices. These modifications are summarized in Table 4-10.

4.7 DATA HANDLING

4.7.1 Summary Description

The data handling subsystem consists of a digital telemetry unit (DTU) and a data storage unit (DSU). Figure 4-34 shows the functional interconnection of these units and their major external interfaces. The subsystem time-multiplexes and formats science and engineering data into a PCM/PSK coded or uncoded data stream suitable for modulating the telemetry carrier signal. Timing and operational signals are provided to the scientific

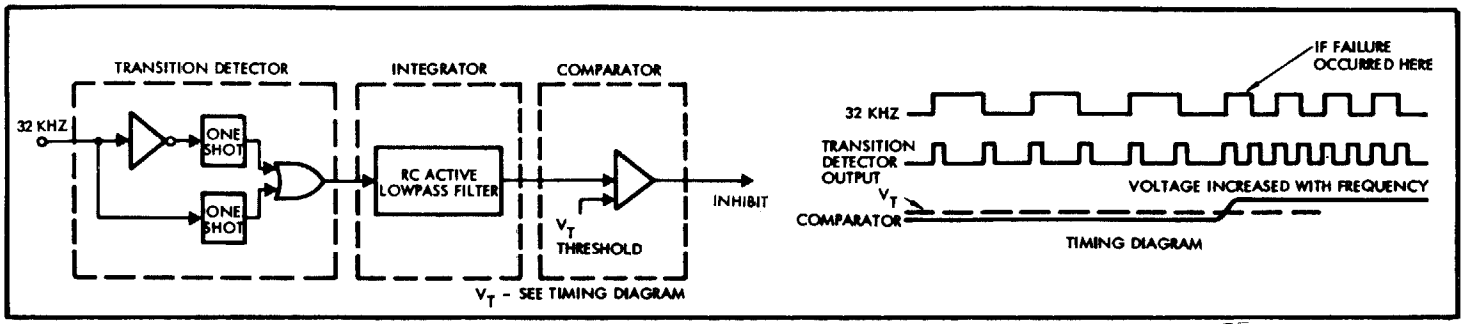

Figure 4-33. Clock Detector Block Diagram

Table 4-10. CDU Configuration Summary

Size:	8 x 7 x 8.9 inches	Previous Use:	Pioneer 10&11
Weight:	9.0 pounds	Redundancy:	Internal
Power:	2.1 watts	No. of slices:	8

Slice No.	Weight (lb)	Description	Modification
1	3.0	Ordnance - capacitor discharge function	None
2	0.99	High-level output control/ sequencer	None
3	0.99	Telemetry conditioning/ undervoltage/thruster counter	Increase SCT counter to 64 Add two thruster counters for redundant SCT's
4	0.76	Signal present control/ telemetry signal conditioning	Revise receiver reverse logic
5	0.74	Low-level output No. 1	Increase pulse commands to full capability
6	0.74	Low-level output No. 2	Increase pulse commands to full capability
7	0.84	Command processor	None
8	0.94	Command memory processor	Redesigned to increase capacity and flexibility, and to include a fail-safe orbit insertion motor firing circuit

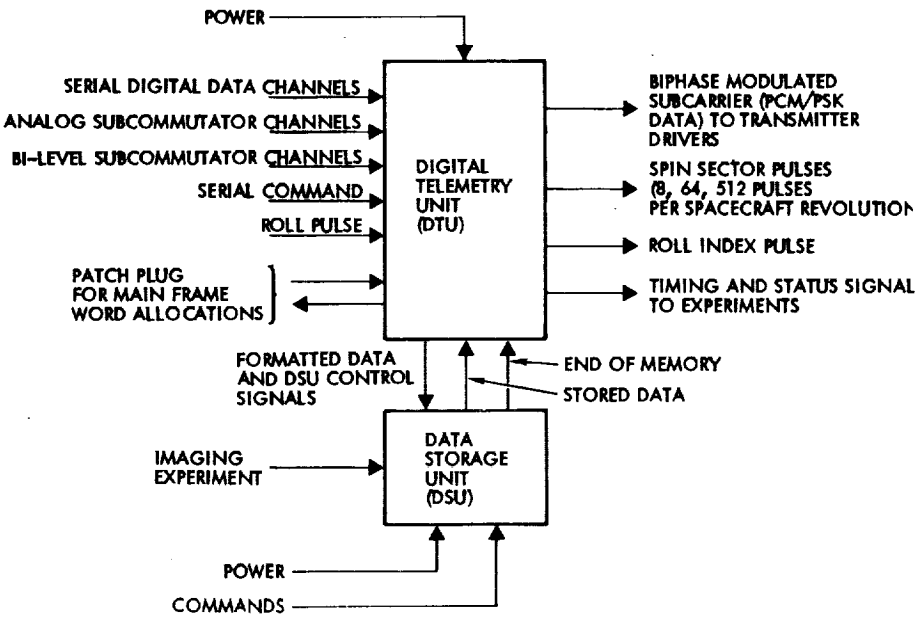

Figure 4-34. Data Handling Subsystem Block Diagram

instruments and spacecraft subsystems. The memory unit will store and send out formatted data upon command. It will also buffer high rate instrument data into the prevailing telemetry bit rate.

All of the investigations required to exploit the imaging system have not been completed. Further studies are required to optimize the subsystem performance. Data compression and concatenated coding are promising techniques which are currently under consideration in a separate study, for application to future outer planet missions. The reference configuration defined in this section does not incorporate these advanced features.

4.7.1.1 Formats

The DTU assembles input data into frames composed of a series of 192 bits. Formats are arrangements of frames. The formats are divided into science and engineering groups. The science group includes two basic science formats shown in Figure 4-35, eight special purpose science formats for science main frame data, and two science formats that are subcommutated in the main frame. The basic science formats each contain 192 bits which includes 144 bits assigned to the scientific instruments, 6 bits to subcommutate the engineering formats, 6 bits to subcommutate the science subframe, 18 bits for frame synchronization and the remainder for identification of the subcommutated data, telemetry mode, bit rate and format. The two basic science formats may be arranged to cater to selected instruments during different mission phases. Each redundant section of the DTU has a patch plug which allows for the rearrangement of the basic science formats without disassembling and rewiring the DTU. The eight special purpose science formats each contain 192 bits of digital data from only one or two scientific instruments (there are no subcommutated or identifying words) and are transmitted only in conjunction with one of the basic science formats, alternating every 192 bits. These special formats

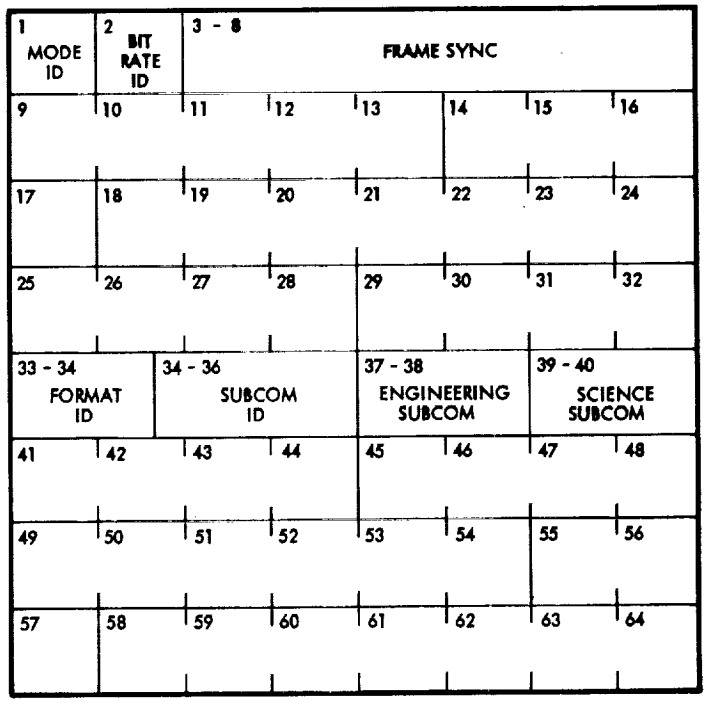

NOTES:

1. FORMATS A AND B ARE THE BASIC SCIENTIFIC FORMATS WITH A WORD SIZE OF 3 BITS
2. SUBCOM ID = SUBCOMMUTATOR IDENTIFICATION
3. EACH BLANK WORD SLOT DENOTES A SERIAL DIGITAL WORD SLOT. FORMATS A AND B ARE BOTH INDEPENDENTLY PATCHABLE IN THE DATA PORTION OF THE MAINFRAME. EACH OF THESE TWO FORMATS HANDLE A MAXIMUM OF 12 DIGITAL INPUT CHANNELS.
4. EACH MAINFRAME WORD SLOT IS SAMPLED AT A RATE OF BR/192, WHERE BR = BIT RATE

Figure 4-35. Mainframe Organization

provide the capability to sample data from certain scientific instruments at a high rate at the expense of reducing the amount of data from the other instruments by one-half. This feature is particularly useful for buffering imaging data.

The engineering data are separated by subsystem into four formats as follows: 1) data handling, 2) electrical, 3) communications, and 4) orientation and propulsion. With a science main frame the engineering formats are subcommutated sequentially in 6 bits of the basic science format. With an engineering main frame the four engineering formats can be transmitted sequentially or each engineering format can be transmitted individually with all four engineering formats subcommutating sequentially at the main frame rate. The separation of the engineering data into formats by subsystem provides high data rates for launch phases, critical maneuvers and diagnostic purposes. The subcommutating science formats, each 192 bits long, also subcommutate 6 bits in the engineering formats at the main frame rate.

4.7.1.2 Modes

The three mutually exclusive modes are real time, telemetry store, and memory readout. A buffer mode, part of the real-time mode, may be used to store high rate data from the imaging experiment.

In the real-time mode, data are transmitted directly without intermediate storage at a bit rate selected by ground command.

In the telemetry store mode, formatted data are simultaneously transmitted and stored. When the memory has been filled, the DTU automatically reverts to real-time operation. The DSU memory can be partially filled and storage subsequently resumed at the location of the last previously stored data.

The memory readout mode provides for accessing formatted data from the DSU for transmission to earth at a bit rate selected by ground command.

4.7.1.3 Performance Characteristics

A summary of the key characteristics of the modified DTU applicable to the orbiter missions is given in Table 4-11.

A summary of the key characteristics of the recommended solid state DSU is given in Table 4-12.

4.7.2 Digital Telemetry Unit (DTU)

A brief description of the Pioneer 10/11 DTU, shown in Figure 4-36, is given as a basis for a discussion of modifications proposed for the Jupiter and Saturn orbiter configurations. The DTU is the heart of the data handling subsystem and processes analog, digital and bilevel (discrete) science and engineering data into a serial time-multiplexed PCM signal which modulates the telemetry carrier. Nearly all elements in the DTU are redundant and selectable by command. A stable, crystal-controlled clock and countdown chain generates the timing signals needed throughout the spacecraft and for transfer of data to the DTU. Utilizing timing signals and the roll reference pulse provided by the attitude control subsystem, a spin period sector generator within the DTU generates an accurate roll-index pulse and spin period sector pulses corresponding to 512, 64, and 8 sectors per spacecraft revolution for the scientific instruments and spacecraft subsystems. This information is also used to determine roll position in relation to the telemetered data and spin rate. A 6-bit analog-to-digital converter is used to encode analog inputs into binary words and is continually checked by encoding three reference voltages. The output of the DTU to the transmitter is a NRZ-L biphase-modulated square-wave subcarrier. The DTU has a patch plug which allows for rearrangement of the two main science formats without disassembly and rewiring of the DTU.

Table 4-11. DTU Characteristics

Parameter	Value
Weight, lb	6.8
Power, W	4.7
Size, in.	11.3 x 7.9 x 5.7 (509 $in.^3$)
Formats	23
Operating modes	Real time Telemetry store Memory readout
Data output	Biphase modulated subcarrier
Data bit rate	Reference Table 4-
Subcarrier (square wave)	32.768 kHz (bit rates $\leq$ 4096 bits/s) 262.144 kHz (bit rates > 4096 bits/s)
Frame size	
Main frame Subframes	192 bits, 3-bit words 384 bits, 6-bit words
Data input channels	114 analog (subframe only) 86 digital 102 bilevel (subframe only)
Analog signal quantization	6 bits
Digital and bilevel signal threshold, V	2
Data coding (by command)	Convolutional, K = 32, R = 1/2
Extended frame counter	Uniquely identifies 8192 data frames
Central timing Clock frequency, MHz Clock stability (long-term) Clock stability (short-term)	 4.194304 $\pm$0.02 percent $\pm$0.002 percent

Table 4-12. DSU Characteristics

Parameter	Value
Weight, lb	9
Power, W	7.5
Size, in.	12 x 6 x 8 (576 $in.^3$)
Operating Modes	Write in Read out
Capacity, bits	1,536,000
Read/write rate, bits/s	Up to 1000
Control	DSU is controlled by DTU in telemetry store mode and by the instrument in the buffer mode (D formats)

C-3

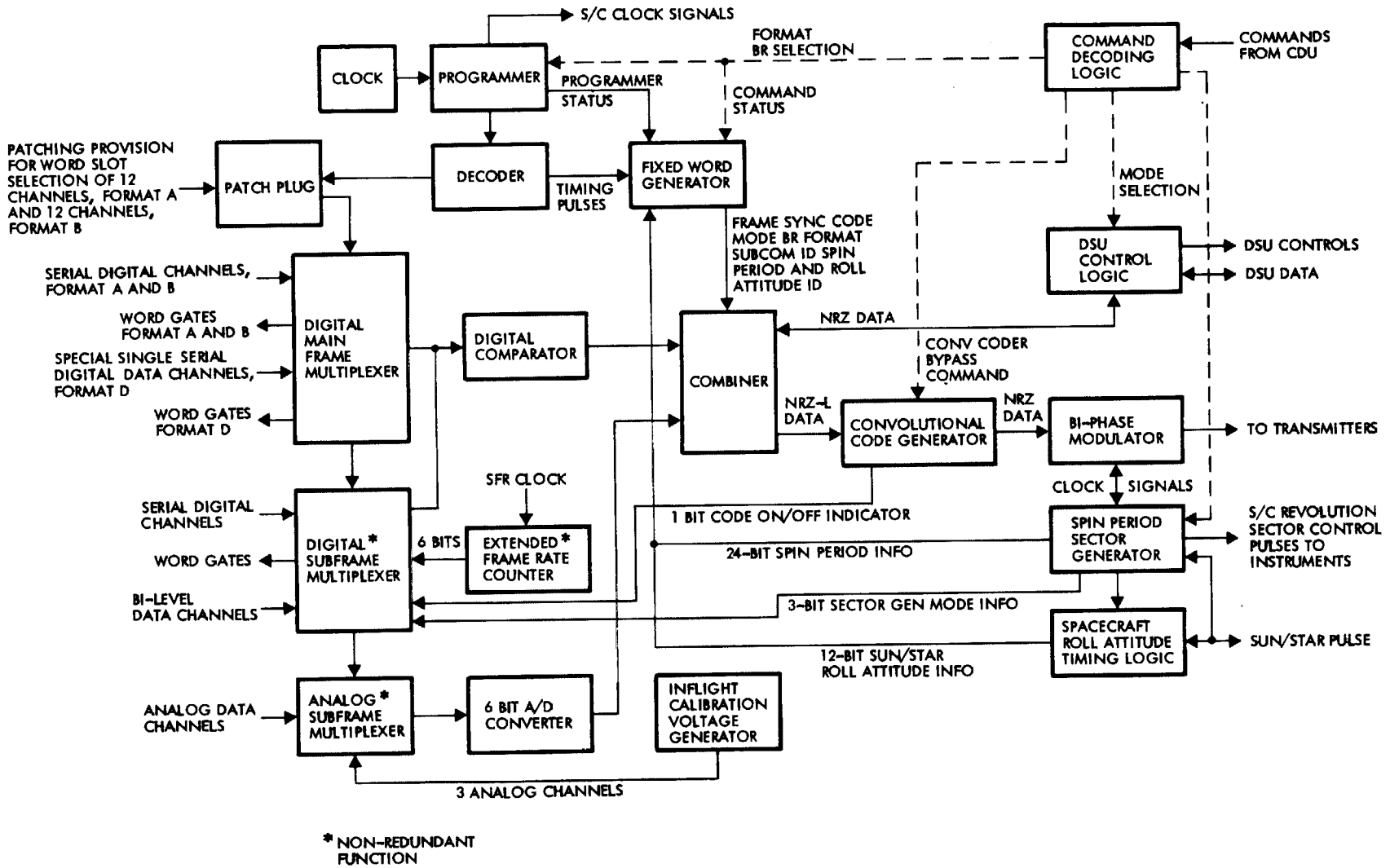

Figure 4-36. DTU Functional Block Diagram (Pioneer 10/11 Configuration)

The convolutional coder, packaged as part of the DTU, codes the formatted data to increase the telemetry efficiency. The telemetry data can be either coded or uncoded by command. The encoder has a multiple-bit shift register and data are shifted in and out of the register at the data bit rate. Logic is provided for generating a pair of parity bits, based on the data in the shift register, for each incoming data bit. Thus, the parity bits are generated and transmitted at twice the data rate. In error-free data, the bits of a pair provide an unambiguous representation of the original data bit. With errors in the data, a decoding process on the ground, utilizing a sequence of parity pairs, provides reconstructed error-free data well beyond normal acceptable error limits without the coding.

4.7.2.1 Modifications

The basic orbiter mission requirements for data handling can be met by modifying the Pioneer 10/11 DTU. The available formats and modes are versatile and easy to adapt to a wide range of science telemetry requirements. The important design driver requirement differing from Pioneer 10/11 is provision for operating at substantially higher data rates — to 33 kilobits per second at Jupiter and 8 kilobits per second at Saturn. This requirement is dictated by imaging experiment requirements to obtain as many pictures as possible.

A high frame rate will be particularly desirable in imaging planetary satellites during close encounters. Typically, a frame rate of N frames per hour corresponds to a telemetry bit rate of about N kilobits per second, assuming a line scan image system with 400 detector cells.

A high frame rate will be particularly desirable in imaging planetary satellites during close encounters. Typically, a frame rate of N frames per hour corresponds to a telemetry bit rate of about N kilobits per second, assuming a line scan image system with 400 detector cells.

The Pioneer 10/11 has eight commandable bit rates from 16 to 2048 bits/s in powers of 2. Operation at higher bit rates required by the orbiter mission will necessitate the following modifications:

1. The A/D converter must be redesigned to operate at the higher data rates

2. The programmer countdown logic and timing circuitry must be modified to provide the faster bit rate(s)

3. The main frame and subframe multiplexer speed must be increased by changing the driver circuits.

These identified changes involve modifications to seven of the existing nine circuit boards.

The command decoder logic within the Pioneer 10/11 DTU is configured to detect and process 8 bit rate commands. In addition, one 3-bit word in the main frame is internally wired to the bit rate identification. Therefore requirements to operate the DTU at more than 8 different bit rates would result in some changes to the decoder logic and rearrangement of fixed word assignments in the telemetry frame. Consistent with the philosophy of minimum modifications, the number of available bit rates was restricted to 8. However, in order to accommodate the expanded range of bit rates, it was necessary to omit some intermediate values. The rationale for the selection of 8 bit rates was to choose the highest bit rates which could be supported by the S- and X- band links at the target planet. Consequently some differences may be noted in the preferred bit rate selection for the Jupiter and for the Saturn Orbiter missions; these are identified in Table 4.7-3. The final choice of bit rates for a given mission ultimately depends on the scientific payload, the effective radiated rf power, and the target planet(s).

Table 4-13. Data Handling Subsystem Bit Rates

Bit Rate (bits/s)	Pioneer 6-9	Pioneer 10/11	Jupiter Orbiter	Saturn Orbiter
32,768			x	
16,384			x	
8,192			x	x
4,096				x
2,048		x		x
1,024		x	x	x
512	x	x	x	x
256	x	x	x	x
128		x		x
64	x	x	x	x
32		x	x	
16	x	x		
8	x			

The increased bit rates will necessitate a subcarrier frequency higher than the 32.768 kHz used for Pioneer 10/11. For efficient demodulation of the telemetry subcarrier, the subcarrier frequency/telemetry symbol rate should not be less than 4. However, DSN flight project interface requirements constrain the minimum subcarrier frequency to 40-50 kHz for symbol rates less than 500 bit/s. Consequently two subcarrier frequencies are required to support the contemplated range of bit rates. It is proposed to adopt 262.144 kHz for bit rates exceeding 4096 bit/s, while retaining the existing subcarrier frequency for the lower range of bit rates. This modification requires a minor change to the programmer.

A detailed accounting of subcommutator word allocations has not been performed. It is recognized, however, that the present Pioneer 10/11 science and engineering subcommutator capacity may be inadequate for the orbiter missions as a result of increased instrument payload and X-band communications housekeeping telemetry. Although not incorporated in the reference design, it is appropriate to consider the possible expansion and/or reapportionment of these subcommutators. The modification consists of providing additional input gates, gate drivers, and control logic. A third subcommutator circuit board would be required along with modifications to the programmer logic.

4.7.3 Data Storage Unit

4.7.3.1 Requirements

The data storage unit (DSU) buffers high rate data from the photo-imaging instrument and stores formatted data from the DTU for later transmission to earth at the prevailing telemetry link rate. In order to size the capacity of the DSU a typical photo-imaging system was considered to be the primary driver requirement. One way that this requirement could be derived assumes an imaging sensor comprising 390 detector elements. The dimension along the array is accommodated electronically, while scanning normal to the array is automatically provided by the rotation of the spacecraft. The required storage capacity is, therefore, 390 TV lines x 390 data samples per TV line (assuming a square frame) x 10 bits per pixel, or 1.521 megabits. It was assumed that imaging would be conducted only when there is real-time contact with the DSN and that only one picture would be stored. The remainder of the instruments time share the memory during non-imaging periods; i.e., cruise, orbital regions near apoapsis, and when the spacecraft is occulted by the planet.

The capacity of the Pioneer 10/11 DSU (49,152 bits) is too small, and the weight would be much too heavy if expanded for this application.

4.7.3.2 Tradeoffs

Various alternative storage techniques were evaluated; a comparison of the key tradeoff parameters is summarized in Table 4-14. The estimated weight, power, and cost entries include the required interface units, where applicable.

A modularized DSU constructed from commercially available medium-scale C-MOS integrated circuits was selected for its favorable performance, weight and cost characteristics and the modular construction which permits optimizing capacity for different mission requirements and which affords a high degree of operational flexibility. There are other off-the-shelf core and plated wire memories with adequate capacity but none can interface directly with the DTU or the scientific instruments. These are

Table 4-14. Candidate Data Storage Units

Memory Type	Capacity (bits)	Weight (lb)	Total Cost ($K)	Power (watts)	Remarks
Core					
Pioneers 10 and 11	49,152	3.5	N/A	0.4 to 1.2	Off the shelf. Compatible DTU interface. Insufficient capacity. Needs three voltages.
EMI	1,100,000	14.0	630	2.0 to 5.5	Off the shelf. Requires major modification or new interface unit. Needs three voltages.
HELIOS	524,288	10.3	?	3.0 to 5.7	Advanced development. Requires new interface unit. German made. Needs three voltages.
Plated Wire					
Minuteman	580,000	16.2	644	1.5	Off the shelf. Requires new interface unit. Needs three voltages
Viking	500,000	9.5	655	1.5	Advanced development. Requires new interface unit. Needs three voltages.
Motorola	768,000	38	650	1.5 to 2.5	Requires new interface unit. Needs two voltages.
Honeywell	544,000	36	560	5	Requires new interface unit. Needs power switching added. Needs four voltages.
Solid State					
Dynamic P-MOS (Multi-Chip)	491,520	2.7	460	4.3	New design using proven technology. Because of timing problems special buffer modes cannot be supplied. Needs three voltages.
Static C-MOS (Multi-Chip)	1,536,000	9.0	800	5 to 8	New design using proven technology. Gives special modes simultaneously to science and provides reconfigurable redundancy. Operationally very flexible. Needs one voltage.

heavier than the preferred C-MOS memory and, because of complex fabrication processes, cost more. Further, the selected modular approach facilitates configuring the DSU as a group of independent memories, providing buffer storage for multiple asynchronous data sources simultaneously, whereas the existing memories are limited to a single input and output. Of course it is possible to cascade several core or wire memories to achieve the modularity, but the cost, weight, and power consumption penalties are excessive.

P-MOS technology offers many of the same advantages as the static C-MOS but since it is dynamic, timing problems limit the special buffer modes. Static P-MOS circuits were not investigated because of their inherently high power consumption

4.7.3.3 Selected Configuration

The selected DSU is comprised of five identical but separate memory units (MU) as shown in Figure 4-37, each with a capacity of 307.2 kilobits. The DSU operates in these modes: telemetry store (TS), memory readout (MRO), and buffer. In the TS mode the DSU accepts formatted NRZ data from the DTU at any of the bit rates selected by command. In the MRO mode formatted data is read out through the DTU. In the buffer mode unformatted imaging data is stored prior to transmission in a D format. Asynchronous data inputs may be routed to specific MU's; alternatively the DSU can be configured as one large storage unit accepting 1.536 megabits from a single source, typically the photo-imaging

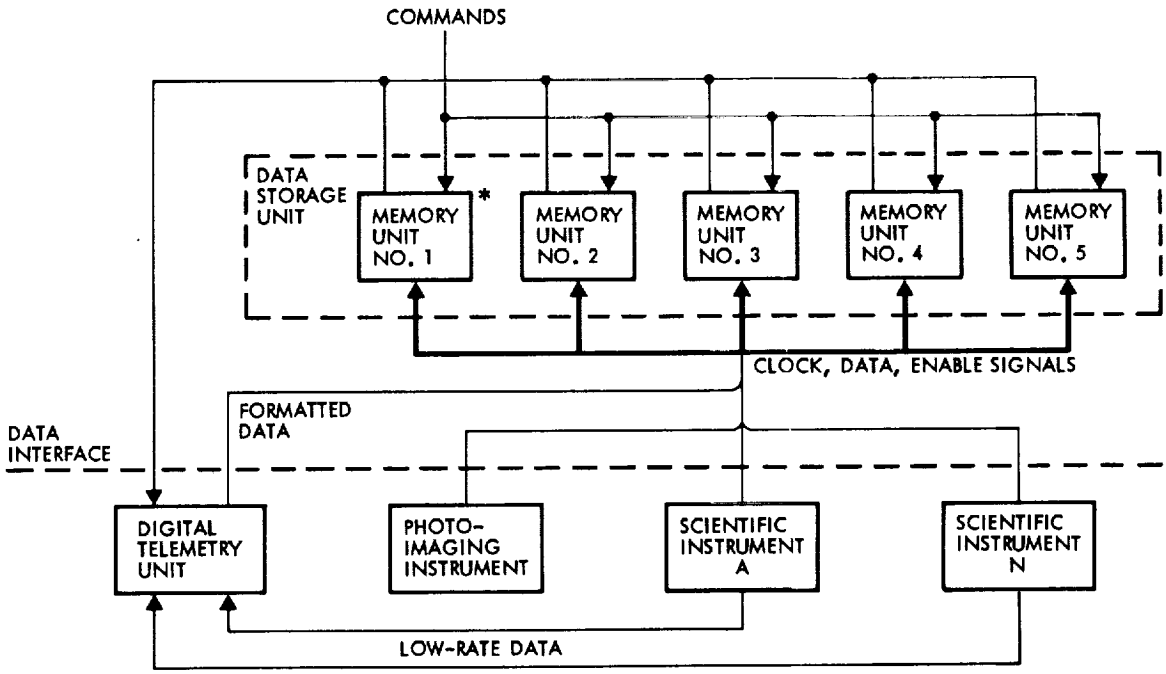

*EACH MEMORY UNIT IS COMPOSED OF TWO IDENTICAL MEMORY MODULES OF 153,600 BIT CAPACITY

Figure 4-37. Data Storage Unit Functional Diagram and Interfaces

instrument. Storage efficiency is improved in this mode by reducing the storage of formatted data (low rate signals, timing and attitude markers, and housekeeping) and storing raw data direct from the science instruments. The instruments process and transfer data at rates and times favorable to the mission objectives constrained only by the total number of bits stored.

The data sources furnish data, clock, and enable signals, which are common to all memory units. Configuration commands control which inputs will be accepted. Clock and enable signals control the write-in rate, slaving the storage to the instrument requirements. When the assigned storage capacity is filled, further inputs are inhibited. Readout of the stored data is controlled by commands routed through the DTU to each MU. Each MU is assigned a "D" format for readout.

Each memory unit consists of 2 identical modules illustrated in Figure 4-38. Each module contains 153.6 kilobits of storage. The memory is organized in a three-dimensional matrix. There are sixty 256-bit strings per plane and 10 planes. The memory module appears as 15,360 10 bit words. The memory has been organized with a 10 bit word to be compatible with the quantization level of the A/D converters associated with the reference imaging system. However, other arrangements are easily accommodated.

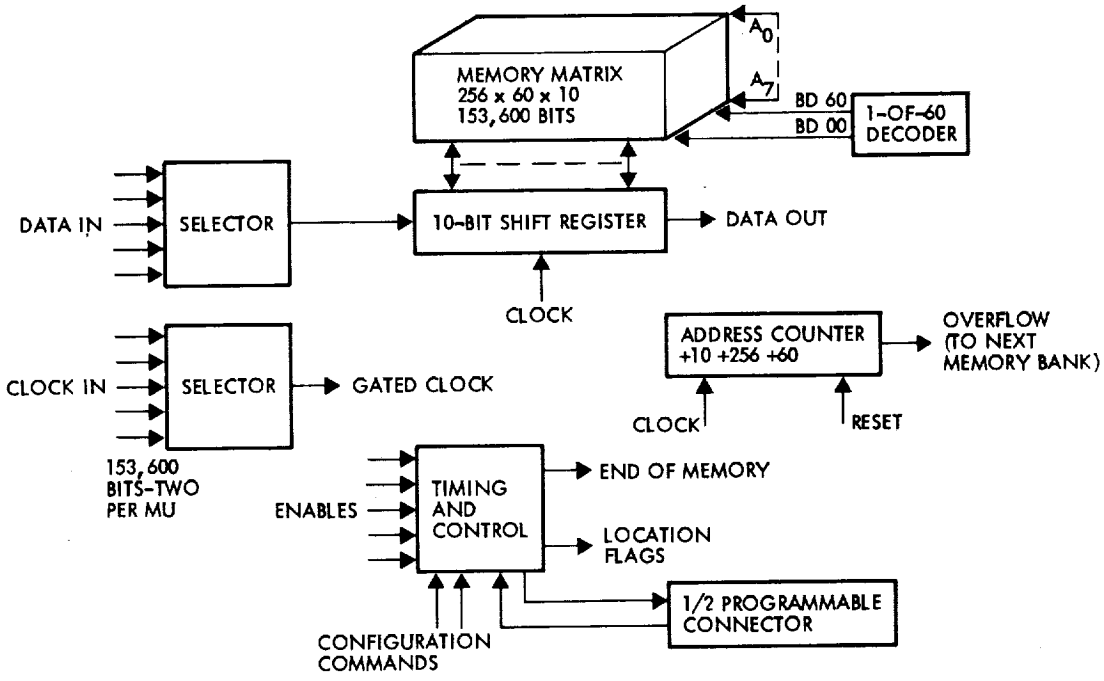

Figure 4-38. Memory Module Block Diagram

During memory load data is shifted serially into the buffer shift register with the data source clock. On the tenth clock, the contents of the register are transferred in parallel to the addressed memory word. Read-out operations are performed in a similar manner. The module appears as a 153,600 bit serial memory to its external interface. These modules can be interconnected to form a single memory unit or they can be used independently.

This memory approach is based on a 256-bit C-MOS chip. A total of 600 chips are required for each module, 1200 per MU, or 6,000 for the total DSU. This type of memory is volatile; i.e., stored data is lost if power is interrupted. Readout is nondestructive.

4.8 COMMUNICATIONS

4.8.1 Functional Requirements

The communications subsystem supports the telemetry, tracking, and command requirements of the orbiter spacecraft throughout the mission. Specifically, the subsystem performs the following functions:

a) Radiates a noncoherent RF signal in the absence of an uplink signal to permit acquisition of the spacecraft by the Deep Space Stations (DSS).

b) Provides a phase-coherent retransmission after acquisition of an uplink signal such that two-way Doppler measurements can be made at the DSS.

c) Receives and demodulates commands from the DSS modulated in a PCM/FSK/PM format.

d) Modulates and transmits scientific and engineering data to the DSS in a PCM/PSK/PM format utilizing a single subcarrier.

e) Generates and processes a conical scan error signal from the RF uplink carrier that is utilized by the attitude control subsystem to precess the spacecraft spin axis toward earth in a closed-loop attitude control mode.

4.8.2 Summary Description

The selected communications subsystem for the orbiter spacecraft retains the Pioneer F/G S-band configuration virtually intact but augmented by an X-band transmission capability to achieve significantly higher data rates. A functional block diagram of the subsystem is shown in Figure 4-39. Revisions to the baseline Pioneer F/G design are enclosed in dashed lines.

A high-gain antenna is provided for communications at maximum data rates and at extreme ranges. The high-gain antenna has a 9-foot diameter parabolic reflector illuminated with dual S- and X-band feed horns to produce narrow pencil beam patterns. The X-band beam is coincident with the spin axis; the S-band beam is tilted slightly to effect a conical scanning action as the spacecraft rotates. A coupled medium-/low-gain antenna with fore and aft elements, respectively, is provided for broad angle communications (S-band only) at intermediate and short ranges. The composite pattern provides near-spherical coverage except for some interference near the normal to the spin axis.

Two frequency-addressable phase-lock receivers are connected to the two antenna systems through a ground-commanded transfer switch and two diplexers, providing access to the spacecraft via either signal path. The receivers and antennas are interchangeable through the transfer switch by ground command or automatically after a preselected fixed period of inactivity. S-band carrier frequencies, compatible with the DSN, are used in conjunction with a PCM/FSK/PM format for uplink transmission.

Except when inhibited by command, the receiver which is locked to an uplink signal provides a phase-coherent drive signal to either of the two redundant S-band transmitter drivers. In the absence of an uplink signal, the activated driver automatically switches to a self-contained auxiliary oscillator. The redundant transmitter drivers are connected to redundant 8-watt S-band travelling wave tube amplifiers (TWTA's) which are coupled through a coaxial transfer switch and diplexer to both the high-gain and medium-/low-gain antennas. S-band carrier frequencies, compatible with the DSN, are used in conjunction with a PCM/PSK/PM format for downlink transmission via the S-band link.

A drive signal available from the S-band transmitter driver is frequency multiplied to X-band by two additional redundant transmitter drivers. These X-band transmitter drivers are connected to redundant TWTA's which

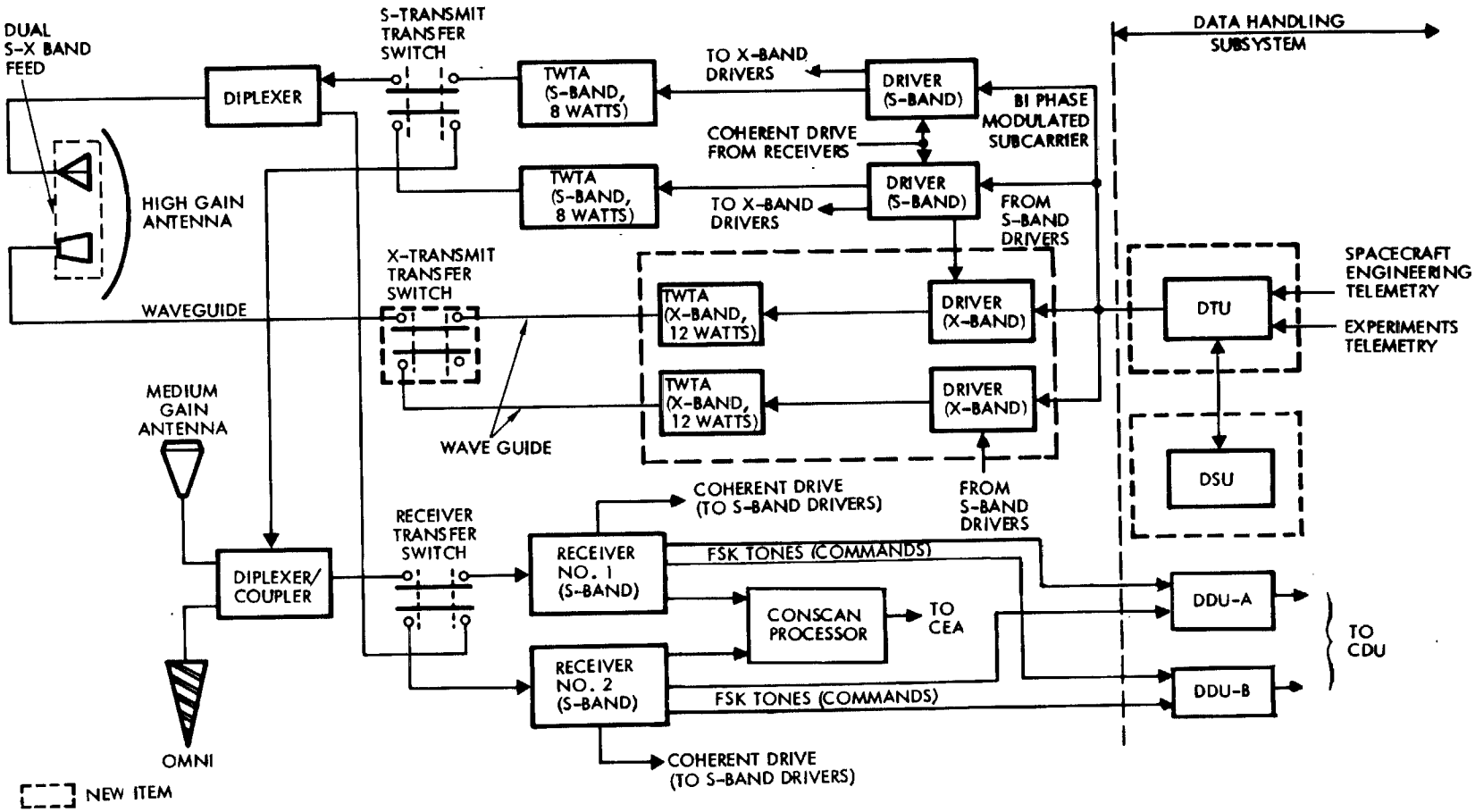

Figure 4-39. Communication Subsystem Functional Block Diagram

are coupled through a RF transfer switch to the high-gain antenna. The X-band transmission frequency is coherently related to the S-band downlink signal by the ratio 11/3 under all operating conditions. Unless inhibited by command, the X-band downlink is coherently related to the uplink signal frequency by the translation ratio 880/221, just as the S-band downlink is related by the ratio 240/221.

A closed-loop RF angle-tracking, or conscan system is used to acquire and maintain the earth-pointing attitude. The spinning spacecraft automatically provides the signal for closed-loop precession by tilting the receiving antenna beam with respect to the spin axis. This antenna gain variation amplitude-modulates the received S-band uplink carrier, producing an error signal which indicates both the amplitude and direction of the pointing error. The S-band high-gain antenna feed is displaced from the focal point to provide the tilt; the medium-gain antenna is permanently tilted.

The amplitude-modulated RF signal is coherently detected by the receiver automatic gain control. The conscan signal processor (CSP) conditions the resultant conscan signal and generates a thruster firing pulse which precesses the spacecraft in a direction to reduce the pointing error.

A summary of the required modifications to the Pioneer F/G communications subsystem is given in Table 4-15.

Table 4-15. Communication Subsystem Modification

Unit	Pioneer F/G Configuration	Orbiter Baseline Configuration
High-gain antenna	9-foot paraboloid; focal point feed	Unchanged
High-gain antenna feed	Cavity-backed, crossed dipole S-band	Dual S- and X-band
Feed movement mechanism	Thermal actuator	Deleted
Medium-gain antenna	Corrugated horn	Unchanged
S-band transfer switch	Procured from Teledyne Microwave	Unchanged
X-band transfer switch	Not applicable	New item
Diplexer	Procured from Wavecom	Unchanged
Diplexer/coupler	Procured from Wavecom	Unchanged
X-band transmitter	Not applicable	13/23-watt unit derived from M-J-S project
S-band transmitter	8-watt TWTA; procured from Watkins/Johnson	Unchanged
S-band driver	50-mW power output	Add buffer amplifier to provide coherent drive to X-band driver
Receiver	Phase lock loop; 20 Hz threshold loop bandwidth	Unchanged
Conscan processor	Digital maximum likelihood estimator	Increase register and accumulator lengths to accommodate 2 rpm spin speed
RF transmission lines	Coaxial (semirigid and flex)	Coaxial and waveguide

4.8.3 Telemetry Link Performance Trades

The increased data rate requirements, dictated primarily by an increased imaging capability envisioned for most of the contemplated outer planet missions, justify seeking a significantly increased downlink telemetry bit rate capability. With the orbiter missions to Jupiter and Saturn, the requirements apply over communication distances from 6 to 11 AU. Therefore, the approach taken to configuring the communications subsystem was to achieve the highest possible bit rate consistent with retaining as much of the simplicity, reliability, and technology of Pioneer F/G as possible and constrained by the available electrical power. The potential alternatives which offer bit rate enhancement and were considered include:

a) Increased S-band power

b) Higher gain antenna

c) Utilization of X-band transmission.

Increasing the S-band transmitter power affords limited bit rate enhancement while retaining the basic Pioneer F/G configuration and avoiding the disadvantages of X-band. However, the transmitter is a major consumer of electrical power; 28 watts or 26 percent of the total spacecraft power is required by the Pioneer F/G TWTA. Even modest increases in RF power have a major impact on the primary power requirements to energize the transmitters due to the relatively low DC-to-RF conversion efficiency. For example, to achieve the identical effective radiated power provided by an 8-watt X-band system would require a 56-watt S-band transmitter which would consume approximately 187 watts of electrical power. This would impose an unreasonable load demand requirement for the power-limited configurations of interest.

In addition to the enormous power consumption, this approach creates increasingly difficult thermal dissipation problems. Another adverse factor is the inability of existing interfacing units, such as the diplexer and transfer switch, to accept the higher RF power without detrimental effects.

Increasing the diameter of the high-gain antenna reflector is, of course, a possible approach to increasing the link gain. The 9-foot diameter Pioneer F/G antenna could be increased if launch vehicle fairing dimensions permit; the Titan/Centaur with the Viking fairing would accomodate a 12-foot diameter reflector. The resultant 2.5 dB enhancement is considered less attractive than either of the other two alternatives because of the severe limitation in bit rate enhancement — less than a factor of two. Also, the increased gain is achieved at the expense of a decrease in beamwidth which impacts attitude control (earth-pointing) accuracy requirements, particularly at X-band frequencies. No consideration has been given to a deployable or unfurlable antenna to obtain further gain improvement because of the substantial complexity and cost impact.

The use of DSN-compatible X-band frequency transmission is a straightforward solution, within the constraints cited, which can support substantially higher bit rates than S-band at a given transmitter power.

Theoretically, an 11.3 dB link gain improvement accrues from increasing the downlink frequency from 2.3 GHz to 8.4 GHz. Practical limitations (e.g., higher antenna pointing losses and atmospheric attenuation) restrict this improvement to approximately 8.5 dB or a factor of 7 in data rate. Further, X-band propagation is weather-dependent, whereas, S-band is independent. Cloud cover or rain can introduce losses ranging from tenths of dB's to several dB's, depending on the density of the cover. Nevertheless, recourse to X-band offers an attractive practical solution.

A data rate of approximately 16 kbit/s at Jovian ranges was the goal for the Outer Planets Pioneer baseline configuration. X-band transmission at 12-watts output offers the only viable means for realizing the objective since the Pioneer F/G 8-watt S-band link is capable of supporting a maximum rate of 1024 bit/s at this communication range.

These telemetry link performance goals are, in general, applicable to the Jupiter orbiter mission. However, a 4:1 data rate reduction is incurred at the maximum range for a Saturn orbiter mission. Alternatively, increased transmitter power can partially offset the greater free-space loss. Considerations of optimum transmitter power, including the possibility of dual-mode operation (two power levels, selectable by command) are discussed in Section 4.8.7.4.

4.8.4 Dual Frequency Transmission

While an X-band telemetry link clearly provides the greatest transmission rate for primary support of the mission science objectives, retention of S-band transmission capability is also essential to perform the following functions:

a) Support tracking and telemetry operations during the critical launch, ascent, and initial Deep Space Station acquisition phases of the mission

b) Provide continuous communications during off-earth-pointing maneuvers (at limited earth-spacecraft ranges)

c) Permit routine data acquisition from the DSN 26-meter diameter antenna network, particularly during routine cruise phase (26-meter DSS operations limited to S-band)

d) Provide a viable auxiliary telemetry link, at reduced bit rate, to back-up and augment the prime X-band system (in case of failure or adverse propagation conditions)

e) Facilitate ground station acquisition of the spacecraft downlink with larger earth-pointing angles than would be possible with the more narrow X-band beamwidth.

In addition, dual frequency radio science occultation experiments will be enhanced if simultaneous S- and X-band coherent transmissions can be provided; relative phase-delay and group-delay measurements are also improved. Moreover, dual frequency capability will facilitate calibration of charged-particle effects which degrade the accuracy of the S-Band Doppler tracking data.

The redundant 8-watt TWTA transmitters developed for Pioneer F/G have been tentatively selected for the orbiter configuration primarily to minimize the required modifications and because of their flight-proven compatibility and performance. However, the substitution of solid-state transmitters is an increasingly attractive option which may prove more cost effective as flight-qualified hardware becomes available. Recent comparative evaluations of TWT's and solid-state devices for deep space S-band applications have shown that the critical DC-RF conversion efficiencies are comparable at power outputs of interest (8 to 12 watts). Moreover, the solid-state units are considerable lighter and less expensive. Therefore, it is recommended that the tradeoff criteria be reevaluated prior to the final selection of an S-band transmitter.

4.8.5 Telemetry System Optimization

The process of optimizing the telemetry system is one of selecting those values of certain parameters which produce the most efficient telemetry system performance. A good measure of efficiency is the amount of total received power required for a particular configuration to achieve the selected error rate criteria.

The optimization procedure reveals two constraints which are not immediately obvious. First, the inherent phase noise of the radio frequency oscillators prevents the choice of an arbitrarily small carrier tracking bandwidth. Thus, the bit error rate will be inordinately high for bit rates much less than the receiver loop bandwidth because of instabilities in the phase reference for demodulating the telemetry sidebands. A lower limit on receiver loop bandwidths is established by the Doppler rates which must be accommodated when the spacecraft is in orbit around the planet. These rates are typically highest in the vicinity of periapsis where scientific interest is greatest. Second, the use of high data rates requires most of the transmitted power to be in the sidebands. However, because of modulation index stability factors in practical designs, at least 10 percent of the available power must be left in the carrier.

It is convenient to consider the ratio of total received power to system noise spectral density (P_T/N_0) and the bit error rate (or frame deletion rate for convolutional coded-sequentially decoded data) as fixed independent parameters, and to maximize the dependent data rate. This method is useful in selecting data rates that are realizable at various ranges and mission conditions.

4.8.5.1 S-Band Link

Selection of the downlink carrier modulation index offers limited flexibility in optimizing the S-band telemetry data rate performance. Figure 4-40 illustrates this concept for three representative values of modulation index. An upper practical limit of 1.15 radians maximizes the achievable data rate at a given communication range by allocating 83 percent of the total power to the data channel. However, this causes the ground station receiver to reach threshold at a lesser range than would occur with lower modulation indices. Reducing the modulation index increases the range at which data can be acquired but with a concommitant reduction in data rate. The lowest useful index is one in which the carrier channel and data channel performance margins are balanced at the minimum acceptable bit rate. Pioneer F/G is limited to 16 bit/s (the lowest bit rate compatible with the DSN is 6 bit/s). Bit rate estimates are based on the nominal $1/R^2$ relationship; additional receiver loss at bit rates less than 256 bit/s has not been included.
included.

Idealized data rate performance curves for the S-band system, based on 8 watts of spacecraft transmitter power and reception by either the DSN 26-meter or 64-meter subnet, are shown in Figure 4-40. The baseline configuration modulation index selection is predicated on ensuring satisfactory S-band telemetry operations at the target planet. For the Jupiter mission the modulation index of 1.15 radians appears optimum; for Saturn the modulation index should be reduced to 1.0 radian.

4.8.5.2 X-Band Link

X-band telemetry reception is limited to the three stations comprising the 64-meter subnet. Figure 4-40 includes data rate predictions for three representative transmitter power levels: 4, 12, and 20 watts at the maximum modulation index (1.15 radians). It is apparent that as little as 4 watts is adequate to support a communication link at the distance of the most remote planet, Pluto. Therefore, the parametric trade of bit rate for maximum range by means of modulation index selection applied to the S-band link offers no advantage in optimizing the X-band link performance. Foremost is the prime requirement to design the link for high data rate performance at Jupiter and Saturn for the orbiter missions. This is achieved by selecting a modulation index of 1.15 radians, the highest index compatible with the DSN. The approach used in selecting the X-band power level for the orbiter spacecraft is to maximize the transmitter power output, consistent with electrical power margins and thermal dissipation considerations.

4.8.6 Ranging

Doppler data is the primary observable used to determine the trajectory of the spacecraft in flight. This information provides a direct measure of the spacecraft radial velocity and a relative measure of its

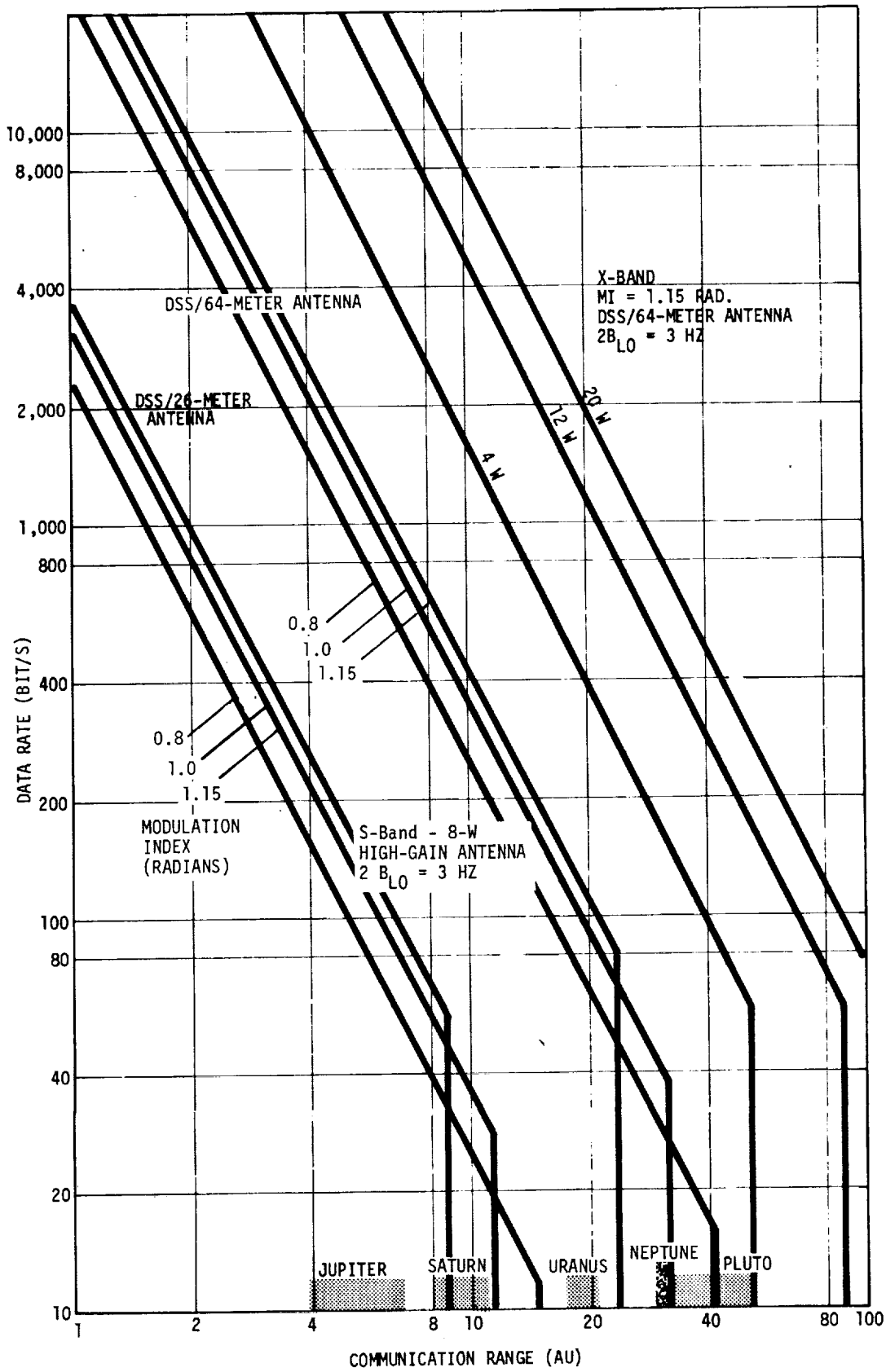

Figure 4-40. Telemetry Link Performance with Modulation Index and Transmitter Power as Parameters

range. A ranging system permits a measurement of the round trip propagation delay which may be directly related to an estimate of the spacecraft range and the properties of the transmission media (electron content). It is, therefore, a navigational tool which also satisfies a scientific requirement for improving ephemeris information for certain types of missions. It may also improve trajectory and orbit tracking accuracy.

A ranging system is conceptually compatible with the communication subsystem for the Pioneer Outer Planets Orbiter. However, actual implementation would necessitate modifications to the baseline Pioneer F/G transponder because it does not have the required wideband response or ranging modulation processing circuits. If ranging were desired, it may be cost effective to select a transponder which includes this function.

4.8.7 Hardware Implementation

4.8.7.1 High-Gain Antenna

The high-gain antenna consists of a 9-foot diameter reflector with a feed system mounted on a tripod support. The modification of the Pioneer F/G configuration is shown in Figure 4-41.

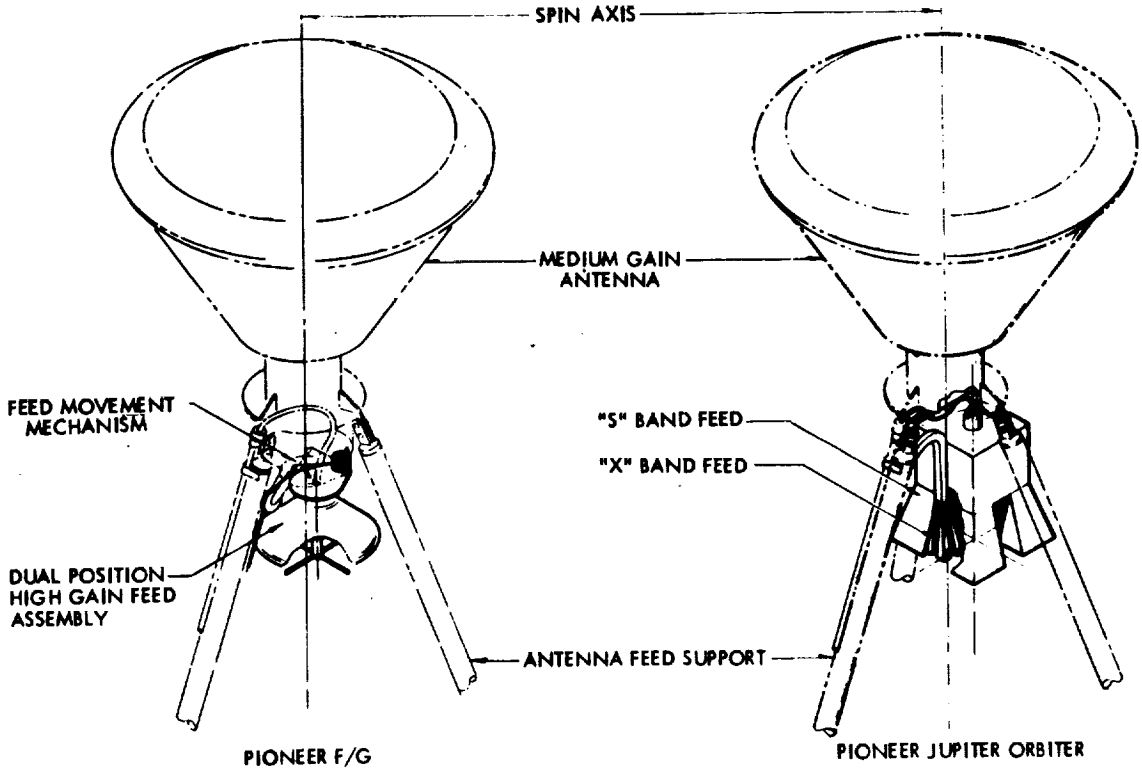

Figure 4-41. Antenna Feed Configurations

The Pioneer F/G high-gain antenna S-band feed and associated feed movement mechanism are replaced with a fixed dual S- and X-band feed. Ridged waveguide horns are used for this application. The S-band horn is permanently offset from the reflector focal point to squint the beam and produce a -2 dB gain crossover. The X-band horn is positioned in one of the S-band waveguide ridges and is coincident with the focal plane axis.

The X-band feed will be coupled to the TWTA via waveguide because of the large losses associated with coax at these high frequencies. This waveguide is routed parallel to, and supported by, one leg of the tripod support. The effect of this waveguide adjacent to the strut on the mechanical stability of the feed system warrants further study, careful design, and development testing. The waveguide must be loosely coupled to the TWTA to permit relative motion between the equipment compartment and the feed. This may be accomplished with a flexible waveguide section or perhaps by a waveguide-coax transition. The attachment of the waveguide to the struts and the induced lateral vibration loads as well as the potential thermal loading of the strut ("hot dog" effect) should be verified by tests.

4.8.7.2 S-Band Transmitter Driver

The required modification to the Pioneer F/G transmitter driver is the insertion of a buffer amplifier following the RF summing network, as shown in Figure 4-42, to obtain a coherent drive signal for the X-band link. Extracting the drive signal at this point ensures coherence between the S- and X-band transmissions independent of the receiver lock status, a feature essential for precision dual frequency occultation experiments. The buffer amplifier also isolates the two output signals to afford protection from a single fault disabling the coherent drive function on both the primary and redundant X-band channels.

4.8.7.3 X-Band Transmitter Driver

The X-band driver performs the functions of frequency-multiplying the coherent drive signal available from the S-band driver and phase modulating the resultant X-band carrier with the 131 kHz telemetry subcarrier. The required power output must be compatible with the input requirements of a 24-watt TWTA. For a TWT gain of 35 dB, the minimum level is approximately 16 mW (+12 dBm), including isolator losses.

The X-band signal frequency must be related to the received S-band signal by the ratio of 880/221. Several methods of synthesizing the X-band signal were considered during the study. The coherent drive presently available from the Pioneer F/G driver is 12f (114.6 MHz). With a minor modification to the existing driver the X-band and S-band downlink signals will maintain the desired fixed-frequency relationship under all operating conditions. This modification contemplates the addition of a buffer amplifier preceding the phase modulated amplifier.

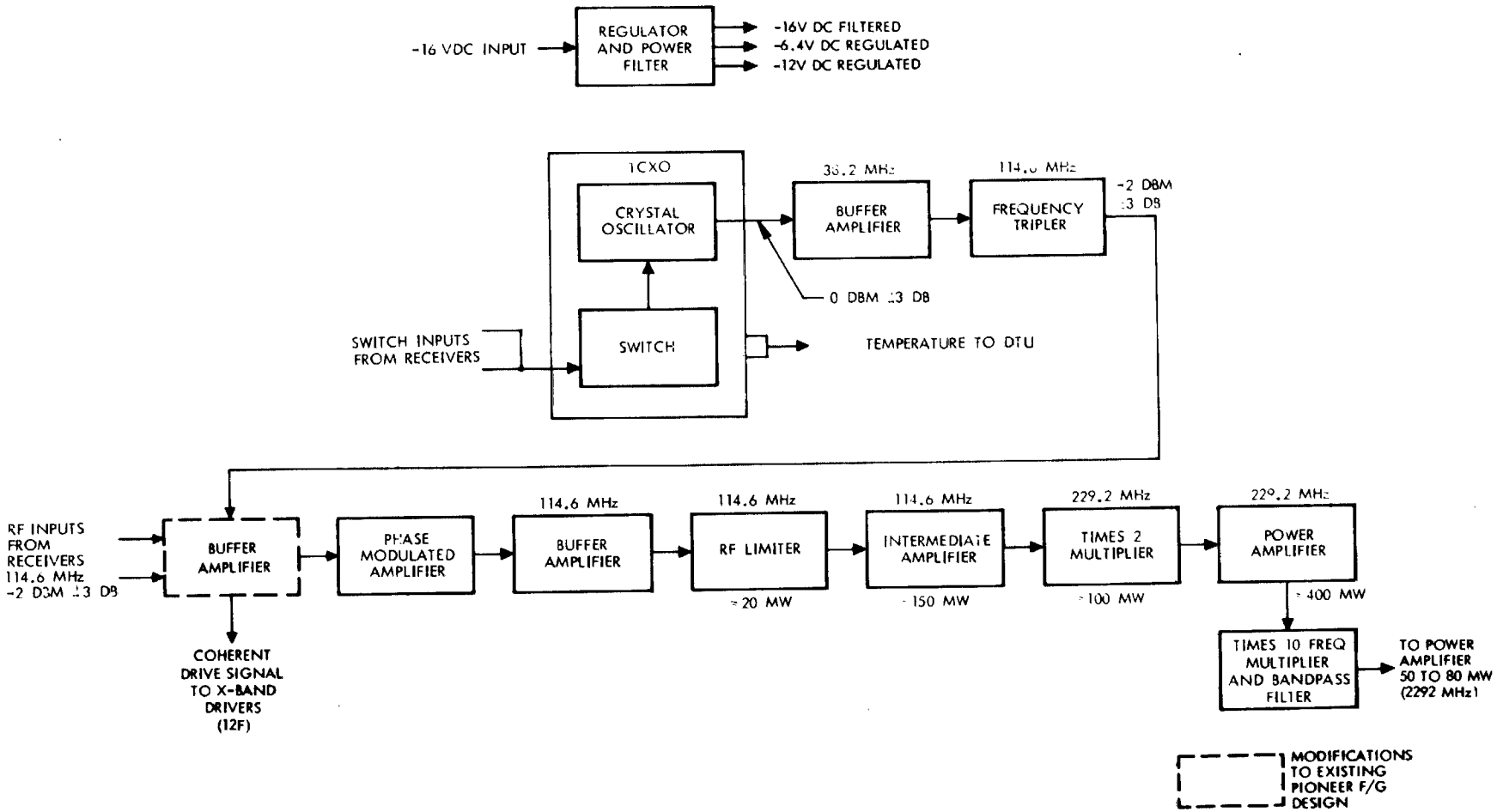

Figure 4-42. S-Band Transmitter Driver Block Diagram

Three different approaches were considered in providing the X-band driver:

- Develop a new design tailored to the specific requirements
- Modify the Motorola X-band transmitter designed for the Mariner-Venus-Mercury-73 program
- Modify the existing Defense Support Program (DSP) S-band transmitter.

A new design requires various frequency multiplier and mixer stages to synthesize the desired X-band signal which is related to the S-band receive frequency by the DSN-compatible translation ratio, 880/221. It is assumed that a compatible drive signal is available at a frequency of 12 f (114.6 MHz) from the S-band driver.

If the design employs multipliers exclusively, a times eleven (x 11) multiplier must be developed, since 11 is a prime factor of the coherence term 880. These high-order multipliers are prone to instability problems and present severe filtering problems. Additional multipliers required are x 2, x 4, and x 5.

Similar devices have been constructed and tested at L- and C-band. A preliminary performance specification for an X-band version includes:

Frequency	8415 MHz
Bandwidth	100 MHz (-0.5 dB)
Required drive power	1 mW
DC power input	1.5 W
RF power output	20 mW
Baseplate temperature	160°F (maximum allowable)
Construction	Hybrid (discrete components and microstrip)

The X-band transmitter designed by Motorola for the Mariner-Venus-Mercury 1973 mission offers another possible approach to meeting the driver requirement. Figure 4-43 illustrates a block diagram of this existing flight proven design. It develops 200 mW output power and consumes 12 watts of DC power. For the orbiter spacecraft application, these levels must be reduced by approximately a factor of ten. This can be accomplished by deleting the final power amplification stage (7 dB gain) and redesigning the following x 5 multiplier to operate at the lower level. In addition an input frequency divider (6) is required to achieve compatibility between the 12f input from the S-band driver and the 2f capability of the Motorola design. The predicted performance parameters of the revised design are 4 watts of input power and 40 mW RF output power.

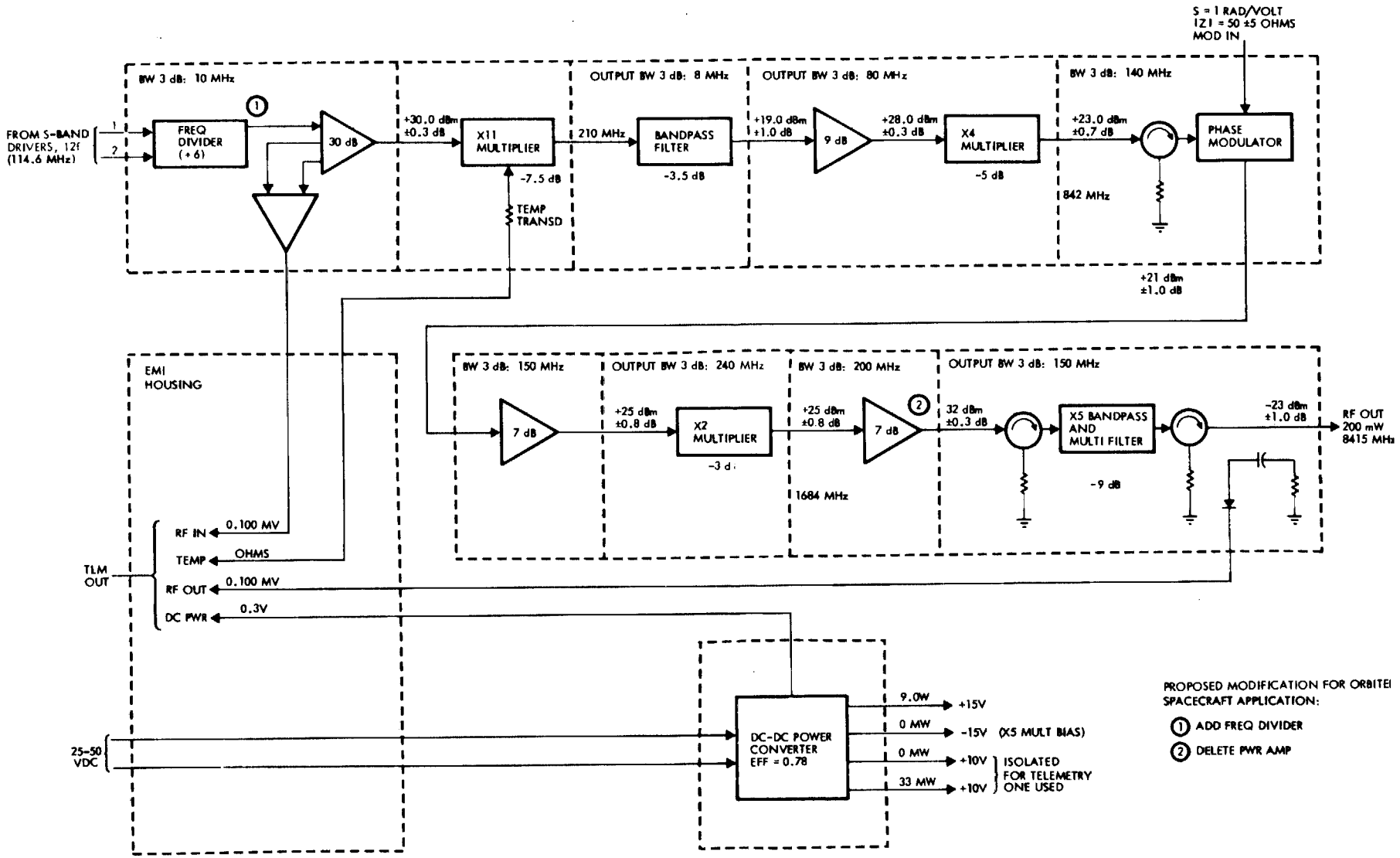

Figure 4-43. Motorola X-Band Transmitter (MVM-73) Modified for Pioneer Outer Planets Orbiter Application

A third approach involves a relatively simple modification of the TRW DSP S-band transmitter, depicted functionally in Figure 4-44. The modification consists of adding a frequency divider, mixer, and three multipliers (x 5, x 2, and x 4), as illustrated by the subassemblies in dashed lines. A balanced varactor quadrupler multiplies the S-band signal to X-band.

A third approach involves a relatively simple modification of the TRW Model-35 S-band transmitter, depicted functionally in Figure 4- . The modification consists of adding a frequency divider, mixer, and three multipliers (x 5, x 2, and x 4), as illustrated by the subassemblies in dashed lines. A balanced varactor quadrupler multiplies the S-band signal to X-band.

The mixer provides a coherent signal at a frequency of 220f, eliminating the requirement for the x 11 multiplier. Minor retuning of the final stage of amplification, from 240f to 220f, may be required to improve its performance as a driver for the new quadrupler.

Table 4-16 summarizes the key performance characteristics of the latter two approaches, reflecting the modifications which have been described.

Table 4-16. Summary Characteristics of Candidate X-Band Transmitter Driver

	Modified Motorola MVM-73	Modified DSP
Input frequency	114.6 MHz (12f)	114.6 MHz (12f)
Drive power required	0 dBm ±2 dB	0 dBm ± 1 dB
Input power	4 watts	2.5 watts
Output frequency	8415 MHz (880f)	8415 MHz (880f)
Output power	40 mW (minimum)	20 mW (minimum)
Modulation	Linear PM (not required)	Linear PM
Size	2 x 6.9 x 8 inches	1.52 x 4.52 x 4.53 inches
Weight	4 pounds	2 pounds
EMI Harmonics of 19.125 MHz	-30 dB	-40 dB
Spurious	-50 dB	-60 dB
Transmitter driver	Add ÷ 6 circuit. Delete power amplifier stage	Add mixer, 3 multipliers (x 5, x 2, x 4) and ÷ 6 frequency divider

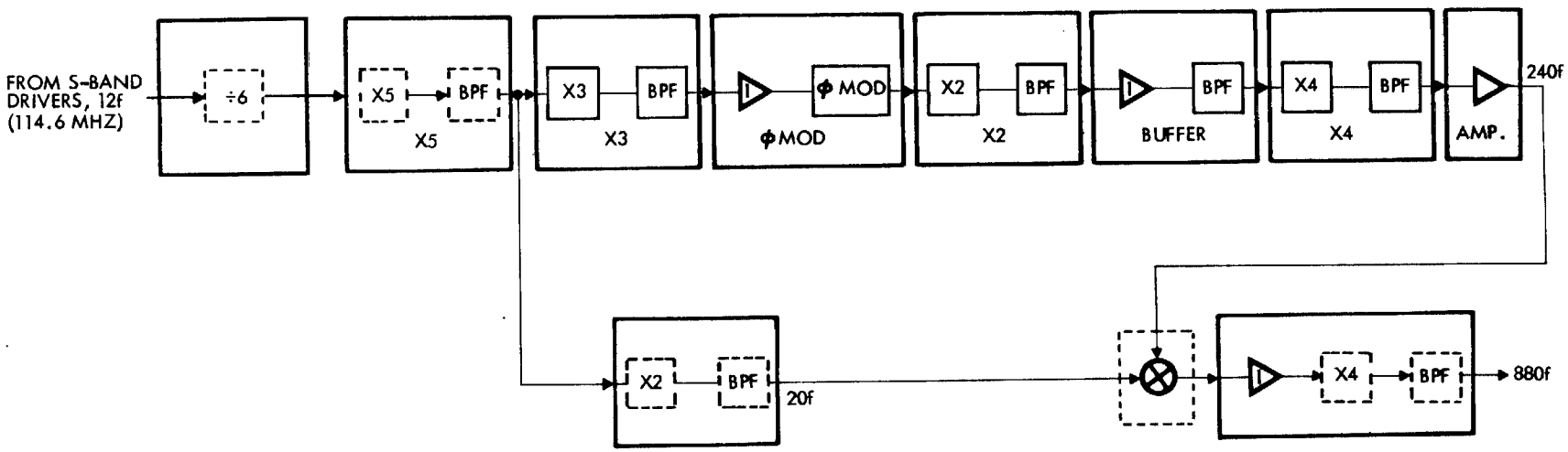

Figure 4-44. TRW S-Band Transmitter Modified for Pioneer Outer Planets Orbiter X-Band Driver Application

The DSP transmitter is recommended for the orbiter spacecraft because development cost and risk are significantly less than for an entirely new design. Secondly, stringent weight and power limitations favor using the DSP approach compared to the Motorola unit although the modifications are more extensive.

4.8.7.4 X-Band TWTA

Solid-state technology at X-band frequencies is not sufficiently advanced at this time to design transmitters capable of developing the required RF power levels. A major disadvantage is the relatively poor DC-to-RF conversion efficiency which severely impacts the electrical power requirements. Therefore, solid-state devices are probably not viable candidates for this application, at least at this time. TWTA's offer a much less risky approach based on existing and proven techniques.

A survey of X-band TWTA development is summarized in Table 4-17.

The Hughes Model 285H 23-watt TWT developed for the Mariner-Jupiter-Saturn (MJS) mission in 1977 is the most promising candidate for the Pioneer Outer Planets Orbiter. Significant improvement in tube efficiency is achieved with a dual-stage depressed collector design. Delivered output power of 24 watts with a tube efficiency of 46 percent has been demonstrated in the laboratory. The specification requirements include dual power levels of 13 watts and 22-24 watts. The composite TWTA (tube and converter) is estimated to weigh approximately 9 pounds.

Procurement specifications for the MJS X-band TWTA transmitter include the following preliminary requirements:

Frequency	8415 MHz
Power output	22-24 watts (high power mode) 13 watts (low power mode)
Gain (minimum)	35 dB
Primary power	30 VDC $\pm$ 2 VDC
Weight	9 pounds
DC-RF conversion efficiency	36 percent (high power mode)

The MJS TWTA is potentially the most attractive candidate for the Pioneer outer planets spacecraft because the similarity of performance requirements for the respective deep space missions will permit its adaptation with minimal modifications.

4.8.7.5 Conscan Processor

The orbiter spacecraft is capable of operation at spin rates as low as 2 rpm to accommodate the special requirements of selected instruments. Relatively minor modifications to the conscan processor are required to prevent register overflow. Those items requiring capacity increases of 1 bit include:

Table 4-17. X-Band TWT Development Status

	MANUFACTURER AND MODEL NUMBER						
	Watkins-Johnson (WJ-130)	Watkins-Johnson (WJ-3703)	Watkins-Johnson (231)	Hughes (227H)	Hughes (237H)	Hughes (219H)	Hughes (285H)
TWT Parameters							
Frequency range	8.5 GHz	8.5 GHz	6-8 GHz	6-8 GHz	7-8 GHz	7.5-8.5 GHz	8.4 GHz
Power output	3.3 watts	25 watts	35 watts	12 watts	40 watts	20 watts	23 watts
Efficiency including heaters	25.5 percent	45 percent	29 percent	33 percent	33 percent	33 percent	43 percent
Saturated gain	37 dB	35 dB	41 dB	40 dB	40 dB	40 dB	35 dB
Development status	Qualified	Developed for JPL TOPS	Space qualified	Developed but not qualified	Developed but not qualified	Developed for NASA Langley; general qualification	Under development for JPL Mariner Jupiter Saturn
Previous usage	IDCSP	None	Nine tubes life tested two years-no failures	None	None	None	None
Power Supply							
- TWT power supply efficiency	85 percent	85 percent (estimated)	85 percent (estimated)	85 percent (estimated)	85 percent (estimated)	85 percent (Gaulton Indus.)	84 percent (JPL estimate)

a) A cos θ accumulator

b) A sin θ accumulator

c) Amplitude estimator

d) Division logic

e) Amplitude comparator.

A more complete discussion of these design modifications and their effect on conscan operations in included in Section 4.6.6.1.

5. SPACECRAFT PERFORMANCE

5.1 ACCOMMODATION OF SCIENTIFIC INSTRUMENTS

5.1.1 Mechanical

The spacecraft is capable of accommodating instruments in which the sensors and electronics must be separated to the extent necessary to achieve either the viewing or environmental requirements of the instrument. Surfaces are provided within an environmentally controlled and protected compartment for mounting the scientific instruments. The equipment compartment is designed so that scientific instruments or sensors can be mounted externally on at least two of its surfaces that are parallel to the spin axis and one that is perpendicular to the spin axis. The surfaces of the equipment compartment on which instruments can be mounted are flat to within 0.001 inch per inch of dimension.

The spacecraft is designed to provide a boom on which to mount a magnetometer sensor weighing no more than 2 pounds. The boom has a flange to support the sensor and provision for cabling between the sensor and remote electronics. The length of the boom (approximately 17 feet) is selected to meet the specified magnetic requirements.

The equipment compartment is designed to provide ready access for mounting, inspecting, and removing instruments with minimum disturbance to other equipment or instruments.

5.1.1.1 Field of View

Openings in the equipment compartment required by instruments within the compartment are mainly in the sidewalls. The openings may have any shape which does not compromise the spacecraft structural integrity or thermal requirements. For instruments having viewing ports through the side panels, a portion of the field of view is blocked by the high-gain antenna.

A pointable science package is provided, allowing the cone angle of the scan to be varied, to permit viewing of the planet from various portions of the orbit. It also could be oriented toward any of the satellites during satellite encounter. An imaging camera, the IR instrument, and the UV instrument are located on the pointable science package.

5.1.1.2 Instrument Mounting and Orientation

Figure 3-5 shows the suggested physical arrangement of payload instruments in the equipment bay of the Jupiter orbiter spacecraft. Most of the instruments are housed in the two payload compartments attached to the opposite sides of the main structure. As in the baseline Pioneer F/G, the plasma analyzer is located on top of the elongated hexagonal science compartment.

The specified orientations and clear field-of-view requirements of the sensors are readily met by the arrangement shown, with the exception of the optical instruments (imaging camera, UV photometer, and IR radiometer) which are located in the articulated package on the -X axis.

The articulated package rotates about an axis parallel to the Y axis, permitting any cone angle from 40 to 175 degrees. Although viewing in the forward direction is partially obscured by the antenna reflector, this limitation is offset by advantages inherent in the selected placement of the instruments:

- Shielding by the antenna dish against direct sunlight and avoidance of a separate, less effective, light shade
- Thermal protection of the instruments inside the payload compartment
- Shielding of the optics against dust impingement during cruise phases and Saturn ring encounter.

Actually, the cone angle range limitation imposed by the selected camera arrangement does not restrict planet or satellite viewing significantly. These bodies are to be observed primarily from the sunlit side which means at cone angles greater than 90 degrees. The relative geometry of the Jupiter and Saturn encounters permits observation of the planet's bright limbs at cone angles greater than 90 degrees practically to the point of terminator crossing.

The only observation objective that would be restricted is that of obtaining images of Saturn's rings under certain back-lighting conditions.

5.1.2 Thermal

Temperatures in the vicinity of the scientific instruments that are mounted within either equipment compartment, or to the exterior surface (within the insulation blanket) of the compartment are maintained between 0 and 90^{o}F when the instrument is powered. Instruments not mounted within the equipment compartments or to exterior surfaces of a compartment (within the insulation) must provide their own temperature control.

5.1.3 Electrical

All scientific instrument loads are supplied from the primary DC bus. Each instrument receives electrical power through an individual, fused, branch circuit. The DC bus voltage, measured in the PCU, is 28 volts, $\pm$1 percent short-term deviation with an additional $\pm$1 percent long-term drift superimposed. Voltage at the terminals of a scientific instrument will be lower by the voltage drop through the fuse and wire of its branch circuit. Typically, this is 0.1 to 0.2 volt. Those instruments requiring other voltages must provide their own converter. If the total load exceeds the power subsystem capability, loads will be dropped in an automatic sequence. The first group to be turned off includes all scientific instruments.

An estimated 60 watts of power is allocated for the scientific instrument payload on the Jupiter orbiter spacecraft. A reduced allocation of 35 watts for the Saturn orbiter configuration is consistent with the payload weight capacity for that mission and the RTG power generation capabilities at the end of the six-year mission.

In case of power shortage due to failure of one RTG, the total power allocation for the experiments has to be reduced and used on a time-shared basis.

Each instrument has provision for maintaining its own electrical load on or off in accordance with a state signal supplied by the spacecraft and controlled by ground command.

The spacecraft provides a cable harness to supply each scientific instrument electrical power, data signals to and from the instrument, and command signals. Cables between the sensors and electronics are supplied with the instruments except for the magnetometer and the meteoroid detectors if included in the science payload.

5.1.4 Signals to the Instruments

The data handling subsystem supplies commands, spacecraft operational status, and timing signals to the scientific instruments, as required. They are similar to those provided for the Pioneer F/G spacecraft and are identified in Table 5-1.

5.1.5 Data from the Instruments

The characteristics of digital, analog, timing, and operational status signals from the scientific instruments to the data handling subsystem are summarized in Table 5-2.

5.1.5.1 Data Handling

The input data signals to the DTU from the instruments consist of serial digital, bilevel, and analog type of signals which are assembled into frames composed of 192 bits. The data handling capability is summarized in Table 5-3.

The serial digital data are accepted in multiple groups of complete 3-bit words in the main frame and as 6-bit words in the subframes. Bilevel data are formatted into groups of 6 bits. All analog data are encoded to 6-bit words. The maximum encoding error due to all analog-to-digital conversion process effects is $\pm$ 1 bit (1.6 percent of full scale).

Mainframe Organization. The mainframe format arrangement is illustrated in Figure 5-1. The size of the mainframe is 64 words (192 bits). Forty-eight words are assigned to a maximum of 12 serial digital data channels for each of two basic scientific (mainframe) formats (A and B). Sixteen words are permanently assigned to fixed words

Table 5-1. Signals Available to Scientific Instruments

Nomenclature	Signal Description	Origin
Mainframe rate pulse	A pulse at the end of each frame	DTU
Science subframe rate pulse	A pulse every 64 frames except when operating in a Format D; then every 128 frames	DTU
Word rate pulse	A pulse generated during the last bit period of each word	DTU
Bit shift pulse	Pulses continuously generated at the operating bit rate	DTU
Roll index pulse	A single pulse per spacecraft revolution	DTU
Sector generator pulse	512 pulses per spacecraft revolution. 64 and 8 pulses per spacecraft revolution.	DTU
32.768 kHz clock (high clock)	A square wave with a 32.768-kHz repetition rate	DTU
2048 Hz clock (low clock)	A pulse train with a 2.048-kHz repetition rate	DTU
Bit rate ID signal	Continuous states indicating operating bit rate. 3-wire connection (1 wire per bit with 000 = lowest bit rate and 111 = highest bit rate)	DTU
Mode ID signal	Continuous states indicating operating mode	DTU
Format ID signal	States indicating operating format	DTU
Word gate	Gate to each instrument to indicate time of reading out digital data to DTU. Separate line for mainframe and subframe digital words	DTU
Function commands	Pulse upon receipt of a ground command. Separate line for each command.	CDU
On/Off commands	Step signal upon receipt of a ground command. Single line connection.	CDU
End of memory	A pulse when DSU reaches last memory location.	DSU

Table 5-2. Data from the Scientific Instruments

Nomenclature	Signal Description
Digital data	A pulse shall indicate "one" and no pulse shall indicate "zero"
Instrument operational status	Bilevel states indicating operational conditions of instruments. Separate line required for each signal.
Analog data	Normalized analog voltage. Separate line required for each word
Data store gate	Gate to DSU to indicate data is to be stored in buffer
Bit shift clock	Clock pulses to DSU for shifting digital data into DSU buffer
Enable signal	Controls assignment of DSU to instruments

Table 5-3. Scientific Instrument Data Handling Capability

Channel Type	Available Channels
a) Serial Digital	
Mainframe format A	12*
Mainframe format B	12*
Special single channel (formats D1 to D8)	8
Science subframe	20
b) Bilevel	
Science subframe	24
c) Analog	
Science subframe	40

*Patchable word allocations

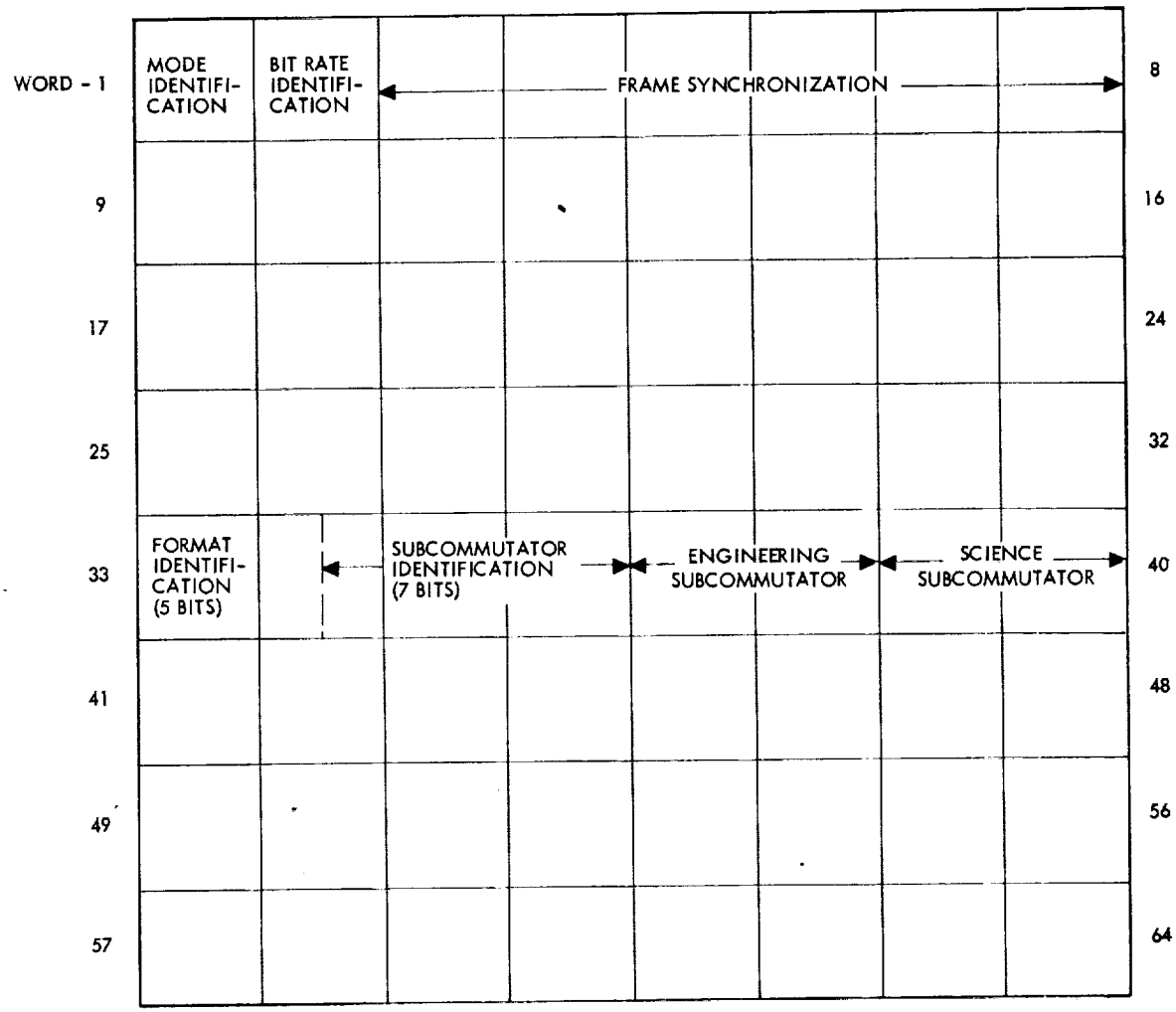

Figure 5-1. Mainframe Organization

for the purpose of synchronization and format, mode, bit rate, and subcommutator identification. The assignment of mainframe word allocations, in word lengths of one or more groups of 3 bits is accomplished by means of a 50-pin patch plug. The rearrangement of mainframe words does not require redesign of, change of permanent wording in, adding to or removing modules or circuits from the DTU. This feature facilitates changes in the format after the telemetry unit has been fabricated and tested.

Each mainframe word slot is sampled at a rate of BR/192 where BR is the bit rate in bits per second.

Science Subcommutator Organization. The science subcommutator accepts analog, digital and status (bilevel) housekeeping information (temperature, mode status, etc.) from the instruments. This subcommutator consists of 64 6-bit words located in the 39th or 40th word positions in the main frame. The subcommutator format arrangement is illustrated in Figure 5-2 where A denotes an analog input converted to 6 bits, D denotes a 6-bit digital word, and B denotes six bilevel inputs.

When the subcommutator is used in format A or B, each subframe is sampled at a nominal rate of BR/12,288 where BR is the bit rate in bits per second.

Special Formats. Eight special formats (D-1 through D-8) are available to enable investigators to sample data from certain instruments at a high rate by reducing the transmission rate of other data. All 192 bits of a D format are allocated to a single instrument (except for format D-2) with data supplied on a single input channel. The selected special format is only telemetered at the main frame rate interleaved with format A or format B, on an alternating basis. Each word in this total format is sampled at a nominal rate of BR/384 where BR is the bit rate in bits per second. The special event channel supplying data is selectable by command.

Buffer Mode Formats. Formats D-1 and D-2 are designated as buffer mode formats, where buffer storage in the DSU is read out when the DTU is operated in these formats. The buffer mode formats are restricted to real-time operation.

Format D-1 is dedicated to a single instrument requiring very high sampling rates. Consequently it is necessary to store the data in the DSU during the fraction of a spacecraft revolution in which sampling occurs for subsequent transmission at the prevailing telemetry rate. As soon as the data sample has been shifted into the DSU, readout of this data commences as the DTU alternates format D-1 with either format A or B at the operating data rate.

Format D-2 is configured to accept data from two instruments. The first 24 bits from one instrument is read out direct, without intermediate storage, i.e., identical to format A or B. The remaining 168 bits from the second instrument are buffered by the DSU, the same as format D-1.

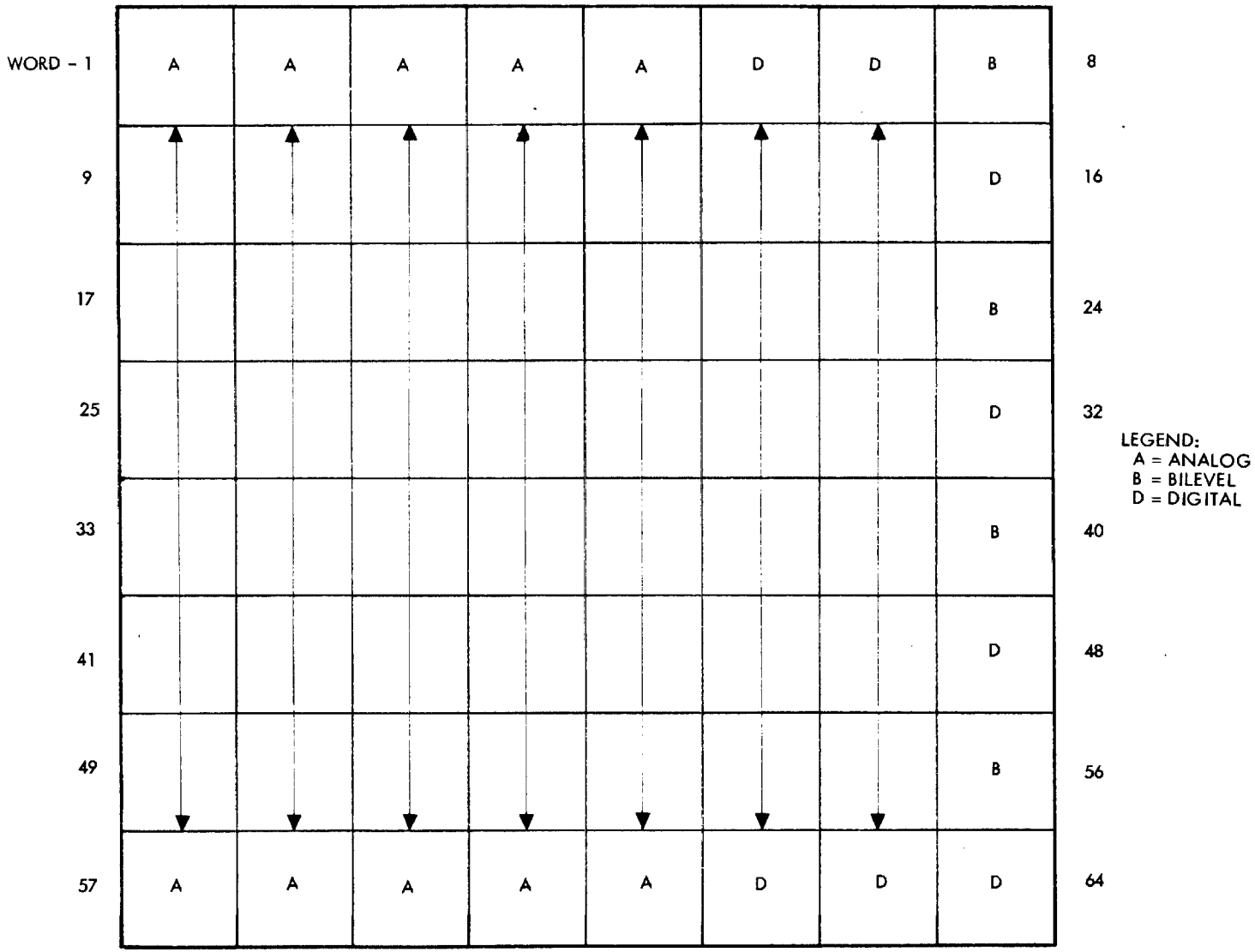

Figure 5-2. Science Subcommutator Organization

Frame Identification. It is possible to identify unambiguously the frame count up to 8192 frames. The telemetry frame count advances by unity for each transmission of a normal 192-bit frame. For main frames containing any of the special D formats the frame count is incremented for each 384-bit transmission.

Bit Rates. The bit rate for sampling the input data is selectable by command and is independent of format and mode. Eight bit rates are provided:

	Jupiter Orbiter	Saturn Orbiter
a)	32,768 bits/s	8,192 bits/s
b)	16,384 bits/s	4,096 bits/s
c)	8,192 bits/s	2,048 bits/s
d)	1,024 bits/s	1,024 bits/s
e)	512 bits/s	512 bits/s
f)	256 bits/s	256 bits/s
g)	64 bits/s	128 bits/s
h)	32 bits/s	64 bits/s

The bit rate is accurate within $\pm$0.02 percent of the specified value.

Accommodation of Data Handling and Telemetry Requirements. The spacecraft provides telemetry data rates of 33 and 8 kbits/s (using the X-band high-power mode) at Jupiter and Saturn, respectively. Use of S-band as a backup mode would only permit data rates of 1024 and 256 bits/s, respectively. The total data rate (approximately 1600 bits/s) of all instruments except the image system can be readily accommodated with X-band transmission. Storage of the science data during earth occultation can be handled comfortably by the data storage unit (DSU) providing a total capacity of approximately 1.5 megabits.

The main concern is accommodation of the image system data requirements in terms of data handling, data storage, and telemetry. An image system with even a relatively small number of sensor cells requires hundreds of kilobits of buffer storage capacity and a large percentage of the available telemetry bit rate. Multispectral imaging implies an increased number of image frames compared to a single instrument and hence, still greater data handling and telemetry requirements.

Figure 5-3 is a nomograph designed for convenient evaluation and tradeoff of image system data requirements versus capabilities. The chart at the lower left gives the bit rates, required to transmit a desired number of image frames per hour, as a function of the number of sensor cells in the array. The diagonal parametric lines indicate the frame rate as well as the number of spacecraft revolutions between exposures. The lower horizontal scale shows the required buffer storage per frame. A typical value of 8 data bits per cell is assumed here.

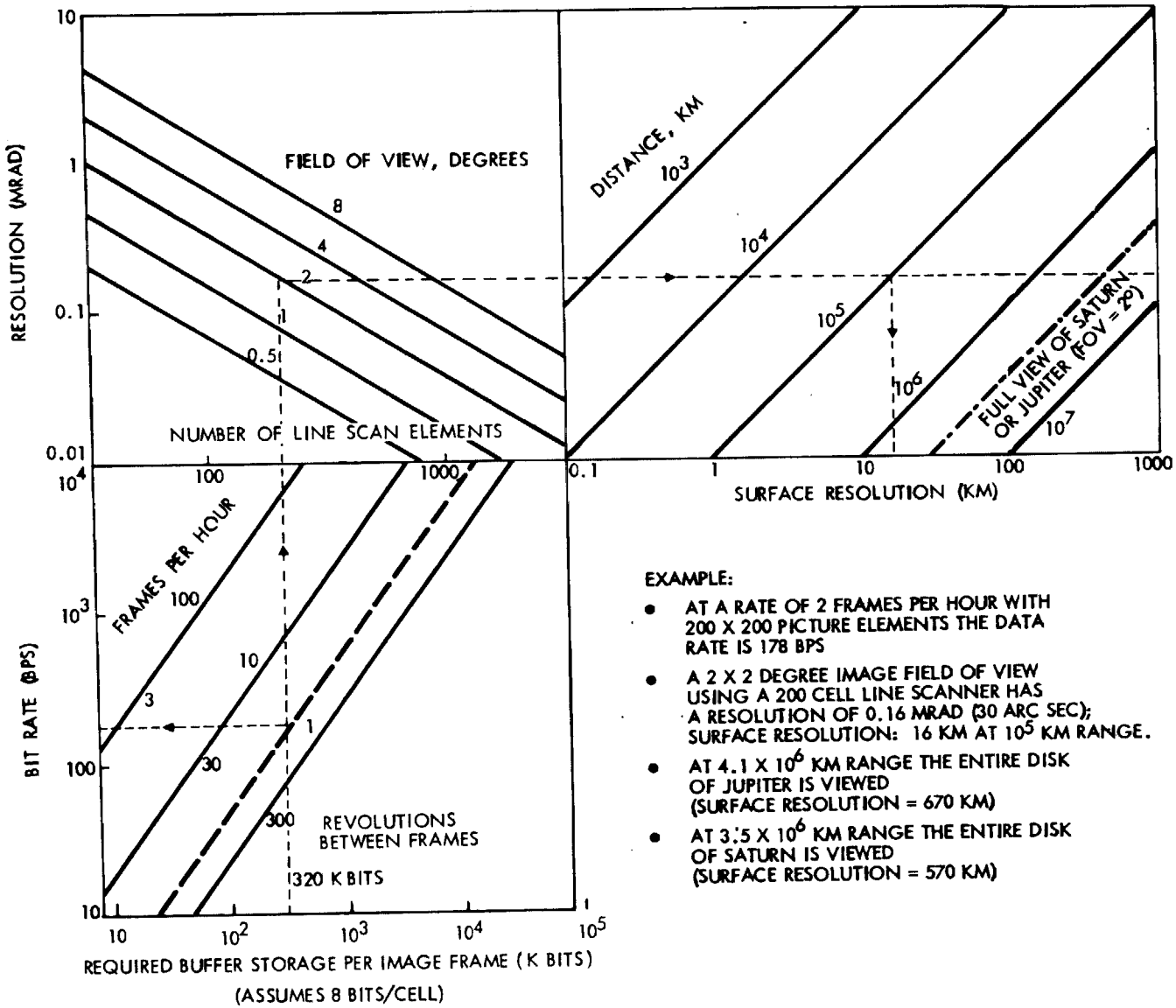

Figure 5-3. Line-Scan Imaging Capabilities and Data Rate Requirements

The chart at the upper left indicates the angular resolution obtainable with a given number of cells and a given field-of-view angle. The chart at the upper right converts angular resolution to surface resolution for a given observation distance. It also shows the distances at which Jupiter's and Saturn's disk would cover the entire field of view of a 2 x 2 degree image system, and the surface resolution corresponding to these distances.

The illustrative example shown in the chart indicates that for a line scanner with 200 image cells the required buffer storage is 320 kbits, and a frame rate of two images per hour corresponds to a bit rate of 178 bit/s. With the less conservative assumption of 6 rather than 8 data bits per cell, the storage requirement would be 240 kbits and the data rate 134 bit/s. With a 2 x 2 degree field of view this line scanner achieves an angular resolution of 0.16 milliradian and a surface resolution of 16 km at a distance of 10^5 km.

Tradeoff options between data requirements and imaging capability can be readily evaluated with the aid of the nomograph. For example, it is evident that doubling the number of line-scan elements for a given FOV-size would unnecessarily improve the surface resolution to 8 km at 10^5 km distance while multiplying the storage and telemetry requirements by a factor of four.

As another example we consider satellite viewing. An increase in FOV-size from 2 x 2 to 4 x 4 degrees would simplify the task of obtaining satellite pictures if the relative encounter geometry is not known accurately in advance. This can be achieved if the cell number is kept unchanged without burdening the telemetry and storage requirements. Surface resolution would then be 32 km at 10^5 km distance (rather than 16 km). Loss of resolution by a factor of two may be justifiable in exchange for increasing the probability of obtaining satellite images by a factor of four in close satellite encounters.

At X-band telemetry bit rates of 2048 to 1024 bit/s the acquisition rates determined in this example can be easily accommodated.

If the communication system is constrained to operate at S-band (as a backup mode), the data rate of 256 bit/s available at Saturn would permit about one image frame per hour.

Of particular interest is the flexible manner in which image system data can be interleaved with other science and engineering data such that under all conditions not more than half of the available telemetry data rate will be allocated to image system data. This flexibility is provided by the interchangeable DTU formats of the baseline Pioneer data handling subsystem that can be directly adapted to the science and engineering telemetry needs of the orbiter mission.

5.1.6 Pointing and Scanning Capabilities

Owing to the spacecraft spin motion all scientific instruments (except those with sensing orientation parallel to the spin axis) perform their in-situ or remote sensing operations by scanning around a stable, inertially fixed axis. The spacecraft provides a method for controlling, automatically or by ground command, the spacecraft attitude to meet the requirements of the scientific instruments and the communications subsystem.

5.1.6.1 Spin Rate

The nominal spin rate after initial despin and appendage deployment is 4.8 rpm ± 10 percent, a compromise between minimizing spin axis drift and minimizing propellant weight required to control the attitude. Imaging experiment smear limitations impose a new minimum spin rate requirement of 2 rpm, typically for limited periods during orbital operations. The spin rate may be controlled over a range from 2 to 15 rpm, with a resolution of 0.003 rpm, by ground commanded pulse firing of the spin control thrusters. The spin period is measured on the spacecraft and telemetered to earth as an engineering measurement.

A retardation of the spin rate due to eddy currents induced in the spinning spacecraft by the interaction of the planetary magnetic field will occur during the orbital phase of the mission. The magnitude of this effect depends on the magnetic characteristics of the spacecraft and the magnetic field encountered at the planet. An estimate of the spin rate change for various Jovian field strengths and periapsis distance, based on the Pioneer F/G spacecraft, is given in Section 4.4.4.1.

5.1.6.2 Roll Attitude Determination

Roll attitude timing data are telemetered to permit correlation of science and engineering data with the spacecraft roll attitude (clock angle). The roll attitude information is accurate to within ±0.5 degree at the nominal spin rate of 4.8 rpm.

5.1.6.3 Pointing Accuracy

The Pioneer spacecraft is normally earth-pointing following an initial orientation maneuver soon after separation from the launch vehicle. The residual pointing error, following a conscan operation using the high-gain antenna, will normally not exceed 0.3 degree. This may be reduced to approximately 0.1 to 0.2 degree by open-loop propulsive operations.

The spacecraft attitude can be measured by means of telemetry data acquired while conical scanning. The accuracy of this attitude information is estimated to be within 0.04 degree when the pointing error is 0.5 degree or less.

5.1.6.4 Attitude Drift

The two most significant environmental disturbances experienced during the Pioneer mission are:

- Solar radiation pressure
- Interaction of planetary magnetic field.

Solar Radiation Pressure. Bombardment of the surfaces of the spacecraft by photons emanating from the sun exerts small but significant forces. Because the center of gravity and center of pressure are not coincident, the resultant torque induces a drift of the angular momentum vector. The angle of solar radiation incidence, as well as the intensity, changes during the mission causing a varying drift rate. The drift rate approaches 0.09 degree/day briefly during the early part of the mission due to the large angle of incidence. However, this rate rapidly decreases by a factor of 10 and is not exceeded during the remainder of the mission.

Magnetic Torque. The interaction of the magnetic field of the planet with the intrinsic magnetic moment of the spacecraft, due to ferromagnetic materials and stray current, induces small moments, parallel and normal to the spin axis. These torques cause small changes in spin rate as well as precessions of the spin axis. The estimated accumulated precession during one Jovian orbit is approximately 0.008 degree, based on the magnetic and inertia characteristics of the Pioneer F/G at 4.8 rpm.

5.2 ATTITUDE CONTROL PERFORMANCE

5.2.1 Operational Modes

There are four basic modes of spacecraft control: precession, ΔV (velocity correction), spinup and despin. In each mode there are a number of ways in which the operation may be performed.

- Precession. A precession can be accomplished in four different ways: fixed-angle, conscan, real-time and programmed.
  - Fixed-Angle. A precession pulse is initiated at one of four fixed angles relative to the phase reference: 0, 90, 180 or 270 degrees, for each command.
  - Conscan. This is a closed-loop precession toward the earth line. Upon command, a thruster pair will fire each third or fourth revolution in a direction to reduce the earth pointing angle, until a threshold is reached which disables the mode.
  - Real-Time. A preselected thruster pair fires upon receipt of a real-time command. The commands must be timed on the ground with the spin phase.

- Programmed. A precession pulse is fired from a preselected thruster pair once per revolution at a programmed angle for a programmed time period. Two precession programs may be stored.

- ΔV. There are three ways of achieving a velocity correction: programmed, real-time, and VSCT.

  - Programmed. A continuous firing of preselected thrusters (fore or aft) or of the 100 lb_f main engine occurs for a programmed time period. A programmed delay (to provide wobble damping) precedes and follows the ΔV firing.

  - Real-Time. This is initiated by ground command and fires a preselected thruster pair for a preselected duration each time a command is received.

- Spinup. Spinup may be by command or automatic.

  - Real-Time. Each time a command is received a single spin-up pulse is fired from the appropriate thruster pair.

  - Automatic. Upon completion of the first programmed precession, unless commanded off, or upon command an automatic spinup to 15 rpm occurs.

- Despin. Despin may occur by real-time command to 16 or 4.8 rpm or may occur automatically to 4.8 rpm.

  - Real-Time. Each time a command is received a single spin-down pulse is fired from the appropriate thruster pair.

  - Initial. Initial despin occurs automatically, being initiated by the DTU sequencer or by ground command. Termination at a nominal 16 rpm occurs when either despin sensor assembly determines that the centrifugal accelera- is proper.

  - Automatic. Upon completion of the programmed ΔV (unless commanded off), or upon command, an automatic despin to 4.8 rpm occurs.

5.2.2 Stored Program

Control of the duration of all programmed functions is redundant so that the expiration of either the primary or redundant time setting will terminate the function. This is a fail-safe feature.

The stored program will occur automatically, once begun, unless interrupted by ground command. The sequence will occur as follows:

Delay
Precession No. 1

Spinup (to 15 rpm), unless inhibited
Delay
ΔV
Spindown (to 4.8 rpm)
Delay
Precession No. 2

This program provides for the completely automatic execution of a velocity correction at any desired angle and the return to earth pointing. The program may be loaded in advance and verified through telemetry prior to execution.

The stored program values are given in Table 5-4.

Table 5-4. Program Storage Parameters

Function	Maximum Value	Quantization	No. of Bits
Precession - 1 angle	360 deg	0.703 deg	9
Precession - 1 magnitude	16,376 sec	8 sec	11
Precession - 1 redundant magnitude	16,320 sec	64 sec	8
Delay	8,128 sec	64 sec	7
ΔV magnitude	8,191 sec	1 sec	13
ΔV redundant magnitude	8,160 sec	32 sec	8
Precession - 2 angle	360 deg	0.703 deg	9
Precession - 2 magnitude	16,376 sec	8 sec	11
Precession - 2 redundant magnitude	16,320 sec	64 sec	8

5.2.3 Thruster Selection

The thruster selections consist of the following:

- Thruster Valve Selection. Commands may preselect which thruster combinations will be used in each mode. These selections remain in effect until changed.
- Maneuver or Mode Enable. The mode may be preselected or is automatically changed during a programmed maneuver. This selects which of the given thrusters are used for precession, ΔV, etc.

- Pulse Duration Selection. The duration of the real-time type pulses may be preselected. This selection changes the frequency of clocks entering redundant counters which determine the pulse duration. The selectable pulse widths are:

  0.03125 second
  0.125 second
  0.5 second
  1.0 second
  2.0 seconds

5.2.4 Control Effectivity

The effectiveness of the thruster firing is dependent on the vehicle mass properties. Table 5-5 shows the nominal effect per second of firing for precession, spin, and ΔV. The data shown reflect mass properties of the Jupiter and Saturn orbiters at beginning of life (BOL), i.e., launch, and end of life (EOL), i.e., propellant depletion. These figures apply approximately to both pulsed and continuous firings. For pulsed firing at pulse lengths other than one second the effects change proportionally.

Table 5-5. Nominal Maneuver Rates (Change per second of thruster firing)

(Two 1.1-lb Thrusters Firing)

Maneuver	Jupiter Mission		Saturn Mission	
	BOL	EOL	BOL	EOL
Precession (deg)	0.88	1.11	1.07	1.11
Spin (rpm)	0.080	0.094	0.090	0.098
ΔV (m/sec)	0.009	0.021	0.015	0.024

The table can be used to determine the rate of maneuvers as well as the minimum quanitifcation of the maneuver.

Note that ΔV firings with the 100-lb_f axial engine provide rates approximately 45 times greater; i.e., from 0.37 to 0.98 m/sec/sec.

5.2.5 Spin Rate

The nominal spin rate after despin and appendage deployment is 4.8 rpm $\pm$ 10 percent. The spin rate can then be adjusted by ground control, with a resolution of 0.003 rpm. The actual spin period may be measured on

the spacecraft and telemetered to the earth. The spin rate achieved by the automatic spinup or despin will have a tolerance of ±10 percent. The despin to 4.8 rpm will require fine adjustment following the completion of the programmed maneuver.

5.2.6 Stellar Reference

The stellar reference assembly (SRA) issues a star pulse whenever a suitable star enters the ±19-degree field of view. It issues a "signal" pulse for sources of energy ≥50 percent of an equivalent Canopus (±0.16 degree accuracy) and a "discrete" pulse for sources of energy >180 percent of an equivalent Canopus (±0.75 degree accuracy). The jitter is about ±0.06 degree. The second mode applies to nonstellar energy sources such as the lighted disk of Jupiter or Saturn. Under normal operation pulses will not be produced in response to Jupiter or Saturn. If pulses do occur, as caused by such a bright source, a saturation of the SRA output occurs, for a maximum of 0.3 second.

The SRA is mounted 25 degrees from the spacecraft Y axis. Since Canopus varies in angle relative to the celestial equator over each year, star delay circuits are provided to enable commanded angle compensation. Circuits are also provided to aid in the acquisition of Canopus and to reduce the probabilities of loss of acquisition or of acquisition of some star other than Canopus.

5.3 PROPULSION PERFORMANCE

5.3.1 Functions of Primary and Auxiliary Propulsion Subsystems

The primary (bipropellant) propulsion subsystem will be used for all major maneuvers where the orientation of the thrust vector coincides with the +Z axis. Although it is normally required that the spin axis always remain earth-oriented, some exceptions are permissible, e.g., the initial trajectory correction maneuver where adequate telecommunications coverage is available via the medium-/low-gain antenna system, and orbit plane change maneuvers that are essential for attaining mission objectives.

The auxiliary (monopropellant) propulsion subsystem will be used as in Pioneer 10/11 for small ΔV corrections during all mission phases, including maneuvers with ΔV components normal to the earthline, and attitude control maneuvers.

Operational modes used by the primary and auxiliary propulsion systems and the execution logic were discussed in Section 5.2.1.

From a performance standpoint it is preferable to use the high-thrust, high-I_{sp} bipropellant system rather than the monopropellant system for all ΔV maneuvers where axial forward thrust is consistent with the spacecraft orientation constraints in order to keep total maneuver time short and to economize propellant expenditure.

If repeated satellite encounters are included in the mission objectives the cumulative ΔV requirements for pre-encounter and post-encounter corrections may be so large as to demand the use of the bipropellant system, even though repeated spin axis reorientations off the earthline may be necessary for this purpose. Thus, if cumulative ΔV maneuvers of 200 m/sec are required for this purpose during the orbital mission phase, propellant savings of 25 to 30 pounds may be achievable, depending on the extent of spin axis reorientation required for each maneuver.

5.3.2 Bipropellant System Performance

The ΔV performance of the N_2O_4/MMH bipropellant system characterized by a specific impulse of 292 seconds is discussed in Section 6.4 (see Figure 6-6). Losses incurred during orbit insertion due to finite burn time and earth pointing constraints are discussed in Section 6.8 and Appendix B. As discussed in Sections 6 and 7 the total main thrust maneuver capability of 2400 and 1600 m/sec of the Jupiter and Saturn orbiters, provided by 115 and 600 pounds of bipropellant mass, respectively, is allocated as listed in Table 5-6.

Table 5-6. Summary of Bipropellant System Performance

	Jupiter Orbiter		Saturn Orbiter	
	ΔV (m/sec)	W_p (lb)	ΔV (m/sec)	W_p (lb)
Orbit insertion	1800	800	1350	542
Plane change	300	176	-	-
Midcourse and orbit corrections	300	176	200	58
Total	2400	1152	1550	600

5.3.3 Monopropellant System Performance

Performance capabilities of the monopropellant hydrazine system, characterized by a specific impulse of 220 seconds for continuous thrusting and 150 to 175 seconds for short-pulse firing were estimated for the Jupiter and Saturn orbiter missions and are given in Table 5-7. The total propellant mass provided is 50 pounds in both missions.

The table includes propellant expenditures for attitude control and ΔV maneuvers. The attitude control maneuvers include:

- spin control operations: initial despin from 60 rpm, spinup and despin maneuvers for main thrust applications and despin/spinup maneuvers for repeated operation at 2 rpm as desired for improved imaging

Table 5-7. Summary of Monopropellant System Performance
(Propellant Expenditures in Pounds)

	Jupiter Orbiter	Saturn Orbiter
A. ATTITUDE CONTROL MANEUVERS		
1. Spin-Up/Down Maneuvers[1]		
• Initial despin to 15 rpm	1.8	1.3
• Spin-up/down (4.8 - 15 - 4.8 rpm) for high thrust maneuvers (six for Jupiter, four for Saturn Orbiters)	14.5	9.0
• Spin-down/up (4.8 - 2 - 4.8 rpm) for improved imaging	6.6	6.2
2. Precession Maneuvers[2]		
• For off-earth ΔV-thrust, average 90 degrees (12 for Jupiter, 8 for Saturn orbiter)	8.2	5.1
• Cumulative small precessions in cruise and orbital phases (estimated)	2.5	5.1
Total for ACS Maneuvers	33.6	26.7
B. ΔV - MANEUVERS		
Remaining propellant mass[3]	16.4	23.2
ΔV maneuver capability[4] (m/sec)	24	46

[1]Average I_{sp} = 220 sec in continuous thrust mode

[2]Average I_{sp} = 150 sec in pulsed thrust mode

[3]Total propellant mass 50 lb_m

[4]Assuming average weight of 1500 (1100) lb for Jupiter (Saturn) orbiter

- precession maneuvers for off-earthline thrusting and for periodic spin axis realignment with the earthline.

Assumptions regarding these maneuver modes are listed in the table. Compared to Pioneer 10/11 the ACS maneuvers require considerably more propellant since

- The spin-moment-of-inertia (I_z) in the deployed configuration is three to four times larger
- The missions have considerably longer nominal durations, and
- Many spinup/down and spin axis reorientation maneuvers are required that do not occur in the Pioneer 10/11 planetary flyby missions.

The ΔV maneuver capabilities provided by the hydrazine system are only 24 m/sec for the Jupiter orbiter and 46 m/sec for the Saturn orbiter; as noted in Table 5-7. These relatively small amounts are considered adequate since they are used to provide a trim maneuver capability. The main propellant system is used to provide midcourse and orbit change maneuver capabilities of 600 m/sec in the Jupiter orbiter mission, but only 220 to 250 m/sec in the Saturn mission (depending on the mission year).

For additional data on maneuver performance in the two missions see Figures 6-29 and 7-14 and Tables 6-8 and 7-3.

5.4 POWER SUBSYSTEM

The design and functional characteristics of the power subsystem are described in Section 4.5. This subsystem consists of two RTG power sources, a power control unit (PCU), an inverter assembly, a central transformer, rectifier and filter assembly, a shunt regulator and shunt radiators.

The multi-hundred watt (MHW) radioisotope generator being developed by GE for use on the LES 8 and 9 satellites was tentatively adoped as power source for the Pioneer Jupiter and Saturn orbiters. The SNAP-19 HPG (high-performance generator) being developed by Teledyne is an alternate power source candidate with four generator units instead of two MHW units, providing adequate power to meet mission requirements.

Figure 5-4 shows the projected power output of two MHW's and four HPG's versus time from launch. The two MHW's are expected to provide a total power of 160 watts during ground operation, 300 watts at the beginning of life in vacuum, decreasing to 265 watts after 3.5 years of operation (Jupiter mission) and to 242 watts after 6 years (Saturn mission). The power budget presented in Table 3-5 shows the two MHW's will support the maximum steady-state loads of the Jupiter (237 watts) and the Saturn (211 watts) orbiters, as well as the maximum pulse loads of 14 watts occurring in the two missions. A requirement for storage batteries (as in Pioneer 10/11) and associated charge control circuitry can thus be avoided, and questions as to reliable long-life battery performance do not have to be considered.

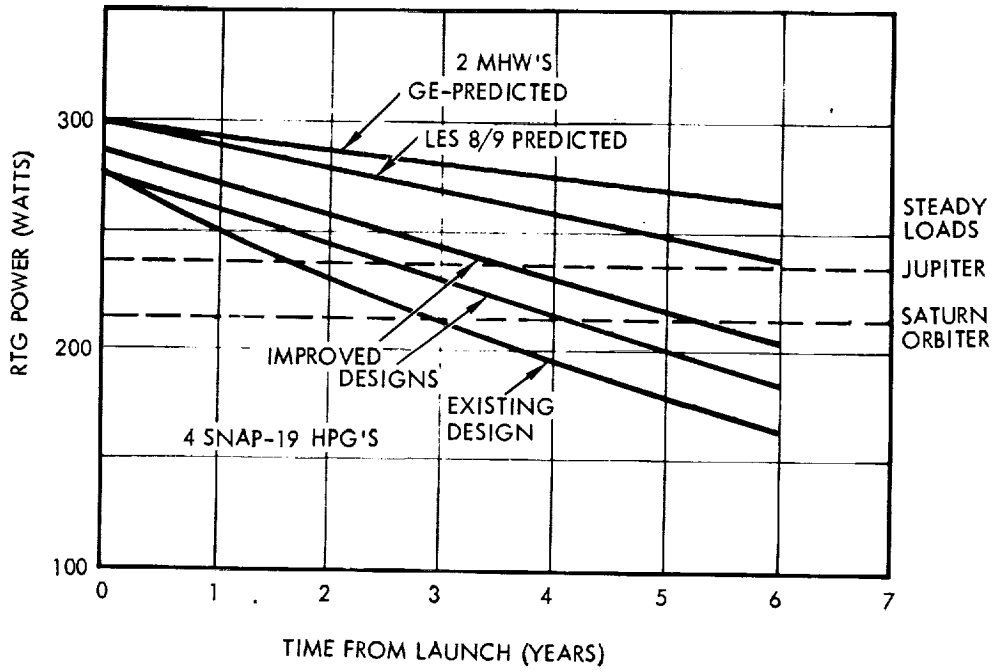

Figure 5-4. RTG Performance Predictions

In case of failure of one MHW unit sufficient power would still be available to support minimum mission requirements, although some of the loads would have to be selectively commanded off in an alternating sequence. For example, the X-band transmitter could be used intermittently for high data rate telemetry of stored science data, while some science experiments are turned off. A single-unit failure would be less disruptive if four RTG's of the HPG type were selected as power sources.

The approach selected to handle the shunt load heat dissipation problem early in the mission when the full available RTG power greatly exceeds spacecraft load requirements is discussed in Sections 4.2 and 4.5.

5.5 COMMUNICATIONS CAPABILITY

5.5.1 Uplink

Control of the spacecraft and scientific instruments operating modes is accomplished by transmission of PCM/FSK/PM modulated S-band signals from the Deep Space Stations. The signal strength at the input to the spacecraft receiver, as a function of the communications range, is depicted graphically in Figure 5-5 for various ground station configurations (antenna diameter and transmitter power) and spacecraft receiving antennas. In the absence of command modulation satisfactory receiver lock, and consequently two-way Doppler tracking, is achieved with an input level of at least -149.8 dBm (receiver threshold). However, an additional 2.8 dB is required when commanding to meet the decoding performance criterion: 10^{-9} probability of executing a false command. A nominal carrier phase modulation index of 1.1 radians is selected to maximize the reception distance for commands.

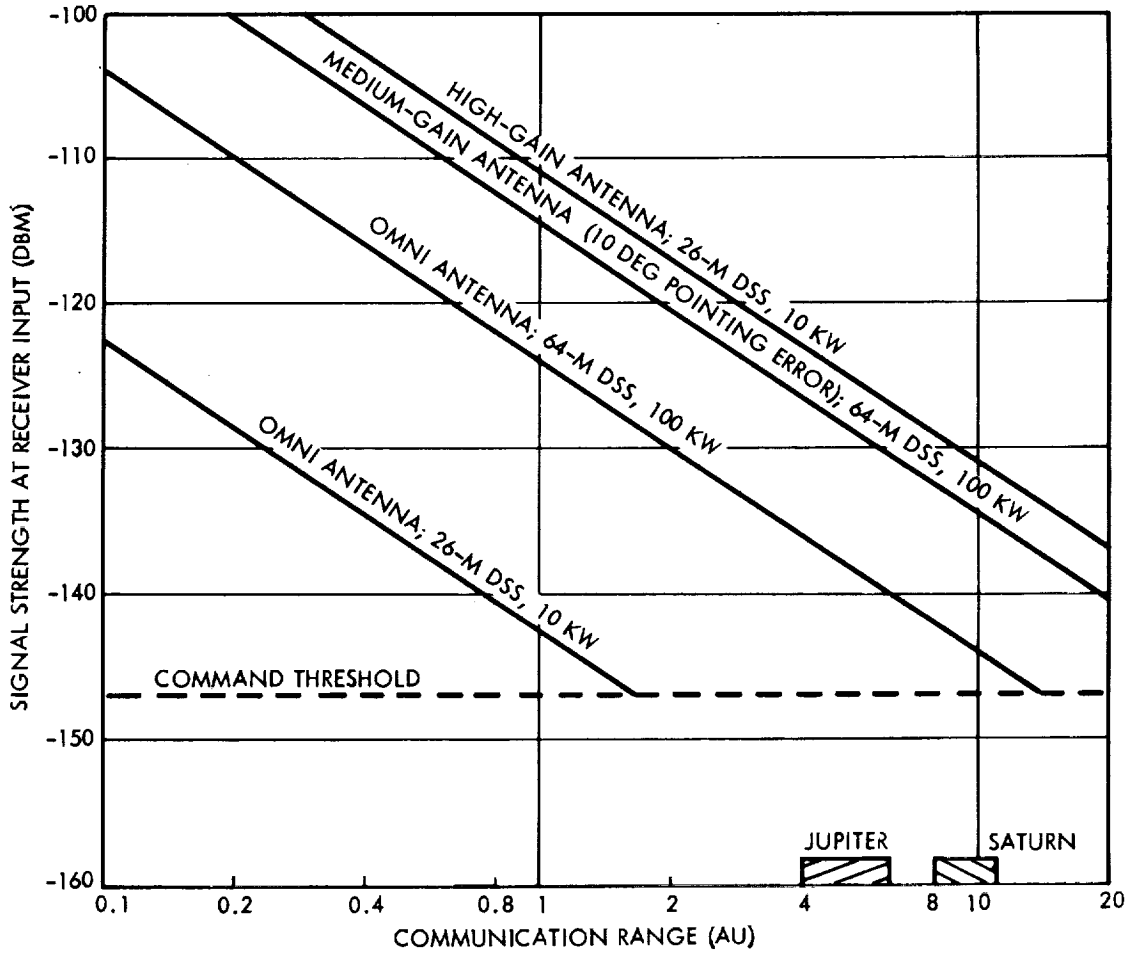

Figure 5-5. Uplink Communications Performance

It is apparent that command control is possible at the extreme range of Saturn, even if the spacecraft is significantly off-earth-pointing and receiving on the omni antenna. However, a 64-meter station and at least 100 kW of transmitter power are required. While a viable downlink is not possible if the pointing error exceeds 2 to 3 degrees, the capability for command access permits open-loop corrective precession maneuvers to recover the earth-pointing attitude and resume normal telemetry operations. Pointing errors as great as 10 degrees may be corrected automatically via closed-loop (conscan) precession using the spacecraft medium-gain antenna and a 64-meter station.

5.5.2 Downlink

Figure 5-6 depicts predicted downlink data rate performance (S- and X-band transmission) achievable with the spacecraft high-gain antenna, based on nominal link parameter values. Increased receiver detection degradation, attributed to imperfect phase coherence in the phase lock tracking loop, causes the data rate capability to diminish faster than the ideal inverse square of the communications range ($1/R^2$) would indicate. Estimates at rates lower than 64 bit/s represent extrapolations of measured empirical data at the higher rates. The telecommunications design control table, Table 5-8 delineates the link parameters which were used in the performance evaluation.

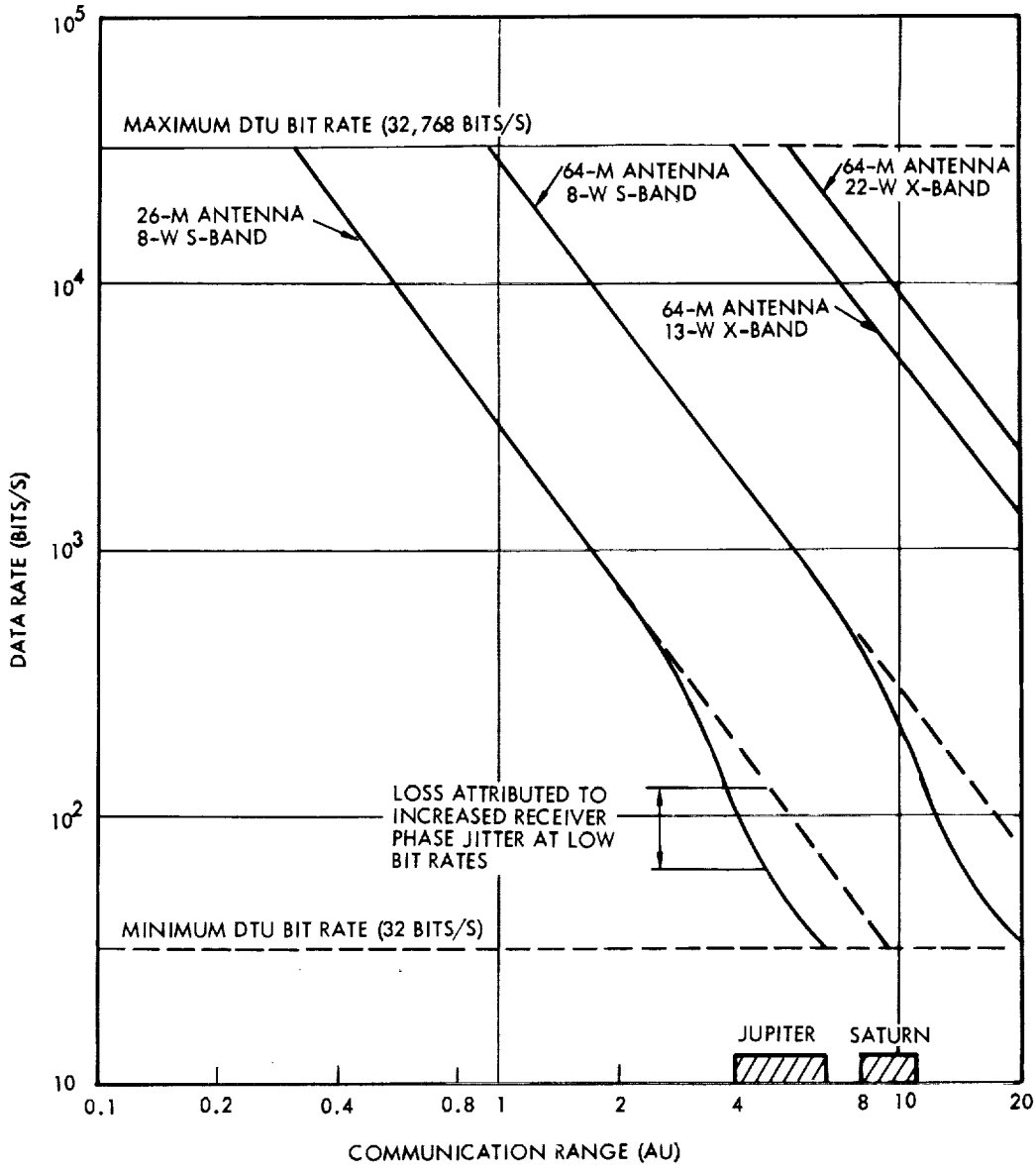

Figure 5-6. Downlink Communications Performance

Table 5-8. Telemetry Link Design Control Summary

Parameter	Nominal Value			Source/Notes
	26-Meter	64-Meter		
	S-Band		X-Band	
1. Frequency (MHz)	2300.0	2300.0	8400.0	
2. Spacecraft transmitter power (dBm)	39.0	39.0	41.3	S-band: 8 watts; X-band: 13 watts
3. Spacecraft coupling loss (dB)	-2.0	-2.0	-1.8	S-band: Pioneer F measured values X-band: Waveguide with 5.5 dB/100 ft loss (8 ft); no diplexer; coax switch with 0.4 dB loss; plus allowance (1 dB) for couplings and VSWR loss
4. Spacecraft antenna gain (dBi)	32.8	32.8	44.1	9-ft parabolic reflector. S-band: Pioneer 10 measured value. X-band: Scaled from S- to X-band.
5. Antenna pointing loss (dB)	-2.2	-2.2	-0.9	S-band pointing error: 1.4 deg. X-band pointing error: 0.25 deg.
6. Polarization loss (dB)	-0.2	-0.2	-0.2	Spacecraft antenna axial ratio: 3 dB (measured). DSS antenna (210-ft) axial ratio: 1.48 dB (JPL document 810-5).
7. Space loss (dB)	-263.1	-263.1	-274.3	Communication range: 1 AU (reference point)
8. Atmospheric attenuation (dB)	0.0	0.0	-0.2	JPL document 810-5
9. Ground station antenna gain (dB)	53.3	61.7	71.5	Referenced to maser input (JPL document 810-5). Includes antenna elevation angle sag.
10. Total received power (dBm)	-142.4	-134.0	-120.7	
11. Ground station system noise temperature (^{o}K)	33	22	27	JPL document 810-5
12. Relative increase in system noise temperature losses (^{o}K)	4	2	6	JPL document 810-5
13. Ground station noise spectral density (dBm/Hz)	-182.9	-184.8	-183.4	
14. Total received power to noise spectral density ratio (dB-Hz)	40.5	50.8	62.7	
Carrier Channel Performance				
15. Carrier modulation loss (dB)	-7.8	-7.8	-7.8	Modulation index: 1.15 radians
16. Carrier power to noise spectral density ratio (dB-Hz)	32.7	43.0	54.9	
17. Carrier loop threshold loop bandwidth (dB)	4.8	4.8	4.8	2 B_{LO} = 3.0 Hz (JPL document 810-5)
18. Carrier loop SNR threshold (dB)	10.0	10.0	10.0	JPL document 810-5
19. Carrier performance margin (dB) at 1 AU	17.9	28.2	40.1	
20. Range for zero carrier margin (AU)	7.8	25.7	101	Modulation index: 1.15 radians
Telemetry Channel Performance				
21. Data modulation loss (dB)	-0.8	-0.8	-0.8	Modulation index: 1.15 radians
22. Available data power to noise spectral density ratio at 1 AU (dB-Hz)	39.7	50.0	61.9	
23. E_b/N_o (dB) required plus receiver loss for a 10^{-3} frame deletion rate at bit rate (bits/s) of ≥1,024	5.0	5.0	5.0	NASA/ARC measurements at JPL CTA-21
256	5.7	5.7	5.7	
128	7.5	7.5	7.5	
≤64	8.3	8.3	8.3	
24. Data power to noise spectral density required for bit rate (bits/s) of 32,768	50.1	50.1	50.1	
16,384	47.1	47.1	47.1	
8,192	44.1	44.1	44.1	
4,096	41.1	41.1	41.1	
1,024	35.1	35.1	35.1	
256	29.8	29.8	29.8	
64	26.4	26.4	26.4	
32	23.4	23.4	23.4	
25. Maximum communication range R(x) in AU at bit rate X R(32,768)	0.3	1.0	3.9	
R(16,384)	0.4	1.3	5.5	
R(8,192)	0.6	2.0	7.8	
R(4,096)	0.9	2.9	11.0	
R(1,024)	1.7	5.6	21.8	
R(256)	3.1	10.1	40.3	
R(64)	4.6	15.1	59.5	
R(32)	6.5	21.2	84	

A range of bit rates extending from 32,768 to 32 bit/s has been investigated to accommodate the anticipated high data rate requirements of photo-imaging instruments as well as the limited capabilities of the S-band link at the extreme planetary ranges. Further, convolutional encoding with sequential decoding, identical to that applied to Pioneer F/G has been

retained to enhance the communication link efficiency. While it is recognized that the DSN is not presently configured to decode convolutionally coded data at rates exceeding 2048 bit/s, it is anticipated that such capability will be introduced to meet the requirements of these and other future missions.

The carrier channel performance is determined by the choice of modulation index, the phase-lock loop noise bandwidth ($2 B_{LO}$), and the threshold signal-to-noise ratio. The constraining design condition is the S-band transmission to the 26-meter antenna ground station at Jovian ranges, operating as a backup for 64-meter operations.* A 3-Hz loop bandwidth is essential to satisfactory performance of this link. Projected DSN capabilities include provision for 3-Hz loop bandwidth receiving capability at selected deep space stations. Design control table entries for the 64-meter receiving station also reflect the use of a 3-Hz loop bandwidth, although the predicted data rate performance is not adversely affected if a wider bandwidth is selected. Moreover, uninterrupted tracking capability through the periapsis region, with attendant high Doppler rates, will necessitate use of wider bandwidths.

Selection of a phase modulation index of 1.15 radians is consistent with maximizing the data rate and meeting the modulation limitations of the DSN, assuming a loop noise bandwidth of 3 Hz. A somewhat lower modulation index is preferred for the S-band link if a wider loop bandwidth is selected or desired. There is no need to adjust the X-band modulation index because the maximum communication range (11 AU) does not approach the carrier-power-limited range (101 AU). A commandable modulation index would permit optimizing the performance for the operating conditions. It has not been incorporated in the orbiter spacecraft configuration because S-band telemetry at extreme ranges is limited to backup support for the prime X-band link.

Figure 5-7 shows the predicted telemetry data rate profiles for the X- and S-band links configured for the orbiter spacecraft, including the estimated receiver detector degradation effects noted above. A maximum of 8 data rates are available and selectable by ground command with the logic provided within the Pioneer DTU. In order to cover as wide a range of data rates as possible, and minimize modifications, it was necessary to omit some intermediate values. Table 4-13 summarizes the available bit rates for Pioneers 6/9, Pioneer F/G the Outer Planets Pioneer baseline, and the tentative orbiter spacecraft. The final selection of bit rates for a given mission may cater to specific scientific requirements, the RF power levels, and the target planet.

*Note that S-band transmission to the 26-meter antenna ground station is insufficient to provide the minimum bit rate of 32 bits/s at Saturn communication distances. The 64-meter antenna would have to be used to receive S-band transmissions.

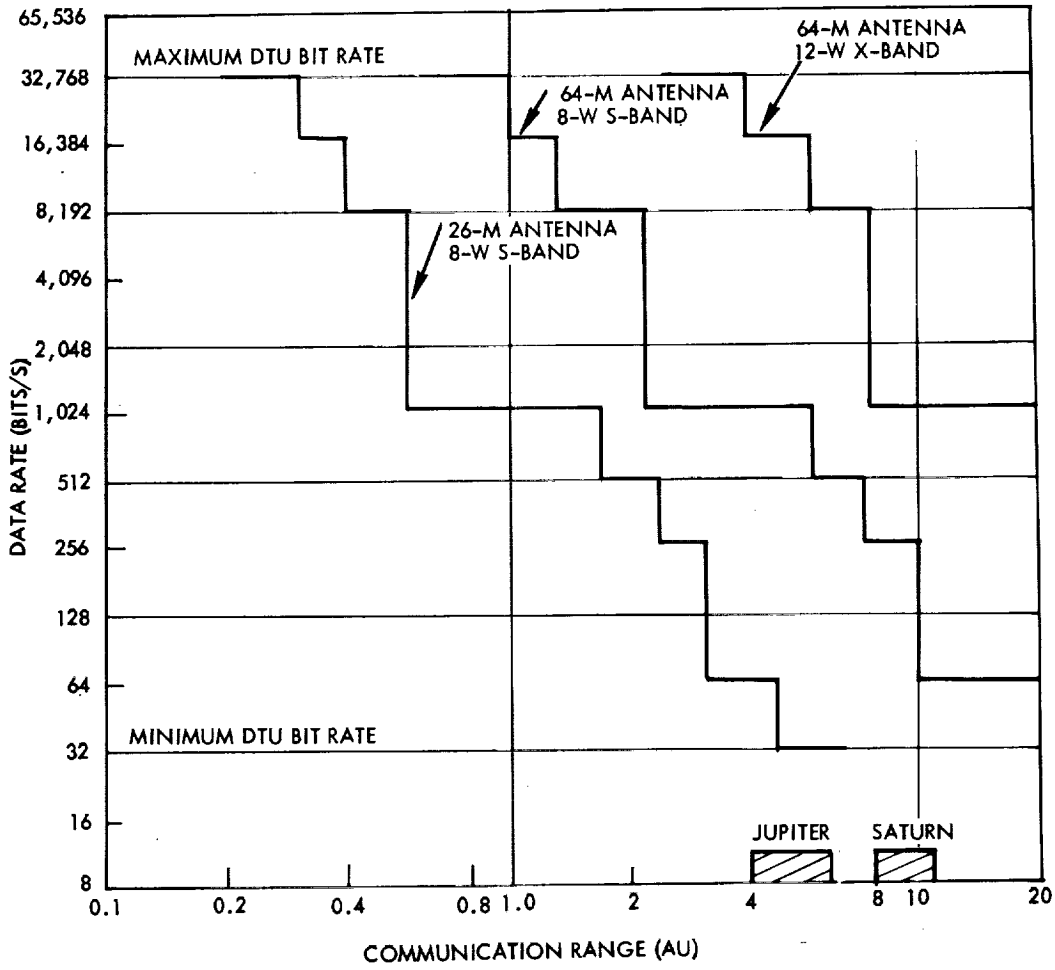

Figure 5-7. Telemetry Bit Rate Versus Range Profile (Jupiter Orbiter)

The data rate profile for the high power (22 to 24 watts) X-band transmission mode is not shown in Figure 5-7. However, the achievable data rate at a given range is approximately twide the rate illustrated for the low-power mode (13 watts). Consequently, the high-power mode affords a maximum data rate of 32,768 kbits/s at Jupiter and 8192 kbits/s at Saturn.

5.5.2.1 Antenna Pointing Errors

The link budgets of Table 5-8 are based on relatively small antenna pointing errors and losses (line 5). For the X-band link the loss is 0.9 dB and the pointing error is 0.25 degree. The pointing errors have the following components, in degrees (Table 5-9):

Table 5-9. S-Band and X-Band Pointing Errors

Component \ Pointing Error (deg)	S-Band	X-Band
Antenna actual electrical axis relative to intended axis*	0.1	0.05
Antenna intended axis relative to spacecraft body Z axis	0.9	0
Spacecraft body Z axis relative to spacecraft spin axis*	±0.09	±0.09
Spacecraft spin axis relative to the earth line	0.4	0.15
Total pointing error	1.44	0.25

*These two quantities root-sum-squared.

The first entry indicates the X-band antenna pattern would be favored in adjusting the feed position with respect to body axes during installation and alignment, but its narrow beamwidth would permit such fine adjustment by pattern measurements. The second entry shows the intended 0.9-degree permanent offset of the medium-gain antenna S-band pattern for conical scanning.

The third entry indicates a range encompassing predictable and unpredictable principal axis tilts due to mass properties effects. (The predictable component is reduced from Pioneer F/G because the center of mass now remains located on the spacecraft centerline, and principal-axis tilt is minimized, with the deployment method adopted for the orbiter).

The fourth entry represents the offset of the spin axis from the earth line. For X-band this component has been reduced about as much as possible. To achieve 0.15 degree requires careful measurements with the conscan signal processor, and correction by open-loop pulses as well as closed-loop homing, as it represents residual error less than the closed-loop threshold setting. The 0.4 degree for S-band tolerates a less accurate earth-pointing procedure, and several days' drift of the spacecraft-earth line since the last earth-pointing update.

The first and third entries, being essentially random and equally distributed in X and Y directions are combined by root-sum-squaring. Otherwise, all entries are added algebraically, to be applicable at the worst point in the spin cycle.

Actually, while careful attention to orientation procedure is required to optimize performance of the X-band link, this is not required during most of the interplanetary cruise phase and part of the orbital phase of the Jupiter and Saturn missions.

5.6 RELIABILITY AND EXTENDED LIFE CAPABILITY

Primary concerns regarding the reliability of the Pioneer Outer Planet Orbiter spacecraft compared with Pioneer F/G include the following:

- Lifetime extension from 2.5 years to 3.5 years in the Jupiter orbit mission, and to 6 years in the Saturn orbit mission.
- Addition of a major new subsystem, i.e., the bipropellant propulsion system and support structure introducing new failure modes that can critically affect mission success.
- Addition of an articulated sensor platform.
- Exposure to uncertain trapped particle radiation and meteoroid flux environments in the vicinity of Jupiter and Saturn during the orbital phase, especially during the close planetary approach at each periapsis passage.

These concerns are mitigated to some degree by several factors. Integrated exposure to environmental effects originating from the sun is not increased because of comparable solar distances involved. Anomalies not related to depletion or wear-out are likely to have a lower incidence rate during the extended part of the mission. By careful selection of orbital characteristics certain known hazard zones in close vicinity of the target planets can be avoided (e.g., zones of maximum trapped radiation fluence near Jupiter based on data obtained from the Pioneer 10 and 11 encounters, and the ring area of Saturn's equatorial plane).

For operational reasons certain components of the spacecraft are in line (in the reliability sense) at later times in the outer planet orbiter missions than their counterparts in the Pioneer F/G flyby missions, and redundancy must be implemented accordingly. Examples are attitude reference sensors, spin control thrusters and critical elements of the added main propulsion system.

5.6.1 Fail-Safe Design Policy

For the Pioneer orbiter missions the following fail-safe policy is proposed and observed:

> The spacecraft should be designed with appropriate redundancy, workarounds and backup capabilities which will eliminate as many electronic, mechanical, and electromechanical failure modes as sources of spacecraft failure as practical. When redundancy or backups are employed, circuits, interfaces between units, and switching circuits

should be designed with fault isolation so that a failure in one unit does not propagate into, or interfere with the operation of, the redundant units or backup modes.

Electrical or electromechanical random single-point failures should be eliminated from equipment which must successfully operate at a high duty cycle throughout the mission, and from equipment which is especially critical to the success of the mission. For the purposes of this single-point failure criterion, failure or degradation from predictable wear-out shall not be regarded as random, and the design should be capable of surviving a single random failure in addition to expected wear-out failures.

The spacecraft should be designed so that it can survive failures occurring when the spacecraft is not being monitored by the ground, since those that occur in deep space require long periods for telemetry detection, problem diagnosis and corrective command transmission.

The above policy is intended to be a firm but not an inflexible guideline to the spacecraft design. In implementing the policy in specific cases, competing factors — such as cost, practicality, schedule, weight, redesign or repackaging of existing equipment, possible introduction of higher probability failures, increased risks of operator errors, etc. — should be taken into account and possibly weigh heavier than the above reliability policy. These considerations should carry more influence in establishing the spacecraft design than numerical reliability calculations alone because the assumptions underlying numerical calculations — exponential probability of failure — have limited applicability to this mission class.

5.6.2 Single-Point Failures

The following single-point failure considerations apply in the Pioneer orbiter spacecraft:

a) Spin Control. As in the Pioneer F/G design, the primary control of spin rate is by two nonredundant thrusters — one to spin up, and the other to spin down. In Pioneer F and G, no backup thrusters were provided, because, in the normal mission, major spin rate changes are not required after 20 days (the second midcourse maneuver). In the orbiter missions, however, repeated spinup and despin maneuvers are necessary 1) to establish an increased spin rate for greater attitude stability during main thrust events, and 2) to establish a lower than nominal spin rate for improved image system operation. These events occur during the final year of the mission; prior to and after entering the planetary orbit phase. This necessitates the addition of a set of redundant spin control thrusters. These additional thrusters are also advantageous in eliminating undesirable precession coupling torques which would occur in the case of a single thruster pair due to unavoidable large variations of the center-of-mass location.

b) Propulsion System. Redundancy is provided in the pressurant and propellant control assemblies of the main propulsion system. As on Pioneer F/G the four velocity/precession control thrusters are a redundant set, i.e., any one of these thrusters could fail without impairing the required control functions. However, in both the main and auxiliary propulsion systems the propellant tanks, including bladders and pressure gauges, are nonredundant. This single-point failure possibility is tolerable primarily because of the great weight and space penalty which would be incurred to attain full redundancy.

c) Conscan Signal Processor. As in the Pioneer F/G design this unit is nonredundant. The function is twofold: to determine, by use of the spacecraft's offset antenna pattern and reception of uplink transmission, the magnitude and direction of the pointing error of the spin axis from the earthline; and to control precession thrusters which will correct this pointing error.

On Pioneers 10 and 11 the conscan unit is being used routinely for attitude determination, but only infrequently for controlling the correction maneuver. (In most cases, attitude is controlled directly by open-loop precession commands.)

However, there is an operational mode in which the pointing error is determined from the downlink transmission by similarly processing on the ground the signal received at the DSN station. The Pioneer orbiter spacecraft, having a permanently offset S-band antenna feed is less likely to have either the primary or backup modes of attitude determination unavailable because of spacecraft equipment failure.

d) Deployment Dampers. Each deployed appendage — two RTG's and the magnetometer boom — has a single rotary viscous damper which serves to restrain the rate of deployment. As in Pioneer F/G, this component is nonredundant. This is justified by the fact that the component is used only once, on the first day of the mission.

5.6.3 Wear-Out Life

Since most of the equipment on the spacecraft is derived from the Pioneer F and G program with a specified mission time of 900 days it is necessary to review that equipment for its ability to survive the longer planetary orbiter missions. The spacecraft must be designed with all expendables and known wear-out phenomena sized for six years.

The fact that most of these components were qualified for a 900-day mission must not be construed as necessarily meaning that their lifetime is limited to that period. Indeed, many of the potentially life-limited components of Pioneer F/G (or similar equipment) have been used on spacecraft with five- or seven-year missions.

Table 5-10 lists the equipment currently identified as potential sources of wear-out, a description of their wear-out phenomena, the circumstances of their use in the orbiter missions, and possible provisions which could be implemented where necessary.

Table 5-10. Life-Limited or Time-Variable Components

Equipment	Aging Phenomena	Comments
Traveling wave tube assemblies	Cathode depletion	State-of-the-art theoretical barium exhaustion times are currently in excess of 100,000 hours (11.5 years). Redundant TWTA's are provided.
	Degradation of insulation in high-voltage power supply causing arcing	State-of-the-art packaging and insulation concepts permit six-year lifetimes to be achieved
Thruster assemblies	Degradation of seal and seating integrity	Thrusters have demonstrated 500,000 pulses life without leakage. Orbiter mission worst case thruster requirement is 5-10,000 pulses. Proper thermal control will provide assurance of seal/seat integrity.
	Catalyst bed degradation from cold starts	The catalyst bed has a design life of 150 cold starts which falls within orbiter mission requirements. The catalyst bed is maintained at temperatures high enough to alleviate the cold start problem.
Propellant expulsion bladders	Long-term degradation under exposure to N_2O_4 or MMH	Mission life exceeds demonstrated endurance of existing Teflon bladders. Additional life testing and/or selection of new materials may be necessary.
Thermal coatings	Long-term aging and discoloration of thermal surfaces	Integrated ultraviolet and particulate radiation is comparable to Pioneer 10/11. No problems anticipated.
Star sensor	Lens fogging from long-term or intensive short space radiation	Integrated solar radiation and electron and proton fluences are comparable to those on Pioneer 10/11, or earth orbiters with one year life
Sun sensors	Degradation of sun sensing devices	Not required beyond first year of mission

5.6.4 Radiation and Micrometeoroid Environment

While the radiation and micrometeoroid environment during transit is comparable to that of the Pioneer 10/11 mission — actually the micrometeoroid flux in the asteroid belt was found to be several orders of magnitude less than anticipated — the orbital phase may present potentially more severe environmental hazards in close vicinity of the target planets.

Estimates of electron and proton radiation levels near Jupiter, based on models of particle fluences assumed during the development of Pioneer F/G and updated by results of the Pioneer 10 Jupiter encounter in December 1973 are discussed in Section 2.1.1.4. By a conservative choice of periapsis altitudes at Jupiter and Saturn, or by timing the flyby events to occur in a zone of low radiation fluence (even at low altitude) the accumulated effects can be held to a level less damaging than that to which Pioneer 10 was exposed during its low inclination flyby at 2.8 R_J closest approach.

Regarding the exposure to micrometeoroid impact in the vicinity of the target planets it can be shown that the predominant relative motion of particles encountered by the spacecraft during the orbital phase is from the rear hemisphere, typically within 30 to 45 degrees of the spin axis. This relative velocity orientation is similar to that of asteroidal micrometeoroids encountered during the cruise phase, such that the micrometeoroid shield and Armalon blanket enclosing the retro-propulsion stage gives effective protection during the orbital phase as well.

5.6.5 Reliability Analysis

This section presents results of the reliability analysis of the proposed Pioneer configurations for the 3.5-year Jupiter and 6-year Saturn orbiter missions.

The analysis uses the baseline Pioneer F/G design (Reference 1) with the modifications identified in this document and in Reference 3, "Outer Planets Pioneer Spacecraft," and Reference 4, "Extended Life Outer Planets Pioneer Spacecraft." The principal changes include the following:

- Addition of the bipropellant main propulsion subsystem
- Addition of a modularized high capacity CMOS DSU
- Addition of two dual-mode X-band transmitters
- Deletion of the storage battery.

Table 5-11 gives a more complete list of the changes from the baseline Pioneer F/G configuration that affect overall reliability. Table 5-12 summarizes subsystem and system reliabilities for the Pioneer F/G, Jupiter orbiter, and Saturn orbiter missions. The table also includes Pioneer F/G reliabilities extrapolated to the mission times of the Jupiter and Saturn orbiter to permit reliability comparisons among the three systems. Reliability versus time characteristics of the three systems are plotted in Figure 5-8. Differences between the Jupiter and Saturn orbiters are mainly due to dissimilar duty cycles of the nearly identical equipment used (e.g., propulsion valves, conscan, and S-band transmitter) whereas differences between the orbiter missions and Pioneer F/G are due to major equipment differences.

Extension of failure rates from the Pioneer F/G reliability model up to six years, as used in this analysis, is probably unduly pessimistic, because these failure rates reflect data based on much shorter missions, including a number of earth-orbiting spacecraft programs. Thus infant failures and failures in the temperature-cycling earth-orbit environment tend to produce failure rates which are too high for the long mission with its unchanging environment. Therefore the 0.45 figure is not a realistic estimate of the probability of mission success of the Saturn orbiter. Nevertheless, the calculations point out those portions of the spacecraft design where reliability augmentation would be comparatively most effective.

Table 5-11. Summary of Equipment Changes to Pioneer F/G for the Jupiter and Saturn Orbiter Missions

Structure Subsystem and Mass Properties Control

- Additional structure to accommodate stage and support spacecraft proper
- Reinforcement of magnetometer and RTG booms
- Increased equipment and structural weight requires increased duty cycling of monopropellant hydrazine system
- Added rotational sensor package with associated drive electronics

Propulsion Subsystem

- Added bipropellant stage including four propellant tanks and one pressurant tank
- Addition of pair of partially redundant spin/despin hydrazine thrusters

Thermal Subsystem

- Additional thermal control demands required for added propulsion stage
- Relocation of louvers to accommodate configuration change
- Deletion of battery thermal control

Attitude Control Subsystem

- Addition of auxiliary roll reference sensor and electronics
- Addition of circuitry to PSE for auxiliary roll reference sensor and to incorporate controls for higher spin rate mode during high thrust ΔV maneuvers
- Addition of valve driver circuits for redundant spin/despin thruster cluster

Data Handling Subsystem

- New high capacity CMOS DSU replaces Pioneer F/G core memory

Communications Subsystem

- Subsystem modification by addition of dual-mode X-band transmitters (13 and 23 watts)
- Movable S-band antenna feed replaced by dual S-band/X-band feeds (all stationary)

Electrical Power Subsystem

- Four SNAP-19 RTG's replaced with two MHW RTG's
- Battery and associated charge and control circuitry deleted

Command Subsystem

- Increased command processor real-time command capability by approximately 20 commands primarily to accommodate new propulsion stage
- Revised command memory capacity to store 16 redundant commands and their associated time tags (formerly 5 nonredundant commands)

Table 5-12. System Reliability Summary

Subsystem	Pioneer F/G t = 21,600 hours	Jupiter Orbiter t = 30,660 hours (3.5 years)	Saturn Orbiter t = 52,560 hours (6.0 years)
Structure	0.9948	0.9947 (0.9946)*	0.9940 (0.9940)*
Propulsion (monopropellant)	0.9508	0.8849 (0.9307)	0.7921 (0.8833)
Propulsion (bipropellant)	-----	0.9474 (------)	0.9109 (------)
Thermal	0.9994	0.9999 (0.9993)	0.9999 (0.9988)
Attitude Control	0.9823	0.9597 (0.9705)	0.9147 (0.9300)
Data Handling	0.9416	0.9744 (0.8945)	0.9127 (0.7599)
Communications	0.9633	0.9295 (0.9362)	0.8445 (0.8524)
Electrical Power	0.9934	0.9975 (0.9906)	0.9942 (0.9839)
Command	0.9679	0.9716 (0.9547)	0.9303 (0.9237)
Meteoroid Hazard	0.9900	0.9900 (0.9900)	0.9600 (0.9900)
System	0.8016	0.6954 (0.7039)	0.4489 (0.4753)

*The numbers in parentheses show the Pioneer F/G reliabilities extrapolated to 3.5 and 6.0 years, respectively, for system comparison.

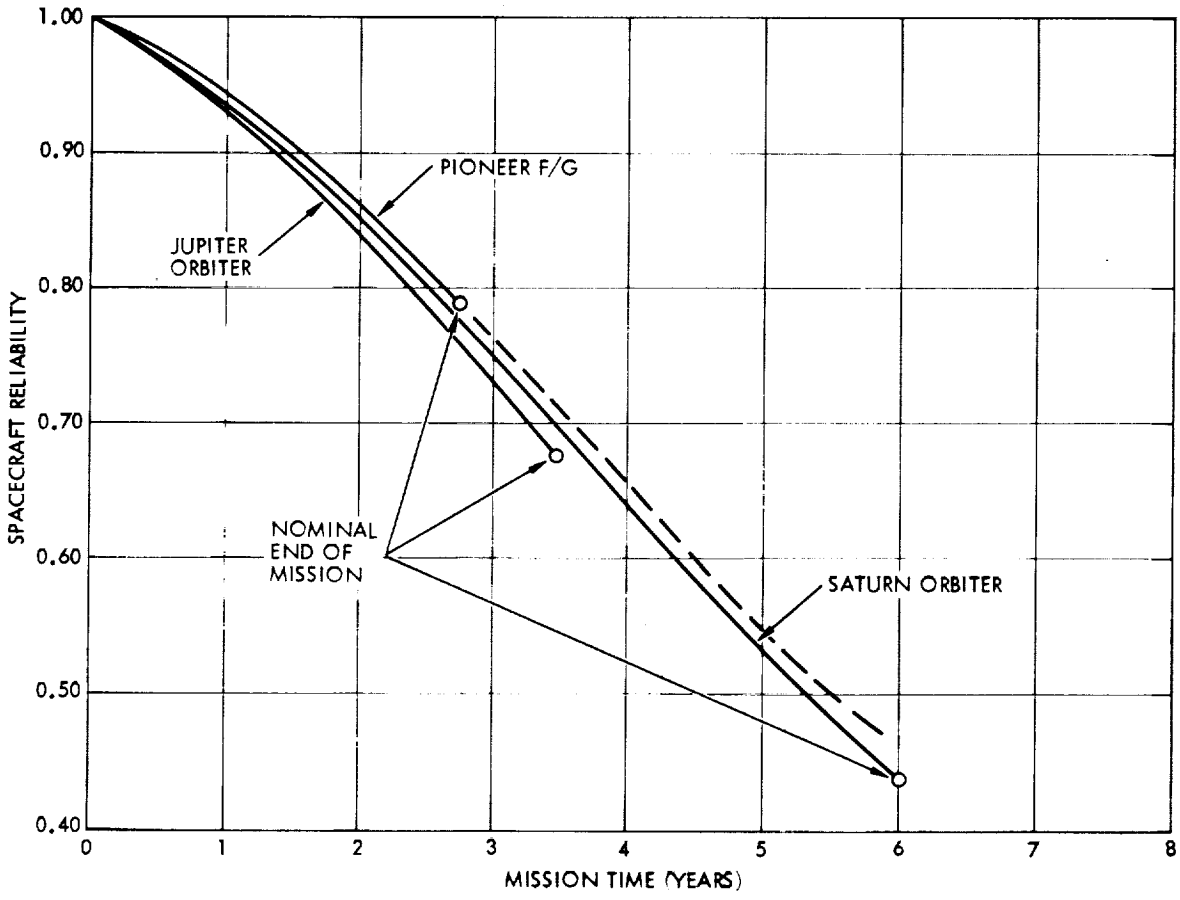

Figure 5-8. Reliability Vs. Time Histories of the Pioneer F/G, Jupiter, and Saturn Orbiter Missions

Before reviewing specific areas, note that the above tabulation includes only the parts of the flight spacecraft considered to be the responsibility of the spacecraft contractor. RTG's and scientific instruments are excluded.

The following subsections present equipment failure rates used in the analysis and identify areas in which significant reliability gains might be realized through the addition of redundancy and configuration modification.

Piece Part and Equipment Failure Rates

The electronic piece part failure rates used in the Pioneer F/G reliability analyses are also applicable to the orbiter spacecraft and are used in this document (see Appendix C). In Reference 15 these failure rates were updated on the basis of actual mission experience of TRW's spacecraft (Reference 16). However, this updating yielded only a small net effect since some generic part failure rates increased and others decreased with respect to the 1970 rate model, depending on in-flight hours of operation and the number of accumulated individual part failures.

The hydrazine thruster reliability model was updated in this study based on orbital information which has become available since the completion of the Pioneer F/G spacecraft development. It should be emphasized, however, that propulsion equipment failure rate data is extremely limited compared to electronic piece parts because of the small number of hydrazine thrusters relative to the number of electronic components on-board any given spacecraft. Thus, owing to the few failures of thrusters experienced in flight the failure rates given in Table 5-13 are extremely conservative.

Table 5-13. Hydrazine Thruster Failure Rates

Failure Mode	Failure Rate ($\times 10^{-9}$)
1) Steady-state burn	8647/second of burn
2) Pulse mode	563/pulse
3) Cold start	485,000/cold start
4) Leak mode	70/hour

Table 5-14 lists the failure rates used in the analysis of the bipropellant system (Reference 17). As mentioned previously, these data have a lower confidence level than failure rates for electronic parts in view of the much more limited data base from which they are drawn.

Table 5-14. Bipropellant System Failure Rates

Equipment	Failure Rate ($\times 10^{-9}$/hr)	Equipment	Failure Rate ($\times 10^{-9}$/hr)
Nitrogen Tank		Heater	
Leak	$\lambda = 26$	Short	1
		Open	1
Temperature Transducer			
Leak	14	Gimbal Bearing	80
Faulty reading	1386		
		Thruster (failure/hour of burn)	
Pressure Transducer		Chamber burnthrough	493,000
Leak	14	Injector failure	400,000
Faulty reading	1386		
		Regulator	
Filter		Leak to space	7
Loss of function	32	Leak downstream	332
		Fail closed	68
Check Valve			
Leak to space	14	Explosive Valve (NC)	
Fail open	45	Fail to fire probability	0.0038
		Premature fire probability	0.0009
Relief Valve			
Leak	214	Explosive Valve (NO)	
Fail closed	50	Fail to fire probability	0.0019
		Premature fire probability	0.0015
Propellant Tank			
Leak	26	Burst Disc	
Bladder	189	Premature burst probability	0.00025
		Fail to burst probability	0.00025
Bipropellant Valve			
Leak to space	7		
Leak downstream	300	Fill Valve (redundant)	
Fail closed	58	Leak to space	113

Subsystem Reliability

Detailed reliability block diagrams are shown in Figures 5-9 through 5-17 for each of the Jupiter and Saturn orbiter subsystems. Brief comments regarding the effects of changes from Pioneer F/G subsystems are given below.

Structure Subsystem. The reliability of the basic structure is not affected by the increased mission duration since structural reliability is assumed to be time-independent once launch is completed.

The structure added to the Pioneer F/G baseline configuration to accommodate the bipropellant system is assumed to have an insignificant effect on structural integrity if high enough design margins of safety are used.

Meteoroid Hazard. Estimates of the probability of noncatastrophic spacecraft failure are based upon the experience of the Pioneer 10 spacecraft during its interplanetary cruise, including the crossing of the asteroid belt, and at the Jupiter encounter. Current hypotheses of the

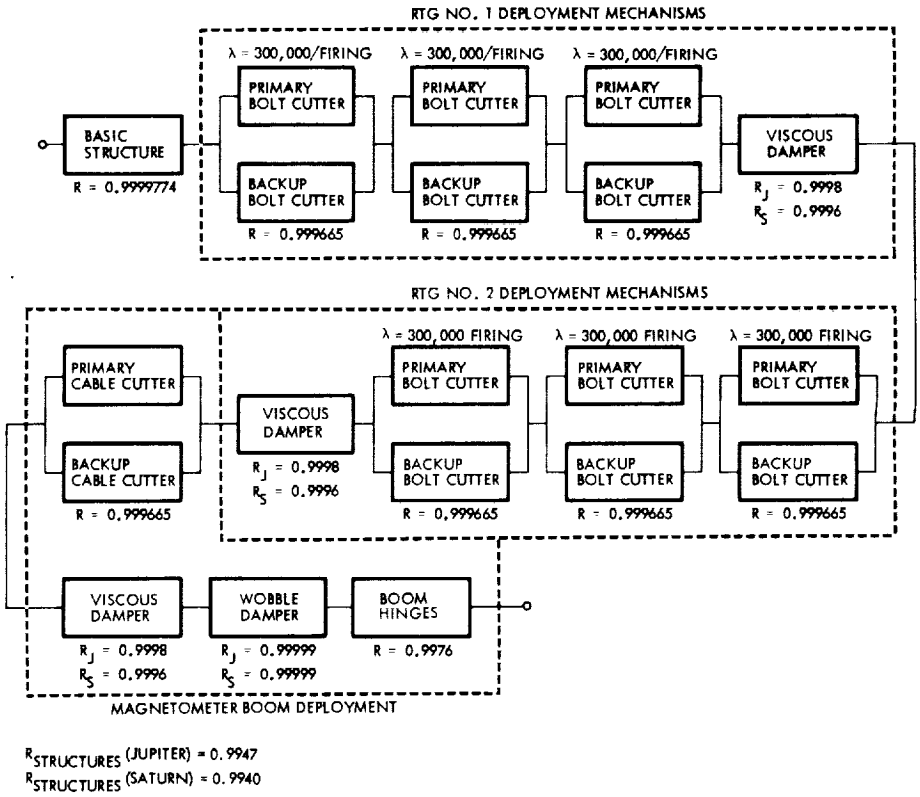

Figure 5-9. Structure Subsystem Reliability Block Diagram

planetary environments of Jupiter and Saturn were also taken into account. These probabilities were estimated to be approximately 0.99 for the Jupiter mission and 0.961 for the Saturn mission.

Hydrazine and Bipropellant Propulsion Subsystems. The additional mission time and the major increase in thruster activity detailed in Table 5-15 significantly decrease the hydrazine propulsion subsystem reliability. The addition of a pair of partially redundant spin/despin thrusters serves to counterbalance the effect of the increased thruster activity, but at the expense of the leak-to-space failure mode.

Table 5-15. Propulsion Activity and Duty Cycling

System	Pioneer F/G	Jupiter Orbiter	Saturn Orbiter
Bipropellant System	No bipropellant system	Six firings for a total of 50 minutes of burn	Four firings for a total of 46 minutes of burn
Monopropellant System			
Each ΔV Thrusters			
Cold starts	7	7	11
Steady-state burn	8500 sec	21,250 sec	31,874 sec
Pulses (125 ms)	7600	10,640	17,100
Each spin/despin			
Cold starts	6	30	24
Steady-state burn	132 sec	1188 sec	792 sec
Pulses (125 ms)	3000	5000	6000

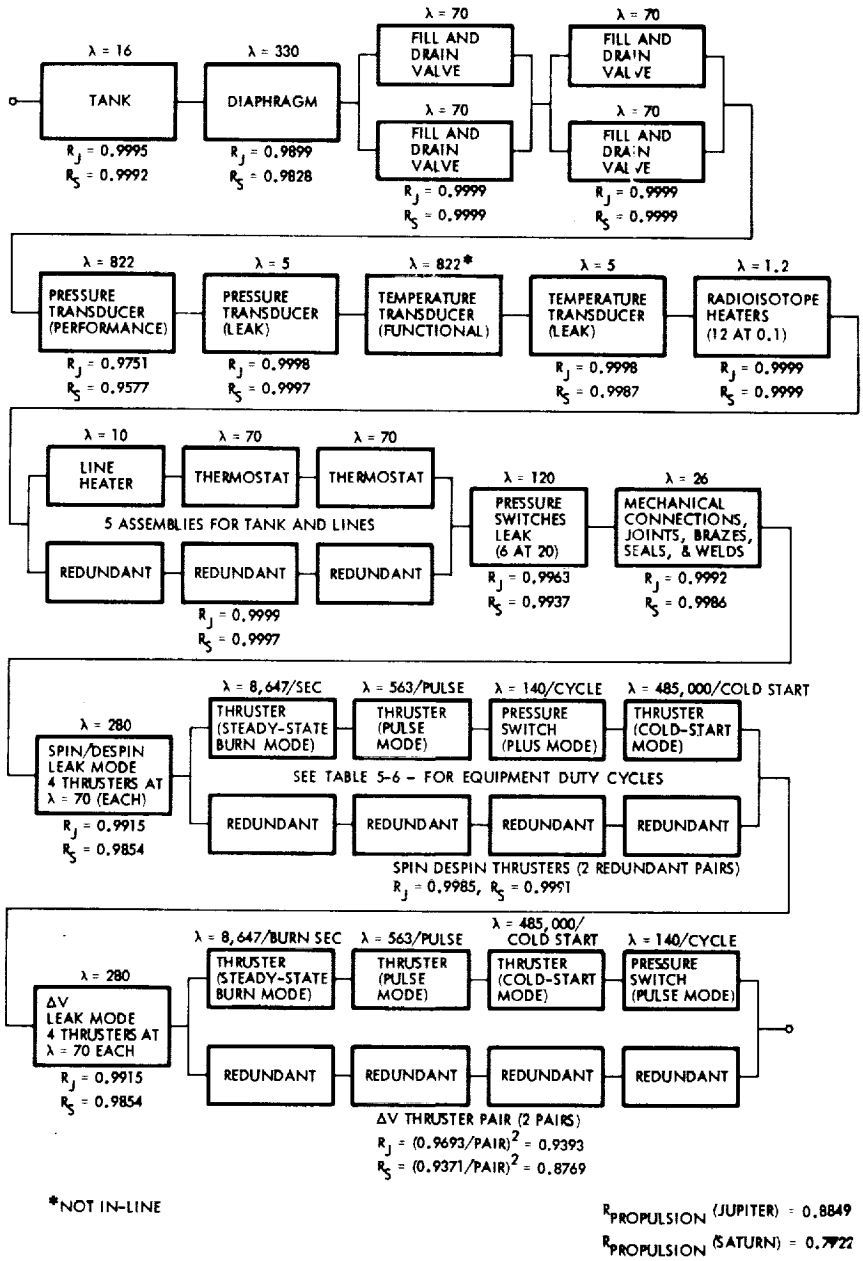

Figure 5-10. Hydrazine Propulsion Reliability Block Diagram

Earlier studies have shown that the RTG radiation environment will probably cause only an insignificant hydrazine degradation. The RTG radiation environment may, however, adversely affect the elastomeric bladder and diaphragm materials in both subsystems.

Passive surface tension devices which are currently being developed and perfected should offer a solution to this potential problem as well as to the more conventional burst and leak problems of bladders and diaphragms. At this time the reliability of the surface tension devices cannot be quantified, but should certainly exceed that of the bladders.

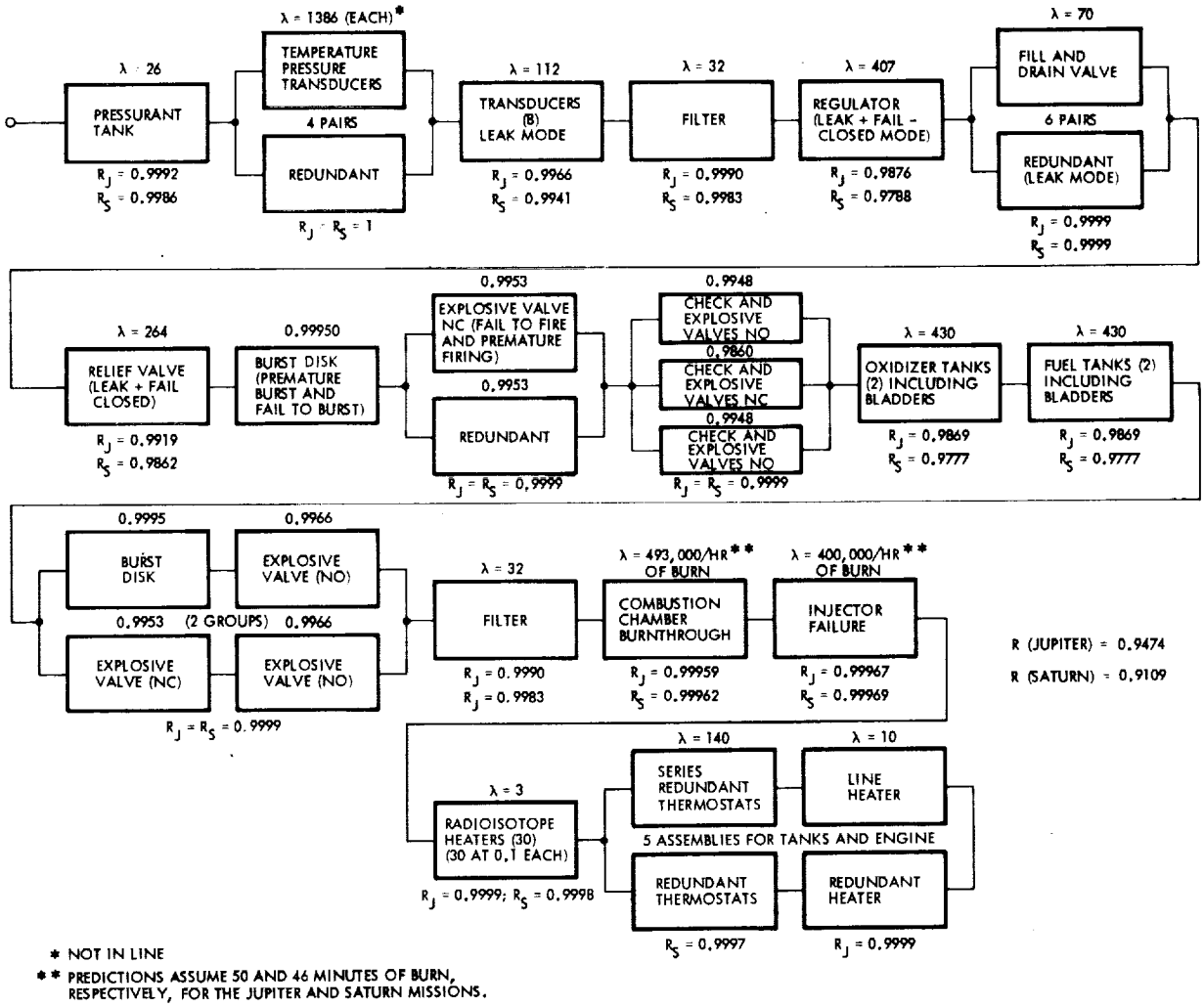

Figure 5-11. Bipropellant System Reliability Block Diagram

The large fuel and oxidizer tanks of the bipropellant system will have an increased vulnerability to the micrometeoroid hazard, but a thin double wall shielding should minimize this hazard with a minimum expenditure of weight.

The current flight-proven bipropellant designs use explosive devices for fuel and pressurant control. Long-life missions may require the replacement of the ordnance devices with solenoid valves since long shelf life reliability characteristics have not been well established.

Thermal Subsystem. A principal change in thermal control reliability characteristics is introduced by the addition of the new propulsion stage. Thermal control of the propellant tanks, feed lines and main retro-engine by electrical and radioisotope heaters adds several failure modes to the overall spacecraft system. Furthermore, the change in the method of waste heat dissipation from the equipment compartment via side louvers adds some

complexity and operating constraints. These changes are taken into consideration in modifying the thermal control subsystem reliability from that used for Pioneer F/G.

The reliability block diagram does not reflect the additional heaters for the new propulsion stage. These additional items are accounted for in the bipropellant stage block diagram.

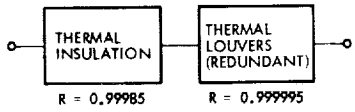

Figure 5-12. Thermal Subsystem Reliability Block Diagram

ACS Subsystem. An auxiliary roll reference assembly has been added for attitude control during periods of ineffectivity of the sun sensor and star reference assembly (in close vicinity of the planet). The ACS subsystem also includes the articulated sensor package drive and electronics. These changes only reflect in a small overall effect on ACS reliability.

Data Handling Subsystem. Five solid-state (CMOS) memory units comprise the Pioneer orbiter DSU. Each unit contains 1200 chips, 1 percent of which may be lost as an acceptable degradation level. It is also assumed that the DSU is required only after arriving at the planet. Thus, a high DSU reliability is achieved.

Communications Subsystem. The 8-watt TWTA's from Pioneer F/G are retained. The X-band TWTA's have been added to the subsystem to permit downlink communication at higher data rates.

Electrical Power Subsystem. The four SNAP-19 RTG's have been replaced by two MHW RTG's with significantly increased power level. This permits the deletion of the battery and simplification of the inverter and power control unit design.

Command Subsystem. The command processor has been enlarged to provide additional commands for control of the bipropellant system and other additional equipment. An enlarged and improved command memory has replaced the existing assembly in Pioneer F/G.

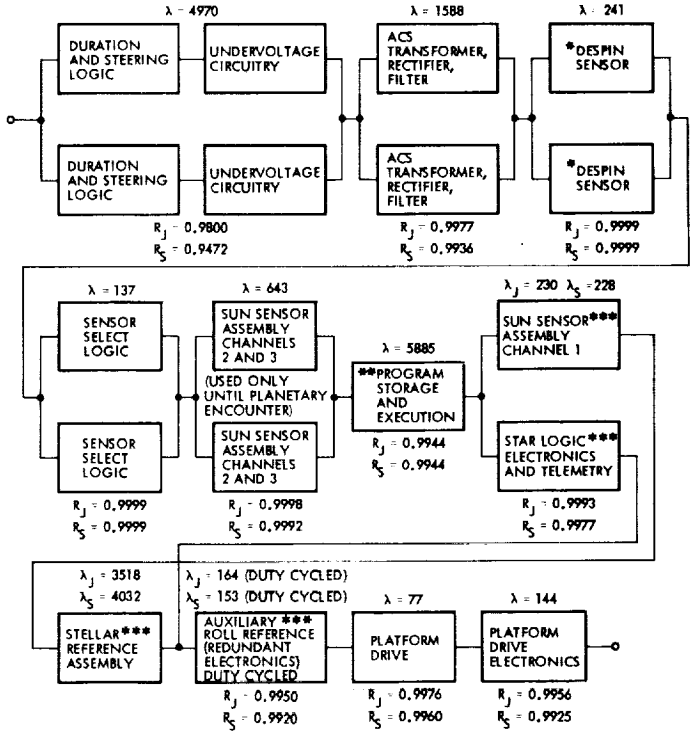

Figure 5-13. Attitude Control Subsystem Reliability Block Diagram

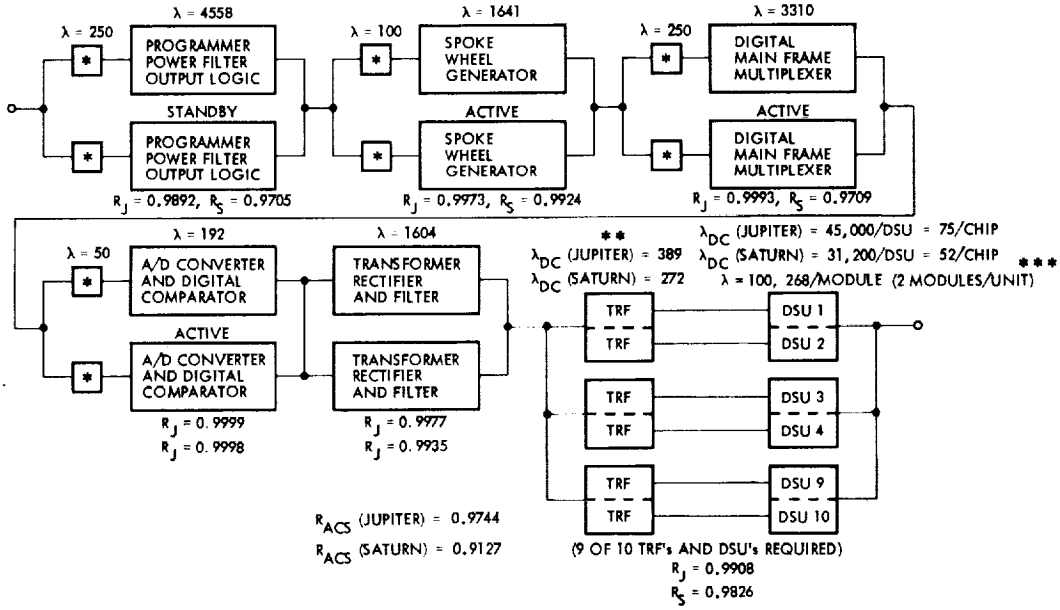

Figure 5-14. Data Handling Subsystem Reliability Block Diagram

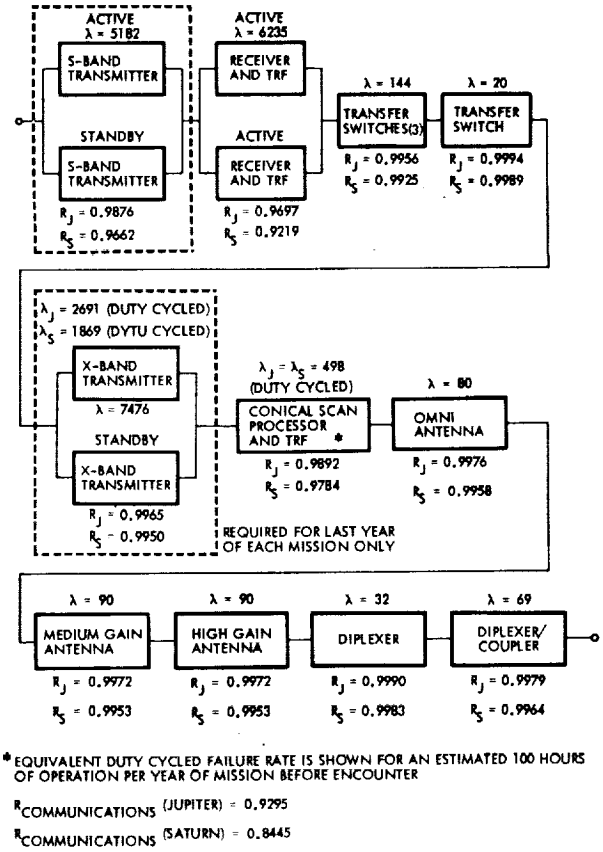

Figure 5-15. Communications Subsystem Reliability Block Diagram

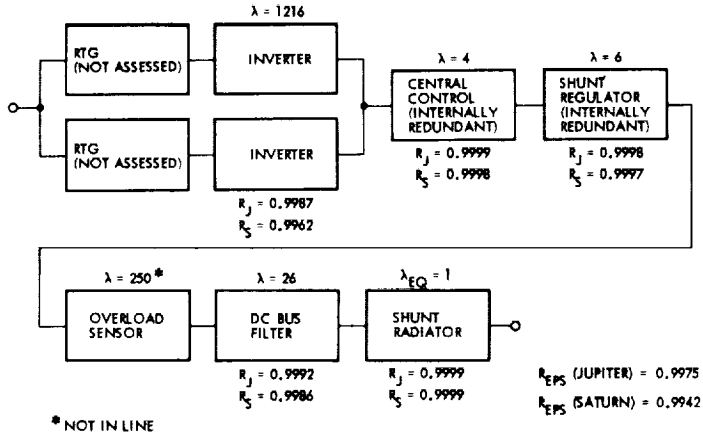

Figure 5-16. Electrical Power Subsystem Reliability Block Diagram

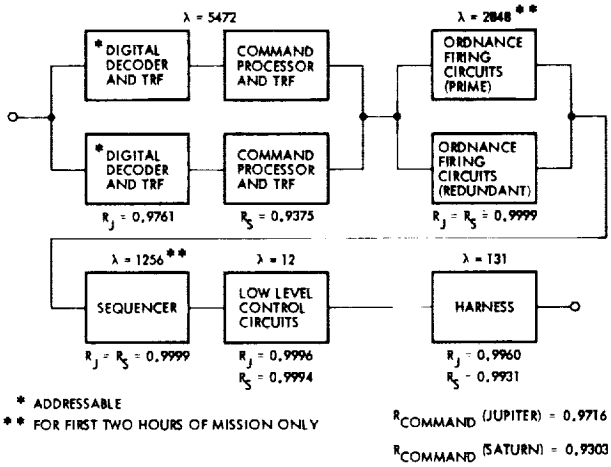

Figure 5-17. Command Subsystem Reliability Block Diagram

5.6.6 Reliability Improvements

Table 5-16 shows the reliability improvements which can be achieved for selected units for both orbiter missions. The units were selected on the basis of potential reliability growth. If all the changes were implemented the Jupiter mission reliability would increase to 0.7824 (from 0.6954) and the Saturn mission to 0.5831 (from 0.4489).

Table 5-16. Selected Reliability Improvements for Individual Spacecraft Units

	Jupiter Orbiter		Saturn Orbiter	
	Nominal	Improved	Nominal	Improved
Propulsion				
Add redundant pressure transducer	0.9749	0.9990	0.9574	0.9976
ACS				
Add redundant channel to DSL and undervoltage circuitry	0.9800	0.9972	0.9472	0.9879
Data Handling				
Add second standby programmer output logic	0.9892	0.9987	0.9705	0.9942
Add second redundant digital main frame multiplexer	0.9893	0.9991	0.9709	0.9959
Communications				
Add standby redundant conscan processor and TRF	0.9892	0.9999	0.9784	0.9995
Add second redundant receiver and TRF	0.9697	0.9947	0.9219	0.9776
Command Subsystem				
Add second redundant digital decoder, command processor, and TRF	0.9761	0.9963	0.9375	0.9844
All of above changes incorporated into the spacecraft system	0.6954	0.7824	0.4489	0.5831

6. MISSION PERFORMANCE OF THE JUPITER ORBITER

6.1 LAUNCH OPPORTUNITIES

Jupiter orbit missions being considered in this report start with the 1981/1982 launch opportunity. Favorable conditions for launching a spacecraft from earth to Jupiter repeat with the synodic period of approximately 400 days, thus shift by about one month in successive years. Figure 6-1 shows the sequence of launch opportunities to Jupiter in the 1970's and 1980's. It also indicates those for Saturn missions, to be discussed in Section 7. The yearly shift of favorable launch seasons is only about half a month in that case because of the 378-day synodic period for earth and Saturn.

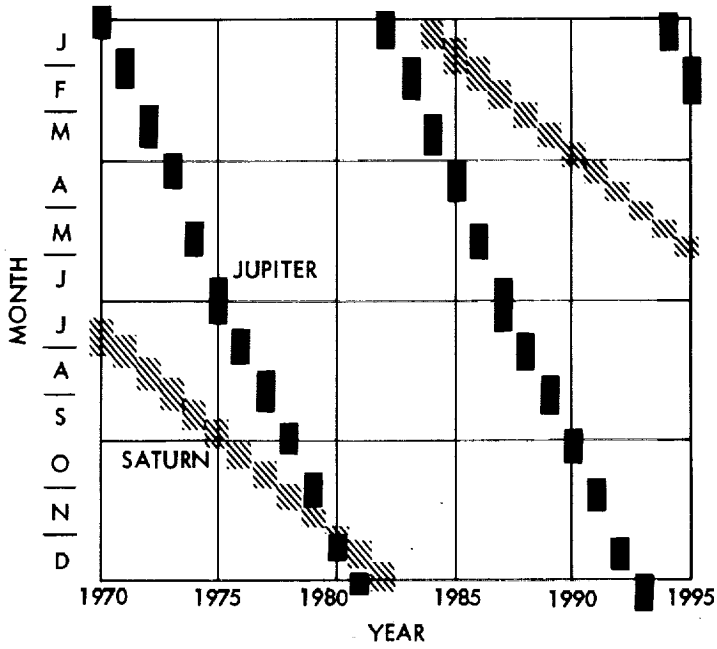

Figure 6-1. Launch Opportunities for Jupiter and Saturn Orbiter Missions in the 1970's and 1980's

Since the orbit of Jupiter is slightly inclined (1.3 degrees) relative to the ecliptic and has a significant eccentricity (e = 0.048), the characteristics of earth-Jupiter trajectories vary with each launch opportunity, completing a cycle in approximately 12 years. These effects are summarized as follows:

- Because of the inclination of Jupiter's orbit, out-of-plane components increase the earth departure velocity requirements twice per cycle. Opportunities with the lowest launch energy requirements correspond to arrival at Jupiter when it is close to the nodal line and occur in July 1975, January 1982 and June 1987.

- The eccentricity of Jupiter's orbit increases trip time and launch energy somewhat once every 12-year cycle, which makes launches in the mid 1980's somewhat more favorable than those in the early 1980's.

- Successive launch opportunities occur with the earth at a different location in its orbit. Because of the inclination of the earth's equator to the ecliptic plane this introduces a variation in the geocentric characteristics (declination and right ascension) of the outgoing asymptote from year to year.

As a result the earth-Jupiter trajectory characteristics vary considerably in the period from 1981 to 1986. Launch energy requirements are at a maximum in 1981-1982 and at a minimum in 1985-1986 for trajectories with short trip times. These variations are indicated in Figure 6-2 for nearly two cycles of the departure energy C_3 at launch opportunities in the 1970's and 1980's.

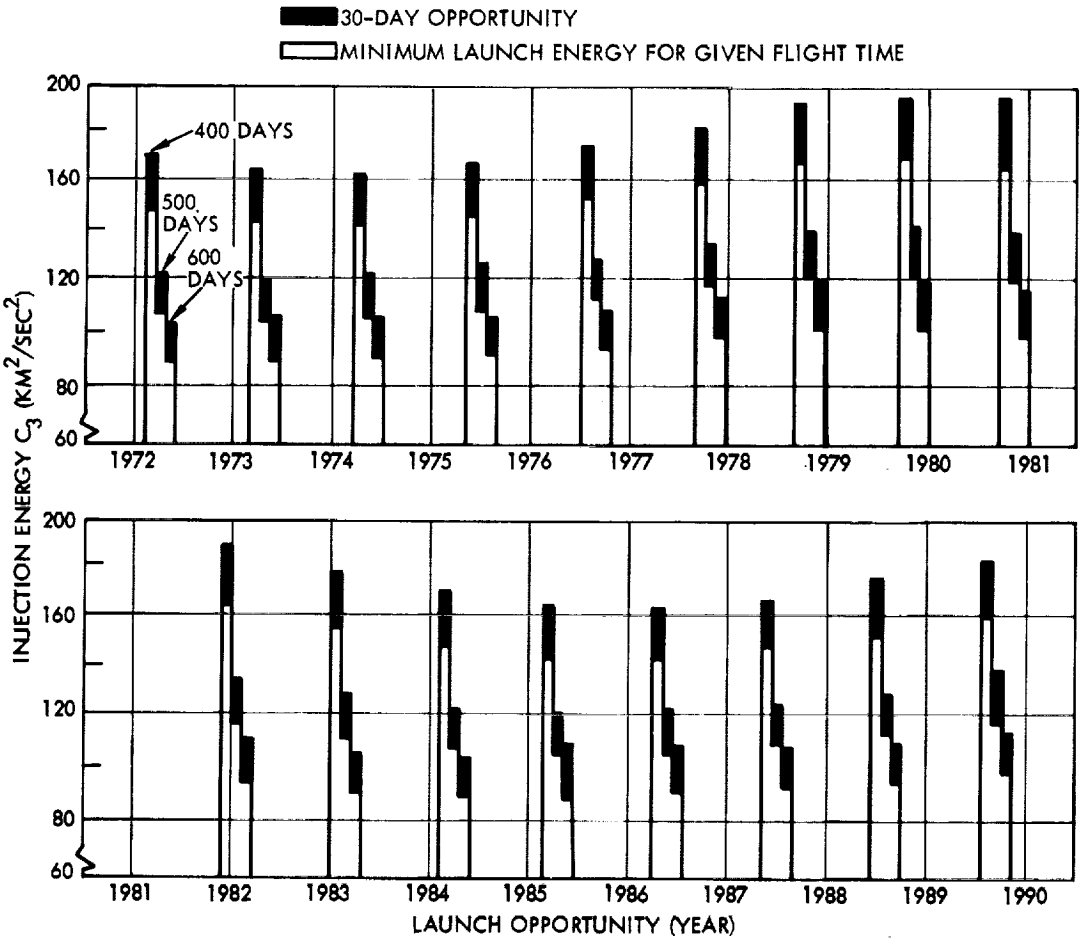

Figure 6-2. Variation of Injection Energy Requirements with Launch Year for 400-, 500-, and 600-Day Earth-Jupiter Transfers

The month of the launch opportunity progresses from December in 1981 to May in 1986 which causes a change in earth declination from +2 degrees in 1981 to values as low as -45 degrees in 1985 for trajectories with the relatively lowest launch energy. Consequently, missions in 1985 and 1986 must be penalized in launch requirements in order to avoid trajectories with excessively large (negative) declination so as to meet azimuth constraints typical for launches from ETR.

Type II trajectories (those in which the spacecraft travels more than 180 degrees around the sun between earth and Jupiter) could alleviate the more severe launch energy requirements, but a considerable increase in flight time would accrue, making this approach unattractive. Therefore, only Type I trajectories are proposed.

The yearly variation in geometrical characteristics of the earth-Jupiter transfer trajectories also reflects in a periodic change in arrival velocity at Jupiter which is shown in Figure 6-3 for flight times of 400, 500 and 600 days. The largest arrival velocities occur for trajectories launched in 1981 and 1982, the lowest for those launched in 1986 and 1987 (see also Section 6-3.

6.2 SELECTION CRITERIA FOR EARTH-JUPITER TRAJECTORIES

Principal criteria for selection of earth-Jupiter trajectories may be divided into those involving operations at or near earth, and those applying at Jupiter.

The significant parameters at earth are:

- Launch energy, C_3, required to inject the spacecraft onto a trajectory to Jupiter.
- DLA, the declination of the launch asymptote, and its influence on the launch azimuth and on the coast time to be sustained by the second stage of the launch vehicle.
- The duration of the launch period (number of consecutive days on which the launch may be conducted) and the launch window (minutes of each launch day, when a launch is possible).

The significant parameters at Jupiter are:

- V_∞, or asymptotic planetocentric arrival velocity, which governs the velocity impulse necessary to attain a given size orbit.
- The declination (in Jovian latitude) of the approach asymptote. This indicates the minimum inclination of the ensuing orbit which can be obtained without a plane change.
- The arrival date at Jupiter, which has several subsidiary considerations. First, to maintain communication, arrival

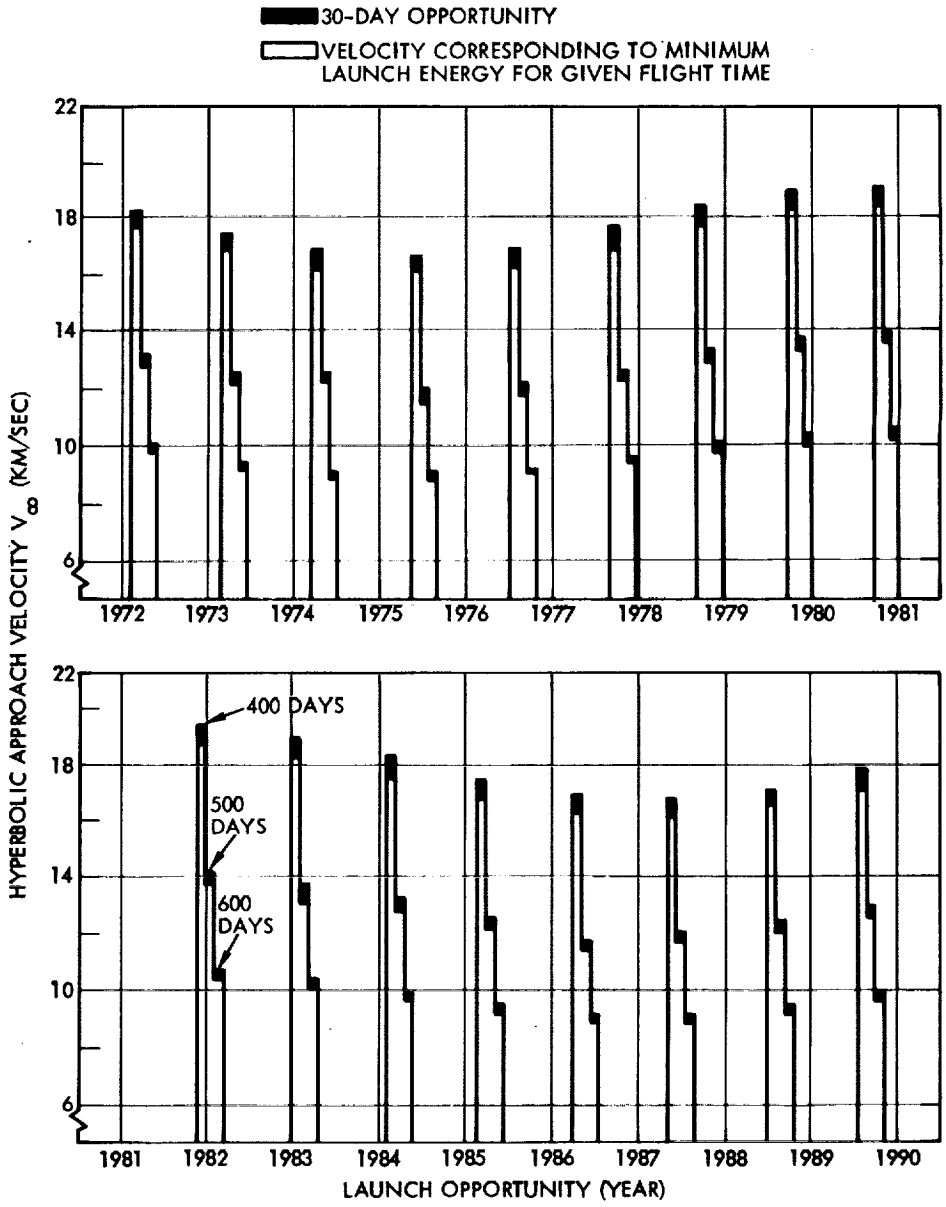

Figure 6-3. Variation of Jupiter Approach Velocity V_∞ with Launch Year for the 400-, 500-, and 600-Day Earth-Jupiter Transfers

at times of earth-Jupiter conjunction is to be avoided. These arrival dates generally correspond to trip times of 700 and 1100 days.

The in-plane direction of the approach asymptote varies with arrival date; thus a certain band of arrival dates is favorable for orbit insertion with the thrust along the earth line. This band corresponds to trip times of approximately 750 to 1000 days.

A third consideration is to aim for specific arrival dates which facilitate close encounters with the Galilean satellites during the Jupiter orbit phase.

The total trip time from earth to Jupiter is the key parameter affecting the launch energy (C_3) and the asymptotic arrival velocity (V_∞) in a given mission year, thus determining the total spacecraft mass that can be launched from earth as well as the propellant mass required for orbit insertion at Jupiter. Generally, trip times of at least 700 to 800 days are desirable for keeping C_3 and V_∞ at sufficiently low values consistent with a large total spacecraft mass and a reasonably low propellant mass. Optimal launch dates are nearly fixed for a given mission year, thus selection of the trip time reflects primarily in the choice of arrival date. Given a preferred trip time the final choice of departure and arrival dates will be influenced by constraints on launch and arrival geometry discussed earlier.

6.3 DEPARTURE ENERGY AND ARRIVAL VELOCITY FOR THE 1981, 1983 and 1985 LAUNCH OPPORTUNITIES

Departure energy and arrival velocity characteristics for trip times ranging from 400 to 1000 days are shown in Figure 6-4 for the 1981, 1983 and 1985 launch opportunities. (Note that the 1981 opportunity extends into January 1982. Data for the 1984 opportunity were omitted in the graph.) The dashed parameter lines of fixed trip times represent portions of the nearly periodic variation of trajectory characteristics repeating approximately every 12 years. Data points of the 1980 launch opportunity are shown to indicate the trend.

The procedure by which the data in Figure 6-4 are derived from the complete set of trajectories available in these mission years (see Reference 18) is illustrated by curves of C_3 and V_∞ versus departure date for fixed values of flight time, applying to the 1981 launch opportunity (Figure 6-5). Allowing a 15-day launch period has the effect of adding a 5 km^2/s^2 increment to the minimum C_3 requirement for each trip time. These C_3 increments are reflected in the data shown in Figure 6-4.

Note that the bar graphs of minimum C_3 and V_∞ values previously presented in Figures 6-2 and 6-3 include a 30-day launch period but are otherwise consistent with the data in Figure 6-5.

It is evident from these data that flight times of at least 700 days are desirable in order to bracket departure energies and arrival velocities within ranges that will yield favorable spacecraft weight characteristics and retro-propulsion requirements. Performance implications of these results will be further discussed in the following section and in Section 6-8.

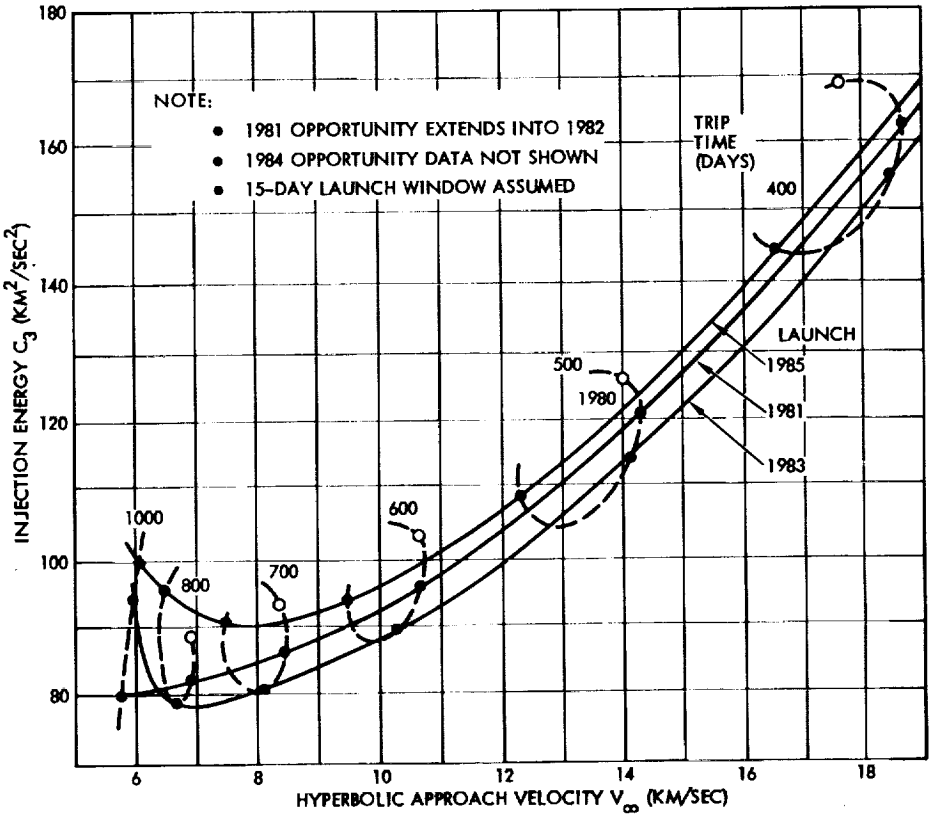

Figure 6-4. Launch Energy and Arrival Velocity Characteristics for 1981 through 1983 Earth-Jupiter Trajectories

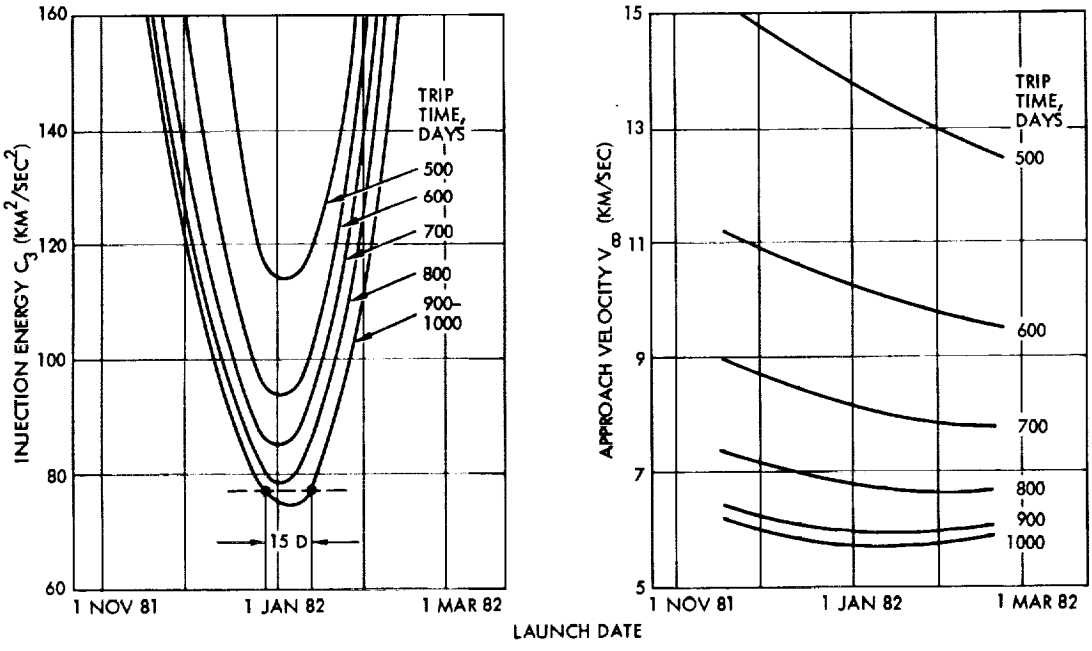

Figure 6-5. Launch Energy and Jupiter Approach Velocity Characteristics for Various Trip Times; 1981 Launch Opportunity

6.4 RETRO-PROPULSION PERFORMANCE CHARACTERISTICS AND TRADEOFFS

The performance of the Pioneer propulsion stage can be assessed by determining the ΔV capability of the stage parametrically as function of propellant weight and spacecraft inert weight. The carpet graph shown in Figure 6-6 gives the ΔV capability versus total injected weight with spacecraft inert weight and usable propellant weight as parameters. These curves were derived for a bipropellant (N_2O_4/MMH) system with 292 seconds of specific impulse.

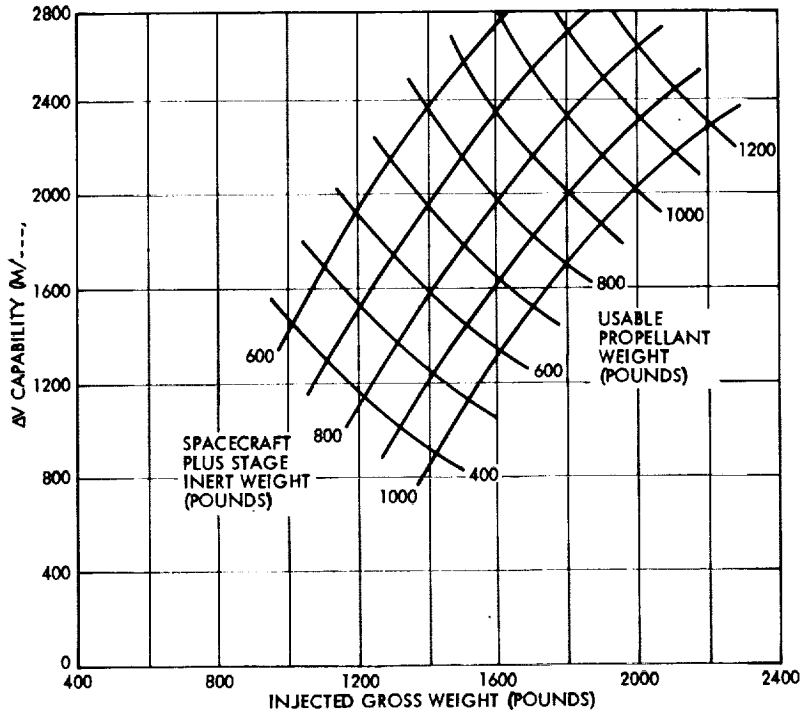

Figure 6-6. ΔV Capability Vs. Injected Weight

Propellant expenditures of up to 50 pounds by the auxiliary hydrazine propulsion system in performing attitude control maneuvers and small midcourse corrections have been neglected in obtaining the performance curves shown in Figure 6-6 thus giving a conservative, low estimate of retro-stage performance. Upper brackets of the stage ΔV capability are obtained by increasing these ΔV values by a percentage equal to the weight fraction of the nominal inert weight that is actually allocated as hydrazine propellant, typically 4 to 6 percent.

The graphs show that an orbiter spacecraft with 900 pounds of inert weight and a usable propellant weight of 1150 pounds has a total ΔV capability of 2400 m/s. In the performance range of interest weight tradeoffs between dry weight and gross injected weight and between dry weight and propellant weight are governed by these relationships:

- The exchange ratio of total injected weight to inert weight with ΔV capability held constant is about 2:1 in the performance range of interest.

- Thus, to maintain a fixed ΔV capability any change in spacecraft inert weight must be accompanied by an equal change in propellant weight.

- An increase or decrease in injected spacecraft weight due to launch vehicle performance variation, change in adapter weight penalty, or change in launch energy requirements is to be apportioned in equal parts to changes of inert weight and propellant weight if the same ΔV capability is to be maintained.

- The exchange ratio $\partial \Delta V / \partial W_{gross}$ is given by $I_{sp}\, g / W_{gross}$. This value is 1.4 to 1.6 m/s per pound in the performance range of interest. Thus addition of 1 pound of propellant to a spacecraft with a fixed dry weight increases the ΔV capability by about 1.5 m/s.

In Figure 6-6 the maximum ΔV performance capability is delineated by the maximum launch vehicle capability ($W_{gross\ max}$), the maximum propellant capacity of the stage ($W_{prop\ max}$) and the lowest achievable dry weight of the spacecraft ($W_{dry\ min}$). This is illustrated in Figure 6-7 by two examples corresponding to conditions where the maximum ΔV capability is determined (a) by the dry weight and propellant weight and (b) by the dry weight and the injected weight limit. The maximum ΔV capability consistent with condition (b) is attained by appropriate variation of the propellant load, such that the three limit curves intersect in one point.

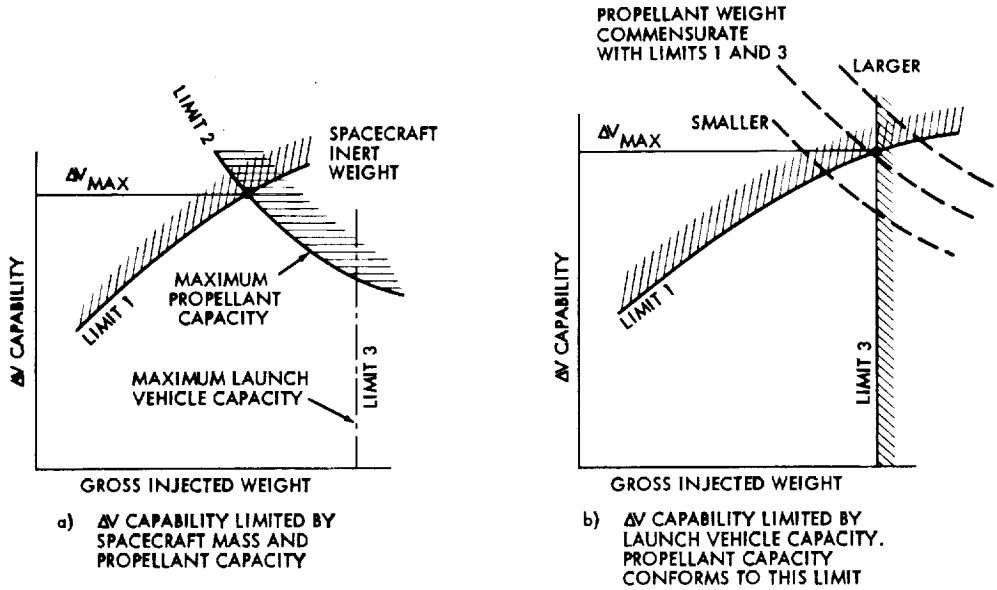

Figure 6-7. ΔV Performance Limits

In the case of the 1981 Pioneer orbiter mission the upper limit of ΔV capability is determined by the spacecraft dry weight and the propellant capacity rather than by launch vehicle capability. The Titan IIIE/Centaur/TE 364-4 provides a margin of several hundred pounds in this mission year. This performance margin can be used to accommodate more demanding launch requirements at subsequent launch opportunities.

6.5 LAUNCH VEHICLE PERFORMANCE

The launch vehicle designated for use in performing the Pioneer Jupiter and/or Saturn orbiter missions in the early 1980's is the Titan IIIE/Centaur D-1T/TE 364-4.* The payload fairing is the nominal 14-foot diameter Centaur shroud also to be used in the 1976 Viking and 1977 Mariner Jupiter-Saturn missions. The dynamic envelope of this shroud is that indicated in the configuration drawing in Section 3.

Figure 6-8 shows the injected gross payload weight capability of this booster versus C_3 for due east launch from ETR with a nominal 100 n mi parking orbit. This performance curve is an updated version of that specified in earlier Pioneer mission studies (References 5 and 12).

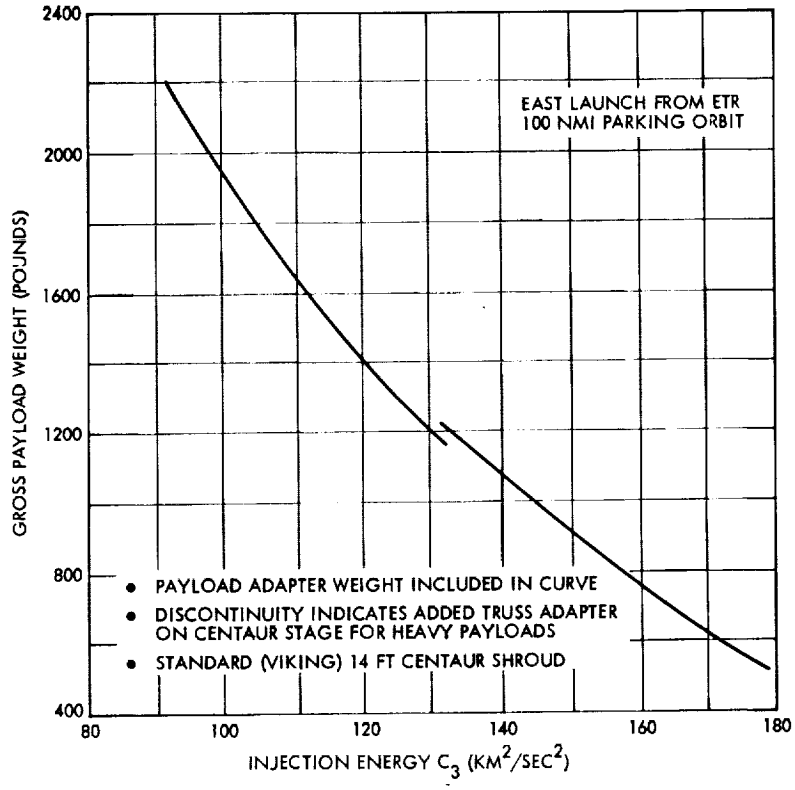

Figure 6-8. Titan IIIE/Centaur D-1T/TE 364-4 Injection Performance

*This designation is still tentative but has been assumed as ground rule for purposes of this report.

A parking orbit coast period of up to 25 minutes can be accommodated by the Centaur stage without weight penalty. Extended coast periods of up to 1 hour can also be accommodated but require an increase in the Centaur attitude control propellant and tankage weight which reflects in a 70-pound payload penalty for parking orbits of up to 1 hour. Actually, in the Pioneer Jupiter and Saturn missions contemplated here extreme coast period durations such as these will not be required.

The discontinuity in the booster performance curve (Figure 6-8) reflects the addition of an adapter truss which is required to reinforce the Centaur stage mount when heavy payloads in excess of 1200 pounds are to be launched.

Note that the gross spacecraft weight given in Figure 6-8 includes the weight of the payload interstage adapter, that is a weight penalty of 50 to 65 pounds depending on the weight of the spacecraft to be carried by this structure. The actual net spacecraft weight injected by the launch vehicle is obtained by subtracting the adapter weight.

For the purposes of this report the injection accuracy of the Titan IIIE/Centaur/TE 364-4 is the same as that given in PC 221 (Launch Vehicle - Pioneer F Spacecraft Interface Document) for the Atlas SLV-3C/ Centaur/TE 364-4 vehicle. The acoustic and vibration environments are the same as those prescribed in PC 210.03 (Pioneer F and G Spacecraft Specification) for qualification and acceptance level testing of the Pioneer F and G spacecraft.

6.6 LAUNCH PHASE

6.6.1 Launch Constraints

The following launch phase constraints may impose operational restrictions and/or performance penalties:

- Duration of the launch period for a given mission year
- Duration of the daily launch window
- Azimuth restrictions on launches from ETR
- Time limitation on parking orbit coast prior to the interplanetary injection burn
- Location of the ground track and the injection burn relative to available ground station coverage.

Performance penalties due to the requirement of a 15-day launch period have been previously discussed in Section 6.3. The maximum C_3 increment corresponding to this requirement is of the order of 5 km^2/sec^2 and reflects in a weight differential of about 100 pounds in typical Jupiter missions.

Constraints due to the minimum daily launch window, the permissible range of launch azimuths and the parking orbit coast capability of the

Centaur stage are interrelated and depend on the required declination of the departure asymptote. This will be discussed below.

The position of available ground tracking and command stations relative to the spacecraft during the launch and pre-injection phase does not impose restrictions other than those included in the permissible range of launch azimuths. Tracking and command capability during and after the injection phase can be provided either by existing ground facilities or by ships stationed appropriately as has been the case in previous interplanetary launches. Thus, no significant new launch restriction is imposed by this requirement.

6.6.2 Declination of Departure Asymptote

Declinations of the departure asymptote for earth-Jupiter launch opportunities between 1981 and 1985 are shown in Figure 6-9 as function of trip time. The declination angles shown, ranging from +2 to -50 degrees, correspond to trajectories with minimum departure energy for the given values of trip time. Favorable declination angles which impose little or no azimuth penalty are associated with the 1981 and 1983 launch years. These declinations, ranging between 2 degrees north and 28 degrees south can be reached either by the direct ascent mode or by orbital ascent with a short coast period at a nearly due east launch azimuth. Declinations more southerly than -28.8 degrees, that are associated with the later launch years in the range of trip times of interest here (i.e., trip times greater than 700 days) require significantly off-east launch azimuths and hence impose some performance penalty.

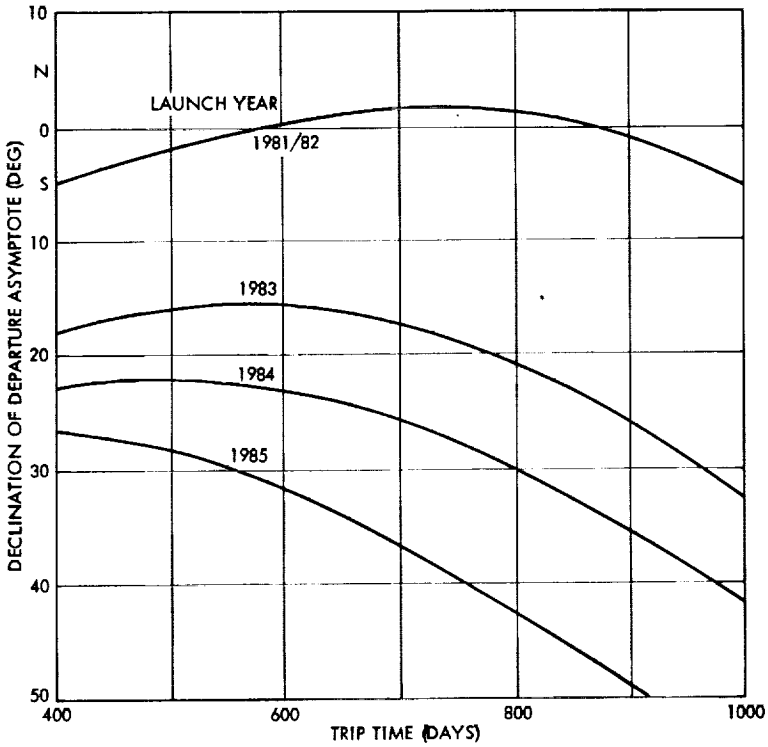

Figure 6-9. Declination of Departure Asymptote Vs. Trip Time for Earth-Jupiter Trajectories

6.6.3 Launch Azimuth and Parking Orbit Coast Time

The required launch azimuth is shown as a function of departure asymptote declination δ in Figure 6-10 for several launch window durations. Off-east azimuth requirements increase rapidly as the declination angle rises above +28.8 degrees or falls below -28.8 degrees. Weight penalties begin to accrue if the off-east angle is significantly greater than 10 degrees, as shown in Figure 6-11 for injection energies of 90 and 120 km^2/sec^2. Thus for $|\Delta\alpha| = 40$ degrees a weight penalty ranging from 57 to 71 pounds must be taken into account for the C_3 values considered here.

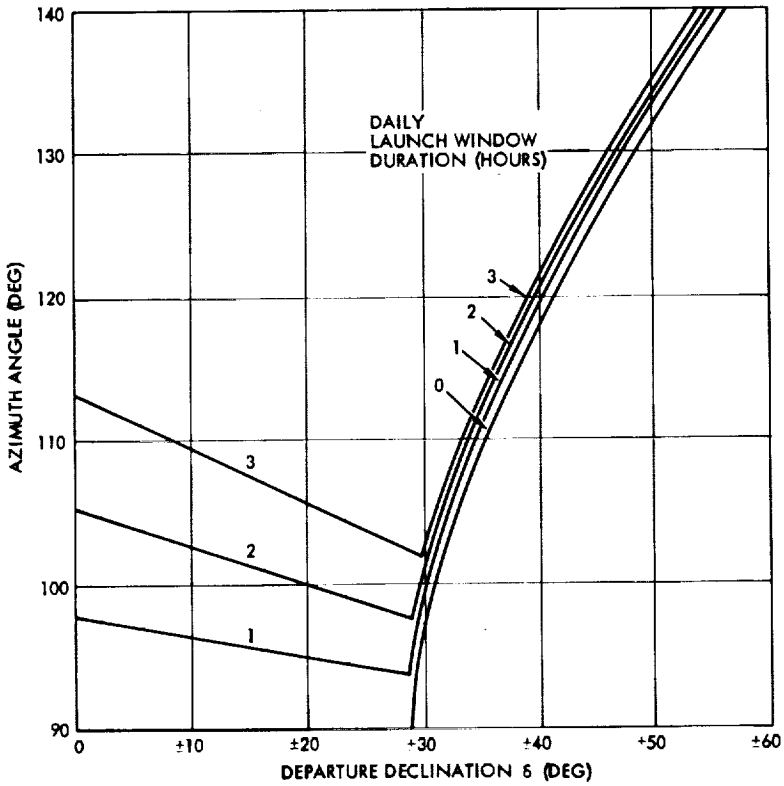

Figure 6-10. Minimum Southerly Azimuth Angles at ETR Vs. Departure Inclination δ

A reasonably short daily launch window of 30 minutes to 1 hour, as such, does not have a significant effect on azimuth angles in either of the two regimes of declination angles $|\delta| \leq 28.8$ degrees or $|\delta| > 28.8$ degrees, as seen in Figure 6-10 and 6-11. The weight penalty corresponding to this change in azimuth angle generally does not exceed 10 pounds.

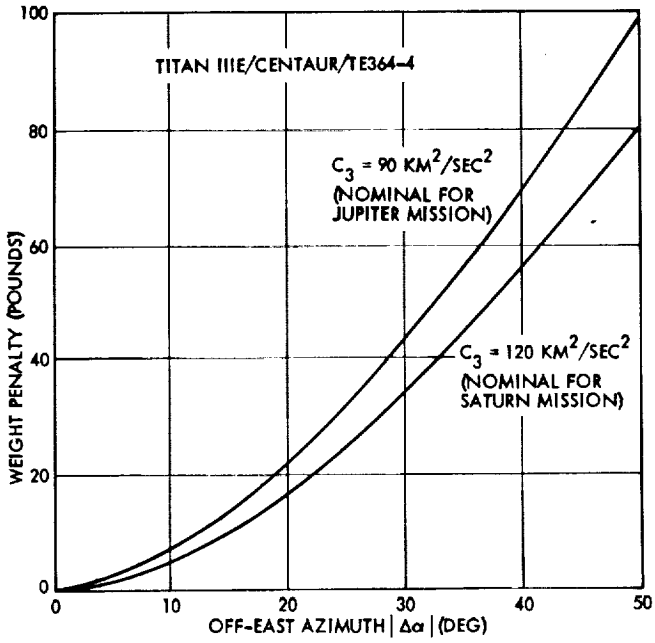

Figure 6-11. Weight Penalty Due to Off-East Launch for Two Values of Injection Energy

Orbital coast time is related to departure asymptote declination and launch azimuth as shown in Figure 6-12. Coast times extending significantly beyond 25 minutes require modifications of the Centaur stage and thus impose weight penalties as explained in Section 6.5. However, for the southerly declinations typical for the earth-Jupiter trajectories being considered the coast periods generally do not exceed 25 minutes. In some instances the direct ascent mode can be used with azimuths in the range of 90 to 114 degrees, i.e., in the sector of azimuth angles at ETR where launch permission is generally granted on a routine basis. The maximum off-east azimuth weight penalty is about 30 pounds in this mode.

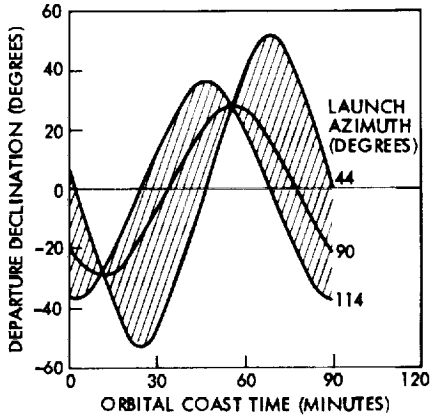

Figure 6-12. Orbital Coast Time Requirements

6.7 SELECTED NOMINAL EARTH-JUPITER TRANSFER TRAJECTORIES

6.7.1 Trajectory Characteristics

On the basis of the selection criteria and constraints discussed earlier, two sample earth-Jupiter trajectories were chosen from data in Reference 18 for the 1981 and 1985 launch opportunities. Their principal characteristics are listed in Table 6-1. The table includes departure and arrival dates, trip time, departure energy C_3, departure and arrival hyperbolic excess velocities and declinations, heliocentric transfer angle, communication distance at arrival, and approach illumination angle (the angle between Jupiter's heliocentric radius vector and the incoming hyperbolic excess velocity). From this angle, the arrival velocity, and the selected periapsis altitude the angle between the velocity vector at periapsis and the earth-line can be derived. This value, as well as the cosine-loss involved with the spacecraft in the nominal earth-pointing mode while performing the Jupiter orbit insertion maneuver at periapsis are also given in the table. This and other orbit insertion performance penalties will be discussed in Section 6.8.

Table 6-1. Selected Earth-Jupiter Sample Trajectories

Characteristics	Trajectory 1	Trajectory 2
Departure date	1 January 1982	14 April 1985
Arrival date	10 March 1984	4 May 1987
Trip time (days)	800	750
Injection energy C_3 (minimum) (km^2/sec^2)	78.97	85.72
Injection energy C_3 (15-day launch period) (km^2/sec^2)	79.23	87.38
Departure hyperbolic velocity (km/sec)	8.89	9.26
Departure asymptote declination (deg)	1.45	-42.7
Inclination relative to ecliptic (deg)	1.38	-5.1
Heliocentric transfer angle (deg)	169.1	164.9
Arrival hyperbolic velocity (minimum) (km/sec)	6.77	6.76
Arrival hyperbolic velocity (15-day launch period) (km/sec)	6.87	6.76
Arrival asymptote declination (deg)	2.9	6.1
Earth-spacecraft distance at arrival (AU)	5.49	5.81
Approach illumination angle*, (deg)	55.6	62.1
Angle between velocity vector at periapsis and earth line* (r_p = 3 R_J) (deg)	-1.5	1.5
Cosine-loss for orbit insertion in earth pointing mode* (percent)	0.034	0.034

*See also discussion in Section 6.8

6.7.2 Trajectory Time History, Pointing Angles and Communication Distances

Figure 6-13 shows the two sample transfer trajectories projected into the ecliptic plane with time marks at 100-day intervals. The time history of communication distances and earth-spacecraft-sun angles during transit is given in Figure 6-14 for the first sample mission.

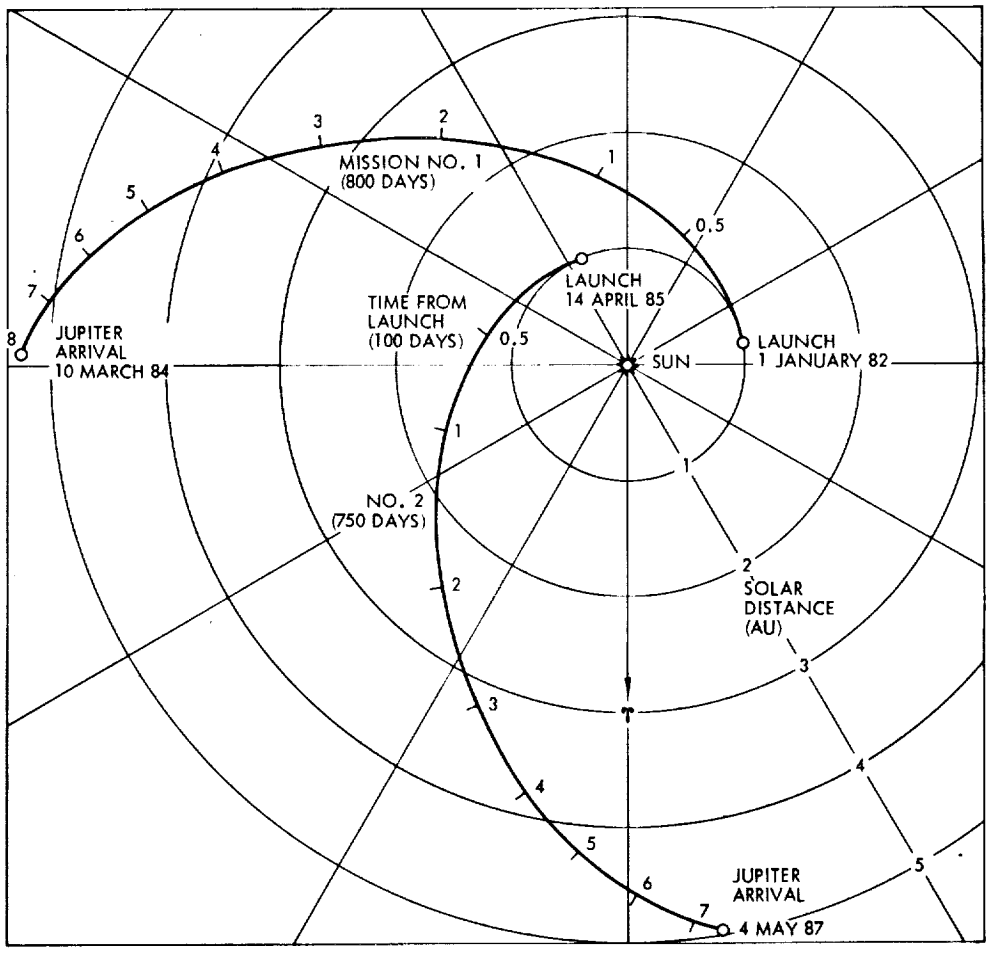

Figure 6-13. Sample Earth-Jupiter Trajectories (Projected Into Ecliptic)

For the spacecraft in orbit about Jupiter, the communication distances and earth-spacecraft-sun angles are presented in Figure 6-15 which shows the relative positions of sun, earth and Jupiter. The relative motion of earth as seen from Jupiter is approximated by a circle of 1 AU radius with time marks indicating monthly intervals. The synodic period of 400 days, rather than one year, is required to complete one revolution. Actually, Jupiter's distance from the sun varies slightly during the time interval in question as shown in the graph. This variation can be taken into account to correct the indicated earth-Jupiter distances if necessary. In the case of the first sample trajectory the earth-spacecraft distance decreases from its initial value of 5.5 AU at the 10 March 1984 arrival date, reaching 4.25 AU after 3.5 months in orbit, then increases to 6.15 AU during the next 6.5 months. The earth-spacecraft-sun angle varies between -12 and +12 degrees. Earth-sun alignments (syzygies) occur around 15 July 1984 and 1 February 1985.

Figure 6-15 also shows a second set of time marks to indicate communication distances and angles occurring during the orbit phase of the second sample trajectory following the arrival on 4 May 1987.

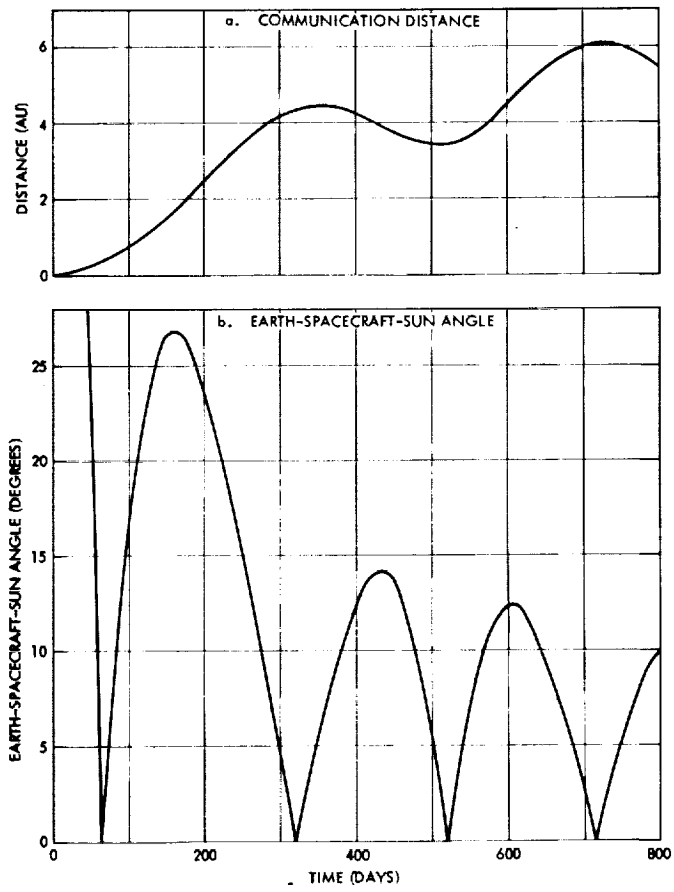

Figure 6-14. Communication Distance and Earth-Spacecraft-Sun Angle Vs. Time During Cruise for Sample Earth-Jupiter Trajectory (Launch: 1 January 1982)

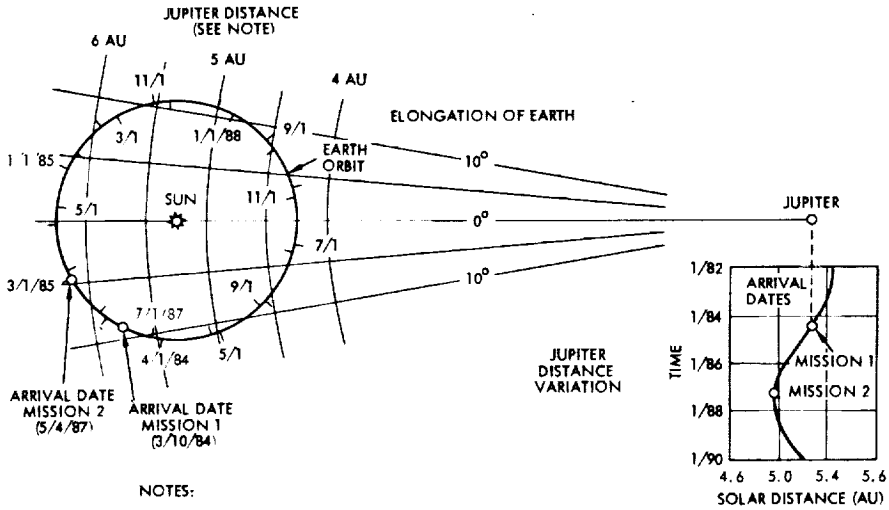

NOTES:

- TIME MARKS INDICATED ON OUTSIDE OF EARTH ORBIT CORRESPOND TO SAMPLE MISSION 1; INSIDE TO MISSION 2.
- RELATIVE DISTANCES AND ANGLES SHOWN APPLY AT ARRIVAL DATE OF MISSION 1.
- CORRECTIONS FOR JUPITER DISTANCE VARIATION WITH TIME ARE INDICATED BY INSERT CHART AT RIGHT.

Figure 6-15. Relative Sun, Earth, and Jupiter Positions During Orbital Phase of Sample Missions 1 and 2

6.8 JUPITER ORBIT INSERTION

6.8.1 Orbit Insertion Retro Velocity Requirements

The retro velocity required to enter an orbit of specified size about Jupiter is minimized if the retro maneuver is impulsive, tangential to the arrival trajectory, and co-apsidal, i.e., occurring at the common periapsis of the hyperbolic arrival trajectory and the elliptical orbit. Tangential thrusting also implies that the elliptical orbit is coplanar with the arrival trajectory.

For a given retro-maneuver ΔV capability, an orbit with minimum apoapsis distance, lowest eccentricity and shortest orbital period is attained if orbit insertion is performed at the closest permissible approach distance. The desired distance depends on scientific mission objectives and is constrained by the maximum acceptable trapped particle radiation level in close vicinity of Jupiter.

Figure 6-16 shows the relation between orbit size, orbital period and orbit insertion velocity requirement. The ΔV values shown correspond to the idealized condition of impulsive, cotangential orbit insertion at periapsis, for a hyperbolic approach velocity V_∞ = 6 km/sec. For example, a 1.8 km/s retro maneuver performed at the periapsis distance of 3 Jupiter radii (R_J) achieves an orbit with 40 R_J apoapsis radius and a period of 12 days. The graph also shows that if this maneuver were performed at 10 R_J it would only achieve a much more eccentric orbit with an apoapsis radius of 100 R_J and an orbit period of 50 days.

Retro ΔV requirements for achieveing specified orbital dimensions increase with the arrival velocity V_∞. As a corollary, the effectiveness of a given ΔV maneuver capability decreases as V_∞ is increased such that only orbits with less tight dimensions can be achieved. The equivalent change in ΔV requirement necessary to compensate for this loss in effectiveness can be determined from the data presented in Figure 6-17 using the retro velocities indicated in Figure 6-16 (for V_∞ = 6 km/s) as reference values. (The basis for this method of determining equivalent ΔV requirements will be discussed in Appendix B.) Consider for example, a change from V_∞ = 6 km/s to 9 km/s. Figure 6-16 shows that for V_∞ = 6 km/s, ΔV = 1500 m/s and periapsis radius of 3 R_J the apoapsis radius would be 50 R_J, and the orbit period 17 days. Figure 6-17 indicates that the increase of V_∞ to 9 km/s is equivalent to a reduction of ΔV by 620 m/s at the given 3 R_J periapsis radius. Thus, the attainable orbit would have an apoapsis radius of 150 R_J and a period of 75 days.

6.8.2 Effects of Finite Thrust Acceleration and Constant Thrust Direction

The data given in Figures 6-16 and 6-17 are based on the assumption of impulsive retro thrust maneuvers. Actually, the maneuver must be performed during a finite time interval at an acceleration level sufficently small to avoid excessive structural loads on deployed appendages. This reflects in a performance penalty which increases with the length of the thrust period because: a) the orientation of the thrust vector is

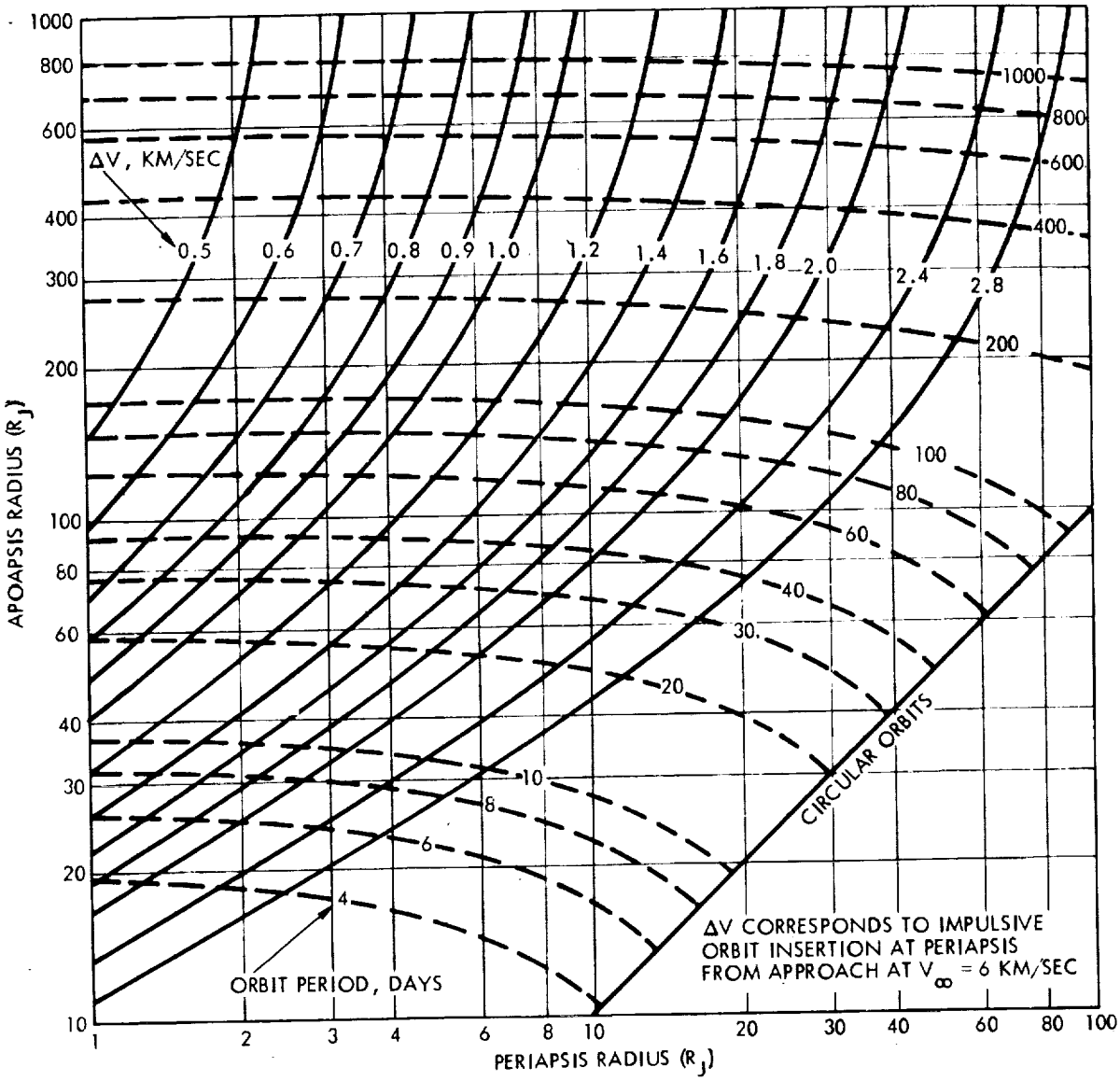

Figure 6-16. Characteristics of Orbits about Jupiter

nontangential during part of the burn period if the maneuver is performed in the fixed earth-pointing mode; b) a part of the maneuver is executed at other than the optimal, smallest distance from the plant. By far the most significant effect is the cosine-loss due to non-cotangential thrust orientation. This fact permits approximation of the performance loss ΔV_L with good accuracy by the simple relation

$$\Delta V_L = \frac{1}{48} \frac{V_{esc_o}^2}{r_o^2} \frac{\Delta t^2}{(r_p/r_o)^3} \Delta V$$

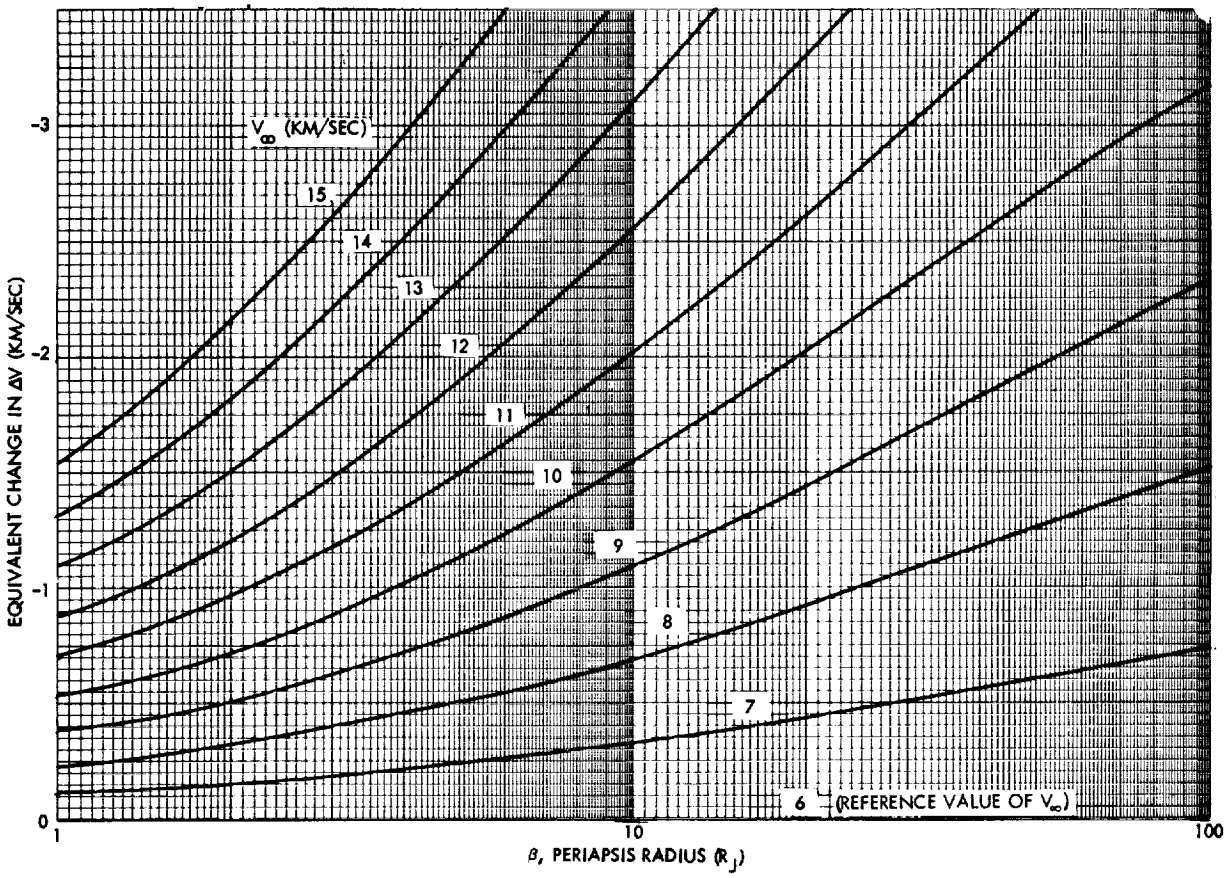

Figure 6-17. Effective ΔV Change with Change in V_∞ for Jupiter Orbits (Nominal ΔV = 6 km/sec)

where

$\Delta t = \Delta V/a$ is the finite burn time

a = thrust acceleration, assumed as constant

V_{esc_o} = escape velocity at surface

r_o = surface radius

r_p = periapsis radius.

In addition to defining the functional dependence of the velocity penalty on burn time and periapsis radius at Jupiter, this equation is also applicable to retro maneuvers at large planets other than Jupiter (e.g., Saturn) through appropriate change of the parameters V_{esc_o} and r_o.

Figure 6-18 shows the ΔV penalty at Jupiter for maneuvers at 2 R_J with retro velocities ranging from 0.5 to 2.5 km/s. The ΔV penalty accruing during a maneuver where the thrust acceleration changes as a result of propellant depletion can also be estimated from this graph. For example, with ΔV = 2 km/s and accelerations varying between 0.05 and 0.08 g's the ΔV penalty will be approximately the mean value between 60 and 25 m/s; i.e., about 40 to 45 m/s. If the periapsis radius is increased to 3 R_J the penalty reduces to 30 percent of this value, or about 15 m/s.

These results show that the selection of a 100 lb_f thruster for the Jupiter orbiter introduces only a minor maneuver performance penalty (see Section 3.7).

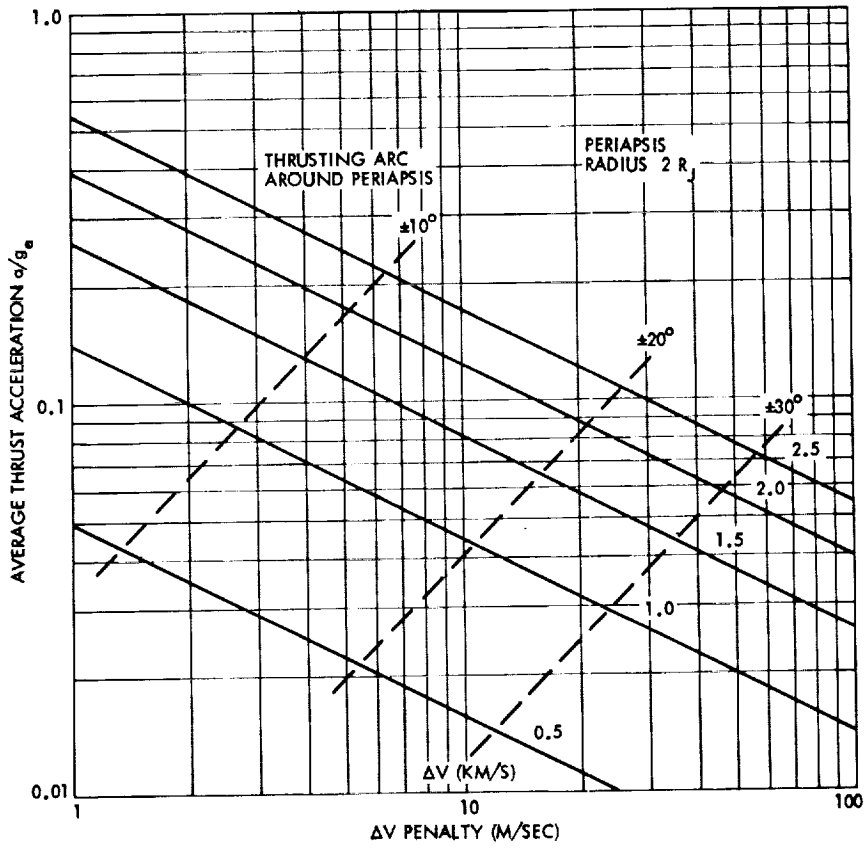

Figure 6-18. ΔV Penalty for Finite Thrust Orbit Insertion at Jupiter

6.8.3 Orbit Insertion in the Earth-Pointing Mode

A principal guideline for operating the retro propulsion system is to perform all maneuvers in the earth-pointing mode in order to avoid loss of communications coverage prior to, during, and after the maneuver phase. The risk of failure to reacquire communications is thereby also

being avoided. However, this requirement imposes a significant constraint on the orbit insertion phase as well as on subsequent maneuvers.

In order to perform an effective orbit insertion in the earth-pointing mode it is necessary to select geometrical conditions of arrival consistent with the requirement that the velocity vector at periapsis be nearly parallel with the earthline. Orbit insertion maneuvers performed with an appreciable misalignment of the thrust vector (i.e., the earthline) from the tangent at periapsis are penalized by cosine losses.*

A detailed discussion of this geometrical pointing constraint, its influence on arrival date selection and performance penalties due to non-optimal arrival dates is contained in Reference 5,Appendix A-6. Additional details applicable to Jupiter missions in the 1981 to 1986 time period are given in Appendix B of this document.

Figure 6-19 shows the deviation Δ from the ideal orientation of the thrust vector at periapsis for arrival conditions of minimum energy trajectories launched in 1981 and 1985 with trip times varying from 700 to

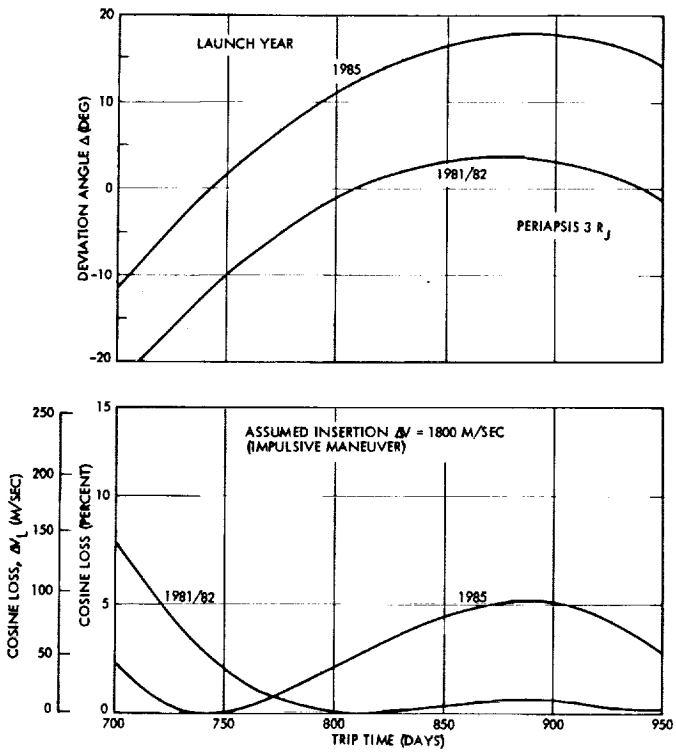

Figure 6-19. Jupiter Orbit Insertion in Earth Pointing Mode: Deviation Angle (Δ) and Cosine Losses (ΔV_L) Vs. Trip Time

*See also Appendix B

950 days. A periapsis radius of 3 R_J is assumed. At the bottom of Figure 6-19 the corresponding cosine-loss is shown. Assuming a retro maneuver ΔV of 1.8 km/s these losses can be as large as 140 m/s and 95 m/s for the two sets of trajectories in the range of trip times shown. In selecting sample trajectories for the 1981 and 1985 opportunities (see Section 6.7) flight times of 800 and 750 days, respectively, were adopted at which these orbit insertion losses are nearly zero.

6.9 JUPITER ORBIT CHARACTERISTICS

6.9.1 Orbit Size

Orbits are contemplated for a Pioneer Jupiter orbiter mission which come to within a fraction of a planet radius of the visible disk of Jupiter, or which remain at altitudes no lower than 4 to 6 radii. Evaluation of data obtained during the Pioneer 10 flyby in December 1973 will influence the selection from a standpoint of survivable radiation hazards. The apoapsis of the orbit from the planet center may range from 30 to over 100 radii.

The purpose of close approaches to Jupiter is to sample that portion of the trapped radiation environment which exists at low altitudes. While the large distances from Jupiter at apoapsis are partly dictated by propulsion considerations, they also cater to the scientific objectives of examining the interaction between the magnetospheric environment of Jupiter and the solar wind, and the optical observation of the planet Jupiter as the spacecraft stands off, slowly moving at high altitude in orbit.

6.9.2 Eccentricity

Regardless of the size of the orbit about Jupiter, a dominant feature is its high eccentricity. This is due to the limited amount of propellant which can be carried by the spacecraft. It is not likely that much more than 2 km/s total velocity increment is available to establish and alter the orbit. The data shown in Figure 6-16 indicate that the apoapsis distance will generally be more than ten times as great as the periapsis distance, under these circumstances. Thus, the eccentricity is greater than 0.8.

For a given periapsis distance of the orbit, the orbit insertion velocity increment decreases as apoapsis distance is raised. Conversely, for a given apoapsis distance, propellant requirements decrease as periapsis distance is lowered.

6.9.3 Orbit Periods

As seen in Figure 6-16, the orbits corresponding to apoapsis and periapsis distances of the ranges described above have orbit periods generally from 10 to 50 (earth) days. Because of the high eccentricity of these orbits, a large part of this time is spent at the greater distances

from the planet. In none of the orbits being considered does the spacecraft spend more than about 10 hours within five R_J of the planet during any single orbital passage. For an orbit with an eccentricity of 0.8, 79 percent of the time is spent at a distance greater than halfway from the planet to apoapsis. For an eccentricity of 0.9, the figure is 80 percent.

Thus, while the orbiter is in continuous orbit about the planet Jupiter, from several points of view it is more appropriate to think of this phase of the mission as repeated, discrete periapsis passages separated by long periods where events are relatively slow moving.

6.9.4 Inclination

An important parameter which influences the inclination of the orbit relative to Jupiter's equatorial plane is the declination of the approach asymptote, a characteristic of the interplanetary trajectory (see Figure 6-9). For the sample missions selected for 1981 and 1985 the declination is 2.9 and 6.1 degrees. (This declination is northerly, implying an arrival from slightly south of the Jovian equator, and a crossing to the north of the equator at the first node crossing.)

The propulsive entry into orbit of Jupiter is most efficient if the orbit plane is coincident with the plane of the approach trajectory. By appropriately targeting the arrival trajectory with respect to the planet, the approach trajectory plane, and hence the orbit plane, can be made to attain any inclination with respect to the equator of Jupiter which is not smaller than the inclination of the arrival asymptote. Thus, inclinations from nearly zero to 90 degrees may be achieved with no penalty in propulsion requirements.

Strictly equatorial-plane orbits, designed to achieve encounters with the Jovian satellites, require additional propellant to change the plane from that initially entered to the desired one. This is best accomplished in a second maneuver in the vicinity of apoapsis of the orbit, rather than as part of the initial orbit insertion maneuver.

Figure 6-20 illustrates the options available in selecting the inclination of an orbit of given size and shape, entered into from a given earth-Jupiter trajectory. It depicts a surface of revolution obtained by rotating one such elliptical orbit about a line through Jupiter parallel to the approach asymptote. Elliptical orbits at various inclinations are indicated by sections through this surface of revolution by planes parallel to the approach asymptote direction.

6.9.5 Orbit Perturbations

Appendix B presents data on the perturbations of the spacecraft orbit about Jupiter which are expected due to the oblateness of that planet. These effects are due to the J_2 term in the gravitational harmonics of Jupiter, a term which is well known, and which dominates all

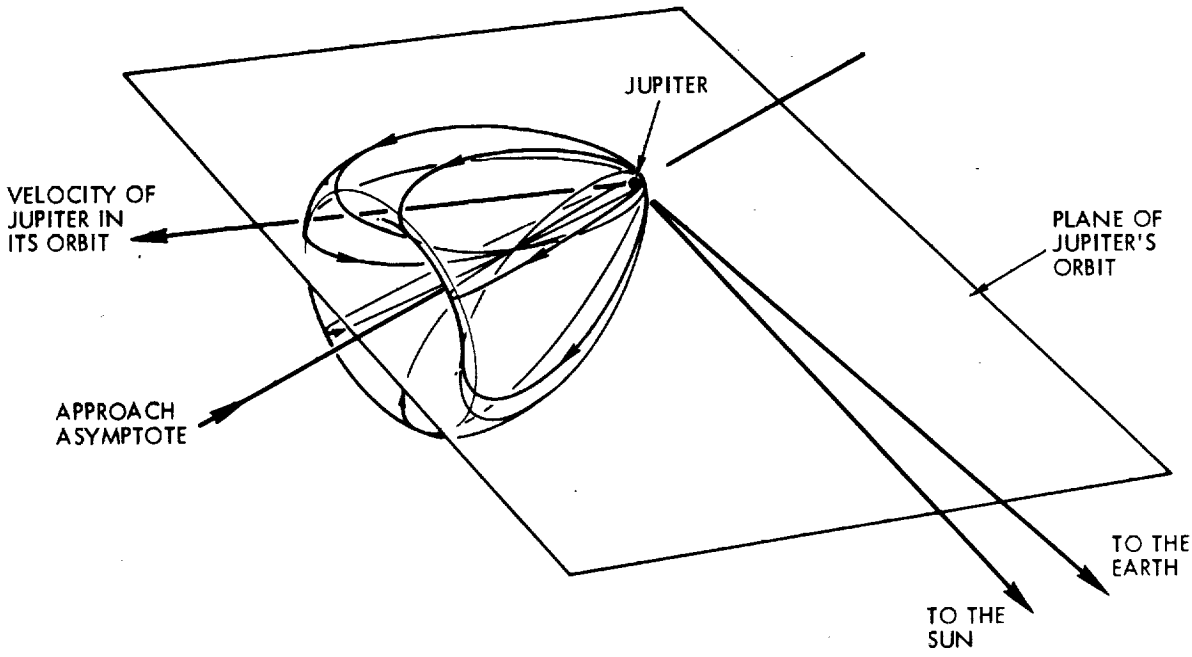

Figure 6-20. Options of Orbit Inclination Attainable at Orbit Insertion

other aspects of nonsphericity of the planet. The nature of the perturbations is the same as those affecting the orbits of satellites of the earth, namely regression of the line of nodes, and advance of the apsides.

The magnitude of these effects is relatively small, when evaluated for the orbits under consideration. For example, posigrade equatorial orbits either 1 x 100 or 2 x 40 Jupiter radii will have a net advance of the line of apsides relative to inertial space equal to the progression of Jupiter in its own 12-year orbit about the sun. Thus, one of these orbits would maintain a constant attitude with respect to the sun line.

Perturbation of the spacecraft orbit by the gravitational influence of the Galilean satellites can also be significant. While massive changes in the spacecraft energy relative to Jupiter, for example, enough to hurl the spacecraft to escape from Jupiter, are not expected from even close encounters with the Galilean satellites, there can be enough deflection of the spacecraft from its nominal orbit to cause it to depart significantly from quasi-synchronous satellite encounter orbits which will be discussed in the following section. Also, if the spacecraft were in an orbit with a very low or grazing periapsis, perturbations induced by a close passage to one of the Galilean satellites could lower periapsis enough to cause entry into the Jovian atmosphere (see also next section).

6.9.6 Satellite Encounter Orbits

While a very significant scientific mission can be performed by a Jupiter orbiter without specific reference to the natural satellites of Jupiter, there is substantial interest in the characteristics of the

Jovian satellites, particularly the four Galilean satellites, and missions have been identified which not only approach these satellites close enough for high resolution imaging, but do so by means of orbits which are in synchronism with the natural synchronism of the first three Galilean satellites, so as to experience repeated patterns of satellite encounter. (Reference 19).

Figure 6-21 shows the repeating figure of syzygy of satellites Io, Europa and Ganymede, an alignment which repeats every 7.05 days, but in an orientation which has regressed 5.2 degrees from the preceding occurrence. Figure 6-22 shows the final orbit, which encounters each of these satellites in each periapsis passage, subject to the slow drifting in and out of optimum passage because of the regression of the syzygy line.

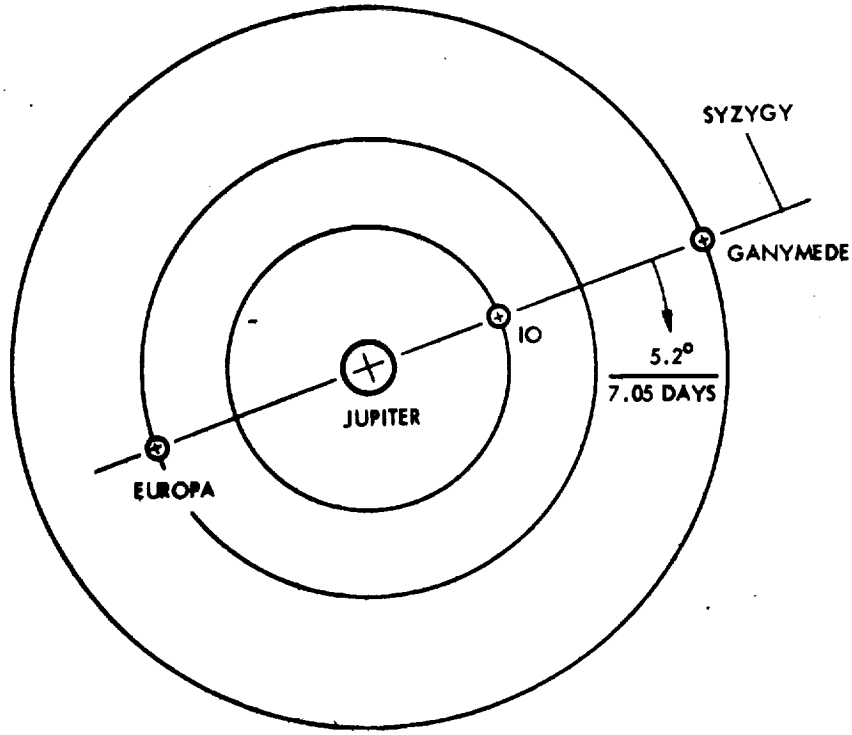

Figure 6-21. Satellite Alignments

By appropriate targeting and close encounters with Galilean satellites orbit perturbations can be achieved that actually help in conducting an extended satellite tour with repeated flyby options. In-plane as well as out-of-plane perturbations can be utilized to advantage to shape the orbit as desired. Table 6-2 lists representative satellite tour encounter histories with up to 11 successive encounter events occurring in a period of less than one year (from Reference 20). The referenced report also covers the navigation and guidance maneuver requirements involved in achieving the successive encounters. Additional work on defining favorable orbit profiles of this type is currently in progress at JPL.

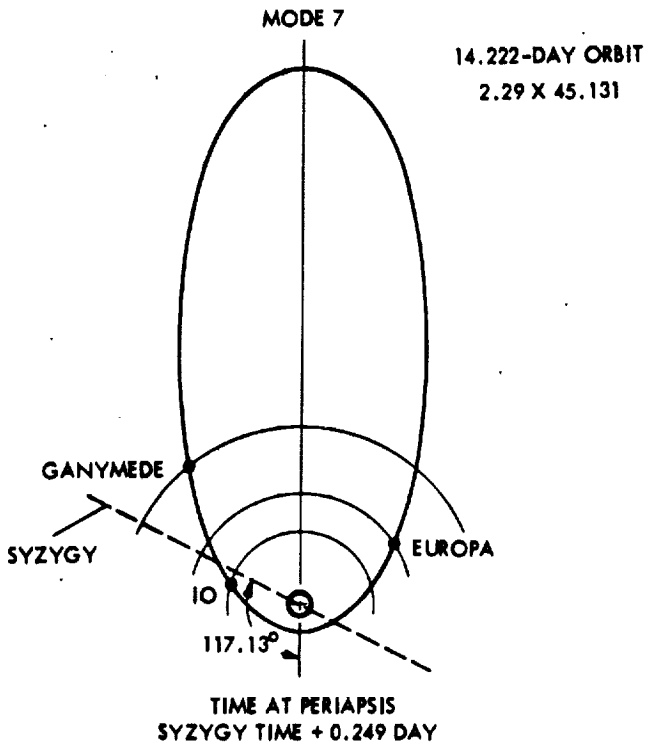

Figure 6-22. Three-Satellite Encounter

Table 6-2. Representative Satellite Tour Encounter Histories* (from Reference 20)

Encounter No.	"Shrinking" Orbit						"Expanding" Orbit					
	Date	Satellite	Distance of Closest Approach (km)	Post-Encounter Orbit			Date	Satellite	Distance of Closest Approach (km)	Post-Encounter Orbit		
				Periapsis (R_J)	Apoapsis (R_J)	Period (days)				Periapsis (R_J)	Apoapsis (R_J)	Period (days)
1	May 11, 1984	Callisto	3855	3.62	56.68	20.40	May 11	Callisto	4618	4.35	63.39	24.48
2	May 31	Ganymede	14868	3.54	54.96	19.49	June 2	Ganymede	16920	4.44	65.92	25.71
3	June 17	Callisto	3504	3.18	52.12	17.91	June 30	Callisto	6931	4.71	68.98	27.55
4	July 7	Europa	2035	3.16	51.50	17.60	July 27	Ganymede	13995	4.78	71.08	28.78
5	July 24	Io	1096	3.14	49.61	16.68	Aug. 24	Europa	82616	4.78	71.34	28.93
6	Aug. 11	Ganymede	2086	2.83	44.60	14.23	Sept. 22	Io	57128	4.78	71.34	28.93
7	Aug. 22	Callisto	10843	2.70	43.85	13.83	Oct. 21	Europa	21068	4.80	72.25	29.45
8	Sept. 6	Europa	1874	2.68	43.46	13.65	Nov. 19	Io	1075	4.80	74.29	30.63
9	Sept. 22	Callisto	4218	2.40	41.94	12.86	Dec. 18	Callisto	13302	4.97	76.59	32.08
10	Oct. 4	Europa	-	-	-	-	Jan. 22, 1985	Ganymede	14651	5.08	80.98	34.77
11	-	-	-	-	-	-	Feb. 23	Callisto	1961	5.71	92.03	42.09

*Initial zenocentric orbit 4 x 60 R_J, period = 22.3 days

6.10 ORBIT CORRECTIONS

Major propulsive maneuvers are required during the orbital phase in order to

- change orbital dimensions
- control the time of periapsis passage
- change the orbital inclination.

Changes in the dimensions of the orbit may be desired as a normal sequence of events associated with a specific mission and its requirements, or they may be instituted for the purpose of trimming orbits to more precise dimensional requirements. For optimum propulsion efficiency, the periapsis radius of an orbit should be changed by a tangential maneuver at apoapsis, the apoapsis radius by a tangential maneuver at periapsis. Appendix B presents the ΔV requirements associated with such changes in orbit size.

Controlling the time of periapsis passage for an orbit of specified dimensions is achieved by successive orbit size changes, with the spacecraft traversing interim orbits for phasing adjustment prior to entering the desired orbit.

Maneuvers to change the orbit plane are performed to obtain an equatorial, or near-equatorial orbit, primarily to achieve favorable conditions for encounters with the Galilean satellites, all of which are in orbits which are very nearly circular and very nearly in the equatorial plane. Multiple encounters with these satellites can be more readily achieved when moving in the same orbital plane.

It was noted earlier that the minimum inclination attainable with an optimum coplanar initial orbit entry is equal to the declination of the approach asymptote to the Jovian equator. While out-of-plane thrusting at the initial orbit insertion maneuver could reduce the inclination of the initial orbit to zero, it is much more efficient to perform a subsequent propulsive maneuver, preferably close to apoapsis, where the required out-of-plane component is much smaller.

Figure 6-23 shows principal parameters involved in defining plane change maneuver requirements, namely the targeting, or aim angle, θ, the initial orbit inclination i and the true anomaly, $\gamma + \zeta$, of the orbital position (node Ω) where the plane change is executed. (The parametrical definition of these quantities is given in Figure 6-24.) The graph indicates the best choice of the initial inclination i and the aim angle such that the plane change maneuver is minimized. It can be seen that the optimum position for plane change maneuver is somewhat prior to apoapsis. The example illustrated is for a 2.29 x 100 R_J orbit, with arrival declinations of 7 and 10 degrees.

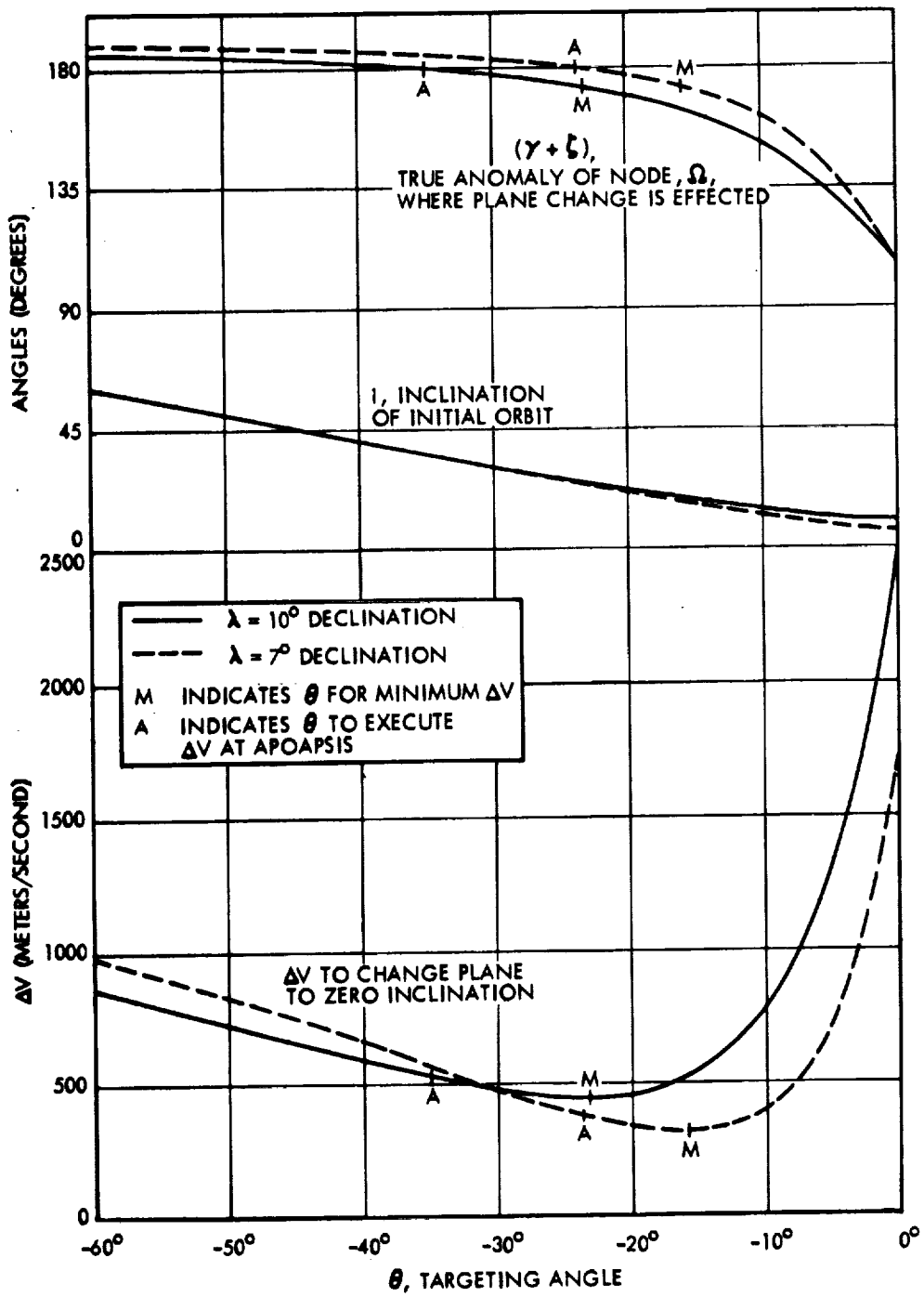

Figure 6-23. Plane Change Maneuver Parameters Vs. Targeting Angle (2.29 x 100 R_J Orbit)

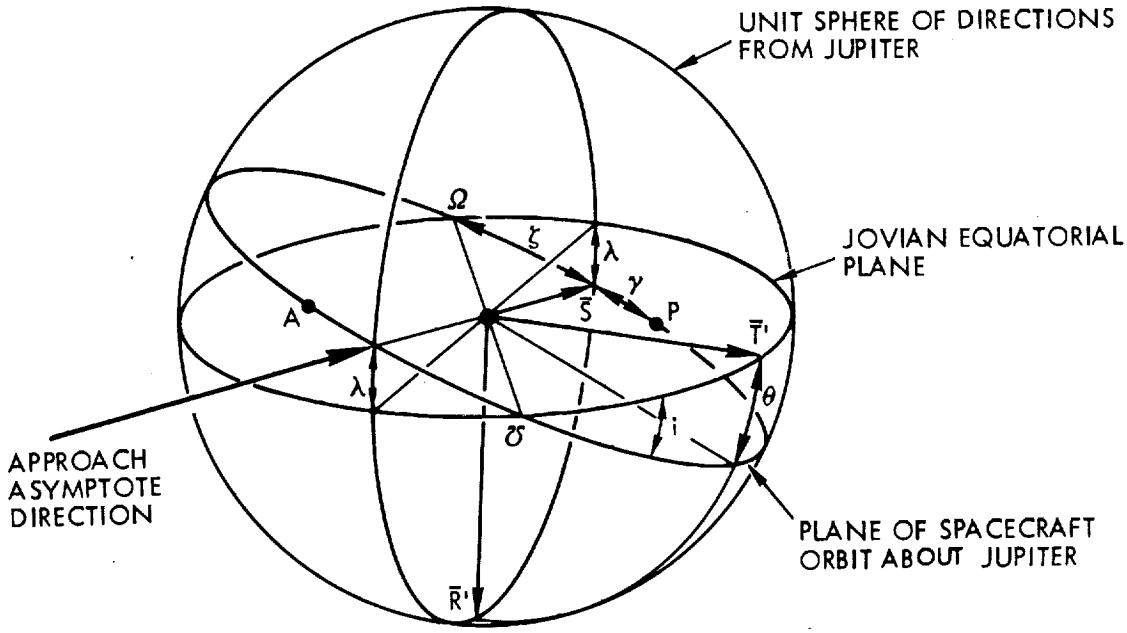

$\bar{R}'$, $\bar{S}$, $\bar{T}'$	UNIT VECTORS OF ORTHOGONAL COORDINATE SYSTEM
$\bar{S}$	UNIT VECTOR ‖ APPROACH ASYMPTOTE
$\bar{R}'$, T'	IMPACT PARAMETER PLANE; T' ‖ JOVIAN EQUATORIAL PLANE
θ	TARGETING ANGLE
P, A	PERIAPSIS, APOAPSIS
Ω, ℧	ASCENDING, DESCENDING NODES
λ	(SOUTHERLY) DECLINATION OF APPROACH ASYMPTOTE
i	INCLINATION OF ORBIT PLANE

Figure 6-24. Geometry of Orbit Plane Inclination

As shown by the example in Figure 6-23 the plane change maneuver involves a very large ΔV expenditure (300 and 400 m/s), even in the optimum case. Hence, the importance of optimizing the orbital parameters that control the maneuver requirements by appropriate choice of the aim angle θ.

The plane change maneuver is, generally, the largest single maneuver of the mission except for the orbit insertion. This is borne out by the ΔV budgets adopted in Reference 21 for several classes of Jupiter orbit missions in the late 1970's and early 1980's. These ΔV budgets listed in Table 6-3 may be regarded as typical.

A-4

Table 6-3. ΔV-Budget for Representative Jupiter Orbit Missions (from Reference 21) in m/sec

Maneuver	Mission Type			
	3-Satellite Encounter, Low Periapsis		2-Satellite Encounter, Medium Periapsis	2-Satellite Encounter High Periapsis[2]
(Launch Year)[1]	(1977)	(1981)	(1976)	(1976)
Orbit insertion	900	1160	1180	1430
(Initial orbit dimensions, R_J)	(2.29 x 100)	(2.29 x 100)	(4.0 x 100)	(6.0 x 100)
Periapsis rotation penalty at insertion	60	0	0	50
Plane change to equatorial orbit	740	180	570	-
Deboost into final orbit	520	520	220	510
(Final orbit dimensions, R_J)	(2.29 x 45.13)	(2.29 x 45.13)	(4.0 x 71.1)	(6.0 x 56.1)
Satellite perturbation trim	60	60	60	60
Total ΔV	2280	1920	2030	2050

Notes:
(1) Launch years in reference mostly in the 1970's but ΔV requirements also assumed as representative for missions in the 1980's
(2) Mission designed for extreme radiation hazard at Jupiter, excludes option of a plane change maneuver.

A matter of practical concern is the feasibility of maintaining the spacecraft in the earth-pointing mode while thrusting. Generally, the orbit trim maneuvers to be performed at periapsis or apoapsis require a thrust orientation parallel to the initial orbit insertion thrust vector, hence parallel with the earth line, assuming that rotation of the nodal line and apsidal line and their influence on the apsidal velocity orientations are small enough to be ignored. Typically these rotations amount to only 1 to 2 degrees in 50 days for the orbit sizes and inclinations considered (see Appendix B).

On the other hand, the large maneuvers involved in performing orbital plane changes require thrust axis and, hence, spin axis orientations perpendicular to the initial orbit plane, which means orientations nearly perpendicular to the earth line. Actually, the spacecraft can execute small trim maneuvers in a direction normal to the spin axis, by using the spin/despin thrusters in the pulsed operating mode. However, this mode would not be adequate for executing the desired large out-of-plane maneuver. To permit a plane change maneuver would require a departure from the operating constraint which nominally prohibits spacecraft reorientations off the earth line at large distances from earth. This exception would appear to be warranted to provide greater mission flexibility, particularly in meeting the important objectives associated with plane change requirements.

6.11 NAVIGATION

Questions addressed in this section concern navigational requirements of outer planet orbit missions and capabilities of earth-based radio guidance used in achieving these missions. Of particular interest are questions related to

- Midcourse navigation during the interplanetary transfer
- Terminal navigation on approaching the target planet
- Effect of inaccuracies at orbit insertion on characteristics of the capture orbit
- Navigation to close encounters with planetary satellites during the orbital phase
- Requirements, if any to use on-board sensors for augmenting earth-based navigation.

Results of previous studies of navigation and guidance in outer planet flyby missions, probe missions, and orbiter missions (References 22, 23, and 24) establish techniques applicable to the Pioneer Outer Planet Orbiter missions and provide data that will be referred to in this section.

For convenience of presentation (and to avoid repetition in Section 7) the discussion will cover navigation capabilities of Jupiter as well as Saturn orbiter missions.

6.11.1 Navigational Requirements

Successful planetary orbit injection and performance of subsequent orbital operations hinge on the accomplishment of a sequence of navigation and guidance tasks, beginning at launch and continuing throughout the mission. These include:

1) Launch and interplanetary injection guidance

2) Midcourse navigation and error correcting

3) Planetary approach navigation and terminal guidance, if necessary

4) Command and execution of orbit injection maneuver to achieve initial capture orbit

5) Orbit phase navigation and trim maneuvers, repeatedly if necessary (see Section 6.10).

Qualitatively, the requirements are similar to those met in earlier planet exploration missions, notably the Mariner 9 Mars orbiter in 1971 (tasks 1 through 5) and Pioneer 10 Jupiter flyby in 1973 (tasks 1 through 3).

The required midcourse and terminal navigation tasks and, in the case of Mariner 9, the orbit injection and trim maneuvers and related navigation tasks were performed with high accuracy using earth-based radio navigation only.

Actually, Mariner 9 also used its high-resolution TV image system to provide optical navigation fixes on approaching Mars, but only as back-up option and for a practical demonstration of the technique. Celestial navigation fixes will be required to augment the accuracy achievable by radio navigation in some outer planet swingby and probe delivery missions (Reference 23).

Planetary approach navigation in the Jupiter and Saturn orbiter mission does not require such augmentation, as will be shown below, since inaccuracies of the initial capture orbit due to approach navigation errors can be readily corrected by subsequent trim maneuvers.

Navigational requirements and accuracies achievable in orbiter missions with close satellite encounters and repeated swingby maneuvers have been investigated in Reference 20. Although a firm requirement has not been established, the use of an on-board navigational sensor may become necessary in such missions.

The Pioneer Outer Planet Orbiter as configured in the present design concept does not include an optical navigation sensor. However, recent studies of a scanning V-slit star mapper by TRW (Reference 25) and related studies by JPL (Reference 23) show this instrument to be a promising candidate for missions that require augmentation of radio-navigation accuracy.

As shown in Reference 12, the star mapper can be incorporated into the Pioneer spacecraft with only minor system modifications, replacing the Pioneer F/G stellar reference assembly that was adopted in the present outer planet orbiter design.

6.11.2 Pioneer 10 and 11 Orbit Determination Accuracy

The high guidance accuracy that can be achieved in outer planet missions by the earth-based radio-navigation and orbit determination technique, as demonstrated by the Pioneer 10 Jupiter flyby in December 1973, is sufficient to meet the planetary orbit injection accuracy requirements of the Jupiter and Saturn orbiter missions. Preliminary data derived from post-encounter analysis of the Pioneer 10 Jupiter flyby indicate that the trajectory uncertainty relative to the planet was within 30 km at the closest approach point.*

Reference 26 presents a detailed analysis of encounter accuracies at Jupiter that were projected for Pioneer 10 and 11 prior to the first Jupiter flyby. Error sources taken into account in the orbit determination process include

- Tracking station location errors
- Signal transmission errors, e.g., interactions with the ionosphere and troposphere
- Errors due to ground station equipment
- Spacecraft-related errors such as gas leaks and solar radiation pressure
- Errors in the assumed physical and orbital characteristics of the target planet.

The best orbit determination accuracy is achieved if principal uncertainties of the computation model, e.g., station location error, target planet mass and ephemeris, as well as spacecraft-related error sources are being updated along with the predicted spacecraft state variables by the weighted least-squares iteration procedure which is used in orbit determination.

Table 6-4 lists best estimates of the Pioneer 10 and 11 Jupiter approach trajectories uncertainties as function of time prior to encounter (from Reference 26).

Figure 6-25(a), (b) shows sequences of 1σ error ellipses of the Pioneer 10 and 11 approach trajectories in the impact parameter (B) plane, illustrating the characteristics listed in Table 6-4. These data show that as a result of the focusing effect of the planetary gravity field a major improvement of the projected trajectory accuracy is achieved compared to

*Final evaluation of the encounter data is still in progress at this time.

Table 6-4. Pioneer 10 and 11 Encounter Accuracy Projections (from Reference 26)

Target Statistics	Pioneer 10				Pioneer 11			
	E-50 to E-20 days	E-50 to E-10 days	E-50 to E-5 days	E-50 to E-1 day	E-50 to E-20 days	E-50 to E-10 days	E-50 to E-5 days	E-50 to E-1 day
Sigma B, km	845	560	322	64	1959	954	417	72
Sigma B·R, km	2460	2317	2231	554	2705	1116	357	93
Sigma B·T, km	670	419	262	71	666	645	606	183
Sigma TCA(1), sec	29	16	16	3.8	32.38	27.52	20.87	5.29
SMAA, km	2460	2321	2244	558	2707	1123	627	204
SMIA, km	668	391	109	3.2	658	633	318	13
Theta(2), deg	91	94	96	97	92.28	97.57	17.34	26.87

(1) TCA = Time of closest approach

(2) Theta = Orientation angle of semi-major axis (SMAA) of error ellipse in B-plane

Notation:
B impact parameter
R, T coordinates of impact parameter plane at Jupiter

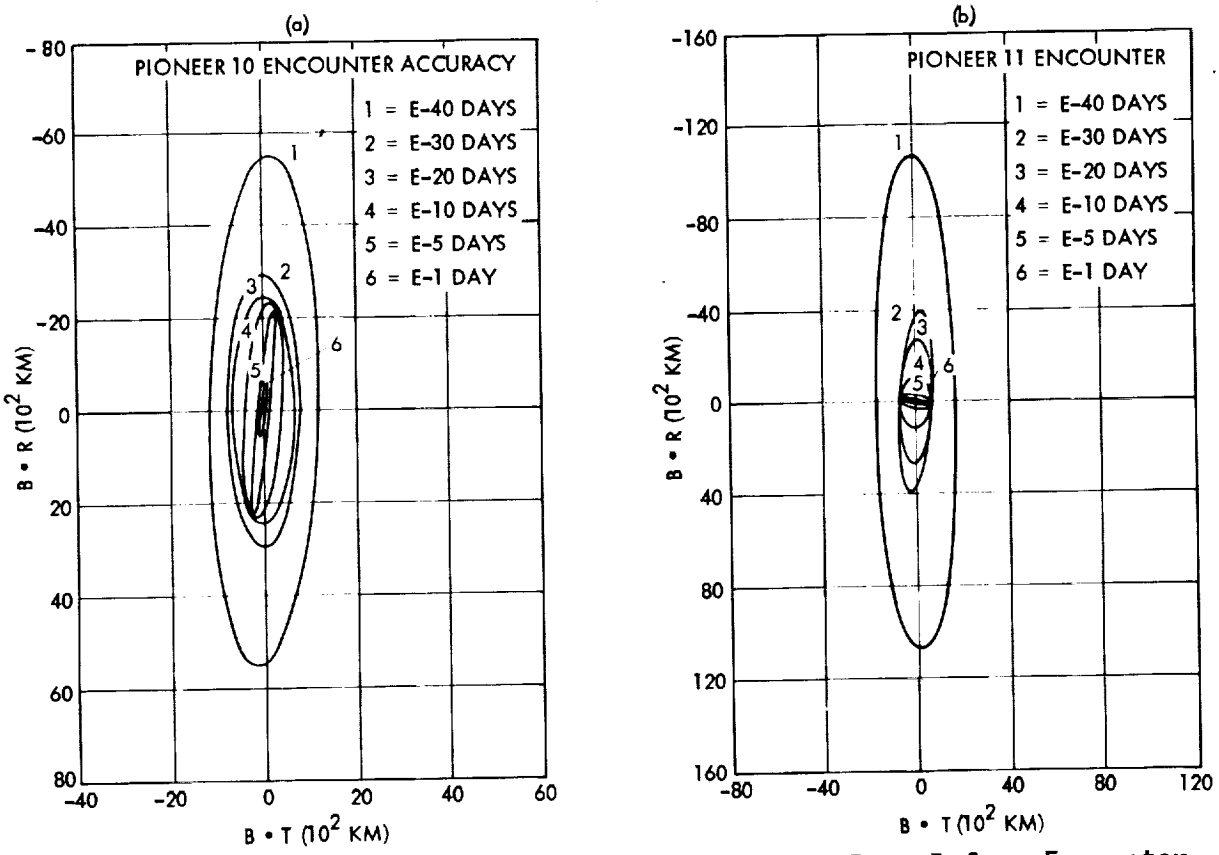

Figure 6-25. 1σ Dispersion Ellipses at Jupiter Vs. Days Before Encounter for (a) Pioneer 10, (b) Pioneer. (Analytical Predictions Based on Two-Way Doppler Data, at 3 mm/sec 1σ-Doppler Error, Reference 26)

the interplanetary cruise accuracy (estimated at about 2000 to 3000 km (1σ)). This is true especially during the last days before the encounter, with the semi-major axis of the 1σ error ellipse being 558 km for Pioneer 10 and 204 km for Pioneer 11, as projected at E-1 day. The higher accuracy of the Pioneer 11 encounter data is explained by the improved knowledge of Jupiter's mass and ephemeris obtained from the preceding Pioneer 10 flyby. The maximum uncertainty of the azimuthal component of Jupiter's ephemeris is expected to be reduced from the a priori best estimates of 750 km (1σ) to less than 400 km as a result of both Pioneer 10 and 11 flybys.*

Further improvements of Jupiter's ephemeris, and similar improvements expected for Saturn from the current maximum uncertainty of 1000 km (1σ), will result from the Mariner 1977 Jupiter/Saturn mission and will increase the confidence of achieving subsequent Jupiter and Saturn orbiter missions with high accuracy by means of radio navigation methods only.

It should be noted that the above analytical accuracy predictions quoted from Reference 26 are conservative, having been derived on the basis of a conventional orbit determination procedure that uses range rate information only. Actually, new data types being used for the first time in Pioneer 10 and 11 include:

1) Precision turn-around ranging obtained through frequency-ramping of the DSN signals and

2) Precision angle measurements obtained by near-simultaneous tracking from Goldstone and Canberra, using these stations for quasi-very-long-baseline interferometry (QVLBI).

The orbit determination accuracy actually achieved for Pioneer 10 demonstrates an improvement by an order of magnitude compared to the conventional radio-navigation techniques used in earlier planetary missions.

6.11.3 Accuracy of Saturn Approach Navigation

An analysis of Saturn approach navigation accuracy was performed in the previously quoted JPL study (Reference 23). Figure 6-26 shows the predicted 1σ dispersions obtainable as a function of time before encounter for the case of "loose" and "tight" station location errors and for different epochs of initiating the tracking and orbit determination process. Data types used in the radio-navigation procedure include: range rate, range, differenced range rate and differenced range. We observe that in the absence of on-board optical navigation the terminal verification accuracy is at best as good as the ephemeris uncertainty of the planet (~1000 km, 1σ). Conclusions derived in Reference 23 state that the best accuracy achievable at Saturn by radio navigation alone meets the requirements of flyby and probe delivery missions but not those of planetary

*Preliminary data received from JPL. Updating of Jupiter's ephemeris from Pioneer 10 encounter data is still in progress.

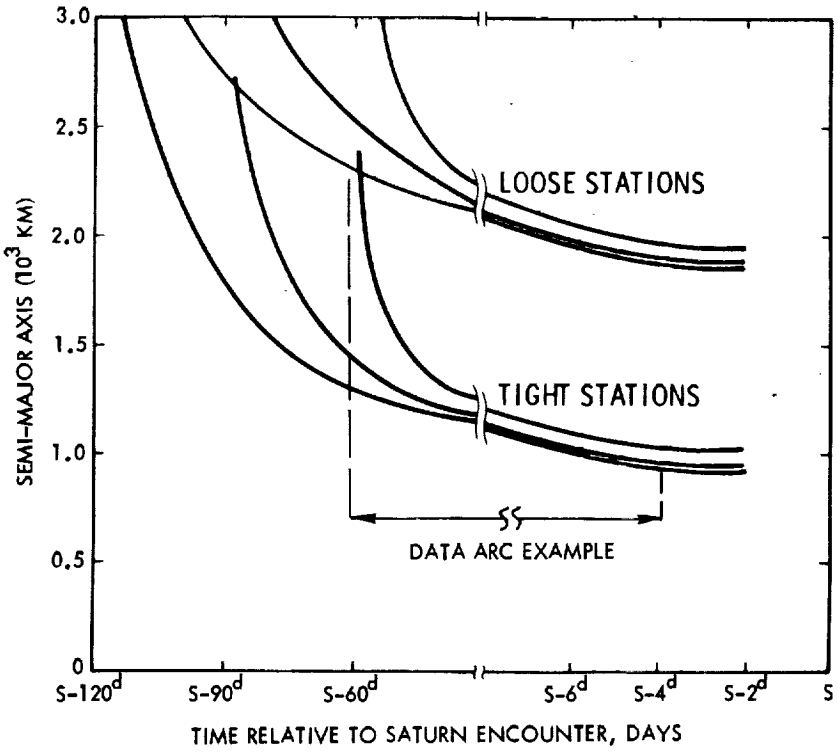

Figure 6-26. Semi-Major Axis of Dispersion Ellipse in $\overline{B}$-Plane for Saturn Approach; Earth-Based Radio Navigation Only (Reference 23)

swingby on a probe mission to Uranus. Saturn ephemeris improvements to be expected from the Mariner Jupiter/Saturn flyby mission (and possibly from the Pioneer 11 mission if it continues to a successful 1979 Saturn encounter after the 1974 Jupiter flyby) would aid navigation capabilities for an orbiter mission in the early 1980's.

6.11.4 Effect of Encounter Accuracy on Capture Orbit Characteristics

Characteristics of the initial capture orbit will reflect the uncertainty of the spacecraft state variables relative to the planet at the time of the injection maneuver. Principal influences of the spacecraft trajectory dispersion at encounter on the parameters of the capture orbit can be summarized as follows.

1) Effect of position uncertainty

- Radial component — Affects the orbit dimensions achieved by the specified insertion velocity increment, ΔV.
- Normal component — Affects out-of-plane elements (orbit inclination and longitude of ascending node).

- Tangential component — Primarily affects the apsidal orientation; may cause an efficiency loss due to change from optimal timing of the insertion maneuver (cosine-loss).

2) Effect of velocity uncertainty

- In-plane components — Affects orbit dimensions and apsidal orientation; may cause cosine losses.

- Out-of-plane component — Affects orbit inclination and nodal position; also causes cosine losses.

Table 6-5 gives results of a preliminary analysis of deviations from assumed nominal capture orbit characteristics at Jupiter and Saturn due to spacecraft position and velocity dispersions. The effect of maneuver execution error is included in the velocity dispersion. The following assumptions are made in this analysis:

1σ position dispersion: (assumed equal in all directions)	300 km at Jupiter 600 km at Saturn
1σ velocity dispersion: (assumed equal in all directions and including ΔV execution errors of 1 percent)	20 m/s at Jupiter 30 m/s at Saturn

The sensitivities $\partial r_a/\partial r_p$ and $\partial r_a/\partial V_p$ of the orbital dimensions to dispersions in periapsis radius r_p and velocity V_p and the sensitivity of the orbit period to apoapsis changes resulting from these dispersions (see Appendix B6) are used in the analysis.

These results indicate that deviations from the assumed nominal capture orbit characteristics are relatively small in the case of Jupiter orbits, but considerably larger for Saturn orbits. In any case, they can be readily corrected by subsequent orbit trim maneuvers. This supports the conclusion that radio navigation accuracy is sufficient for achieving successful orbit insertion at Jupiter and Saturn.

For comparison, it is interesting to consider the Mars orbit insertion accuracy achieved by Mariner 9, the only planetary orbiter mission by U.S. spacecraft to date. Planned and actual capture orbit characteristics are listed in Table 6-6. Because of the low periapsis altitude of that mission (40 percent of the planet's radius) the orbit inclination and apsidal orientation are more sensitive to dispersions of the periapsis location than those of the Jupiter and Saturn orbits assumed in Table 6-5. The small actual dispersion (+48 km) of the Mariner's periapsis distance is representative of radio navigation and guidance capabilities of the early 1970's in a mission to a nearby planet.

Table 6-5. Effect of Periapsis Dispersions on Capture Orbit Characteristics

	Jupiter				Saturn			
Nominal Periapsis Radius r_p/R_J	2		4		2		3	
Nominal Apoapsis Radius r_a/r_J	20	40	20	40	40	80	40	80
Δr_a due to Δr_p [1], 10^3 km	36.0	132.0	10.5	37.5	264	960	126	456
Δr_a due to ΔV_p [1], 10^3 km)	3.3	12.3	2.4	9.0	40.2	150	34.2	132
$\Delta r_{a_{(RSS)}}$, 10^3 km	36.2	132.6	10.8	38.6	267.0	971.6	130.6	474.7
$\Delta r_{a_{(RSS)}}$, percent	2.5	4.6	0.8	1.4	11.1	20.1	5.4	9.8
ΔT_p due to $\Delta r_{a_{(RSS)}}$ [1], days	0.152	0.761	0.045	0.222	2.65	13.4	1.30	6.52
ΔT_p due to $\Delta r_{a_{(RSS)}}$, percent	3.5	6.3	0.9	1.7	15.8	30.0	7.3	14.1
$\Delta\omega$, degrees	0.12		0.06		0.28		0.19	
$\Delta\Omega$ [2], degrees	0.05		0.08		0.13		0.16	
Δi, degrees	0.12		0.06		0.28		0.19	
Assumed Dispersions								
Δr_p, km	300				600			
ΔV_p, m/sec	20				30			

[1] Sensitivities $\partial r_a/\partial r_p$, $\partial r_a/\partial V_p$ and $\partial T_p/\partial r_a$ given in Appendix B.6

[2] Initial orbit inclination assumed to be 30 degrees

Table 6-6. Capture Orbit Characteristics of the Mariner Mars (1971) Mission

	Planned	Actual
Orbit period	12.43 ± 1.33 hours	12.567 hours
Periapsis altitude (h_p)	1350 ± 285 kilometers	1398 kilometers
Apoapsis altitude (h_a)	23,330 ± 1366 kilometers	17,982 kilometers
Orbit inclination to equator (i)	64.0 ± 3.0 degrees	64.3 degrees
Apsidal orientation (ψ)	140 ± 2.4 degrees	139.7 degrees

6.11.5 In-Orbit Navigation

It is necessary, of course, that adequate in-orbit navigation be performed prior to the trim maneuvers designed to compensate for imperfections of the nominal maneuvers. At least one-half orbit is available for tracking to provide such navigation in each case. Regarding the critical parameters, orbit period, apsis radii, and time of periapsis passage, there should be little difficulty in achieving the required accuracy by means of the normal doppler tracking derived from the coherent uplink and downlink operation via the spacecraft transponder.

However, since doppler tracking is insensitive to the inclination of the orbit about the earth line, auxiliary data are required for determination of the orbit inclination and the orientation of the line of nodes relative to the equatorial plane. Such data may be obtainable from the entry and exit times of solar eclipses provided the orbit plane is not coplanar with the earth and sun lines. In the case of Saturn orbits the times of ring crossing and the entry and exit times of earch occultation by the rings can provide additional auxiliary orbit determination data. Methods of detection of these event times, accuracy of detection, and influence of measurement errors on orbit determination require further analysis.

6.11.6 Approach Guidance Maneuver

Since the accuracy of predicting the actual spacecraft position and velocity at the point of closest approach improves rapidly during the final days before the encounter, a small terminal correction maneuver may be desirable at that time. Such a maneuver will generally include components parallel and normal to the earth line (i.e., the spacecraft spin axis orientation).

Since reorientation of the spacecraft for maneuver purposes is ruled out during the critical pre-encounter phase it will be necessary to use axial ΔV thrusters in combination with spin/despin control thrusters to obtain the desired thrust vector orientation. The spin/despin thrusters are operated in the pulsed mode. Precession coupling due to thrust vector offset from the center of mass is compensated by the ΔV/precession control thrusters.

Typically, the correction maneuver will not require more than a few m/s, e.g., a lateral maneuver of 2 m/s performed at a distance of 5×10^6 km, about five days before the encounter, shifts the impact parameter by 1000 km. This maneuver can be performed by operating the spin or despin thrusters in pairs in two-second pulses twice per revolution for a total of 10 minutes. This indicates that the desired terminal corrections can be performed without burdening spacecraft operations significantly.

If terminal maneuvers are to be avoided altogether, it is still possible to use later tracking data to update the commanded orbit insertion velocity, thereby compensating for known residual errors in periapsis location, and thus to achieve a capture orbit with very nearly the desired apoapsis distance and orbit period.

6.12 OPERATIONAL SEQUENCES AND TIME LINES

This section discusses the operation of the Pioneer Jupiter orbiter spacecraft from injection by the launch vehicle into transfer orbit through the encounter with Jupiter and the Galilean satellites. Emphasis is placed upon events and operations of the orbiter which are unlike those of Pioneer F and G. Operational commonality with Pioneer F and G is noted wherever applicable.

6.12.1 Summary of Operational Sequence for a Typical Mission

Table 6-7 summarizes the flight operations required for a particular orbiter mission. A mission including a three-satellite encounter (Europa, Io and Ganymede) was selected to demonstrate, as fully as possible, the flexibility of spacecraft operation. The first segment of the mission sequence has been condensed, since it is identical to that of Pioneer F and G. Sections 6.12.3 and 6.12.4 discuss, in some detail, those operations peculiar to the orbiter.

6.12.2 Post-Launch Operations

The operations commencing with separation of the spacecraft from the launch vehicle third stage and ending with the termination of the initial orientation maneuver are identical to Pioneer F and G (Reference 1). These operations include spin rate reduction from a nominal 60 rpm to near 15 rpm, RTG and magnetometer boom deployment, and initial orientation to earth pointing, or near-earth pointing.

6.12.3 Spacecraft Maneuver Operations

Three types of spacecraft maneuvers are required during a mission:

- Changing the orientation of the spin axis (performed open-loop or closed-loop)
- Increasing or decreasing the spacecraft spin rate
- ΔV maneuvers, performed in either the +Z or -Z direction with two one-pound thrusters, or in the +Z direction with the main (high-thrust) engine.

Open-Loop Maneuvers

These attitude control maneuvers are required to reorient the spacecraft for velocity corrections. As in Pioneer F and G, commands are loaded into the program storage and execution (PSE) logic of the control electronics assembly for timing and firing of the precession control thrusters in relation to the pulses from the sun sensor assembly. The PSE also controls the elapsed time over which these thrusters are fired, thereby controlling the spacecraft spin axis precession angle along the reorientation rhumb line. After velocity correction, the spacecraft precession control thrusters are fired in response to stored commands in the PSE, returning the spin axis to the nominal prior orientation.

Table 6-7. Flight Operations Summary. Three-Satellite Encounter Mission

Operation	Approximate Time		Requirements	Remarks
1. Launch	1-1-82	L	Liftoff through separation from launch vehicle	Initiated by launch vehicle
2. Post launch	1-1-82	L	Despin, deployment, initial orientation	Initated by spacecraft sequencer
3. Earth pointing	Periodically throughout mission		Conical scan homing on earth through uplink signal	Performed on command
4. First midcourse correction	1-5-82	L + 5	Orient ≤180 degrees Spin to 15 rpm ΔV firing Despin to 4.8 rpm Reorient ≤180 degrees	VP thrusters* SC thrusters** 100-pound thruster SC thrusters VP thrusters
5. Second midcourse correction	1-21-82	L + 20	Orient ≤90 degrees ΔV firing Reorient ≤90 degrees	VP thrusters VP thrusters VP thrusters
6. Spacecraft opposition	6-23-82	L + 70		Sun-earth-spacecraft alignment
7. Spacecraft conjunction	11-6-82	L + 315		Earth-sun-spacecraft alignment
8. Spacecraft opposition	6-4-83	L + 520		Sun-earth-spacecraft alignment
9. Spacecraft conjunction	12-10-84	L + 710		Earth-sun-spacecraft alignment
10. Approach science	2-19-84 to 3-9-84	L + 780	Point science package toward Jupiter	
11. Enter magnetosphere	3-6-84	L + 796		
12. Periapsis (1) orbit entry	3-10-84	E = L + 800	Spin to 15 rpm ΔV firing Despin to 2 rpm	SC thrusters 100-pound thruster SC thrusters (Earth-line maneuver; enter 2.29 x 107 R_J orbit)
13. Occultation	3-10-84	E + 0.1	Coherent operation, S- and X-band	Duration three hours
14. Initial orbit science	3-10-84 to 6-7-84	E + 0.3 to E + 89	All instruments. Particles and fields instruments routinely.	Science interrupted by earth pointing about every third day, and ΔV maneuvers
15. Plane change	3-24-84	E + 14	Orient ~90 degrees Spin to 15 rpm ΔV firing Despin to 4.8 rpm Reorient ~90 degrees	VP thrusters SC thrusters 100-pound thruster SC thrusters VP thrusters
16. Apoapsis (1) Periapsis trim maneuver (if required)	4-4-84	E + 25	ΔV firing	VP thrusters (earth-line maneuver)

*Velocity/precession thrusters

**Spin control thrusters

Table 6-7. Flight Operations Summary. Three-Satellite Encounter Mission (Continued)

Operation	Approximate Time	Requirements	Remarks
17. Periapsis (2) Orbit time trim	4-30-84 E + 50	Spin to 15 rpm ΔV firing Despin to 4.8 rpm	SC thrusters 100-pound thruster SC thrusters (Earth-line maneuver; change to 2.29 x 90 R_J orbit)
18. Jupiter opposition	5-11-84 E + 62		Sun-earth-Jupiter alignment
19. Apoapsis (2)	5-18-84 E + 69		
20. Periapsis (3) Apoapsis reduction maneuver	6-7-84 E + 89	Spin to 15 rpm ΔV firing Despin to 4.8 rpm	SC thrusters 100-pound thruster SC thrusters (Earth-line maneuver; change to 2.29 x 47 R_J orbit)
21. Satellite encounter orbit science	6-7-84 to end of mission E + 89	All instruments Imaging, IR, UV instruments pointing to Jupiter, apoapsis to periapsis; to satellites at encounters	Science interrupted by earth pointing about every third day.
22. Apoapsis (3)	6-15-84 E + 97		
23. Periapsis (4) Orbit time trim Enter satellite-synchronous orbit	6-23-84 E + 105	Spin to 15 rpm ΔV firing Despin to 4.8 rpm	SC thrusters 100-pound thruster SC thrusters (Earth-line maneuver; change to 2.29 x 45.2 R_J orbit)
24. Occultation	2 to 5 hours after number 23		
25. Io encounter	6 hours after number 23		
26. Ganymede encounter	20 hours after number 23		
27. Apoapsis (4)	6-30-84 E + 112		
28. Europa encounter	10 hours before number 29		
29. Periapsis (5) Final trim maneuver (if required)	7-7-84 E + 119	ΔV firing	VP thrusters (Earth-line maneuver; 2.29 x 45.1 R_J orbit)
30. Occultation	2 to 5 hours after number 29		
31. Io encounter	6 hours after number 29		
32. Ganymede encounter	20 hours after number 29		Items 28, 30, 31 and 32 repeat each periapsis (14-day intervals)

Closed-Loop Maneuvers

Closed-loop precession maneuvers utilize the conical scan signal processing of the uplink RF signal to establish earth pointing and commands to the precession control thrusters. Operation is the same as in Pioneer F and G.

Spin Rate Adjustment

For spin rate adjustment paired thrusters are used which can be commanded in real time or operated via stored commands in the PSE of the CEA. These thrusters are commanded in a continuous rather than a pulsed mode.

Maneuver Sequence Using High-Thrust Engine

All ΔV maneuvers which use the high-thrust engine will be performed at elevated spin rates (15 rpm). The sequence of events, starting with the spin axis in the nominal earth-pointing orientation and the spin rate at the nominal value of 4.8 rpm is as follows:

- Command the spin thruster to achieve the nominal spin rate increase
- At termination of spinup, verify on ground spin period via sun sensor (or star sensor) pulses
- Trim spin speed (if necessary)
- Allow time for decay of residual wobble
- Command and execute ΔV maneuver
- Determine spin rate via sun sensor (or star sensor) pulses
- Command the despin thruster return to nominal spin rate
- Verify and trim the spin speed (if necessary)
- Correct earth pointing error (closed loop) via conscan and precession control thrusters.

For high-thrust maneuvers at other than the nominal earth-pointing orientation the above sequence is modified by introducing steps to precess the spin axis (in the open-loop mode) to the desired thrust orientation and to return it to the nominal orientation after completion of the ΔV maneuver.

The sequence for velocity adjustment performed by the precession control thrusters is unchanged from that used in Pioneer F and G.

6.12.4 Typical Operations In Jupiter Orbit

The mission sequence summary of Section 6.12.1 typifies the operation of a Jupiter orbiter in a three-satellites (Europa, Io, and Ganymede) encounter mission. Operational aspects are expanded here based on the above sections and Sections 3 and 4.

A number of spacecraft maneuvers are required to insure execution of the mission. These maneuvers include orbit entry, plane change, orbit trimming, earth pointing updating and spin rate corrections, to be discussed below.

Deboost and Orbit Trimming

Figure 6-27 shows the location of impulsive velocity maneuvers that are required to synchronize the spacecraft position with respect to the Jovian and satellite positions. The operation numbers are referred to Table 6-7 and are the following at periapsis:

Operation 12: Deboost to 107 R_J apoapsis

Operation 17: Periapsis time trim

Operation 20: Deboost to 45 R_J apoapsis.

Near apoapsis a plane change maneuver (Operation 15) required to obtain zero inclination is performed during the first orbit.

The largest velocity change (deboost) will be performed while earth pointed. Subsequent ΔV adjustments at periapsis will not require a precession maneuver, in spite of motion of the earth during the first and second orbits, because cosine losses are very small. Only the plane change ΔV maneuver will require a reorientation as described above.

Earth Pointing Updates

Correction of the spin axis pointing direction will be required on a periodic basis as a result of one or more of the following:

- Disturbance torques
- Geometry dependent effect due to relative motion of spacecraft and earth.

Updating of earth pointing can be performed in the closed-loop mode utilizing the conical scan signal processing, or in the open-loop mode by commanding the precession thrusters "on" for a given duration at the appropriate time in the spin cycle. Updating will not be scheduled while making scientific measurements near Jupiter or satellites.

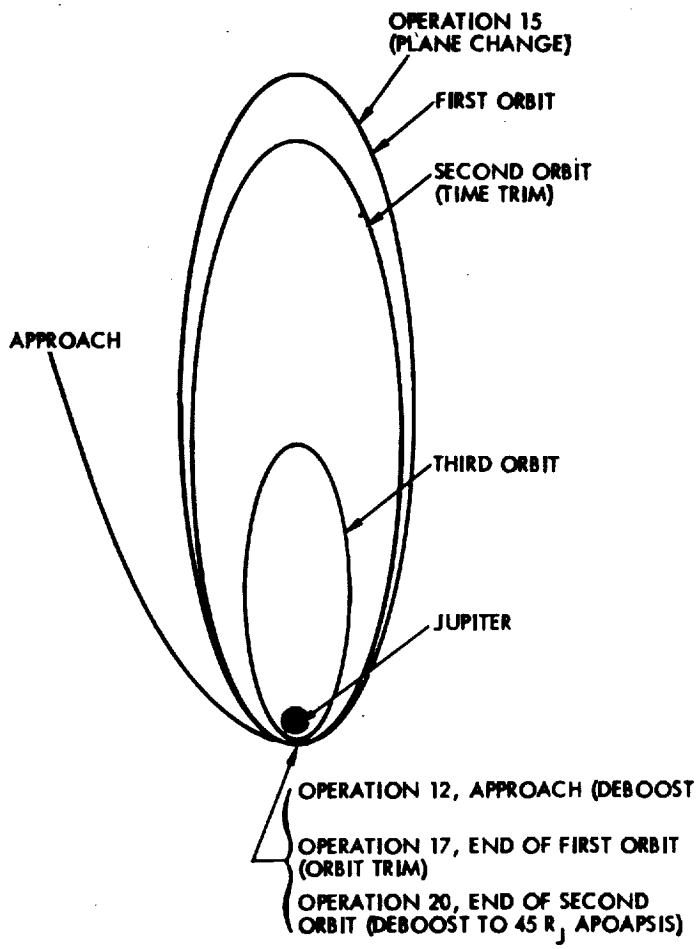

Figure 6-27. Orbit Adjustment

Figure 6-28 shows updating of earth pointing during the orbital phase for the 14.2-day and 45-day orbits near the time when the earth lies between the sun and Jupiter. The earth-line is rotating at an average rate of approximately one degree every four days, as seen from the spacecraft. Slight changes in this rate during each orbit are due to the orbital motion of the spacecraft. Spin axis pointing corrections of one degree are performed whenever the pointing error reaches 0.5 degree.

Spin Rate Changes and Corrections

Repeated major spin rate changes are required a) to attain a high rate (15 rpm) for increased stability during thrust phases, b) to attain a low rate (2 rpm) for improved image system operation, and (c) to restore the nominal spin rate (4.8 rpm) after each of these excursions.

Spin rate variations may occur because of induced eddy currents and magnetic field interaction. Spin rate retardation will be most pronounced near periapsis. Determination of spin rate and corrective thruster firing, if necessary, will be performed after each Jupiter pass when scientific data gathering is complete.

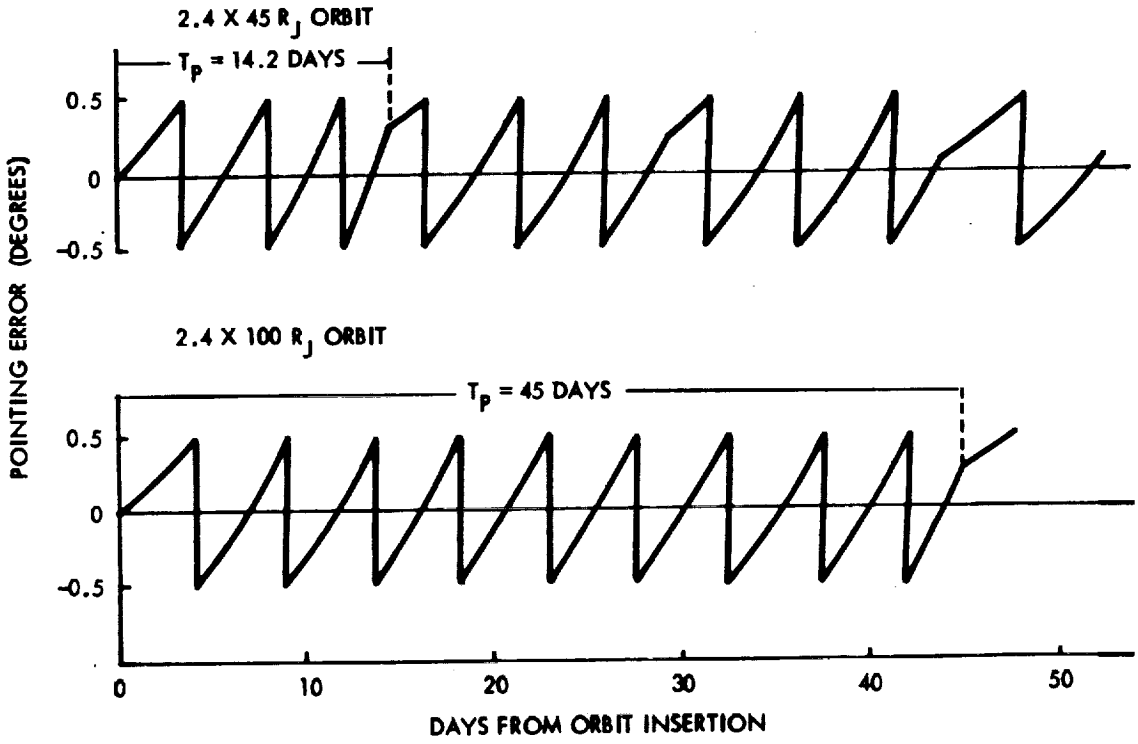

Figure 6-28. Updating of Earth-Pointing During Orbital Phase

Science Payload Operation

Science payload operations required in a typical Jupiter orbit mission are summarized in Section 5.1. The operation of the rotatable sensor package during each passage of Jupiter is of particular interest. The servo drive reorients the package each spin revolution so that the field-of-view of the sensors is pointed nominally at the center of the object being viewed. Reindexing parameters required in the drive logic are selected such that the actual cone angle tracks the idealized cone angles in an open-loop sense. For improved tracking of the actual, non-uniform cone angle changes the drive motor stepping rate, or the number of steps per roll pulse, can be varied at appropriate times during each orbital pass. The package is reindexed at every spacecraft revolution so that several complete images of Jupiter can be obtained by the line scan camera during each pass.

6.13 PERFORMANCE SUMMARY

6.13.1 Orbit Performance Chart

Figure 6-29 is a nomograph designed to permit convenient parametric evaluation of overall performance characteristics of the Pioneer Jupiter orbiter.*

- Performance is measured in terms of ΔV maneuver capability, as indicated by the ordinate of the upper quadrants of the chart.
- The upper right quadrant determines ΔV capability as function of injected spacecraft weight with inert weight and propellant weight as parameters.
- The upper left quadrant shows the orbit dimensions achievable depending on the insertion maneuver ΔV and the arrival velocity, V_∞.
- The two lower quadrants show the influence of launch vehicle performance in terms of injected weight vs. injection energy C_3 (right quadrant), and the influence of the choice of trajectory characteristics (left quadrant).

The curves used in the nomograph present data previously shown in Figures 6-4, 6-5, 6-8, 6-16, and 6-17.

In the example illustrated by dashed lines the gross spacecraft weight of 2100 pounds** injected by the Titan/Centaur launch vehicle at a departure energy $C_3 = 90\ km^2/s^2$ has a total ΔV capability of 2450 m/s, assuming an inert spacecraft weight of 900 pounds and a usable propellant weight of 1200 pounds. The trajectory characteristics (lower left) indicate that at the 1985 launch opportunity an injection energy of $91\ km^2/s^2$ can achieve a 700-day transfer trajectory to Jupiter with a hyperbolic arrival velocity V_∞ of 7.5 km/s. At this arrival velocity an injection maneuver of 1800 m/s can achieve an orbit of 3 x 50 Jupiter radii, having a 17-day period. The available maneuver capability of 2350 m/s (obtained from the total ΔV capability of 2450 m/s by allowing 100 m/s for midcourse maneuvers) thus provides about 550 m/s for orbit change maneuvers in addition to the required 1800 m/s injection maneuver. For conservatism we have assumed that all attitude control (precession and spin control) propellants are still on board when the ΔV maneuvers are performed.

*This nomograph was designed by W. J. Dixon of TRW Systems and first used in a 1970 study of Jupiter and Saturn orbiters.

**Allowing for 65 pounds of interstage adapter weight that is included in the launch vehicle performance curve.

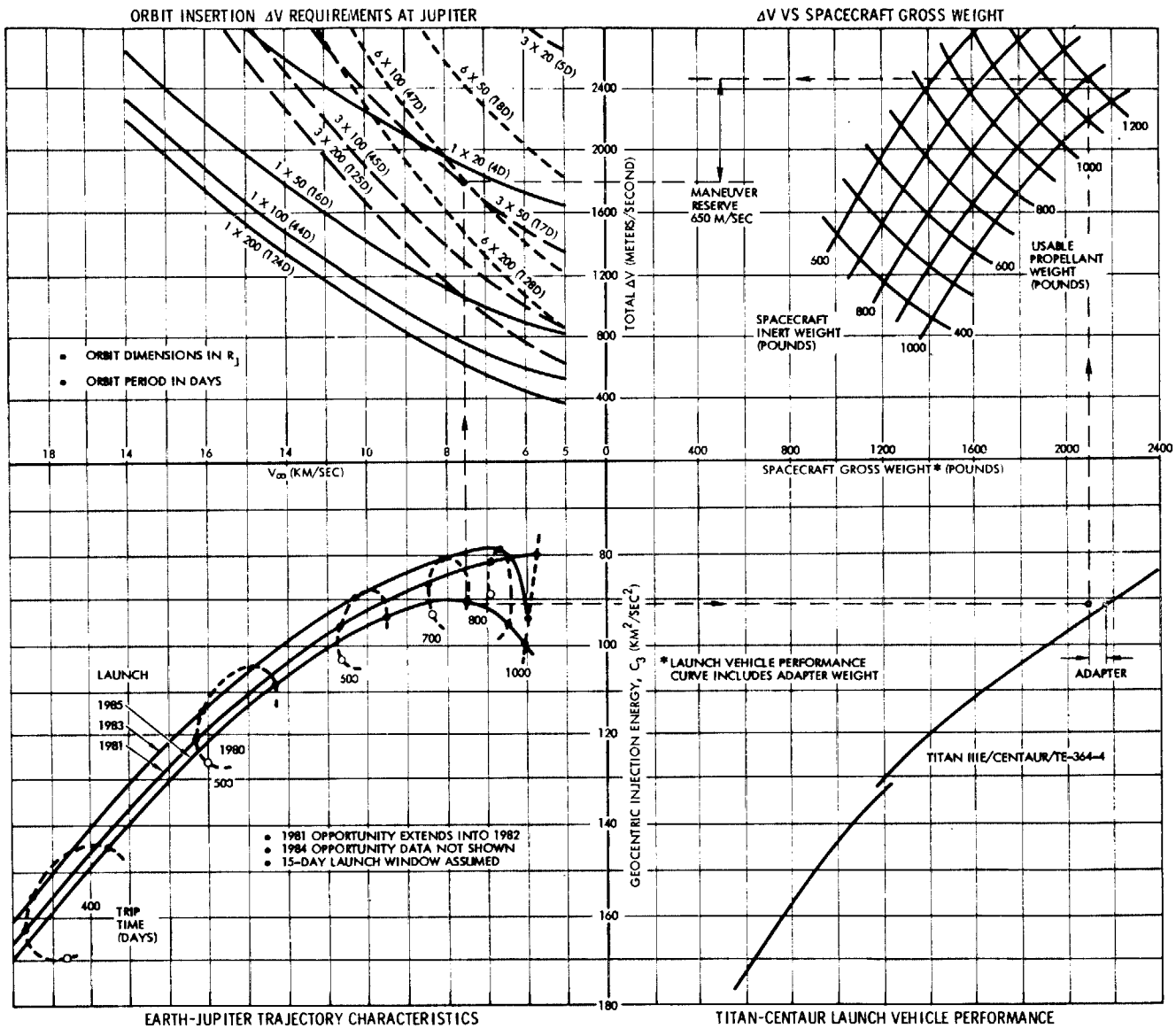

Figure 6-29. Jupiter Orbit Insertion Performance Chart

For a change in conditions from those illustrated by the above example, the chart shows that a reduction of trip time has the twofold effect of 1) increasing the required injection energy, thus reducing the total spacecraft weight, propellant capacity and hence, ΔV capacity, and 2) increasing V_∞, thus increasing the eccentricity of the orbit achievable with a given ΔV allocation. For example, a 100-day reduction in trip time would increase C_3 by 4 km^2/s^2 causing a 100-pound reduction in spacecraft injected weight, a 100-pound reduction in propellant weight and thus a 140 m/s reduction in ΔV capability. The trip time reduction also increases V_∞ to 9.5 km/s which in turn increases the ΔV requirement for achieving a 3 x 50 R_J orbit to 2220 m/s. As a result, the ΔV allocation for orbit changes would be reduced from 550 m/s to 130 m/s. If, on the other hand, the orbit change ΔV allocation is to be held constant at 550 m/s the 100-day trip time variation would require a change in the dimensions of the achievable capture orbit from 3 x 50 to 3 x 100 Jupiter radii.

These examples illustrate the utility of the performance nomograph. It should be noted that more detailed aspects of mission performance covered previously in this section are omitted in the nomograph:

- Launch phase penalties
- Orbit insertion penalties
- Deviation from optimum transfer trajectory characteristics (except for 15-day launch window allowance).

6.13.2 Spacecraft Performance Summary in 1982 and 1985 Sample Missions

Performance characteristics of the Jupiter orbiter in the selected 1982 and 1985 sample missions (Section 6.7) are summarized in Table 6-8.

The less demanding launch energy requirements in 1981/1982 reflect in a greater unused margin of launch vehicle capability (394 pounds) in the first mission. The weight margin in the second mission (launch in 1985) is only 119 pounds. These data reflect a conservative tank size selection:

1) Limiting the propellant weight to the maximum weight capability available in the mid-1980's, avoiding propellant off-loading at earlier mission years and an attendant increase in dynamic loads due to propellant sloshing

2) Reducing propulsion system dry weight

3) Allowing a greater margin for weight contingencies that may accrue in subsequent design studies.

Table 6-8. Performance Summary of Jupiter Orbiter

Launch year	1981/82	1985
Trip time, days	800	750
Injection energy C_3, km^2/sec^2	79.3	87.4
Maximum launch vehicle weight capacity, lb	2600	2350
Launch weight penalty (estimated), lb	15	40
Adapter weight allowance, lb	65	
Injected gross spacecraft weight, lb	2126	
Launch vehicle capability margin, lb	394	119
Total usable propellant weight, lb	1202	
- Propellant used in transit, lb	30	
- Propellant used for orbit insertion*, lb	978	
- Propellant used for orbit change*, lb	174	
Science payload weight, lb	120	
Spacecraft less usable propellant, lb	924	
Arrival velocity, km/sec	6.9	6.8
Total ΔV capability at arrival*, m/sec	2280	
Orbit injection ΔV*, m/sec	1800	
Allowance for orbit changes*, m/sec	480	
Initial orbit dimensions, R_J	3 x 46	3 x 45
Orbit period, days	14.94	14.49

*Bipropellant weights and maneuver capabilities only

7. MISSION PERFORMANCE OF THE SATURN ORBITER

Principal considerations regarding launch phase constraints, trajectory selection criteria, orbit insertion requirements and constraints, orbit characteristics and orbit changes previously discussed for the Pioneer Jupiter orbiter also apply to the Saturn orbiter mission. Drawing on the data presented in Section 6, this section only covers specific characteristics of the Saturn orbiter that differ from those of the Jupiter orbiter. To facilitate performance comparisons, the Saturn orbiter characteristics will be presented in the same format with back reference to the corresponding Jupiter orbiter characteristics stated in Section 6.

7.1 LAUNCH OPPORTUNITIES, LAUNCH PHASE CHARACTERISTICS, DEPARTURE AND ARRIVAL VELOCITY

Launch opportunities for Saturn missions occur about once every year governed by the 378-day earth-Saturn synodic period. The yearly launch seasons for Saturn missions in the 1970's and 1980's were previously shown in Figure 6-1 together with those for Jupiter missions.

Indirect missions via Jupiter swingby are not being considered because of the greatly increased hyperbolic approach velocities at Saturn and the excessively large retro ΔV requirements that would result from this mission mode. Note also that indirect mission opportunities via Jupiter do not occur during the time period considered in this report.

Variations of launch energy requirements in the 1970's and 1980's are shown in Figure 7-1 for flight times ranging from 500 to 1625 days, corresponding to those for Jupiter missions (Figure 6-2), but governed by the 15-year interval between successive nodal crossings of Saturn's orbit around the sun. For long flight times the launch energy has a minimum at the 1986 launch opportunity.

Variations in arrival velocity at Saturn with launch year are shown in Figure 7-2, corresponding to Figure 6-3 for Jupiter missions. An appreciable variation is noted only for missions with short trip times, with maxima occurring at 1987/1988.

Figure 7-3 summarizes the departure energy and arrival velocity requirements for the 1982, 1984 and 1986 mission years with trip times ranging from 800 to 1800 days, corresponding to Figure 6-4 for Jupiter missions. The 1982 launch opportunity extends into 1983. The 1985 opportunity is omitted in the graph. As in Figure 6-4 it should be noted that the data reflect a 15-day launch window and only show the minimum energy departure envelope.

Declinations of the launch asymptote are shown in Figure 7-4 for launch years between 1982 and 1986 with trip times ranging from 800 to 1800 days, corresponding to Figure 6-9 in the case of Jupiter missions. The launch declinations are northerly in 1982, with a maximum of 20 degrees for a 1500-day trip time. Small north and south declinations occur during the 1985 opportunity. In 1986 all declinations are southerly,

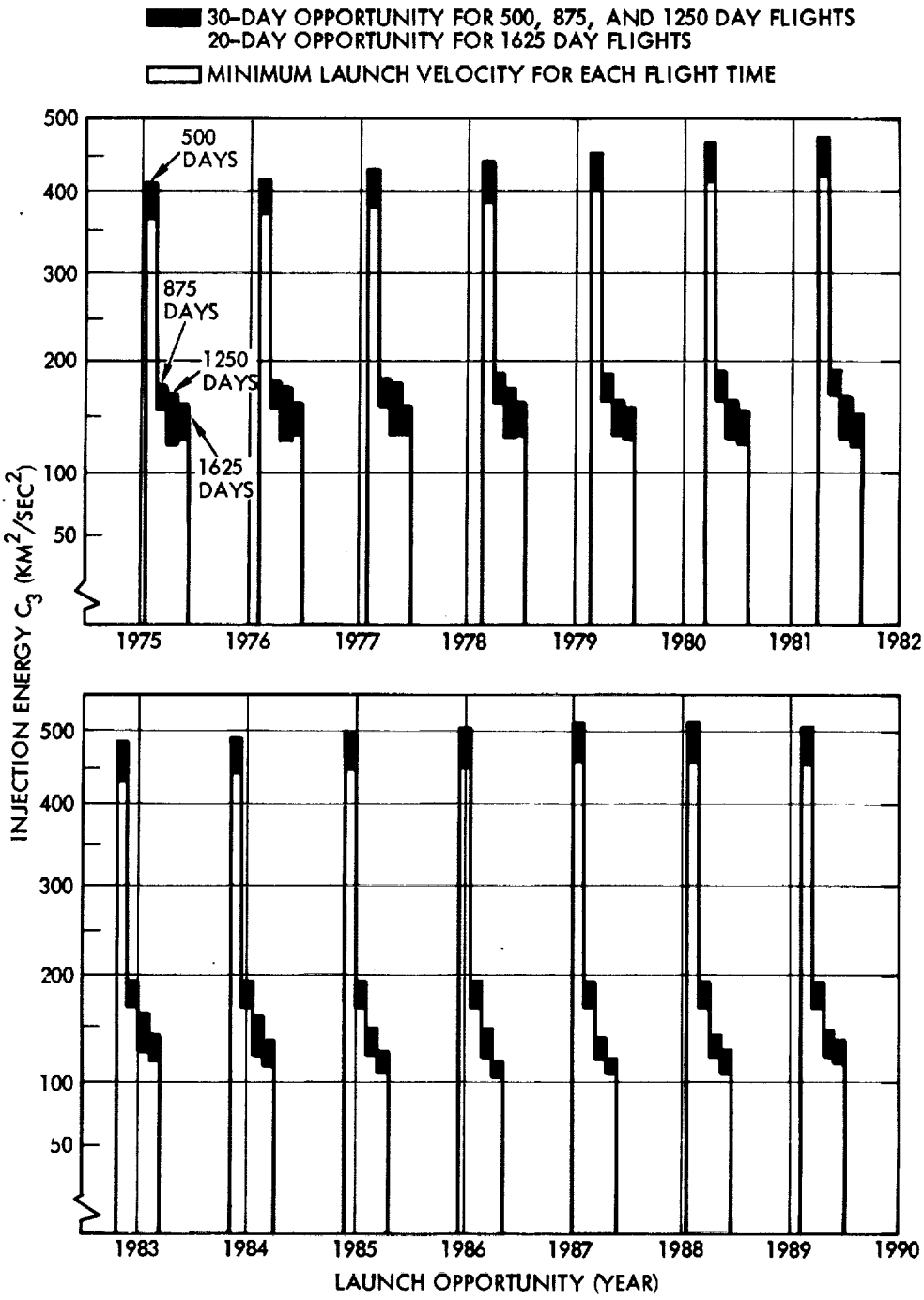

Figure 7-1. Variation of Injection Energy Requirements with Launch Year for 500- to 1625-Day Earth-Saturn Trajectories

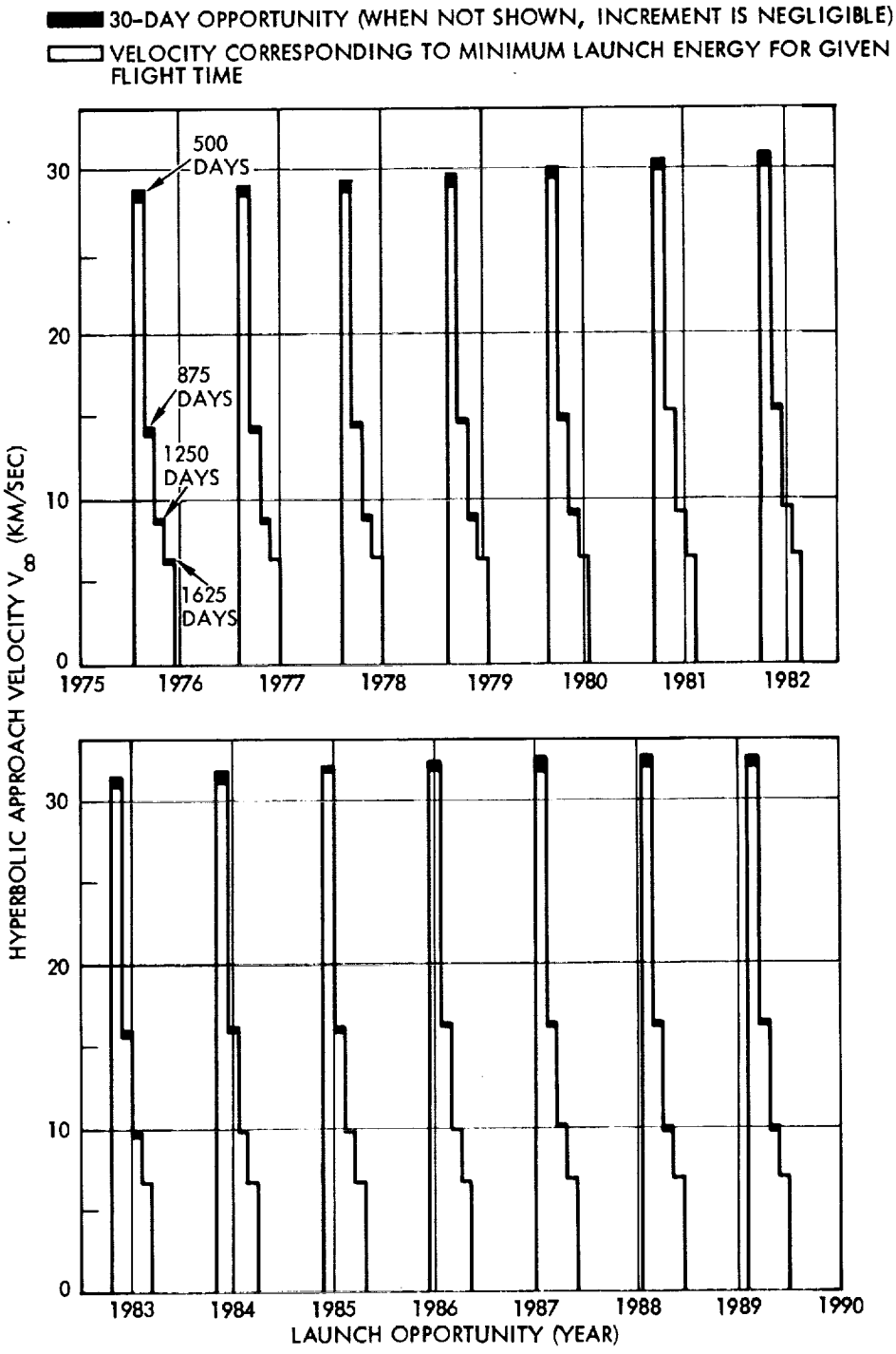

Figure 7-2. Variation of Saturn Approach Velocity V_∞ with Launch Year for 500- to 1625-Day Earth-Saturn Transfers

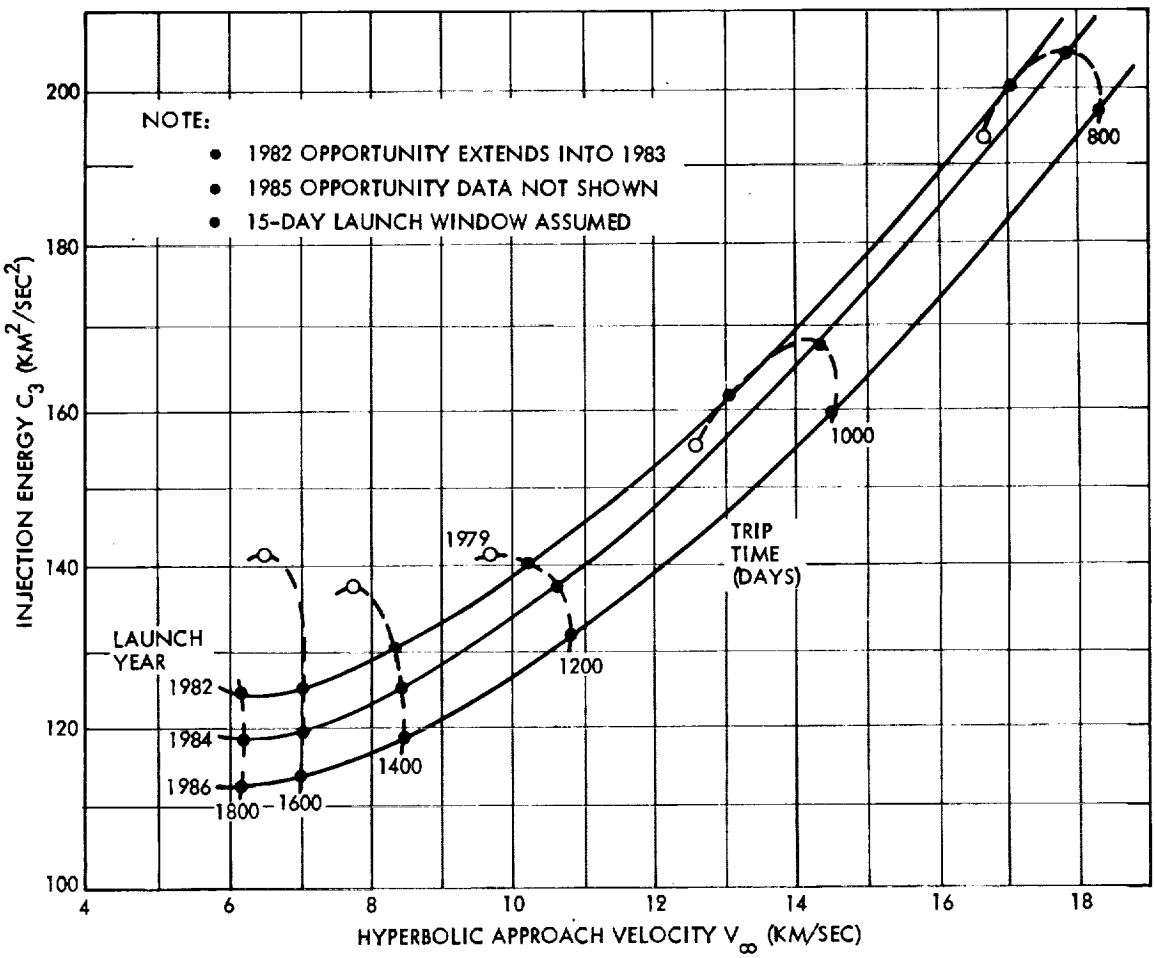

Figure 7-3. Launch Energy and Arrival Velocity Characteristics for 1982, 1984, and 1986 Earth-Saturn Trajectories

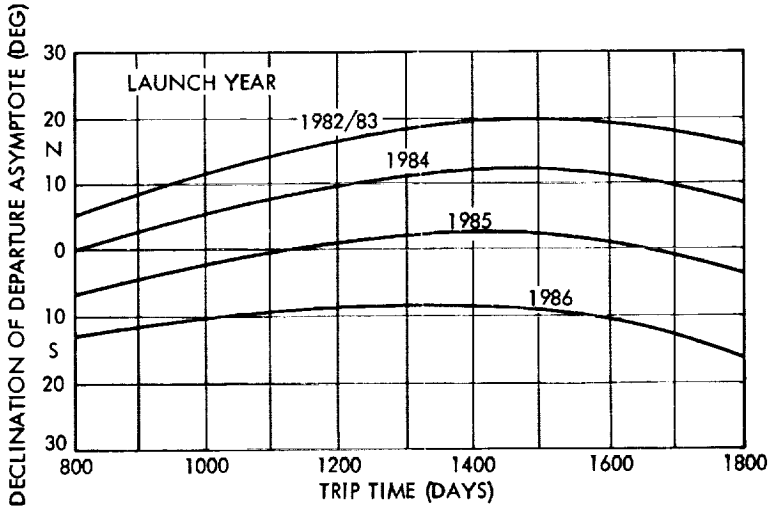

Figure 7-4. Declination of Departure Asymptote Vs. Trip Times for Earth-Saturn Trajectories

between -8 and -16 degrees. Thus, the later launch opportunities are more favorable not only in terms of the launch energy requirements but also with regard to avoidance of launch azimuth penalties and extended orbital coast times.

7.2 SELECTED NOMINAL EARTH-SATURN TRANSFER TRAJECTORIES

On the basis of the selection criteria and constraints discussed previously two sample earth-Saturn transfer trajectories were chosen from data in Reference 18 for the 1982 and 1986 launch opportunities. Their principal characteristics are listed in Table 7-1, corresponding to Table 6-1 for Jupiter missions.

Table 7-1. Selected Earth-Saturn Sample Trajectories

Characteristics	Trajectory 1	Trajectory 2
Departure date	5 Jan. 1983	29 Jan. 1986
Arrival date	10 Dec. 1987	3 Jan. 1991
Trip time (days)	1800	1800
Injection energy C_3 (minimum) (km^2/sec^2)	122.5	108.0
Injection energy C_3 (15-day launch period) (km^2/sec^2)	123	116.1
Departure hyperbolic velocity (km/sec)	11.1	10.8
Departure asymptote declination (deg)	14.2	-15.4
Inclination relative to ecliptic (deg)	3.47	-0.73
Heliocentric transfer angle (deg)	159.0	167.9
Arrival hyperbolic velocity (minimum) (km/sec)	5.89	6.1
Arrival hyperbolic velocity (15-day launch period) (km/sec)	5.95	6.1
Arrival asymptote declination (deg)	-12.8	-21.7
Earth-spacecraft distance at arrival (AU)	10.97	10.97
Approach illumination angle,* (deg)	60.8	58.4
Angle between velocity vector at periapsis and earth line* (r_p = 3 R_S) (deg)	+2.5	0
Cosine-loss for orbit insertion in earth pointing mode* (percent)	0.1	0

*See discussion in Section 6.8

Figure 7-5 shows the sample trajectories projected into the ecliptic plane, with time marks at 100-day intervals. Figure 7-6 shows the time history of communication distances and earth-spacecraft-sun angles during transit. Corresponding data for the sample earth-Jupiter trajectories were shown in Figures 6-13 and 6-14.

Figure 7-7 shows the relative geometry between the spacecraft in Saturn orbit, the earth and sun (corresponding to Figure 6-15 for the Jupiter orbiter). In the case of the first sample trajectory the earth-spacecraft distance decreases from its initial value of 11.0 AU at the 10 December 1987 arrival date to 9.1 AU after 5.5 months in orbit, then

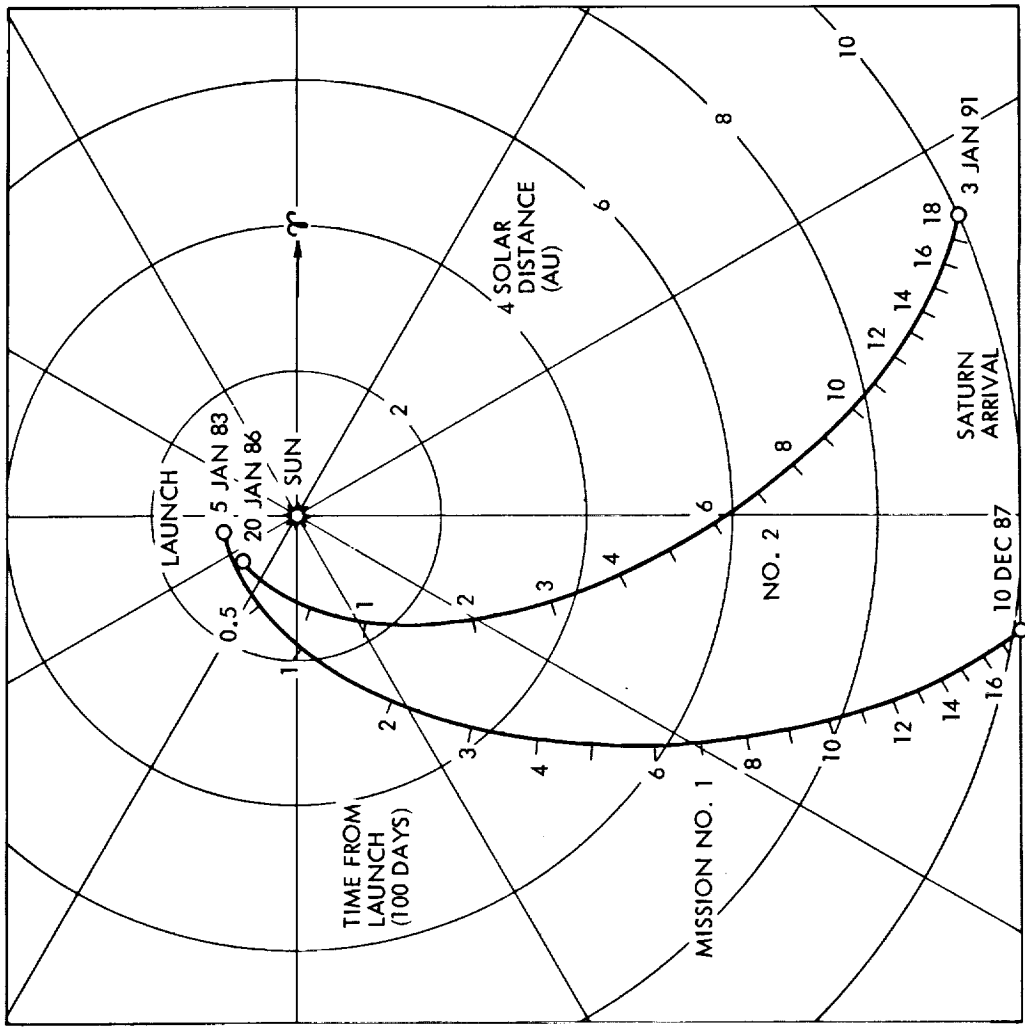

Figure 7-5. Sample Earth-Saturn Trajectories (Projected Into Ecliptic)

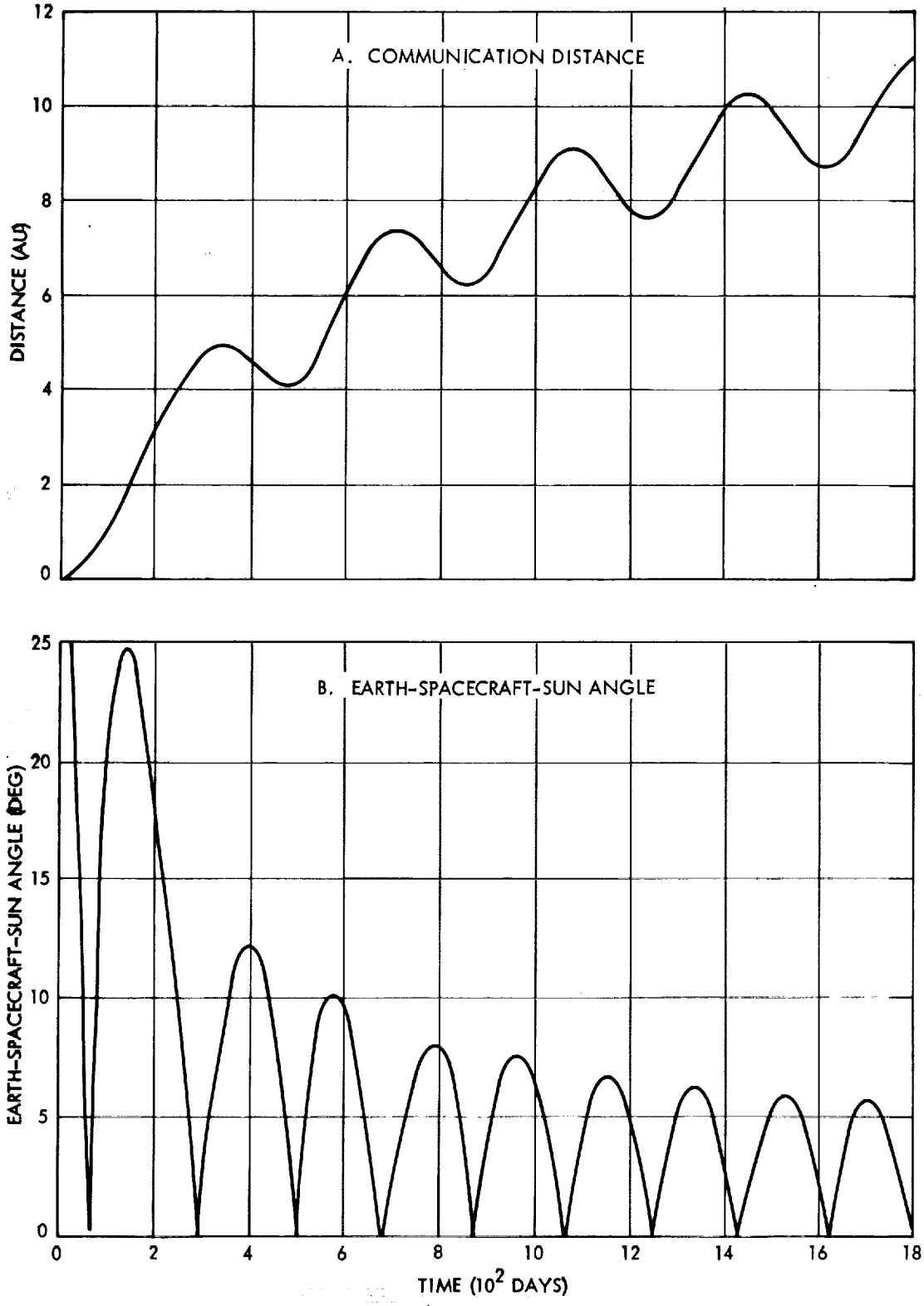

Figure 7-6. Communication Distance and Earth-Spacecraft-Sun Angle Vs. Time During Cruise for Sample Earth-Saturn Trajectory (Launch: 5 January 1983)

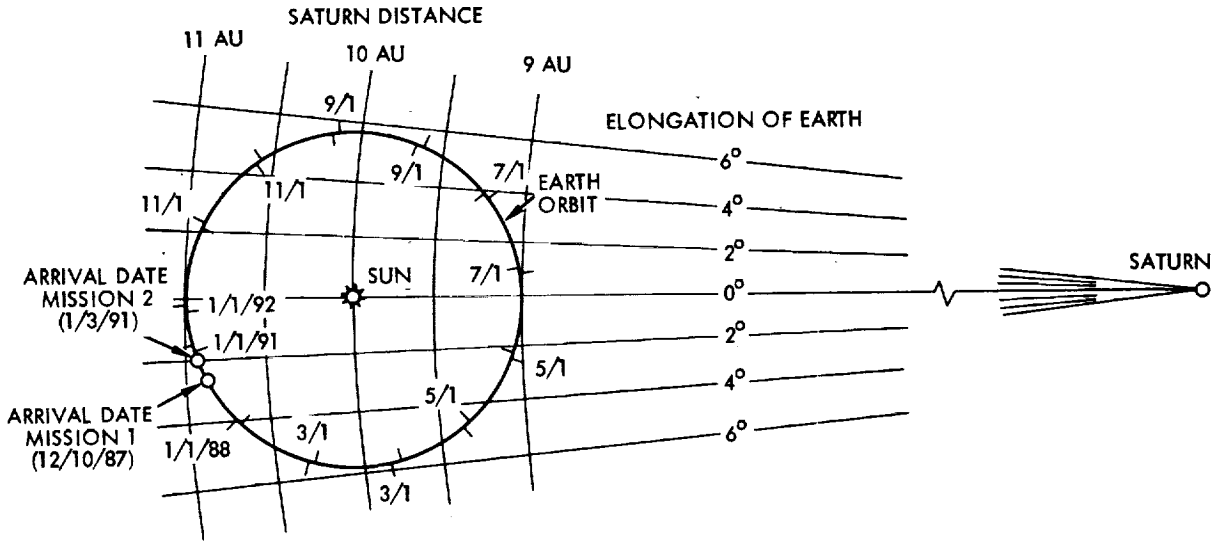

NOTE:

- TIME MARKS INDICATED ON OUTSIDE OF EARTH ORBIT CORRESPOND TO SAMPLE MISSION 1, INSIDE TO MISSION 2.
- RELATIVE DISTANCES AND ANGLES SHOWN ARE APPROXIMATELY VALID FOR BOTH MISSIONS 1 AND 2.

Figure 7-7. Relative Sun, Earth, and Saturn Positions During Orbital Phase of Sample Missions 1 and 2

increases again to 11.1 AU during the next 6.3 months. The earth-spacecraft-sun angle varies between -6 and +6 degrees. Syzygies occur around 20 May 1988 and 30 November 1988.

A second set of time marks indicates communication distances and angles occurring during the orbit phase of the second sample trajectory, following arrival on 3 January 1991.

7.3 SATURN ORBIT INSERTION

7.3.1 Orbit Insertion Retro Velocity Requirements

Figure 7-8 is a parametric plot of orbital period and retro-maneuver ΔV requirements in terms of orbit dimensions for V_∞ = 6 km/s. As in the corresponding plot for Jupiter orbits (Figure 6-16) it is assumed that the orbit insertion maneuver is performed impulsively and under idealized conditions. A change in arrival velocity from the nominal value of 6 km/s is equivalent to a reduction of ΔV as shown in Figure 7-9 (cf. Figure 6-17 for Jupiter orbit insertion). Thus, for example, with an increase of hyperbolic arrival velocity to 7 km/s and orbit insertion at 3 Saturn radii the equivalent reduction in ΔV is 270 m/s. Assuming a retro-maneuver ΔV of 1400 m/s, the apoapsis radius would be increased from 50 R_S to 100 R_S as a result of this change in arrival velocity, and the orbital period from 26 to 67 days. Comparison with the orbit insertion characteristics

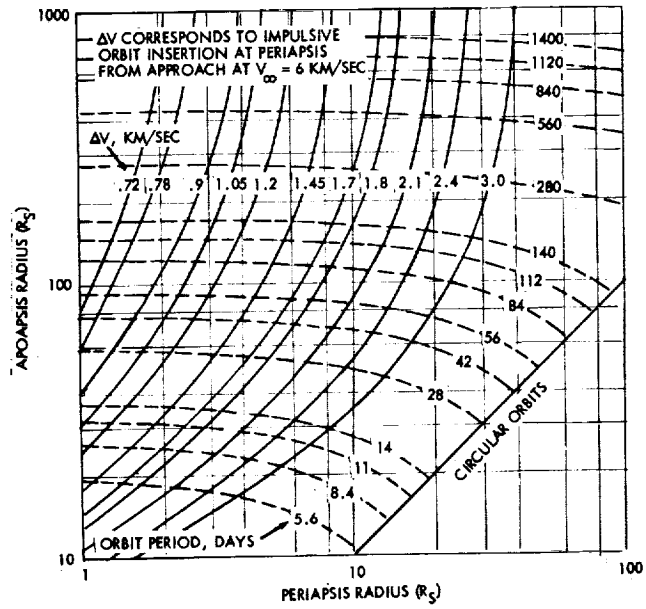

Figure 7-8. Characteristics of Orbits about Saturn

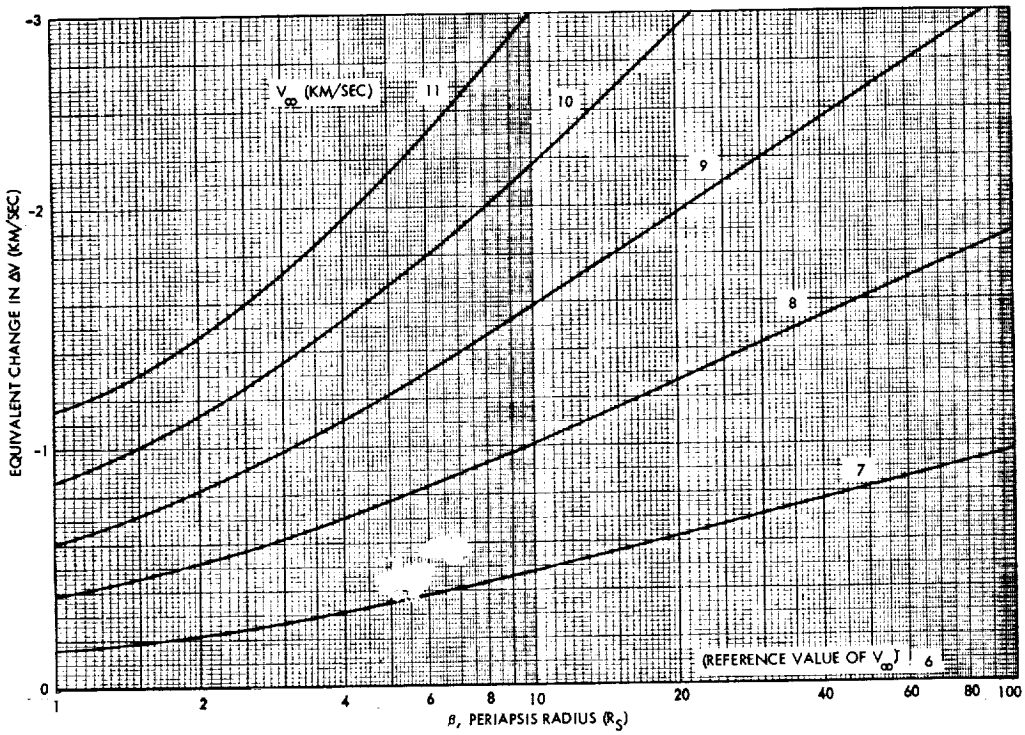

Figure 7-9. Effective ΔV Change in V_∞ for Saturn Orbits (Nominal V_∞ = 6 km/sec)

at Jupiter shows that Saturn orbits are much more sensitive to increases in arrival velocity. This characteristic and the limited propellant load available makes the selection of long flight time trajectories with low arrival velocities, close to 6 km/s, an essential mission constraint for the Saturn orbiter.

7.3.2 Influence of Ring Particle Impact Hazard on Orbit Selection

Injection at periapsis distances appreciably lower than 3 R_S where acceptable orbit dimensions can be achieved without exceeding the available ΔV capability becomes problematic because of the ring particle impact hazard.

An upper bound of the number of particle impacts during the ring plane crossing adopted from an earlier Saturn flyby mission study (Reference 12) is given in Table 7-2.* These results are based on the current model of particle flux density in Saturn's rings as defined in Reference 7. The total cross-section area of the propulsion stage exposed to the particle flux is about 1.5 m^2. The ring crossing is assumed to occur at the distance of 2.30 R_S. (It is noted that just inside the perimeter of ring A, at R = 2.29 R_S, or 600 km closer to the planet, the estimated particle number density in NASA's model is six times greater than at 2.30 R_S.)

Table 7-2. Upper Bound of Number of Hits Sustained by Propulsion Stage During Saturn Ring Plane Crossing

Number of Hits N_i	By Particles of	
	Radius r_i (cm) or Larger	Mass m_i (grams) or Larger
4.7	0.1	4.2×10^{-3}
3.1	0.133	0.01
0.96	0.287	0.1
0.31	0.62	1.0

Assumptions:

- Ring plane crossing at 2.3 R_S
- Velocity component perpendicular to ring plane: 8 km/sec
- Intercept angle relative to spacecraft -Z axis: 4.5 deg
- Exposed area of propulsion stage: 1.5 m^2
- Particle density: 1 gram/cm^3

*See also Figure 2-2 in Section 2.1.1.3)

As shown in Table 7-2, the upper bound of the number of hits sustained by the (shielded) area of the propulsion bay by particles of radius 0.1 cm (mass = 4.2 x 10^{-3} grams) is 4.7 per ring crossing. The number of hits by particles of radius 0.62 cm (mass = 1.0 gram) is 0.31 per crossing. According to the model assumed the number of hits decreases by a factor of about 3 with each order-of-magnitude increase in particle mass.

These estimates are on the conservative side, assuming an upper bound of particle flux and a relatively close ring crossing distance.

Concern with ring particle impact hazard in future Saturn mission planning is evidenced by the fact that the projected closest approach distance in the 1977 Mariner Jupiter/Saturn flyby mission is between 4 and 5 R_S and the distance at ring plane crossing is 5 R_S or larger.

It is advantageous for purposes of minimizing retro ΔV requirements to exploit the fact that the periapsis distance can be made appreciably less than the minimum permissible distance at the ring plane crossing if the spacecraft orbit is inclined to the equator and the periapsis is located sufficiently far off the ring plane crossing points (nodes). Figure 7-10 illustrates this condition with the periapsis located symmetrically between the nodal points of the orbit plane.

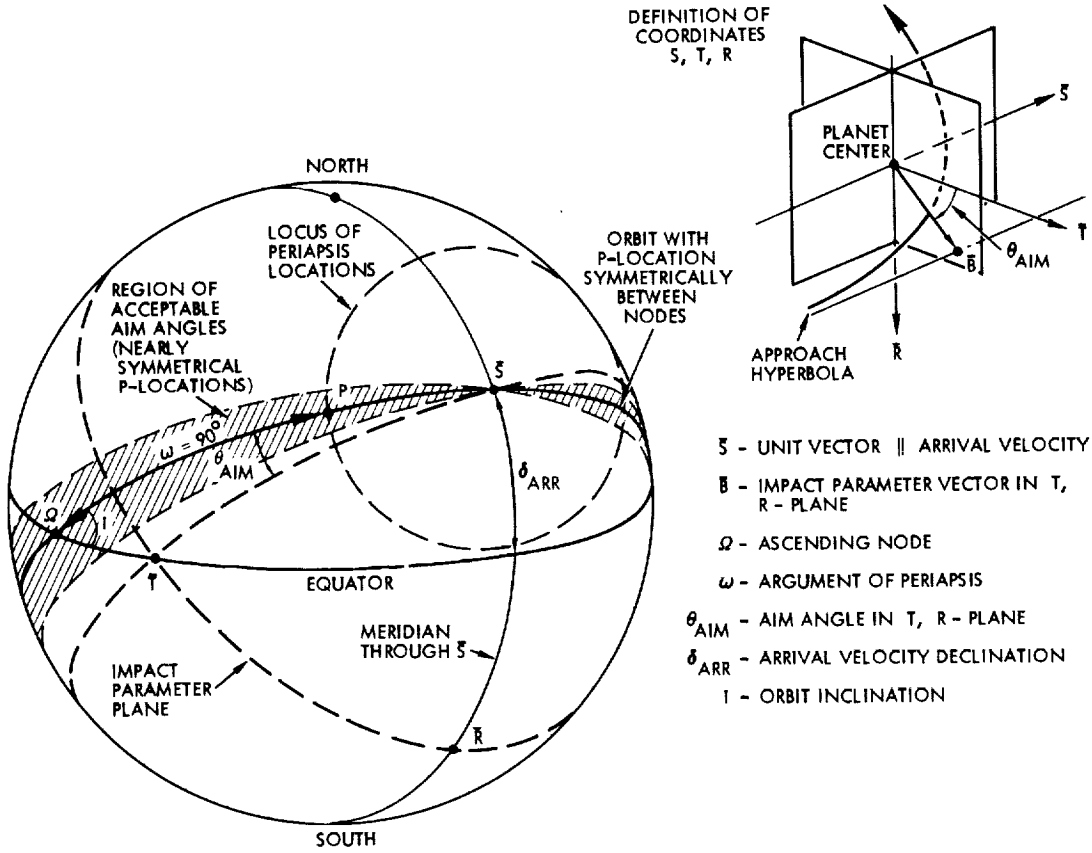

Figure 7-10. Geometry of Saturn Orbit with Periapsis Located Symmetrically Between Nodes

Principal parameters that govern the orbital geometry in three-dimensional space (see Figure 7-10) are the declination δ_{arr} of the arrival velocity vector and the aim angle θ_{aim} of the planetocentric approach trajectory. θ_{aim} is defined as the orientation of the $\overline{B}$ vector relative to the T axis in the impact parameter plane as illustrated by the sketch at the upper right in Figure 7-10. While δ_{arr} is fixed for a given heliocentric transfer trajectory, the aim angle θ_{aim} can be selected according to preferred planetary approach and orbit characteristics.

The geometrical relations illustrated in Figure 7-10 show that the orbital inclination (i) and the argument of the periapsis (ω) as measured from the ascending node (Ω) are controlled by the choice of aim angle, θ_{aim}. The aim angle which minimizes the orbit inclination ($i_{min} = \delta_{arr}$), is different from that which places the periapsis location (P) symmetrically between the ascending and descending nodes, at ω = 90 degrees. Orbits with periapsis locations in the vicinity of the symmetrical case correspond to a limited range of aim angles, as indicated by the shaded region in Figure 7-10. Constraints imposed on the aim angle to assure that the ring crossing distance is greater than a specified boundary r_B are shown in Figure 7-11 as function of the periapsis distance r_p. (Distances r_B and r_p indicated in this graph are normalized with respect to Saturn's radius.) It is noted that the aim angle constraints narrow down to a small range as the periapsis distance approaches half the value of the specified ring crossing distance r_B. The minimum value $r_p \simeq 1/2\ r_B$ corresponds to the symmetrical case, ω = 90 degrees. This condition reflects the fact that for large orbital eccentricities the distance at the semi-latus rectum is approximately twice that at the periapsis since these orbits are closely approximated by parabolas.

Figure 7-12 shows the ΔV reduction achievable by lowering the periapsis to distances closer than the specified minimum ring crossing distance. Two cases are illustrated with ring crossing distances set at 2.3 R_S (nominal outer perimeter of Saturn's Ring A) and 3 R_S, and with apoapsis distances ranging from 40 to 100 R_S. The resulting ΔV reduction can be as large as 400 and 700 m/s, respectively, at the corresponding lower limit of possible periapsis distances. This amounts to 27 and 47 percent, respectively, of the total available ΔV capability, assumed to be 1500 m/s. The results show that an optimum choice of the periapsis location is very important in planning the Saturn orbit mission and that tight constraints on selecting the aim point and orbital inclination are to be accepted in order to make the most effective use of the limited ΔV capability of the Saturn orbiter spacecraft.

7.3.3 Effect of Finite Thrust Acceleration and Constant Thrust Direction

The ΔV penalty resulting from non-impulsive orbit insertion at Saturn and at constant thrust direction, dictated by the earth-pointing mode, is smaller by a factor of 2 than in the case of Jupiter orbit insertion

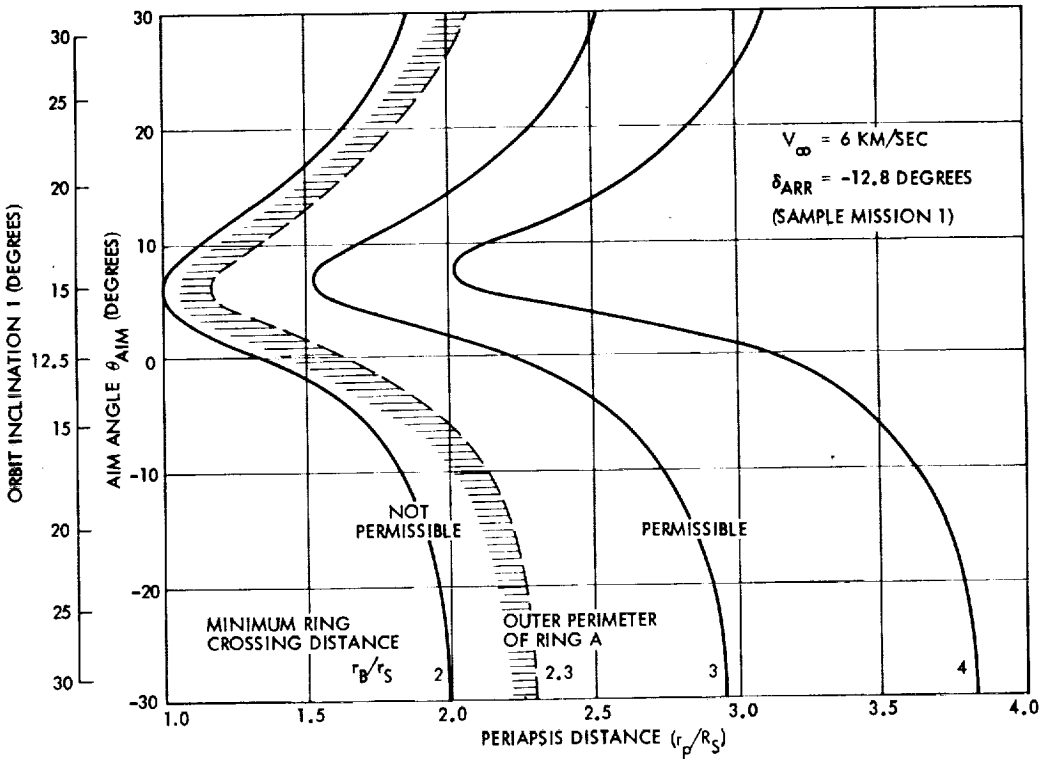

Figure 7-11. Boundary of Permissible Aim Angles and Orbit Inclinations

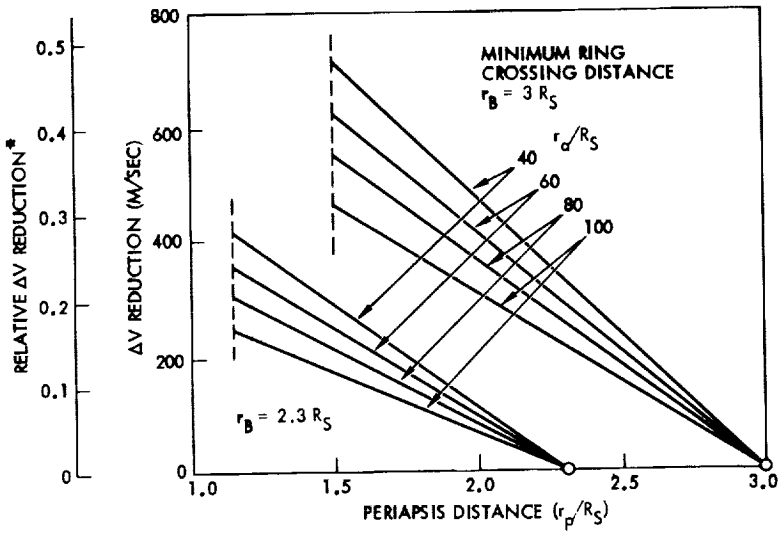

*RELATIVE ΔV - REDUCTION BASED ON NOMINAL ΔV CAPABILITY OF 1500 M/SEC

Figure 7-12. ΔV Reduction Through Lowering of Periapsis Distance

(see Figure 6-18) if performed at the same relative periapsis distance, r_p/r_o. This is explained by the fact that ΔV_L is proportional to V_{esco}^2/r_o^2 as discussed in Section 6.8.2. In the range of retro ΔV maneuvers assumed for the Saturn mission, and with thrust accelerations 30 to 40 percent larger (because of the smaller gross spacecraft weight) the ΔV penalty only amounts to about 5 m/s if the periapsis distance is 2 R_S.

7.3.4 Orbit Insertion in the Earth-Pointing Mode

Referring to the discussion in Section 6.8.3 and Appendix B, constraints on the selection of arrival conditions dictated by the earth-pointing maneuver requirement were analyzed for the Saturn orbiter. Figure 7-13 shows the deviation angle, Δ, of the earth line from the optimum (tangential) thrust orientation and the resulting cosine losses, for earth-Saturn trajectories in 1982 and 1986 with trip times ranging from 1400 to 1900 days. (See Figure 6-19 for Jupiter orbits.)

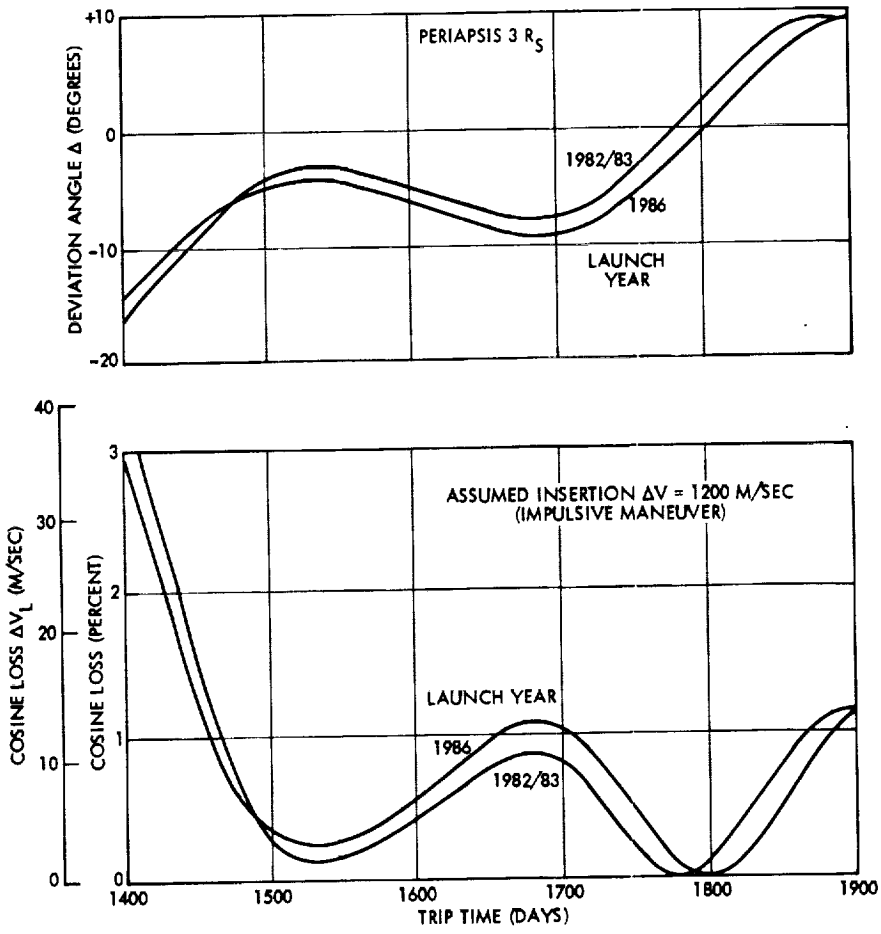

Figure 7-13. Saturn Orbit Insertion in Earth-Pointing Mode: Deviation Angle (Δ) and Cosine Losses (ΔV_L) Vs. Trip Time

It is seen that the choice of an 1800-day trip time in the sample trajectories selected for 1982 and 1986 is nearly ideal for minimizing this ΔV penalty. It can be shown that, in general, this ΔV penalty remains quite small, i.e., less than 10 m/s over a relatively much wider range of trip times as compared to Jupiter missions.

7.4 SATURN ORBIT CHARACTERISTICS

Compared to the Jupiter orbits discussed in Section 6, orbits achievable about Saturn are more highly eccentric, and the initial orbit inclination cannot be significantly changed, owing to the more limited maneuver capability of the Saturn orbiter spacecraft. However, a sufficient ΔV capability margin will be available for orbit modifications that may be dictated by scientific objectives, e.g., to achieve encounters with some of Saturn's satellites.

Orbit Inclination

The initial orbit inclination is at least equal (in magnitude) to the declination angle δ_{arr} of the arrival velocity vector, i.e., 12.8 degrees for the 1983 sample trajectory, and 21.7 degrees for the 1986 sample trajectory. A major plane change maneuver cannot be considered since even a 10-degree change performed at the apoapsis of a 2 x 50 R_S orbit would require a maneuver velocity of 175 m/s. Actually, completion of the mission without a change of the initial orbit inclination appears reasonable since the inclined orbit permits better global coverage of planetary features and better observation of ring phenomena than in equatorial orbit. However, opportunities for achieving repeated satellite encounters are less favorable under these conditions.

It is proposed to utilize the ΔV capability (100 to 300 m/s) remaining after orbit injection for trim maneuvers that would be required for close encounters with selected satellites. Eight of the ten known satellites of Saturn are within the range of a 2 x 50 R_S spacecraft orbit.

Generally, the encounter velocities are not much increased by noncoplanar intercept conditions unless the encounter occurs close to apoapsis or periapsis. For example, in the case of a coplanar 2 x 50 R_S spacecraft orbit the relative velocity of a Titan encounter (at a radius of 20.2 R_S and at a true anomaly of 151 degrees) would be 6.6 km/s. This velocity would increase by only six percent if the spacecraft orbit were inclined by 60 degrees.

In-Plane Orbit Trim Maneuvers

As shown in Section 6.10 and Appendix B.6 the eccentricity of the orbit and hence the orbital period are highly sensitive to trim maneuvers at periapsis. E.g., a one-day change of the period of a 2 x 50 R_S orbit (from 22.4 to 23.4 days) can be achieved by a 15 m/s velocity change at periapsis. This property permits the repeated time adjustments required for satellite encounters with a reasonable maneuver economy.

Maneuvers performed at apoapsis to change the periapsis radius are economical because of the leverage provided by the high orbital eccentricity. It may be desirable after achieving the initial capture orbit at a low periapsis radius to raise the periapsis in order to minimize spacecraft exposure to the particle environment close to the rings in subsequent orbital passes. The velocity increment at apoapsis required to raise the periapsis of a 2 x 50 R_S orbit by 1 R_S is 230 m/s. At a 100 R_S apoapsis distance the required velocity would only be 103 m/s.

Orbit Perturbation

Orbit perturbations due to Saturn's oblateness are nearly as small as at Jupiter, as shown in Appendix B.5. The nodal regression of a 2 x 50 R_S orbit with 30-degree inclination is only 0.03 degree per day. The apsidal advance rate is 0.004 degree per day. Although this rate is a more sensitive function of orbit inclination than the nodal regression (at i = 60 degrees the apsidal advance is 0.047 degree per day), there is no cause for concern about the long-term drift of the periapsis closer to the ring crossing point and possible increased ring particle impact hazard since at the maximum rate considered here the periapsis would drift only about 1 degree per orbit.

7.5 NAVIGATION

Navigation characteristics of the Saturn orbiter mission were discussed in Section 6.13 in conjunction with those of the Jupiter orbiter. It should be noted that greater navigational errors which occur in the Saturn mission cruise and encounter phases propagate into orbital accuracy as follows:

- Cruise navigation errors are roughly twice as large as in the Jupiter mission.
- Approach navigation errors are also about twice as large owing to the greater ephemeris uncertainty of Saturn.
- The sensitivity of the capture orbit apoapsis to position errors at injection is more than three times larger at Saturn owing to the greater orbital eccentricity. As derived in Appendix B.6 the increase in sensitivity is proportional to m (2 + m), where $m = r_a/r_p$. Due to the more limited maneuver capacity of the Saturn orbiter, the apsidal ratio m is 50 to 100 percent larger than at Jupiter which explains the large increase in apoapsis sensitivity.
- Similarly, the sensitivity of the orbital period increases strongly, typical in the ratio of 2:1. The resulting large dispersions in the dimension and period of the capture orbit can be corrected by subsequent trim maneuvers. The greater orbital sensitivity which magnifies the orbital dispersion of course also facilitates the performance of the correction maneuvers. Periapsis position uncertainty, about twice as large as in the Jupiter mission, is still

small enough to preclude concern with the feasibility of a safe orbit injection at the relatively small periapsis distance of 2 to 3 planet radii.

7.6 OPERATIONAL SEQUENCE

The operational sequence during the launch, cruise and arrival phase is essentially similar to that discussed for the Jupiter orbiter mission (Table 6-7). The greater target distance may require additional midcourse maneuvers without actually imposing new operational requirements. The orbital phase differs from that of the Jupiter orbiter only in terms of the reduced number and magnitude of projected orbit change maneuvers, notably the omission of a major plane change maneuver.* Because of the similarities between the two mission profiles a detailed description of the operational sequence can be omitted.

7.7 PERFORMANCE SUMMARY

The nomograph for parametric evaluation of Pioneer Saturn orbiter performance characteristics shown in Figure 7-14 is similar to the Jupiter orbiter nomograph (Figure 6-29), except for the trajectory data presented in the upper and lower left quadrants. C_3 vs. V_∞ characteristics of earth-Saturn trajectories launched in 1982, 1984 and 1986 (lower left) are those previously shown in Figure 7-3. Saturn orbit dimensions achievable as function of orbit insertion ΔV vs. arrival velocity V_∞ (upper left) are derived from data presented in Figures 7-8 and 7-9.

The example illustrated in the nomograph assumes a mission launched in 1984 with a trip time of 1800 days, characterized by $C_3 = 118$ km^2/s^2 and $V_\infty = 6.2$ km/s. The gross injected weight is 1400 pounds. The inert weight is assumed as 850 pounds and the total usable propellant weight as 550 pounds. This provides a total ΔV capability of 1400 m/s of which 100 m/s are allocated to midcourse and approach guidance maneuvers, and 100 m/s for orbit trim maneuvers. 1200 m/s allocated to the orbit insertion maneuver can achieve a Saturn orbit with dimensions of 3 x 100 R_S at the arrival velocity of 6.2 km/s. The orbit period would be 67 days. Other orbit dimensions achievable with this ΔV allocation would be 2 x 50 R_S (22 days) and 1 x 25 R_S (7 days). We note that for shorter trip times and hence larger arrival velocities the orbital eccentricities would increase very rapidly. A somewhat greater performance margin would be available for a 1986 mission, permitting a propellant load of 650 pounds with a total ΔV capacity of 1547 m/s, or permitting an increase of inert weight by about 75 pounds if the ΔV capability is kept the same as in the

*With generally longer orbital periods in the Saturn mission more time is available between critical events, a factor which mitigates the longer communication round-trip time delay (~2.8 to 3 hours).

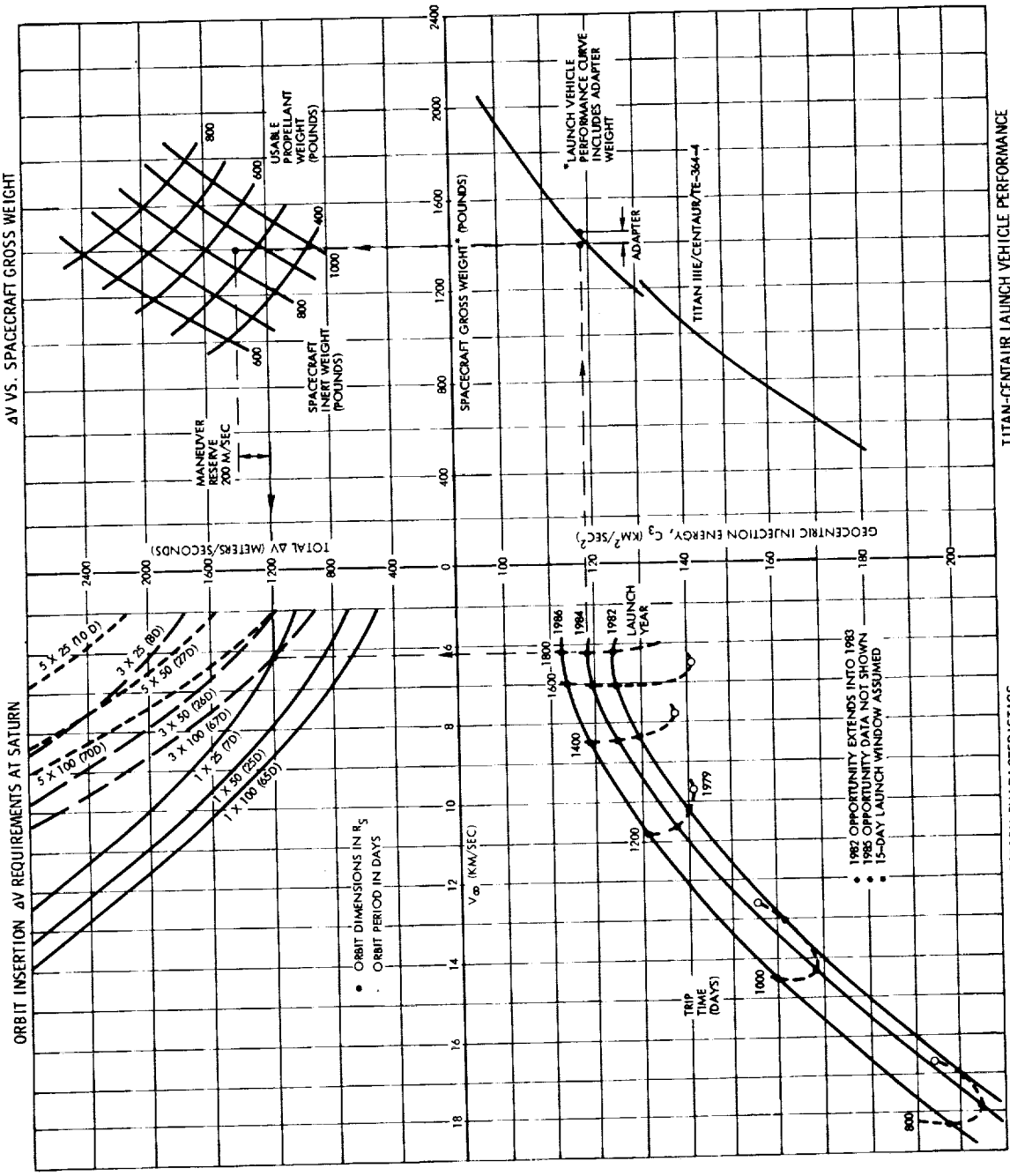

Figure 7-14. Saturn Orbit Insertion Performance Chart

previous example. We also note that in the 1982 mission year the total ΔV capability is limited to 1100 m/s. Orbital dimensions achievable in this case would be 2 x 100 R_S requiring an injection velocity of 950 m/s with almost no margin for subsequent trim maneuvers. Performance characteristics for the 1986 mission are summarized in Table 7-3.

Table 7-3. Performance Summary of Saturn Orbiter

Launch year	1986
Trip time, days	1800
Injection energy C_3 [1], km^2/s^2	113
Maximum launch vehicle weight capacity, lb	1600
Launch weight penalty (estimated), lb	30
Adapter weight allowance, lb	50
Injected gross spacecraft weight, lb	1470
Launch vehicle capability margin, lb	50
Total usable propellant weight, lb	650
- Propellant used in transit, lb	30
- Propellant used for orbit insertion,* lb	542
- Propellant used for orbit change,* lb	58
Science payload weight, lb	70
Spacecraft less usable propellant, [2] lb.	813
Arrival velocity, km/s	6.2
Total ΔV capability at arrival,* m/s	1547
Orbit injection ΔV,* m/s	1350
Allowance for orbit changes,* m/s	197
Initial orbit dimensions, R_S	3 x 75
Orbit period, days	42

[1] Assumes 15-day launch window

[2] Less than Jupiter orbiter by 104 to 111 pounds

* Bipropellant weights and maneuver capabilities only

8. CONCLUSIONS

The results presented in this report show that the baseline Pioneer F/G spacecraft design can be readily adapted, with some modifications, to the requirements of Jupiter and Saturn orbit missions. The spacecraft would be launched by the Titan III E/Centaur/TE 364-4, which presents a launch environment and interfaces comparable to the Atlas/Centaur/TE 364-4 that was used for the Pioneer 10 and 11 Jupiter flyby missions, except for providing a larger (14-foot) standard payload fairing.

The major configuration change is the attachment of a new, external propulsion module to provide the requisite large maneuvering capability for planetary orbit insertion and orbit modification. Typically, the added ΔV capability is 2100 m/sec and 1400 m/sec, respectively, for Jupiter and Saturn orbit missions in the 1981 to 1985 time period.

The propulsion system uses conventional earth-storable hypergolic bipropellants (N_2O_4/MMH) of the type successfully flown on the Mariner 9 (1971) Mars Orbiter and in several earth orbital applications. An engine with 100 lb_f thrust level was selected as a compromise between higher thrust levels, desired for most effective planetary orbit insertion, and lower thrust levels which would minimize the structural loads on deployed appendages, giving a maximum thrust acceleration of about 0.1 g when the propellant tanks are empty.

Although it would be desirable to use the same propulsion module in both the Jupiter and Saturn orbiter applications, it was found preferable to adopt custom designed propulsion modules with different propellant capacity for the two missions, since reduction of inert weight is essential for best performance in the weight-critical Saturn orbiter spacecraft.

In the interest of system commonality in both missions it would actually be possible to use the lower capacity Saturn orbiter propulsion module in the Jupiter mission but only at a considerable performance sacrifice. The injected weight capability of the Titan/Centaur launch vehicle would not be fully utilized in that case.

Modifications of the Pioneer baseline configuration are necessitated by:

a) The attachment of the propulsion module and the interface requirements associated with this change (e.g., rearrangement of thermal control louvers to equipment compartment sidewalls)

b) Accommodation of a larger science payload complement (as large as 120 lb_m in the Jupiter mission) and catering to higher data rate telemetry and data handling requirements of more sophisticated payload instruments such as a high-resolution line scan image system

c) Use of uprated RTG power sources, i.e., MHW generators replacing the SNAP-19 units of the baseline Pioneer spacecraft, to provide additional power needed for the enlarged payload complement, greater telemetry bit rate capability, for thermal control and operation of the added propulsion module, and to meet the extended mission duration

d) Various minor changes in engineering subsystems such as added command capability for spacecraft operation in new mission modes (e.g., the retro-propulsion maneuver) and new science payload support requirements (e.g., operation of articulated sensor platform).

In summary, none of the modifications adopted in the design of the Pioneer Outer Planets Orbiter require the use of novel technology or entail significant new development risks. The modifications in the power subsystem and other electrical subsystems are based on hardware evolution common to other concurrent or recent spacecraft programs, such as the use of S-band/X-band downlink communications and increased transmitter power (Viking and Mariner Jupiter/Saturn spacecraft); MHW power generators (MJS spacecraft); N_2O_4/MMH propulsion module (Mariner 9 and Mariner Jupiter Orbiter) and high data capacity solid-state C-MOS data storage system (High Energy Astronomical Observatory).

Reliability characteristics of the outer planet orbiters have been analyzed with particular attention to the extended mission life of 3.5 and 6.0 years for the Jupiter and Saturn orbiters, respectively. Nominal mission success probabilities of 0.70 and 0.45 determined by this analysis can be improved by selected addition of redundancy in critical components, especially the propulsion, attitude control, communication and data handling subsystems. Thus, by a modest improvement program the reliability of the Saturn orbiter can be raised to about 0.6, while that of the Jupiter orbiter is comparable to Pioneer F/G even without further improvement.

Recommended areas for future study include:

- Payload instrument definition in greater detail
- Review of science payload accommodation requirements and capabilities based on payload definition
- More detailed definition of operational modes and sequences, and implementation by the command subsystem
- Additional study of ground system interfaces and mission operations
- Effect of new planetary orbit modification concepts such as satellite tours and swingby maneuvers (orbit pumping and cranking) on spacecraft operations, navigation and guidance requirements.

In addition, the possible adaptation of Pioneer F/G with less extensive modification to a more modest Jupiter orbiter mission should also be studied as an alternative to the design concept presented in this report. Of particular interest in this context is the possible use of Pioneer F/G spare units and qualification test hardware (appropriately refurbished) in a Pioneer H Jupiter orbiter mission of lesser scope, as currently envisioned under a joint NASA/ESRO sponsored feasibility study program.

REFERENCES

1. "Pioneer F/G Spacecraft Operational Characteristics Study Final Report," 71-7531.9-14, TRW Systems Group, Redondo Beach, California, 23 April 1971.

2. "The Pioneer Mission to Jupiter," NASA SP-268.

3. "Outer Planets Pioneer Spacecraft," NASA/Ames Research Center, 15 April 1974.

4. "Extended Life Outer Planets Pioneer Spacecraft," NASA/Ames Research Center, 5 March 1974.

5. "Study of Follow On Pioneer Missions to Jupiter, Pioneer Jupiter Orbiter Mission," (four volumes), 20406-6004-RU-00, TRW Systems Group, Redondo Beach, California, August 13, 1971.

6. "The Planet Jupiter (1970)," NASA SP-8069, December 1971.

7. "The Planet Saturn (1970)," NASA SP-8091, 1972.

8. J. C. Beckman, J. R. Hyde, and S. I. Rasool, "Exploring Jupiter and its Satellites with an Orbiter," Astronautics & Aeronautics, September 1974.

9. "Study of Alternate Retro-Propulsion Stage Configurations for the Pioneer Outer Planet Orbiter," 22303-6003-RU00, TRW Systems Group, November 30, 1973.

10. "Study of Orbit Insertion Propulsion for Spinning Spacecraft," Jet Propulsion Laboratory, October 18, 1971.

11. "A Feasibility Study of Developing Toroidal Tanks for a Spinning Spacecraft," MCR-73-223, Martin Marietta Corporation, September 1973.

12. "Saturn Uranus Atmospheric Entry Probe Mission, Spacecraft System Definition Study, Final Report," 23267-6001-RU-00, TRW Systems Group, July 15, 1973.

13. "Pioneer Spacecraft Operation at Low and High Spin Rates," 22303-6002-RU00, TRW Systems Group, October 5, 1973.

14. T. W. Price and D. L. Wong, "Space Storable Propellants Demonstration Module," presented at AIAA/SAE 9th Propulsion Conference, Las Vegas, Nevada, November 1973.

15. "Pioneer F/G Final Report Spacecraft System Reliability Prediction," 71-2286.2-008, TRW Systems Group, 22 January 1971.

16. "Demonstrated Orbital Reliability of TRW Spacecraft," D-00735-73-2286.145, TRW Systems Group, Redondo Beach, California, December 1973.

17. "Comparative Reliability Study of Monopropellant and Bipropellant Jupiter Mission Systems," Final Report, TRW Systems Group, November 14, 1969.

18. "Planetary Flight Handbook, Part 7, Direct Trajectories to Jupiter, Saturn, Uranus, and Neptune," NASA SP-35.

19. J. C. Niehoff, "Touring the Galilean Satellites," AIAA Paper 70-1070, August 1970.

20. J. C. Beckman and D. B. Smith, "The Jupiter Orbiter Satellite Tour Mission," presented at AAS/AIAA Astrodynamics Conference, Vail, Colorado, July 16-18, 1973.

21. "Preliminary Mission Designs for Jupiter Orbiter Missions," NASA TM X-2565, May 1972.

22. D. W. Curkendall and V. J. Ondrasik, "Analytic Methods of Orbit Determination," presented at AAS/AIAA Astrodynamics Conference, Vail, Colorado, July 16-18, 1973.

23. "Advanced Pioneer Planetary Probe Mission Guidance and Navigation Requirements, 760-88, Jet Propulsion Laboratory, Pasadena, California, 15 November 1973.

24. T. C. Hendricks, E. D. Vogt, and D. V. Byrnes, "Navigation and Dispersion Analysis for Probe Missions to Jupiter, Saturn, and Uranus," presented at AAS/AIAA Astrodynamics Conference, Vail, Colorado, July 16-18, 1973.

25. "Feasibility Test for a V-Slit Star Mapper for Pioneer Spacecraft Terminal Navigation, Final Report," R 7537.2-451, TRW Systems Group, Redondo Beach, California, November 1973.

26. "Encounter Phase Orbit Determination Strategy and Accuracy for Pioneer 10 and 11," 616-44, Jet Propulsion Laboratory, Pasadena, California, September 1, 1973.